HYDRAULIC MACHINES: TURBINES AND PUMPS

Second Edition

Grigori Krivchenko

LEWIS PUBLISHERS
Boca Raton Ann Arbor London Tokyo

205487

Library of Congress Cataloging-in-Publication Data

Krivchenko, G. I.

Hydraulic machines: turbines and pumps/G. I. Krivchenko.—[2nd ed.]

p. cm.

Includes bibliographical references and index.

ISBN 1-56670-001-9

1. Hydrualic machinery. I. Title.

TJ840.K76 1993

621.2—dc20 93-8853

CIP

1996 00379

LN79397

This book contains information obtained from authentic and highly regarded sources. Reprinted material is quoted with permission, and sources are indicated. A wide variety of references are listed. Reasonable efforts have been made to publish reliable data and information, but the author and the publisher cannot assume responsibility for the validity of all materials or for the consequences of their use.

Neither this book nor any part may be reproduced or transmitted in any form or by any means, electronic or mechanical, including photocopying, microfilming, and recording, or by any information storage or retrieval system, without prior permission in writing from the publisher.

CRC Press Inc.'s consent does not extend to copying for general distribution, for promotion, for creating new works, or for resale. Specific permission must be obtained in writing from CRC Press for such copying.

Direct all inquiries to CRC Press, Inc., 2000 Corporate Blvd., N.W., Boca Raton, Florida 33431.

© 1994 by CRC Press, Inc.
Lewis Publishers is an imprint of CRC Press
No claim to original U.S. Government works

International Standard Book Number 1-56670-001-9

Library of Congress Card Number 93-8853
Printed in the United States of America 1 2 3 4 5 6 7 8 9 0
Printed on acid-free paper

Contents

Preface ix

About the Author xi

SECTION 1 MAIN DEFINITIONS

Chapter 1 Hydraulic Machines and Hydraulic Energy 3
1.1. Hydraulic Machines 3
1.2. Energy of Fluid (Water) 8

SECTION 2 HYDRAULIC TURBINES

Chapter 2 Parameters and Kinds of Turbines 17
2.1. Turbine Head 17
2.2. Turbine Capacity (Power) 21
2.3. Principal Turbine Types 22
2.4. Applications of Turbines of Various Classes and Kinds 28

Chapter 3 Turbine Design 31
3.1. Axial-Flow, Adjustable Blade (Kaplan) Turbines . . . 31
3.2. Horizontal Axial-Flow Turbines 39
3.3. Mixed-Flow (Diagonal) Adjustable Blade Turbines . 43
3.4. Radial-Axial-Flow (Francis) Turbines 45
3.5. Pelton Turbines 50
3.6. Small Hydroelectric Power Plant Turbines 54
3.7. Shafts and Bearings 55
3.8. Development of Turbine Designs 59

Chapter 4 Turbine Power Regulating Mechanisms 61
4.1. Guide Vane Operating Gear 61
4.2. Runner Blade Operating Gear of Adjustable Blade Turbines 63
4.3. Operating Gear of the Pelton Turbine Regulating Needle 66

Chapter 5 Theoretical Fundamentals of the Turbine Working Process 69
5.1. Water Flow Created by the Wicket Gate of the Reaction Turbines 69
5.2. Kinematics of Water Flow in Reaction Turbine Runner 72
5.3. Operating Conditions (Regime) of the Turbine 77

5.4. Turbine Energy Equation 79
5.5. Operating Process of Impulse [Pelton] Turbines . . . 85
5.6. Turbines of One Type and Similarity Laws for Their Modes of Operation 86
5.7. Reduced Turbine Parameters 90
5.8. Specific Speed 93
5.9. Mode of Water Motion in the Turbine Runner 97

Chapter 6 Supply and Discharge Elements of Turbines 101
6.1. Turbine Cases 101
6.1.1. Types of Turbine Cases 101
6.1.2. Design of Turbine Cases 102
6.1.2.1. Design of the Average Velocities . . . 109
6.1.2.2. Design of a Spiral Case 112
6.2. Draft Tubes 114
6.2.1. Performance 115
6.2.2. Types of Draft Tubes 118
6.2.1.1. Straight Draft Tubes 118
6.2.1.2. Elbow-Type Draft Tubes 119

Chapter 7 Cavitation and Permissible Suction Lift 125
7.1. Cavitation 125
7.2. Turbine Cavitation Coefficient and Permissible Suction Height 132
7.2.1. Determining the Cavitation Coefficient 135

Chapter 8 Turbine Characteristics 139
8.1. Kind of Characteristics 139
8.1.1. General Characteristics 140
8.1.2. Linear Characteristics 143
8.2. Determination of Characteristics by Model Tests . . 144
8.3. Plotting the Characteristics of the Adjustable Blade Turbines 148
8.4. Conversion of Model Parameters to Full-Scale Equipment 151
8.4.1. Losses in Turbine and Balance Characteristics 152
8.4.2. Determination of Efficiency of a Full-Scale Turbine 154
8.4.3. Theoretical Basis of Hydraulic Efficiency Correction Formula 157
8.5. Plotting Linear Characteristics Based on Universal Characteristics 160
8.6. Plotting Operation Characteristics 161
8.7. Runaway Characteristics of Turbines 164

8.8. Axial Loads Acting on the Turbine Runner 167
8.9. Comparing Turbines of Different Types via Their Characteristics 168

Chapter 9 Selecting Turbines for Hydroelectric Power Plants (HEPPs) 171
9.1. Hydroelectric Unit and Powerhouse of HEPP 171
9.2. Nomenclature of Reaction Turbines 173
9.2.1. Turbine Type Marks and Range Chart 173
9.2.2. Specific Speed of Turbines 176
9.2.3. Axial-Flow Adjustable Blade Vertical Turbines 177
9.2.4. Axial-Flow Adjustable Blade Horizontal Bulb-Type Turbines 179
9.2.5. Mixed-Flow Adjustable Blade Turbines 179
9.2.6. Propeller-Type Axial-Flow and Mixed-Flow Turbines 182
9.2.7. Radial-Axial Flow Turbines 182
9.2.8. Turbine Mass or Weight Data 182
9.3. Selecting Reaction Turbines Using Reduced Characteristic Parameters 185
9.3.1. Calculation Procedure 185
9.4. Peculiarities in Selecting Pelton Turbines 191
9.5. Hydroelectric Power Plant Operation Curves 196
9.6. Total Characteristics of HEPP Turbines Operating in Parallel 197

Chapter 10 Automation, Installation, and Operation of Turbines 201
10.1. Turbine Automatic Control Systems 201
10.1.1. Oil Pumping Unit 202
10.1.2. Control Cabinet 203
10.1.3. Design Features of Automatic Controllers for Adjustable Blade Turbines 204
10.1.4. Peculiarities of Automatic Control in Pelton Turbines 206
10.1.5. Turbine with Pressure Regulator 207
10.2. Installation of the Turbines 209
10.3. Operation of the Turbines 213

SECTION 3 PUMPS

Chapter 11 Basic Characteristics of Pump Installations and Types of Pumps 219
11.1. Heads of Pump Installation 219

11.2. Pump Capacity 224
11.3. Types of Pumps. 225
11.3.1. Positive Displacement Pumps 226
11.3.2. Rotodynamic Pumps 230
11.3.3. Classification of Pumps 232

Chapter 12 Working Process of Impeller Pumps 235
12.1. Kinematics of Flow 235
12.2. Main Energy Equation. 239
12.3. Pump Operation and Operation Similarity Conditions. 243
12.4. Specific Speed 248
12.5. Structure of Flow 252
12.6. Pump Energy Losses 253

Chapter 13 Construction of Impeller Pumps 255
13.1. Types 255
13.2. Cradle-Mounted Pumps 256
13.3. Double-Entry Pumps 258
13.4. Axial-Flow Pumps 260
13.5. Mixed-Flow Pumps 263
13.6. Vertical Centrifugal Pumps 265
13.7. Multistage Pumps 266
13.8. Some Elements of Impeller Pump Construction . 270

Chapter 14 Cavitation in Pumps 277
14.1. Cavitation and Permissible Suction Lift 277
14.1.1. Permissible Vacuum Suction Lift 278
14.1.2. Net Positive Suction Head 280
14.2. Converting Cavitation Characteristics vs Changes in Pump Rotational Speed 282
14.2.1. Vacuum Suction Lift 282
14.2.2. Net Positive Suction Head 283
14.3. Pump Specific Speed Cavitation Coefficient 285

Chapter 15 Characteristics of Impeller Pumps 287
15.1. Kinds 287
15.2. Theoretical Characteristics 290
15.3. Experimental Determination of Pump Characteristics 292
15.4. Dependence of Pump Characteristics on Specific Speed 294
15.5. Converting Pump Characteristics 295

Chapter 16 Pump Selection 297
16.1. Pump Units of Pump Plants and Installations . . 297
16.2. Characteristic of Water System and Actual Delivery of Pump 301
16.3. Nomenclature of Pumps 302
16.3.1. Pump Designation 303
16.3.2. Nomenclature of Impeller Pump 305
16.3.2.1. Centrifugal Cradle-Mounted Pumps 305
16.3.2.2. Centrifugal Double-Entry Pump 306
16.3.2.3. Centrifugal Vertical Pump 306
16.3.2.4. Vertical Axial-Flow Pump 306
16.3.2.5. Horizontal Axial-Flow Pump . . 307
16.4. Parallel Connection of Pumps to a Common Pipeline 308
16.5. Series Connection of Pumps to a Common Pipeline 311
16.6. Selection of Pumps 312

Chapter 17 Operation of Impeller Pumps 317
17.1. Starting 317
17.2. Delivery Control of the Impeller Pump 322
17.2.1. Control by Gate Valve or by Throttling . 322
17.2.2. Control by Varying Pump Speed of Rotation 323
17.2.3. Control via Bypassing 325
17.2.4. Control by Changing the Impeller Blade Angle 325
17.2.5. Control by Changing the Circulation of Flow Before the Entrance to the Impeller 326
17.2.6. Control by Changing the Number of Pumps 326
17.3. Installation of Impeller Pumps 327
17.4. Cavitation and Abrasive Wear of Pumps 328
17.5. Unstable Operation of Pump 332
17.6. Pump Sumps 335

Chapter 18 Special Pumps 339
18.1. Dredge Pumps 339
18.2. Well Pumps 346
18.2.1. Well Pumps with Transmission Shaft 346

18.2.2. Immersion Motor Well Pumps 348
18.3. Hydraulic Pumped-Storage Plants Pumps 350
18.4. Jet Pumps 353
18.5. Vacuum Groundwater Lowering Installations . . 360
18.6. Air Lift 361
18.7. Hydraulic Ram 363

SECTION 4 REVERSIBLE HYDRAULIC MACHINES (PUMP-TURBINES)

Chapter 19 Characteristics of Reversible Hydraulic Machines 367
19.1. Application 367
19.2. Reversibility of Hydraulic Machines and Principal Characteristics of Pump and Turbine Modes 368
19.3. Determining the Parameters of Reversible Pump-Turbines via Generalized Characteristics 373
19.4. Circular Characteristic of the Impeller Hydraulic Machine 376
19.5. Types of Reversible Pump-Turbines and Their Universal Characteristics 378

Chapter 20 Constructions of Reversible Hydraulic Machines (Pump-Turbines) 385
20.1. Radial-Axial Flow Pump-Turbines 385
20.2. Mixed-Flow Reversible Pump-Turbines 387
20.3. Multistage Reversible Pump-Turbines 392
20.4. Double-Wheel Reverisble Pump-Turbines 393

Main Symbols 397

Appendices: Measuring Units and Their Conversion 399

Bibliography 403

Index 405

Preface

Hydraulic machines, pumps, turbines, and in the last few decades, reversible pump-turbines, are widely used in many branches of industry, agriculture, energy production, municipal economy, and construction, and consequently, large numbers of specialists must work with hydraulic machines in their daily practice. These specialists are of two groups: persons who design and manufacture different hydraulic machines, and rather more numerous, persons interested in the use and maintenance of hydraulic machines. Although the problems and tasks of both groups are different they are strongly interconnected. Such links are based on the necessity of realizing the best and most profitable transformation or use of flowing liquid energy. It is the basic approach of this volume.

Principally, the book concerns the types and construction of hydraulic machines and the mechanical aspects of their operation, the most important parameters such as heads, discharges, power, capacity efficiency, cavitation factors, reliability, and others. The items that characterize the performance of pumps, turbines, and reversible pump-turbines are analyzed in detail. These characteristics are vital to their selection for use in waterworks systems and structure design and for establishing the best conditions for their maintenance.

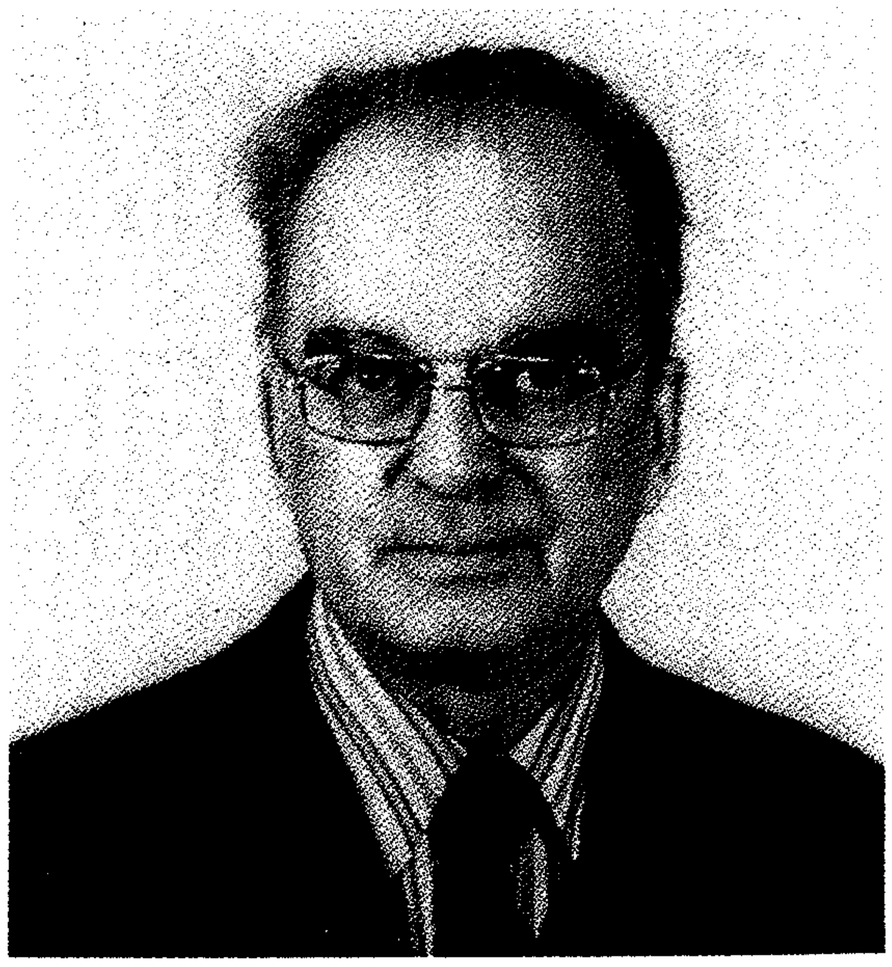
The book contains a large number of drawings of different constructions and designs of hydraulic machines. The volume also contains charts and other concrete data that can be employed for the selection and determination of the operational properties of hydraulic machines.

Some portions of text are supplemented by numerical examples. The aim of these examples is not only to illustrate the use of calculation methods and formulas, but is also important for a more complete understanding of the problems and influence of acting factors.

This book is based on the course given to students of the Moscow Institute of Civil Engineering; on the vast experience of persons involved in designing hydroelectric stations, pumping plants, and other waterworks systems; and on laboratory and field investigations. The book has been updated several times and has been published in Russian, Chinese, and English. This second edition includes such items as losses in hydraulic machines and their efficiency, cavitation factors, and the use of generalized parameters, whereby the base of the discussions has been widened. Several new chapters devoted to pump sumps, runner and impeller axial and radial thrust, as well as other topics, have been added; additional examples have been introduced.

The book is divided into four sections: general discussion, those devoted to turbines, pumps, and pump-turbines. The sections dealing with turbines and pumps are composed so that they can be studied separately. This is convenient for use by different types of specialists.

The Author



Grigori Krivchenko received the first scientific degree of Doctor (D) in 1947 and the highest degree Doctor of Science (D.Sc) in 1966. Both were received at the Moscow Institute of Civil Engineering, where he was professor, leading courses in hydraulic machines and hydroelectric power stations. At the same time, he brought about a wide activity in research and designing of hydraulic machines, hydro-energy, and pumping systems.

Professor Krivchenko was a member of the Technical Council of the Ministry of Energy and Electricity, an expert of the State Planning Committee, a consultant of the State Designing Institute "Hydroproect" and others. He has published many articles and books including Water Hammer and Turbines Regulation, (1951); Governing Regimes of Kaplan Turbines (1960); Automation of Turbines (1964); Pumps and Turbines (1970); Hydromechanical Transients in Power Plant Installations (1975); Hydraulic Machines (1978, 1983, 1986); Hydroelectric Power Plants (1983, 1987).

From 1991 Dr. Krivchenko served as visiting professor in "Technion"-Israel Institute of Technology.

Dr. Krivchenko has a wide experience in academic and practical work in hydraulic machinery and in hydraulic engineering.

HYDRAULIC MACHINES:
TURBINES AND PUMPS

Second Edition

SECTION 1

Main Definitions

CHAPTER 1

Hydraulic Machines and Hydraulic Energy

1.1. HYDRAULIC MACHINES

The term hydraulic machine indicates a device in which mechanical energy is transferred from the liquid flowing through the machine to its operating member (runner, piston, etc.), or from the operating (working) member of the machine to the liquid flowing through it. Hydraulic motors (hydraulic turbines) are hydraulic machines in which the operating member receives energy from the liquid flowing through it, and the inlet energy of the liquid is greater than the outlet energy of the liquid. Where energy is transmitted from the working member to the flowing liquid and the energy of the liquid at the inlet of the hydraulic machine is less that the outlet energy indicates a hydraulic machine known as a pump.

Hydraulic turbines[1] are designed for service at hydroelectric power plants (HEPP) where they drive electric generators. The schematic diagram of a HEPP is shown in Figure 1.1a. Water is directed from the headwater (HW) via a pressure conduit to the turbine and is discharged into the tailwater (TW). In the turbine, the water's energy is converted into the mechanical energy of the rotating shaft. The shaft rotates the rotor of the electric generator (hydraulic generator); where the mechan-

[1]As the book considers only hydraulic turbines, the term "hydraulic" is omitted after this point.

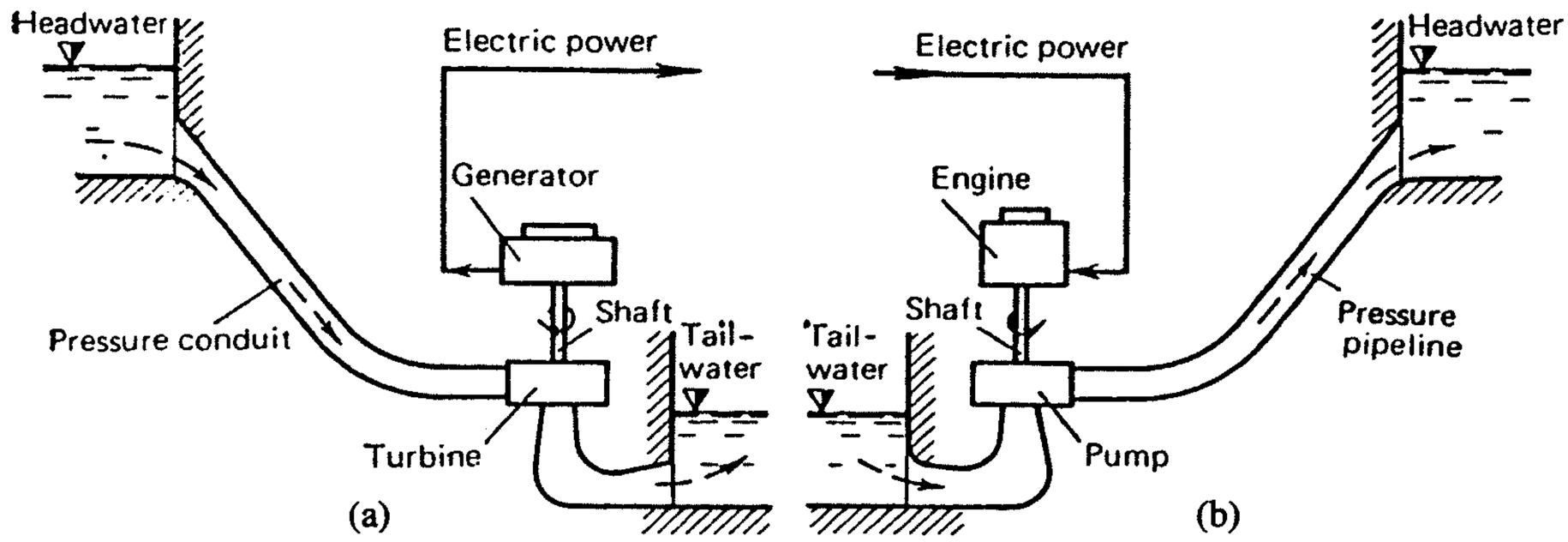


FIGURE 1.1. Turbine (a) and pump (b) installations.

ical energy is converted into electric power that is supplied to consumers via high-voltage transmission lines, sometimes for distances of 1000 km or more. A turbine coupled with a generator is called a hydroelectric unit, the characteristic parameters of which are the head (determined by the difference between the elevations of the HW and TW)and capacity or power. At various HEPPs heads vary widely—from several meters (low-head HEPP) to 700 to 1000 m and above (high-head plants). The capacity of a hydroelectric unit may amount to several tens or hundreds of kilowatts (micro- or small units) and reach 600,000 to 700,000 kW and even more (large and extra-large hydroelectric units).

Illustrated in Figure 1.2 is a vertical hydraulic unit with a low-head turbine (vertically arranged shaft or axis of rotation). Units of this kind are presently installed in hydroelectric plants with heads up to 50–70 m constructed on lowland rivers such as the Columbia, Parana, Volga, and Dnepr. In the last few decades low-head plants (< 10 to 15 m) have been fitted with horizontal bulb-type units (Figure 1.3). These plants include the Kiev, Kanev, and Jenpeg HEPP.

Figure 1.4 depicts a hydraulic unit comprised of a high-head turbine, which differs materially from a low-head unit as is clear from Figure 1.2. Such hydraulic units, rated at 200 to 700 MW each, are installed at many high-power HEPPs and have heads up to 500 to 600 m.

The most characteristic dimension of a turbine is the diameter of the runner, D_1. Turbines with D_1 not greater that 1.5 to 2.5 m are classified as small. The D_1 of large turbines measures as much as 7.5 to 10.5 m.

Turbines are manufactured by a rather complicated branch of the heavy engineering industry and require that large-size metal-cutting machine tools be available, as well as special design offices and research laboratories. Turbine manufacture has experienced rapid development since the second half of the 19th century. Specialized companies engaged in the development and manufacture of turbines include Voith

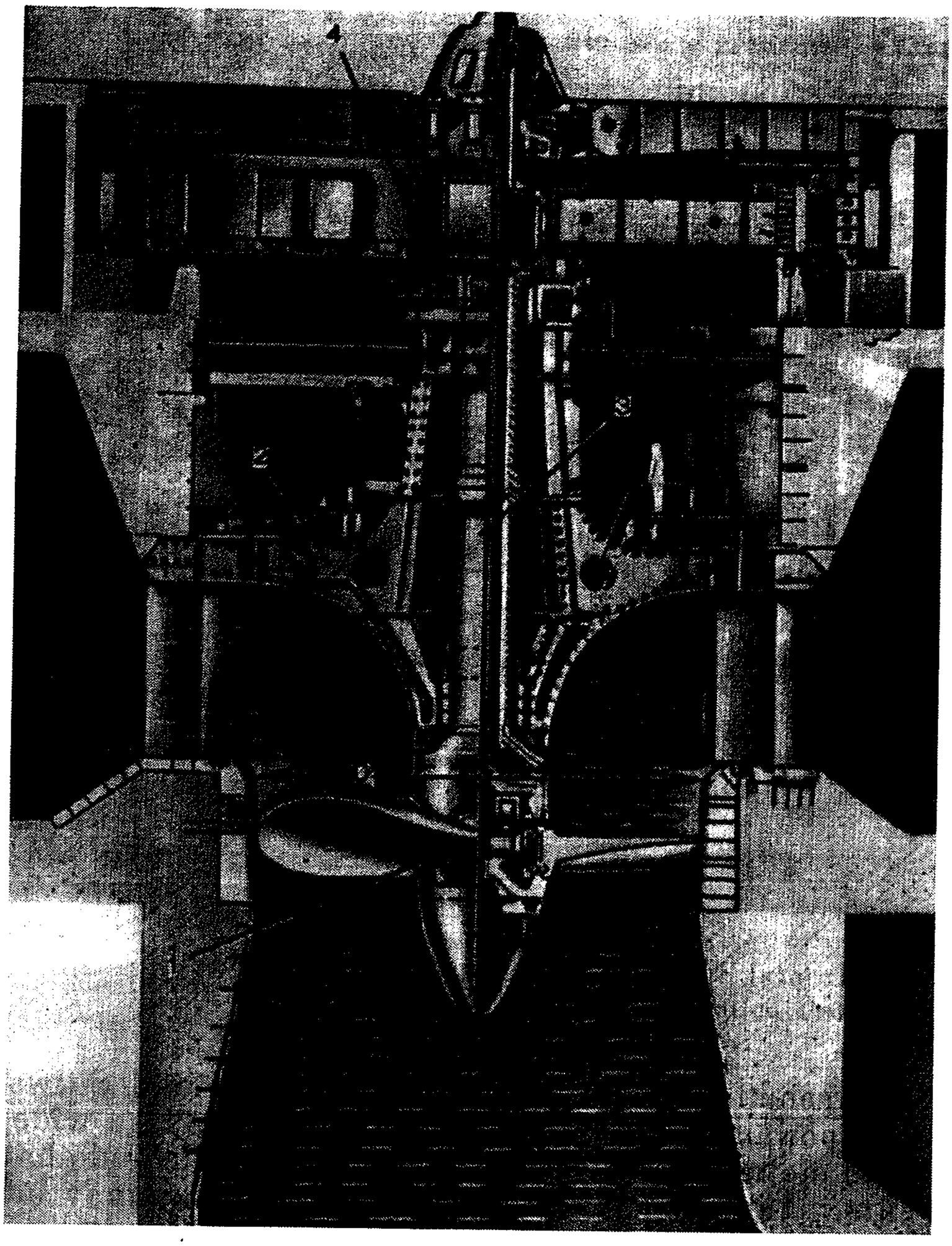


FIGURE 1.2. Vertical hydraulic unit with low-head turbine. 1 — runner; 2 — turbine cover; 3 — shaft; 4 — electric generator.

Co. (Germany), Escher Wiss and Charmilles (Switzerland), Riva (Italy), KMW (Sweden), Hitachi and Toshiba (Japan), Neyrpic (France), Saint Petersburg Metal Works (StPMW), Kharkov Turbine Works (KhTW) (the Ukraine), and CKD-Blansko (Czechoslovakia).

Pumps are designed for transferring liquid [2] and are operated at pumping stations or pumping units. The schematic diagram of a pump is

[2] Machines that handle gases are called compressors, blowers, and fans.

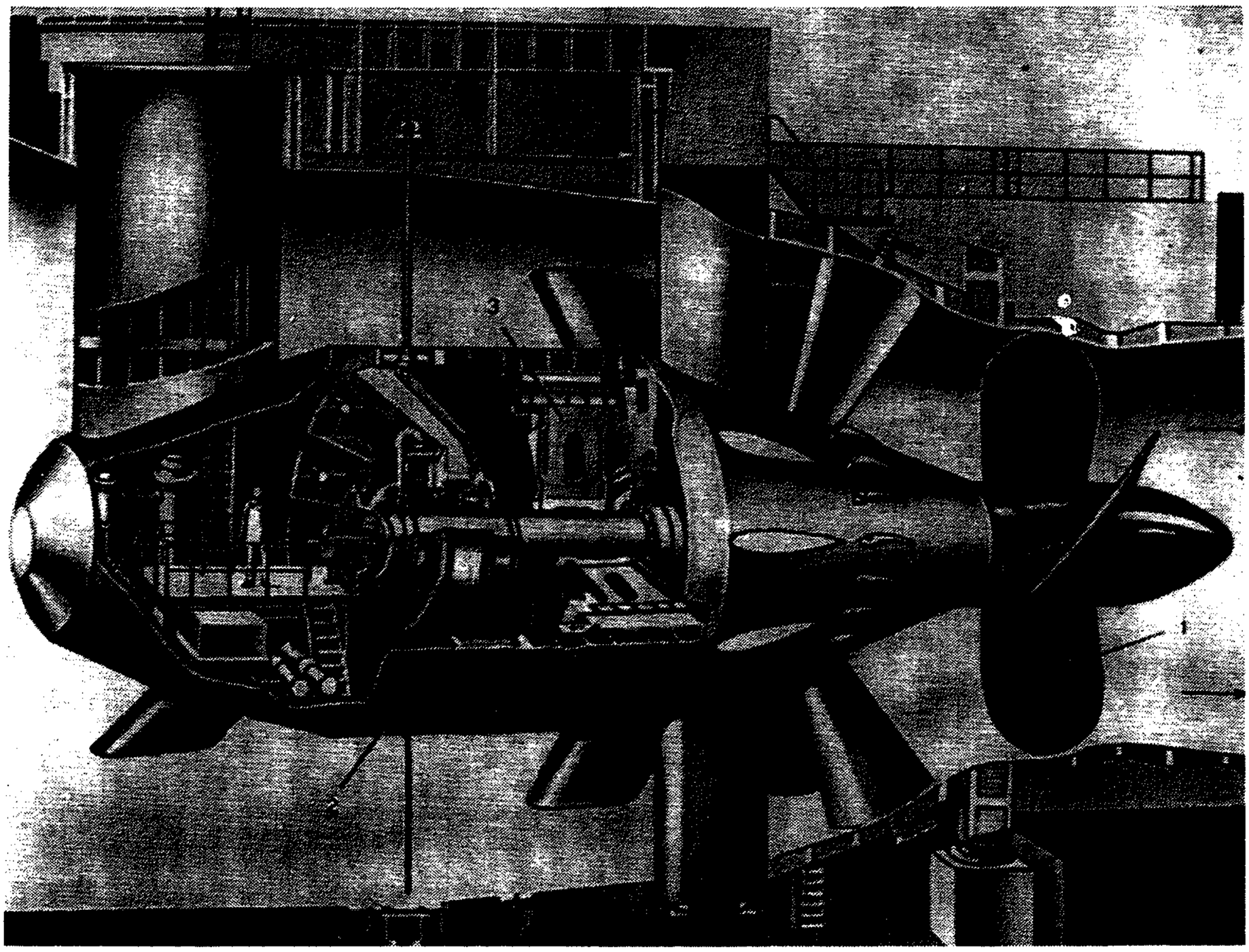


FIGURE 1.3. Horizontal low-head bulb-type hydraulic unit. 1 — runner; 2 — steel bulb; 3 — electric generator.

shown in Figure 1.1b. Pumps are driven by electric motors, but use is sometimes made of internal combustion engines as drives, especially for mobile units. In special cases pumps are driven by steam, gas, or hydraulic turbines.

Water is drawn by the pump from the lower reservoir (TW) and delivered into the upper basin (HW). As water is pumped the mechanical energy of the motor that is imparted to the pump is converted into the energy of the liquid, which forces it to flow upward through the pipeline.

The parameter characteristic of pumps is the head or pressure they create. The head is required to overcome the difference between the levels in the (HW) and (TW), and the amount of water or another liquid delivered by the pump. Pumps are manufactured in a wide range of types and sizes, with heads ranging from 5 to 10 m to 600 to 800 m and above, and deliveries ranging from 1 to 5 L/s to 3 to 40 m^3/s and more.

Pumps are used in many different fields. They are used as the principal equipment in pumping plants or in pumping installations in

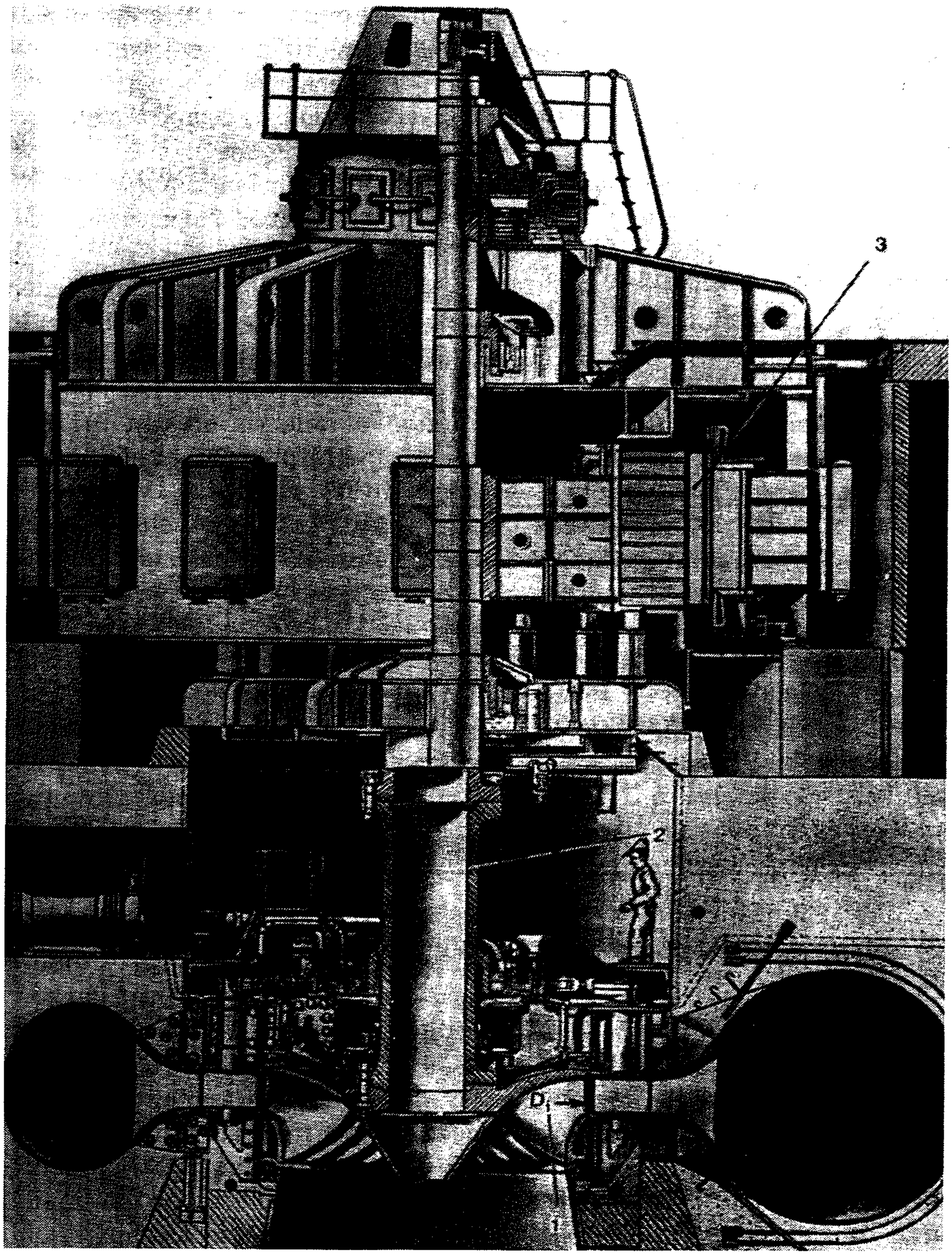


FIGURE 1.4. High-head hydraulic unit. 1 — runner; 2 — shaft; 3 — electric generator.

different technological processes. Pumps find application in water supply systems; irrigation works; sewage and drainage systems; thermal, fossil, and nuclear electric stations; cooling systems; structure construction works; in the mining industry for pit dewatering, drawdown underground water levels and slurry of pulp (water-ground mixture) conveyence; and in many other fields. To serve the demands, and extremely wide variety of classes and types of pumps are necessary.

In addition to the manufacturers of turbines mentioned above, many plants specialize in pump manufacture, for instance, Sulzer (Switzerland), Jeumont (France), Boving (England).

Reversible hydraulic machines (pump-turbines) have found ever-widening application due to intense construction of hydraulic pumped-storage hydroelectric plants, (HPSP) designed for carrying peak loads and improving operational conditions of electric systems. During the nighttime hours when power consumption diminishes greatly, the hydraulic units of pumped-storage plants are performing pumping operations and accumulating energy by pumping water from the TW into the HW (Figure 1.1b). During peak (daytime) hours the units change over to turbine operation and deliver power into the consumer electric system (Figure 1.1a). It therefore follows that a reversible machine can be used both as a pump and a turbine.

Technological progress in the manufacture of hydraulic machines is ensured by the extensive research work conducted at the plant and at specialized research laboratories and institutes. The further improvement of hydraulic machines aims to perfect the energy characteristics of turbines and pumps, to raise their operational reliability to decrease the cost of equipment and structures, to reduce operating costs, and to improve automation and control systems.

1.2 ENERGY OF FLUID (WATER)

The operation conditions for hydraulic machines—turbines at HEPPs and pumps at pumping plants and units considered above— show that both in turbines and pumps the energy of liquids is converted. In turbines the energy of liquid is converted into the energy of rotation, which is transferred to the electric generator, and in pumps the energy received form the drive motor is converted to the energy of the liquid. Thus, it is necessary to specify the hydraulic factors characterizing liquid motion and its energy.

Water pressure in different parts of the flow passage through a hydraulic machine is of great importance in assessing the energy as well as other characteristics of machine performance. Thus the determination of pressure must be considered in greater detail. It must be borne

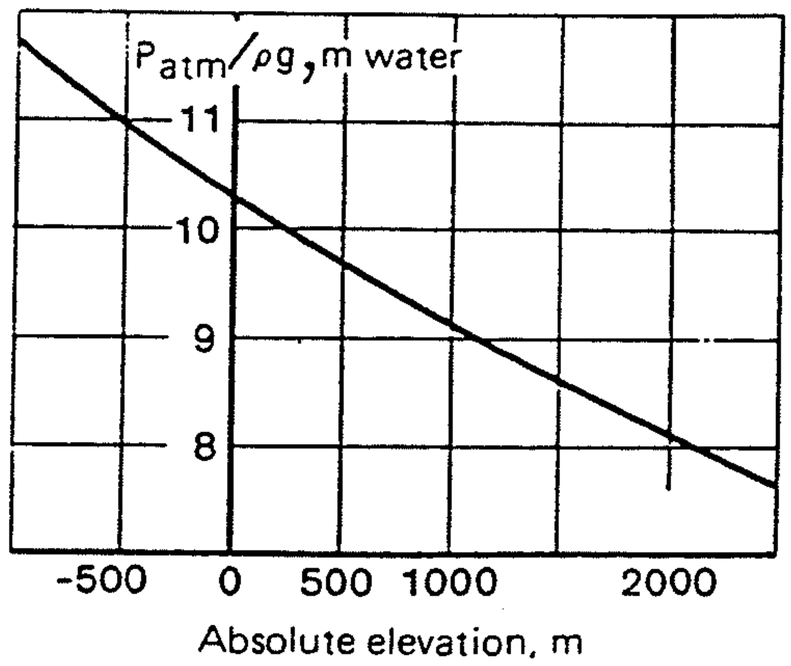


FIGURE 1.5. Atmospheric pressure vs absolute elevation.

in mind that absolute pressure p_a and excessive, or gauge, pressure p are distinguished, with

$$p_a = p_{atm} + p \tag{1.1}$$

where p_{atm} is the atmospheric pressure depending on the elevation above sea level. At sea level p_{atm} = 100,000 Pa = 0.1 Mpa.

The quantity $p_{atm}/\rho g$ is measured in meters of liquid column; ρ is the density of liquid, equal for fresh water to 1000 kg/m^3; and g is the free fall acceleration, equal to 9.81 m/s^2. The dependence of atmospheric pressure, meters of water column, on the absolute elevation is plotted in Figure 1.5; atmospheric pressure can be specified approximately by the following formula:

$$\frac{P_{atm}}{\rho g} = 10.3 - \frac{\nabla}{900} \tag{1.2}$$

where ∇ is the absolute elevation.

The excessive pressure is associated with the piezometric height, meters of water column, by the relationship $H_p = p/\rho g$ (Figure 1.6a),

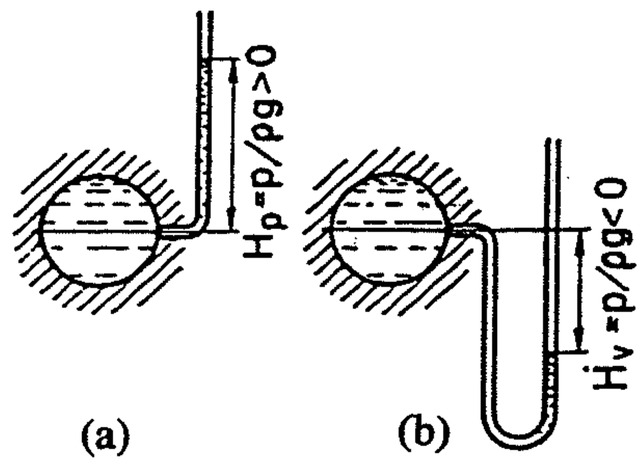


FIGURE 1.6. Determining liquid pressure.

i.e.,

$$p = \rho g H_p$$

where p is pressure, in pascals and H_p is the piezometric height measured in meters of water column.

If the absolute pressure at a point is below atmospheric pressure, the piezometric height of the level, measured in meters of water column, is negative ($H_p = p/\rho g < 0$) or equal to the suction lift H_v (Figure 1.6b); in other words it corresponds to a vacuum—pressure below atmospheric. Then, absolute pressure is specified by the formula

$$p_a = p_{atm} - \rho g H_v \tag{1.3}$$

Specific energy of a flow through stream filament (stream tube) in its given cross-section can be determined in respect to:

1. The weight of the flowing liquid (weight force in newtons)

$$e = \frac{p}{\rho g} + z + \frac{v^2}{2g} \quad (\text{J/N or m})$$

2. The volume discharge of the flowing liquid

$$e_v = p + \rho g z + \rho \frac{v^2}{2} \quad (\text{J/m}^3 \text{ or Pa})$$

3. The mass discharge of the flowing liquid

$$e_m = \frac{p}{\rho} + gz + \frac{v^2}{2} \quad (\text{J/kg or m}^2/\text{s}^2)$$

Here, p is pressure (Pa), z is elevation measured from some datum level (m), v is velocity (m/s), p is density (Kg/m^3), and g is gravity acceleration (generally, $g = 9.81$ m/s^2). Therefore, specific energy includes three components: pressure energy, potential (position) energy (connected with acting on liquid mass forces), and kinetic energy. All three forms of specific energy expression e, e_v and e_m are equally valid. The first form e (Figure 1.7) is most widely used as it allows a very illustrative geometric interpretation (all elements have a length dimension). In some cases however, this form cannot be applied; for example, in satellites, where $g = 0$. For such conditions, e_v is more convenient. Mass specific energy must be used in cases in which a flow of compress-

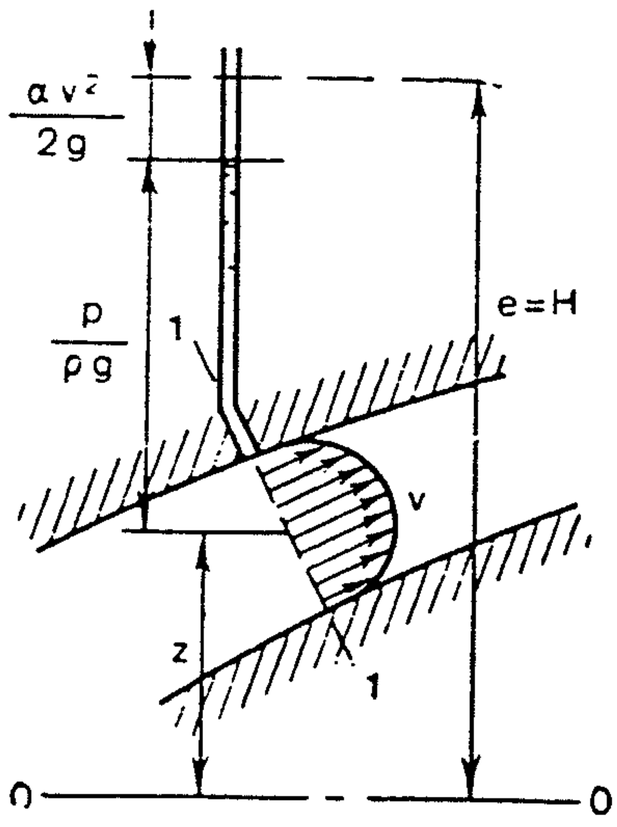


FIGURE 1.7. Determining specific energy of flow liquid.

ible liquid is considered, or when pressure changes sufficiently influence the density of flowing liquid. It must be kept in mind that for these cases it is sometimes important to take into account the internal energy of the flowing liquid by introducing the thermodynamics characteristics.

The notion of specific energy can be applied to the whole flow, but in this case it represents some averaged value and it is necessary to note how this averaging has been achieved. The most simple condition, in which the sum of the first two items (pressure and position) can be accepted as a constant in the cross-section ($p/\rho g + z = \text{const}$) or as a pressure distribution over the cross-section, follows the hydrostatic law. This takes place when the mass forces do not depend on z, for example, when streamlines are straight-lines or have a small curvature, and one does not have to take centrifugal forces into consideration. In such cases it is necessary to find only the average value of kinetic energy. If the mean flow velocity is determined as ratio $V = Q/F$, where Q is the discharge and F is the area of cross-section for which streamlines are normal, the expression for the average kinetic energy will be proportional to αv^2; α is the kinetic energy correction factor (Coriolis). Thus, specific energy for a flow for a given cross-section 1–1 (Figure 1.7) is

$$e = \frac{p}{\rho g} + z + \frac{\alpha v^2}{2g}$$

$$e_v = p + \rho g z + \rho \alpha v^2/2$$

$$e_m = \frac{p}{\rho} + gz + \alpha v^2/2 \qquad (1.4)$$

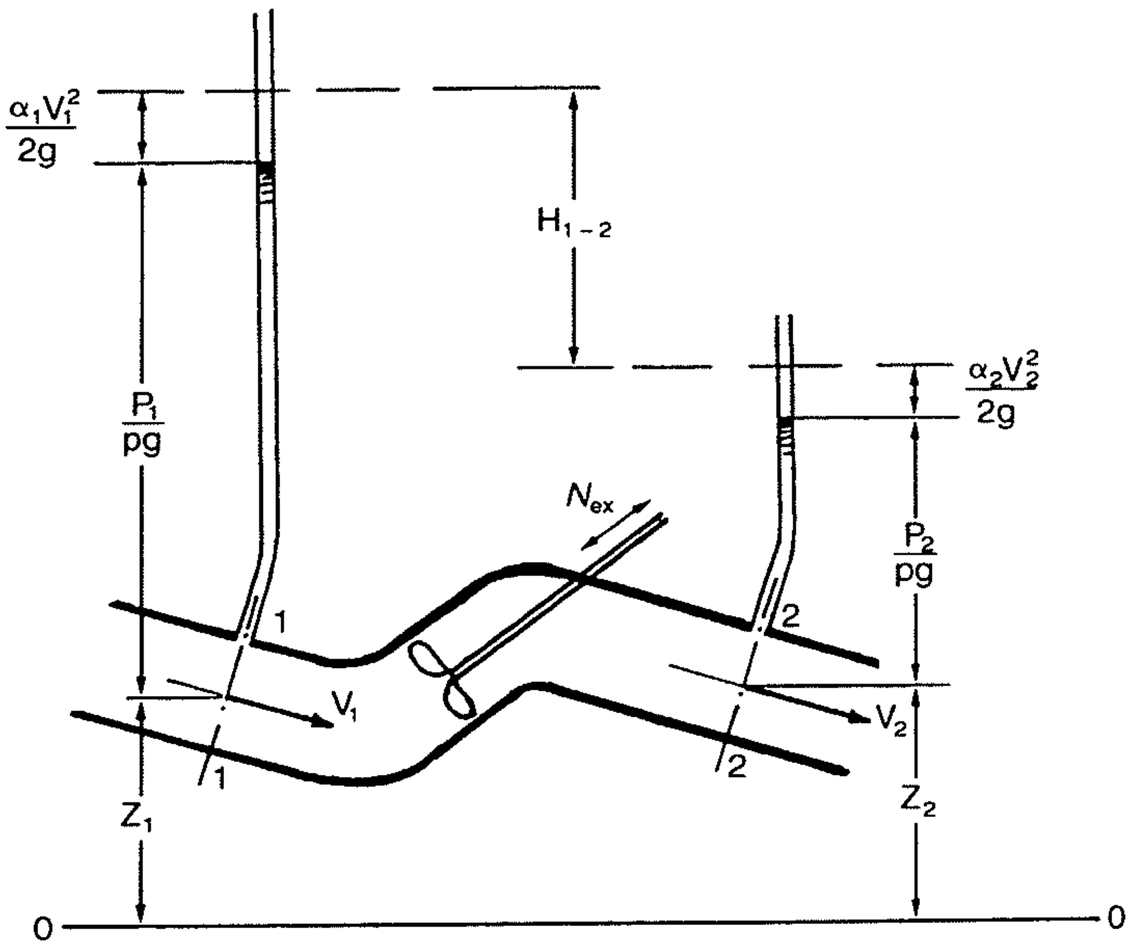


FIGURE 1.8. Geometric representation of Bernoulli's equation.

and the correction factor for kinetic energy is:

$$\alpha = \frac{1}{Fv^3}\int_F u^3 dF \tag{1.5}$$

where u is the local velocity.

The power of flowing liquid over a given datum elevation N_l(W) can be determined if its specific energy and discharge are known:

$$N_l = e(\rho g Q)$$

$$N_l = e_v(Q)$$

$$N_l = e_m(\rho Q) \tag{1.6}$$

Absolute liquid power exists between two cross-sections, 1–1 and 2–2 (Figure 1.8), where any arrangement can be located that is capable of exchanging energy with the liquid and of changing the flow power on N_{ex}. In such conditions it is possible to have $e_2 > e_1$, if the arrangement increases liquid energy. The absolute power $N_{1\text{-}2}$ therefore will be:

$$N_l(1\text{-}2) = |N_{l1} - N_{l2}| = |e_1 - e_2|\,\rho g Q$$

Denoting $|e_1 - e_2| = H_{1\text{-}2}$ for the head:

$$N_{l(1\text{-}2)} = \rho g Q H_{1\text{-}2} \quad \text{(W)}$$

Allowing for clean fresh water, $\rho = 1000$ kg/m^3:

$$N_{l(1\text{-}2)} = 9.81QH_{1\text{-}2} \quad \text{(kW)} \tag{1.7}$$

It is now possible to give a general form of the Bernoulli equation for incompressible fluid and for steady-state motion when $\partial v/\partial t = 0$ (Figure 1.8):

$$\frac{p_1}{\rho g} + z_1 + \frac{\alpha_1 v_1^2}{2g} = \frac{p_2}{\rho g} + z_2 - \frac{\alpha_2 v_2^2}{2g} + h_{1\text{-}2} \pm h_{ex} \tag{1.8}$$

Here, $h_{1\text{-}2}$ is the hydraulic losses (friction and local or minor) that occur between cross-sections 1–1 and 2–2 and h_{ex} is the external increase or decrease of liquid specific energy (accordingly $\pm$ is applied), which can be determined by:

$$h_{ex} = \frac{N_{ex}}{\rho g Q}$$

In the absence of the energy arrangement, $h_{ex} = 0$ and Equation 1.8 become a well-known Bernoulli equation.

SECTION 2

Hydraulic Turbines

CHAPTER 2

Parameters and Kinds of Turbines

2.1 TURBINE HEAD

The installation of a turbine at a HEPP is shown schematically in Figure 2.1a. Water is supplied to the turbine from the headwater (HW) (forebay) through the water intake and the pressure conduit (inlet; Section 1–1 of Figure 2.1). Having passed through it, water is discharged from the draft tube (outlet; Section B–B of Figure 2.1) into the tailwater (TW) (afterbay) or into a tailrace conduit. The difference between the elevations in the HW and TW is called the static head of the HEPP H_{st} (meters):

$$H_{st} = z_{hw} - z_{tw} \tag{2.1}$$

The head of a turbine H (meters) is the difference between the specific energies e_1 and e_{out} at the turbine inlet and outlet, respectively:

$$H = e_1 - e_{out} \tag{2.2}$$

According to Equation (1.4):

$$e_1 = \frac{p_1}{\rho g} + z_1 + \frac{\alpha_1 v_1^2}{2g}$$

where v_1 is the average velocity (Section 1–1 of Figure 2.1). To determine the term $p_1/\rho g$, use Bernoulli's equation (1.8) for the data

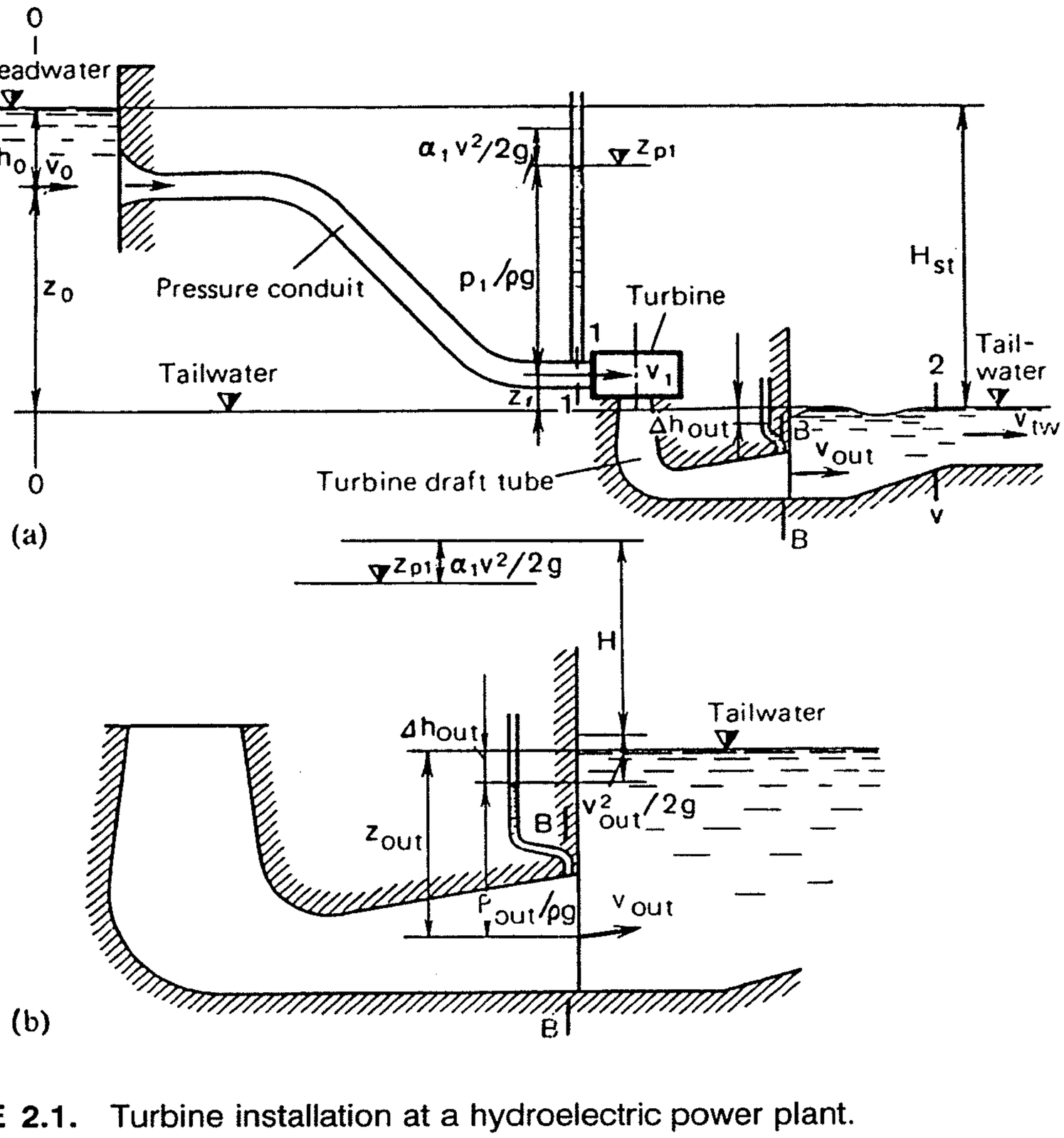


FIGURE 2.1. Turbine installation at a hydroelectric power plant.

sections 0–0 in the forebay and 1–1 at the turbine inlet (Figure 2.1a) about the afterbay elevation:

$$\frac{p_0}{\rho g} + z_0 + \frac{\alpha_0 v_0^2}{2g} = \frac{p_1}{\rho g} + z_1 + \frac{\alpha_1 v_1^2}{2g} + h_{loss}$$

where $p_0/\rho g = h_0$, and h_{loss} is hydraulic losses through the headrace and local losses (at the water intake inlet, bends, and others). Allowing for $h_0 + z_0 = H_{st}$, from the equation, we determine the piezometric height $p_1/\rho g$ (Figure 2.1a):

$$\frac{p_1}{\rho g} = H_{st} - z_1 + \frac{\alpha_0 v_0^2}{2g} - \frac{\alpha_1 v_1^2}{2g} - h_{loss} \tag{2.3}$$

If the outlet section of the turbine is referred to the afterbay (TW) (Section 2–2 of Figure 2.1), then the specific energy e_{out} about the TW

elevation will be equal to

$$e_{out} = e_2 = \frac{\alpha_{tw} v_{tw}^2}{2g}$$

In the final analysis, in accordance with Equation 2.2 the turbine head is specified by the relationship

$$H = H_{st} - h_{loss} + \frac{\alpha_0 v_0^2}{2g} - \frac{\alpha_{tw} v_{tw}^2}{2g} \tag{2.4}$$

This head is referred to as the net head of a turbine unit.[1]

As the difference in the velocity heads in Equation 2.4 is small it can be ignored. Thus, the expression for the turbine head appears as follows:

$$H = H_{st} - h_{loss} \tag{2.5}$$

Equation 2.5 is widely used in turbine design. It should be borne in mind that h_{loss} is the sum of all the hydraulic losses in the conduits supplying water to the turbine from the forebay and in the conduits through which water is discharged from the turbine into the afterbay. When calculations are designed to check on the warranted turbine capacity and efficiency, the head is determined in accordance with the adopted international code. Then, the outlet energy is taken about the outlet section of the draft tube B–B (see Figure 2.1a and b); the pressure is determined from the readings of the installed piezometers. The level in these piezometers often happens to be below the afterbay elevation by Δh_{out} (Figure 2.1b). This quantity is called the recovery drop, which results from the recovery of a fraction of the kinetic energy

[1] The difference between the specific energies in the forebay and afterbay is called the gross head, $H_g = e_0 - e_2$, or

$$H_g = H_{st} + \frac{\alpha_0 v_0^2}{2g} - \frac{\alpha_{tw} v_{tw}^2}{2g}$$

i.e., it differs from the net head by the amount of hydraulic losses.

of the water at the draft tube outlet, $\alpha_{out}v_{out}^2/2g$, and leads to an increase of the utilized head[2]

$$e_{out} = -\Delta h_{out} + \frac{\alpha_{out}v_{out}^2}{2g}$$

while for $\alpha_{out} = 1$

$$H = H_{st} - h_{loss} + \frac{\alpha_0 v_0^2}{2g} + \Delta h_{out} - \frac{v_{out}^2}{2g} \tag{2.6}$$

Example 2.1

Compare the heads determined by different formulas for the following conditions: $H_{st} = 18.0$ m; $v_0 = 0.2$ m/s; $v_{tw} = 1.6$ m/s; $v_{out} = 2.8$ m/s; $h_{loss} = 0.6$ m; $\Delta h_{\text{out}} = 0.16$ m (assume $\alpha_0 = 1$ and $\alpha_{tw} = 1$).

Solution

From Equation 2.4:

$$H = 18.0 - 0.6 + \frac{0.2^2}{19.6} - \frac{1.6^2}{19.6}$$

$$= 18.0 - 0.6 + 0.002 - 0.13 = 17.27 \text{ m};$$

From Equation 2.5:

$$H = 18.0 - 0.6 = 17.4 \text{ m};$$

From Equation 2.6:

$$H = 18.0 - 0.6 + \frac{0.2^2}{19.6} + 0.16 - \frac{2.8^2}{19.6}$$

$$= 18.0 - 0.6 + 0.002 + 0.16 - 0.4 = 17.16 \text{ m}.$$

The obtained results show all formulas specify very close heads. The greatest divergence, 0.24 m, occurs between Formulas 2.5 and 2.6;

---

[2] If the level in the piezometers is above the afterbay elevation, not only does recovery of kinetic energy take place at the outlet, but also additional losses. Then, $\Delta h_{\text{out}} < 0$ and the head diminishes.

however, this is $< 1.5\%$. The relative disagreement diminishes with increasing head.

2.2 TURBINE CAPACITY (POWER)

The head H calculated by Equation 2.2 shows to what extent the specific energy of water (Joules per newton) diminishes as it flows through the turbine. As the discharge of the turbine is Q (m^3/s), and weight flow rate is ρgQ (N/s), then the energy lost by the liquid per second as it flows through the turbine, i.e., the power N_l removed by the turbine from the flowing liquid, amounts to

$$N_l = \rho gQH \tag{2.7}$$

Only a fraction of this power is transferred to the turbine shaft, however, because losses occur in the turbine that are accounted for by the turbine efficiency η:

$$\eta = N/N_l \tag{2.8}$$

where N is the shaft power. Formulas 2.7 and 2.8 are used to determine the net capacity (power) of the turbine:

$$N = \rho gQH\eta \tag{2.9}$$

where N is expressed in watts. Turbines are operated usually with unpolluted freshwater for which $\rho = 1000$ kg/m^3. Under these conditions, with $g = 9.81$ m/s^2 and taking into account that 1000 W = 1 kW, we obtain

$$N = 9.81\, QH\eta \tag{2.10}$$

Q and H are expressed in Equation 2.10 in units of cubic meters per second and meters, respectively, and N is expressed in kilowatts. This formula is widely used in designing HEPPS and turbines.

Turbines are operated with sufficiently high efficiencies that under the most favorable operating conditions fall within 0.92 to 0.95 or 92 to 95%; under maximum load conditions turbine efficiencies are within 0.88 to 0.93 or 88 to 93%.

Example 2.2

Determine the flow rate through a turbine of a HEPP rated at 508 MW at a head of 93 m.

Solution

For a maximum load we assume an efficiency equal to 92% ($\eta = 0.92$). From Equation 2.10 it follows that

$$Q = \frac{N}{9.81 H \eta} = \frac{508\,000}{9.81 \times 93 \times 0.92} = 607 \text{ m}^3/\text{s}$$

2.3. PRINCIPAL TURBINE KINDS

A turbine is designed to convert the mechanical energy of the water flowing through it into the useful energy of the rotating shaft. With regard to this the principal characteristic of a turbine is the shape and arrangement of its flow passage, which consists of three main elements: the runner (wheel), which is the working member of the turbine; devices that supply water to the runner; and devices through which water is discharged from the runner.

A great number of turbine kinds exist, but only four find application in hydraulic power engineering: axial, mixed-flow, radial-axial, and impulse turbines. Let us consider their arrangement and principles of operation.

Axial-Flow (Kaplan) turbines are low-head machines. They are used with small heads ranging from 1 to 3 to 60 to 70 m. The schematic diagram of an axial-flow turbine is shown in Figure 2.2. The runner of the axial-flow turbine, consisting of runner blades (1), secured in casing (2) with a cone, is connected to a shaft (3). The number of runner blades may vary from four to eight. The greater the head, the greater the number of runner blades. The blades may be rigidly secured at a certain angle of inclination. The turbine thus is referred to as a propeller turbine. However, usually the blades are adjustable; i.e., on the run, the blade angle may be varied depending on operating conditions (load, head). Such turbines are called adjustable blade or Kaplan turbines. Adjustable blade turbines are of a more intricate design than propeller turbines, but their energy indices are higher.

The runner with the shaft is the rotating part of the turbine. The runner diameter D_1 characterizes the size of the turbines. As illustrated in section A–A of Figure 2.2 (meridional) the flow enters the runner and leaves it in an axial direction. This is the reason that turbines of this kind are called axial-flow turbines. Water is supplied to the runner along the turbine case (4), through stayring (5), and the wicket gate (6).

The turbine case usually consists of a trapezoidal cross-section made from concrete. Steel turbine cases having round cross-sections are constructed only at relatively high heads (> 50 m).

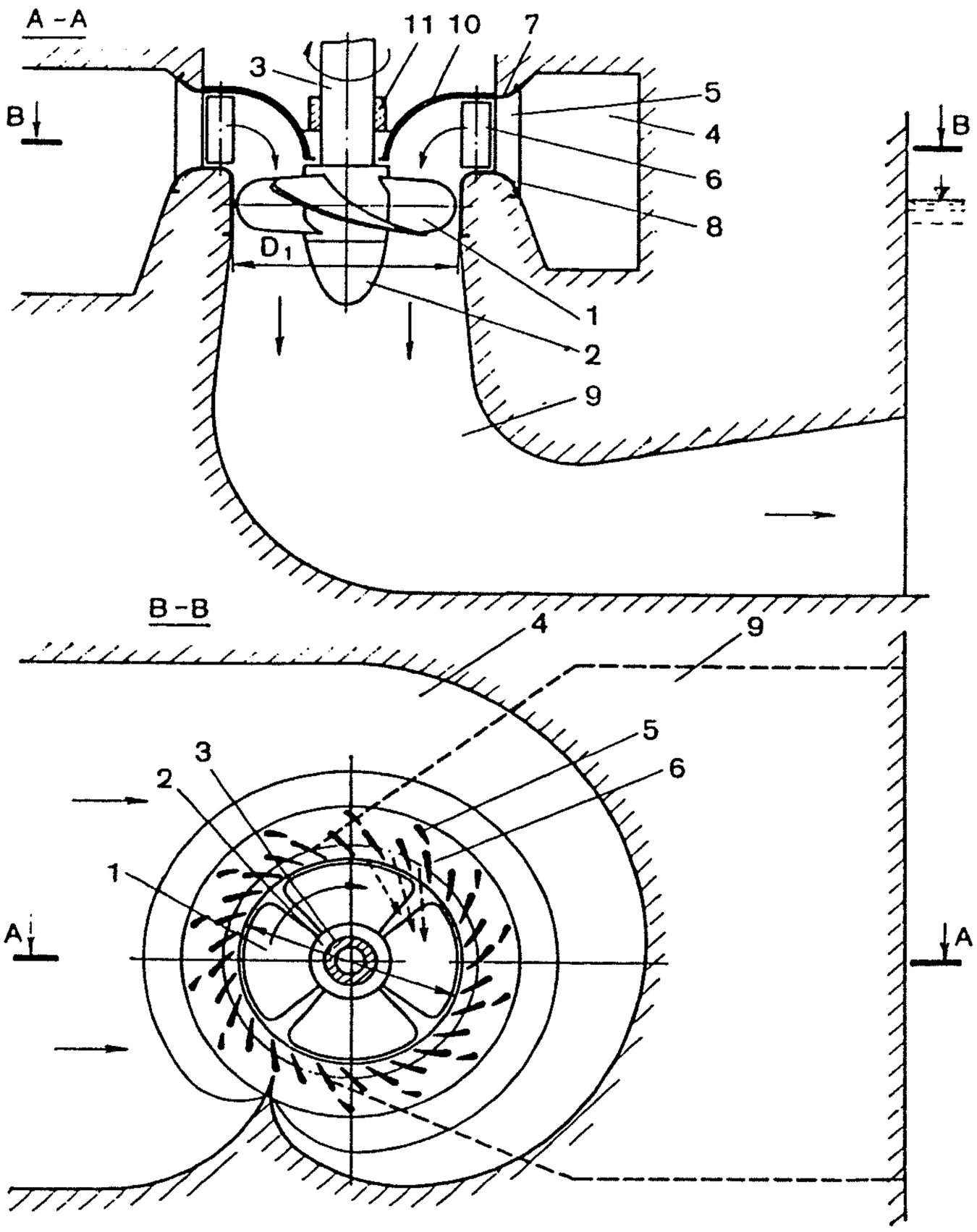


FIGURE 2.2. The axial-flow turbine.

The stayring vanes are designed for transmitting the load from the top support band (7) of the stayring to the lower (8) i.e., the stayring strengthens the structure. To reduce the entrance hydraulic losses, the stayring vanes are streamlined.

The wicket gate is built from 20 to 32 guide vanes (6) that form a circular vane cascade, imparting rotation to the flow in front of the runner blades. This manifests itself in that the velocity vector v_0 is directed at the guide vane outlet at some angle to the radius (Fig. 2.2, section B–B). In addition, the guide vanes are used to regulate turbine power (capacity). To this end each guide vane can be turned about its pivot pin, and when all vanes are turned simultaneously through some angle the opening a_0 changes from a maximum value (Figure 2.3a) to zero (figure 2.3b). The flow rate and power of the turbine change in accordance with Equation 2.10.

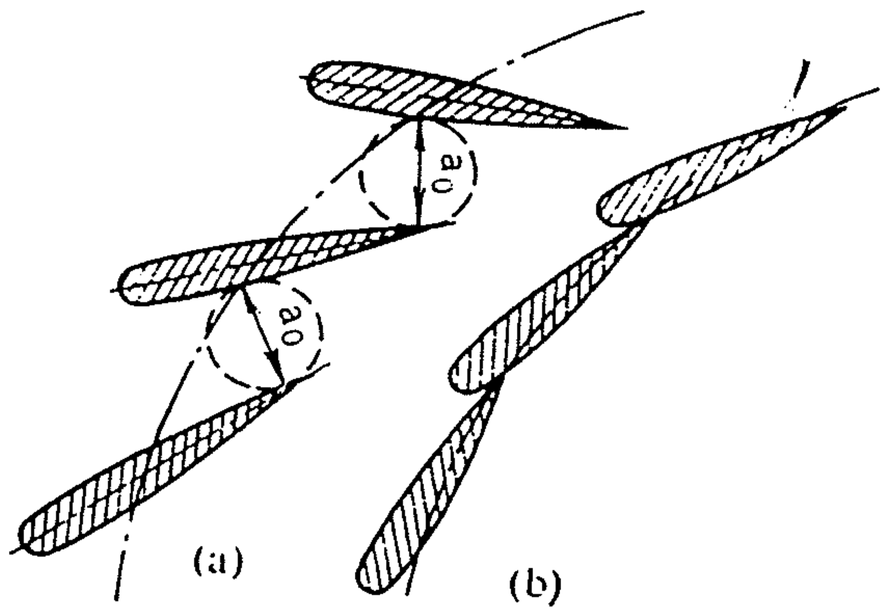


FIGURE 2.3. Adjustment of turbine flow rate by the wicket gate.

Water is discharged from the runner through the draft tube (9 of Figure 2.2), which is a diffusor. The draft tube ensures a smooth decrease of flow velocity upstream of the afterbay. Such a reduction in velocity makes it possible to diminish the kinetic energy of the flow at the turbine outlet and thereby raise turbine efficiency. The draft tube of high-capacity turbines is always made of concrete.

The turbine cover (10), which takes up the load created by water pressure, is an important design element of the axial-flow turbine. In addition, the guide vane pivot pins are secured on the cover, which mounts the turbine guide bearing (11), restricting radial displacement of the shaft and runner.

A more general view of an axial-flow turbine is shown in Figures 1.2 and 1.3.

Mixed-flow turbines have been in development over the last few decades. They differ from axial-flow turbines in that the runner blades are mounted at an angle to the axis rotation (shown in Figures 3.12 and 3.14).

Radial-axial turbines, also known as Francis turbines, are medium-head hydraulic machines. They are used with heads ranging from 40 to 60 to 500 to 700 m. The schematic diagram of a radial-axial Francis turbine is depicted in Figure 2.4. The runner of this turbine consists of 12 to 17 blades forming an annular cascade. The blades (1) are rigidly fixed in the crown (2′) and the band (2″) by virtue of which the runner acquires the required strength and rigidity. The runner is connected to the shaft flange (3). Cone (12) of the runner ensures better conditions for water exiting the runner blades. The runner and shaft constitute the rotating part of the turbine. The runner diameter over the inlet edges of the blades, D_1, characterizes the size of the radial-axial (Francis) turbine.

The meridional section A–A of Figure 2.4 shows that the flow enters the runner in the radial direction and leaves the runner in the axial direction, which lends the name, radial-axial turbine. Water is supplied

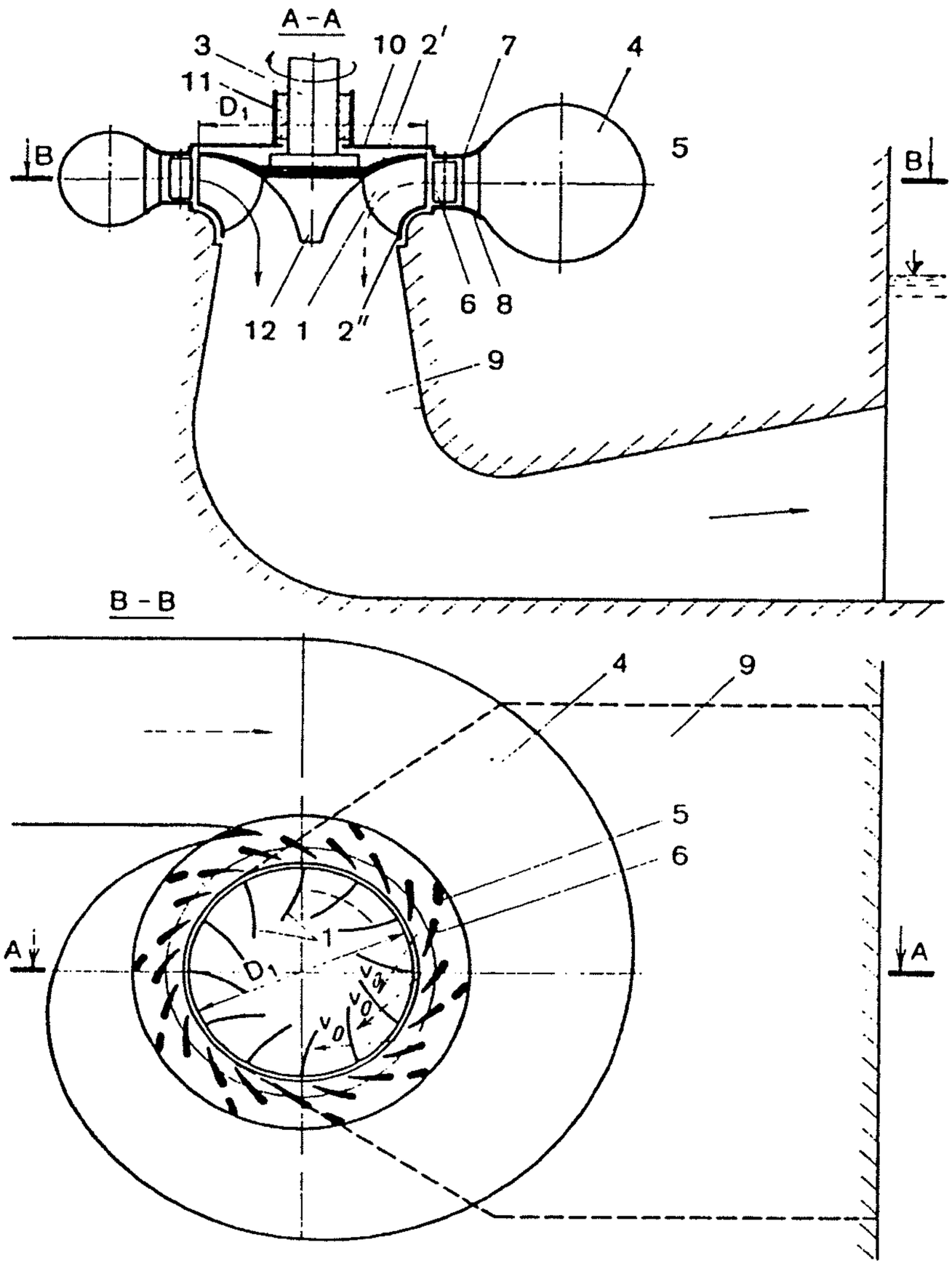


FIGURE 2.4. The radial-axial turbine.

to the runner through the spiral case (4), stayring (5), and wicket gate (6). The external view of the runner of a radial-axial turbine is illustrated in Figure 2.5. The spiral case of the turbine is usually made of steel, and is of a circular cross-section so as to improve the conditions under which the case walls take up the water pressure load. The stayring vanes are designed for transmitting the load from the upper stayring band (7) to the lower (8). Therefore, the main purpose of the stayring is to ensure strength. Hydraulic entrance losses are diminished by streamlining the vanes and setting them in the direction of the flow.

The wicket gate consists of 20 to 24 guide vanes (6) which are designed to ensure the required direction of velocity upstream of the runner inlet (Figure 2.4, section B–B) and for regulating the rate of water flow through the turbine and its capacity by turning the vanes and changing the opening a_0 (Figure 2.3).

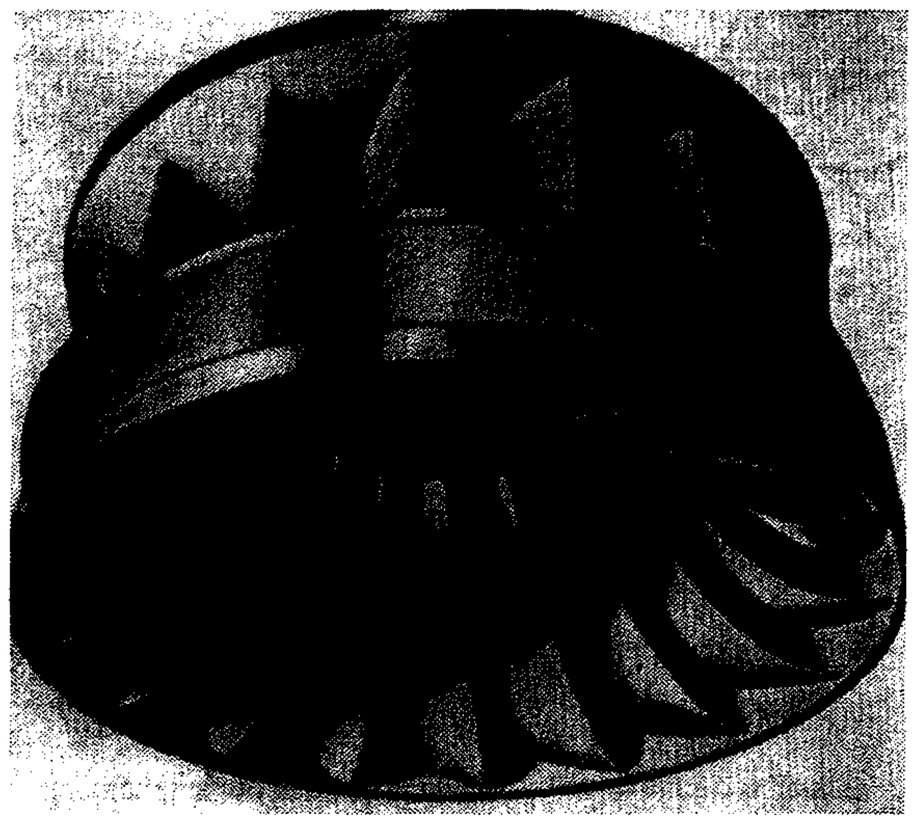


FIGURE 2.5. Runner of the radial-axial turbine.

The water is removed from the runner by means of the draft tube diffuser (9), ensuring smooth reduction of velocity and a lesser kinetic energy of the flow at the turbine outlet.

An important component part of the radial-axial turbine is cover (10), in which the turbine guide bearing (11) is secured. Also secured in the cover are the pivot pins (6) of the guide vanes and their operating gear. The turbine cover takes up large hydraulic loads and must be sufficiently strong and rigid.

Pelton turbines (free-jet) are high-head turbines operated at heads over 400-600 m. The schematic diagram of a Pelton turbine is depicted by Figure 2.6. The main component elements of the turbine are the nozzle (1) to which water is supplied from pipeline (2) and the runner (3) is secured on the shaft (4). The nozzle and the runner are mounted above the water level so that the runner rotates in the air. Acted upon by the head H the jet of water is forced for the nozzle with a velocity v_j, which is found from the relationship

$$v_j = \varphi\sqrt{2gH} \tag{2.11}$$

where the velocity factor $\varphi = 0.98$ to 0.99. Allowing for the heads at which Pelton turbines are employed, it is clear that the velocity v_j is very high; for instance, at a head $H = 600$ m, the velocity $v_j = 105$ m/s, and with $H = 1500$ m, $v_j = 165$ m/s.

As water flows through a nozzle the jet constriction effect takes place, resulting in the jet diameter d_j being smaller than the nozzle diameter.

The runner (3) consists of a disk with 12 to 40 buckets (5). Each bucket has two curvilinear surfaces separated by a spear (6) (Figure 2.6,

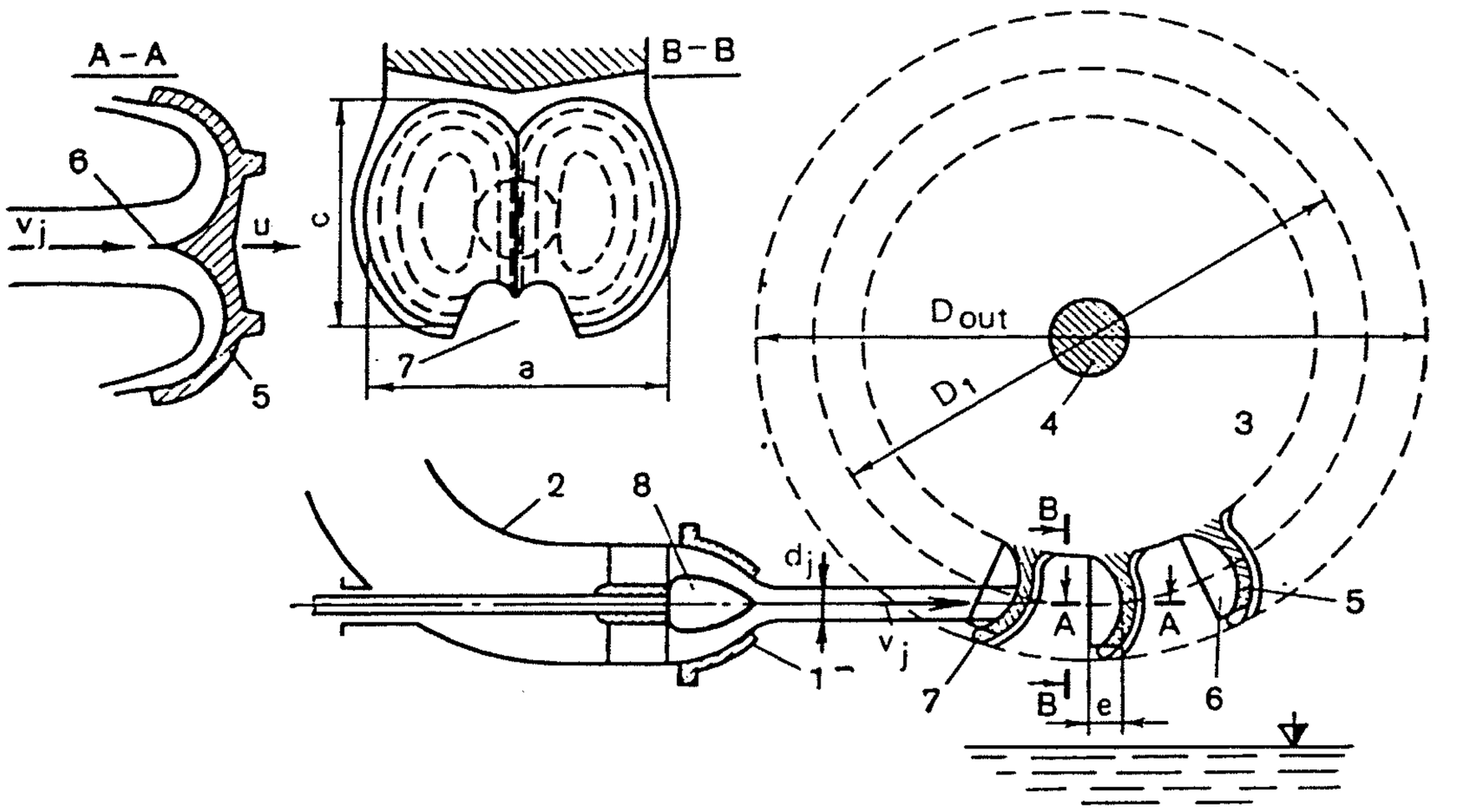


FIGURE 2.6. The Pelton turbine.

section A–A and B–B). The runner is mounted in way that the spears coincide with the direction of the jet. As the jet enters a bucket the spear divides it into two equal parts and each flows past the curvilinear surface (section A–A). At the expense of a change in the water velocity and its direction, a moment of the runner forms and rotates the runner together with the shaft. Because the water enters the runner blades at a very high velocity, high requirements are imposed on the accuracy capabilities of the machine and surface finish. To prevent the back of the bucket from impacting against the jet during rotation, a special slit (7) is made.

The capacity of the Pelton turbine is regulated by varying the rate of water flow through it. This is ensured by needle (8). When the needle is moved in Figure 2.7a water flows through the complete cross-sectional area of the nozzle at the largest flow rate (the jet diameter d_j is at maximum). As the needle is drawn out the nozzle cross-sectional area decreases, the jet diameter diminishes, and the flow rate from the nozzle decreases accordingly (Figure 2.7b).The needle may fully cover the nozzle, and thus the flow rate is equal to zero (Figure 2.7c).

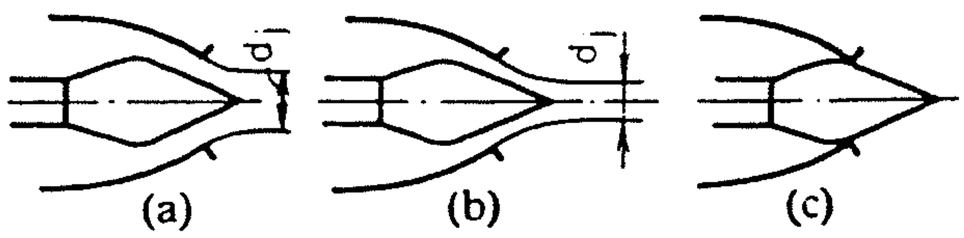


FIGURE 2.7. Flow rate varying by needle.

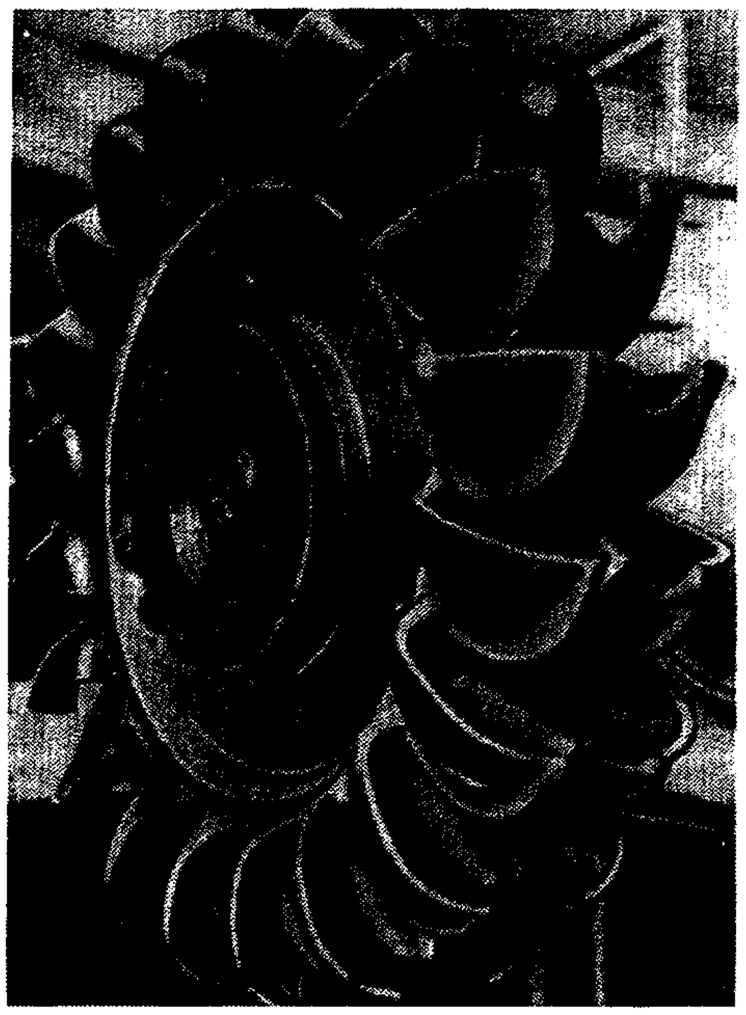


FIGURE 2.8. Pelton turbine runner.

An external view of a Pelton turbine runner is shown in Figure 2.8. The dimensions of the buckets of a Pelton turbine (Figure 2.6) runner are as follows: $a = (2.8 \text{ to } 3.6)\ d_j$; $c = (2.5 \text{ to } 2.8)\ d_j$ and $e = (0.9 \text{ to } 1.0)\ d_j$. All component elements of the Pelton turbine bear against the casing and water splashing is prevented by housing, neither of which are shown in Figure 2.6.

2.4 APPLICATIONS OF TURBINES OF VARIOUS CLASSES AND KINDS

Axial-flow and radial-axial flow turbines differ radically from Pelton turbines (see above). The flow in axial-flow and radial-axial-flow turbines is continuous over the entire length of the flow passage; the runner rotates in water and the water flows continuously past its blades. These features of axial-flow and radial-axial-flow turbines permit the runner to utilize all components of the energy of the water flowing through the turbine: pressure energy and kinetic energy (Equation 1.4). Accordingly, the flow velocity at the runner inlet is comparitively low, even at high heads.

The runner of a Pelton turbine rotates in the air and only some of the buckets interact with the water at any given time. The Pelton turbine runner is capable of utilizing only the kinetic energy of water; i.e., all the energy of water must be converted only into kinetic energy

upstream of the runner, and such energy conversion is ensured by the nozzle. Therefore, water (jet) velocity must be very high upstream of the wheel (Equation 2.11). The axial-low, radial-axial, and Pelton turbines are classified based on this fundamental difference. Axial-flow and radial-axial-flow turbines are classed as reaction (pressure) turbines and Pelton and other similar turbines are classed as active (impulse) machines.

The application of turbines of different classes and kinds based on their heads is given in Figure 2.9. Axial-flow, adjustable blade (Kaplan) turbines, and propeller turbines are used with low heads—up to 70 m. Heads within 40 to 100 m permit the application of mixed-flow adjustable blade or propeller turbines. Radial-axial Francis turbines are used with heads from 40 to 700 m and Pelton turbines with heads over 400 m. It follows that high-capacity reaction (pressure) turbines cover a wide range of heads, from 1-2 to 600-700 m, and active (impulse) turbines find application at higher heads.

It ought to be borne in mind that for low-capacity turbines rated at between 100 to 3000 kW their field of application has a lesser head

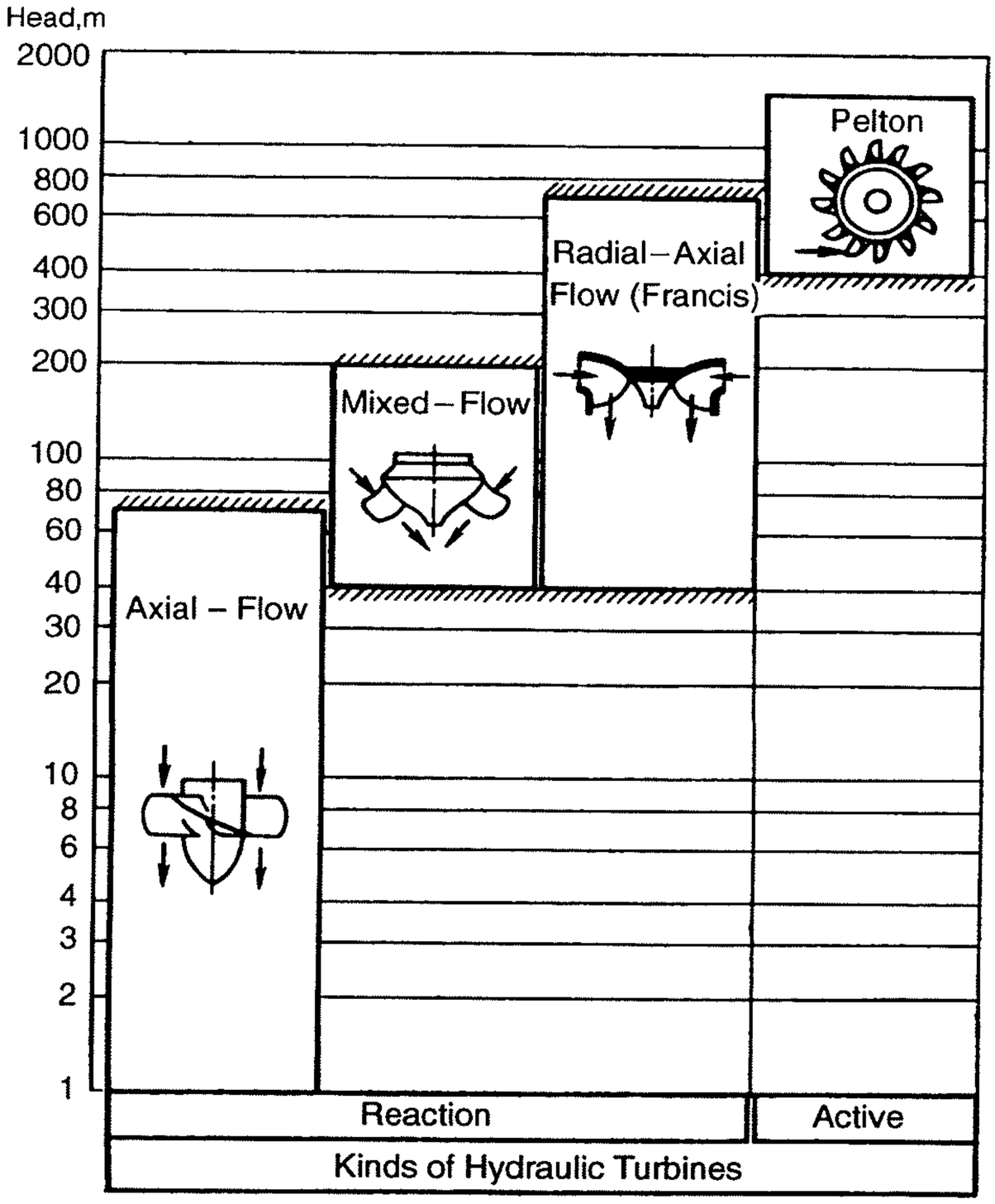


FIGURE 2.9. Application of turbines of different kinds.

limit. For instance, radial-axial turbines may happen to be suitable at heads within 20 to 25 m, and Pelton turbines may find application at heads within 150 to 200 m. Some kinds of turbines may be suitable for the same application. At heads of 50 to 70 m axial-flow, mixed-flow and radial-axial turbines may find application. The choice of an optimal solution is made on the basis of comparing the operation and cost data of various possible alternatives.

CHAPTER 3

Turbine Design

3.1. AXIAL-FLOW, ADJUSTABLE BLADE (KAPLAN) TURBINES

The design of axial-flow, adjustable blade (Kaplan) turbines is discussed in this chapter with regard to a turbine mounted at a HEPP on the Dnepr River, shown in Figure 3.1 (heads within 9.6 to 16.9 m, power rating 58 MW, runner diameter $D_1 = 8.0$ m). The part of the turbine from which the water supply emanates consists of the turbine case, stayring, and wicket gate. It should be noted that the designs of the component elements are common to all reaction turbines.

The turbine stayring is composed of a number of vanes (1) that are of an elongated streamline cross-section. Stayring vanes may be anchored in the reinforced concrete (Figure 3.2(a)), or to ensure a greater rigidity and strength, the vanes are interconnected by means of steel circular bands, upper and lower (Figure 3.2(b)). Individually mounted vanes are used only at comparatively low heads and large turbine diameters, and a stayring with bands is used at higher heads. The use of bands is obligatory when the turbine case is made of steel or has a steel lining (Figure 3.7).

The wicket gate consists of guide vanes (2) (Figure 3.1) secured in the lower ring (3) and in the turbine cover (4) by means of pivot pins, making is possible to set the vanes at an angle. The characteristic parameters of the wicket gate are

1. The number of guide vanes z_0. The wicket gate of large axial-flow turbines operated at a low head comprises 32 vanes; at higher heads there are 24, and sometimes 20 guide vanes.

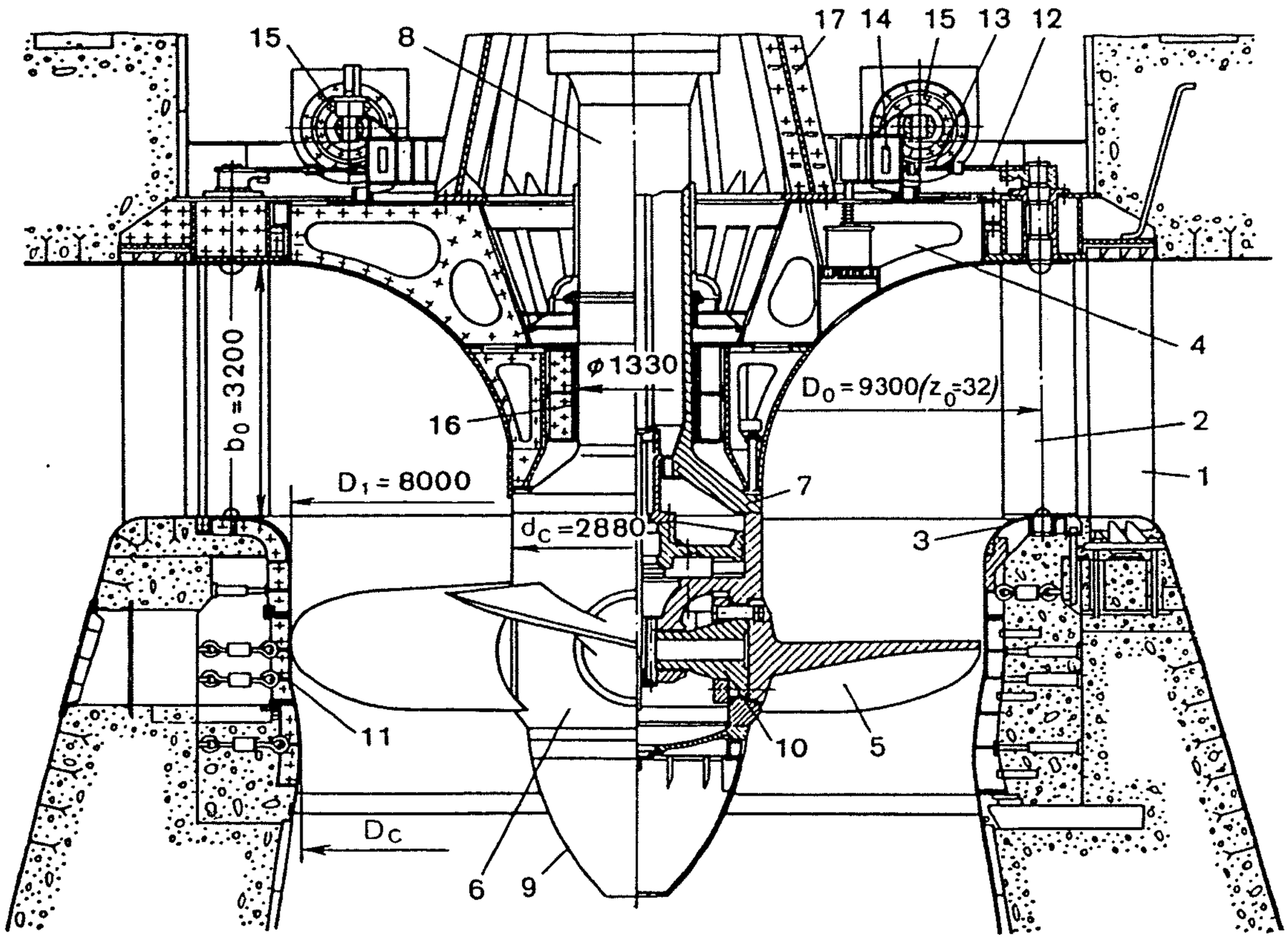


FIGURE 3.1. Axial-flow, adjustable blade turbine of Kremenchug HEPP, located on the Dnepr River. 1 — stayring vanes; 2 — guide vanes; 3 — lower ring; 4 — turbine cover; 5 — runner blades; 6 — runner hub; 7 — shaft flange; 8 — shaft; 9 — runner cone; 10 — turbine case; 11 — sliding block; 12 — guide vane arm; 13 — link; 14 — adjustment ring; 15 — servomotors; 16 — bearing; 17 — generator thrust bearing support structure.

2. The height of the wicket gate b_0 (in Figure 3.1 $b_0 = 3.2$ m). Use is sometimes made of dimensionless quantities referred to as the diameter; to a great extent these quantities characterize the type of turbine. The relative height $\bar{b}_0$ of the wicket gate is

$$\bar{b}_0 = b_0/D_1 \tag{3.1}$$

where D_1 is the turbine diameter (for the case considered $D_1 = 8$ m and $\bar{b}_0 = 3.2/8.0 = 0.4$). The relative height $\bar{b}_0$ in axial-flow turbines falls within 0.45 to 0.35 (the smaller values pertain to greater heads).

3. The diameter over the guide vane pivot pins D_0 (in the example treated $D_0 = 9.3$ m). The relative diameter of the wicket gate is

$$\bar{D}_0 = D_0/D_1 \tag{3.2}$$

for the turbine considered $\bar{D}_0 = 9.3/8.0 = 1.16$. For different turbines $\bar{D}_0$ varies within 1.16 to 1.25 (increases with a lesser number of guide vanes in the wicket gate).

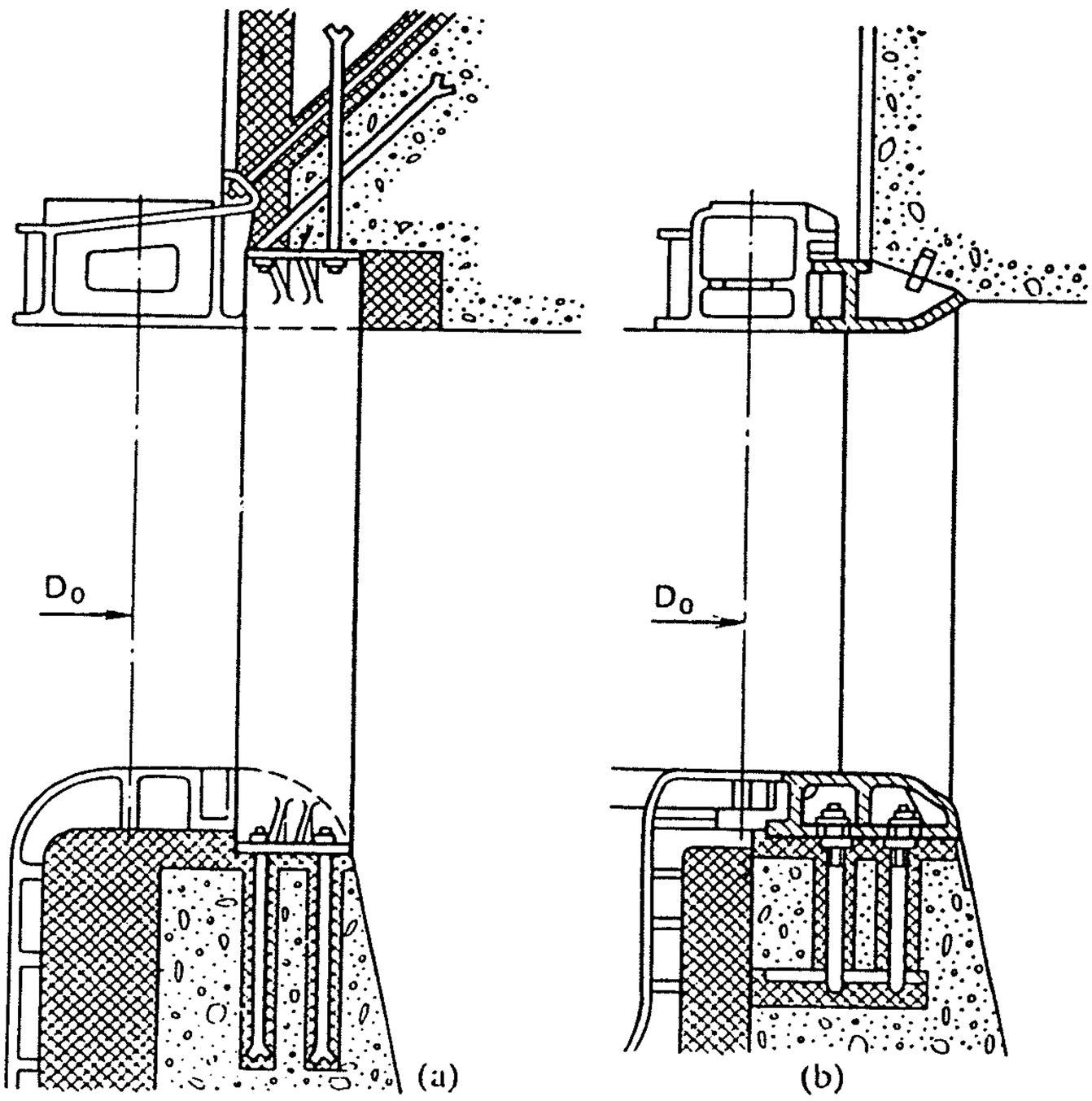


FIGURE 3.2. Axial-flow turbine stayring.

Figure 3.3 illustrates the design of the wicket gate of the Djerdap-Iron Gate HEPP on the Danube River, one of the largest axial-flow, adjustable blade turbines (heads within 17.5 to 35.5 m, $D_1 = 9.5$ m, rated power 178 MW). The lower pivot pin (4) of each guide vane (1) bears against a bushing force fit in the lower ring (2), and the upper pivot pin (5) bears against two bushings force fit in the bearing (6) mounted on the upper ring (3) of the wicket gate (located sometimes in the turbine cover). The bushings are made from polymer materials (requiring no lubrication), bronze (requiring periodic lubrication with grease), wood plastic, and laminated lignin plastic (requiring water lubrication).

The lever (7) set on the upper end of the pivot pin is connected to the regulating ring (9) by means of a pullrod (8). The elements (7), (8), and (9) form the guide vane operating gear, which make it possible to change the opening of the wicket gate, a_0, from zero (complete closing) to $a_{0\,max}$ (for the case considered $a_{0\,max} = 700$ mm).

The kind of wicket gate predetermines the direction of water flow. In the wicket gate (shown schematically in Figures 3.1 and 3.3) the stream surfaces are close to the planes normal to the turbine axis. This type of wicket gate is referred to as radial. When the stream surfaces are almost conical, the wicket gate is called conical (Figure 3.4(a)). When

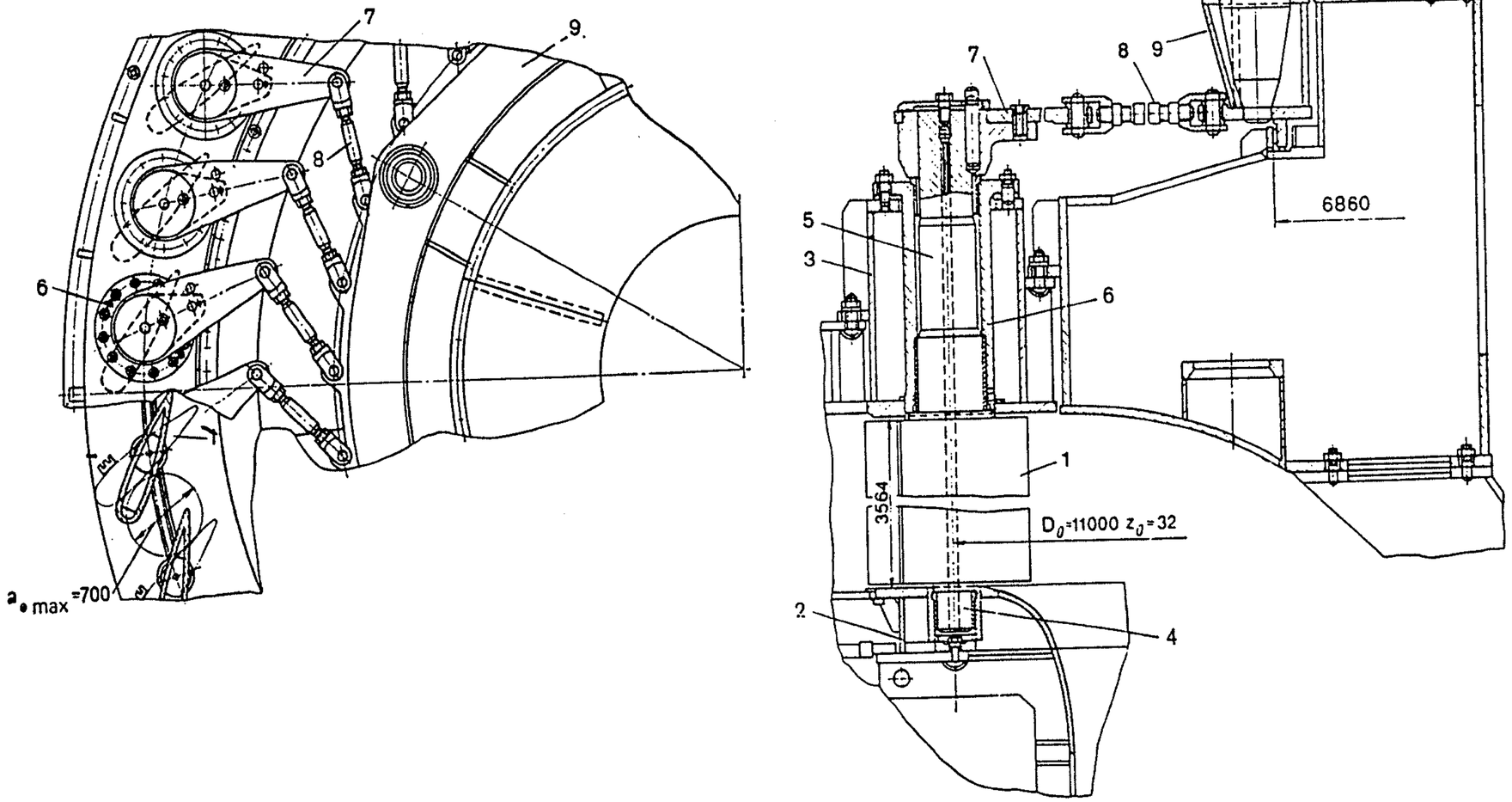


FIGURE 3.3. Wicket gate of turbine at Djerdap-Iron Gates HEPP.

the surfaces are close to cylindrical, the wicket gate is termed axial (Figure 3.4(b)).

The main parts of the runner (Figure 3.1) are the blades (5) and the hub (6) in which the blades are fastened. The runner is bolted to the lower flange (7) of shaft (8). The cone (9) is designed to lessen the losses associated with vortex formation, and pulsation is secured to the outlet end of the case.

The blade of the runner of an axial-flow turbine (Figure 3.5) consists of the blade proper and the flange. The blade is relatively thin and is formed as a curvilinear surface on which interaction with the water flowing through the turbine takes place, causing the conversion of the hydraulic energy into the rotational energy of the runner and the shaft. The flange is used to secure the bland to the flange of the pivot, and aids in securing the blade in the bushing ((10) in Figure 3.1).

The cylindrical blade sections shown schematically in Figure 3.5 give an idea of the form of the blade: the sections located closer to the flange, root sections, are thicker and steeper; the peripheral sections are thinner and flatter. Such a form is determined by the hydraulic conditions under which water flows past the vane and by strength. The load taken up by the vane is very large and distributed over the entire surface (for instance, in a turbine 9.5 m in diameter having six blades, at a head of 30 m, the load on each blade amounts to 2700 kN). The action of the blade is similar to a cantilever beam carrying a distributed load,

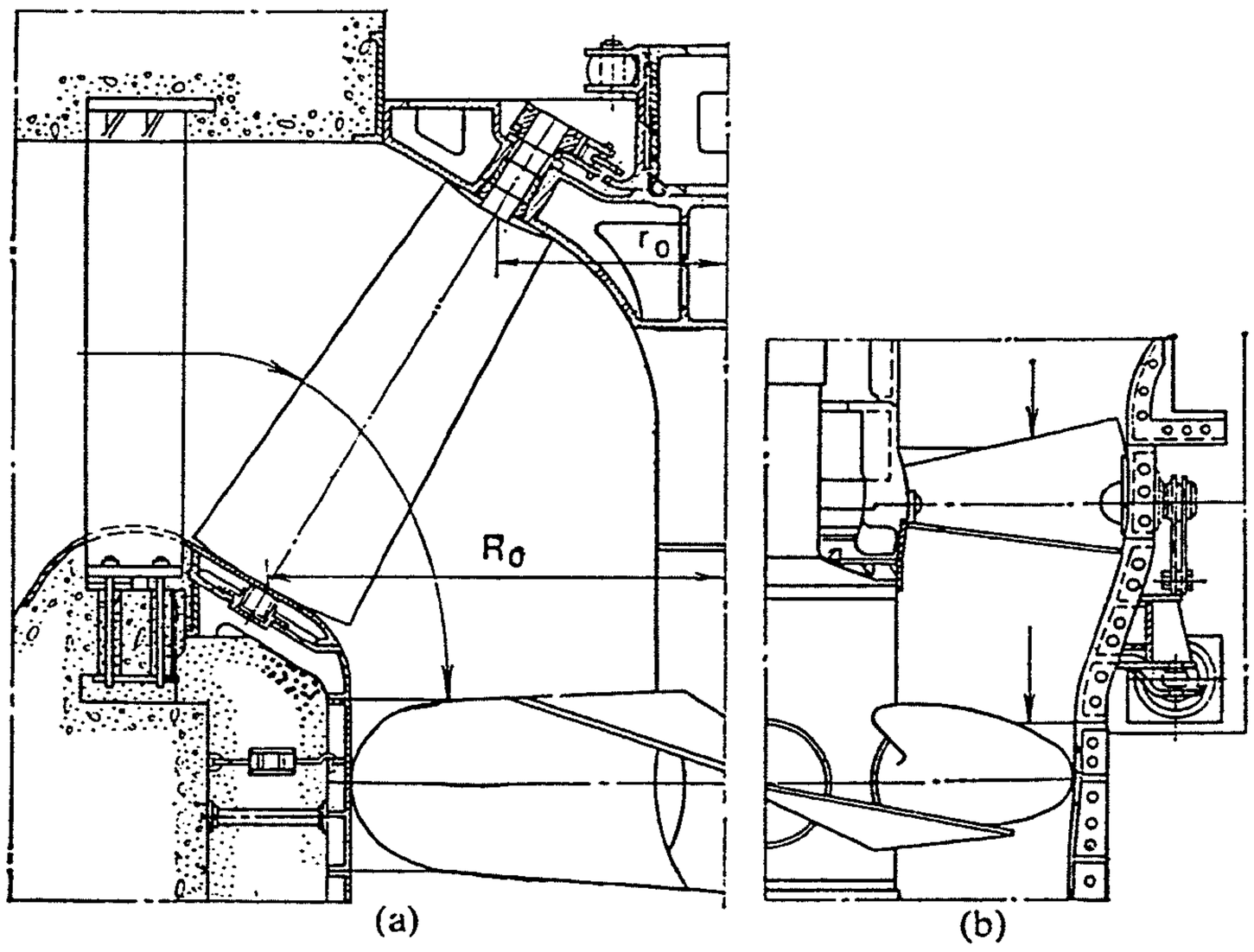


FIGURE 3.4. Conical (a) and axial (b) wicket gates.

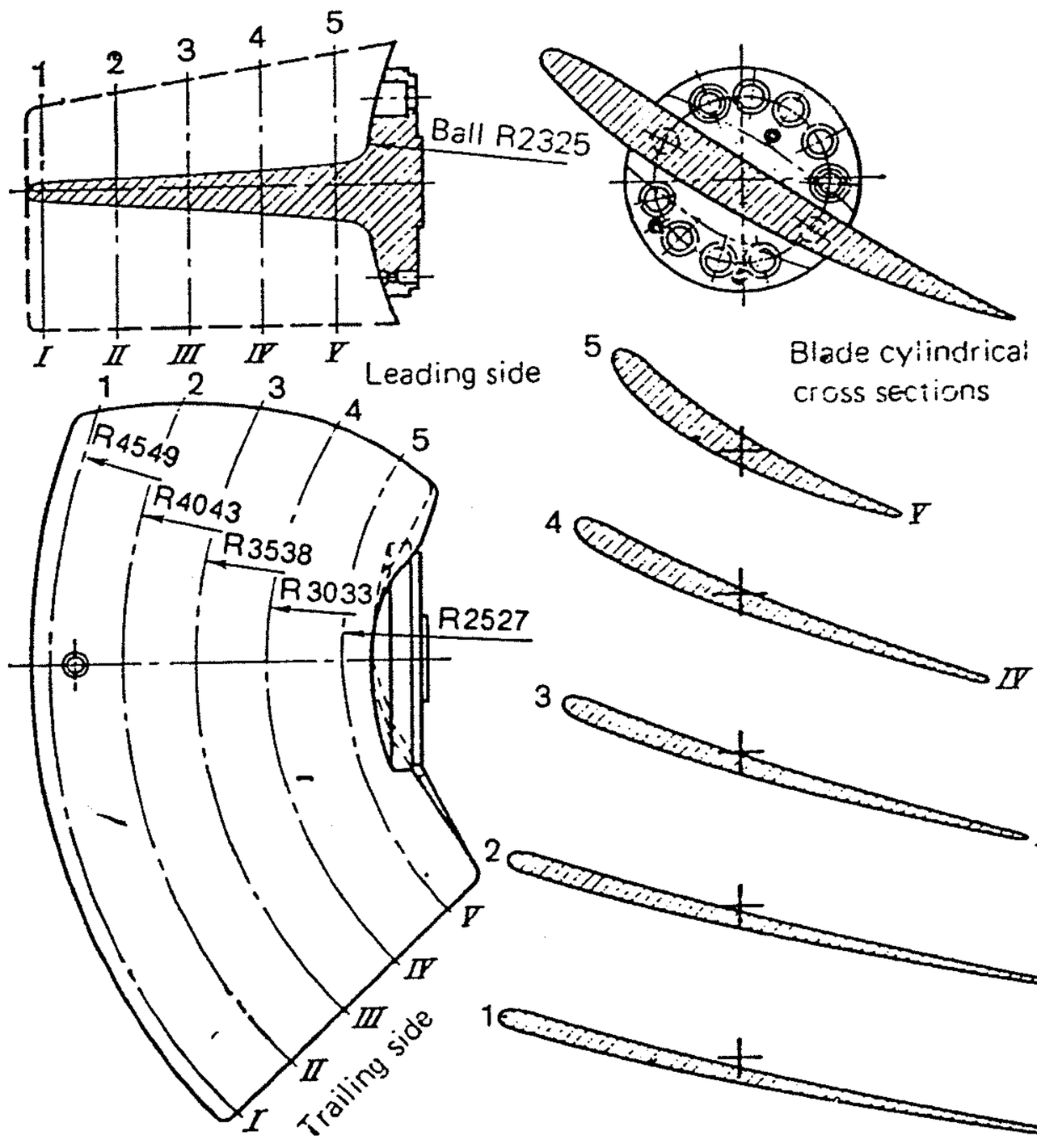


FIGURE 3.5. Blade of an axial-flow turbine runner.

and the bending moment, especially in the root sections, is very large. This requires a corresponding section moment of resistance.

The runners of adjustable blade (Kaplan) turbines permit the blades to be turned "on the go," i.e., to change the blade angle, as illustrated in Figure 3.6. Some design blade position is assumed as the reference

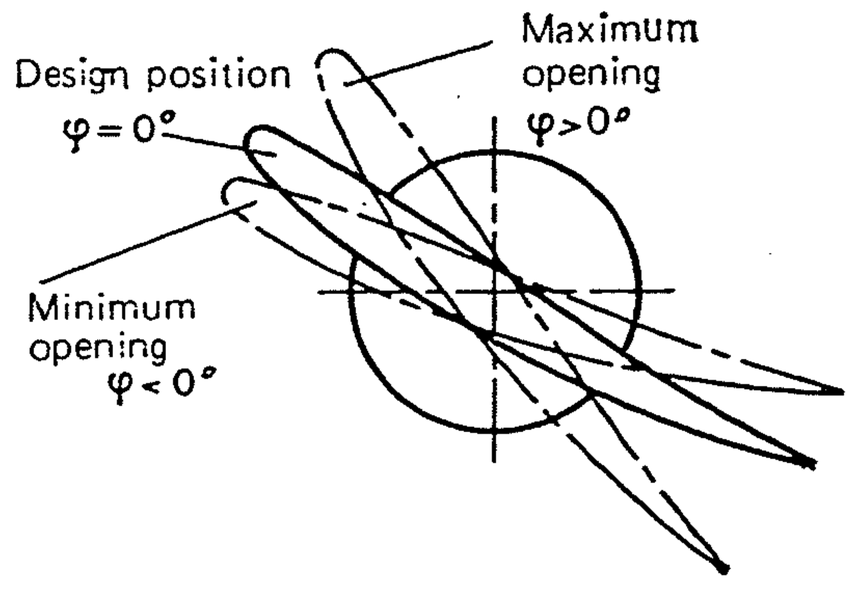


FIGURE 3.6. Turning of axial-flow turbine blades.

point for the blade angle φ. In this case $\varphi = 0$ is a "design position," which corresponds to the zone of maximum efficiency. When the blade angle ensures a maximum opening, $\varphi > 0$; when the blade angle is diminished, $\varphi < 0$. Another reference point for the blade angle is sometimes used, for instance, the plane perpendicular to the runner axis of rotation (in this case the angle is always positive). The blade angle is chosen in strict accordance with the opening of the wicket gate and with account taken of the acting head. The relationship

$$\varphi = f(a_0, H) \tag{3.3}$$

the so-called combinator dependence, is set in such a way that a maximum turbine efficiency is ensured under all operating conditions. It follows that two power regulations are possible in adjustable blade turbines: regulation by changing the opening of the wicket gate, and regulation by varying the runner blade angle. This is a great advantage from the power-generation point of view, but leads to a more complicated design, especially that of the runner, which requires very powerful blade operating gear.

Some axial-flow turbines have a fixed vane angle. Such machines are referred to as propeller turbines. They have a simpler design, cost less, and have only one power-regulating element—the wicket gate. Their power-generating properties are somewhat worse, the average efficiency is less.

Axial-flow turbines are employed in a wide range of heads, from the lowest 1 to 3 m up to 60 to 70 m (Figure 2.9). It is clear that a change in the available head necessitates a change in the form of the runner, which is characterized by the number of blades and the diameter of the hub or by its relative value:

$$\bar{d}_c = d_c/D_1 \tag{3.4}$$

For the turbine depicted in Figure 3.1, $d_c = 2.8$ m and $\bar{d}_c = 2.8/8 = 0.35$. Larger heads require blades with a larger surface. This can be attained initially by the size of a blade, and then the number of blades must be increased. The blade fastening conditions and arrangement of the blade-operating gear make a turbine hub of a larger diameter necessary. As an example Figure 3.7 the schematic diagram of the axial-flow adjustable blade (Kaplan) turbine installed at a HEPP constructed on the Tuloma River in Russia. The turbine is rated at about 60 MW at heads of 51 to 62 m. The diameter of the turbine runner $D_1 = 4.2$ m, the number of blades $z_1 = 8$, and the hub diameter $d_c = 2.07$ m. It follows that $\bar{d}_c = 2.07/4.2 = 0.5$.

The turbine hub causes constriction of flow, especially at a relatively large diameter, subsequently leading to deterioration of turbine operating conditions. In addition, to preserve small clearances between the tips of the blades and the turbine hub when the blade angle is changed as well as to diminish leakage, the central part of the case has a spherical shape, as shown in Figures 3.1 and 3.7. The diameter of the spherical part of the hub $\bar{d}_{c.s}$ is 0.03 to 0.05 times greater than $\bar{d}_c$ and flow constriction is augmented.

The runner casing ((11) in Figures 3.1 and 3.8) has a thick steel lining secured in concrete by means of anchors and pullrods (Figure 3.8(b)). The extent of the lining and fastening are traced to the fact that when the turbine is in operation the casing walls take up large pulsating loads from water pressure, and the loads are capable of shaking and damaging the lining of the casing.

Of material importance to adjustable blade turbines are the clearances or gaps between blade tips and the casing. The less wide the gap, the less the leakage, and the higher the turbine efficiency. The admissible gap is usually $\delta = 0.001\ D_1$ (with a diameter of 9.5 m the gap measures about 10 mm). To maintain a constant gap when the blade angle pit is changed, the turbine runner casing must be spherical. However, difficulties may be encountered when mounting the assem-

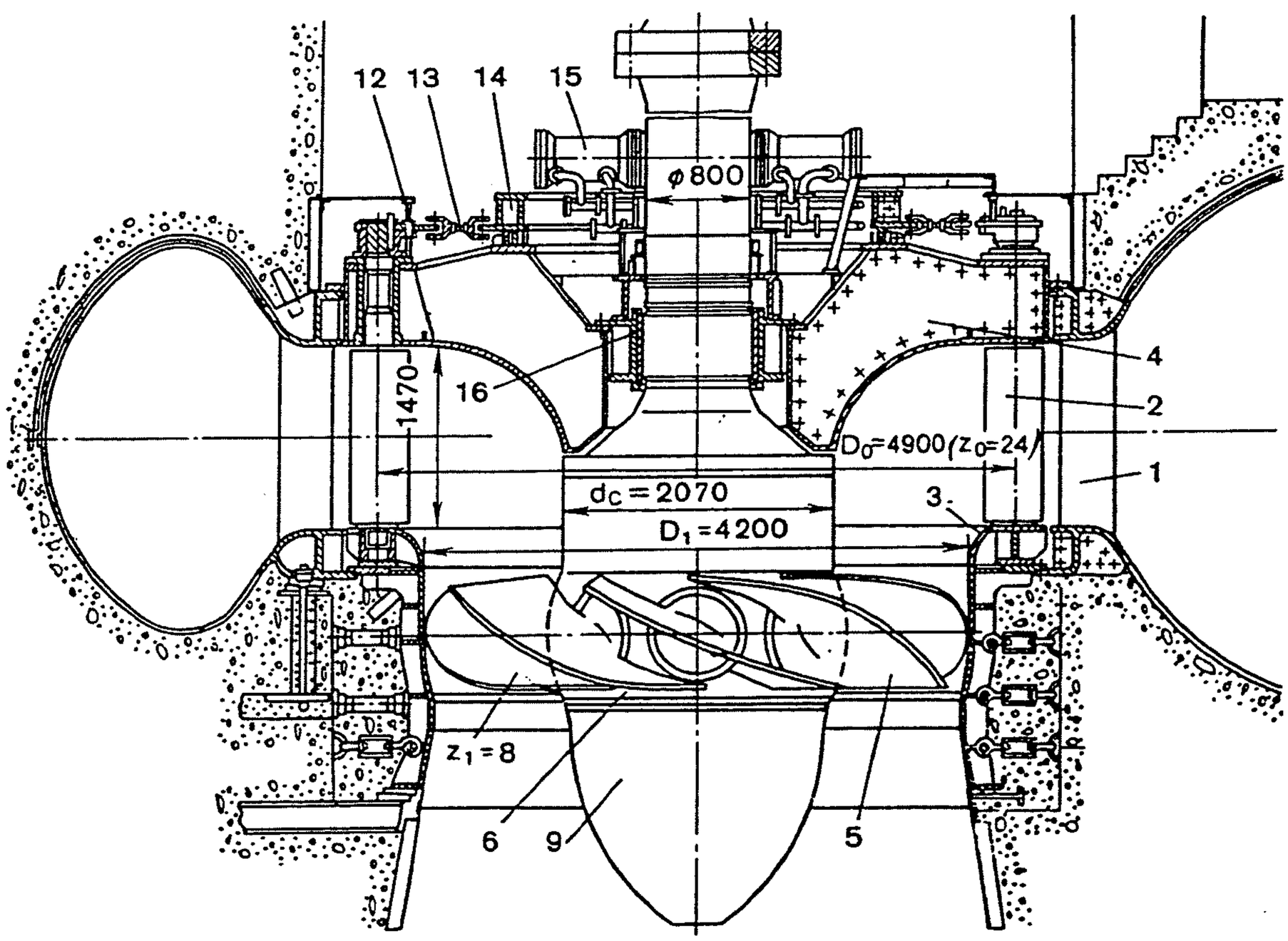


FIGURE 3.7. Axial-flow adjustable blade turbine of Verkhne-Tuloma HEPP (numbered parts are identified in Figure 3.1).

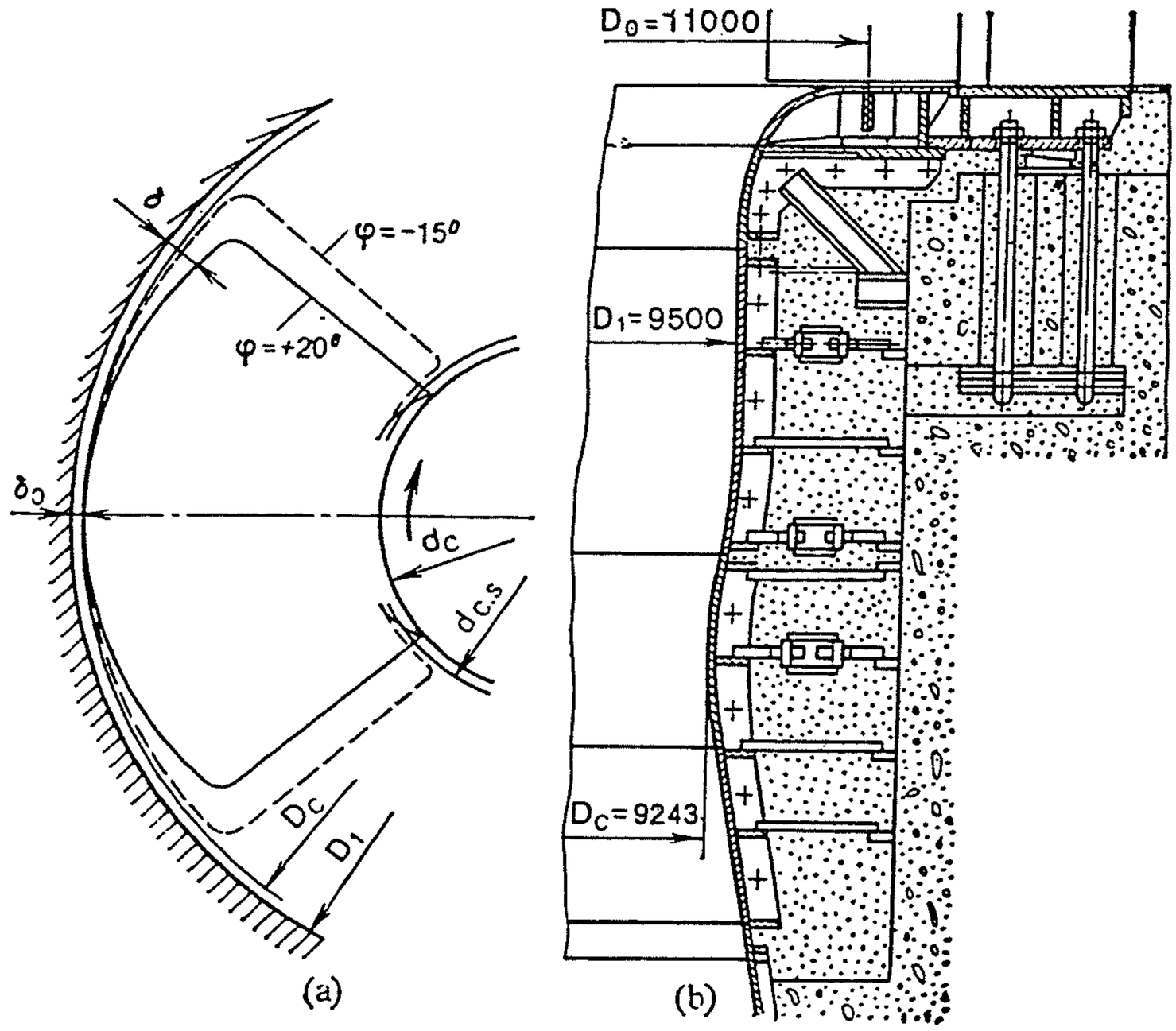


FIGURE 3.8. Axial-flow turbine runner case.

bled runner in its place. Thus, the part of the casing atop the adjustable blade axis is cylindrical. The lower outlet part of the casing is spherical, but not over its entire height, so that a minimum outlet diameter D_c is not smaller than (0.98 to 0.96 D_1 (in Figure 3.8(b), $\overline{D}_c = 9243/9550 = 0.973$). A lesser cross-section causes a drop in turbine power and efficiency. With a casing of this form the gap δ_0 remains constant at the adjustable blade axis. When the blade angle φ is increased the gap δ increases, especially at the inlet end of the blade (Figure 3.8(a)).

The turbine cover ((4) in Figures 3.1 and 3.7) covers the space on top of the runner; it accommodates the upper pivots of the guide vanes and supports the regulating ring (14). The cover houses the guide bearing (16) of the turbine. The structure of the generator thrust bearing ((17) in Figures 1.2 and 3.1) often bears against the turbine cover. This bearing takes up the axial load created by the rotating parts of the unit. Safe turbine operation is ensured by making the cover sufficiently strong and rigid.

3.2. HORIZONTAL AXIAL-FLOW TURBINES

These turbines are widely used for submerged or bulb-type hydroelectric units with generator, placed in a steel bulb exposed to water

flow. The features of the powerhouse of a low-head HEPP fitted with bulb-type hydroelectric units are made clear in studying the layout of the Kiev a hydro constructed on the Dnepr River by the Kharkov Turbine Works (KhTW) which has a head of 5.6 to 11.8 m; the hydroelectric units are rated at 23 MW (Figure 3.9). In the bulb-type hydroelectric unit water flow must make a minimum number of turns throughout the unit, and, of paramount importance, water must flow in a straight line through the draft tube (compare with Figures 2.2 and 2.4). This results in lesser hydraulic losses and a higher turbine efficiency, especially at high rates of water flow. Turbines of this type produce 20 to 35% more power than vertical turbines of the same size. Figure 1.3 is a schematic diagram of a bulb-type hydroelectric unit, and Figure 3.10 provides a general view of one of the largest bulb-type units, comprising a 7.5-m turbine manufactured at the St. Petersburg Metal Works (StPMW).

A major concern associated with horizontal hydroelectric units is to ensure the reliable performance of bearings, especially of the turbine

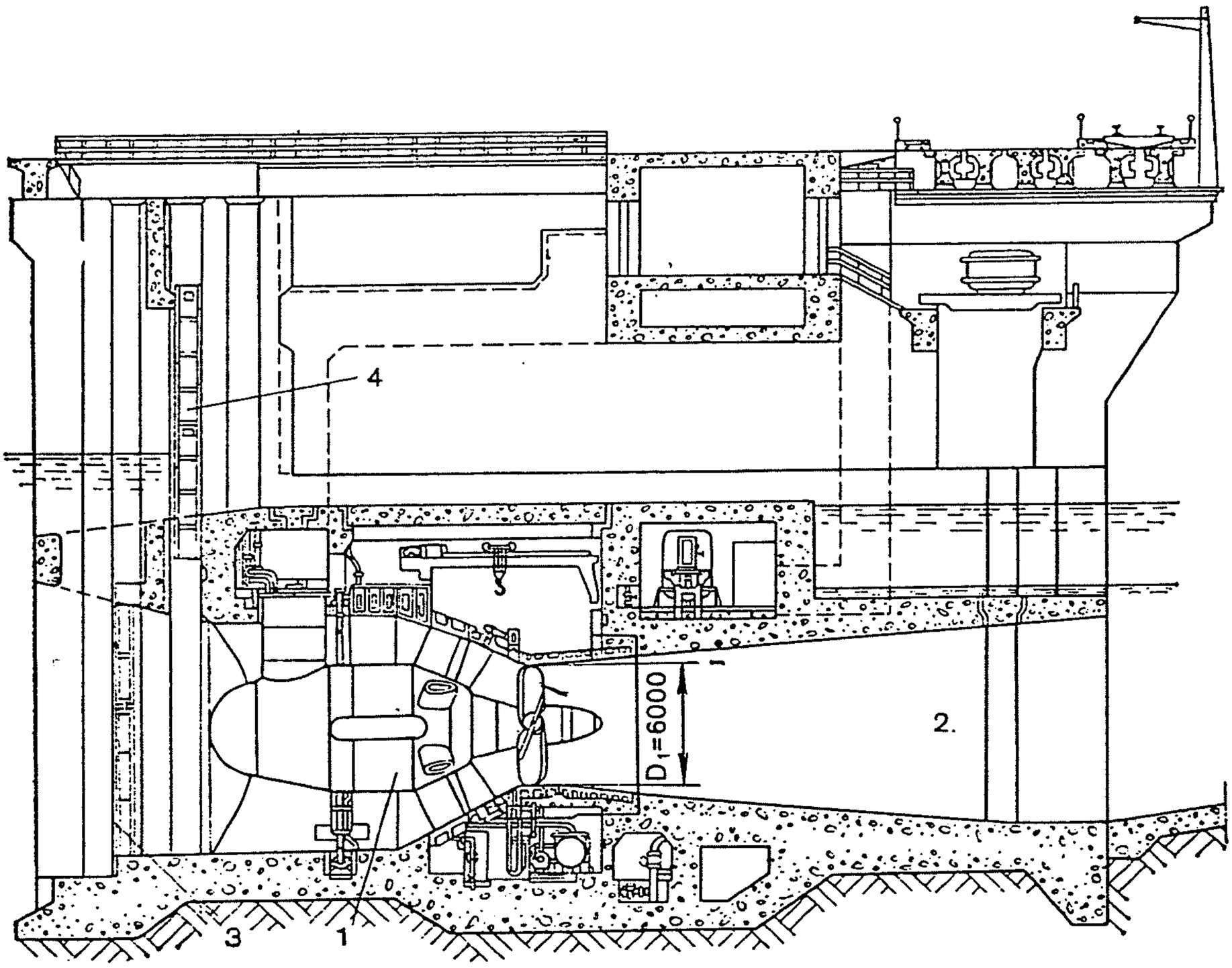


FIGURE 3.9. Powerhouse of Kiev HEPP with bulb-type horizontal hydroelectric units. 1 — Bulb-type hydroelectric unit (turbine and generator); 2 — draft tube; 3 — trashrack; 4 — gates of overflow spillway.

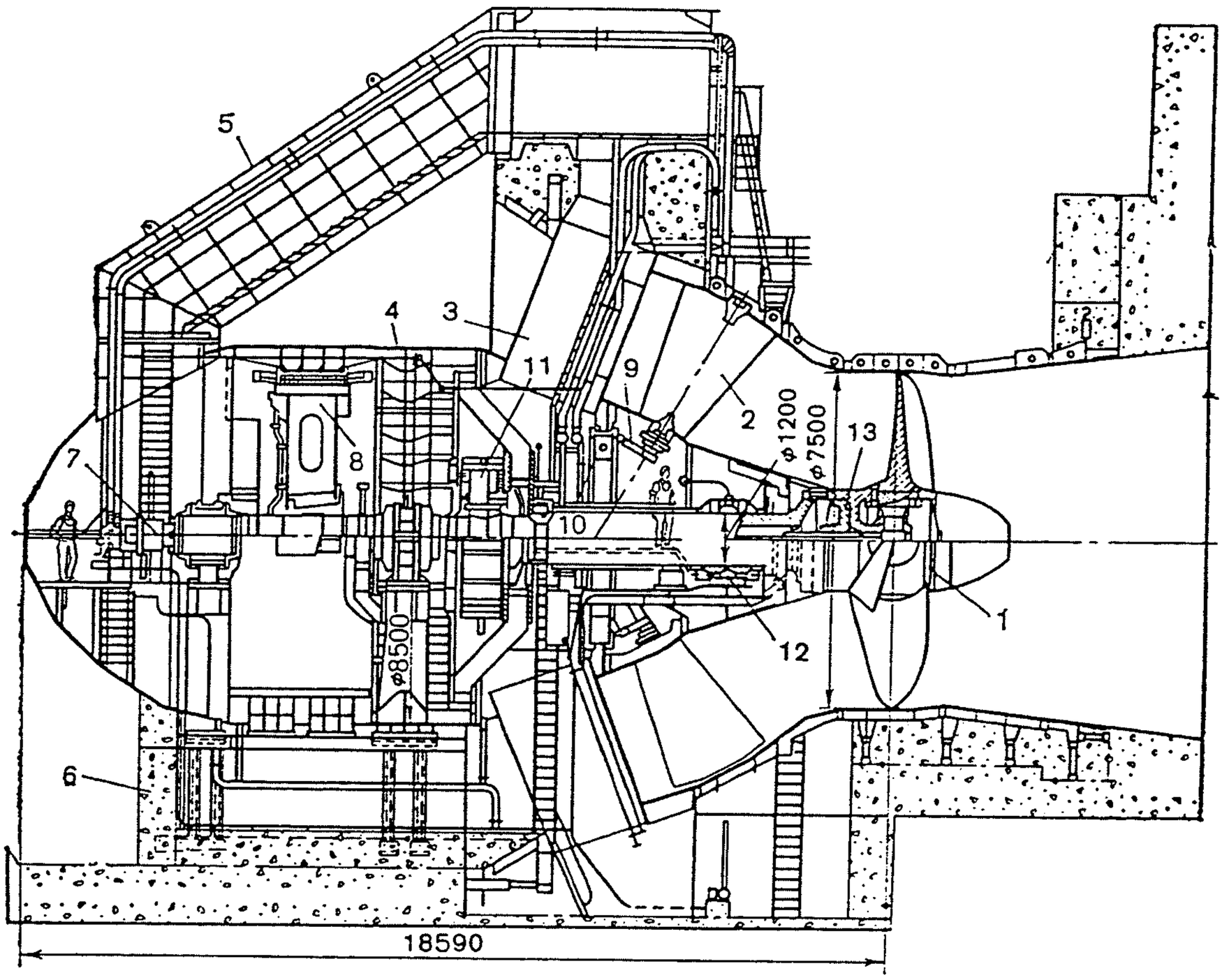


FIGURE 3.10. Bulb-type unit with a 7.5-m diameter turbine. 1 — Runner; 2 — guide vanes; 3 — support columns; 4 — bulb; 5 — service line shaft; 6 — concrete pedestal; 7 — oil collector; 8 — generator rotor; 9 — vane arms; 10 — adjustment ring; 11 — thrust bearing; 12 — turbine shaft bearings; 13 — runner body.

bearing (Figure 3.10, (12)) that takes up a large radial load caused by the overhang-mounted runner. The tendency, therefore, is for the center of gravity of the runner to be as close as possible to the bearing.

In some bulb-type hydroelectric units a step-up gear is placed between the shafts of the turbine and the generator. This step-up gear increases the rotational speed by 8 to 12 times as compared with the turbine speed. This makes it possible to reduce the dimensions of the generator and the diameter of the bulb.

Very large axial-flow horizontal turbines (8.2 m in diameter with bulb units, manufactured by Kvaerner Co.) were installed at the Sidney A. Murray, Jr. Hydropowerstation (Mississippi River) in 1990. The principal parameters of the turbine are as follows: heads, maximum 6.25 m, minimum 2.6 m, rated (design) 4.9 m (therefore, the head is rather low); rated power, 25 MW; speed, 52.2 rpm; and number of turbines in the station, 8. One of the peculiarities of these turbines is that they have rigidly fixed guide vanes and regulation is carried out only by turnable

runner blades. In the standing-still position the sluicegate, located in the draft tube, must be closed. The other peculiarity is the use of a two-stage step-up gearbox with 11.5 speed ratio. It made it possible to use a normal electric generator, at 600 rpm, and decrease the bulb diameter from 9.4 to 6.6 m. The result was an approximately 25% increase of the inlet area at the same station block dimensions.

Hydropower plants with 4 to 5 m heads constructed on the Moselle River (Germany) operate bulb-type hydroelectric units rated at 3.5 to 4.6 MW, and incorporate turbines with diameters $D_1 = 4.6$ to 4.8 m and step-up gears 87/750 to 67/750 rpm.

A special type of horizontal hydroelectric unit with an axial turbine is the so-called straight-flow unit, distinguished by the fact that the generator rotor is set on the peripheral edges of the turbine runner. It should be noted that the idea of such a design was suggested as early as 1919, but was not realized until the end of 1930-th, when, Escher-Wiss

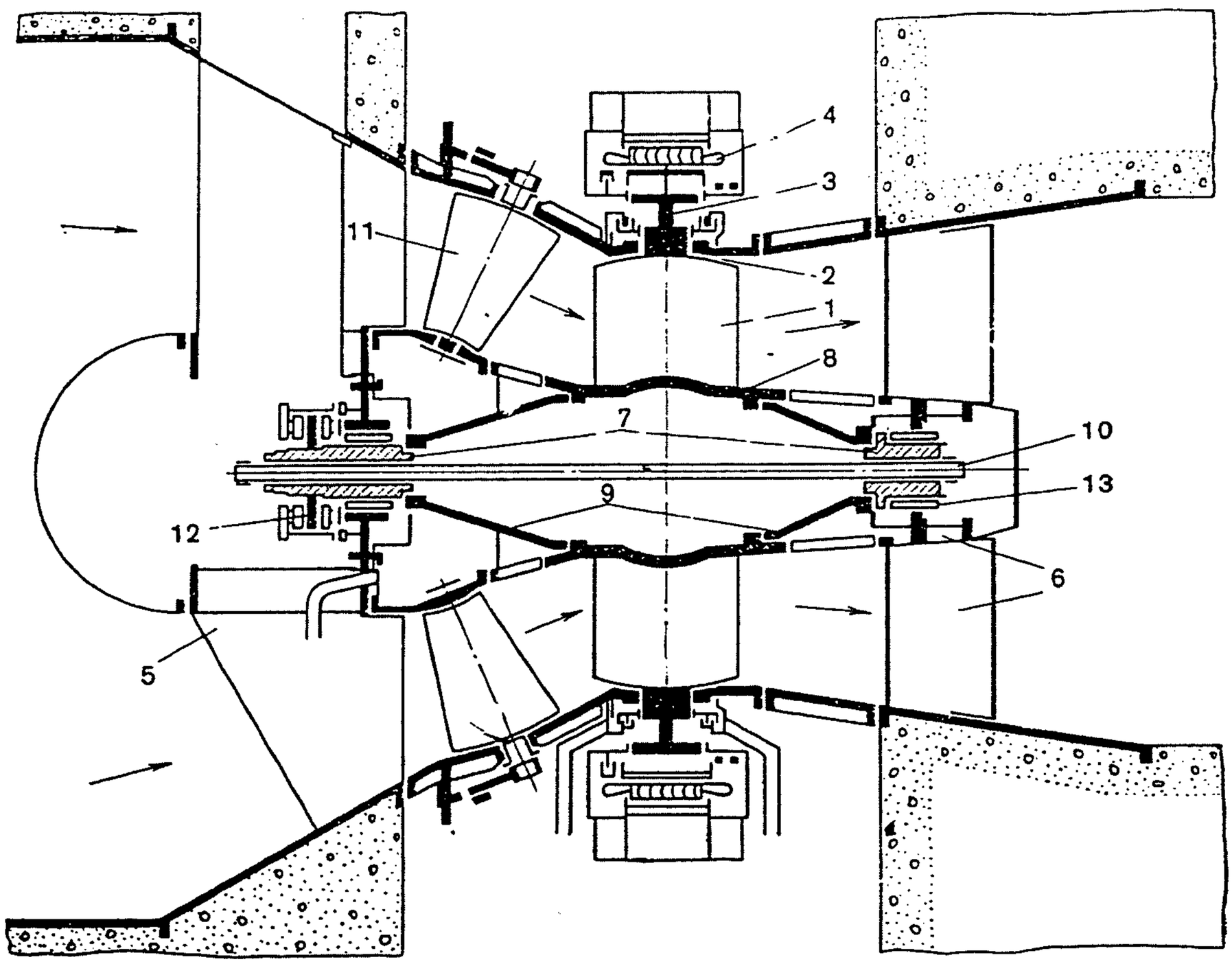


FIGURE 3.11. Straight-flow unit (Straflo). 1 — Runner blades; 2 — runner rim; 3 — generator rotor rim; 4 — generator stator; 5, 6 — support columns; 7 — shaft journals; 8 — body; 9 — shaft cone inserts; 10 — tension rod; 11 — guide vanes; 12 — thrust and guide bearing; 13 — guide bearing.

produced about 70 low-power straight-flow hydroelectric units over a period of 15 years. Straight-flow units of this type have not found wide application, however, due to the difficulty of protecting the generator against moisture penetration.

It is necessary to note that intense work toward the creation of horizontal hydroelectric units was undertaken in connection with the plan and dėsign of tide power plants (TPP). The result of this work during the 1950s was the construction and commissioning of the first high-power TPP, La Rance (France) in 1968. The station was fitted with 24 horizontal bulb-type hydroelectric units; the rated power of each was 10 MW. The turbine runner is 5.35 m in diameter with four adjustable blades, 95 rpm, and has a straight connection with the electric generator shaft. The turbines operate under heads 3 to 11 m in both directions (basin to sea or sea to basin) and also can be used for pumping operations, which aim to increase the acting head on 1 to 2.5 m. Thus, the units work in an extremely wide range of regimes.

In the last few decades researchers have returned to the straight-flow unit idea. They were stimulated by construction plans for a TPP in the Bay of Fundy (Canada). The consequence of this work was the creation of a new hydroelectric unit, referred to as Straflo. Its simplified scheme is shown in Figure 3.11. Straflo was installed in the experimental Annapolis Royal TPP, put into operation in 1984. The parameters of this unit are turbine rated power, 17.8 MW; runner, 7.6 m diameter with fixed blades; operation head range, 1.4 to 7.1 m (rated 5.5); rotation speed 50 rpm.

3.3. MIXED-FLOW (DIAGONAL) ADJUSTABLE BLADE TURBINES

The largest high-power mixed-flow turbines (developed and constructed at the StPMW) are installed at the Zeisk HEPP in Russia. These units, rated at 215 MW, operate with heads 74.5 to 97.3 m, and have the runner diameter of 6.0 m (Figures 3.12 and 3.13). The stayring, guide vanes, and the guide vane operating gear are similar to those of axial-flow turbines. The main difference is in the form and design of the runner and its casing. Runner blades (1) with pivots (2) are secured in spherical-shape case (3) at an angle of 45° to the runner axis of rotation. Each pivot carries lever (4) connected by a ball-and-socket joint to pull rod (5), which is moved by the piston of servomotor (6). This results in the simultaneous turning of all runner blades through the same angle. The case is of a rather large diameter and $\bar{d}_c$ may range from 0.56 to 0.65 with nine to ten blades. However, the runner case of these turbines does not cause local constriction of water flow. The runner casing (7) is spherical, and this makes it possible to maintain a small gap between

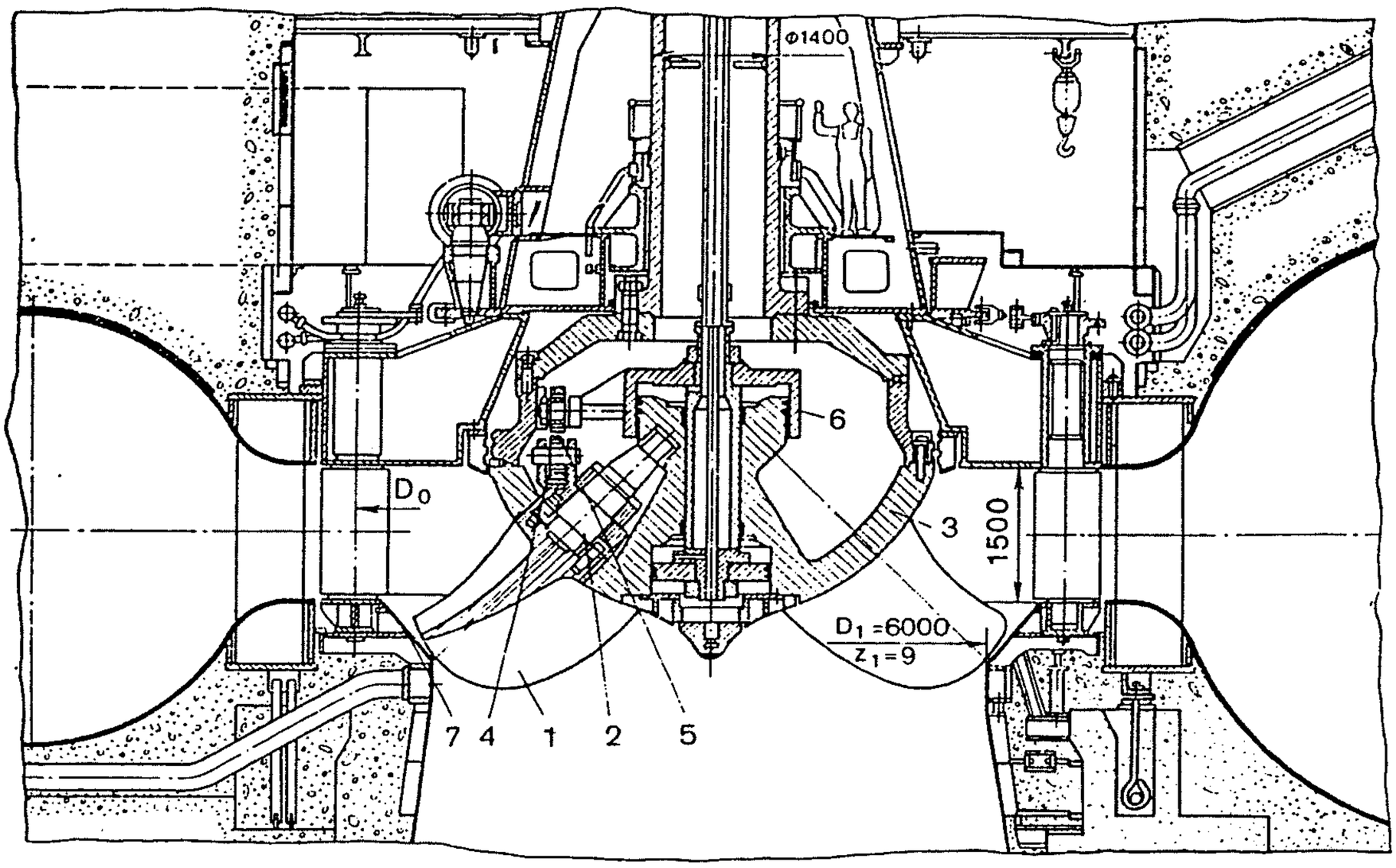


FIGURE 3.12. Mixed-flow adjustable blade turbine.

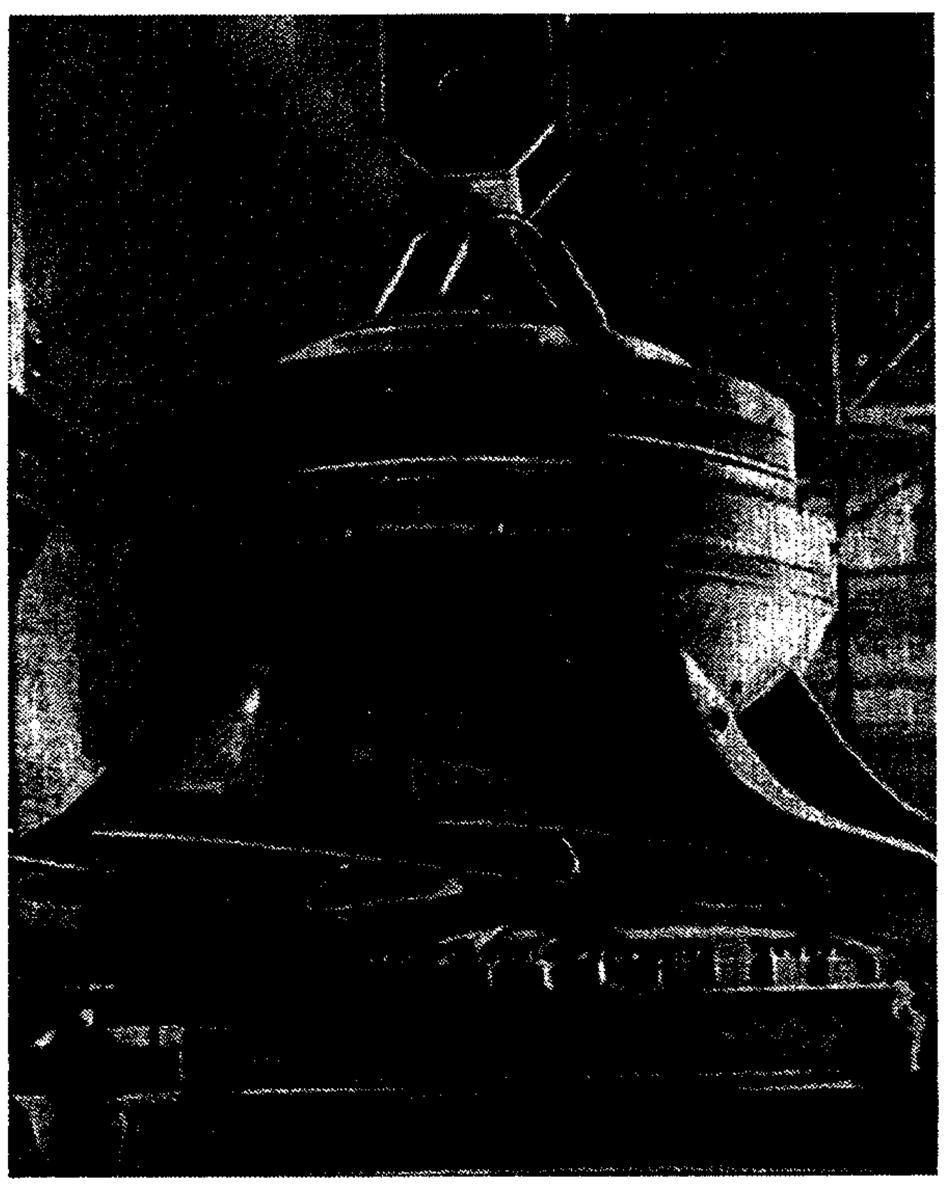


FIGURE 3.13. Runner of mixed-flow adjustable blade turbine of Zeisk HEPP during installation.

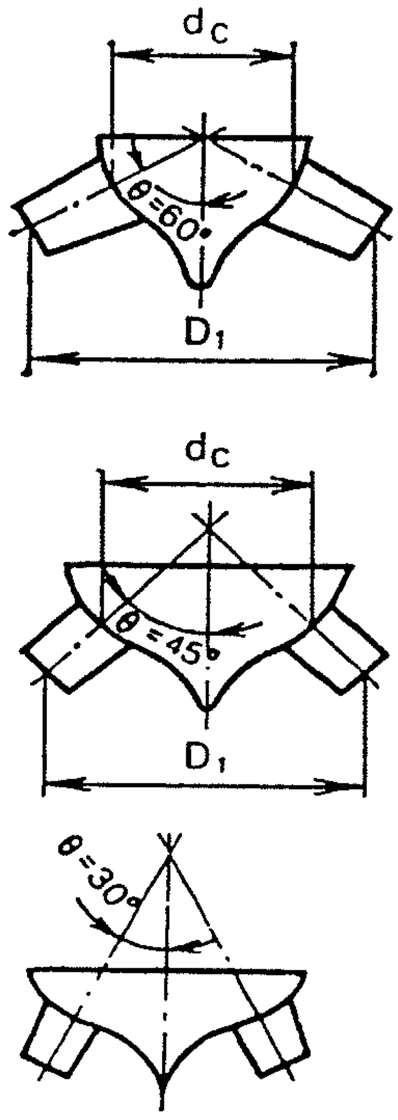


FIGURE 3.14. Shapes of runners of mixed-flow turbines.

the casing and ends of the runner blades. The gaps affect the power-generating characteristics of mixed-flow turbines appreciably; they must not exceed $1/1000\ D_1$ (smaller gaps are desirable).

The characteristic diameter D_1 of the mixed-flow turbine is determined by the intersection of the blade turning axes with the runner case (Figures 3.12 and 3.14). The relative minimum diameter of the runner case (throat) amounts to (0.95 to 0.98) D_1. It should be noted that while in axial-flow turbines D_1 determines the maximum diameter of the runner. In mixed-flow turbines the diameter determined over the inlet blade edges is larger than D_1.

Mixed-flow turbines may have not only a different number of blades, but also a different blade angle θ (Figure 3.14). The angle diminishes with increasing head. The approximate relations are as follows: heads from 40 to 80 m, $\theta = 60°$; heads from 60 to 130 m, $\theta = 45°$; heads from 120 to 200 m, $\theta = 30°$.

3.4. RADIAL-AXIAL-FLOW (FRANCIS) TURBINES

The design of radial-axial turbines is clarified by considering the turbine constructed by StPMW for the Sayano-Shushenskoye HEPP located on the Yenisey River of central Siberia (Figure 3.15), with heads

from 175 to 220 m. The parameters of the turbine are as follows: power rating, 650 MW at a design of 194 m (turbine power may reach 735 MW at a head of 212 m and more); runner diameter $D_1 = 6.77$ m; and rotational speed, $n = 136.4$ rpm (there are ten hydroelectric units at the HEPP).

The water supply system consists of the turbine spiral casing (not shown in the schematic) with a steel lining welded to strong upper and lower steel bands of the stayring (a) and (b), and stayring vanes (1). The wicket gate consists of guide vanes (2) whose pivots are supported in bearings (5) secured in the turbine cover (4). The cover is bolted (6) to the upper stayring band.

The operating gear of the guide vanes is similar to that used in axial- and mixed-flow turbines. It consists of levers (12) set on the upper pivots of the guide vanes, ball joints, pullrods (13 and 14), and servomotors (15).

The sealing of the wicket gate, ensuring minimum leakage when fully closed, is attained by diminishing the end gaps, tight fit of the blades, or with the aid of rubber or machined metal gaskets made from stainless steel.

The runner consists of crown (9), band (10), and blades (11), and these components are an integral rigid part. The crown is used to connect the runner to the lower flange (7) of the shaft (8) whose outside diameter measures 1.945 m. Cone (18) secured to the crown is designed to prevent the formation of a vorticity zone in the water flow.

The runner of the radial-axial (Francis) turbine has a solid, nondetachable design. It may be shipped by rail, if its diameter does not exceed 4.75 m; runners of greater diameter can be delivered to the construction site via water transport, as was used for the Sayano-Shushenskoye HEPP and to deliver turbine runners 6.3 m in diameter to the Aswan HEPP located on the Nile River.

Runners also may have a detachable design for assembly in situ. For instance, the runners of turbines that are 5.5 m in diameter, intended for the Bratsk Hydro on the Angara River (central Siberia), have been manufactured at the works in halves and assembled at the construction site.

Water pressure is high upstream of the runner and is low downstream of the runner. Often, a vacuum sets in the low-pressure zone. It follows that when the turbine is in operation, water may leak between the rotating and fixed elements, and these leaks will lower the turbine efficiency. The leaks are reduced by means of special seals. The turbine shown in Figure 3.15 is fitted with the so-called slot seals (19) whose performance is based on the creation of a small gap between a rotating part and a fixed part (1.5 to 2.5 mm). Sometimes the duct resistance coefficient is increased by making widened grooves. Labyrinth seals are

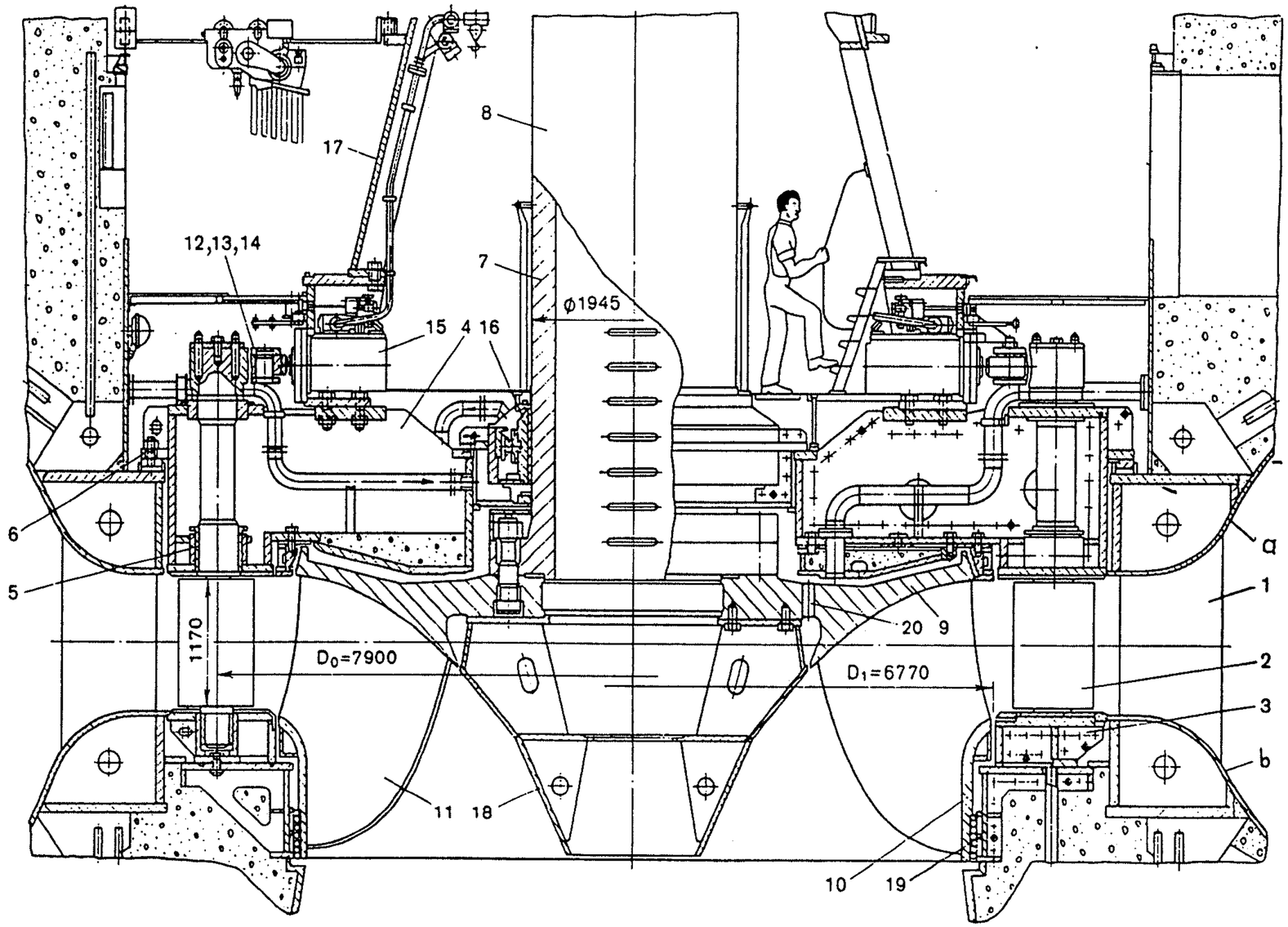


Figure 3.15. Radial-axial flow turbine. 1 — Stayring vanes; a and b — upper and lower stayring bands; 2 — guide vanes; 3 — wicket gate lower ring; 4 — turbine cover; 5 — support bearings of guide vane upper pivot; 6 — attachment of cover to stayring upper band; 7 — shaft flange; 8 — shaft; 9 — runner crown; 10 — runner band; 11 — runner blades; 12, 13, 14 — operating gear levers and pullrods; 15 — servomotors; 16 — bearing; 17 — generator thrust bearing support; 18 — cone; 19 — runner band seals; 20 — balancing hole.

used in turbines at very high heads (Figure 3.17). The runner crown requires a seal in cases in which discharge (balancing) holes occur (20 in Fig. 3.15 and 5 in Fig. 3.17). These holes, which create free communication between the space above the runner crown and the lower-pressure region underneath the runner, reduce the hydrodynamic loads, creating an axial load that is taken up by the thrust bearing. The crown illustrated in Figure 3.15 has a groove seal and the crown in Fig. 3.17 has a labyrinth seal.

The turbine cover (4) is a strong, welded structure that absorbs great loads from the guide vanes that are acted upon by water pressure as well as loads coming from the thrust bearing support (17). The cover mounts the turbine guide bearing (16).

The turbines of the Grand Coulee Hydro (built by the Allis Chalmers Company), located in Washington state, have unique parameters. Figure 3.16 is a view of the station's hydroelectric unit incorporating a radial-axial Francis turbine rated at 700 MW with a head of 87 m (see Figure 3.15 for the corresponding reference numbers). The heads vary

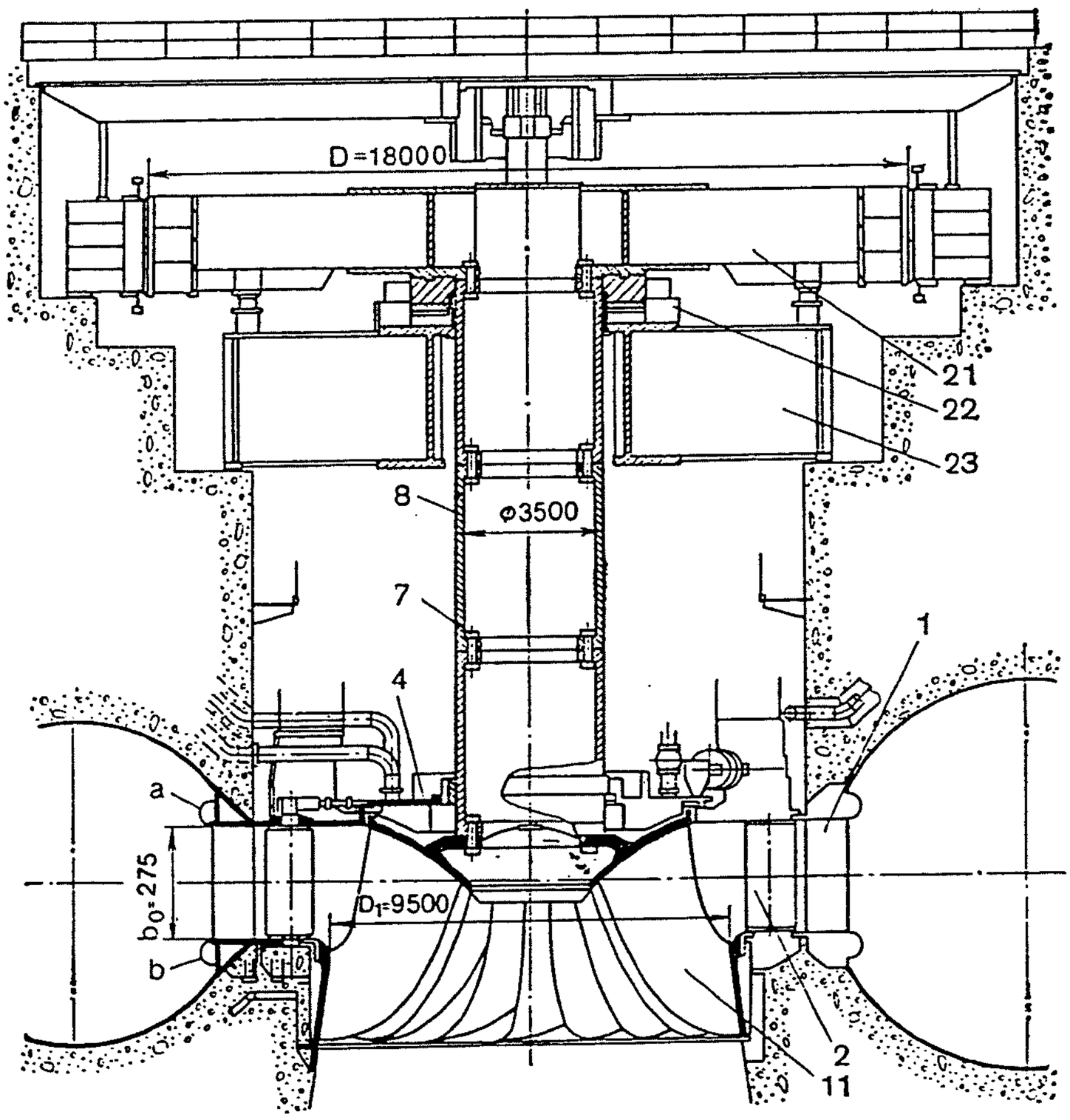


FIGURE 3.16. Hydroelectric unit at Grand Coulee HEPP.

from 67 to 108 m, the runner diameter is 9.5 m, and the rotational speed $n = 85.7$ rpm. The generator thrust bearing (22) is mounted on a strong spider (23). The diameter of the generator rotor (21) measures about 18 m. The hollow shaft (8) of the hydroelectric unit has a 3.5-m outside diameter O.D. and consists of three parts, each 4.5-m long, that are interconnected by means of internal flanges (7). The ring-shaped stayring bands *a* and *b* have semiround guides which facilitate the fabrication and reduce the width of the turbine spiral casing.

The turbines installed at the Inguri Hydro (Georgia) (Figure 3.17) are typical high-head radial-axial (Francis) turbines. They were developed and manufactured at the KhTW. At the design head of 325 m, the power rating of the turbines is about 250 MW. The maximum head is 404 m. The rotational speed is $n = 250$ rpm. It should be noted that an increase in the head causes a material change in the shape of the water passage. The relative height of the wicket gate diminishes; here, $\bar{b}_0 = 0.45/4.5 = 0.1$; for a head of about 200 m (Figure 3.15), $\bar{b}_0 = 0.17$; and for a head of 90 m $\bar{b}_0 = 0.29$. The outlet diameter of the runner

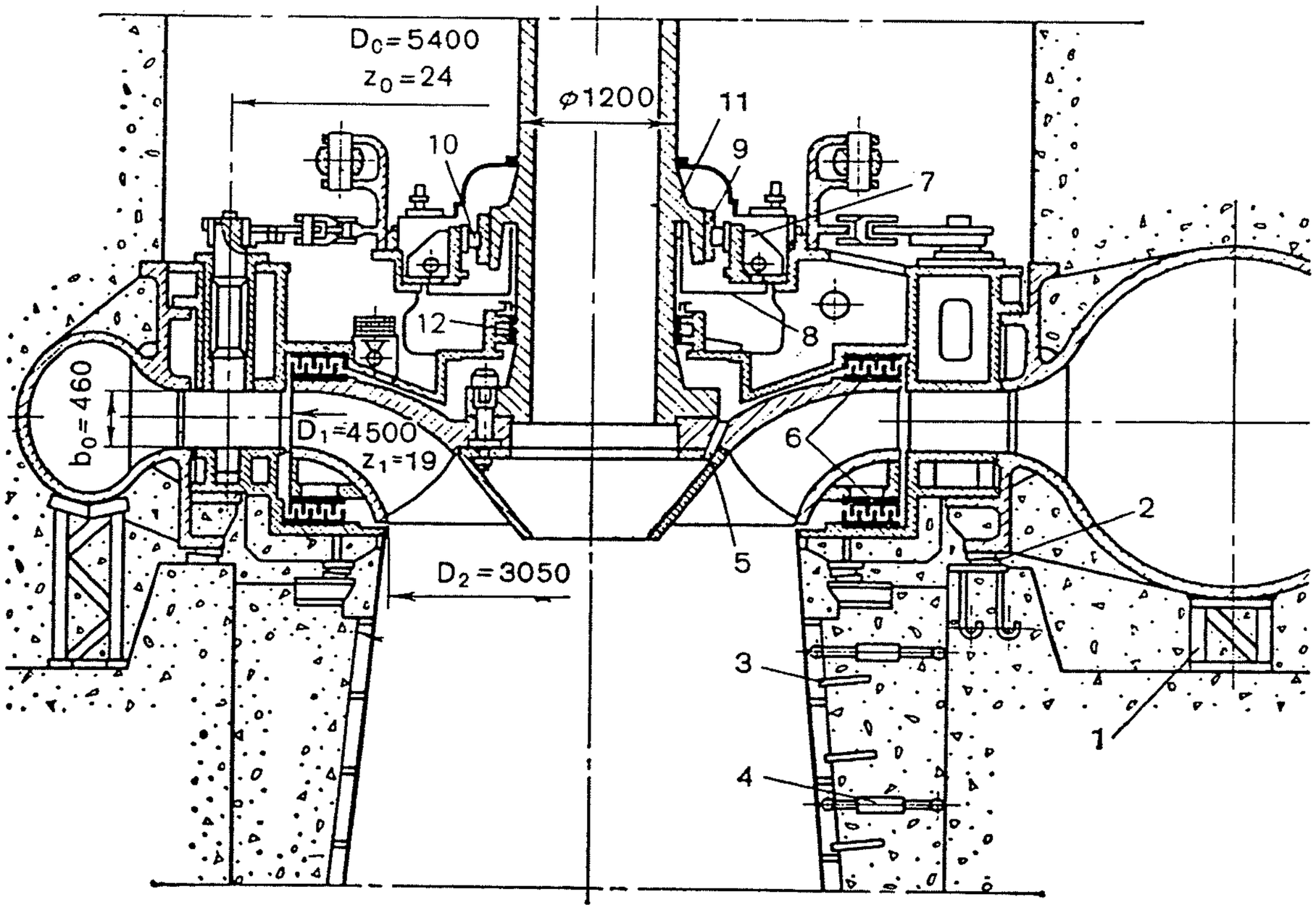


FIGURE 3.17. The Inguri HEPP turbine. 1, 2, 3, 4 — Mounting elements: pedestals, wedges, steel lining of draft tube with anchors, and turnbuckles; 5 — balancing holes; 6 — runner labyrinth seals; 7–10 — members of turbine bearing with oil lubrication; 11 — shaft with support part at bearing; 12 — water seal.

also diminishes. In Figure 3.17 $\overline{D}_2 = D_2/D_1 = 3050/4500 = 0.68$; in Figure 3.15 $\overline{D}_2 \approx 1.0$; in Figure 3.16 $\overline{D}_2 = 1.06$.

3.5. PELTON TURBINES

The design of Pelton turbines depends to a great extent on the total number of nozzles, i.e., on the number of acting jets. An increase in the number of jets leads to a corresponding increase in turbine power, with the diameter of the wheel, or runner, remaining the same. The most widely encountered designs of Pelton turbines are shown schematically in Figure 3.18. The position of the turbine shaft divides Pelton turbines into two groups: horizontal and vertical. A different number of jets may be supplied to the runner. In horizontal turbines, the runner is acted upon by one jet (a) and two jets (b) requiring special branching of the water supply conduit. The encompassing (spiral) water supply conduit of the vertical turbines makes it possible to provide easily a different number of branches and jets, for instance, two (c), four (d), six, and sometimes an odd number of jets. The turbine may have one or two runners. Horizontal hydroelectric sets (Pelton turbines) with one (A) and two (B) runners often find application. Vertical hydroelectric units as a rule use a turbine with one runner (C), but the installation of two runners (D) is also possible in principle.

The creation of Pelton turbines involves a number of difficulties. One is the design of the runner and, in particular, fastening the blades or buckets. It is simple to manufacture each bucket individually, and then secure them on the disk. The buckets of Pelton turbines perform under

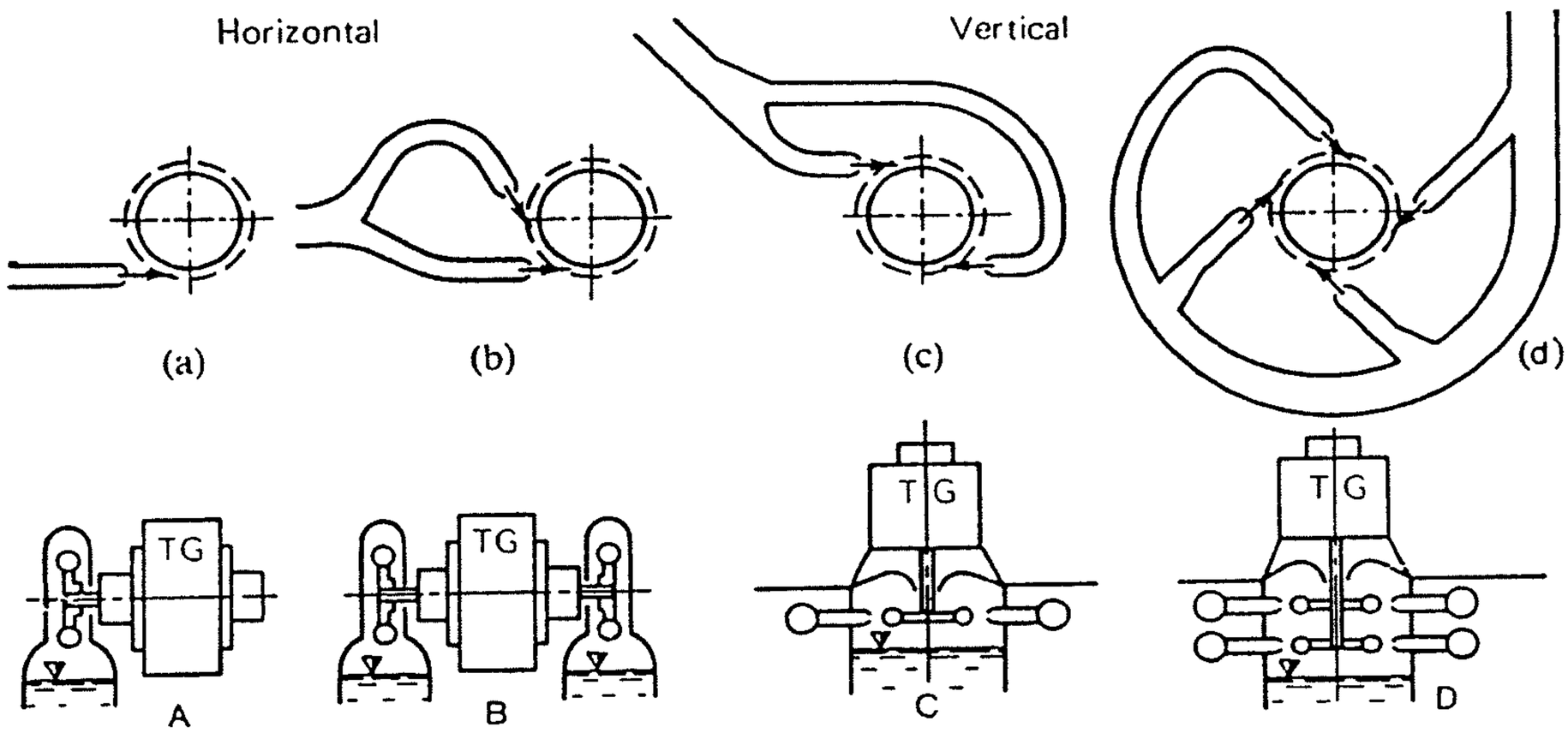


FIGURE 3.18. Designs of Pelton turbines. TG = turbine generator.

very heavy conditions. In contrast to reaction turbines, wherein the load imparted to the blades by the water flow remains constant, the buckets of Pelton turbines are acted upon by a maximum force coming from water pressure only when the bucket passes through the jet. The load is then removed. It follows that performance under conditions of an abruptly alternating load causes fatigue of the metal and loosens or weakens fastenings. A great number of detachable joint designs exist in which buckets are fixed with the aid of bolts, studs, clamping rings, and other fixtures.

In the last few decades use has been made of nondetachable, one-piece cast and welded-cast runners, which has been made possible by the advances gained in the casting and welding technologies for alloyed steels. A one-piece cast runner of a Pelton turbine, 2.69 m in diameter, is depicted in Figure 2.8. Sometimes an integral group of buckets is cast, then the disk is assembled of three to six parts.

Water is supplied to Pelton turbines through long pressure conduits, the material importance of which are the supplementary loads caused by the water hammer originating when the nozzles are closed rapidly and the flow rate, or discharge, diminishes. The power of Pelton turbines may be reduced temporarily without closing the nozzle, i.e., diminishing the rate of water flow. To this end the jet must be deflected from the buckets by means of a deflector (Figure 3.19(a)) or a jet divertor (Figure 3.19(b)) that is mounted downstream of the nozzle. The deflector may change the direction of the jet depending on the magnitude of its travel. The device functions in the following manner: When it is necessary to diminish turbine power rapidly, a command pulse is applied and the deflector shifts rapidly (in 2 to 3 s), ensuring the required drop of power, and the rate of flow is preserved. At the same time, a command impulse is applied to close the needle, but the latter moves slowly and the flow rate changes slowly, respectively, and this precludes the origination of a large water hammer (the whole shift of the needle for 20 to 40 s). As the needle closes the nozzle, the deflector clears the jet and the system is set in the position of normal operation.

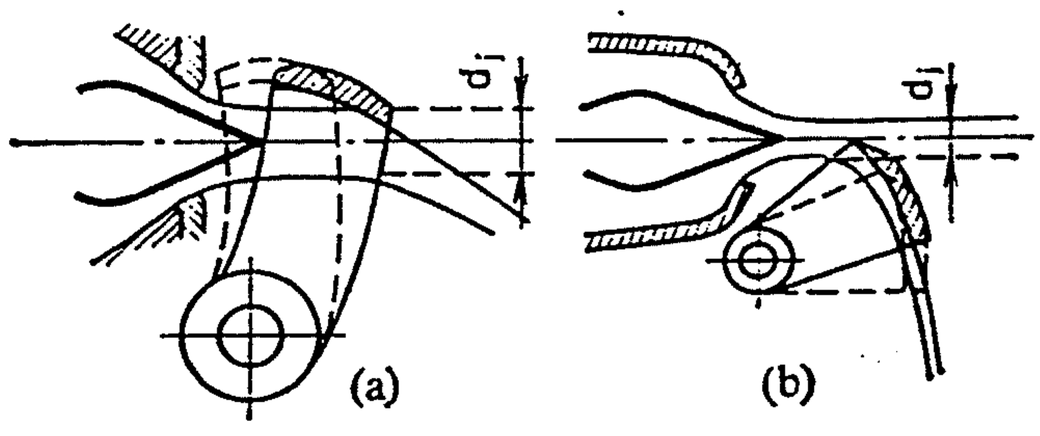


FIGURE 3.19. Operation of the deflectors.

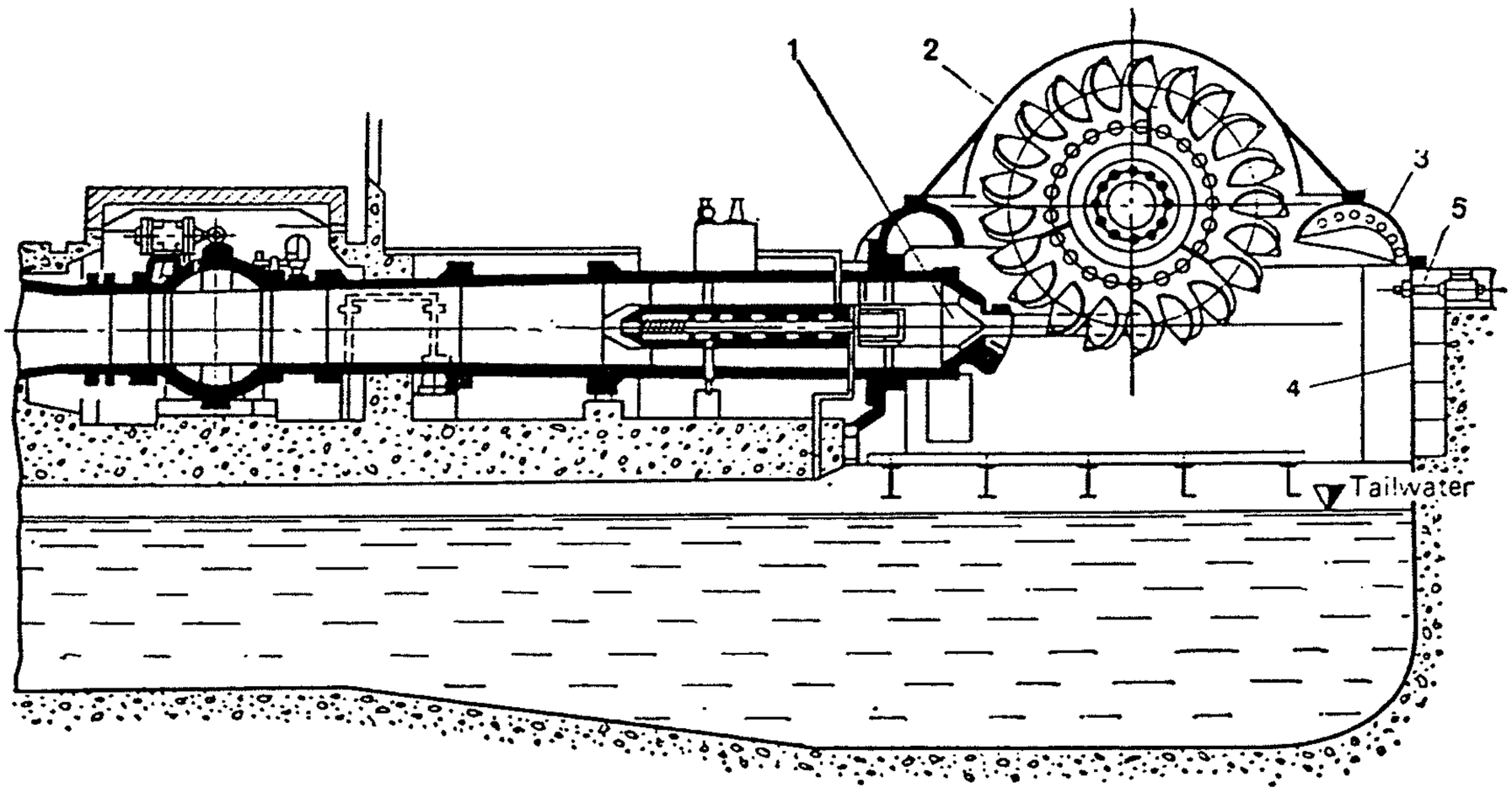
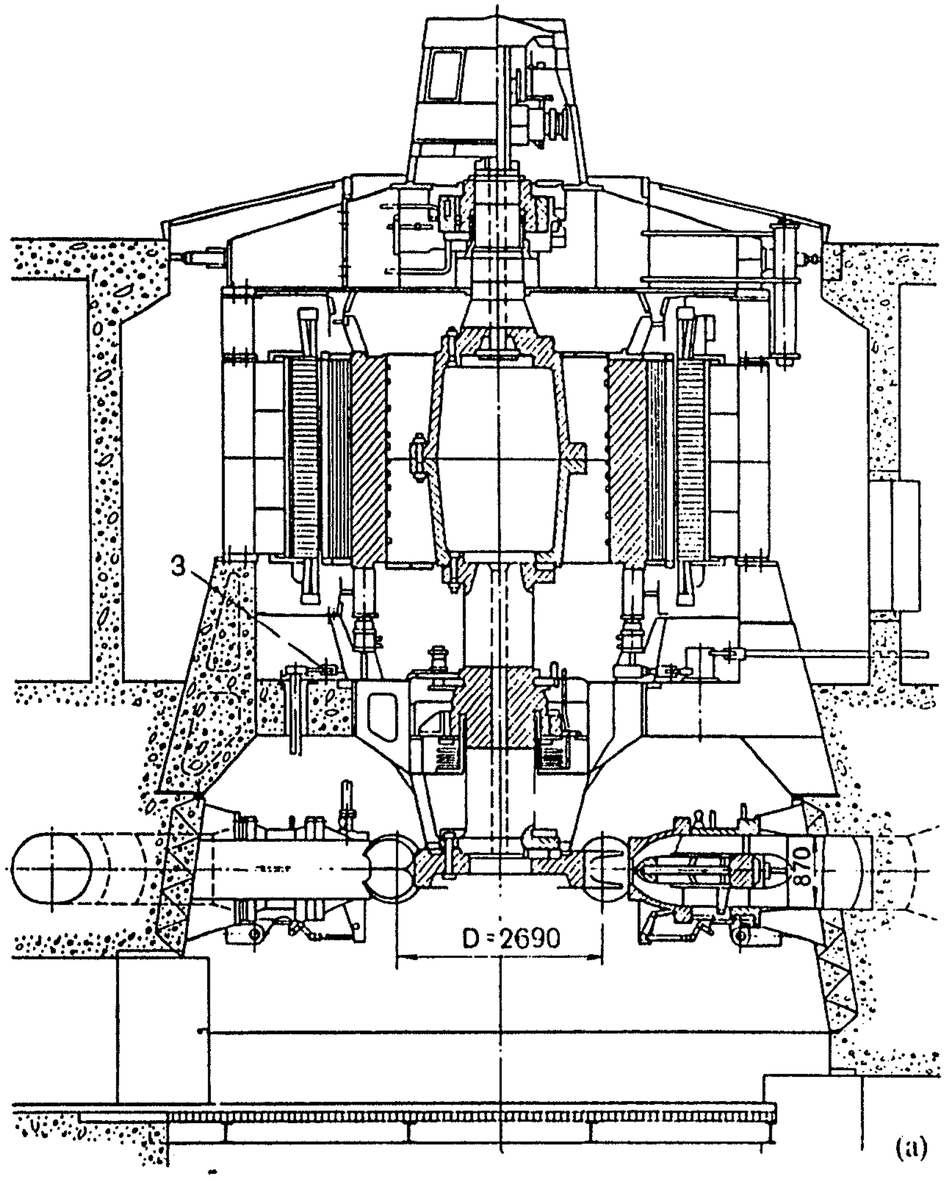


FIGURE 3.20. Pelton turbine at the Cimego Hydro.

Figure 3.20 illustrates the horizontal Pelton turbine installed at the Cimego Hydro (Italy), rated at 110 MW (head is 721 m, $D_1 = 3.5$ m, $n = 300$ rpm, $d_j = 0.31$ m; the turbine has two runners installed as shown in Figure 3.18(B). In this turbine use is made of the so-called straight-flow needle (1) with a built-in (tube-type) operating gear (Figure 4.8 (b)). Such design permits a straight water supply to the nozzle without turning, which contributes to a higher density and stability of the jet and a higher turbine efficiency. The bulb-type regulating needle gear has found wide application.

The turbines operated at the Cimego Hydro have a casing (2) covering the runner and special attention is paid to the deflector (3) that must prevent both water entrainment and the throwing of water into the upper part because this creates additional losses. It is necessary to place the strong steel baffle (4) that takes up the jet when the deflector acts downstream of each nozzle. To speed up turbine shutdown when necessary, a small braking nozzle (5) is provided, and water may be supplied from the water supply line.

Figure 3.21 is a schematic view of the vertical hydroelectric unit mounted at the Sestrimo Hydro (Bulgaria), incorporating a Pelton turbine manufactured at the CKD-Blansko (Czechoslovakia) works. It is a six-jet Pelton turbine rated at 135.8 MW, operating with heads ranging from 501 to 539 m, having a one-piece cast runner, $D_1 = 2.69$ m, $n = 333.3$ rpm, fitted with a straight-flow (bulb-type) needle-operating gear. The illustration shows deflectors or jet deviators (1) and baffles (2) on which the jet impinges. The deflectors are controlled by a servomotor with the aid of shafts, levers, and pullrods (3). Particular



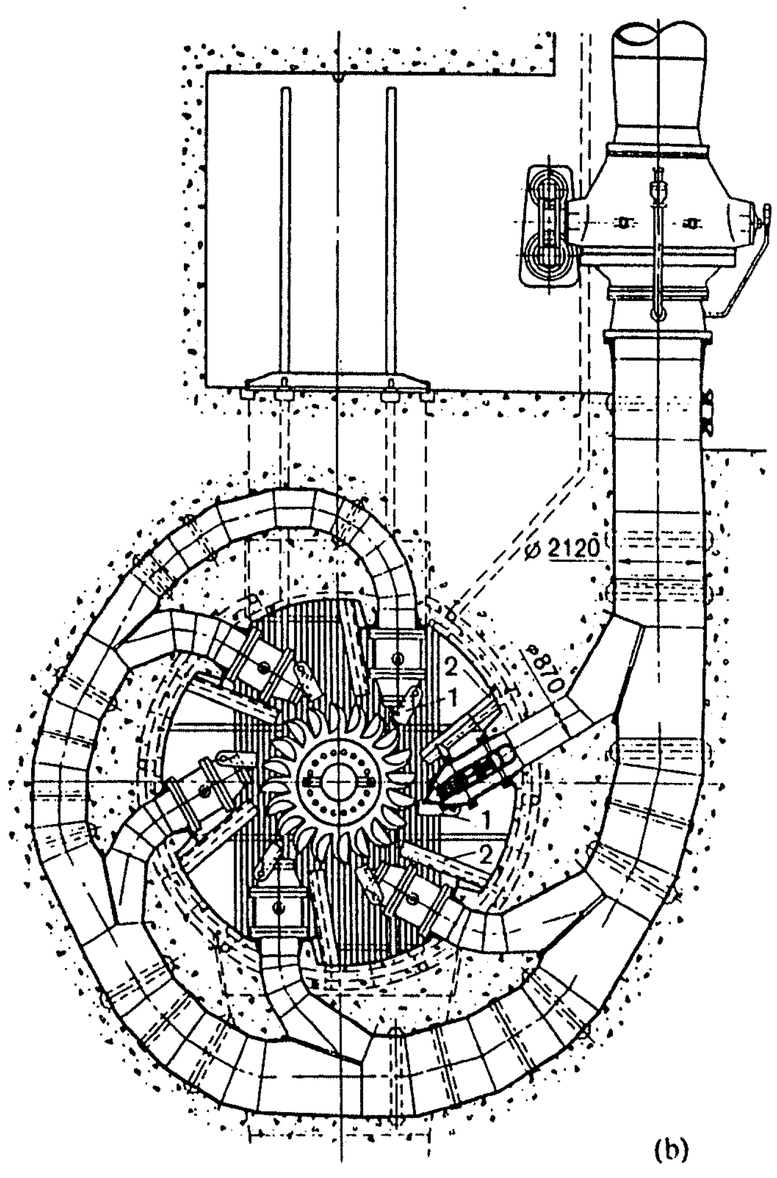


FIGURE 3.21. Vertical Pelton turbine unit of the Sestrimo Hydro.

attention must be paid to the large overall dimensions in planning the water distributing conduit; the maximum water velocity in it is about 8 m/s upstream of the bulb-type needle-operating gears.

3.6. SMALL HYDROELECTRIC POWER PLANT TURBINES

The use of the term small HEPPs indicates stations of a power rating from tens of kilowatts to 5000 to 10,000 kW (units of lesser power are referred to as micro-HEPPs). Presently, the construction of such plants in many countries has received considerable attention. Small HEPPs operate hydroelectric units of the types described above, with runner diameters from 35 cm up to 160 to 225 cm. The cost of such power plants is reduced by using turbines of simpler design.

Figure 3.22(a) shows a hydroelectric unit incorporating a radial-axial (Francis) turbine installed in an open pit. The unit is designed for a flow rate of up to 10 m^3/s. The horizontal hydroelectric unit shown in Figure 3.22(b) incorporates a bulb-type turbine having an S-shaped draft tube designed for a flow rate of up to 15 m^3/s. When operating with low heads of 5 to 12 m, the shaft of the turbine is connected to the

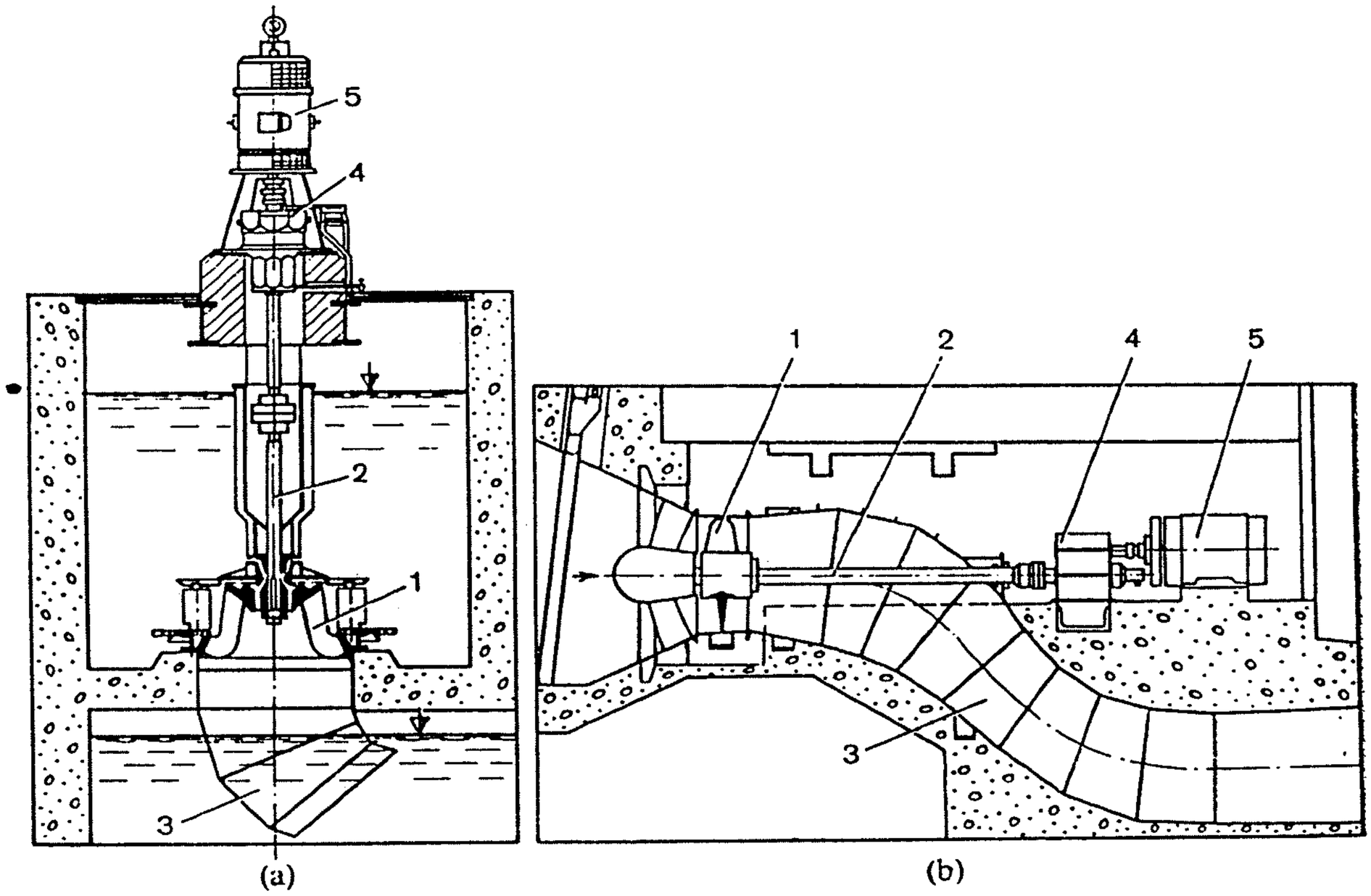


FIGURE 3.22. Reaction turbines of a small HEPP. 1 — Runner; 2 — turbine shaft; 3 — draft tube; 4 — gearing; 5 — generator.

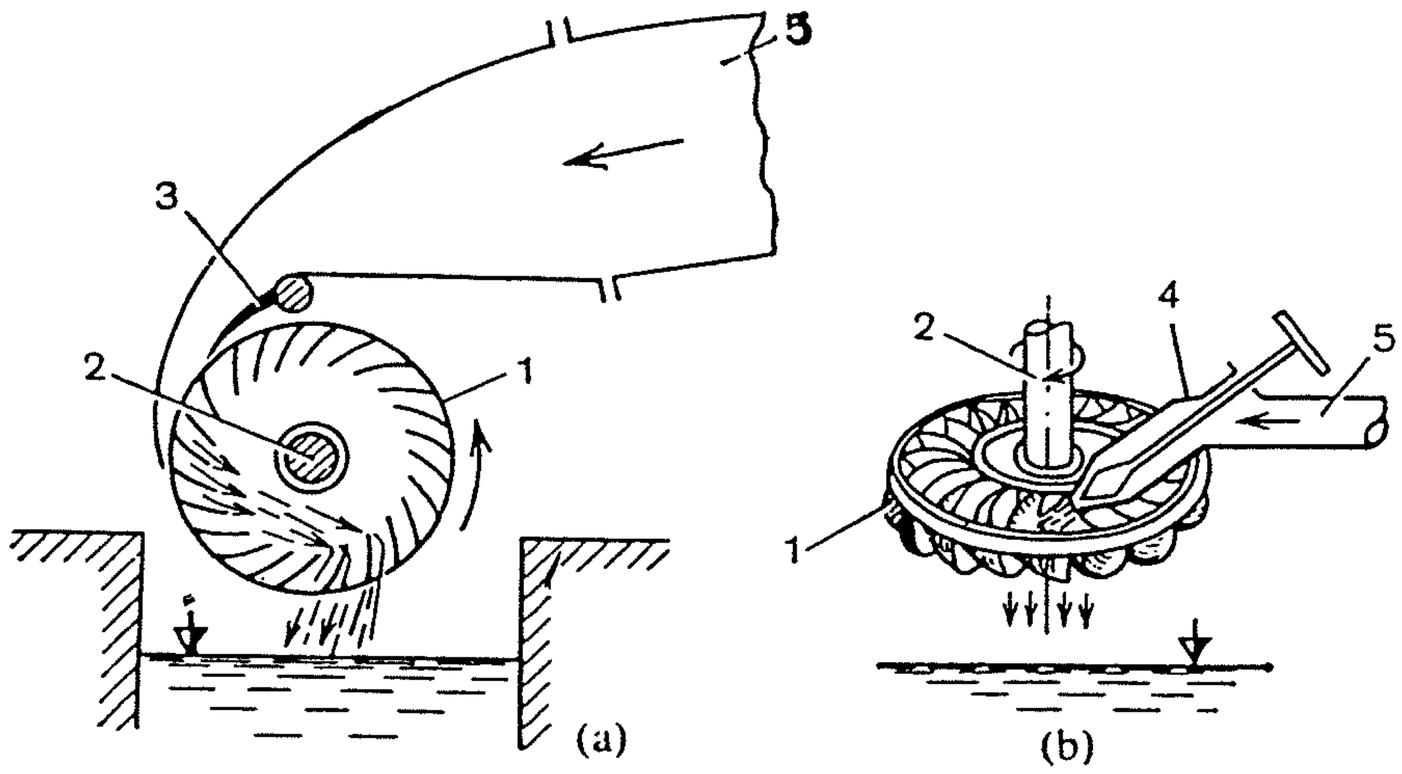


FIGURE 3.23. Impulse turbines of a small HEPP. 1 — Runner; 2 — shaft; 3 — swiveled gate; 4 — nozzle with adjustment needle; 5 — pipeline.

generator shaft via a speed-up gear. Higher heads permit the use of horizontal radial-axial turbines with a frontal casing and an elbow-type draft tube (see Figure 6.1(b)).

With heads up to 10 m, the so-called double-flow or cross-flow Banki turbines also find application. These turbines (Figure 3.23(a)) have a cylindrical runner with a horizontal axis installed atop the afterbay elevation. Water is supplied to the turbine in a rectangular section of a swiveled gate. These turbines are classed as active, they are distinguished by simple design and manufacture. However, their efficiency is somewhat lower than that of reaction turbines, partly due to the loss of head which can be traced to high installation of the units.

Another type of active turbine that may be used at small HEPPs with high heads are the so-called inclined-jet Turgo turbines. These turbines (Figure 3.23(b)) differ from Pelton turbines in that the runner has a greater number of blades on which the jet thrown from the nozzle impinges at an angle to the axis of rotation of the runner.

3.7. SHAFTS AND BEARINGS

The shaft of a vertical unit turbine is acted upon by the torque transmitted from the runner to the generator rotor and by axial thrust determined by the weight of the rotating parts (runner) and hydrodynamic axial forces imparted to the runner by the flowing water. It follows that the shaft works mainly in torsion and tension. The shaft of horizontal units takes up an additional load, the bending moment.

If shafts have a sectional built-up design, the turbine shaft and the shaft of the generator are connected rigidly by means of a flange

(Figures 1.2 and 1.4). In some cases hydroelectric units have a solid shaft (Figures 3.12 and 3.15).

Turbine shafts always have a hollow design. The shafts are either one-piece forged together with the flanges (Figure 3.24(a)) or one-piece cast design (Figure 3.24(b)). The cylindrical part of the shaft is forged from a casting, and to the ends of the cylindrical part cast or forged flanges are welded. Use is also made of one-piece shafts (Figure 3.24(c)); the main part of the shaft is welded into two half-cylinders (troughs), fabricated from thick steelplate by bending, and the welded shaft flanges are then welded. Shafts of the first two designs have found the widest application, but one-piece forged shafts are used only when shafts of comparatively small diameter (< 1400 mm) are required.

The outside diameter D_s (millimeters) of shafts used in vertical hydroelectric units may be determined approximately from the following formula

$$D_s = 105\,(N/n)^{0.35} \tag{3.5}$$

where N is the rated turbine power in kilowatts, and n is the rotational frequency in revolutions per minute.

Turbine bearings support the rotating parts of the hydroelectric unit. Vertical turbines have only a guide bearing that takes up radial loads that may be caused by the water flow asymmetry within the limits of the runner, as well as by the insufficient balancing of rotating parts.

Two kinds of bearings are used in turbines: with oil and water lubrication. Water-lubricated bearings consist of metal elements on which a thick layer of rubber is vulcanized. Bearings of this kind are shown in Figures 3.1, 3.7, and 3.15. The main component parts of water-lubricated bearings (Figure 3.25) are the housing (1), which is

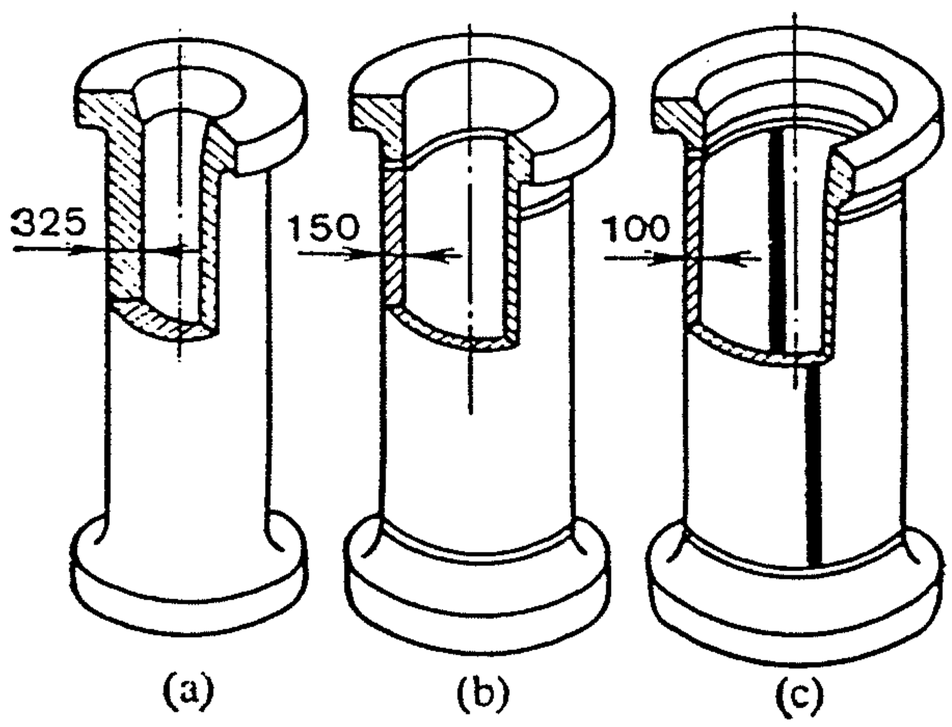


FIGURE 3.24. Shaft designs.

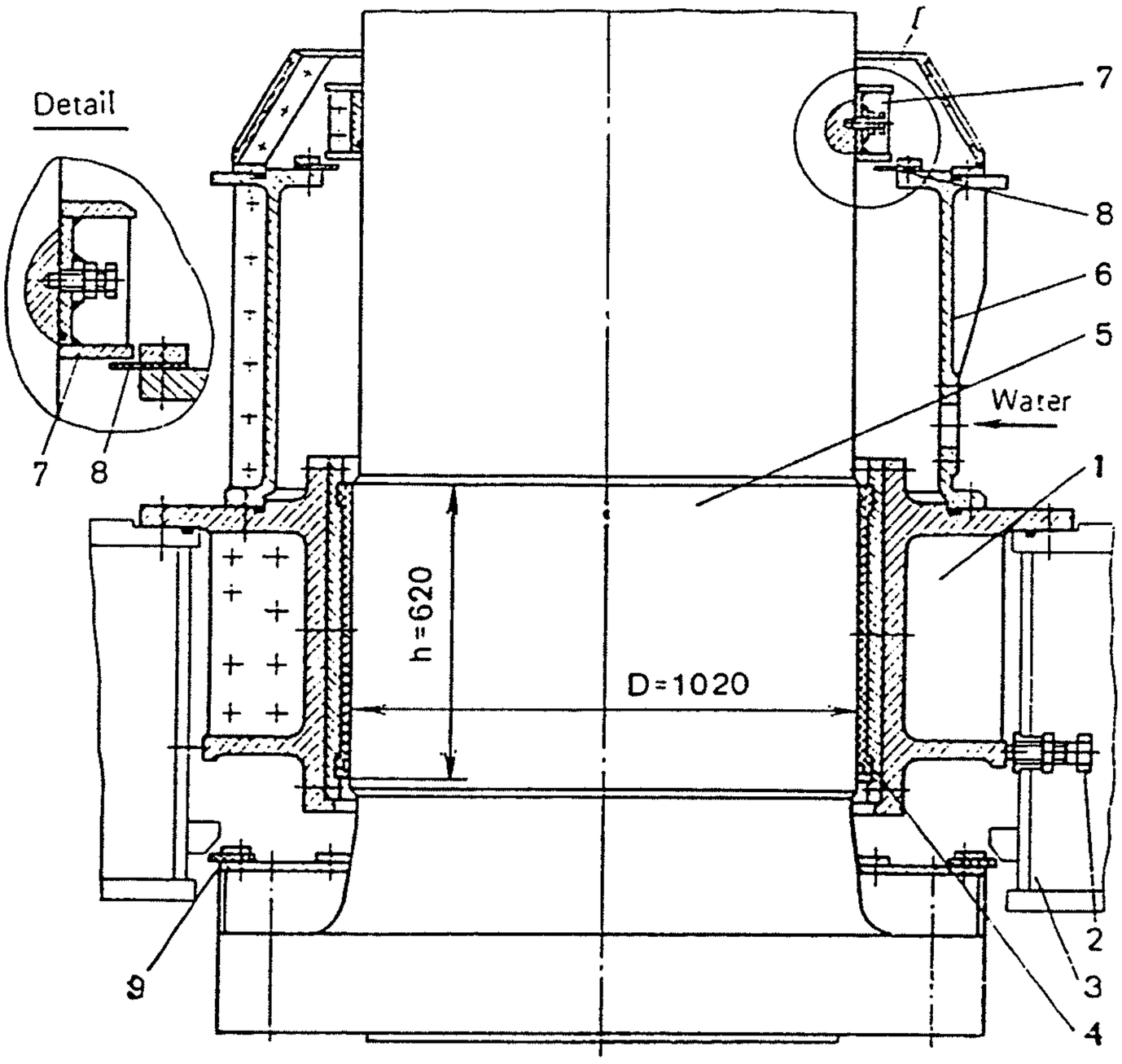


FIGURE 3.25. Water-lubricated bearing with rubber shells.

aligned by means of staybolts (2) and secured in the turbine head cover (3) and bearing shells (4). The latter are constructed of circumferential bent steel segments covered with a layer of special rubber about 20 mm thick achieved via vulcanization. On the surface of the rubber that bears against the shaft there are longitudinal grooves which ensure better water flow into the clearance between the rubbing parts. The part of the shaft that accommodates the bearing is protected against corrosion by a stainless steel liner (5). Water is supplied to the bearing from a water conduit into the upper bath (6) secured on the bearing housing. Figure 3.25 shows an end face rubber sealing (I) consisting of a ring (7) set on the shaft (the lower part of the ring is made of stainless steel) and a flexible rubber ring (8) fastened on the cover of the water bath. Water pressure holds the rubber ring to the steel ring and seals the clearance. A provision is also made for repair seals (9) which are brought into service during turbine repair. This kind of seal is of special importance when turbines are installed far below the afterbay elevation.

The advantages of water-lubricated bearings lie in their simple design, reliability, and long service life; they must not be protected against exposure to water on the side of the rubber during operation. The long service life, however, is ensured only with a continuous supply of

lubricating water at a pressure not lower than 0.15 to 0.20 MPa, provided that the lubricating water does not contain abrasive particles (the water supplied to the bearing must not contain total solids exceeding 0.1 g/L). Water not only lubricates the bearing (the coefficient of friction between the shaft and shells amounts to 0.05 to 0.005), but also ensures cooling. Cooling is of paramount importance because the thermal conductivity of rubber is low. Thus, when the water supply to the bearing is interrupted for any reason, the temperature of the shells rises rapidly and they may fail.

An oil-lubricated bearing (self-lubricated) is depicted in Figure 3.17 (7 to 10). The main parts of the bearing are (see Figure 3.26) the housing (1) and reservoir (2) fastened on the turbine cover and babbit-lined[1] blocks (3) pressed to the guide band (5) of the shaft by staybolts (4). The bearing is filled with turbine oil, ensuring reliable lubrication.

Oil temperature is maintained within permissible limits by circulating it through a water-cooled space located on the turbine cover. Oil circulates via centrifugal force in the direction shown by the arrows in Figure 3.26 through pipes (6) and (7) connected to the water-cooled space. Oil is sometimes cooled by means of tubular coils (arranged in the bearing reservoir) through which water flows. When oil-lubricated bearings are employed, of utmost importance is the seal ((12) in Figure 3.17) that must preclude penetration of water into the bearing.

Oil-lubricated bearings are used when warranted by operating conditions and turbine design, and also when it is difficult to ensure the supply of clean water for lubrication.

If one were to look at vertical turbine design (Figures 2.2 and 2.4), it seems that turbine guide bearings work without any sufficient *lateral (radial) force*. The reality is quite different. In turbines exist two types of lateral forces transmitted to the guide bearing: constantly directed and rotating. The first is caused by lack of full axial symmetry of the flow in the runner (influence of spiral case). The rotating forces have two sources:

1. The deficiency in balance of the unit rotating parts (the most important are the turbine runner and the electric generator rotor). The value of this force P_{dis} is proportional to *dis-balance radius e (millimeters), to rotating mass (kilograms), and to* n^2 *(n-rotation speed). Its frequency* $f_{dis} = n/60$ (Hz).
2. The existence in some operational regimes of so-called rotation flow break, in which flow separation occurs on the part of the lattice foils, and this zone moves in the direction of rotation or its opposite. The frequency of such zone motion (rotation) is $< f_{dis}$.

---

[1] Babbit—an alloy containing tin, lead, antimony, copper; the steel-on-babbit friction coefficient is 0.01 to 0.005, with perfect lubrication.

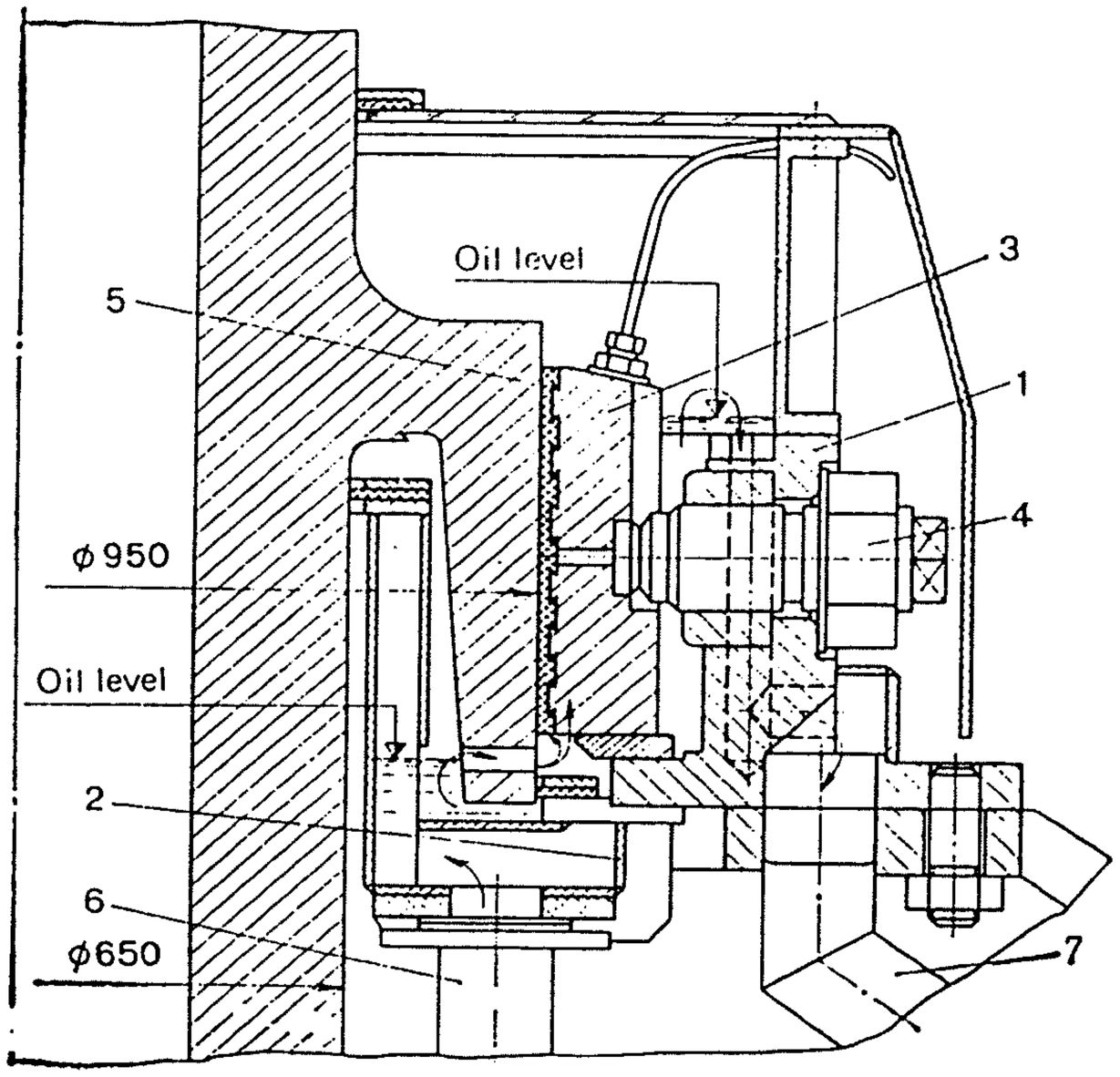


FIGURE 3.26. Oil-lubricated bearing.

In order to design a reliable turbine guide bearing it is necessary to accept the maximum total lateral (radial) force P_r that can be expected with high probabilty. This force (kilonewtons) can be determined by the practical formula

$$P_r = (0.6 - 0.8)\frac{M}{D_1}$$

Here, M is rotation shift moment ($M = (60/2\pi)(N/n)$ and N (kilowatts) rated power, n in revolutions per minute), and D(meters) is turbine diameter.

3.8. DEVELOPMENT OF TURBINE DESIGNS

Hydraulic wheels were probably the first mechanical motors invented and used by humans. These motors were various water wheels—overshot type, breast type, undershot type, etc.—that had been used up to the mid-19th century, and even find application today. These machines–structures reached amazingly large dimensions and ensured high (for the time) power. The main shortcomings of these machines consisted in their cumbersome design and low speed, 4 to 10 rpm.

Hydraulic machines brought into operation by hydrodynamic reaction were created comparatively recently. During the 1750s, Euler,

investigating the Segner's wheel, developed the theoretical fundamentals of operation of reaction hydraulic machines, which are still of great importance. The first turbines suitable for practical purposes were created in France by Fourneyron in 1827 to 1834, and in Russia by N. E. Safonov in 1837. These were centrifugal turbines with fixed guide vanes in which water moved from the center to the periphery. After this period, the design of water turbines advanced rather rapidlly. From 1847 to 1849 the English engineer, Francis, while working in the United States, created a reaction turbine of improved design by arranging the wicket gate (guide vanes) in such a way that it covered the runner and the water moved from the periphery to the center (centipetal turbine). Such an arrangement has proved to be very convenient and is widely used.

A wicket gate with adjustable blades was suggested by Fink in 1880. In the same year Pelton invented the bucket turbine, and a patent for discharge regulation with the aid of a needle was granted to Doble in 1900. Turbine improvement also extended into the 20th century. Of greatest importance is the 1913 invention of Victor Kaplan of Czechoslovakia, the axial adjustable blade turbine with double regulation, which permitted improvement of power-generating characteristics. A patent was granted to Kaplan in 1917. The first adjustable blade Kaplan turbine with a diameter of 0.6 m was commissioned on March 26, 1919, at a hydro constructed on the Velma River (with a head of 3 m). The considerable advantages of the adjustable blade Kaplan turbines over the Francis turbines, especially at low heads, have contributed to their rapid development and wide application. Of great importance to the construction of low-head hydroelectric units was the creation in the 1950s of horizontal bulb-type units fitted with axial-flow turbines. Originally much was undertaken in this field in France, where the construction of high-power TPPs was planned. Bulb-type hydroelectric units rated at up to 10 MW were installed at the La Rance Hydro (France). In subsequent years large-scale studies were conducted, resulting in the creation of large bulb-type hydroelectric units mounted at a number of HEPPs.

Early in 1950 Deriaz (England) developed a mixed-flow (diagonal) pump-turbine for pumped-storage electric power plants (PSPP), and Kviatkovski (Russia) developed a mixed-flow (diagonal) turbine. Both types have been used in some stations.

New types of hydraulic machines and hydroelectric units are also currently being created. Efforts are underway to improve the power generating and operation characteristics, increase the reliability, durability, and reduce the mass and cost.

CHAPTER 4

Turbine Power Regulating Mechanisms

4.1. GUIDE VANE OPERATING GEAR

The operating gear must ensure that all turbine guide vanes are set at the same angle (equal values of a_0) as any opening of the wicket gate, from $a_0 = 0$ to $a_0 = a_{max}$ (Figure 2.3). The schematic of the most widely employed guide vane operating gear is shown in Figure 4.1. The levers (1) set on the upper pivot of the guide vanes (protruding from the top of the turbine cover) are connected to the regulating ring (3) ((7, 8, 9) in Figure 3.3) by means of shackles and pull rods (2). These three elements constitute the major portion of the guide vane operating gear. Figure 4.1a shows the guide vane operating gear in the fully closed position. If the regulating ring turns counterclockwise, all levers will turn through the same angle, as will the guide vanes, and the turbine will be opened. Figure 4.1b shows the operating gear in the fully opened position. It follows then that in order to change the turbine power it is necessary to turn the regulating ring.

To preclude damaging the guide vanes or the guide vane operating gear when a solid object carried by the water flow is jammed between the closing vanes, a provision is made for weakened links, shear pins, and explosive bolts.

The servomotors of the wicket gate are designed to turn the regulating ring and change the opening of the guide vanes so as to regulate turbine power. Inasmuch as tremendous forces originate in the operating gear, caused by the action of water flow on the guide vanes and also

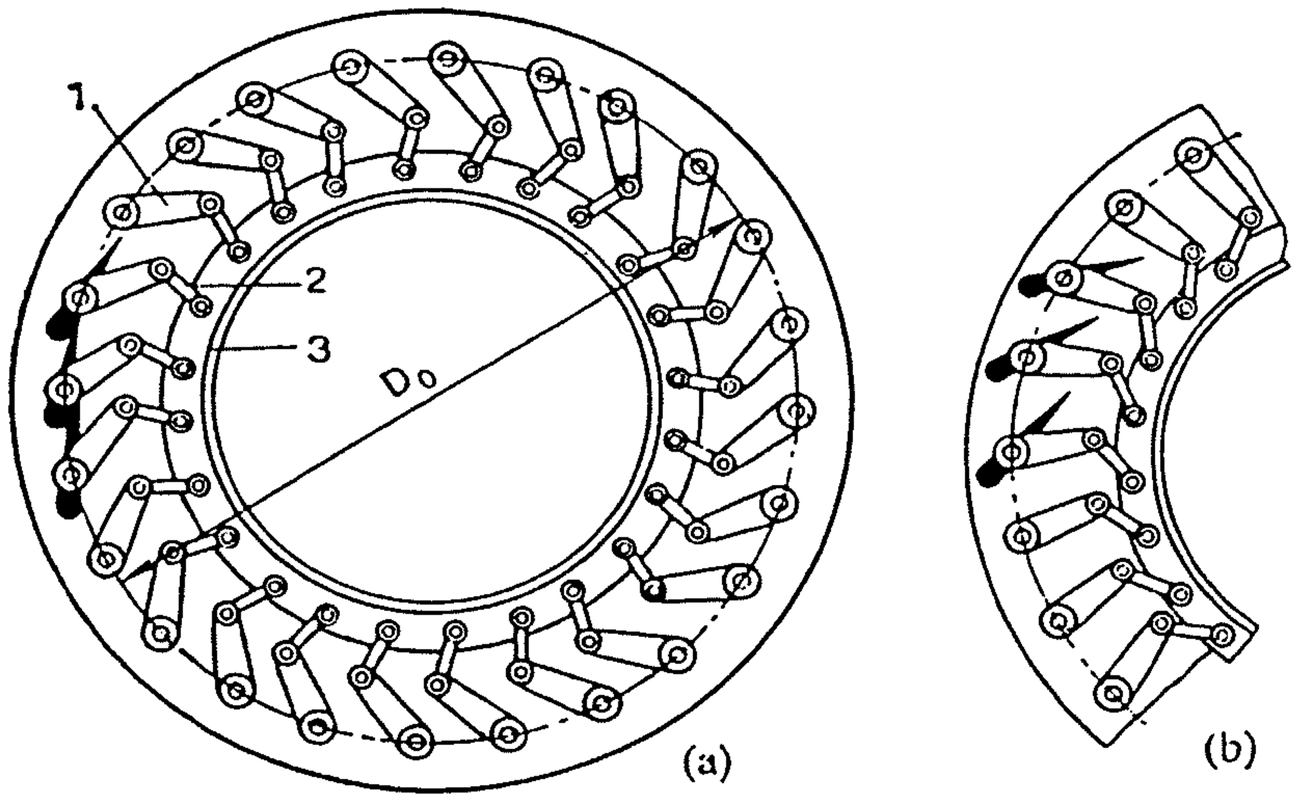


FIGURE 4.1. Guide vane operating mechanism.

by frictional forces, the servomotors must be capable of developing the displacement forces required, and at the same time effect smooth and accurate opening of the turbine wicket gate. Hydraulic servomotors (hydraulic motors) possess these properties. The servomotors are operated using high-pressure oil and find use in all regulating systems of high-power turbines.

The servomotors operating the turbine guide vanes that have found the widest application are presented schematically in Figure 4.2. Each of the two servomotors consists of a cylinder and a piston that is connected by a pullrod to the regulating ring (the pullrods of the servomotors (15) shown in Figure 3.1 are connected to the regulating ring (14)).

Servomotors operate in the following way: The branching pipe A runs to spaces A of the cylinder, and tube B runs to spaces B of the cylinder. If a high-pressure oil is supplied to pipe A and pipe B is

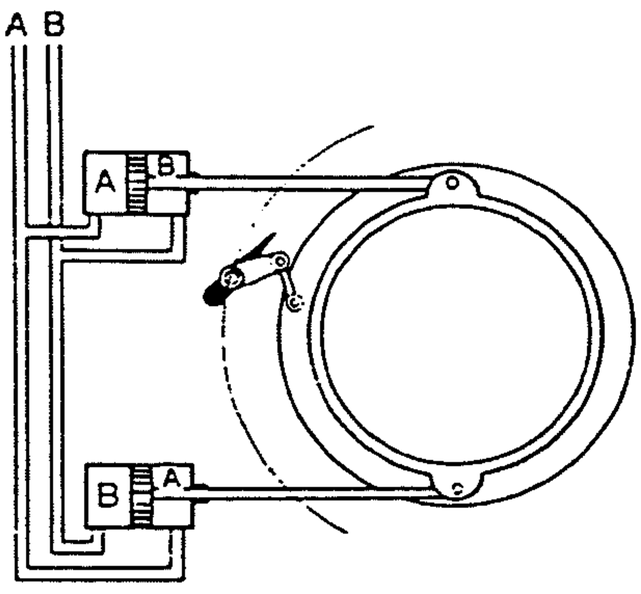


FIGURE 4.2. Guide vane operating gear with two cylindrical servomotors.

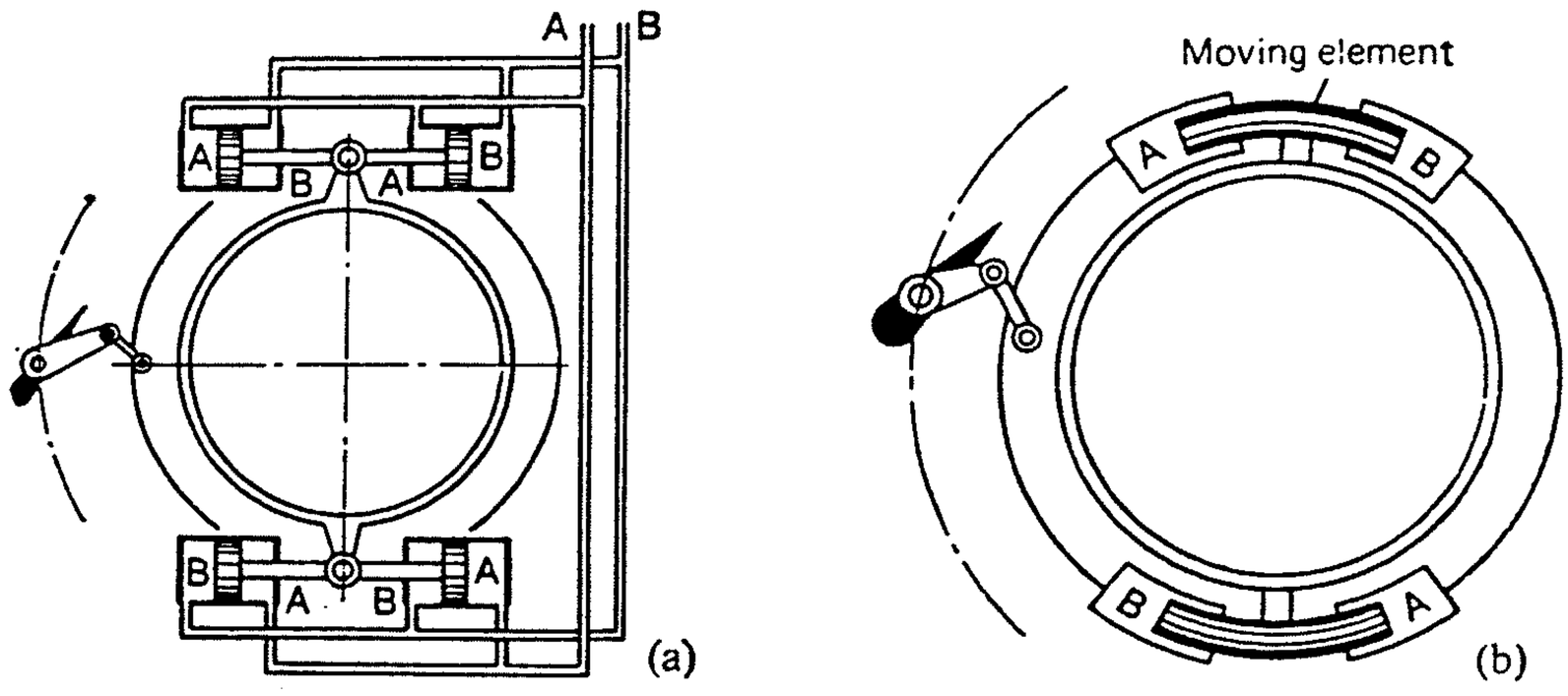


FIGURE 4.3. Guide vane operating gear with (a) two twinned and (b) anchor-ring servomotors.

connected to the return line, the servomotor pistons and rods will move, forcing the regulating ring to turn clockwise. The turbine is thereby closed. Alternatively, if high-pressure oil is supplied to pipe B and pipe A is connected to the oil return line, the regulating ring will turn counterclockwise and will open the turbine (Figure 10.1).

A guide vane operating gear with four servomotors is often encountered. In this case the servomotors are arranged on the turbine cover (Figure 4.3a). Such operating gear permits the use of smaller diameter

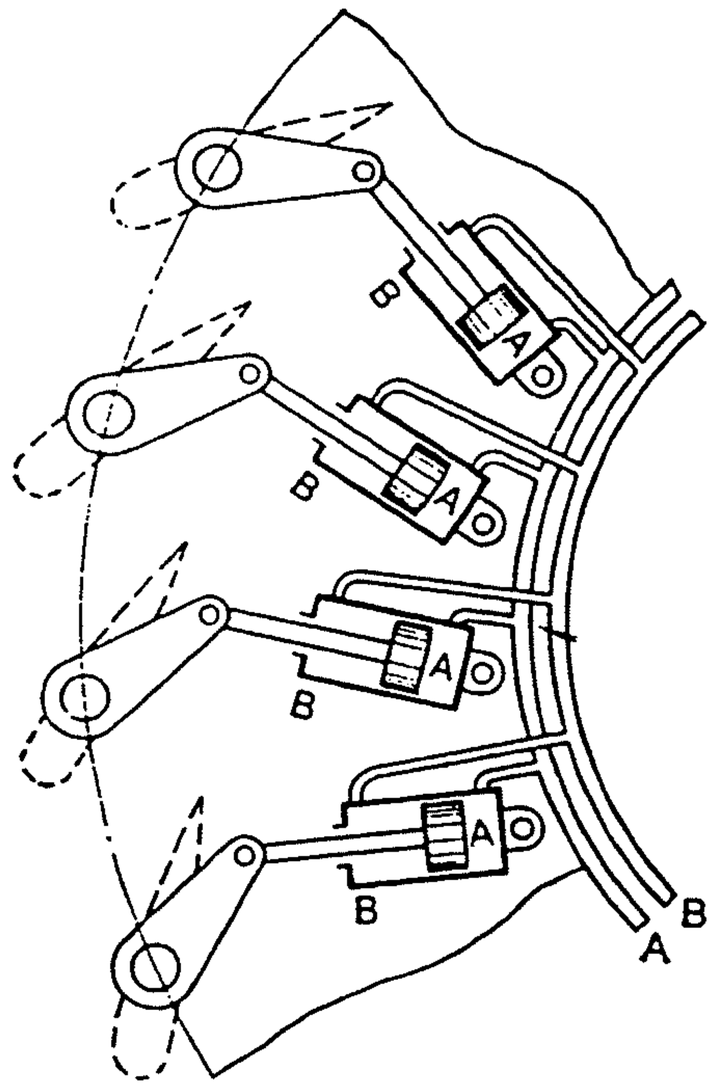


FIGURE 4.4. Guide vane operating gear with individual servomotors.

servomotors and shorter pullrods. Such a servomotor is shown in Figure 3.7, (15).

Anchor-ring servomotors of various types are used. The schematic diagram of these servomotors is given in Figure 4.3b, These servomotors differ from that described above in that the moving element (ME) is in the form of an anchor ring. Its large radius is attributed to its center coinciding with the axis of revolution of the regulating ring. This makes the use of intermediate links (pullrods with articulated joints) unnecessary in connecting the servomotor to the regulating ring.

In large, high-power radial-axial (Francis)-type turbines individual servomotors for each guide vane are sometimes used (Figure 4.4). Such a design is shown in Figures 3.15 and 20.2. This design permits one to do away with the heavy regulating ring and makes the use of weakened links in the guide vane operating gear obsolete. The number of servomotors becomes equal to the number of guide vanes (20 to 24), however, and this complicates control of the guide vanes. To circumvent this, the performance of the servomotors is synchronized by fitting special synchronizing devices.

4.2. RUNNER BLADE OPERATING GEAR OF ADJUSTABLE BLADE TURBINES

The angle and accurate setting of the blades, usually within 30° to 40° (for instance, from $\varphi = -15°$ to $\varphi = +20°$), without stopping the turbine (i.e., with a rotating runner), must be ensured in runner blade operating gear. The operating rings of the blades must be capable of overcoming the tremendous water pressure, centrifugal, and frictional forces in the blade pin bearings, they must be arranged in a very confined space in the runner hub, and feature an exceptionally high reliability because their repair requires complete disassembly of the component units.

Figure 4.5 is the schematic diagram of runner blade operating gear. Blade pivot (2), having two supports in housing (3) and (4) is connected to the blade flange (1). The lever (5) set on pivot (2) is connected by pull rod (6) to piston (7) of the runner servomotor. Displacement of the piston (7) through pullrod (6) results in turning of the pivot (2) and the blade (1). Downward piston travel results in greater blade angle. The piston is displaced and retained in the required position by high-pressure oil supplied through the piston regulating system (not shown in the schematic diagram).

A great number of designs of the runner blade operating ring exist, differing mainly in the way in which the servomotor piston is connected to the levers. Two examples are given below.

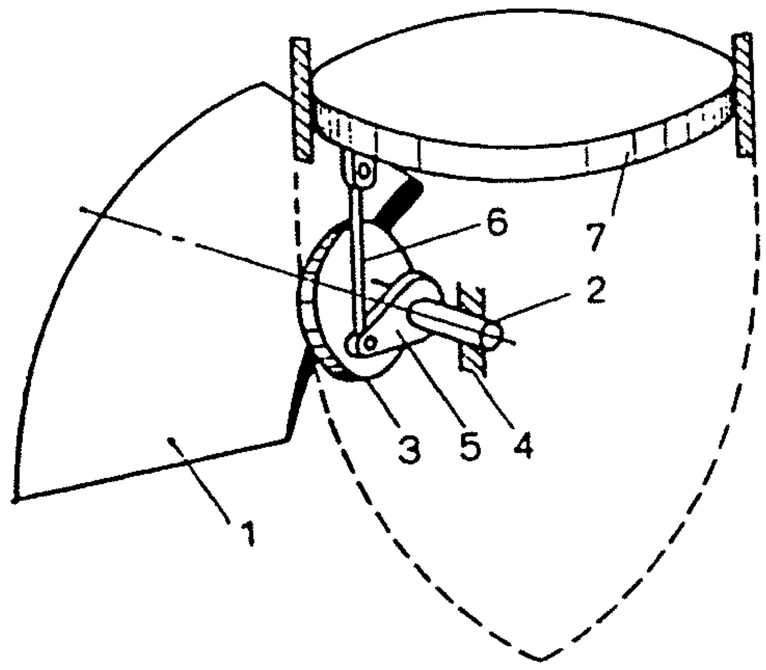


FIGURE 4.5. Adjustable blade runner operating gear.

Figure 4.6 shows a sectional view of the runner casing of a respectable high-head axial-flow turbine ($D_1 = 7.2$ m; head, 25 to 32 m; number of runner blades, $z_1 = 7$, $\bar{d}_c = 0.5$). In the illustration (1) is the runner bearing hub; (2) is the blade; (3) is the pivot with flange; (4) and (5) are the plain bearings; (6) is the lever; (7) is the servomotor piston, 3.15 m in diameter; (8) is the cups rigidly connected to piston (7); (9) is the pull rod hinging the cup and piston with the pin of the blade lever. The servomotor cylinder of this design is formed by the upper part of the runner casing. The piston is displaced by high-pressure oil supplied through the pipe (10) into the rod end of the cylinder, and through pipe (11) into the head end of the cylinder. The middle pipe (12) serves to drain the lower part of the runner hub. The oil supply line consists of two concentric pipes (10) and (11) which are run through the central passage in the shaft and are connected to the high-pressure oil bushing located in the upper part of the hydroelectric unit, usually above the upper spider (see Figure 10.3).

Figure 4.7 presents a cross-section view over the runner casing of a low-head axial-flow turbine ($D_1 = 10.3$ m; head, 6.5 to 14.7 m; $z_1 = 4$, $\bar{d}_c = 0.35$ (the reference numbers of corresponding parts are as in Figure 4.6). Blades (2) are fastened in hub (1) with the aid of pivot flange (3) in plain bearings (4) and 5. Pullrods (9) hinge blande levers (6) to piston 7, 2.6 m in diameter. This ensures equal turning of all blades during piston travel. Oil is supplied to the rod end via pipe 10 and into the head end via pipe 11. The piston is prevented from turning by a round pin on the cylinder wall.

The dimensions of the runner hub can be decreased by placing the servomotor either between the flanges of the turbine and generator shafts or in the hub of the generator rotor.

Runner servomotors are capable of providing large positioning forces. Thus, in the turbine shown in Figure 4.7 oil pressure is 4 MPa, and with

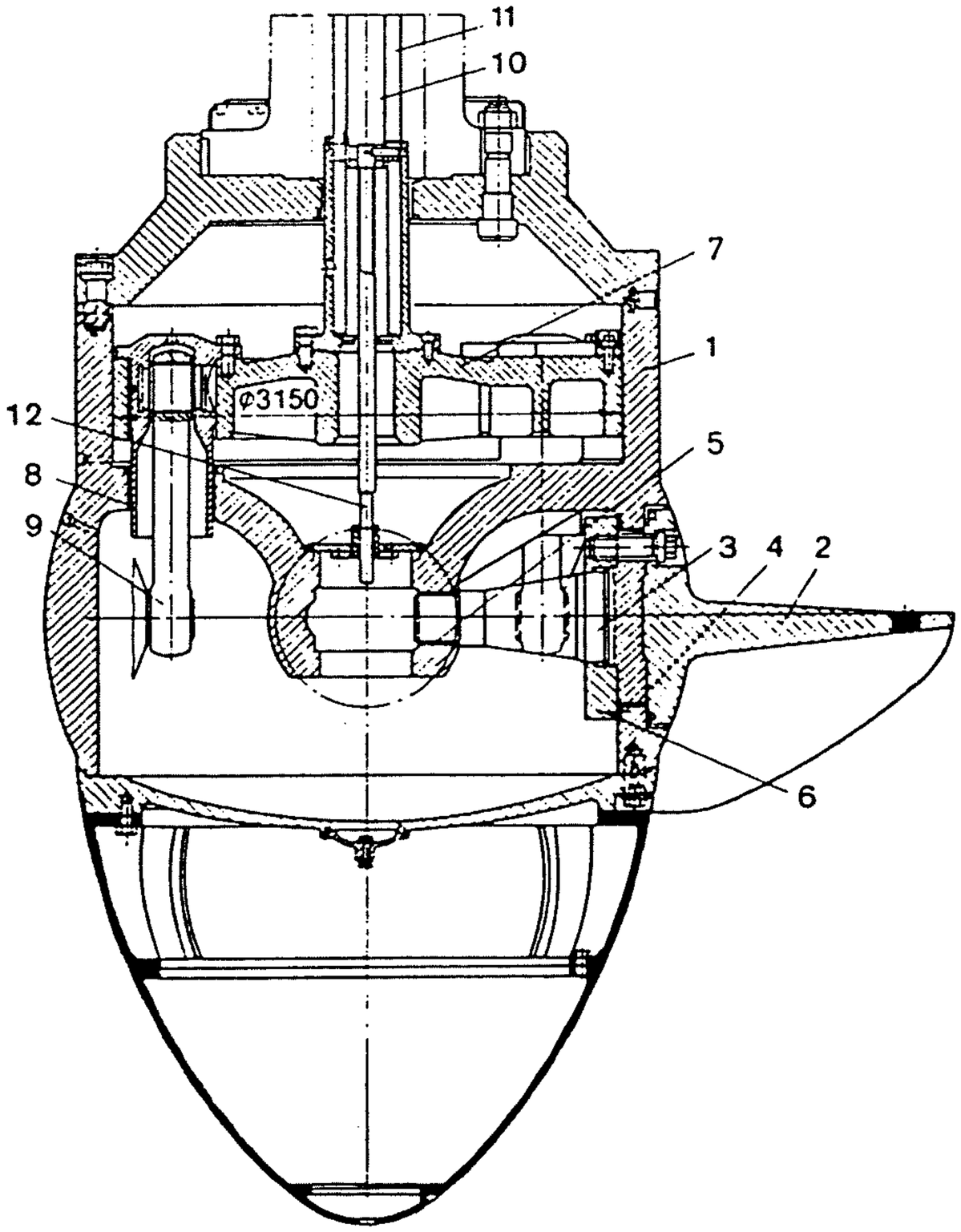


FIGURE 4.6. Blade operating gear of high-head turbine runner. The key is delineated in text.

a servomotor piston 2.6 m in diameter, the maximum force amounts to 21,500 kN. The complete shift of the servomotor piston is about 0.3 m.

The blade operating gear in mixed-flow (diagonal) turbines is similar to that of the turbine shown in Figure 4.5, but because the blade pivots are at an angle to the piston displacement axis of the servomotor (Figure 3.12), the levers must be connected to the pullrods and piston via ball-and-socket joints. The great number of blades (9 to 11) means that the blade operating gear of the mixed-flow turbine has a more complicated design as compared to axial-flow turbines, thus a larger diameter casing is required ($\bar{d}_c = 0.5$ to 0.65).

4.3. OPERATING GEAR OF THE PELTON TURBINE REGULATING NEEDLE

The rate of flow through the Pelton turbine and the power of the turbine itself are regulated by shifting the needles, thereby changing the

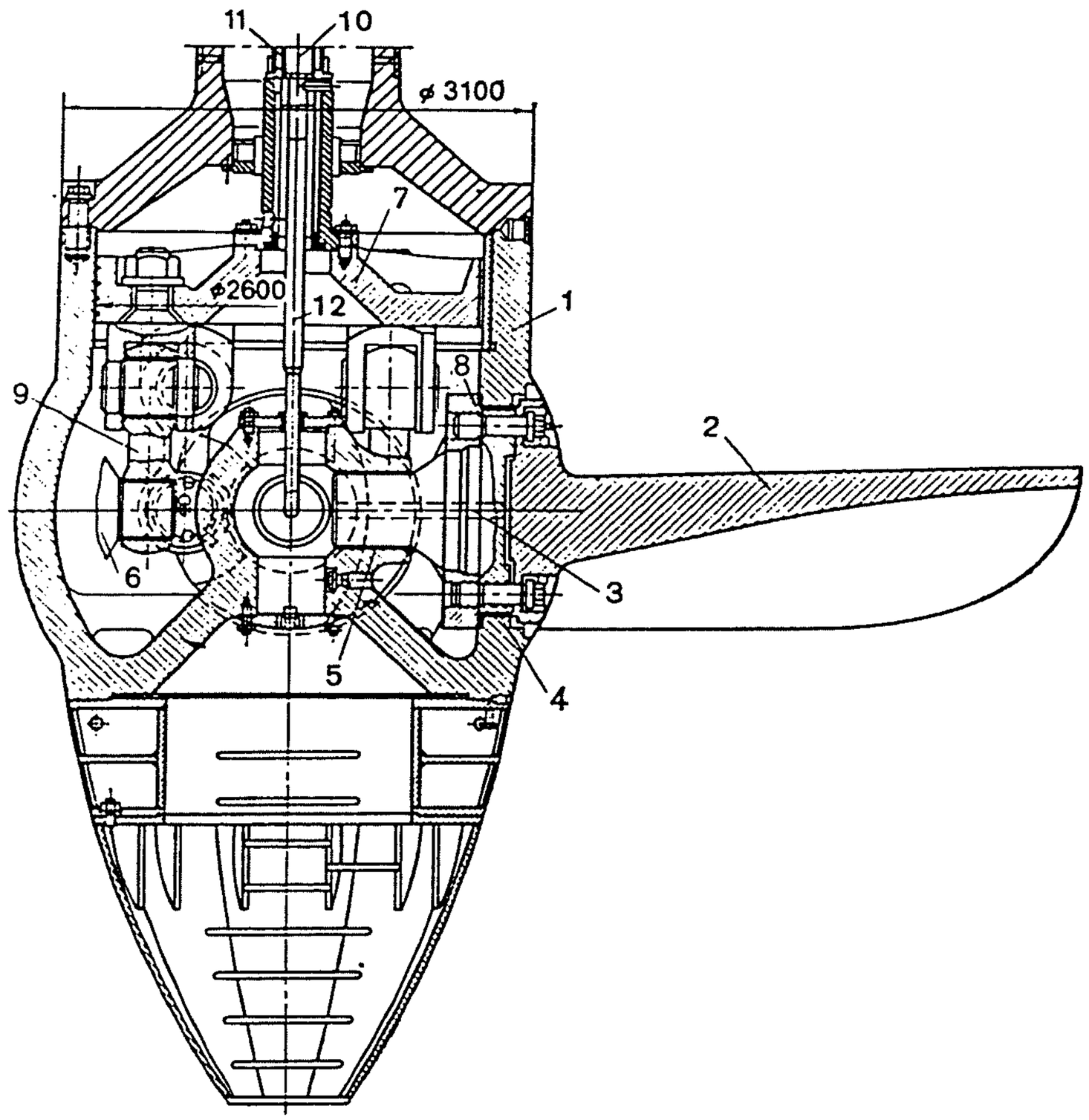


FIGURE 4.7. Blade operating gear of low-head turbine runner. The key is delineated in text.

flow area of the nozzles. The needle-operating gear is shown in Figure 4.8a. The needle (2) is fixed on the end of the long rod (3) connected to the piston of the hydraulic servomotor (4). The needle is aligned and radial displacement is prevented by a guide sleeve and spacer ribs (5). This design requires a rather sharp turn of the water supply conduit directly upstream of nozzle (1), and this diminishes the density of the jet at the nozzle outlet and impairs the power-generating characteristics of the turbine due to the origin of reverse flows at the turn. In the last few decades use has been made of the so-called straight-flow nozzle (1), depicted in Figure 4.8b. The needle (2) is fastened on short rod (3) connected to the piston of servomotor (4). The servomotor is made in the form of a bulb which is secured in the center of a tube by ribs (5). The bulb is exposed to water flow, which makes it unnecessary to turn the water supply conduit (Figure 3.20).

This regulating nozzle (1) performs in the following manner. If oil is supplied under pressure to pipe A, and pipe B is connected to the

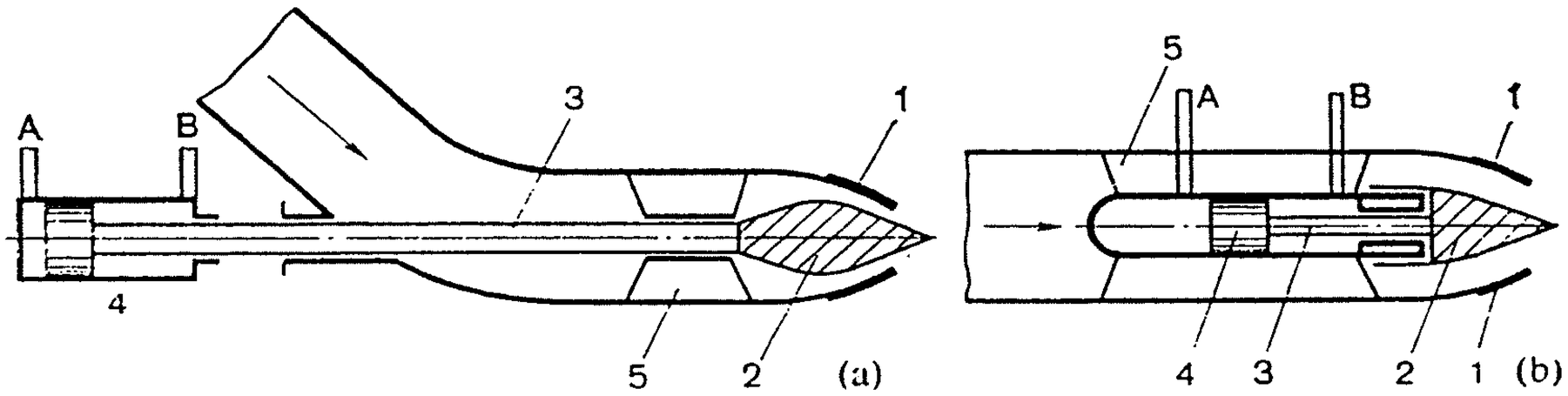


FIGURE 4.8. Pelton turbine regulating needle operating gear. The key is delineated in the text (Section 4.3).

return main, then due to the pressure drop across the piston the needle will shift to the right, closing the nozzle and decreasing the rate of flow. On the contrary, if high-pressure oil is supplied to pipe B and pipe A is connected to the return main the needle will move in the direction that opens the nozzle. These are only the main composing elements of the regulating system. Of no less importance are the devices that ensure retaining the needle in the necessary position. This requires a feedback device (not shown in the illustration) as well as a device that coordinates the shifting of all turbine needles and the position of the needles and the deflectors (not shown in the schematic diagram). A more detailed scheme is found in Figure 10.4.

CHAPTER 5

Theoretical Fundamentals of the Turbine Working Process

5.1. WATER FLOW CREATED BY THE WICKET GATE OF THE REACTION TURBINES

In all reaction turbines the water flow in front of the runner is formed by the wicket gate, which is an annular cascade of guide vanes, as can be seen in Figures 2.2 and 2.4. This cascade is characterized by the form of the profiles and the chord spacing of the cascade. The blade profile is said to be symmetric (Figure 2.3) when the middle line of the profile is straight, and asymmetric when the middle line is curved (Figure 5.1). As can be seen from Figure 5.1 the distance between adjacent profiles over the middle lines t is the cascade pitch, and the chord length L is the length of the profile. The ratio L/t indicates the density of the cascade. Inasmuch as the guide vanes must ensure complete closure of the turbine (Figure 2.3b), the ratio L/t is always greater than unity ($L/t > 1$), and is usually equal to 1.1. It follows that the wicket gate is a sufficiently dense cascade. At the inlet at the diameter D_{02} the direction of liquid (water) velocity $\mathbf{v}_0$ is close to the direction of the blade outlet edges $\alpha_0 = \alpha_{w \cdot g}$ (Figure 5.1).

For a radial-flow wicket gate, commonly used with reaction turbines, the vector $\mathbf{v}_0$ may be presented as the sum of two components

$$\mathbf{v}_0 = \mathbf{v}_{0r} + \mathbf{v}_{0u}$$

where $\mathbf{v}_{0r}$ is the radial component and $\mathbf{v}_{0u}$ is the peripheral component.

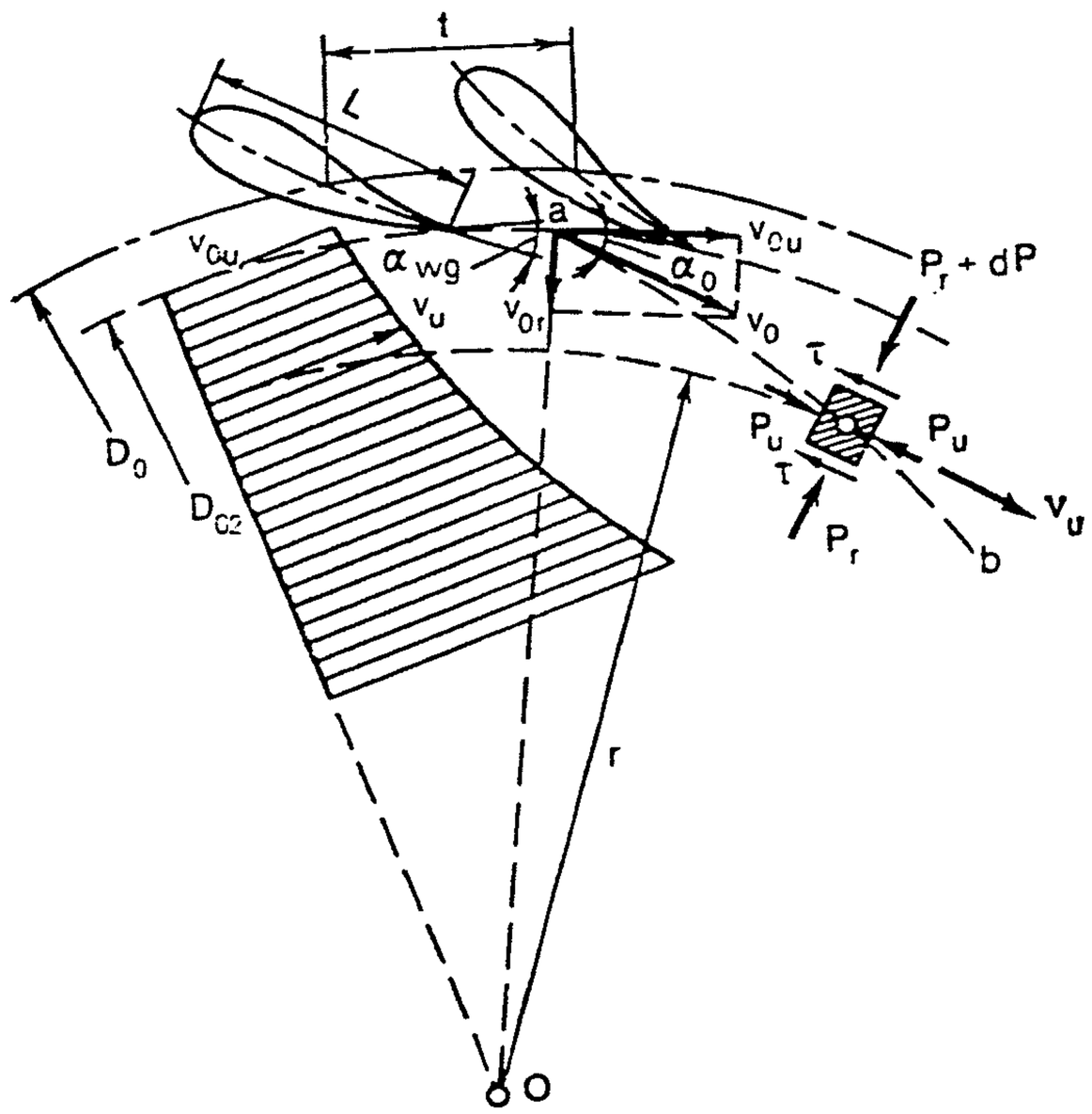


FIGURE 5.1. Flow created by wicket gate.

Knowing the flow rate through the turbine, Q, and the dimensions of the wicket gate, the radial component is specified by the formula

$$v_{0r} = Q/\pi D_{02} b_0 \tag{5.1}$$

where b_0 is the height of a guide vane (Figure 3.1).

Denoting by α_0 the angle formed between $\mathbf{v}_0$ and $\mathbf{v}_{0u}$, we obtain

$$v_0 = v_{0r}/(\sin \alpha_0) \tag{5.1a}$$

and the peripheral component is determined from the relationship

$$v_{0u} = v_0 \cos \alpha_0 \tag{5.1b}$$

The presence of the peripheral component $\mathbf{v}_{0u}$ indicates that the flow is rotated about axis 0 downstream of the wicket gate. Swirling water is specified by the so-called circulation Γ, generally expressed by the formula

$$\Gamma = \int_S \mathbf{v}_0 \cos(\mathbf{v}\,\mathbf{dS})\, dS \tag{5.2}$$

where S is the closed contour drawn inside the flow (Figure 5.2), and $\mathbf{v}\,\mathbf{dS}$ is the angle α between the directions **v** and **dS**. It is clear from Equation 5.2 that the circulation Γ is measured in square meters per second. For an averaged flow downstream of the wicket gate on the outlet diameter D_{02} the circulation is equal to

$$\Gamma_0 = \pi D_{02} v_0 \cos \alpha_0 \tag{5.2a}$$

It follows from Equation 5.2a that the wicket gate creates the flow circulation Γ_0.

Between the ends of the guide vanes and the inlet edges of the runner blades (which can be called the "prerunner" space), the water is in free flow; the stream line is presented by curve a–b in Figure 5.1.

To determine the way in which velocity changes let us consider the elementary mass m at the radius r in the stream line. Let us make use of the angular-momentum equation; for the considered mass the time derivative of the moment about some axis is equal to the sum of the moments of all external forces acting upon this mass about the same axis. This law is expressed by formula

$$\frac{d(mv_u r)_0}{dt} = \sum M_0 \tag{5.3}$$

where m is the mass of liquid in the volume considered, v_u is the peripheral velocity component, r is radius, and $\sum M_0$ is the sum of the moments of external forces acting on the considered mass about axis 0.

Consider the external forces in Figure 5.1. The pressures acting in the radial directions P_r and $P_r + dP$ form no moment about the center 0. The pressures acting onto the end faces P_u are equal for an averaged flow and also do not create a moment about 0. The low tangential forces τ, which are due to liquid friction, may be ignored. In the final

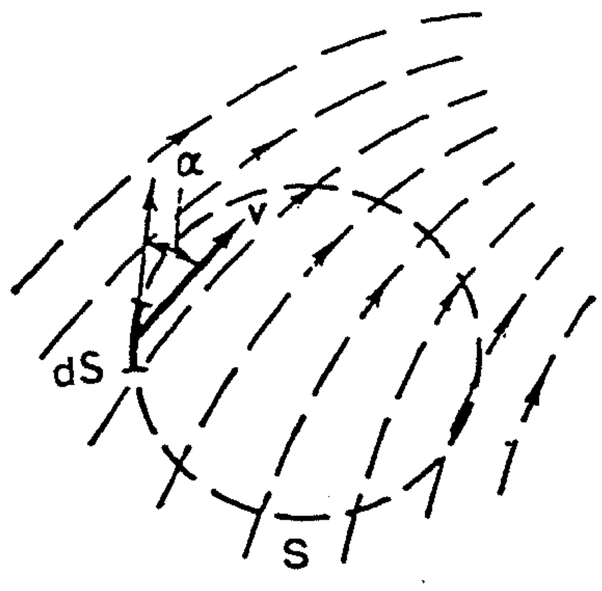


FIGURE 5.2. Determination of flow circulation.

analysis we obtain that for water in free flow we may assume that $\sum M_0 = 0$, and this means that

$$\frac{d(mv_u r)}{dt} = 0 \qquad mv_u r = \text{const}$$

From this an extremely important dependence follows:

$$v_u r = \text{const} \tag{5.4}$$

determining the conditions of free liquid flow and referred to as the law of conservation of velocity momentum.

The relationship (Equation 5.4) shows that as axis 0 is approached the peripheral component of velocity increases and at radius r

$$v_u = v_{0u} \frac{0.5 D_{02}}{r}$$

i.e., curve $v_u(r)$ is a hyperbola (Figure 5.1). When we take into account $\Gamma = 2\pi r v_u$, it follows from Equation 5.4 that the constant circulation condition with liquid in free flow is

$$\Gamma = \Gamma_0 = \text{const} \tag{5.4a}$$

Thus, the circulation is created by the wicket gate in the space between the guide vanes and runner preserves.

5.2. KINEMATICS OF WATER FLOW IN REACTION TURBINE RUNNER

The energy of liquid is converted into mechanical shaft energy in the turbine runner at the expense of the interaction between flow and the runner blades, constituting a rotating cascade of profiles.

When water flow in the runner is investigated this motion is considered to be a compound of two motions: relative and transportation. The relative motion of the water is fixed by an "observer" positioned on the runner. The pattern of relative motion may be documented by photographing it with a camera that rotates along with the runner. Transportation motion defines the motion of the runner proper and of its blades. This motion is always rotational in turbines. The sum of the relative and transportation motions is called absolute motion.

If we denote the vector of the velocity of relative motion by **w** and the vector of velocity of transportation motion by **u**, then the vector of absolute velocity **v** is specified by the vector sum

$$\mathbf{v} = \mathbf{u} + \mathbf{w} \tag{5.5}$$

Thus, the vectors **v**, **u**, and **w** are interrelated via the parallelogram, or triangle, of velocities.[1]

A study of turbine designs shows that the forms of each runner is different, and each changes considerably with various heads. It is necessary, therefore, to determine some general principles on the basis of which the geometric characteristics of various runners may be defined permitting us to plot a parallelogram of velocities.

The determination of flow in the turbine runner, including quantifying velocities and pressure distribution by solving general hydrodynamics equations is rather complicated. Reliable data concerning turbine operation can be established using the so-called layer-flow approach and some averaging methods.

Let us consider the most general case—the runner of a radial-axial flow turbine. All points on the leading edge of runners, denoted by (1) (Figure 5.3), and the points of the trailing edge (2), are projected onto the meridional section of the turbine. Let us divide the flow downstream of the wicket gate into several layers (six in this case) of equal area and height and project the trajectory of each layer in the runner onto the meridional plane. We obtain curves (shown by dotted lines), with the surface of rotation of each representing the stream surfaces, i.e., the surfaces that the moving liquid does not intersect.

Thus, the curves on the meridional plane are sections of the stream surface. It is clear that to establish a full pattern of water flow in the runner, it is necessary to consider motion over all meridional stream surfaces. For the sake of simplicity we may consider the most characteristic curve, the middle stream surface *pk*, and use it to analyze the conditions of the flow.

Imagine that the middle stream surface (curve *pk*) intersects the runner blades. These sections will be three-dimensional. To facilitate construction, the sections are projected onto a plane, preserving the actual values of the angles. (If line *pk* is close to a straight line, this can be accomplished by developing a conical or cylindrical section; if curvilinear, by mapping.) The practical application of the described method will be clear from a further consideration of several specific cases.

---

[1]The following notations are assumed: vectors **v**, **u**, **w**, and their lengths (values) v, u, w, respectively.

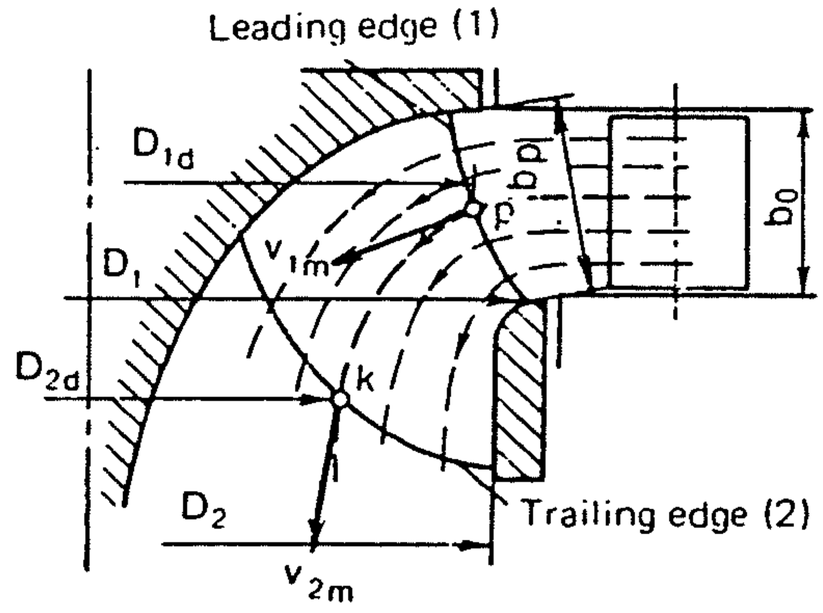


FIGURE 5.3. Meridional flow in a radial-axial flow turbine.

The section of the runner of a radial-axial turbine is illustrated in Figure 5.4a, where D_{1d} and D_{2d} are design diameters of the inlet (1) and outlet (2) of the blade edges. As seen in Figure 5.3, these diameters are smaller than the rated inlet diameter D_1 and outlet diameter D_2. The direction of the runner blades at a given point is determined by the angle δ that forms between the tangent to the middle line of the blade profile, and drawn to the side opposite that of runner rotation.

The operating conditions of the turbine are preset by two parameters: the flow rate Q and rotational speed n of the runner. When the dimensions of the runner are given it is possible to determine the components of the velocity parallelograms. The transportation (peripheral) velocity is expressed by the formula

$$u = \pi Dn/60 \tag{5.6}$$

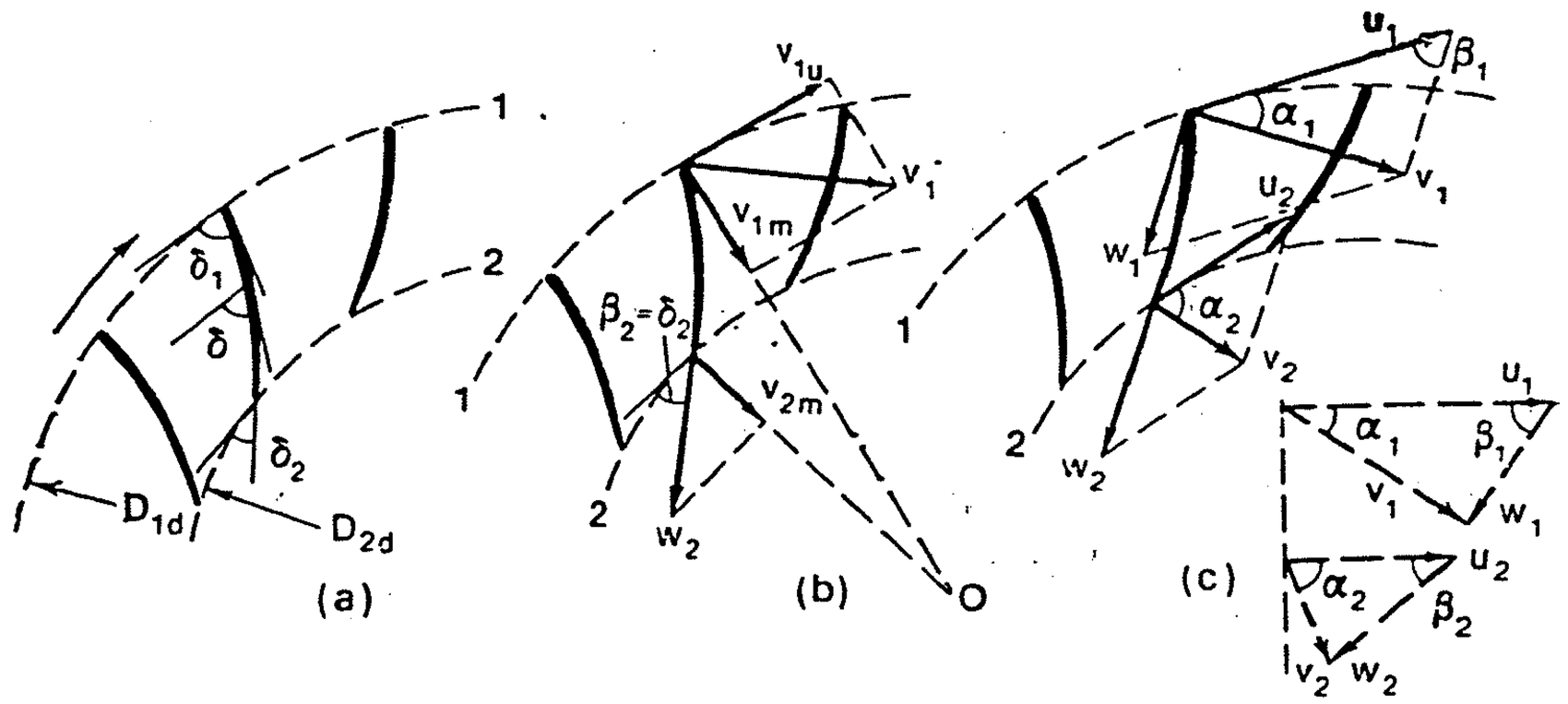


FIGURE 5.4. Velocity parallelograms and triangles of a radial-axial flow turbine runner.

The projection of the vector of absolute velocity on the meridional plane, the meridional component v_m (v_{1m} and v_{2m} are shown in Figure 5.3) can be approximately found from the relation

$$v_m = Q/F_i \tag{5.7}$$

where F_i is the summary flow area in the runner normal to the stream surfaces. The other required components depend on the section considered. For instance, in the inlet section (1) of the runner of a radial-axial turbine $F_i = \pi D_{1d} b_d$, where b_d is the height of the inlet opening of the runner, and from formula (5.7)

$$v_{1m} = \frac{Q}{\pi D_{1d} b_d} \tag{5.8}$$

The peripheral component v_{1u} depends on the conditions under which the water flow leaves the wicket gate and in conjunction with Equation 5.4 it will be equal to

$$v_{1u} = v_{0u} \frac{D_{02}}{D_{1d}} \tag{5.9}$$

The absolute velocity at the runner inlet is specified by the vector sum (Figure 5.4b)

$$\mathbf{v}_1 = \mathbf{v}_{1m} + \mathbf{v}_{1u} \tag{5.10}$$

Knowing $\mathbf{v}_1$ and in accordance with Equation 5.6,

$$u_1 = \pi D_{1d} n/60$$

we plot the velocity parallelogram and determine $\mathbf{w}_1$ (Figure 5.4c). The form of the velocity parallelogram depends on the angle α_1 between u_1 and v_1, and β_1 between u_1 and w_1. A velocity triangle is sometimes plotted (dotted line) instead of the parallelogram.

In the outlet section (2) of the runner

$$u_2 = \pi D_{2d} n/60 \quad \text{and} \quad v_{2m} = Q/F_2$$

In addition, because the cascade of the runner blades is rather dense, we may approximately assume that the relative velocity is a directed tangent to the blade, i.e.,

$$\beta_2 = \delta_2 \tag{5.11}$$

According to Figure 5.4b, it follows from this condition that

$$w_2 = v_{2m}/\sin \delta_2 \tag{5.12}$$

Knowing $\mathbf{u}_2$ and $\mathbf{w}_2$ and in accordance with Equation 5.5, we plot a parallelogram (Figure 5.4c) and find $\mathbf{v}_2$. The form of the outlet parallelogram is specified by the angles α_2 and β_2. The velocity triangle is plotted with a dotted line. Such a triangle may be plotted not only for the inlet and outlet sections, but also for intermediate sections. These triangles determine the vectors $\mathbf{v}_i$, respectively, and may be used to construct the trajectory of absolute liquid motion in the runner. The shape of these trajectories is shown in Figure 5.5. We should concentrate our attention on the rather important conclusion that the form of the trajectories of absolute motion does not depend on the magnitude of the velocity v, and is determined only by its direction. If the cover and band of the turbine runner were transparent, the form of the trajectories of absolute motion could be photographed using a stationary camera.

In axial-flow turbines the stream surface is close to cylindrical (Figure 5.6a), i.e., $D_{1d} = D_{2d} = D_d$; the design diameter can be calculated as the average over the area:

$$D_d = \sqrt{0.5(D_1^2 + d_c^2)} \tag{5.13}$$

Development of the cylindrical section of the runner is shown in Figure 5.6b. The special inset translates to:

$$u_1 = u_2 = u = \frac{\pi D_d n}{60}$$

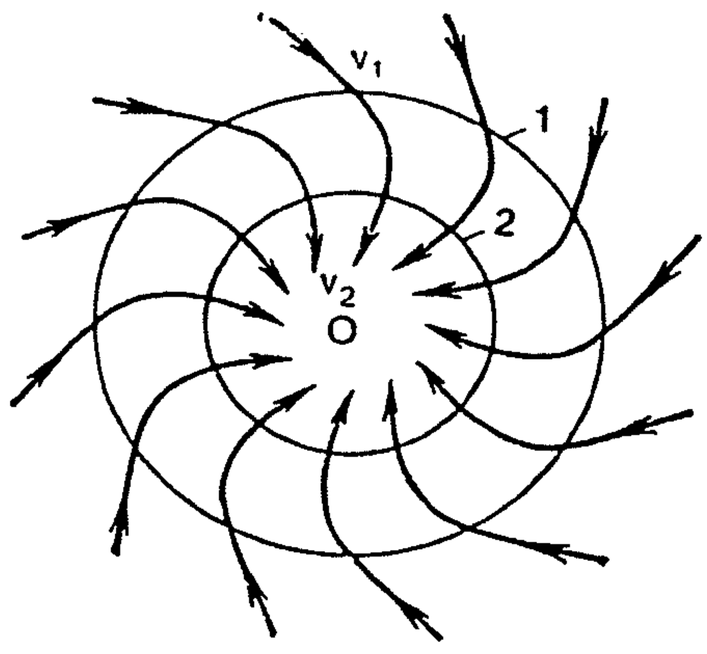


FIGURE 5.5. Trajectories of liquid absolute motion in a radial-axial flow turbine.

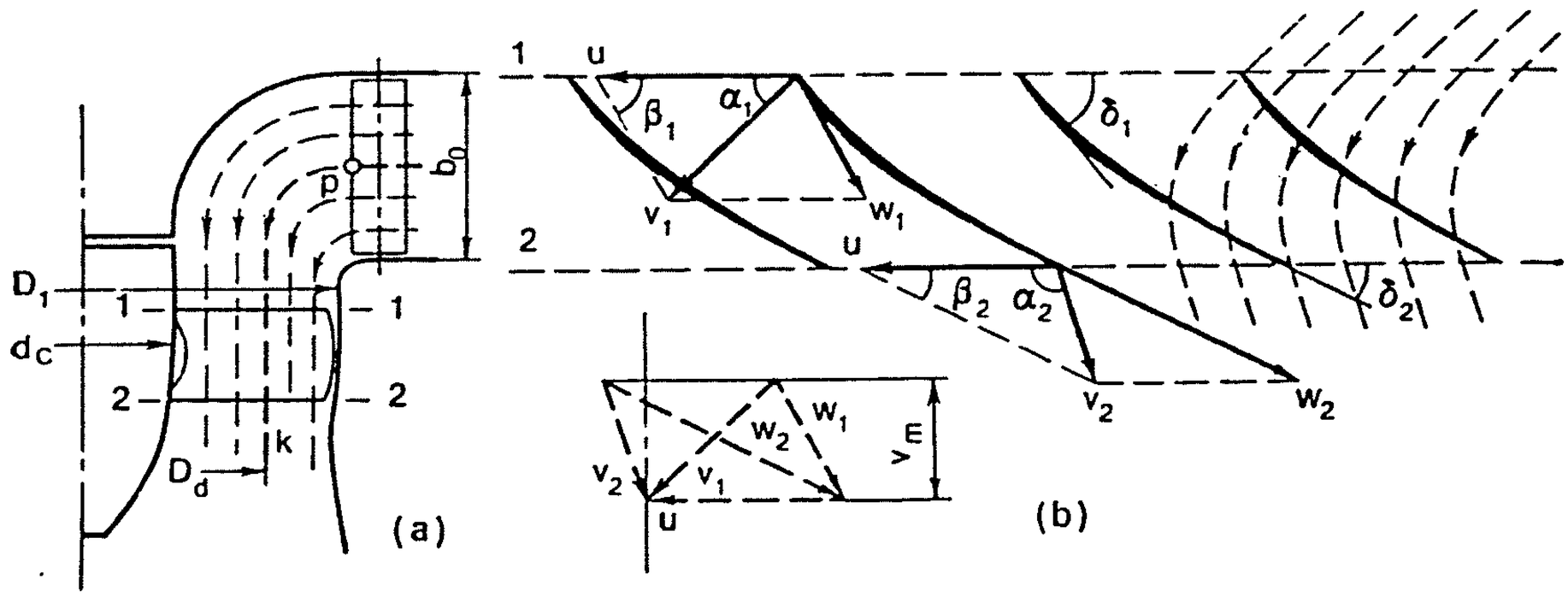


FIGURE 5.6. Flow in axial-flow turbine.

and

$$v_{1m} = v_{2m} = v_m = \frac{4Q}{\pi(D_1^2 - d_c^2)}$$

The velocity in the inlet edges (1) is determined as a vector sum:

$$\mathbf{v}_1 = \mathbf{v}_{1m} + \mathbf{v}_{1u}$$

with v_{1u} from Equation 5.9. The absolute velocity $\mathbf{v}_2$ is plotted in accordance with Equation 5.5, taking into account Equations 5.11 and 5.12. The resulting velocity parallelograms are shown in Figure 5.6b. The velocity triangles on the inlet and outlet edges are superposed (dotted line), inasmuch as they have an equal base u and an equal altitude v_m. The trajectories of the absolute motion of water in the runner are shown on the right by dotted lines.

5.3. OPERATING CONDITIONS (REGIME) OF THE TURBINE

The construction of velocity parallelograms (triangles) considered in Section 5.2, shows that for a given runner at a constant opening of the wicket gate ($\alpha_0 = \text{const}$) the form of the velocity parallelograms, specified by the angles α and β, depends on rotational speed n and the rate of flow Q. Let us examine how the n and Q parameters affect the flow.

Assume the turbine operates with a constant Q and a varying rotational speed, n. Then $\mathbf{v}_1$ will remain constant on the inlet edges (1) of the runner, because according to Equation 5.10 $\mathbf{v}_1$ is independent of n. Only $\mathbf{u}_1$ and $\mathbf{w}_1$ will change, as shown in Figure 5.7a. The plot shows that the vector of relative velocity $\mathbf{w}_1$ changes direction. At a low

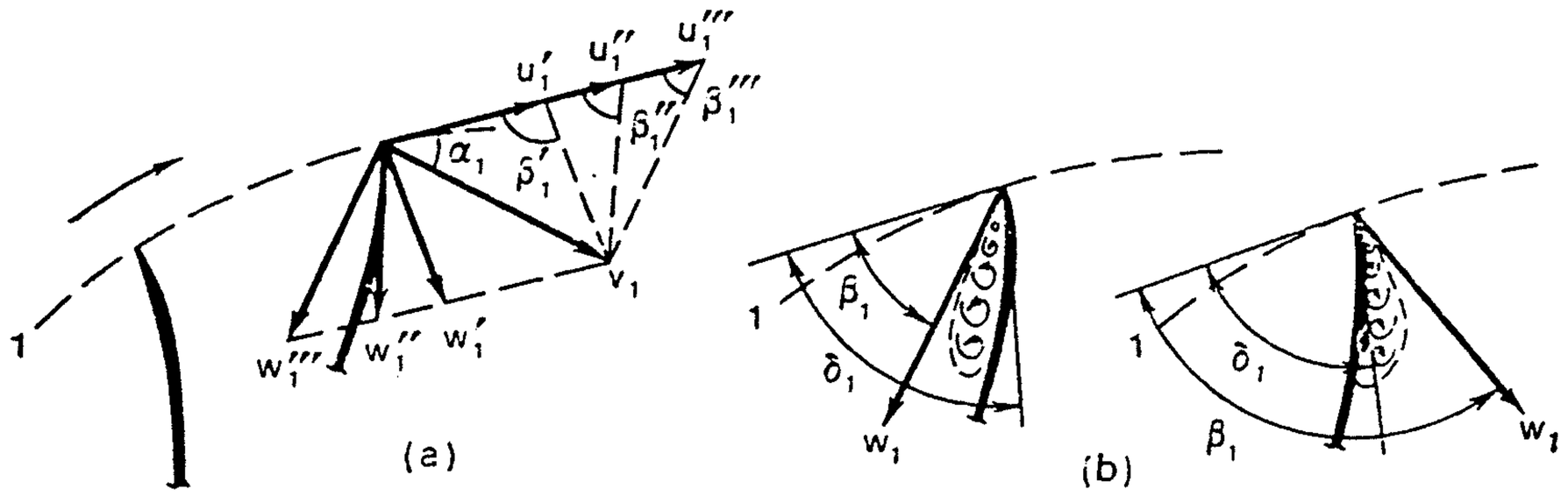


FIGURE 5.7. Flow at leading (inlet) edges of the runner blades.

rotational speed the vector $\mathbf{w}_1$ deflects in the direction of rotation, $\beta_1' > \delta_1$, and at a high speed $\mathbf{w}_1$ deflects in the opposite direction, $\beta_1''' < \delta_1$. When $\beta_1 \leqq \delta_1$ liquid flows on the blade inlet edge at an angle that (see Figure 5.7b) is accompanied by the creation of vorticity regions which cause additional losses of energy (shock loss). The mode of shock-free entry, when $\beta_1 = \delta_1$, is the most favorable.

The relative velocity $\mathbf{w}_2$ on the outlet blade edges (2), in accordance with Equation 5.12, depends only on the flow rate Q and angle δ_2. In other words, it is independent of n. However, inasmuch as $\mathbf{u}_2$ is proportional to n, the absolute velocity $\mathbf{v}_2$ (according to Equation 5.5) will depend on n as well. This dependence can be easily determined by examining the velocity parallelograms on the outlet edges of the runner of a radial-axial turbine (Figure 5.8a) and of an axial-flow turbine (Figure 5.8b). The parallelograms shows the angle α_2 to decrease with increasing n and $\mathbf{u}_2$ and the vector $\mathbf{v}_2$ to turn toward the direction of rotation. As this occurs the following may be noted:

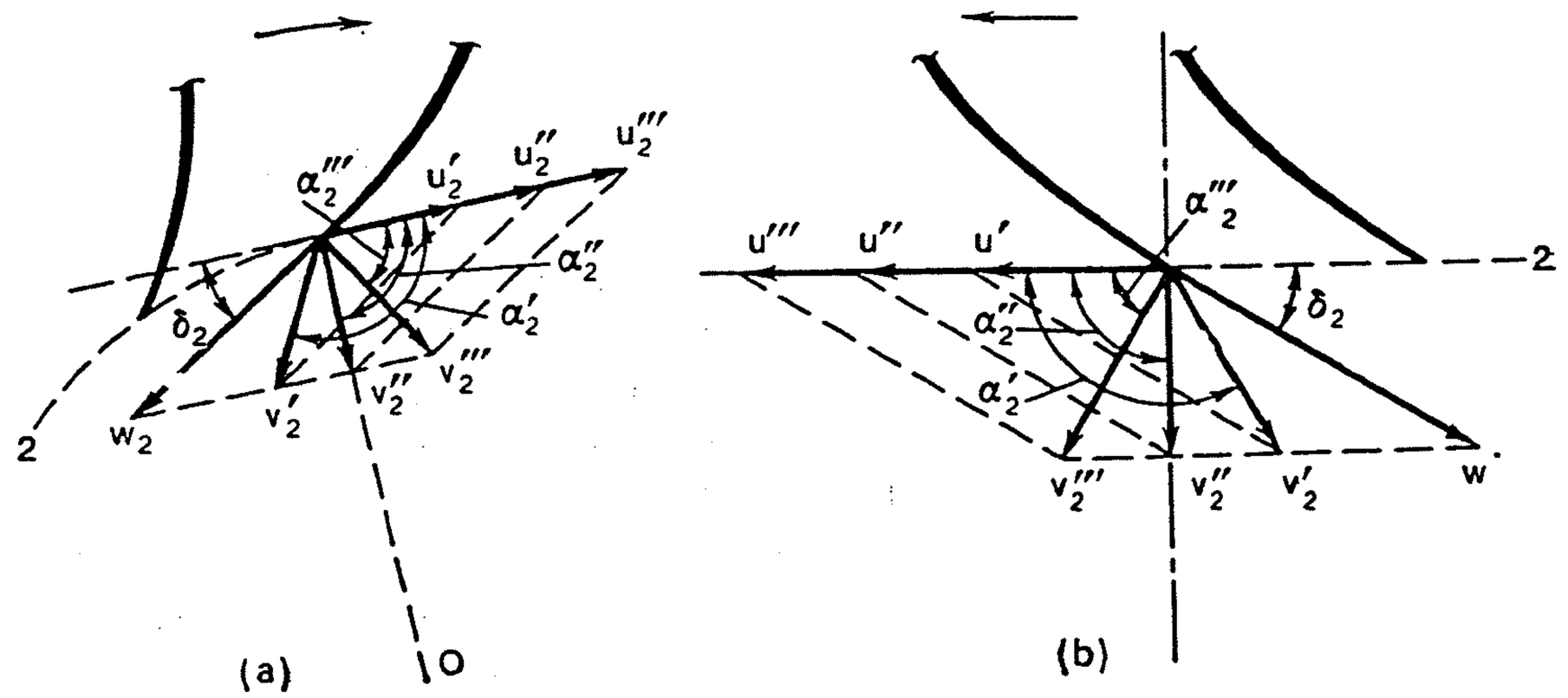


FIGURE 5.8. Flow at trailing (outlet) edges of the runner blades.

1. Although the flow rate is constant the magnitude of the velocity vector $\mathbf{v}_2$ depends on n and its minimum length corresponds to the condition in which the vector $\mathbf{v}_2$ lies in the meridional plane (directed toward the center or parallel to the axis of rotation); i.e., $\alpha_2 = 90°$.
2. In the general case the flow downstream of the runner is twisted (circulation $\Gamma_2 \neq 0$). If $\alpha_2 < 90°$, the direction of the twist coincides with the runner rotation direction, but if $\alpha_2 > 90°$, the flow rotates in the opposite direction. Circulation $\Gamma_2 = 0$ only at $\alpha_2 = 90°$.

The mode of flow corresponding to the condition $\alpha_2 = 90°$, where v_2 is minimal and $\Gamma_2 = 0$, is referred to as the mode of normal outflow (exit). The mode of turbine operation close to the normal outflow mode is characterized by the smallest losses. This is the most favorable because the losses at the runner outlet are generally proportional to v_2^2.

The mode of operation that ensures both shock-free entrance and normal outflow, and ensures a maximum turbine efficiency, is referred to as the optimal mode of operation or operating conditions. Thus, *operating conditions* (*regime*) *of the turbine are determined by the form of the velocity parallelogram.*

5.4. TURBINE ENERGY EQUATION

Let us determine the power-generating characteristics of the flow in the runner by making use of the angular-momentum equation (Equation 5.3) for the runner section shown in Figure 5.4, and single out, reference surfaces (1) and (2), the region, including the runner blades (Figure 5.9). For the steady-state averaged flow within the singled-out region, $v_u r$ does not change with time, consequently, $d(v_u r)$ is equal to the difference $v_{1u} r_1 - v_{2u} r_2$ on the reference surfaces. The mass of liquid flowing through the runner in time dt is

$$m = \rho Q \, dt$$

Under these conditions the angular-momentum equation is

$$\rho Q(v_{2u} r_2 - v_{1u} r_1) = \sum M_0 \tag{5.14}$$

The sum of the moments of the external forces about the axis of rotation, $\sum M_0$, acting upon the singled-out volume of liquid, is determined as follows. The moment of the pressure forces acting on the surfaces of rotation (1) and (2) (see Figure 5.9) and the surface of the rim is equal to zero. The gravitational forces produce no moment because their center of application coincides with the axis. The only

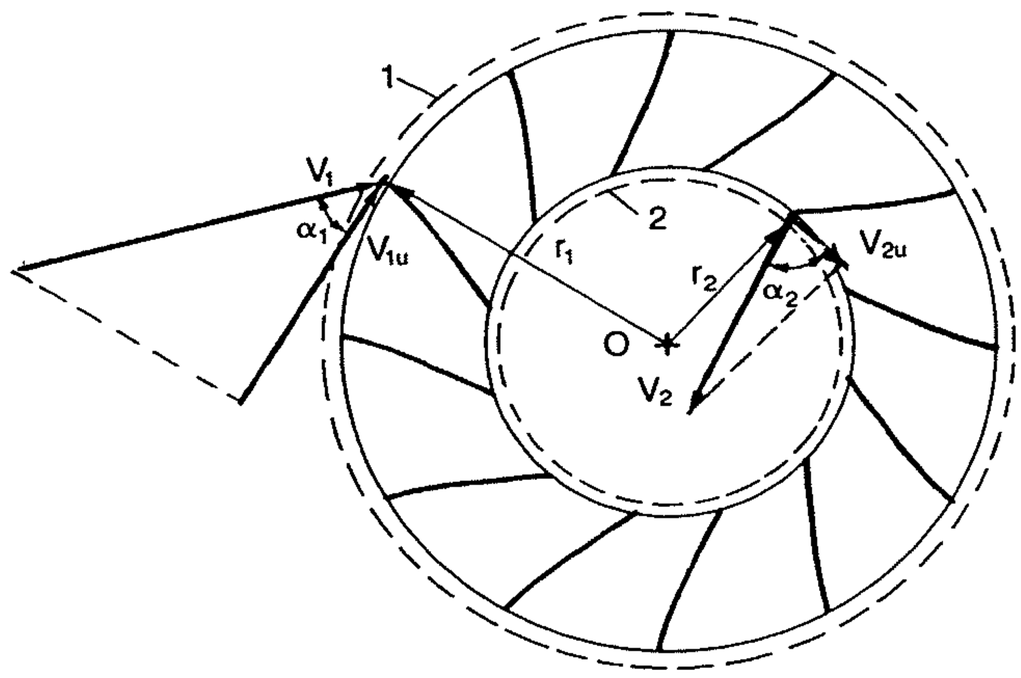


FIGURE 5.9. Velocities at leading and trailing edges of the runner blades.

forces remaining are those of friction on the confining surfaces and the pressure and friction forces of the liquid on the blades. The two groups of forces produce a moment about the axis, but the first group is small and may be ignored. The only moment remaining is that acting upon the liquid from the side of the runner blades M; the moment of the runner created on the blades by the liquid will be equal to $-M$.

In the final analysis, expanding the terms v_{1u} and v_{2u} in Equation 5.14, we obtain

$$M = \rho Q(0.5D_{1d}v_1 \cos \alpha_1 - 0.5D_{2d}v_2 \cos \alpha_2) \tag{5.15}$$

Using the expressions for the mean circulation, similar to Equation 5.2 in front of the inlet edge (1)

$$\Gamma_1 = \pi D_{1d}v_1 \cos \alpha_1$$

and downstream of the outlet edge (2)

$$\Gamma_2 = \pi D_{2d}v_2 \cos \alpha_2 \tag{5.16}$$

it is possible to express the moment of the runner by the difference between the mean inlet and outlet circulations

$$M = \frac{\rho Q}{2\pi}(\Gamma_1 - \Gamma_2) \tag{5.17}$$

Equation 5.17 is rather demonstrative. It shows that torque is created on the runner only when its blades change the flow circulation. Γ is assumed to be positive when $\mathbf{v}_u$ coincides with the direction of the peripheral velocity **u**.

Knowing the moment and assuming an angular velocity for the runner, it is possible to determine the power created by it

$$N_r = M\omega \tag{5.18}$$

where M is expressed in terms of newton meters, ω in $(\text{seconds})^{-1}$, and N_r in watts. Yet, turbine capacity is known to be specified by Equation 2.9. This makes it possible to set up the equality.

$$M\omega = \rho g Q H \eta_h$$

where H is the head of the turbine and η_h is the hydraulic efficiency. Substituting M into this formula from Equation 5.15 and allowing for $\omega 0.5 D_{1d} = u_1$ and $\omega 0.5 D_{2d} = u_2$ where u_1 and u_2 are peripheral velocities, we obtain

$$H\eta_h = \frac{1}{g}(u_1 v_1 \cos \alpha_1 - u_2 v_2 \cos \alpha_2) \tag{5.19}$$

Using Equation 5.17, Equation 5.19 takes the form

$$H\eta_h = \frac{\omega}{g 2\pi}(\Gamma_1 - \Gamma_2) \tag{5.20}$$

Formulas 5.19 and 5.20 represent the main energy equation of turbines or the Euler equation. The left side, $H\eta_h$, is the energy expressed in joules received by the runner from the liquid (weighing 1 N) passing through the runner blades. The right side contains the kinematic parameters of the flow up- and downstream of the runner. The main energy equation shows the relationship between the power-generating and kinematic parameters in a turbine.

Euler's equation, represented in Equation 5.20, permits us to draw the following essential conclusions.

1. For turbine energy characteristics, the principal importance is the structure of the flow before and after the runner.
2. As noted above, the most favorable operating conditions as far as efficiency is concerned are close to the conditions of normal discharge, where circulation $\Gamma_2 = 0$, or is small. $\Gamma_1 = \Gamma_0$ are the circulations created by the guide vanes. Hence, it is possible to determine the required value of Γ_0 depending on H and ω.
3. As water flows through the turbine runner the flow circulation must diminish. It follows that the runner "gobbles up" the circulation created by the wicket gate (guide vanes).

Of interest is another form of main turbine energy equation which permits a better understanding of the mechanism of energy conversion by the turbine runner. This can be derived from Bernoulli's equation, although in this case it is necessary to use the equation as written for relative motion. Imagine a disk rotating at a speed, n (in revolutions per minute), on which tube (1–2) is fastened (Figure 5.10). Liquid flows through this tube from section 1 to section 2 with a velocity w (with respect to the tube). Considering Bernoulli's equation, *0–0* takes on the following appearance about the datum plane:

$$\frac{p_1}{\rho g} + z_1 + \frac{w_1^2}{2g} - \frac{u_1^2}{2g} = \frac{p_2}{\rho g} + z_2 + \frac{w_2^2}{2g} - \frac{u_2^2}{2g} + h_{1-2} \quad (5.21)$$

where h_{1-2} is losses of head through section 1–2; u_1 and u_2 are peripheral velocities (transportation motion). The distinguishing characteristic is that under the conditions considered, the specific energy of the liquid flowing along the tube may diminish or increase depending on the value of the peripheral velocities u_1 and u_2. It is exactly this property that is used in the turbine runner whose ducts, formed by the runner blades, represent a system of "tubes."

It follows from Equation 5.21 that

$$\frac{p_1}{\rho g} + z_1 - \frac{p_2}{\rho g} - z_2 = \frac{w_2^2 - w_1^2}{2g} + \frac{u_1^2 - u_2^2}{2g} + h_{1-2} \quad (5.21a)$$

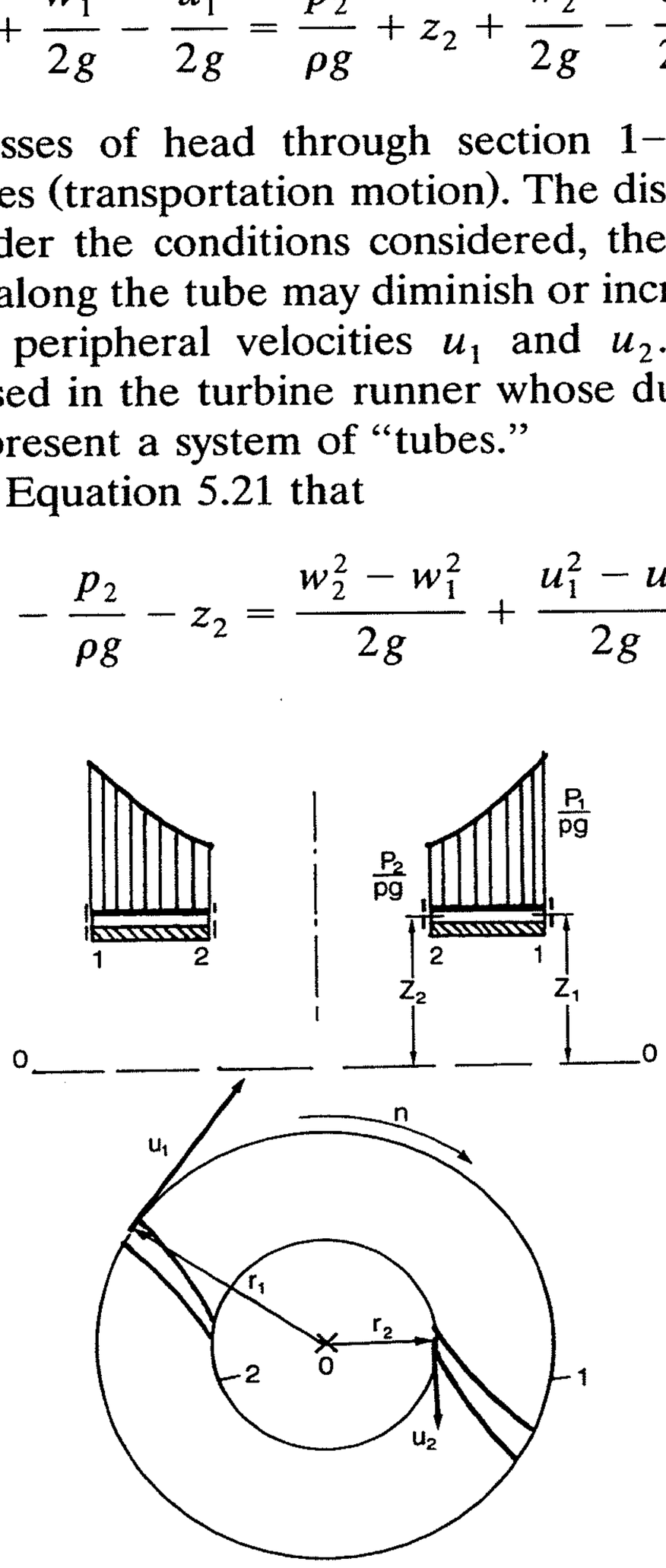


FIGURE 5.10. Bernoulli's equation for relative motion.

The specific energy of liquid upstream of the runner is

$$e_1 = \frac{p_1}{\rho g} + z_1 + \frac{v_1^2}{2g}$$

The specific energy of liquid at the runner outlet is

$$e_2 = \frac{p_2}{\rho g} + z_2 + \frac{v_2^2}{2g}$$

The difference between the specific energies gives runner's head:

$$e_1 - e_2 = \left(\frac{p_1}{\rho g} + z_1 - \frac{p_2}{\rho g} - z_2\right) + \frac{v_1^2}{2g} - \frac{v_2^2}{2g} = H_r$$

Replacing the expression in brackets at the right side of Equation 5.21a, we obtain

$$H_r = \frac{w_2^2 - w_1^2}{2g} + \frac{u_1^2 - u_2^2}{2g} + h_{1-2} + \frac{v_1^2 - v_2^2}{2g}$$

Using $H_r - h_{1-2} = H\eta_h$, we obtain another form of main turbine equation

$$H\eta_h = \frac{v_1^2 - v_2^2}{2g} + \frac{u_1^2 - u_2^2}{2g} + \frac{w_2^2 - w_1^2}{2g} \tag{5.22}$$

which clearly shows the direct dependence of $H\eta_h$ on the velocity triangles upstream and downstream of the turbine runner. Equation 5.22 explains the relation between the form of the runner and the turbine head. In axial-flow turbines $u_1 = u_2$ and, consequently, $H\eta_h$ is specified only by the absolute and relative velocities. These velocities cannot be too high, for otherwise great losses are suffered. This restricts the use of axial-flow turbines with respect to head. With greater heads, H, use is made of mixed-flow (diagonal) and radial-axial flow turbines, in which the difference between the peripheral velocities u_1 and u_2 is seen; the higher the head H, the more important is that factor. This explains the increase of the ratio of D_1/D_2 of high-head turbines (Figures 3.15 to 3.17).

Example 5.1

Using Euler's equation, determine the speed characteristics of a turbine, i.e., the dependence $M(n)$, $\eta(n)$, and $N(n)$ for the following conditions $a_0 = \text{const}$, $H = \text{const}$.

Solution

Under the given conditions we may approximately assume that $Q =$ const. Then, according to Equations 5.2a and 5.4a $\Gamma_1 = \Gamma_0 =$ const. As demonstrated in Section 5.3, the outlet circulation Γ_2 depends on n. At $n = 0$ (the runner does not revolve), $\Gamma_2 < 0$ (approximately, $\Gamma_2 = -\Gamma_1$). As speed n increases, Γ_2 rises, passing through $\Gamma_2 = 0$. Circulation then becomes positive. The variation of Γ_1 and Γ_2 is plotted on a chart (Figure 5.11). The difference yields $(\Gamma_1 - \Gamma_2)$. Hence, with the aid of Equation 5.17 we obtain the monotonously decreasing curve $M(n)$. The efficiency curve may be plotted through three points

$$(1) \qquad n = 0, \quad \eta = 0, \quad N = 0$$

$$(2) \qquad \Gamma_2 = 0, \quad \eta = \eta_{max}, \quad N = N_{max}$$

$$(3) \qquad (\Gamma_1 - \Gamma_2) = 0, \quad \eta = 0, \quad N = 0$$

These three points (see Figure 5.11) permit us to draw two important practical conclusions: the turbine apparently must be operated in the region of maximum efficiencies, i.e., in the region of speeds $n_1 - n_2$. For an idly running turbine the maximum rotational frequency (speed) to which the runenr accelerates is determined by point $M = 0$. This is the runaway speed n_{run} against which the strength of all rotating parts of the turbine unit must be calculated.

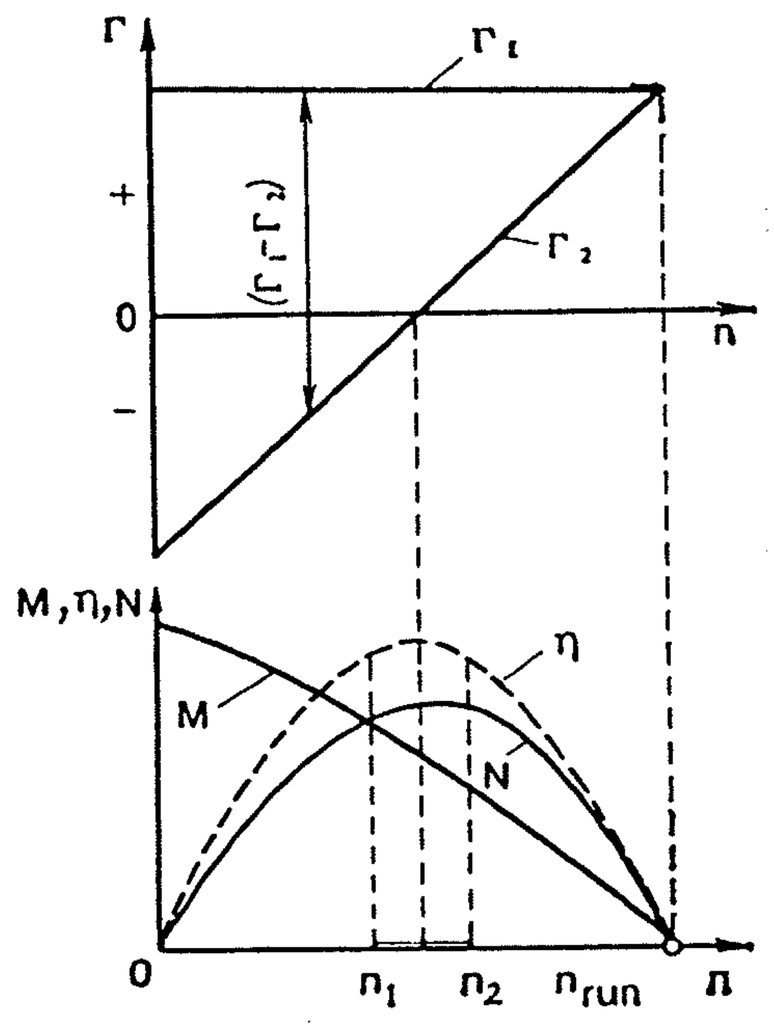


FIGURE 5.11. Plotting the turbine speed curve using Euler's equation.

5.5. OPERATING PROCESS OF IMPULSE [PELTON] TURBINES

Active Pelton turbines (Figure 2.6) differ from reaction (pressure) turbines in that (1) their runner rotates in the air and is only capable of utilizing the kinetic energy of the liquid, and (2) the water behaves in a simultaneous fashion only on some of the blades (buckets). These two factors determine some of the peculiarities associated with the operating process of Pelton turbines.

At all openings the direction and velocity of the jet v_j (Equation 2.11) remain constant; the factor φ changes very little. The velocity at the inlet edge of the blade (bucket) (1) is practically equal to the jet velocity: $\mathbf{v}_1 = \mathbf{v}_j$ (v_c in Figure 5.12).

The peripheral velocity for the given section of (bucket) blades located at a distance r from the axis of rotation is specified by the expression

$$u_1 = u_2 = u_r = 2\pi rn/60$$

(the average radius $r_{av} = 0.5D_1$ in Figure 2.6).

In this case the velocity parallelogram $\mathbf{w}_1 = \mathbf{v}_1 - \mathbf{u}_1$ transforms into a straight line on the inlet edge of the blade (Figure 5.12b) and $\mathbf{w}_1$ coincides with the direction of the jet. To ensure shock-free entry the angle of the inlet edge δ_1 (Figure 5.12a) must be at a minimum (spear).

The velocity parallelogram for the outlet edge is determined by the fact that as water flows along the blade the relative velocity changes little and we may assume $w_2 = w_1$, and the direction of the velocity coincides with δ_2. In the final analysis we get (Figure 5.12c)

$$\mathbf{v}_2 = \mathbf{w}_2 + \mathbf{u}_2$$

As the exit angle δ_2 is small, the plotted parallelogram is elongated. The velocity v_2 is also small, notwithstanding the large velocities w_2 and u_2. Analogous to Figure 5.8 it is easily seen that a change in speed

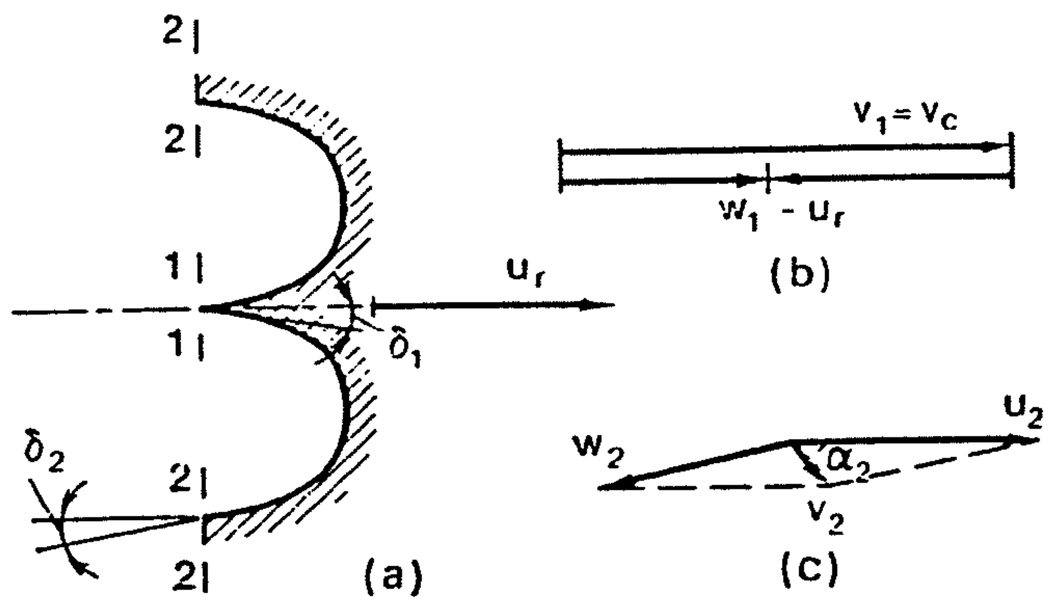


FIGURE 5.12. Flow kinematics in the runner of the Pelton turbine.

n at constants Q and w will cause a change of the angle α_2 and velocity v_2. The minimum magnitude of v_2 corresponds to $\alpha_2 = 90°$; this is the condition of a normal exit.

The kinematics of liquid flow show that the runner of a Pelton turbine also changes the moment of fluid velocity about the axis of rotation and, consequently, the torque of the runner many be determined via Equation 5.14. In the final analysis we may use the Euler equation in the form of Equations 5.19 and 5.22. (Equation 5.20 is unsuitable because it precludes the use of the definition of circulation.)

Equation 5.22 yields interesting results. If we bear in mind that the peripheral velocities on the inlet and outlet edges are equal ($u_1 = u_2$), and the relative velocity diminishes somewhat as the liquid moves along the blade due to friction ($w_2 < w_1$), then it follows from Equation 5.22 that

$$H\eta_h = \frac{v_1^2 - v_2^2}{2g} - \frac{w_1^2 - w_2^2}{2g}$$

Taking into account that according to Equation 2.11 and the assumed condition $v_1 = v_j$; $v_1^2/2g = \varphi^2 H$, we obtain

$$\eta_h = \varphi^2 - \frac{w_1^2 - w_2^2}{2gH} - \frac{v_2^2}{2gH} \tag{5.23}$$

Formula 5.22 indicates that the hydraulic efficiency η_h is the sum of three terms, allowing for the losses in the nozzle, the blades, and the exit, equal to $v_2^2/2gH$. This substantiates the requirement that the blade surface be strictly smooth and the velocity v_2 decreased. These factors ensure better power-generating quality for the Pelton turbine.

5.6. TURBINES OF ONE TYPE AND SIMILARITY LAWS FOR THEIR MODES OF OPERATION

The type of turbine is determined by the form ("geometry") of its liquid passage, the duct. In other words, the turbines of one type have similar liquid passages. It should be emphasized that the size of a turbine does not determine its type.

In accordance with the definition, two turbines of one type but of different size meet the following conditions:

1. All turbine corresponding angles are alike:

$$\delta_{11} = \delta_{12} \qquad \delta_{21} = \delta_{22} \qquad \delta_{i1} = \delta_{i2} \tag{5.24}$$

2. The ratio of corresponding dimensions is constant:

$$\frac{D_{11}}{D_{12}} = \frac{D_{21}}{D_{22}} = \frac{b_{01}}{b_{02}} = \cdots \tag{5.25}$$

The operational modes of turbines of one type will be similar if the geometrical similarity of velocity parallelograms or triangles at corresponding points in the liquid passage remains valid. Thus, when operating conditions are similar

1. All corresponding velocities must be similarly directed, i.e., all corresponding angles are equal:

$$\alpha_{i1} = \alpha_{i2} \qquad \beta_{i1} = \beta_{i2} \tag{5.26}$$

   In connection with this property similar modes of operation or operating conditions are sometimes referred to as isogonal.
2. The ratios of all velocities at corresponding points i must be constant:

$$\frac{v_{i1}}{v_{i2}} = \frac{u_{i1}}{u_{i2}} = \frac{w_{i1}}{w_{i2}} = \text{const} \tag{5.27}$$

Based on the above definitions it is possible to define regularities governing the relationship between the parameters of turbines of one type under conditions of similar modes of operation.

Problem

There are two turbines of one type but of different sizes, D_1 and D_2, heads H_1 and H_2. The guide vane angles and the runner blade angles are equal: $\alpha_{01} = \alpha_{02}$ and $\varphi_1 = \varphi_2$. What ratios of speed n_1 and n_2 and discharges Q_1 and Q_2 must be ensured for their modes of operation to be similar?

Solution

First, make use of the geometric (Equations 5.24 and 5.25 and the kinematic ratios (Equations 5.26 and 5.27). Then, based on Equation 5.6,

$$\frac{u_{11}}{u_{12}} = \frac{\pi D_1 n_1}{\pi D_2 n_2} = \frac{D_1 n_1}{D_2 n_2} \tag{5.28}$$

From Equation 5.8 we obtain

$$\frac{v_{1m1}}{v_{1m2}} = \frac{Q_1 \pi D_2 b_{02}}{\pi D_1 b_{01} Q_2}$$

Taking into account that according to Equation 5.25 $b_{01}/b_{02} = D_1/D_2$, we obtain

$$\frac{v_{1m1}}{v_{1m2}} = \frac{Q_1 D_2^2}{Q_2 D_1^2} \tag{5.29}$$

According to Equation 5.27, when operating conditions are preserved, $u_{11}/u_{12} = v_{1m1}/v_{1m2}$, we come to the equality

$$\frac{D_1 n_1}{D_2 n_2} = \frac{Q_1 D_2^2}{Q_2 D_1^2} \qquad \frac{Q_1}{n_1 D_1^3} = \frac{Q_2}{n_2 D_2^3}$$

Generalizing this result, we write the kinematic condition for the similarity (preservation) of turbine modes of operation

$$\frac{Q}{nD^3} = \text{const} \tag{5.30}$$

Now, make use of the energy (power) ratios, allowing for the fact that these turbines operate under different heads H_1 and H_2 and have hydraulic efficiencies η_{h1} and η_{h2}. Writing the main equation in the form of Equation 5.19 for each turbine we have

$$gH_1\eta_{h1} = u_{11}v_{11}\cos\alpha_{11} - u_{21}v_{21}\cos\alpha_{21} \tag{5.31}$$

$$gH_2\eta_{h2} = u_{12}v_{12}\cos\alpha_{12} - u_{22}v_{22}\cos\alpha_{22} \tag{5.31a}$$

It follows from the similarity conditions of Equations 5.26 and 5.27 and from Equation 5.28 that

$$\alpha_{11} = \alpha_{12} \qquad \alpha_{21} = \alpha_{22} \qquad \frac{u_{11}}{u_{12}} = \frac{v_{11}}{v_{12}} = \frac{u_{21}}{u_{22}} = \frac{v_{21}}{v_{22}} = \frac{D_1 n_1}{D_2 n_2}$$

or

$$\cos\alpha_{11} = \cos\alpha_{12} \qquad \cos\alpha_{21} = \cos\alpha_{22}$$

Hence,

$$u_{12} = u_{11}\frac{D_2 n_2}{D_1 n_1} \qquad v_{12} = v_{11}\frac{D_2 n_2}{D_1 n_1}$$

$$u_{22} = u_{21}\frac{D_2 n_2}{D_1 n_1} \qquad v_{22} = v_{21}\frac{D_2 n_2}{D_1 n_1}$$

Substituting the obtained relationships into the right side of Equation 5.31, we get

$$gH_2\eta_{h2} = \left(\frac{D_2 n_2}{D_1 n_1}\right)^2 (u_{11}v_{11}\cos\alpha_{11} - u_{21}v_{21}\cos\alpha_{21}) \quad (5.31b)$$

Dividing Equation 5.31 by 5.31b results in the expression

$$\frac{H_1\eta_{h1}}{H_2\eta_{h2}} = \left(\frac{D_1 n_1}{D_2 n_2}\right)^2$$

The above expression permits us to find the speed ratio

$$\frac{n_1}{n_2} = \frac{D_2}{D_1}\sqrt{\frac{H_1}{H_2}}\sqrt{\frac{\eta_{h1}}{\eta_{h2}}} \quad (5.32)$$

Substituting the found ratio n_1/n_2 into the kinematic condition for similarity, Equation 5.30,

$$\frac{Q_1}{n_1 D_1^3} = \frac{Q_2}{n_2 D_2^3}$$

we get the discharge ratio

$$\frac{Q_1}{Q_2} = \left(\frac{D_1}{D_2}\right)^2\sqrt{\frac{H_1}{H_2}}\sqrt{\frac{\eta_{h1}}{\eta_{h2}}} \quad (5.33)$$

The ratio of powers can be easily found from Equation 2.10 $N_1 = 9.81Q_1H_1\eta_1$ and $N_2 = 9.81Q_2H_2\eta_2$, using Equation 5.33

$$\frac{N_1}{N_2} = \left(\frac{D_1}{D_2}\right)^2\frac{H_1}{H_2}\sqrt{\frac{H_1}{H_2}}\frac{\eta_1}{\eta_2}\sqrt{\frac{\eta_{h1}}{\eta_{h2}}} \quad (5.33a)$$

Formulas 5.30, 5.32, 5.33, and 5.33a are called the laws (formulas) of similarity, which are used widely. When the similarity conditions are preserved, hydraulic efficiency changes only slightly, and often it is accepted that $\eta_{h1}/\eta_{h2} = 1$.

Example 5.2

An investigation of a turbine model, $D_m = 0.3$ m in diameter, operated with a head $H_m = 3.5$ m, has shown that optimal operating conditions having the highest efficiency are ensured at a speed $n_{m\cdot\text{opt}} = 430$ rpm and a discharge $Q_{m\cdot\text{opt}} = 0.15$ m^3/s. Find the speed $n_{t\cdot\text{opt}}$, the discharge $Q_{t\cdot\text{opt}}$, and the power $N_{t\cdot\text{opt}}$ of a full-scale turbine of the same type, having a diameter $D = 5.0$ m and operating with a head $H = 90$ m.

Solution

Assuming $\eta_{h\cdot m}/\eta_{h\cdot t} = 1$, Equation 5.32 yields

$$n_{t\cdot\text{opt}} = n_{m\cdot\text{opt}}\frac{D_m}{D}\sqrt{\frac{H}{H_m}} = \frac{430 \times 0.3}{5}\sqrt{\frac{90}{3.5}} = 131 \text{ rpm}$$

From Equation 5.33 we find that

$$Q_{t\cdot\text{opt}} = Q_{m\cdot\text{opt}}\left(\frac{D}{D_m}\right)^2\sqrt{\frac{H}{H_m}} = 0.15\left(\frac{5}{0.3}\right)^2\sqrt{90/3.5} = 211 \text{ m}^3/\text{s}$$

It is better to calculate turbine power or capacity via Equation 2.10. The efficiency must be assumed. Under optimal operating conditions $\eta_{\text{opt}} =$ 92 to 95%. We assume $\eta_{\text{opt}} = 0.93$ and obtain $N_{t\cdot\text{opt}} = 9.81 \times 90 \times 211 \times 0.93 = 172{,}000$ kW.

5.7. REDUCED TURBINE PARAMETERS

It is possible to manufacture turbines of different sizes and use them in a wide range of heads, speeds, discharges, and power. Consequently, to characterize a turbine of a given type, some indices or characteristics reduced to common standard conditions are required; e.g., with respect to the head or diameter. It is customary to assume turbine characteristics recalculated to a head, $H = 1$ m, and diameter, $D = 1$ m. These parameters are referred to as reduced (unitary) and are denoted n'_1, reduced rotational frequency (speed), and Q'_1, reduced discharge. Using the recalculation formulas (Equations 5.32 and 5.33), with no account

taken of a change of hydraulic efficiency, and using the assumed turbine parameters n, H, and D, we obtain

$$\frac{n'_1}{n} = \frac{D}{1}\sqrt{\frac{1}{H}}$$

or

$$n'_1 = \frac{nD}{\sqrt{H}} \tag{5.34}$$

The recalculation formulas also permit us to obtain

$$\frac{Q'_1}{Q} = \left(\frac{1}{D}\right)^2 \sqrt{\frac{1}{H}}$$

where

$$Q'_1 = \frac{Q}{D^2\sqrt{H}} \tag{5.35}$$

The reduced (unitary) parameters n'_1 and Q'_1 (sometimes denoted as $n_{1,1}$ and $Q_{1,1}$) that are widely used for turbine characteristics are dimensional values. It follows from Equations 5.34 and 5.35 that both have the same dimension $L^{1/2}/T$ (L meaning length, and T meaning time). For example, if $L - m$ and $T - s$ their dimension is $m^{1/2}/s$. However, taking into account the origin of their derivation (via 1, 1 indices), they are often referred to as reduced speed for n'_{I} (revolutions per minute) and as reduced discharge for Q'_{I} (m^3/s or L/s) (see Figures 8.8, 8.11, and 9.11).

The reduced parameters can be transferred easily into dimensionless forms. For this to occur it is necessary to refer the parameters not to $H(m)$ but to gH ($\mathrm{m}^2/\mathrm{s}^2$). The formulas, thus are

$$n'_{10} = \frac{nD}{\sqrt{gH}} \tag{5.36a}$$

$$Q'_{10} = Q/D^2\sqrt{gH} \tag{5.36b}$$

where index 0 indicates the dimensionless form.

The different forms of the reduced parameters or coefficients also find use in turbine practice:

n_{s0} can be described as the rotation speed 1/s of a given type of turbine with a diameter D_s, that under mass head gH equal to 1 m^2/s^2 its discharge Q_s is equal to 1 m^3/s.

Equation 5.38b is the universal form of specific speed, and can be applied to all types of hydraulic rotodynamic machines; e.g., turbines, pumps (see Equation 12.28b), and reversible pump-turbines. In the future this form may find a wide use. For the present, however, dimensional values of n_s are used in practice. Therefore, it is very important when dealing with concrete data of n_s to find out the dimensions in which they are given.

When discussing n_s, the values are viewed as numerical quantities without dimension. The quantities are measured in revolutions per miture (discussed in the Section in which the derivation of n_s is described).

Determining Q and n through reduced parameters, according to Equations 5.36 and 5.37, we get

$$n_s = 3.65 \frac{n'_{\mathrm{I}} \sqrt{H}}{D_1} \frac{\sqrt{Q'_{\mathrm{I}} D_1^2 \sqrt{H\eta}}}{H^{3/4}}$$

and, finally,

$$n_s = 3.65 n'_{\mathrm{I}} \sqrt{Q'_{\mathrm{I}} \eta} \tag{5.39}$$

The most important property is that the value of specific speed does not depend on the diameter of the turbine, thus, it is the compound characteristic of the turbine type. The specific speed is usually determined for a turbine operated under conditions that ensure a rated power. It fully specifies turbine properties, the form of the runner (i.e., the kind), and the type of turbine. For turbines of various types, the specific speed n_s (see Equations 5.38, 5.39) varies over the following ranges:

Turbines	n_s
Adjustable blade axial flow (Kaplan)	1200–450
Adjustable blade mixed-flow	500–300
Radial-axial (Francis)	400–80
Impulse (Pelton)	50–10

Looking at Figure 2.9 it is clear that the larger the head the less the specific speed of the turbine.

As mentioned previously, the specific speed value drastically influences turbine properties and their reduced parameters. This is proved by Figure 5.16, which represents the averaged connection between Q'_{I} and n'_{I} with n_s, determined according to Equations 5.38 and 5.39 for rated turbine head and power. The data are given for radial-axial (Francis) and for vertical adjustable blade (Kaplan) turbines with elbow-type draft tubes (Figure 2.2).

Example 5.5

For the planned hydroelectric power plant having a rated head $H = 60$ m and a unit rated power of 40,000 kW, turbines with specific speeds of 220 or 310 can be used. What will the difference be in parameters and what are the recommendations?

Solution

According to Equation 2.10, taking $\eta = 0.92$ for the rated conditions, the turbine discharge is

$$Q = \frac{N}{9.81H\eta} = \frac{40{,}000}{9.81 \times 60 \times 0.92} = 73.9\ \mathrm{m}^3/\mathrm{sec}$$

From Figure 5.16 the reduced parameters for given values of specific speed are

n_s	= 220	310
Q'_{I}	= 840	1230
n'_{I}	= 70	80

For $n_s = 220$ (from Equation 5.37)

$$D = \sqrt{\frac{Q}{Q'_{\mathrm{I}}\sqrt{H}}} = \sqrt{\frac{73.9}{0.84\sqrt{60}}} = 3.37\ \mathrm{m}$$

and from Equation 5.36

$$n = \frac{n'_{\mathrm{I}}\sqrt{H}}{D} = \frac{70\sqrt{60}}{3.37} = 160.9\ \mathrm{rpm}$$

For $n_s = 310$

$$D = \sqrt{\frac{73.9}{1.23\sqrt{60}}} = 2.9\ \mathrm{m} \qquad n = \frac{80\sqrt{60}}{2.9} = 213.7\ \mathrm{rpm}$$

Therefore, the larger the n_s, value the smaller the diameter, and accordingly all dimensions of the turbine, the higher the speed of rotation. Both factors are profitable; therefore, if we take into account only these factors, the option using $n_s = 310$ is preferable. (A further analysis can be found in Example 7.1.)

5.9. MODE OF WATER MOTION IN THE TURBINE RUNNER

Section 5.2 considers the conditions for the motion of an averaged flow in the turbine runner. It is now possible to obtain the relationship that specifies the torque of the runner and as well as the energy equation. Some peculiarities associated with water motion in the runner are elucidated below.

The main factor determining the pattern of flow in the runner is the interaction between the moving blade and water which creates the torque of the runner. First, we must discover the regularities governing the action of the water flow on the body exposed to it. Let us consider the simplest case: flow around an individual profile (aerofoil) by an infinite steady-state flow (plane problem). At an infinite length upstream of the profile, the water is in undisturbed flow, which is characterized by a constant velocity v_∞ (Figure 5.13a). As the flow approaches the profile its action on the flow becomes stronger, and this manifests itself in curving the flow stream lines, the change in the distance between them. The stream lines become more dense on top of the profile and more spaced beneath it. Inasmuch as the flow rate between two flow lines is constant (the line of flow may be conceived to be a rigid boundary), the velocities consequently increase atop the profile, as compared to v_∞, and decrease underneath the profile.

If we consider a perfect, or ideal, liquid moving without losses, and we assume pressure to be constant at infinity (pressure flow is considered), then according to Bernoulli's equation, pressure must drop at the

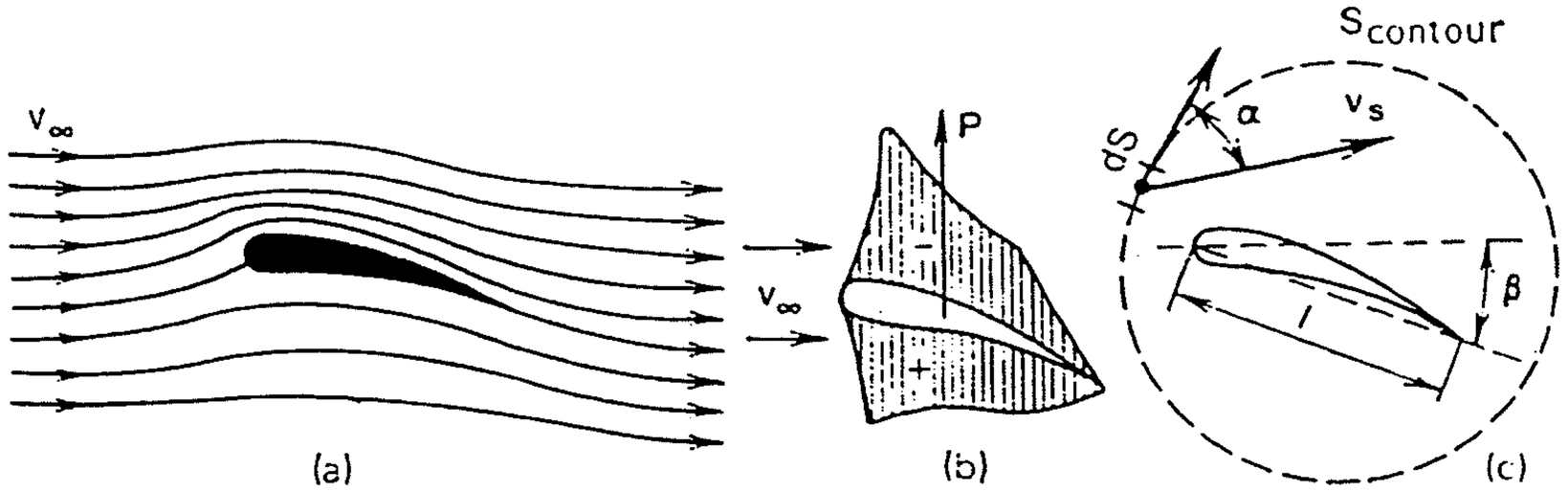


FIGURE 5.13. Flow around the aerofoil section.

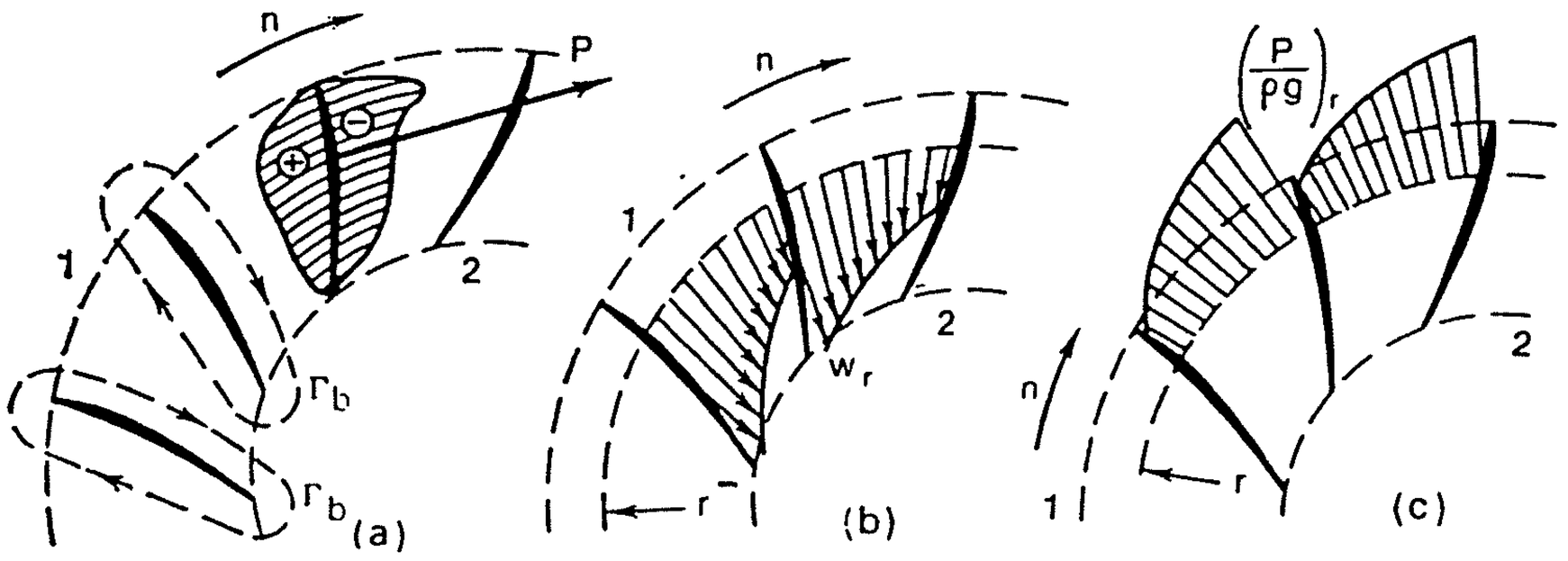


FIGURE 5.14. Flow in the blade space of the runner of the radial-axial flow turbine.

top of the profile, at the expense of a change in velocity, and increase underneath the profile. It is exactly this that is responsible for the action of flow on the profile (Figure 5.13b), the resultant P of which is the so-called lift force. It is clear that a similar lift force will appear if liquid is at rest and the profile moves within it at velocity v_∞.

The lift force per meter of the profile width is determined by the Kutta-Joukovski theorem:

$$P = \rho v_\infty \Gamma \tag{5.40}$$

where ρ is the density of the liquid (water, in this case); v_∞ is velocity; and Γ is the circulation created by the profile in the closed contour embracing it (Figure 5.13c), determined by Equation 5.2.

The principal conclusion that can be drawn from the Kutta-Joukovski theorem is that the action of the liquid on the profile exposed to it is determined by the velocity circulation created around the profile. In other words, for the flow to act on the profile exposed to it a circulation Γ must exist around this profile.

On the runner blades the resultant force P is directed toward the sense of rotation. P appears because of the difference in the pressures on the face and back sides of the blade (illustrated in Figure 5.14a).

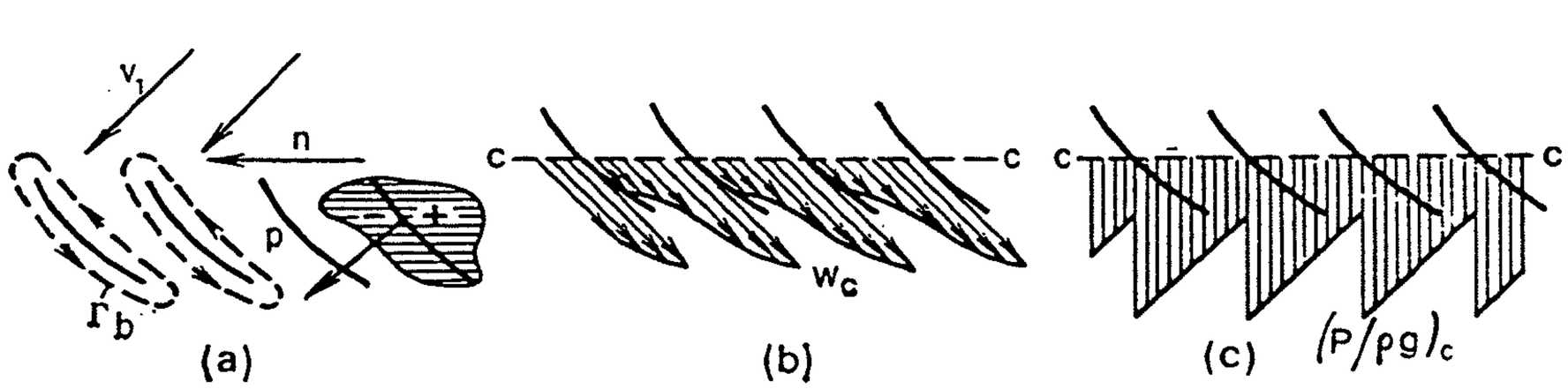


FIGURE 5.15. Flow in the blade space of the runner of the axial-flow turbine.

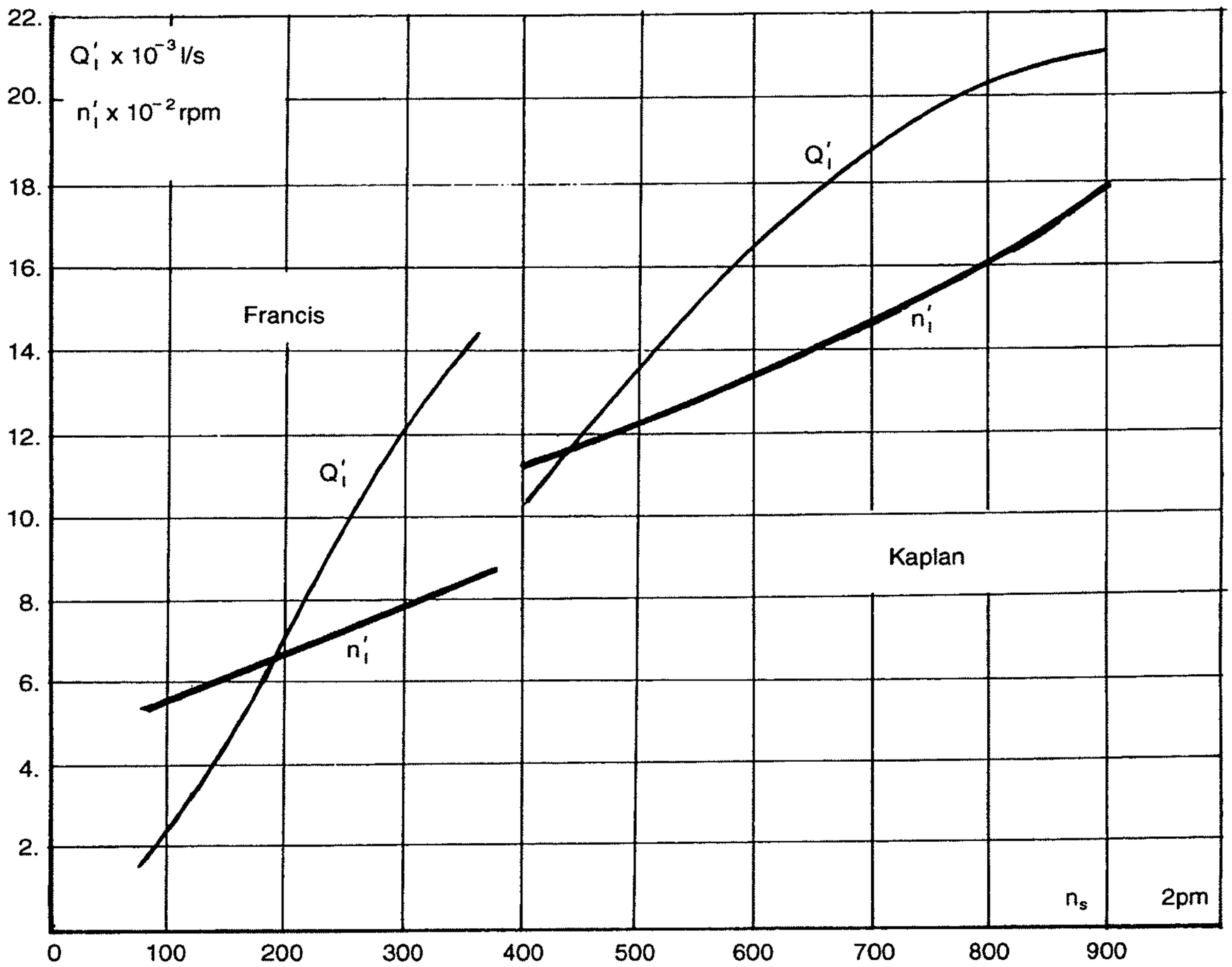


FIGURE 5.16. The dependence of reduced parameters from rated specific speed in turbines.

This is a result of the blade circulation, Γ_b, whose direction is shown by the dotted line in Figure 5.14. The summation of the common averaged flow, directed in radial-axial flow turbines from the periphery to the center, and the secondary flow caused by the circulation Γ_b, results in a decrease in the velocity of the liquid at the face of the blade, and increases at the back of the blade. This creates a difference in pressure on the blade. As a result water flows with a nonuniform velocity through the runner ducts—at a lower speed on the face side and at a higher speed at the back (Figure 5.14b); the pressures are nonuniform accordingly (Figure 5.14c).

A similar nonuniform distribution of velocities and pressures, caused by blade circulation Γ_b, exists in the runner ducts of axial-flow turbines (Figure 5.15a to c).

The considerable nonuniform flow in runner blades brings about greater hydraulic losses, and may also be responsible for pulsation and vibration.

The dependence of reduced parameters n'_I and Q'_I from rated specific speed is shown in Figure 5.16.

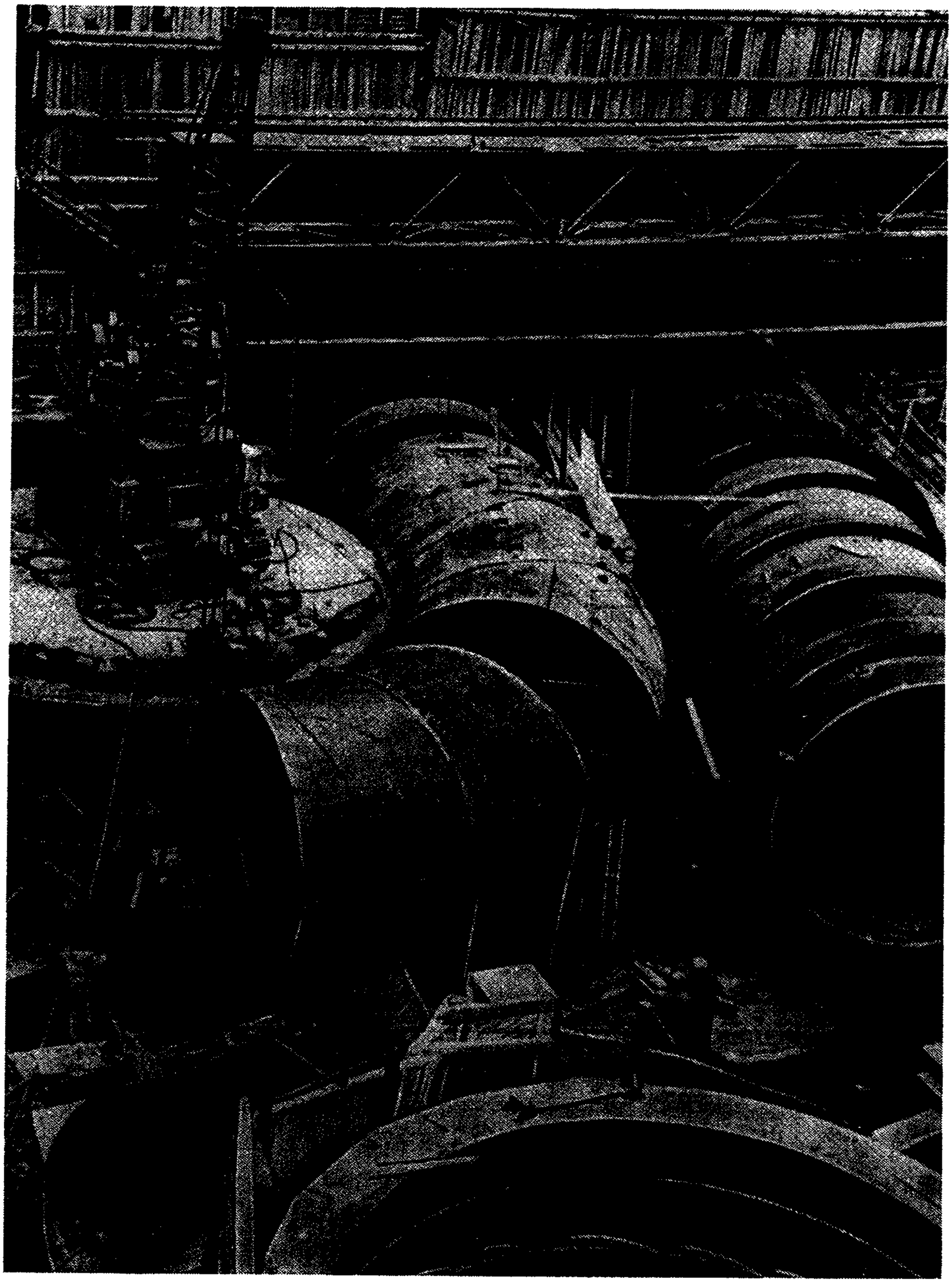


FIGURE 6.4. Erection of steel turbine cases.

6.1) is not satisfied, other solutions regarding the spiral case must be undertaken.

The most widespread designs of spiral turbine cases are those in which a fraction of the load constituted by the internal water pressure is transferred to the reinforced concrete of the powerhouse of the HEPP. Thus, the steel lining of the Nurek Hydro is designed to take up one

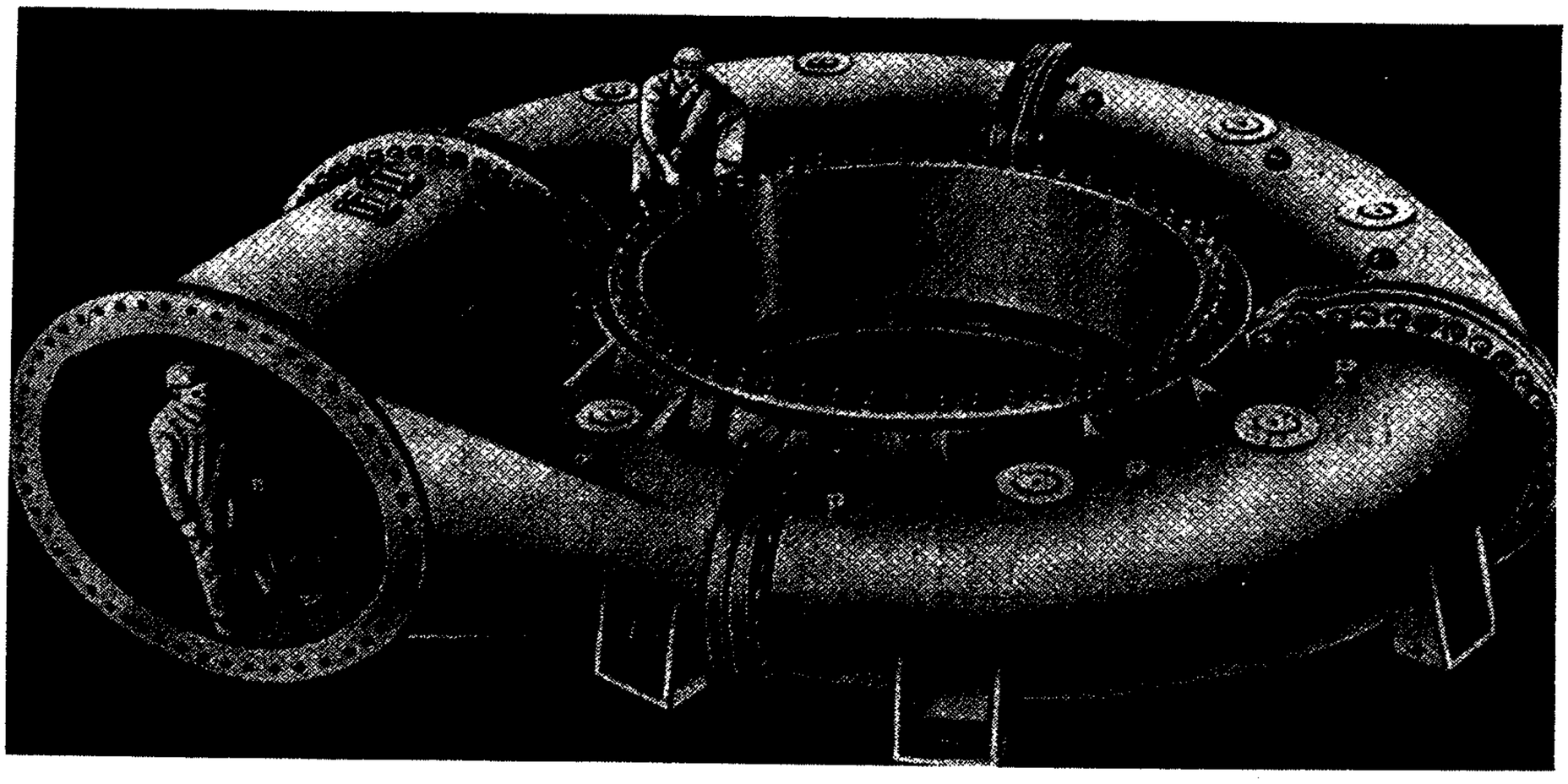


FIGURE 6.5. Steel cast turbine case of the Yabloniza Hydro.

third of the water pressure (with the hydraulic hammer amounts to 4 MPa), and two thirds of the load is taken up by reinforced concrete (provision is made for strong, annular reinforcing bars shown in Figure 1.4). This transfer of part of the load that acts upon the shell casing is employed in the turbines installed at the Sayano-Shushenskoye HEPP (Figure 3.15).

It is possible to use a two-pipeline spiral turbine case. The conceptual design of such a scroll elaborated for 7.5-m diameter turbines is illustrated in Figure 6.7. The special feature of this spiral case is that water is supplied to the turbine through two pipelines. Each joins with one half of the scroll that covers one half of the stayring. The diameter of the inlet sections of each of the two halves of the scroll will be almost 1.5 times smaller than when a common spiral case is used. The thickness of the steel plates from which the case is made will diminish accordingly.

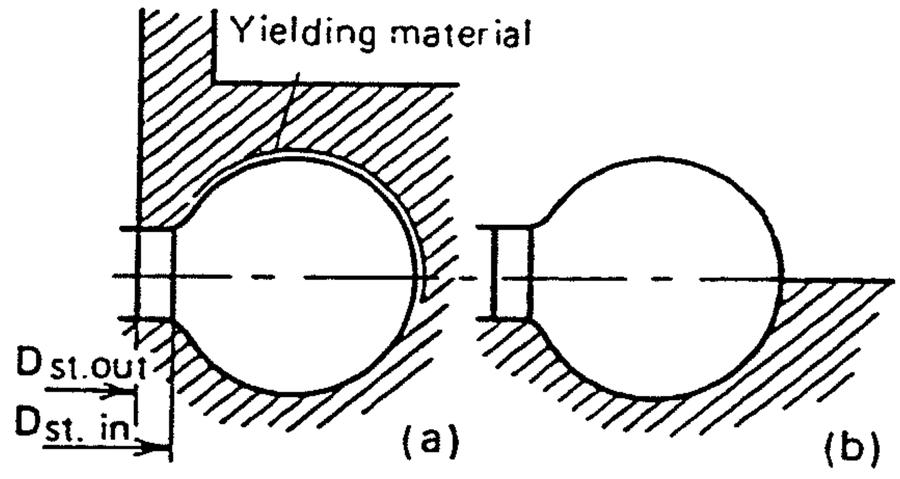


FIGURE 6.6. Installation of steel turbine cases.

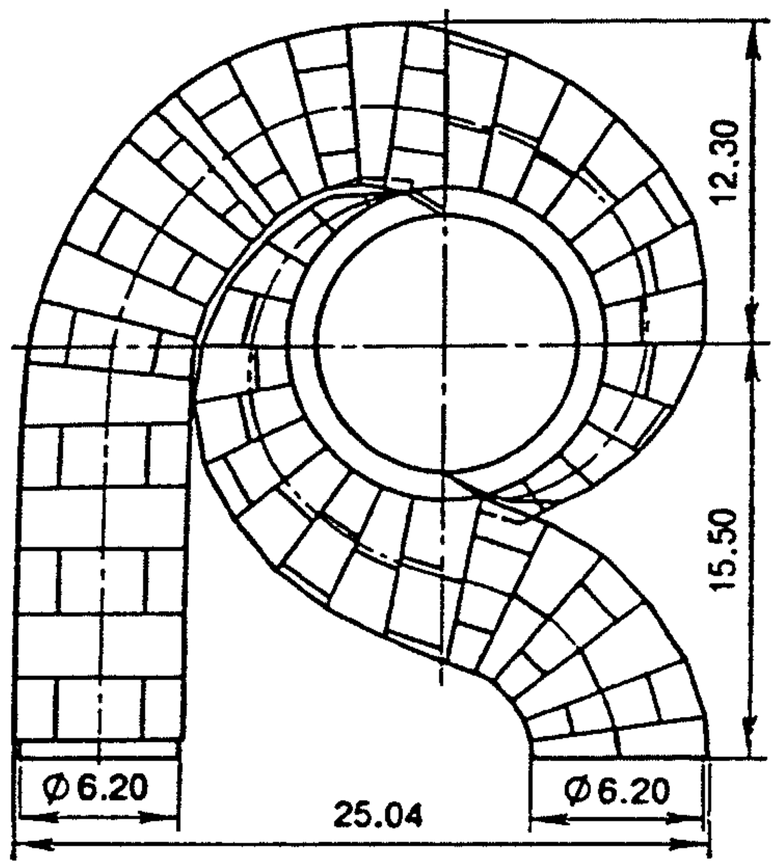


FIGURE 6.7. Two-pipeline spiral case.

Concrete turbine cases differ from the steel in that they have a trapezoidal cross-section and a lesser coverage angle φ_{cov} equal to 180° to 270°. It is clear from Figure 6.8 that φ_{cov} depends on the maximum turbine head H_{max}. Applications are known where lesser coverage angles $\varphi_{cov} = 135°$ were assumed. This was based on the requirement that the stayring be located in the middle of the powerhouse, in accordance with the layout of the house.

The height (b) (Figure 6.9) of the trapezium-shaped concrete cases is usually greater than the trapezium midline (a). This is done with the intention of diminishing the overall dimensions of the case, but primarily it is done to reduce the width (midline) B_{sp}.

Three forms of concrete turbine cases are distinguished: developed downward with a constant upper base elevation (Figure 6.9a); developed

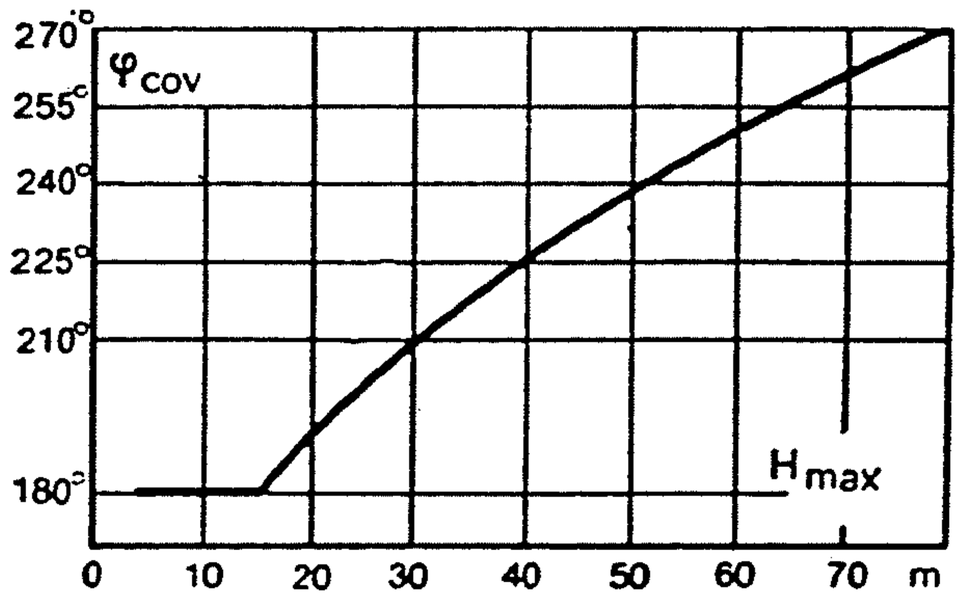


FIGURE 6.8. Coverage angle vs. head in concrete spiral cases.

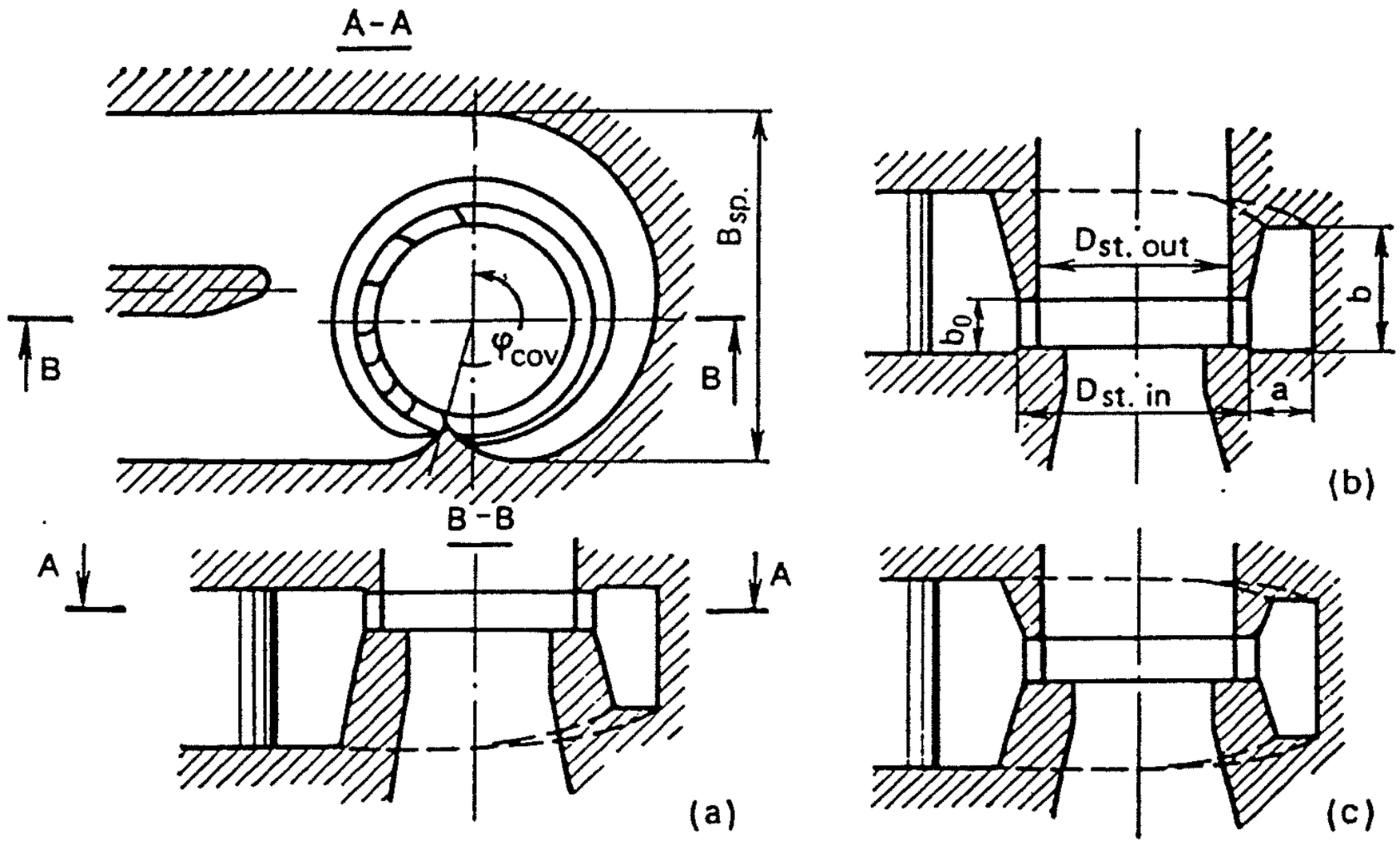


FIGURE 6.9. Concrete turbine cases.

upward with a constant elevation of the lower base (Figure 6.9b); and T-shaped with a variable elevation of the upper and lower bases (Figure 6.9c). The selection of a cross-section of a concrete turbine case is predetermined by the conditions of the most suitable layout of the HEPP powerhouse.

One of the essential features of concrete turbine cases is that water is supplied to a considerable part of the wicket gate perimeter directly from the water conduit. It is clear from Figure 6.9 that water is supplied to the stayring and guide vanes under less favorable conditions, due to an abrupt change in velocity direction in the stayring and guide vanes. To ensure better conditions under which water may enter the guide vanes, curvilinear stay vanes are arranged in the right quarter of the spiral in front of the baffle vane (Figure 6.9), with shorter distances between the stay vanes. The possible use (for low-head turbines) of rectangular-shaped turbine cases is occasionally considered, for such cases simplify the shape of construction elements and facilitate the use of prefabricated reinforced concrete elements.

Concrete spiral cases with heads over 50 m are lined with a facing constructed of 10- to 16-mm thick steelplates. This lining serves mainly as an antiseepage guard, but is accounted for when calculating the strength of the turbine case. The lining must be anchored securely in the concrete.

The design and size of the turbine case are determined by the turbine manufacturer; however, in designing a HEPP it is necessary to

determine the expected size of the turbine cases and to consider possible variations in the shapes and sizes of the cases to bring them into better compliance with the HEPP layout and it structural elements. With this in mind, the principles underlying the design of turbine cases are considered in the following. One of the most important parameters is the width of the turbine case, B_{sp}, whose relative magnitude is

$$\overline{B}_{sp} = B_{sp}/D_1$$

where D_1 is the turbine runner rated diameter. The dependence of the relative width on the design (rated) head H_r is plotted in Figure 6.10. The spread of points corresponding to some HEPPs is great. Especially in the case of concrete turbine cases, the spread is primarily associated with the difference in the shape of the cross-sections.

Because the turbine case directly abuts on the stayring it is necessary to know its dimensions (characterized by the relative height $\overline{b}_0$) and the relative diameters, where the inlet and outlet tips of the stay vanes are located, $\overline{D}_{st\cdot in}$ and $\overline{D}_{st\cdot out}$, $\overline{D}_{st\cdot in} = D_{st\cdot in}/D_1$, and $\overline{D}_{st\cdot out} = D_{st\cdot out}/D_1$ (Figures 6.6 and 6.9). The height $\overline{b}_0$ given on the outline drawings of turbines depends on their types. The size of the stayring changes, but not as strongly. For turbines operated with concrete cases $\overline{D}_{st\cdot in} = 1.5$ to 1.55 and $\overline{D}_{st\cdot out} = 1.3$ to 1.35; greater values are at $D_1 < 4.0$ m. For turbines with steel spiral cases $\overline{D}_{st\cdot in} = 1.55$ to 1.64 and $\overline{D}_{st\cdot out} = 1.33$ to 1.37; greater values pertain to $D_1 < 3.2$ m. In addition, for heads over 100 m, $\overline{D}_{st\cdot out}$ and $\overline{D}_{st\cdot in}$ increase by 0.03 to 0.07.

The basic condition for the hydraulic design of a turbine case is a uniform rate of water flow into the stayring and the wicket gate over the entire perimeter. It follows from the above that the flow rate Q_φ through a given section of the spiral determined by the angle φ (Figure

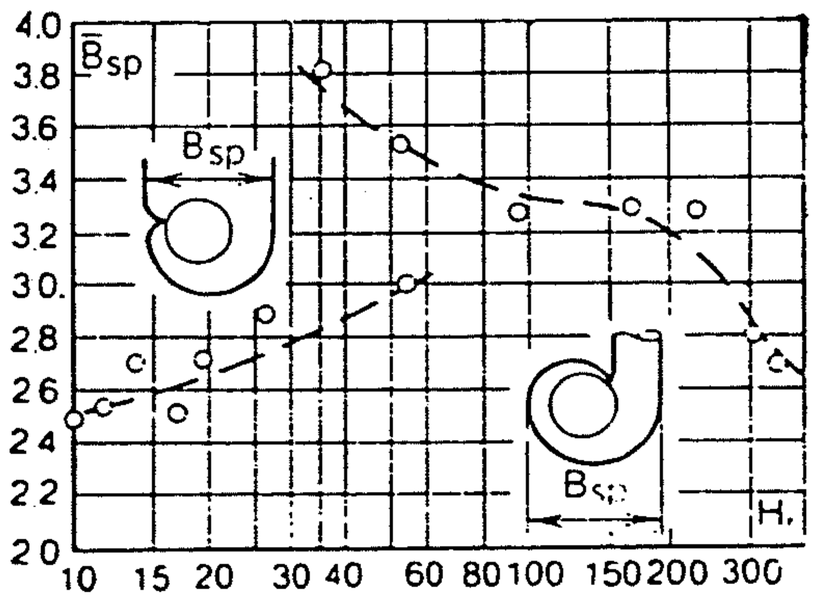


FIGURE 6.10. Turbine case width vs. head.

6.11) will be expressed by

$$Q_{\varphi} = Q\frac{\varphi}{360^{\circ}} \tag{6.2}$$

Here, Q is the total turbine discharge, and φ is the angle measured from the end of the spiral tooth. The rate of water flow through the inlet section of a turbine spiral case is

$$Q_{sp\cdot in} = Q\varphi_{\text{cov}}/360^{\circ} \tag{6.2a}$$

The dimensions of sections of a spiral case are determined on the basis of two hypotheses: (1) by the given values of the average peripheral component of velocity $v_{u.av}$ and (2) by the given direction of flow velocity at outlet diameter of the staryring $D_{st.out}$, i.e., directly in front of the wicket gate. Let us consider the design methods based on each of the hypotheses.

6.1.2.1. Design of the Average Velocities

This is carried out either by the law of constancy of the average velocity

$$v_{u.av} = v_{sp.in} = \text{const}$$

where $v_{sp.in}$ is the average velocity in the inlet section of the spiral 0–0 (Figure 6.11) or by the law of decreasing average velocity

$$v_{u.av} = f(\varphi)$$

where $v_{sp.av}$ diminishes with decreasing φ as shown in Figure 6.12.

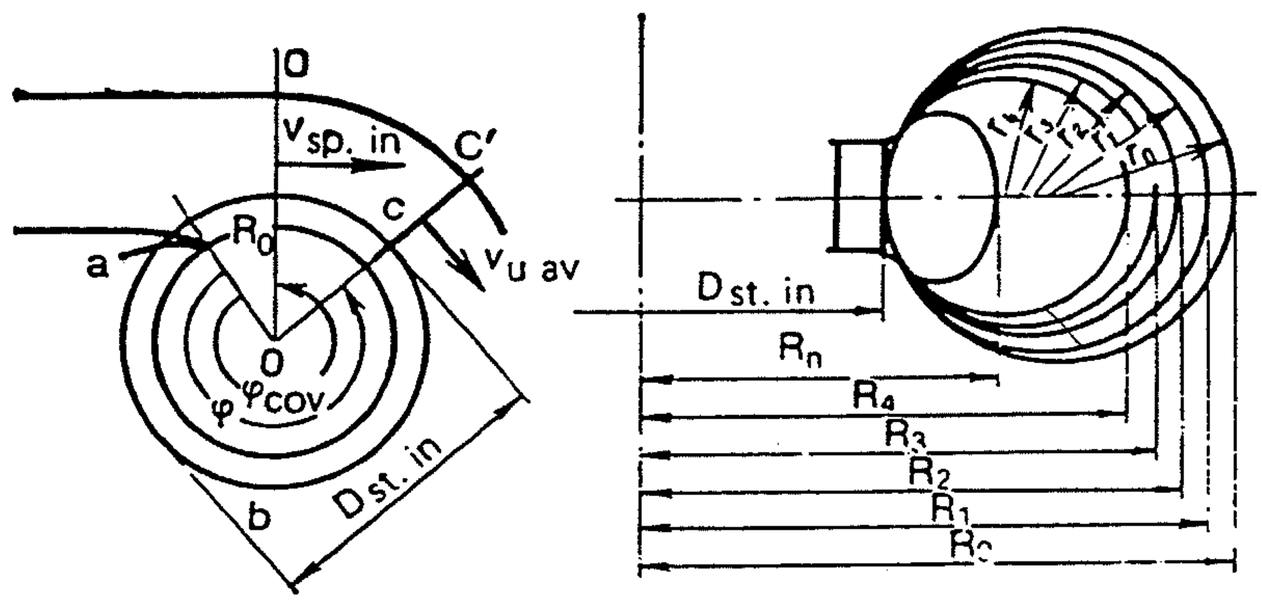


FIGURE 6.11. Calculating the metal spiral case.

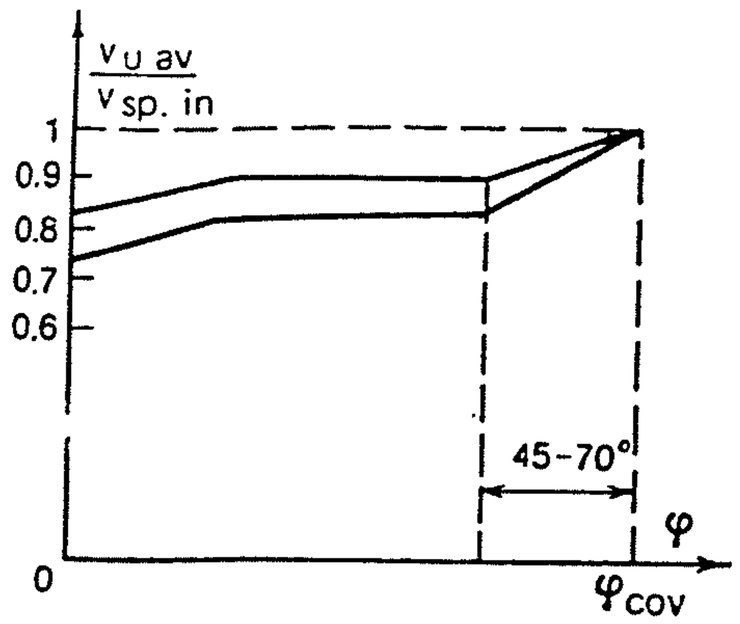


FIGURE 6.12. Reduction of average velocity along spiral.

It is preferable to have a higher average velocity in the inlet section, $v_{sp.in}$, because this results in decreasing dimensions of the spiral turbine case; however, at the same time, with excessive increase of $v_{sp.in}$ the losses rise considerably (the efficiency diminishes) and the discharge capacity of the turbine drops. The curve $v_{sp.in} = f(H_r)$, where H_r is the rated turbine head plotted on the basis of current experience, is illustrated in Figure 6.13. The design of the spiral that is based on decreasing average velocity (Figure 6.12) makes it possible to increase $v_{sp.in}$ by 10 to 20% (the greater values pertain to concrete turbine cases) as compared to Figure 6.13. No noticeable deterioration occured in the power-generating characteristics of the turbine.

With a known variation in average velocity along the spiral, it is possible to find the corresponding area of the meridional section of the spiral turbine case

$$\mathbf{F}_{\varphi} = \frac{Q_{\varphi}}{v_{u.av}(\varphi)360^{\circ}} \tag{6.3}$$

and in the case where $v_{u.av}$ = const, it is assumed that $v_{u.av} = v_{sp.in}$.

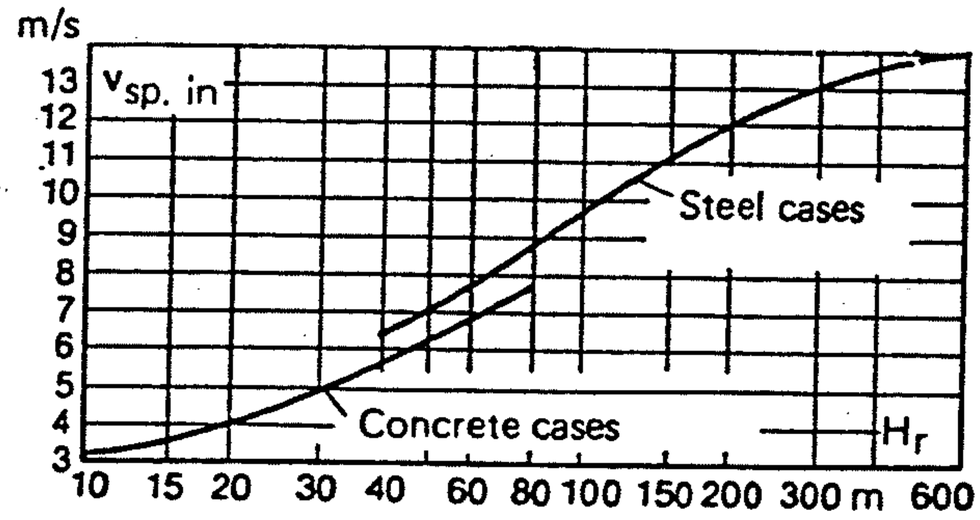


FIGURE 6.13. Spiral inlet cross-section average velocity vs. head.

The overall dimensions of a steel spiral turbine case with a round cross-section are easily determined: different values of the angle φ are assumed and corresponding areas and radii are calculated for each angle (Equation 6.3)

$$r_\varphi = \sqrt{F_\varphi / \pi}$$

The circumferences (circles) of the sections are described in such a way that they touch the upper and lower stayring bands, as shown in Figure 6.11.

For concrete spiral cases, first, the coverage angle φ_{cov} is determined (Figure 6.8), and using Equation 6.3, assuming $\varphi = \varphi_{cov}$ and $v_{u.av} = v_{sp.in}$ (Figure 6.13), the area of the inlet section of the spiral $F_{sp.in}$ is calculated. The form of the cross-sectional area (Figure 6.9) is selected and the inlet section is drawn on the basis of the layout of the powerhouse. In so doing, the following conditions are taken into account: $b_0/a_0 \leq 2$ to 2.5, the angles δ_1 and δ_2 are assumed equal to 15° to 30° (Figure 6.14). It is necessary to adopt a common method of plotting the intermediate sections. The method is preset by curves formed as the vertical wall intersects the top and the bottom. Three alternatives are possible (Figure 6.14d): sections (a) uniform decrease in the height and width; (b) a more rapid decrease in the height; and (c) a more rapid decrease in the width. Form (c) is the most squeezed and form (b) is the widest.

It is convenient to construct a concrete spiral case by plotting it as shown in Figure 6.15. Take the value of φ_{cov} (Figure 6.8), and using Equation 6.3, find the area

$$F_{sp.in} = \frac{Q_{\varphi_{cov}}}{v_{sp.in} 360°} \tag{6.3a}$$

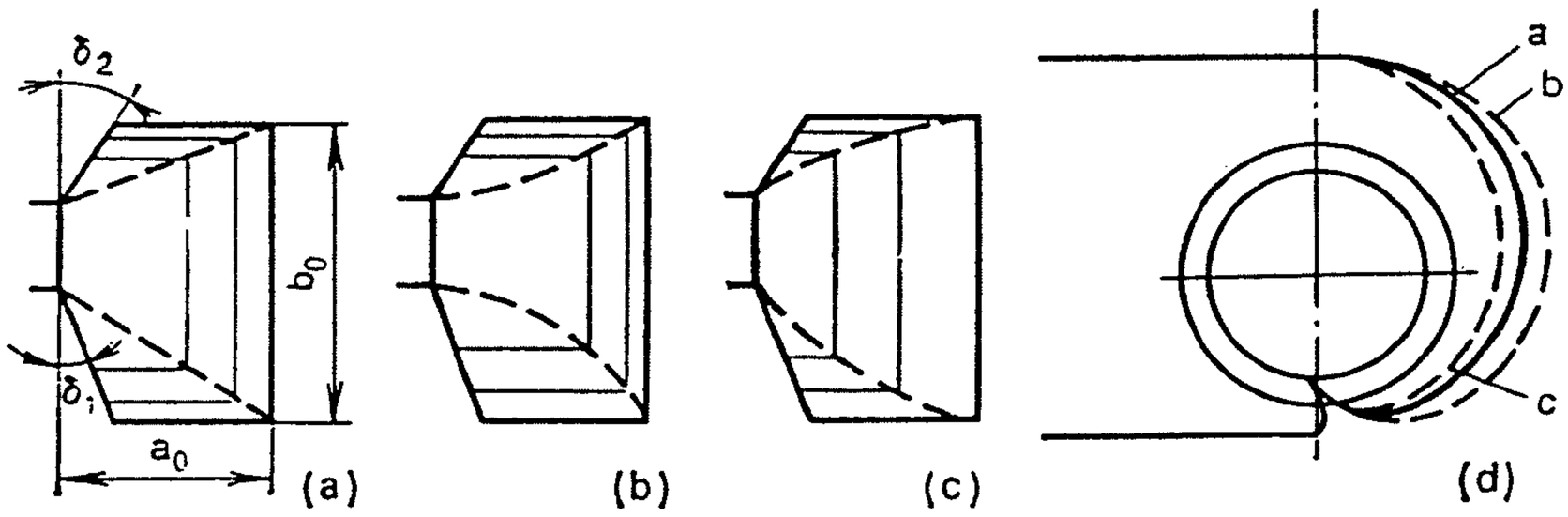


FIGURE 6.14. Designing intermediate cross-sections of concrete spiral cases.

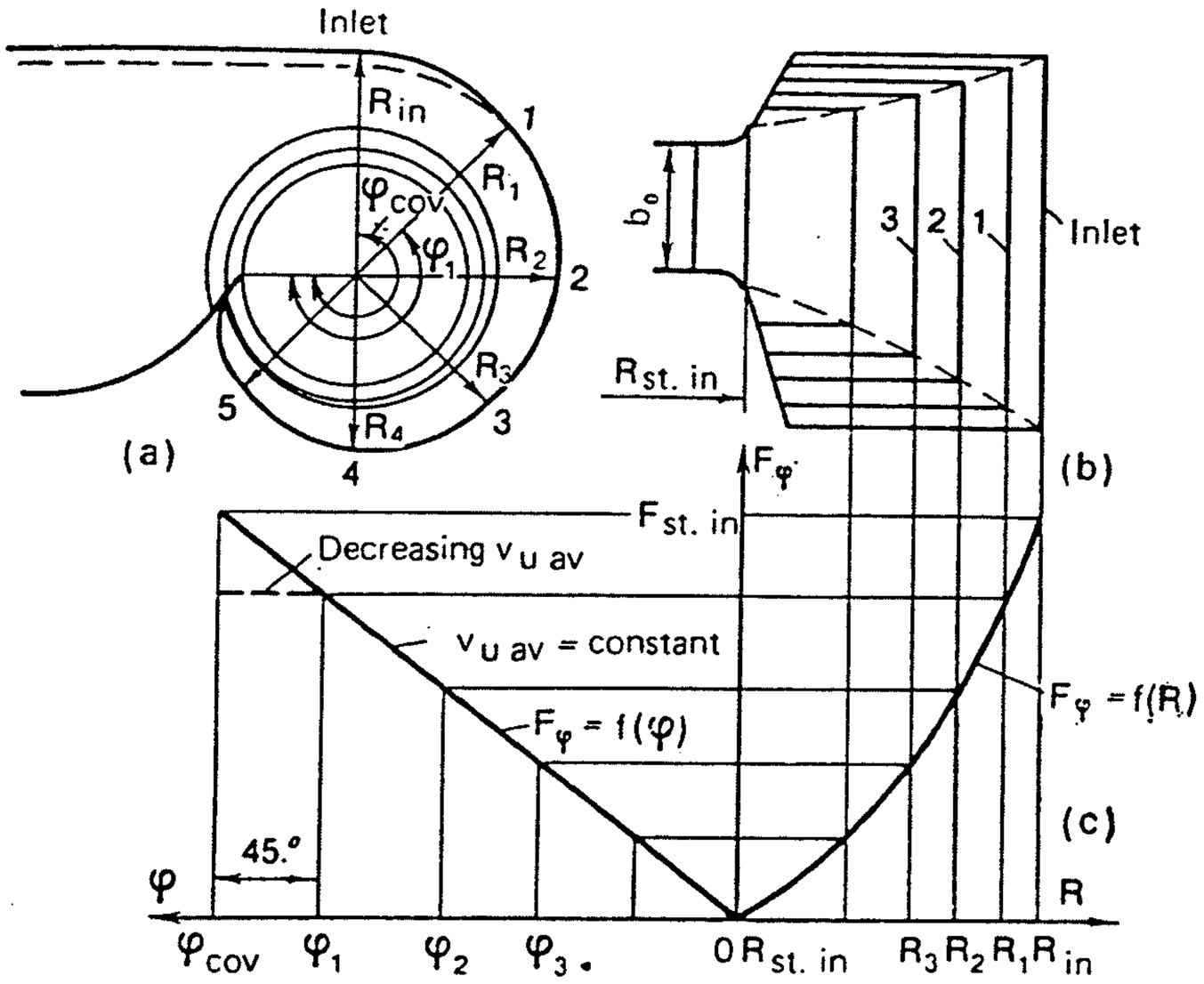


FIGURE 6.15. Graph for determining dimensions of concrete spiral cases.

According to the conditions governing the layout of the powerhouse of the HEPP, the form and dimensions of the inlet section are selected in accordance with $F_{sp.in}$. By the known dimensions of the stayring ($R_{st.in}$ and b_0), the "found" section is plotted (inlet in Figure 6.15b). Selecting the law governing the variation of the section lengthwise (dotted lines), we plot several intermediate sections (1, 2, 3, . . .). A twin chart is plotted underneath the section (Figure 6.15c): $F_\varphi = f(R)$ and $F_\varphi = f(\varphi)$, according to Equation 6.3. Projecting the intermediate sections on the curves of the twin chart, the corresponding values of $R_1, R_2, \ldots$ and $\varphi_1, \varphi_2, \ldots$ that permit plotting the spiral in plan (Figure 6.15a) are determined.

If the size of the inlet section must be decreased, use then can be made of the law of decreasing velocity at an angle of about 45° (shown by the dotted line in Figure 6.15a).

6.1.2.2. Design of a Spiral Case Based on Velocity Direction

This design is based on a given inlet velocity direction at the wicket gate with account taken of the nonuniform distribution of velocities over the section. Entering the spiral, as is clear from Figure 6.16a, the flow possesses a moment of velocity about the center 0. This makes it possible to apply to the water flow through the spiral case the law of constance of the velocity moment (Equation 5.4) in accordance with

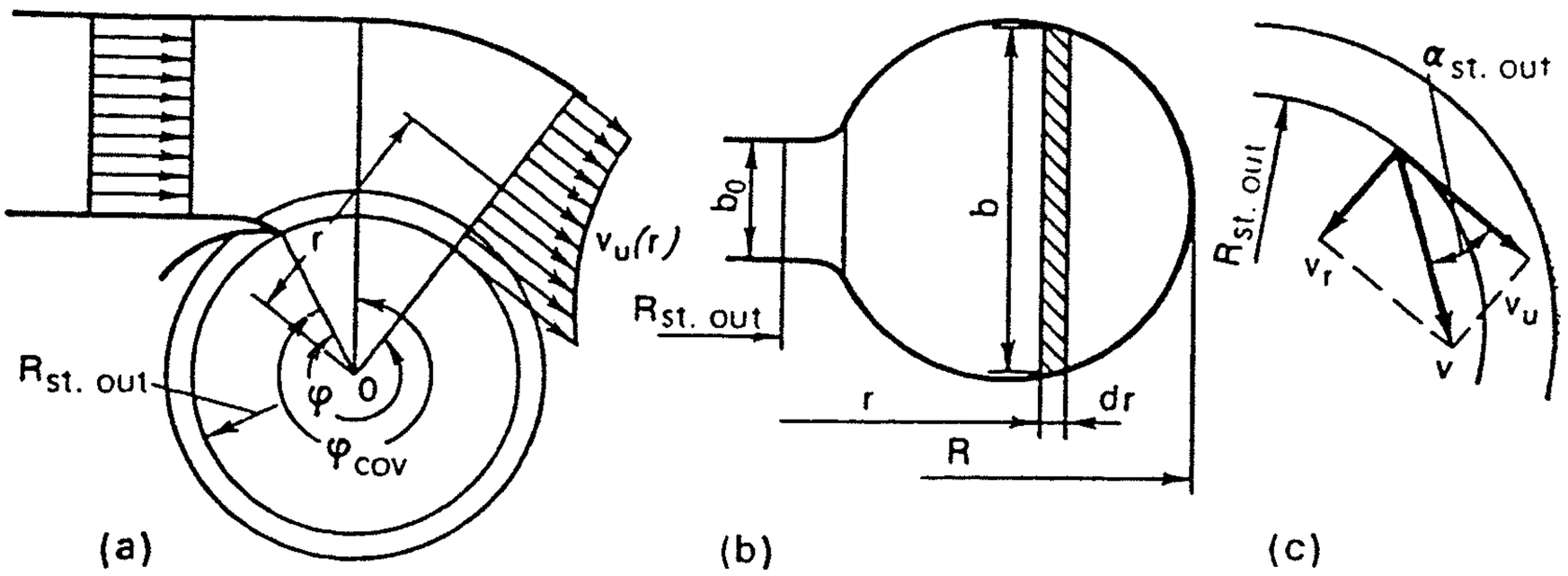


FIGURE 6.16. Calculating the spiral case according to the assigned direction of velocity at the inlet to the wicket gate.

which

$$v_u = K/r \tag{6.4}$$

The factor K is constant. According to Equation 6.4, the velocity distribution curve $v_u(r)$ is a hyperbola. The factor K may be determined by the discharge Q_φ with account taken of Equation 6.2 and Figure 6.16b:

$$Q_\varphi = \frac{Q\varphi}{360^\circ}\int_{R_{st.out}}^{R} v_u b(r)\,dr = K\int_{R_{st.out}}^{R}\frac{b(r)}{r}\,dr \tag{6.5}$$

where $b(r)$ is the height depending on r.

Then we find

$$K = \frac{Q\dfrac{\varphi}{360^\circ}}{\displaystyle\int_{R_{st.out}}^{R}\frac{b(r)}{r}\,dr} \tag{6.6}$$

The average radial velocity component v_r at the stayring outlet is specified by the expression

$$v_r = \frac{Q}{\pi D_{st.out} b_0} \tag{6.7}$$

Of the greatest importance is the direction of velocity at the inlet of the wicket gate, $v_{st.out}$, i.e., the angle $\alpha_{st.out}$ (Figure 6.16c), which, with account taken of Equations 6.4 to 6.7, is specified from

$$\tan \alpha_{st.out} = \frac{v_r}{v_u} = \frac{QR_{st.out}}{\pi D_{st.out} b_0 K} = \int_{R_{st.out}}^{R} \frac{b(r)}{r}\, dr \Big/ \left(2\pi b_0 \frac{\varphi}{360^\circ}\right) \quad (6.8)$$

Formula 6.8 indicates that:

1. the angle $\alpha_{st.out}$ is independent of the discharge Q;
2. with a constant K the angle $\alpha_{st.out}$ preserves a constant value over the entire perimeter of the wicket gate; and
3. the angle $\alpha_{st.out}$ depends on the form and size of the spiral case.

It is common practice to design spiral cases at $\alpha_{st.out}$ = const with that angle selected so that it coincides with the angle of the guide vanes at the most important mode of turbine operation.

The required dimensions of the turbine case are calculated in the following manner: The inlet section $F_{sp.in}$ is determined from Equation 6.3 for preset dimensions of the stayring and the accepted φ_{cov}; it is possible to take $v_{sp.in}$ with the aid of Figure 6.13a. The shape and size of the inlet section are chosen, and for this section (using Equation (6.6), we find the factor K substituting in the formula the angle φ_{cov} for φ. Equation 6.8 is used to check the angle $\alpha_{st.out}$ and the dimensions of the section are corrected until this angle coincides with the required one; this will determine the final value of K. Then we construct several intermediate sections, as shown in Figure 6.15b, and for each of them the discharge Q_φ is calculated from Equation 6.5.

Knowing Q_φ it is easy to find the corresponding angle φ using Equation 6.2. This specifies the position of the given section and makes it possible to draw the plan view of the spiral. The design of the spiral case is carried out in this way with K = const. It has been suggested that lesser values of $\alpha_{st.out}$ be assumed as compared to its optimal value at an angle $(\varphi_{cov} - \varphi) \leq 45^\circ$ to 60°. This allows a decrease in the size of the inlet section without appreciable deterioration of the power-generating characteristics.

6.2. DRAFT TUBES

In reaction turbines after-the-runner water flows through a draft tube and is discharged into the tailwater (TW) pool. The draft tube materially affects the power-generating properties of turbines, espe-

cially low-head turbines. In addition, the draft tube determines the dimensions of the lower part of the powerhouse of a HEPP and the elevation of the base. Great attention is thus devoted to the determination of the form and dimensions of draft tubes in designing HEPPs.

6.2.1. Performance

Consider the hydraulic characteristics of draft tubes. The average velocity at the inlet of the draft tube, v_2 (section 2–2 in Figure 6.17), depends on the mode of turbine operation and is determined by the parallelogram of outlet velocities (Figure 5.8). Let us determine the absolute pressure in section 2–2 when the turbine is in operation, $p_{a2}/\rho g$. To this end we set up Bernoulli's equation for sections 2–2 and 5–5 (outlet section) about the TW pool

$$\frac{p_{a2}}{\rho g} + z_2 + \frac{\alpha_2 v_2^2}{2g} = \frac{p_{a5}}{\rho g} + z_5 + \frac{\alpha_5 v_5^2}{2g} + h_{suc}$$

where $p_{a5}/\rho g = h_5 + p_{atm}/\rho g$ (h_5 is the depth of section 5–5 below the level of the TW pool); p_{atm} is atmospheric pressure; $z_5 = -h_5$; h_{suc} are the hydraulic losses in the draft (suction) tube.

The installation height of a turbine with respect to the TW level, referred to as the suction height H_s, is measured from a definite turbine plane (Fig. 7.9). With no great error we may assume that $z_2 = H_s$.

Then, Bernoulli's equation yields

$$\frac{p_{a2}}{\rho g} = \frac{p_{atm}}{\rho g} - \left(H_s + \frac{\alpha_2 v_2^2}{2g} - \frac{\alpha_5 v_5^2}{2g} - h_{suc} \right) \tag{6.9}$$

The result obtained shows that the draft tube creates a lower pressure (vacuum) underneath the turbine runner, the vacuum being the sum of

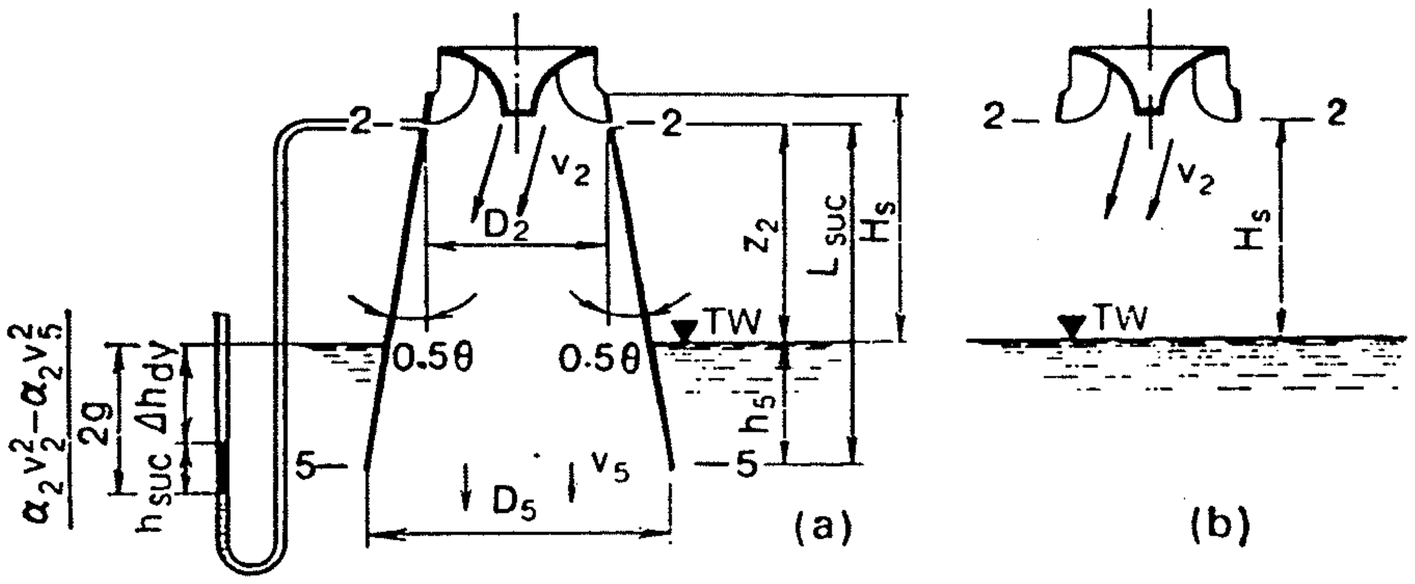


FIGURE 6.17. Hydraulic characteristics of draft tubes.

two parts: static fall of pressure, H_s, which is independent of the discharge and dynamic fall of pressure

$$\Delta h_{dy} = \frac{\alpha_2 v_2^2}{2g} - \frac{\alpha_5 v_5^2}{2g} - h_{suc}$$

which is specified in the main by the diffusion action of the draft tube and increasing it with a rising flow rate.

The power-generating characteristics of the draft tube are described next. The average specific energy of water, e_2, in section 2–2 in Figure 6.17 with respect to the TW pool is determined from the trinomial

$$e_2 = \frac{p_2}{\rho g} + z_2 + \frac{\alpha_2 v_2^2}{2g} \tag{6.10}$$

where $p_2/\rho g = p_{a2}/\rho g - p_{atm}/\rho g$ and α_2 is the nonuniformity factor (of Coriolis) determined from Equation 1.5.

The energy e_2 with which water leaves the runner cannot be utilized by the turbine and must be regarded as a loss. The tendency is to reduce e_2 and thus to increase the turbine efficiency. The specific energy e_2 is reduced by the draft tube, which is a smoothly widening diffusor. Substitution of $p_2/\rho g$ from Equation 6.9 into expression 6.10 for e_2 gives

$$e_2 = -\left(H_s + \frac{\alpha_2 v_2^2}{2g} - \frac{\alpha_5 v_5^2}{2g} - h_{suc}\right) + H_s + \frac{\alpha_2 v_2^2}{2g} \tag{6.11}$$

and, finally,

$$e_2 = \frac{\alpha_5 v_5^2}{2g} + h_{suc} \tag{6.12}$$

The result obtained is rather interesting. It appears that in the presence of a draft tube the lost energy e_2 consists of outlet losses $\alpha_5 v_5^2/2g$ and internal losses h_{suc}. The lost energy e_2 can be diminished by increasing the outlet cross-sectional area F_5 (this results in the reduction of v_5); however, in such a case, the losses h_{suc} must not increase too much. These losses are specified by two factors: the friction on the walls, which is comparatively small, and vorticity losses caused by the diffusivity.

With axial flow continuous water flow is ensured. Here, minimal losses are suffered and the taper (cone) angle θ must be small ($\theta < 8°$), or from one side $0.5\theta < 4°$, as shown in Figure 6.17. In turbines θ may be increased to 12° to 14° and more without causing greater loss and

gaining some reduction of the losses. This can be achieved if the flow downstream of the runner and at the inlet into the draft tube is not axial but slightly twisted. We can achieve this by selecting suitable operating conditions when the angle $\alpha_2 \neq 90°$, and criteria $\Gamma_2 \neq 0$ (some deviation from said normal exit condition). Then the appearing centrifugal forces prevent flow separation from the walls.

If a reaction turbine with a positive suction head ($H_s > 0$) can operate without a draft tube (Figure 6.17b) and the water is discharged into the atmosphere with velocity v_2 and falls into the TW pool, the exit energy e_2 will be:

$$e'_2 = \frac{\alpha_2 v_2^2}{2g} + H_s \tag{6.13}$$

Comparing Equation 6.13 to 6.12 we find that the draft tube increases the energy used by the turbine by

$$\Delta H_{suc} = H_s + \frac{\alpha_2 v_2^2}{2g} - \frac{\alpha_5 v_5^2}{2g} - h_{suc} \tag{6.14}$$

From Equation 6.14 it follows that the draft tube permits

1. complete utilization of the energy corresponding to the turbine installation height above the TW level (it is of importance only at $H_s > 0$); and
2. the use of a considerable fraction of water kinetic energy at the runner outlet.

The efficiency, or recovery factor, of a draft tube η_{suc} is specified by the following expression:

$$\eta_{suc} = \frac{\frac{\alpha_2 v_2^2}{2g} - \frac{\alpha_5 v_5^2}{2g} - h_{suc}}{\frac{\alpha_2 v_2^2}{2g}} \tag{6.15}$$

For good draft tubes of a great length η_{suc} reaches 85 to 90%.

Estimate what fraction of the total energy made available to a turbine belongs to the kinetic energy of water flow downstream of the runner. This fraction is specified by the ratio

$$\frac{e_{2kin}}{H} = \frac{\alpha_2 v_2^2}{2gH} \tag{6.16}$$

The approximate dependence of e_{2kin}/H on the head for complete turbien power is plotted in Figure 6.18. As is seen in the figure, the kinetic energy downstream of the runner in low-head turbines may be equal to 50 to 90% or even more of the total energy H; only in high-head turbines is it equal to $< 10\%$ at $H > 100$ m. It follows that the possibility of using (restoring) the kinetic energy e_2 determines to a great extent the effectiveness of turbines, and indicates the great importance of draft tubes, especially at low heads.

6.2.2. Types of Draft Tubes

6.2.2.1. Straight Draft Tubes

The simplest is the conical draft tube (Figures 6.17a and 6.19a) that possesses good power-generating characteristics; however, the tube must be of a considerable required length L_{suc}. For high-power vertical turbines this makes it necessary to construct the base at a considerable depth, which results in a greater cost for the HEPP. With this in mind, draft tubes of this type find application only in small-power turbines.

Other types of straight draft tubes are depicted in Fig. 6.19. The effectiveness of a conical draft tube may be somewhat increased and its length reduced by making use of the curvilinear generating line (Figure 6.19a). A further development of this idea leads to the so-called flare-type draft tube (Figure 6.19b), whose outlet section 5–5 is cylindrical. To improve the performance of the flare-type draft tube it is advisable

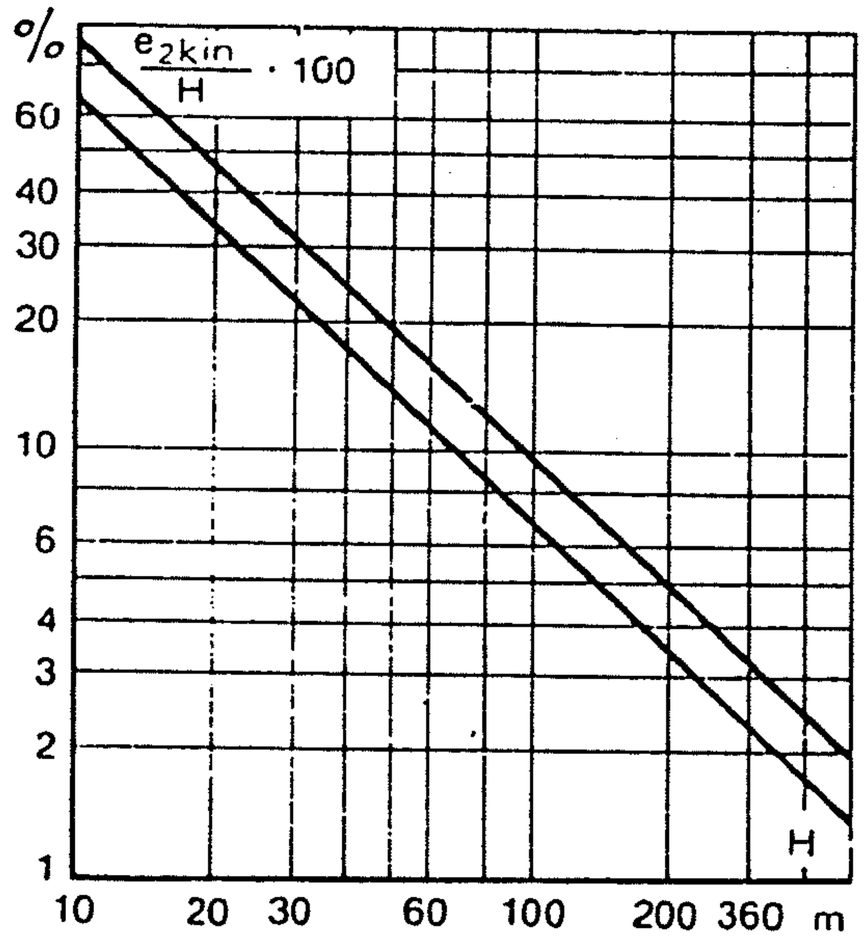


FIGURE 6.18. Relative kinetic energy downstream of runner vs. turbine head.

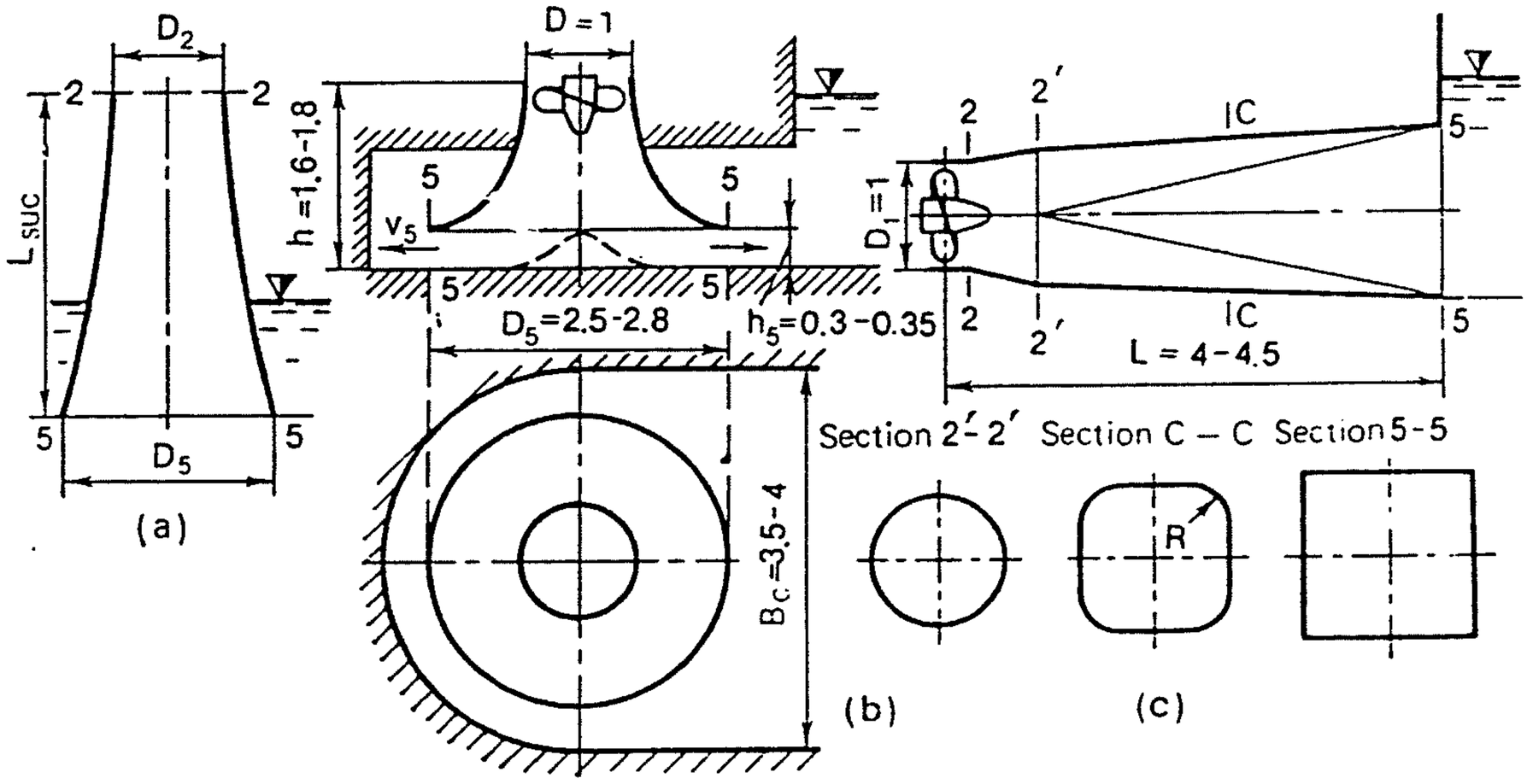


FIGURE 6.19. Straight draft tubes.

to construct a conoid by the center of such a tube (shown by the dotted line). Up to the present, these tubes have not found wide application.

Horizontal turbines, especially bulb-type machines (Figure 3.9) are operated with straight draft tubes (Figure 6.19c). The tube is round between sections 2–2 and 2′–2′ and a smooth transition to a square or rectangular form is effected toward the exit section 5–5. Investigations have shown that the transition from round to square or rectangular forms must be effected over a great distance. In this case the cone angle θ must not exceed 14° to 16°. In the last few years all-length round draft tubes have been used on some plants.

The average cone angle θ at the middle is determined by reducing the cross-sectional area to a circle. For instance, for the tube shown in Figure 6.19c, between the sections 2′–2′ and 5–5 $(L_{2-5})F_{2'} = \pi D_{2'}^2/4$ and $F_5 = h_5 B_5 = \pi D_5^2/4$, where $D_{2'}$, and D_5 are the reduced diameters and h_5, B_5 the height and width of exit 5–5 section. Then

$$\theta = 2 \arctan \frac{\sqrt{F_5} - \sqrt{F_{2'}}}{\sqrt{\pi} L_{2'-5}} \tag{6.17}$$

6.2.2.2. Elbow-Type Draft Tubes

These are used in almost all HEPPs where high-power vertical turbines operate (Figures 2.2 and 2.4). Such a draft tube (Figure 6.20) comprises three main parts: (A) cone, (B) elbow, and (C) discharge

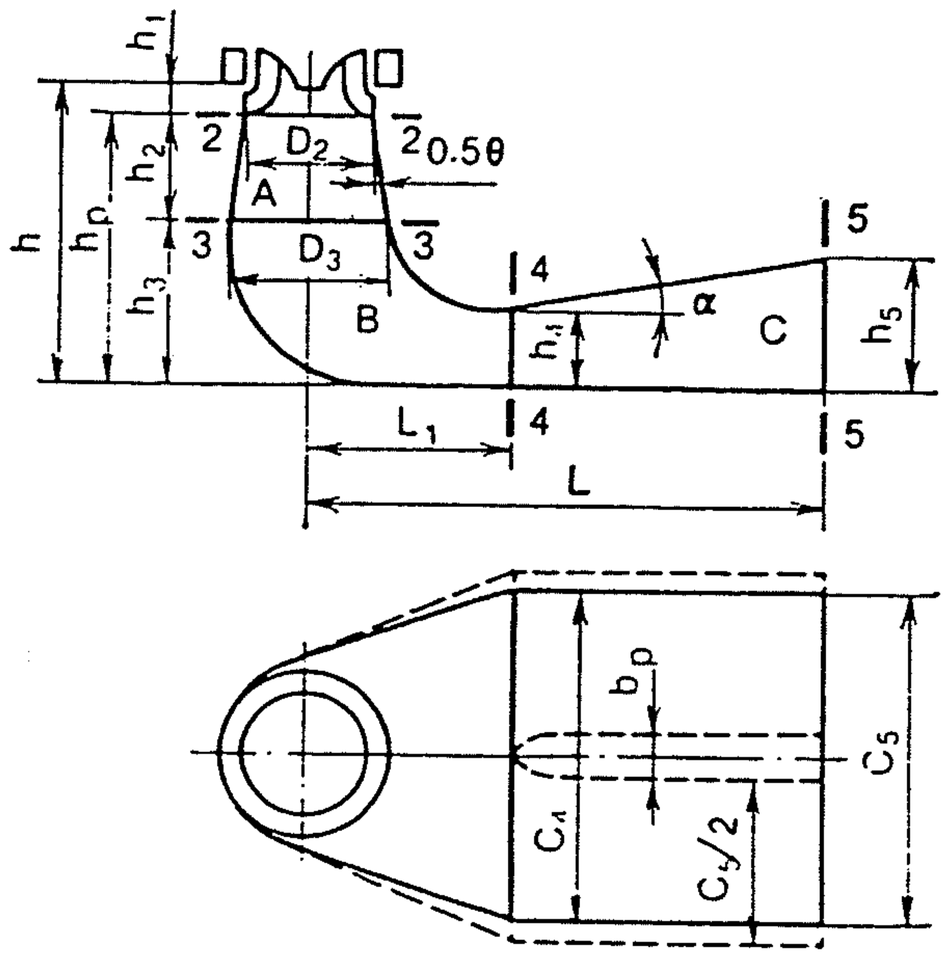


FIGURE 6.20. Elbow-type draft tube.

diffuser. Within the limits of the cone the cross-sectional areas are round, then follow a smooth change to rectangular cross-sections with a more rapid increase in the width. The rectangular sections are preserved in the diffuser, with the cross-sectional area increasing at the expense of the height (the top of the diffuser has a slope angle α).

The most characteristic dimension of the elbow-type draft tube is the height h, taken from the bottom of the wicket gate (the actual height of the tube h_p is smaller and equal to the sum of the cone height h_2 and height of the elbow h_3), and the length of the tube L (in fact, it is only the length of the horizontal part of the tube).

Because the elbow of the bent draft tube causes additional hydraulic losses as compared with a straight draft tube, thorough selection of the forms and dimensions of the elbow is required.

Elbow-type draft tubes having a simplified geometry are widely applied (Figure 6.21). One of the special features of this elbow is that it is formed from simple surfaces: conical (1), cylindrical (2) and (3), face (6), and planes (4, 5, and 7). This simplifies creating the formwork (shuttering). The elbow may be symmetrical in plan or have a shifted central line to the discharge diffuser (shown by a dotted line in Figure 4.21). However, many turbine manufacturers prefere smoothly outlined elbows with the curvilinear cross-sections.

The dimensions of the draft tube are chosen based on the inlet diameter D_3 and height of the tube h. The inlet diameter is fully specified by the type of the runner and its size. The problem concerning the height $\bar{h} = h/D_1$ is more involved. Draft tubes find application with a height $\bar{h}$ equal to 1.9, 2.3, 2.5, 2.7, and higher. The greater the height

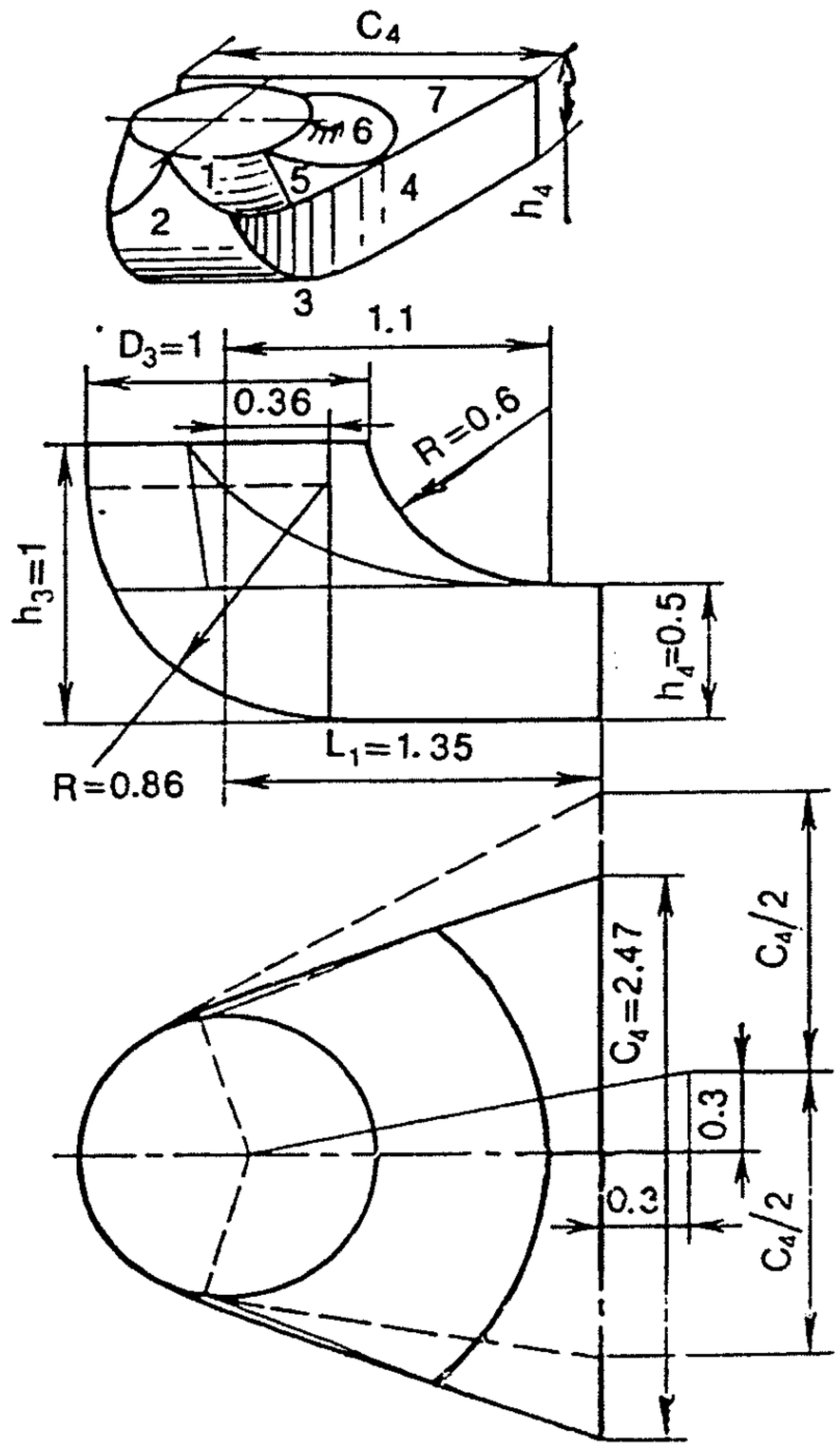


FIGURE 6.21. Simplified elbow of elbow-type draft tube.

$\bar{h}$, the longer the conical part h_2, the less the average velocity in the elbow and, consequently, the less the hydraulic losses. As to the power-generating characteristics, a higher draft tube is given preference.

At the same time, the volume of work and the cost of HEPPs augment with increasing $\bar{h}$. That is why the height of the draft tube is determined on the basis of engineering cost considerations. Most axial-flow adjustable blade turbines are operated with draft tubes having a height $\bar{h} = 1.9$ to 2.5. Radial-axial turbines use draft tubes with a height $\bar{h} = 2.5$ to 3.0.

Small-size high-head turbines are sometimes operated with draft tubes having a steel, split detachable conical part so as to facilitate access to the runner during repairs. Then the height of the tube increases to $\bar{h} = 3$ to 3.5.

The width of a draft tube $B_5 = B_4$ is larger, thus $\bar{h}$ is greater. Therefore, for $\bar{h} = 1.9$, $B_5 = 2.2D_1$, and for $\bar{h} = 2.7$, $B_5 = 2.8D_1$. When B_5 exceeds 10 to 12 m, to make the foundation of the HEPP lighter and to decrease the spanning of gates in the diffuser, one or sometimes two

piers b_p are installed in the diffuser (Figure 6.20). In doing so, care must be taken to preserve the total clear width B_5. This is achieved by the use of an elbow with a large cone angle in Figure 6.21 $B_4 = 2.47D_3$.

Assessing (when required) how the change in the length of a draft tube L affects the power-generating characteristics of a turbine can be done on the basis of outlet losses, assuming

$$\psi_{out} = v_5^2/2gH \tag{6.18}$$

For instance, when the use of a shorter diffuser is contemplated so that v_5 will increase from 3.0 to 4.0 m/s, then at a head $H = 12$ m the shortening of the diffuser will result in the increase of ψ_{out} from 0.038 to 0.068, i.e., the exit losses will increase by 3.0% and the efficiency will reduce correspondingly.

The widely used designs of elbow-type draft tubes are depicted in Figure 6.22. The nonsymmetrical draft tube (Figure 6.22a) makes it easier to define the outline of the powerhouse (the contour of a spiral draft tube is shown by the dotted line). To reduce the scope of work in constructing a HEPP the diffuser part of the draft tube is often placed at an incline (up to 12°). Then the height of the outlet cross-section h_5 is preserved.

In underground (submerged) and half-open HEPPs a greater height of the draft tube does not result in a conceivable increase in cost, i.e., power plants of this type use draft tubes with $\bar{h} > 3.5$ (Figure 6.22b).

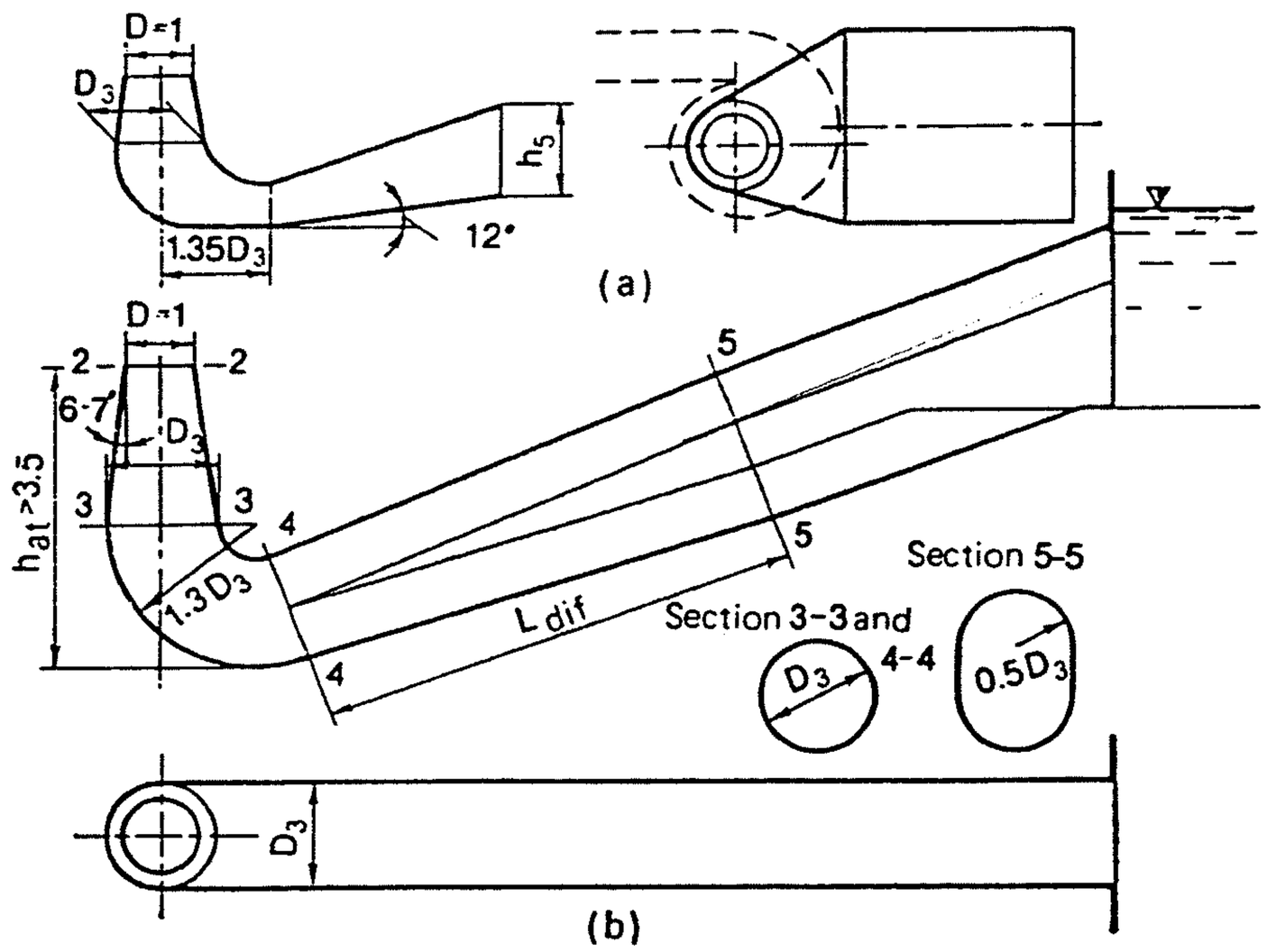


FIGURE 6.22. Various designs of elbow-type draft tubes.

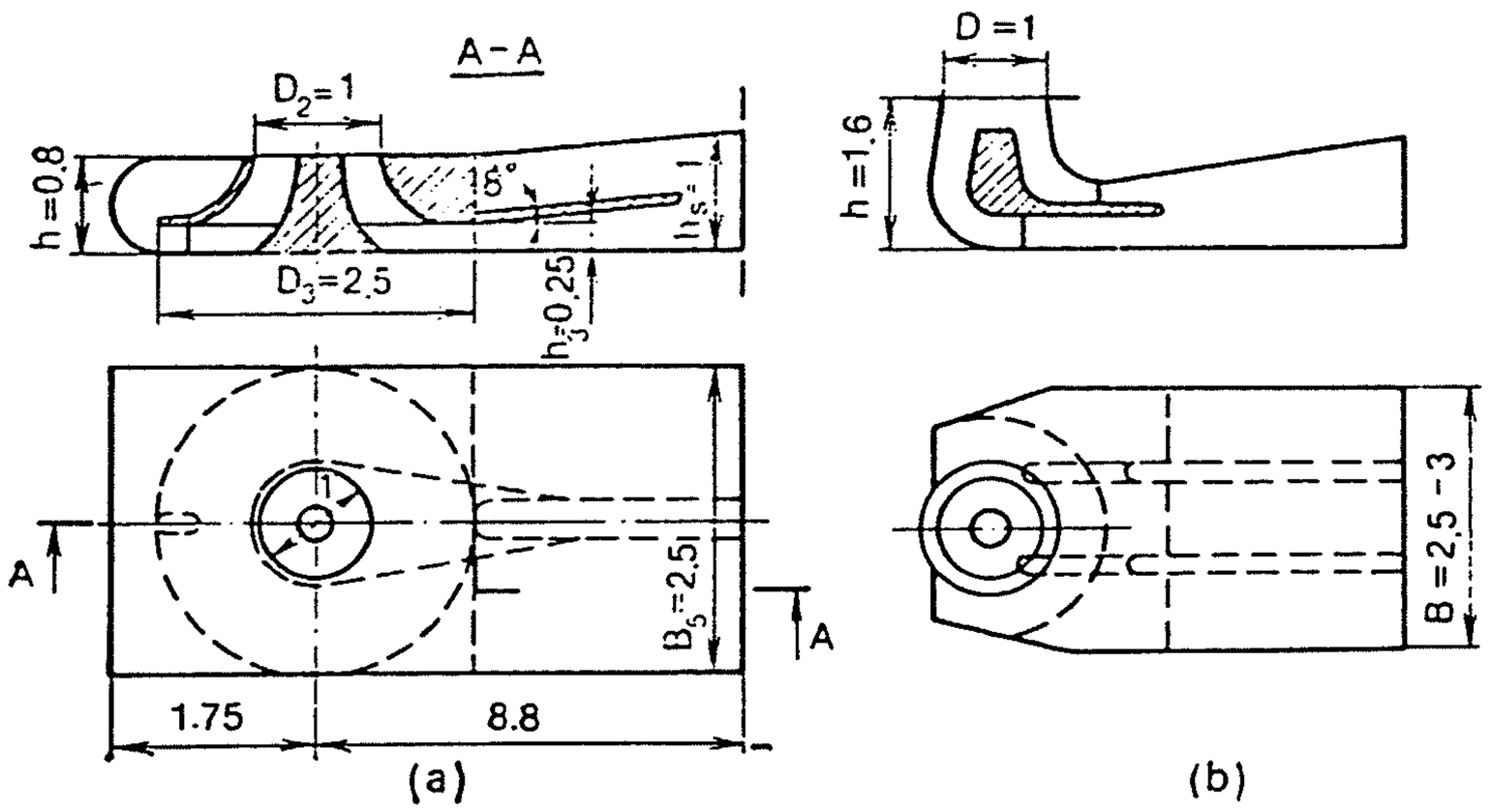


FIGURE 6.23. Proposed low elbow-type draft tubes.

Measures are taken to limit the width so as to make it possible to leave the pillars of rock between workings. This is attained at the expense of the height of the conical part and a rather long diffuser L_{dif} that may have a slope angle up to 30°. The elbow is made with a constant section, and has the form of a torus. Within the limits of the diffuser its sections change from round to oval with the same cone angle (width D_3 in plan). The draft tube proper ends in section 5–5, but in underground plants it is often prolonged to serve as a part of a constant section pressure conduit. Sometimes the end of the draft tube has a rectangular section.

On numerous occasions a lesser height of the draft tube $\bar{h}$ makes it possible to reduce the scope of work and the cost of construction. Therefore, research has been conducted aiming to develop low-elbow draft tubes. Two kinds of these tubes having a height $\bar{h} = 1.2\,(\bar{h}_{d.t} = 0.8)$ and $\bar{h} = 1.6$ are illustrated in Figure 6.23. In both cases use has been made of an internal conoid. However, in the type of draft tube shown in Figure 6.23a, the principle of a bell mouth is used, yet in the type depicted in Figure 6.23b the conoid is interlinked with the elbow. These draft tubes have found no application, but the creation of low elbow-type draft tubes still constitutes an important problem.

Horizontal radial-axis turbines, especially small power, use short elbow-type draft tubes (Figure 6.1b). Because the turbine shaft passes within the limits of the elbow, and due to short conical part downstream of the runner, the efficiency of short elbow-type draft tubes is lower than that of normally bent draft tubes.

CHAPTER 7

Cavitation and Permissible Suction Lift

7.1. CAVITATION

A study of the operating conditions of a turbine with a draft tube has shown that lower pressure is created underneath the runner (Equation 6.9). In addition, Figures 5.14 and 5.15 show that as water flows past the blades of the runner, the pressure is reduced more at the back of the blades. Thus, in some part of the flow passage of a hydraulic machine, the pressure may be rather low (a high vacuum). These operating conditions have their peculiarities, which may give the appearance of cavitation (the formation of discontinuities, or cavities, in a turbulent liquid flow).

One of the factors defining the flow of a liquid at a low pressure is the tensile strength of the liquid. According to test results, clean water free of solid and gaseous admixtures is able to withstand a tension of between 0.2 and 0.3 MPa, and under special conditions up to 10 to 25 MPa. Theoretically, the tensile strength of water is even greater. However, the tensile strength of ordinary water is determined not by its strength, but by the pressure of saturated water vapor, $p_{w.v}$, the magnitude of which depends on the temperature of the liquid (Figure 7.1). This may be explained by the fact that water taken from channels (waterways) and even from water conduits contains a great number of fine solid and gaseous inclusions serving as weak points (the nuclei). The dissolved air contrained in water (in the form of air bubbles upon a reduction in pressure) also contributes to the formation of nuclei.

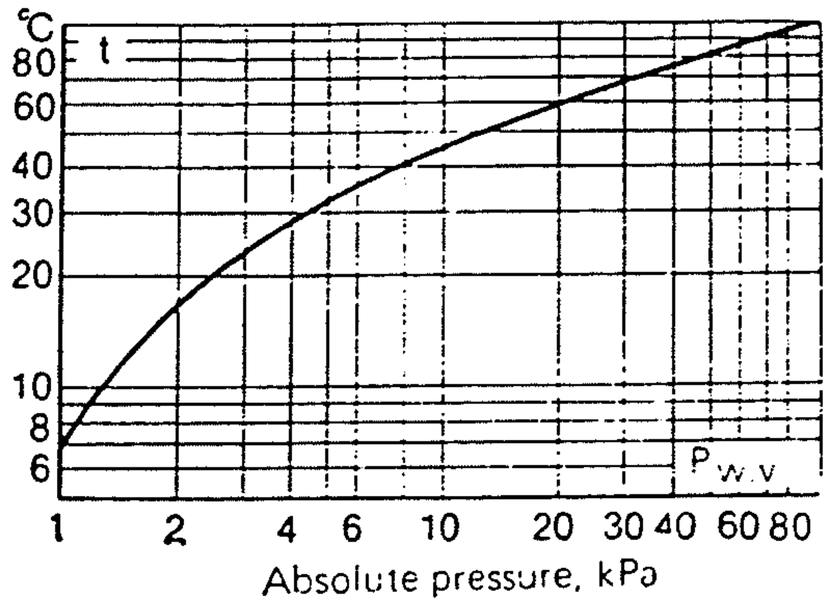


FIGURE 7.1. Saturated water vapor pressure vs. temperature.

When water pressure drops below that of saturated water vapor the intensive transition of the liquid into a gaseous state (steam) is initiated at the nuclei boundary, and local discontinuities, cavities, form which are filled mainly with water vapor. After cavities have formed, no further drop in pressure takes place because it is compensated for by a rapid increase in the volume of cavities. With an increase in pressure the cavities close (collapse) and the vapor condenses instantaneously. As illustrated in Figure 7.1, the saturated water vapor pressure is equal to atmospheric pressure at a temperature of 100°C, and this determines the boiling point. At an elevation of 2200 m above sea level atmospheric pressure is equal to 80 kPa and water boils at 93°C. If the atmospheric absolute pressure is reduced to 2 kPa, water may boil at a temperature below 20°C.

The formation of discontinuities in water can be illustrated experimentally. Fill with water a cylinder with piston so that the space under the piston is free of air bubbles (Figure 7.2a). Next, pull the piston upward with a force P. At first the piston will resist pulling and no perceptible displacement of the piston will take place, but when the

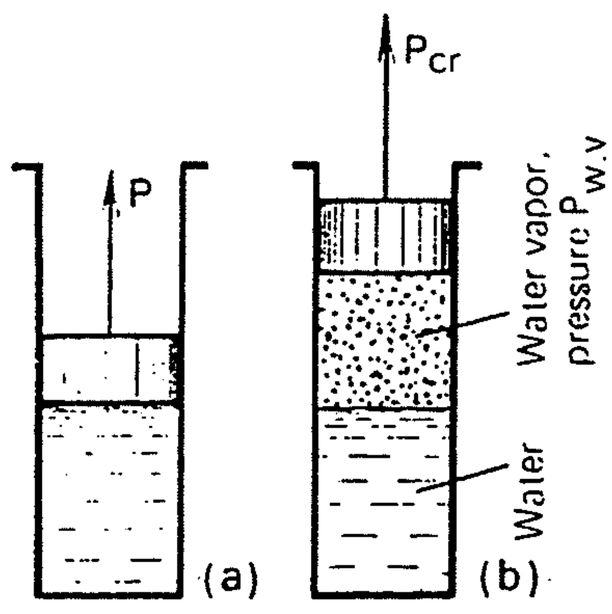


FIGURE 7.2. Static discontinuity in water.

applied force P exceeds some critical value, $P_{er} = F\ (p_{atm} - p_{w.v})$, where p_{atm} is atmospheric pressure and F is the area of the piston, the piston will begin to move upward and a space will form between the piston and the liquid, filled mainly with water vapor at a pressure of $p_{w.v}$ (Figure 7.2b). Then, no matter how much the piston is displaced up or down, as long as the cavity exists, the pressure above the piston will remain constant, equal to $p_{w.v}$. This phenomenon is referred to as the formation of static discontinuity in liquid.

In the event of turbulent flow the phenomenon develops in another way. Turbulent flow is characterized by the fluctuation of velocities and pressures at each point; this occurrence is especially intense in the boundary zones. It follows that the instantaneous pressure at a point of turbulent flow is specified by two components:

$$p_{a.inst} = p_a + p' \tag{7.1}$$

where p_a is the time-averaged absolute pressure, and p' is the fluctuation component. An approximate pattern of variation of $p_{a.inst}$ is shown in Figure 7.3. Imagine that the average pressure p_a in a turbulent flow diminishes and approaches the pressure of saturated water vapor. Then, even at $p_a > p_{w.v}$, local cavities will quickly form and collapse (i.e., fluctuate). With a decreasing p_a; the number of cavities increases, but they will also fluctuate.

If flow regions with still-lower pressure are found, cavities may form and be preserved during the entire time that the flow passes through this region. The existence of such a cavity consists of two phases, formation and growth, the period of time that the flow passes through the region in which the pressure drops (vacuum becomes higher); collapse occurs in the region in which the pressure increases. Under such conditions the cavities may become large, and as they collapse very large pressures arise in the points (centers) of their collapse (condensing). The most important factor in these cases is that these pressure fluctuations have a high frequency, 10 to 20 kHz.

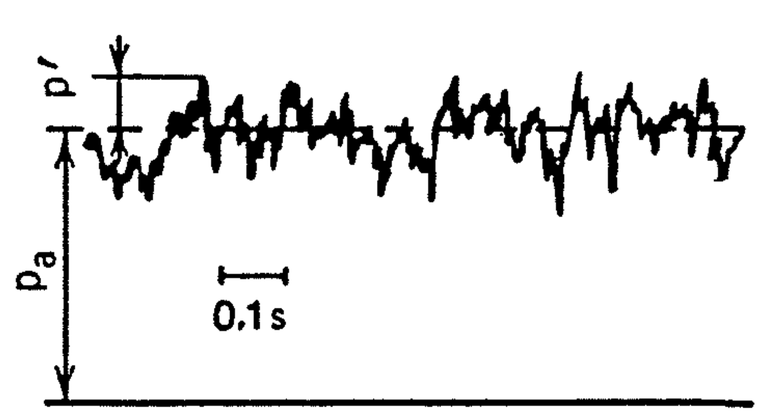


FIGURE 7.3. Pressure fluctuations in turbulent flow.

The cavitating flow has the following effects on hydraulic machines:

1. with a sufficiently developed cavitation the hydraulic losses increase, resulting in a lower efficiency and a lesser discharge;
2. in the presence of cavitation in a hydraulic machine a characteristic noise "cracking" is heard, and a higher than normal vibration appears; and
3. when a hydraulic machine is operated under cavitation conditions, surfaces erode rather rapidly at the places at which cavities collapse.

Cavitation erosions are caused principally by the mechanical action of the cavitating flow, which manifests itself in water hammers originating when cavities collapse on a flow boundary surface or close to it. This harmful action is peculiar in that the frequency of the hydraulic hammers is very high. The hammers cause the phenomenon of materials fatigue. The destruction of steel takes the form of fatigue flaking, knockout of crystals, and the surface of the affected metal becomes sponge-shaped (Figure 7.4). The intensity of the erosion is sometimes rather high and may reach an annual depth of 10 to 40 mm. This necessitates frequent repairs and change of working members, and results in considerably higher costs for operating hydraulic machines. The wear of blades and other surfaces exposed to cavity flow also results in a supplementary reduction of efficiency and a corresponding drop in the power generated at a HEPP.

In addition to the above-considered mechanical actions, cavity flow instigates chemical and electrical phenomena. The role of these factors has not been elucidated as yet, but it is clear that they contribute to a higher intensity of cavitation erosion.

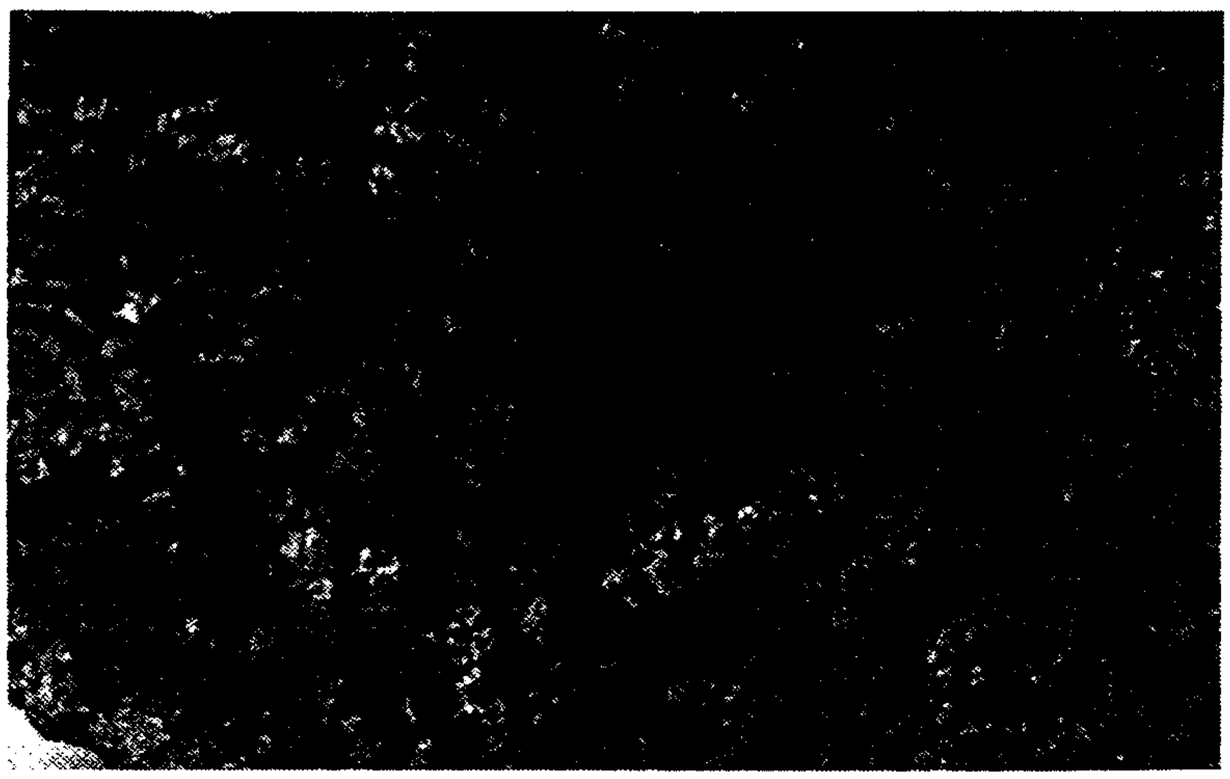


FIGURE 7.4. Cavitation erosion of steel surface.

The characteristic types of cavitation in hydraulic machines are as follows (Figure 7.5): (a) *profile*, originating when blades are exposed to cavity flow in the region of a lower pressure; (b) *slotted*, when liquid flows at a great pressure drop through slots (clearances), for instance, clearances between the runner blades and the turbine case; and (c) *local*, caused by the liquid flowing past irregularities, individual drop walls, fins (ribs), etc. (for instance, bolt heads).

Cavitation, mainly profile type, may take different forms or development stages (Figure 7.6): (a) *bubble cavitation*, in the course of which the discontinuities appear in the form of individually moving bubbles, or cavities; (b) *zonal or sheet cavitation*, characterized by the presence of a continuous cavity filled with pulsating vortexes of the liquid; (c) *separating cavitation*, in which a cavity is not filled with the liquid; and (d) *supercavitation*, in the course of which the cavity space is so developed that it closes up outside the profile boundaries. Each of these forms has its specific properties. The bubble and sheet forms of cavitation manifest themselves most intensely in acoustic (noise) and erosion action, but tell comparatively little about the hydrodynamic characteristics of flow. Separation and (especially) supercavitation change the hydrodynamic characteristics of flow. This affects the discharge, capacity, and efficiency of hydraulic machines.

The above consideration shows that cavitation acts to deteriorate the power-generating and operational characteristics of hydraulic machines. In other words, cavitation is a dangerous phenomenon that must not be permitted during the normal operation of hydraulic machines. Therefore, it is necessary to establish a definite criterion for no-cavitation operation of hydraulic machines. No-cavitation originates in a hydraulic machine if at all points of the flow passage pressure p_{ai} will be higher than the pressure $p_{w.v}$ of saturated steam (water vapor). No cavitation occurs when the following condition is valid

$$p_{at} > p_{w.v} \tag{7.2}$$

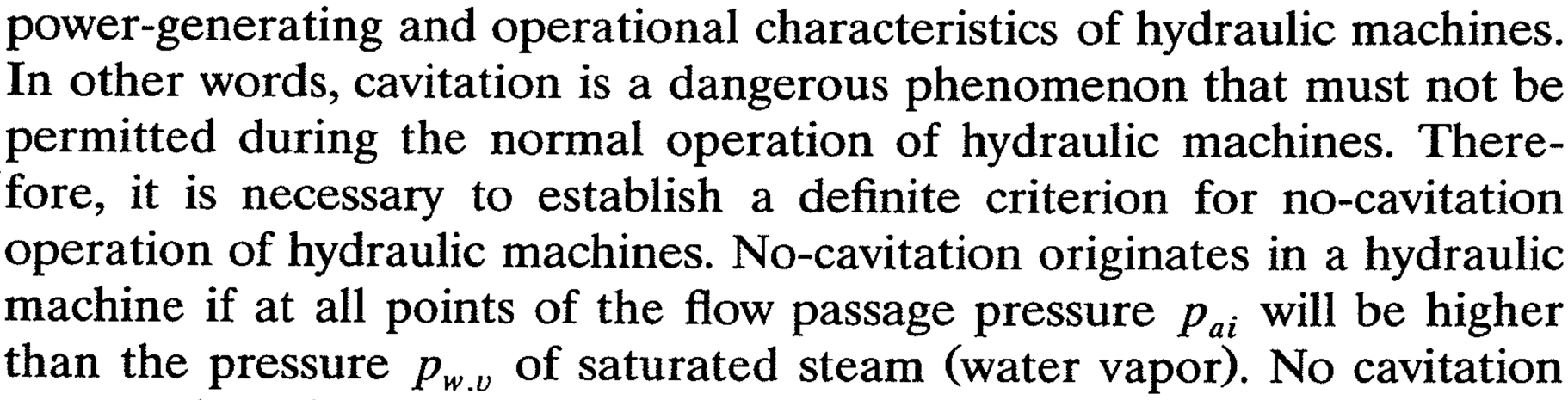


FIGURE 7.5. Types of cavitation in hydraulic machines.

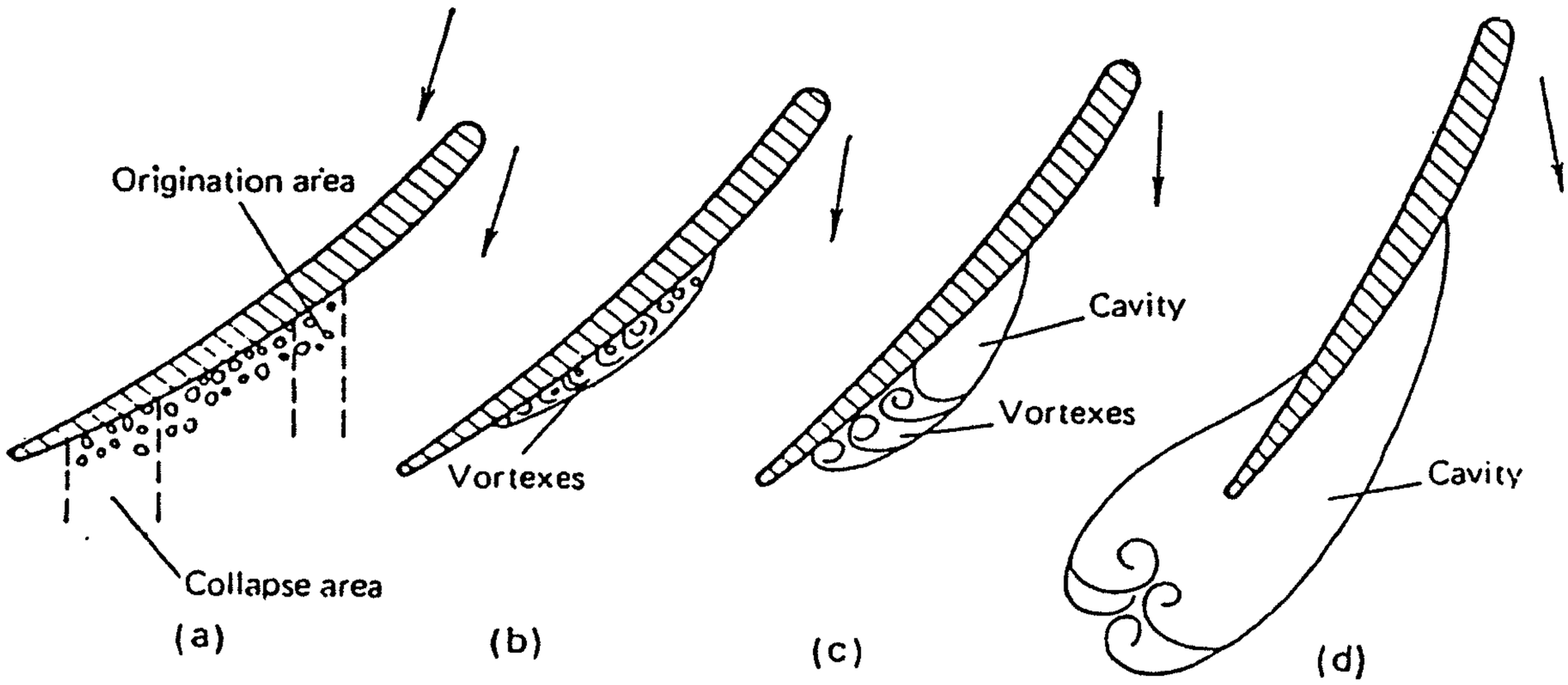


FIGURE 7.6. Stages (forms) of cavitation.

Condition 7.2 can be viewed as the general criterion of no-cavitation operation, but its practical use is very difficult as real pressures in all points of the flow inside the operating machine generally are not known. Thus, no-cavitation requires more acceptable methods. The appropriate approach is the determination of the so-called "cavitation factor" or coefficient σ.

Imagine that any hydraulic arrangement S exists through which some flow passes (Figure 7.7). Velocity (v) and absolute pressure (p_a) in characterized or control section 1–1 can be calculated or measured. Now, using Bernoulli's equation it is possible to express the relation between v_i and p_i, velocity and pressure at any point i, inside S flow and v and p_a values:

$$\frac{p_a}{\rho g} + \frac{\alpha v^2}{2g} = \frac{p_i}{\rho g} + \frac{\alpha_i v_i^2}{2g} + \zeta_{1-i}\frac{v^2}{2g}$$

The last item represents the losses on the way from 1–1 to i (ζ_{1-i} resistance coefficient). The pressure drop will be

$$\frac{p_a - p_i}{\rho g} = \frac{\alpha_i v_i^2}{2g} - \frac{\alpha v^2}{2g} + \zeta_{1-i}\frac{v^2}{2g}$$

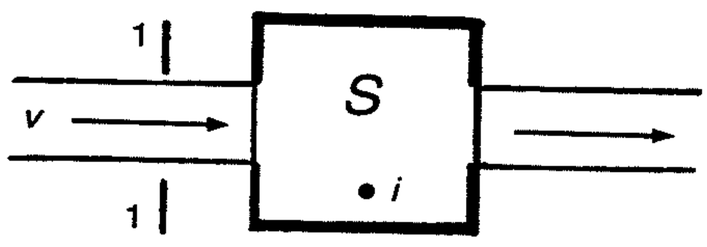


FIGURE 7.7. Determination of the cavitation coefficient.

It is assumed that a definite relation between velocities exists so

$$v_i = k_i v$$

Here, k_i is a velocity factor that is constant for similar flow geometry. From the above written equation, denoting

$$\sigma_i = \alpha_i k_i^2 - \alpha + \zeta_i$$

we obtain the formula

$$\sigma_i = \frac{p_a - p_i}{\rho \frac{v^2}{2}} \tag{7.2a}$$

Here, σ_i is a dimensionless coefficient of the pressure drop between the control section 1–1 and any given point i inside S. As we check for the possibility of cavitation it is necessary to find a point i for which p_i will be minimal or for which σ_i will be maximal.

If all data concerning the flow inside S (pressures) are known, σ can be determined (calculated) using Equation 7.2a. However, such data are not generally available and σ must be determined experimentally. This can be done by gradually decreasing p_a and increasing v until the incipient cavitation in S arises. This would be revealed by external indications such as change in delivery coefficient or efficiency, specific noise, visual examination, etc. For this critical case the value of σ can be determined because p_a and v in section 1–1 are known, and p_i is equal to the pressure of saturated liquid (water) vapor $p_{w.v}$:

$$\sigma_{cr} = \frac{p_a - p_{w.v}}{p^{v^2/2}} \tag{7.2b}$$

The found σ_{cr} can be called incipient or critical cavitation coefficient.

Equation 7.2b may be used for all operational conditions (different p_a and v) in which cavitation does not exist. This value is designated as σ_{op}, the operation cavitation coefficient. Therefore, the desired criterion of no-cavitation operation of S can be expressed as

$$\sigma_{op} > \sigma_{cr} \tag{7.2c}$$

In other words, to prevent cavitation the operational cavitation coefficient must be larger than critical. It is also important to emphasize that for similar operational modes (regimes) the σ_{er} preserves practically constant value.

Nevertheless installation of turbines and pumps is carried out taking in account criterion 7.2c it gives not absolute guarantee that cavitation will not take place. This can be connected to two factors:

1. σ_{cr} is determined after cavitation begins, and accepted safety factors sometimes do not adequately suppress cavitation.
2. Alternately, these safety factors, which are at times rather large, lead to increased structures and installation costs.

Therefore, before durable hydraulic equipment is built or is purchased it is necessary to know the ability of that equipment to resist cavitation erosion of different metals. Some data are given in Table 7.1.[1]

The parts of hydraulic machines in which intensive cavitation can be expected (runner, blades, wicket gates, seals, and others) often are manufactured from stainless steel or have a stainless protection cover. These have the best cavitation erosion resistance characteristics.

Table 7.1. Cavitation Erosion Resistance Factors

Type of Metal	Respective Resistance Factor
Cast aluminum bronze	1.5
Cast stainless steel (18% Cr, 8% Ni)	1.0
Cast stainless steel (12% Cr)	0.65
Welded mild steel	0.14
Ordinary cast steel	0.12
Brass	0.08
Cast iron	0.06

7.2. TURBINE CAVITATION COEFFICIENT AND PERMISSIBLE SUCTION HEIGHT

It is possible to apply the criterion of Equations 7.2 in order to establish no-cavitation operation conditions for turbines. Assume that a certain point C is known in the runner where absolute pressure p_{ac} is minimal (Figure 7.8). The absolute pressure at C point p_{ac} can be determined using Bernoulli's equation for relative motion (Equation

[1]The data given in Table 7.1 are oriented to standard test method using magnetostriction installation, which is characterized by a respectively weak but very high frequency of stress pulsation (up to 10 to 20 kHz). Other test methods such as the high-speed flow chamber or jet-shock installations create a different action on the tested sample and show a different cavitation resistance result. Nevertheless, the general relations are similar to those shown in Table 7.1.

5.21), written between C and exit section 2–2 for the datum level of tailrace water elevation in the tailwater (TW)

$$\frac{p_{ac}}{\rho g} + H_s + \frac{w_c^2}{2g} - \frac{u_c^2}{2g} = \frac{p_{a2}}{\rho g} + H_s + \frac{w_2^2}{2g} - \frac{u_2^2}{2g} + h_{c-2}$$

which gives

$$\frac{p_{ac}}{\rho g} = \frac{P_{a2}}{\rho g} + \frac{w_2^2 - w_c^2}{2g} - \frac{u_2^2 - u_c^2}{2g} + h_{c-2} \tag{7.3}$$

Substituting $p_{a2}/\rho g$ from Equation 6.9 and defining the losses resistance coefficient ζ_{c-2} and ζ_{suc}

$$h_{c-2} = \zeta_{c-2}\frac{w_c^2}{2g} \qquad h_{suc} = \zeta_{suc}\frac{v_2^2}{2g} \tag{7.4}$$

which gives

$$\frac{p_{ac}}{\rho g} = \frac{p_{atm}}{\rho g} - \left(H_s + \frac{\alpha_2 v_2^2}{2g} - \frac{\alpha_5 v_5^2}{2g} - \zeta_{suc}\frac{v_2^2}{2g}\right)$$

$$+ \frac{w_2^2 - w_c^2}{2g} - \frac{u_2^2 - u_c^2}{2g} + \zeta_{c-2}\frac{w_c^2}{2g} \tag{7.5}$$

Using the similarity formula (Equation 5.27) it is possible for a given mode (regime) of operation to express all the velocities through one velocity, say, v_2:

$$v_5 = k_{v5}v_2 \qquad w_c = k_{wc}v_2 \qquad u_2 = k_{u2}v_2 \qquad u_c = k_{uc}v_2 \tag{7.6}$$

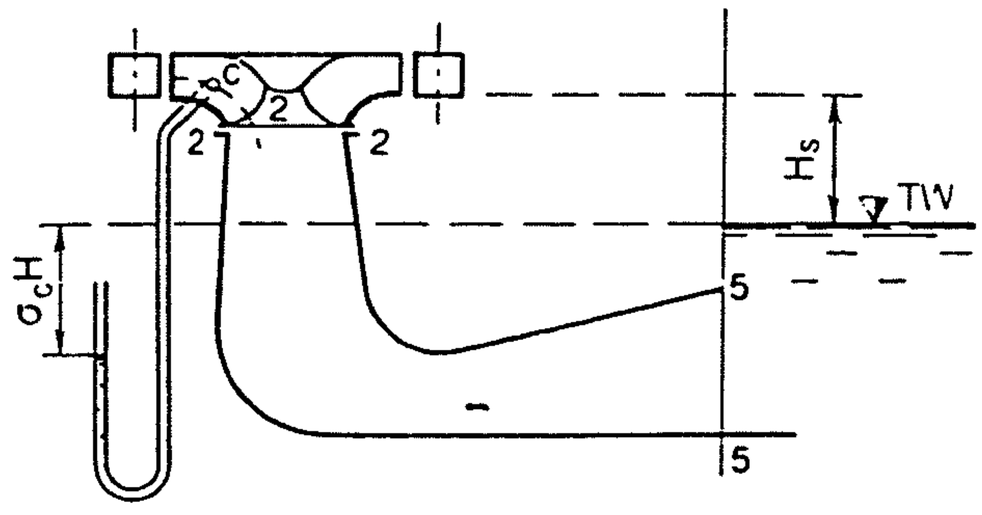


FIGURE 7.8. Determining the cavitation coefficient.

Substituting these in Equation 7.5 gives

$$\frac{p_{ac}}{\rho g} = \frac{p_{atm}}{\rho g} - H_s - (\alpha_2 - \alpha_5 k_{v5}^2 - \zeta_{suc} - k_{w2}^2 + k_{wc}^2 + k_{u2}^2 - k_{uc}^2 - \zeta_{c-2} k_{wc}^2)\frac{v_2^2}{2g} \tag{7.7}$$

The velocity v_2 is dependent on the discharge Q and the area of the 2–2 cross-section $F_2 = \pi D_2^2/4$ or defining $D_2 = k_{1,2} D_1$, where coefficient $k_{1,2}$ for a given type of the turbine (geometry) is constant. Introducing reduced discharge Q'_{I}, fixed for a given regime, according to Equation 5.37, we have

$$v_2 = \frac{Q}{F_2} = \frac{Q'_{\mathrm{I}} D_1^2 \sqrt{H}}{\pi k_{1,2}^2 D_1^2/4} = \frac{4}{\pi k_{1,2}^2} Q'_{\mathrm{I}} \sqrt{H} \tag{7.8}$$

Denoting by σ,

$$\sigma = \left(\frac{4}{\pi k_{1,2}^2}\right)^2 \frac{1}{2g}(\alpha_2 - \alpha_5 k_{V5}^2 - \zeta_{suc} - k_{w2}^2 + k_{wc}^2 + k_{u2}^2 - k_{uc}^2 - \zeta_{c-2} k_{wc}^2)(Q'_{\mathrm{I}})^2 \tag{7.9}$$

we get

$$\frac{p_{ac}}{\rho g} = \frac{p_{atm}}{\rho g} - H_s - \sigma H \tag{7.10}$$

As mentioned previously, coefficient σ is the cavitation coefficient. It shows what fraction of the turbine head is the dynamic rarefaction in the flow passage of a turbine (Figure 7.8). As seen from Equation 7.9, under similar modes of operation the cavitation coefficient σ must be preserved practically constant because the values of all factors k_i and a_i and the reduced discharge Q'_{I} are preserved.

At first glance, σ (given in Equation 7.9) sufficiently differs from the σ in Equation 7.2a, but it actually does not. Similar results will be gained if we accept as a reference velocity $v = \sqrt{2gH}$, as proposed by Thoma in 1924. In this case

$$\sigma = \frac{p_a - p_i}{H}$$

Knowing the value of p_{ac} (see Equation 7.10), we can now express the no-cavitation formula (Equation 7.2) in the following form:

$$\frac{p_{atm}}{\rho g} - H_s - \sigma H > \frac{p_{w.v}}{\rho g} \tag{7.11}$$

Equation 7.11 is used to find the value of the suction height

$$H_s < \frac{p_{atm}}{\rho g} - \frac{p_{w.v}}{\rho g} - \sigma H \tag{7.12}$$

In order to achieve no-cavitation in a turbine, the suction height must be limited. (The dependence of atmospheric pressure on above-sea level elevations (p_{atm}) was first discussed in the section surrounding Equation 1.2.) For cold water we may assume $p_{w.v}/\rho g = 0.3$ m (Figure 7.1). Under these conditions Equation 7.12 for fresh water acquires the following appearance:

$$H_s \leq 10 - \frac{\nabla}{900} - \sigma_t H \tag{7.13}$$

where σ_t is the design cavitation coefficient of the turbine and ∇ is the absolute level of the TW pool.

Equation 7.13 is used in determining the permissible suction height and assigning the mounting elevation for the turbine when designing a HEPP.

7.2.1. Determining the Cavitation Coefficient

It is impossible to determine σ from Equation 7.9 due to the absence of data concerning the inlet factors. It follows that this formula makes only a structural estimation. The quantitative values of the cavitation coefficient σ are determined via experiment on a special cavitation rig (see Figure 8.6). The σ values correspond to the instant cavitation initiates and are referred to as critical.

In calculating the permissible suction height H_s from Equation 7.13, the design cavitation coefficient for a turbine σ_t is determined by the critical value of σ with the introduction of the safety factor k_σ, which is assumed to be equal to $k_5 = 1.1$ and 1.2. (For high-head turbines $H > 300$ to 400 m, although sometimes it is larger, up to 1.5 to 1.7 m.)

$$\sigma_t = k_\sigma \sigma \tag{7.14}$$

Equation 7.9 shows that the cavitation coefficient must depend on the type of turbine (rapid increase with increasing Q'_I or the specific speed n_s) and the mode of operation.

The values of σ are usually taken from the turbine characteristics (see Chapter 8). The generalized dependence $\sigma = f\ (n_{s.nom})$, where $n_{s.nom}$ is specific speed (see Equation 5.38) for conditions of rated (maximum) turbine power and rated head, based on test data, is shown in Figure 7.9. The range of possible deviations for turbines of different types is indicated. The average value of σ for these conditions can be calculated from the empirical formula

$$\sigma = \frac{(n_{s.nom} + 30)^{1.8}}{200{,}000} \tag{7.15}$$

Equation 7.15 asserts that the turbine cavitation coefficient increases rapidly with increasing specific speed of a turbine.

When the critical cavitation coefficient is experimentally determined, the location of the cavitating zone inside the machine is unknown. If the tests are carried out on a prototypical machine, as is generally done for pumps, this fact is not sufficiently important. However, when the coefficient is being determined for a model on the prototype machine (as a rule with much larger dimensions), the zone must be located. The problem is where to place the reference plane from which the suction head H_s is measured. If this plane is located beneath the cavitation zone, the cavitation conditions as determined in Equation 7.12 for real installation will be worse because the real pressure in the cavitation zone will be less than expected. Fundamentally, therefore, the reference plane must not be located below the cavitation zone.

Taking this into account, Figure 7.10 shows the placement of the reference plane which reads the suction head H_s, as determined by

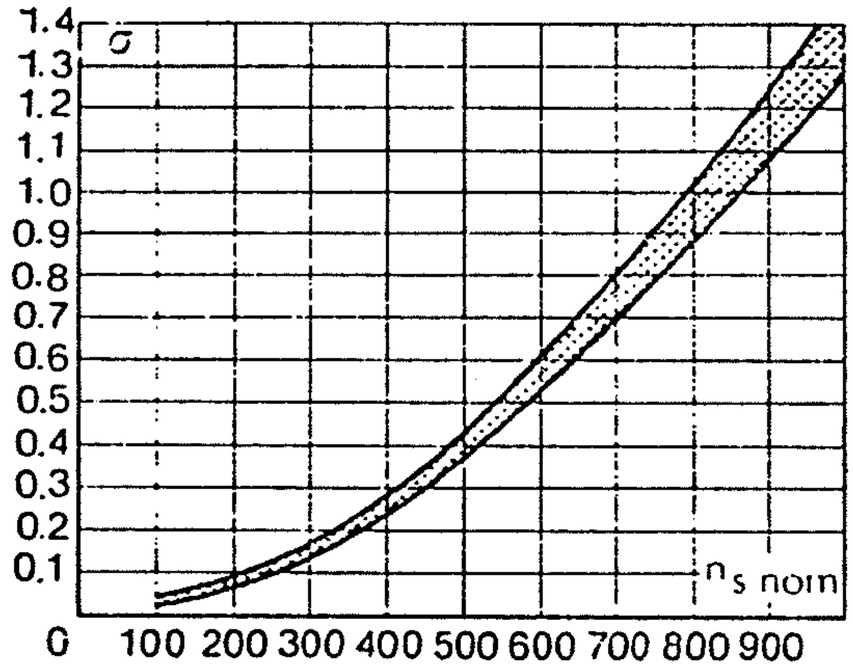


FIGURE 7.9. Cavitation coefficient vs. specific speed at nominal (maximum) load.

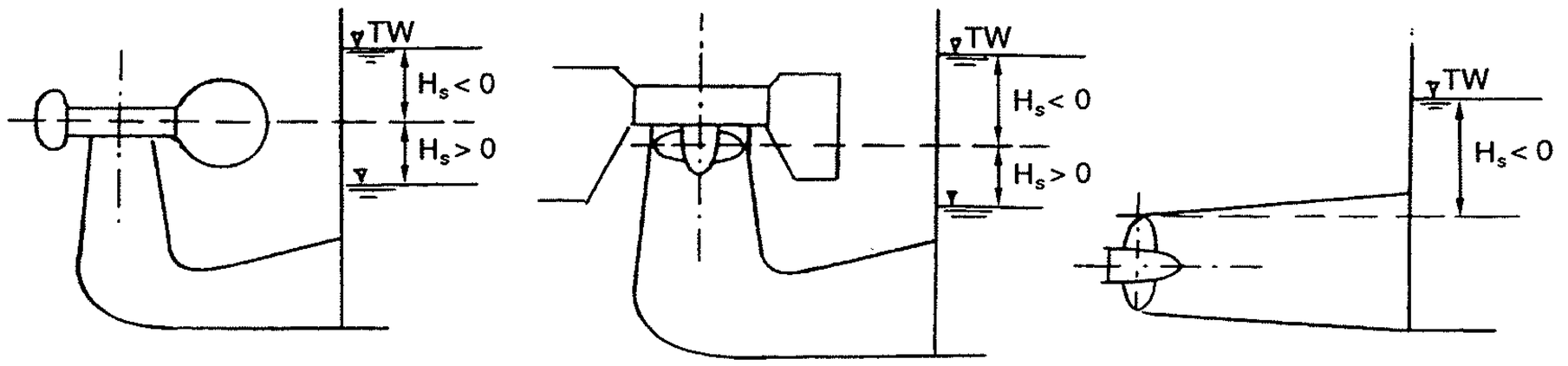


FIGURE 7.10. Measuring suction lift H_s in different turbines.

Equation 7.13 for different turbines. For vertical radial-axial (Francis) and mixed-flow (diagonal) turbines, H_s is read from the middle of the wicket gate; for vertical axial-flow turbines, H_s is read from the axis of the runner blades; for horizontal turbines, H_s is read from the upper point of the runner.

Example 7.1

For the conditions given in Example 5.5 and for absolute tailrace elevation $\nabla = 350$ m, determine the allowable suction head for turbine options with $n_s = 220$ and $n_s = 310$.

Solution

1. For $n_s = 220$. Using Equation 7.15

$$\sigma = \frac{(220 + 30)^{1.8}}{200{,}000} = 0.104$$

Accepting safety factor $k_\sigma = 1.15$ from Equation 7.14, $\sigma_t = 0.12$, and from Equation 7.13

$$H_s = \leq 10 - \frac{350}{900} = 0.12 \times 60 = 2.4 \text{ m}$$

2. For $n_s = 310$

$$\sigma = \frac{(310 + 380)^{1.8}}{200{,}000} = 0.18 \qquad \sigma_t = 0.207$$

$$H_s = 10 - \frac{350}{900} = 0.207 \times 60 = -2.82 \text{ m}$$

Thus, for $n_s = 220$, the turbine can be installed 2.4 m above tailrace, but for $n_s = 310$, the turbine must be submerged below tailrace at

2.82 m. The transition from $n_s = 220$ to the larger specific speed $n_s = 310$ demands the lower turbine installation at 5.22 m. Accordingly, deepening the power station construction and its base will be necessary. The advantages of the option of higher n_s values (revealed in Example 5.5) and the deficiency connected with H_s make it clear that to find the best solution, a thorough economic analysis must be carried out.

CHAPTER 8

Turbine Characteristics

8.1. KIND OF CHARACTERISTICS

When designing a HEPP, selecting the types of turbines, determining the main parameters (size, speed, efficiency, installation elevation, etc.), and assigning the most expedient operating conditions for the the installed equipment, sufficiently complete data on turbine properties must be available. The data are presented in the form of characteristics that define all the required turbine parameters for different operating conditions.

It follows from studying the working process in Chapter 5 that turbine operation must be determined by:

1. geometric factors which are fixed by the shape of the flow passage (type of turbine), dimensions (diameter D_1), and the opening of the wicket gate or needle a_0 (for adjustable blade turbines featuring double regulation) as well as by the runner blade angle φ;
2. kinematic factors, which prescribe the mode (regime) of turbine operation and which must include two independent variables: speed n and discharge Q, as seen in from Equation 5.30.

Expressing the condition for the mode of operation similarity from Equation 5.32, we obtain

$$\frac{nD}{\sqrt{H\eta_h}} = \text{const} \tag{8.1}$$

Thus, for a given diameter D and efficiency η, H and n will be the variables determining the mode of operation. This form of the similarity condition is more convenient for turbines than is Equation 5.30 because the head is usually given and the discharge is determined. Consequently, all the parameters that characterize the performance of a turbine of a given type may be expressed generally by the following functional relationships:

$$\begin{aligned} Q &= f_Q(D, a_0, H, n) \\ N &= f_N(D, a_0, H, n) \\ \eta &= f_\eta(D, a_0, H, n) \\ &\times \cdots \end{aligned} \tag{8.2}$$

These relationships are even more complicated for adjustable blade turbines because they include an additional variable—the runner blade angle φ. For instance,

$$\eta = f_\eta(D, a_0, \varphi, H, n) \tag{8.3}$$

Actual relationships 8.2 and 8.3 are referred to as turbine characteristics, usually presented graphically. It must be borne in mind that in the system of characteristics (Equation 8.2) the division of variables into independents and functions is conditional and may be interchanged. For instance, instead of the opening a_0, Q may be assumed to be an independent variable, thus, $N = f(D, Q, H, n)$; yet the opening would become a function of $a_0 = f_a(D, Q, H, n)$. It is important that the number of variables be completely determined. For turbines with a single regulation (radial-axial, propeller type, mixed-flow, and Pelton), there are four independent variables. For turbines with a double regulation (adjustable blade), there are five independent variables.

It is impossible to present graphically functions of the four independent variables. Therefore, it is necessary to plot characteristics for which a portion of the variables are replaced by constant parameters. Two types of characteristics are used: general and linear.

8.1.1. General Characteristics

General characteristics have two defining parameters and present the dependence of a given parameter on two independent variables. Several types of general characteristics exist.

Operating characteristics are plotted for given turbine diameter D, and constant rotation speed n because under normal condition in

hydroelectric stations turbine speed is maintained constant. The expression of such head-power characteristic is

$$\left.\begin{aligned} \eta &= f_\eta(N, H) \\ H_s &= f_{H_s}(N, H) \end{aligned}\right\} \text{ at } D_1 = \text{const}, n = \text{const}$$

This characteristic is depicted in Figure 8.1 for a radial-axial turbine with $D_1 = 6.3$ m, and $n = 88.3$ rpm. The graph shows the isolines of efficiency and the permissible suction height H_s. It follows that for any operating conditions the value of these parameters may be determined. For instance, at $H = 60$ m, $N = 150$ MW, $\eta = 91.5\%$, and $H_s = 1.8$ m.

It is possible to plot a head-discharge operating characteristic at $D_1 = \text{const}$ and $n = \text{const}$ (Figure 8.2). The graph shows the isolines of efficiency and power N.

The characteristics depicted in Figures 8.1 and 8.2 have the limiting lines (with a shading); the lower lines correspond to the greatest opening of the wicket gate and the upper corresponds to rated generator power.

Universal characteristics. The properties of a given type of turbine are generally specified by the speed-discharge characteristic, which is plotted at constant values of D_1 and H. Inasmuch as this usually defines the common properties of turbines of a given type, it is plotted in reduced parameters at $D_1 = 1$ m and $H = 1$ m. The speed-discharge characteristic for a radial-axial turbine is shown in Figure 8.3. The

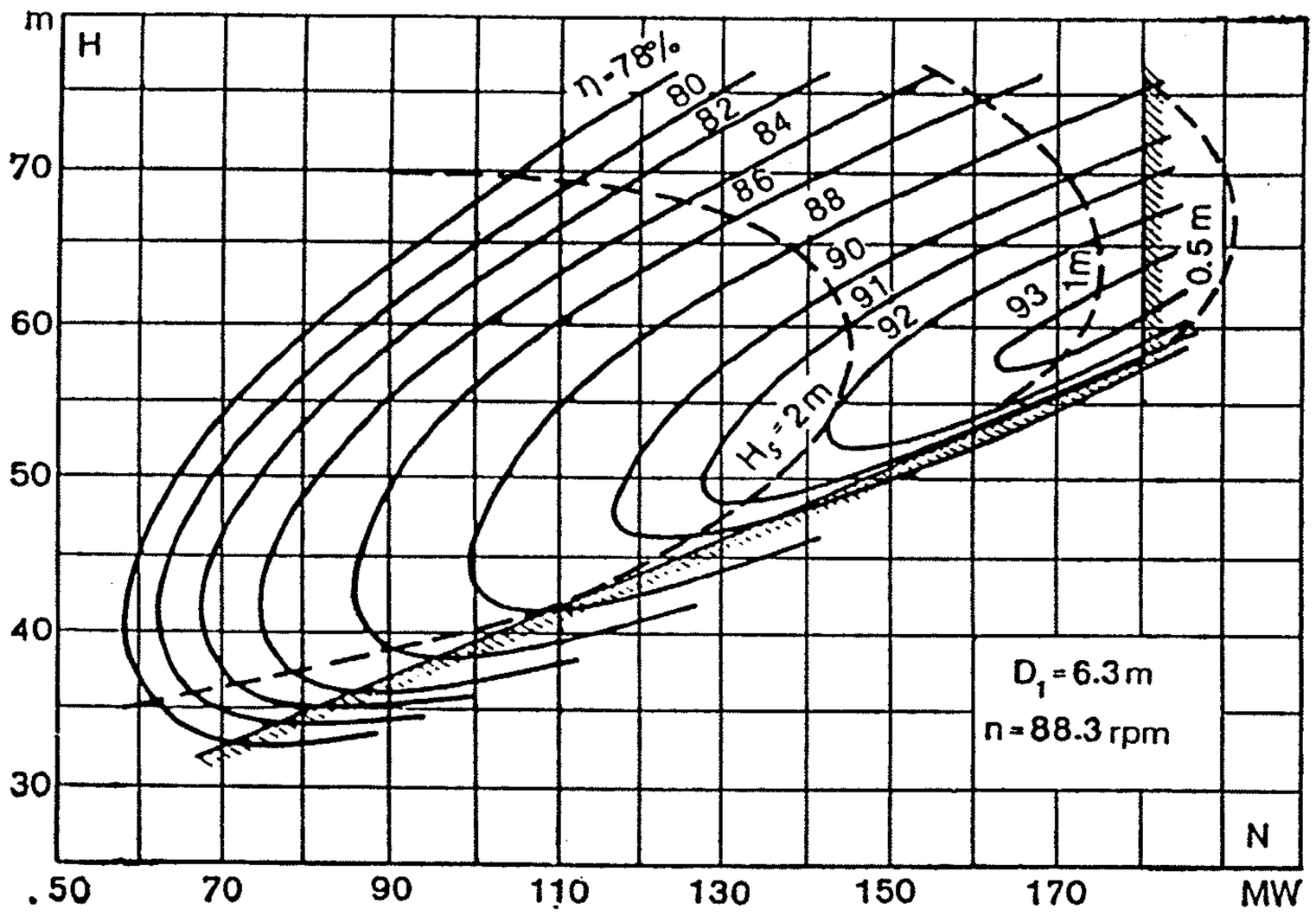


FIGURE 8.1. Operating head-power characteristic of turbine.

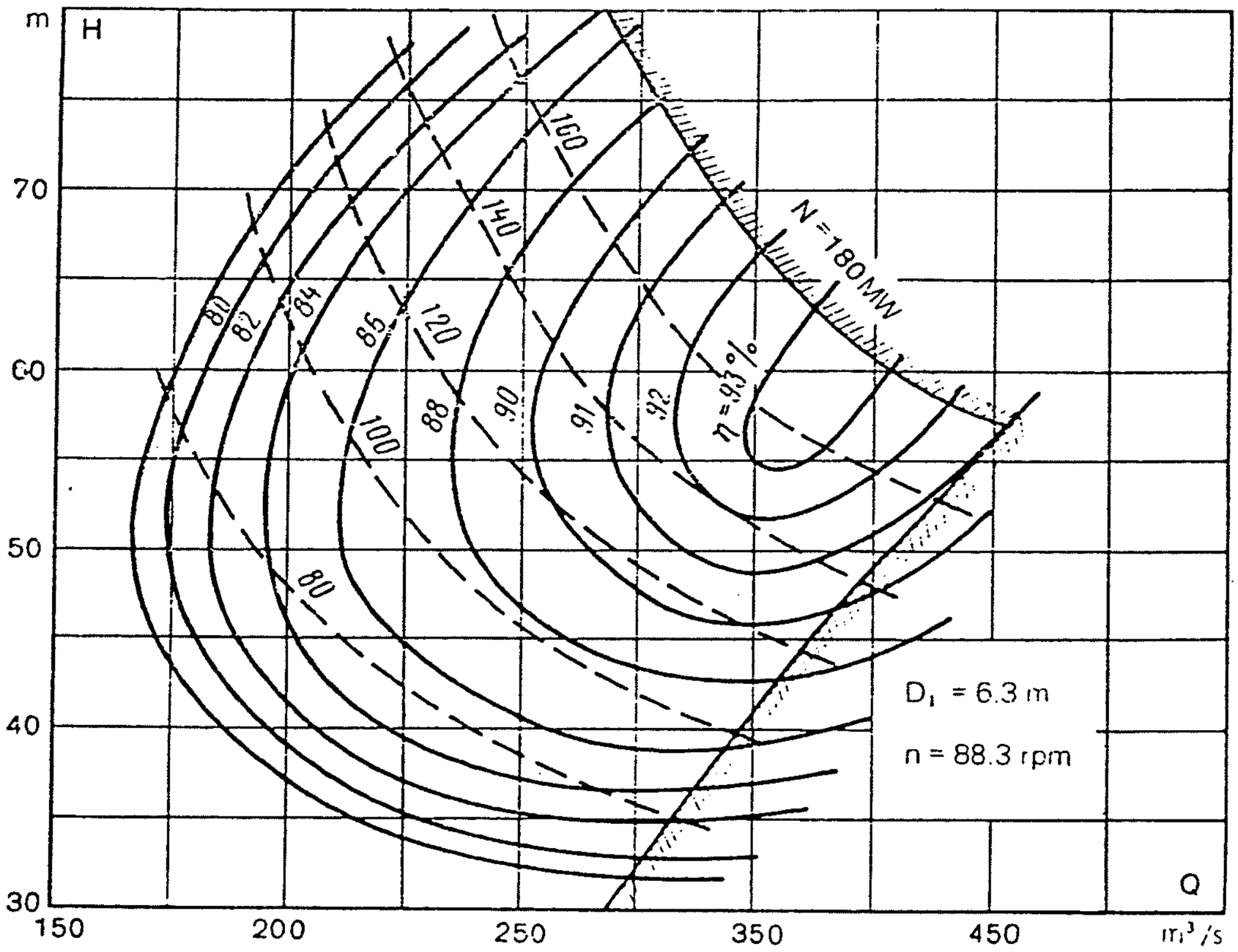


FIGURE 8.2. Operating head-discharge characteristic of turbine.

variables n'_1 and Q'_1 are plotted on the axes (see Equations 5.34 and 5.35). The isolines of the hydraulic efficiency, the cavitation coefficient σ, and the openings of the wicket gate a_0 are also plotted in the graph.

Sometimes the universal characteristic is plotted in dimensionless coordinates ψ and φ (Equation 5.37a).

The universal characteristics is also plotted using the results of model testing (model characteristic) and all quantities (η, σ, a_0, etc.) are given for the model. With this in mind, the size of the model (diameter) is always shown in the characteristic, and overall drawing to scale is given, including the turbine case and the draft tube.

An important point about the characteristic is the optimal mode of operation corresponding to an absolute maximum efficiency. A line of the 5% power margin (95% N_{max}) is often given. To the right of this line, only a 5% increase in power may be gained and usually it is inadvisable to enter into this zone.

The universal characteristic fully covers the properties of turbines of a given type, and using the recalculation Equations (5.36 and 5.37), permits determination of all the required parameters and plotting of any other characteristics of a turbine of this type for the given parameters. To this end, diameter of the model D_m and the approximate head at which tests were conducted are indicated within the characteristic.

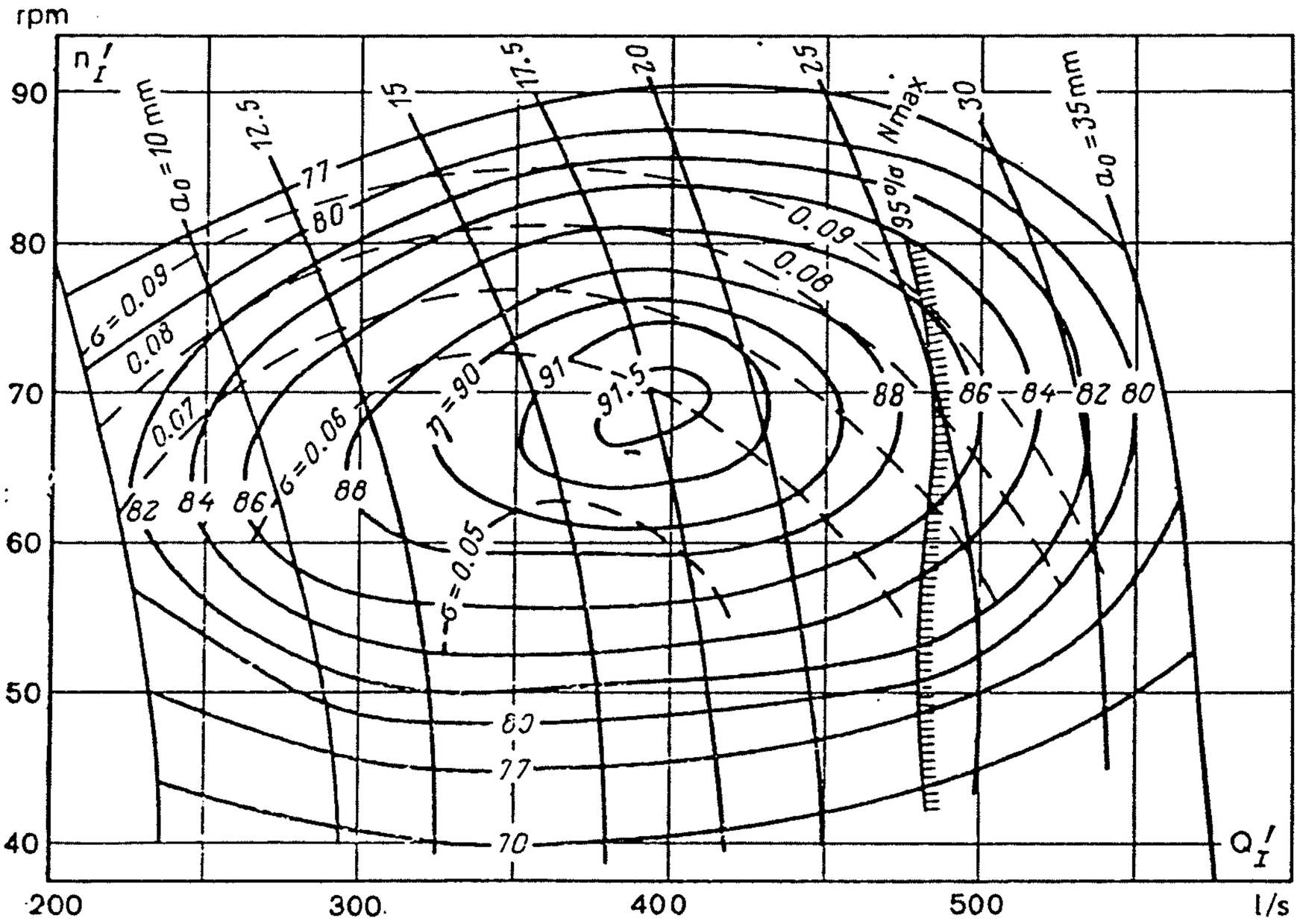


FIGURE 8.3. Universal characteristic of radial-axial flow turbine ($D_m = 460$ mm, $H = 4$ m).

8.1.2 Linear Characteristics

Linear characteristics are plotted with dependence on one variable which supplies the name of the characteristic. In doing so, three parameters are assumed to be constant. For instance, a linear power characteristic shows the dependence of turbine parameters on its power: $\eta = f_\eta(N)$ at $D_1 = \text{const}$, $n = \text{const}$, and $H = \text{const}$. A characteristic of this kind is shown in Figure 8.4. It is easily seen that the given linear

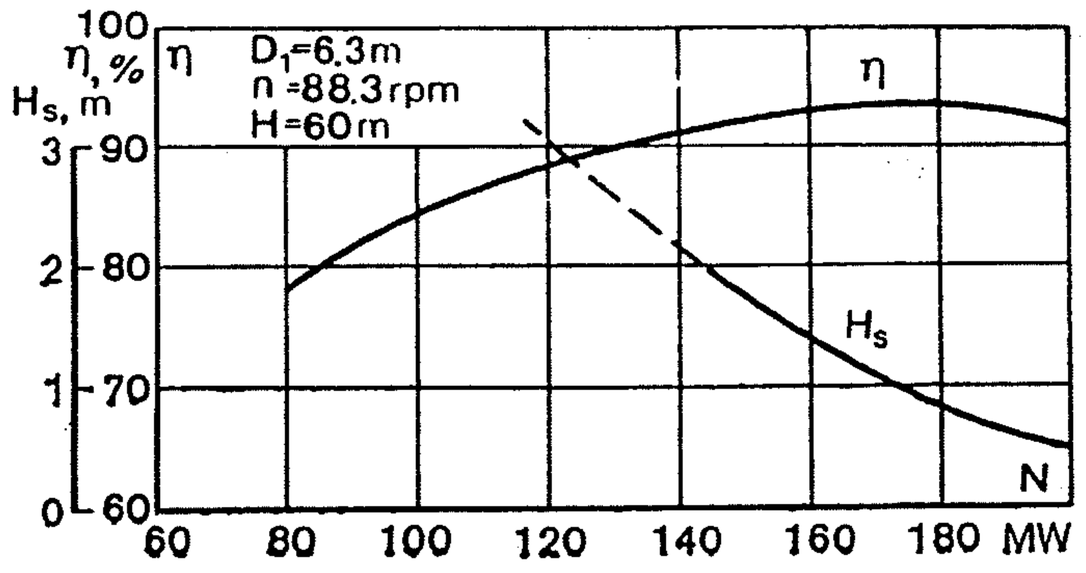


FIGURE 8.4. Linear power characteristic.

characteristic is a section of the operating power head — a characteristic shown in Figure 8.1 at $H = 60$ m.

Other linear characteristics may be plotted:

$$\text{speed: } N = f_N(n) \text{ at } D = \text{const}, a_0 = \text{const}, \text{ and } H = \text{const}$$

$$\text{head: } N = f_N(H) \text{ at } D = \text{const}, a_0 = \text{const}, n = \text{const}$$

Each linear characteristic is some section of the operating characteristic. They not only fully cover the properties of turbines, but are most simple and visual, which is why they are often used to compare the properties of turbines of different types and kinds.

8.2. DETERMINATION OF CHARACTERISTICS BY MODEL TESTS

Although the hydromechanical design of turbines is continuously improving, sufficiently complete, reliable characteristics of turbines, which would cover a wide range of operating conditions, can be only obtained experimentally. When turbines are designed by calculation, it is common practice to work out several alternate forms of the flow passage. These forms are assessed and developed on the basis of the data obtained by model testing on special test rigs. The results of the tests conclude that universal (model) characteristics are obtained to plot operating and other characteristics for full-scale conditions.

Two types of rigs are used: the power test rig, which tests turbines for performance under no-cavitation conditions, and the cavitation rig, used to determine cavitation properties. The power test rigs are designed for testing turbine models from 250 to 460 (800) mm in diameter, and the cavitational rigs are designed for testing turbines that are 250 to 460 mm in diameter.

The power test rig (Figure 8.5) consists of tanks of the headwater (HW) (1) and tailwater (TW) (2), vessel (3), and pump (4). The turbine model (5) is mounted between the two tanks, and geometric similarity is ensured for both the turbine spiral case and the draft tube. When the model is in operation water flows through the turbine from tank (1) into tank (2) where the flow rate is measured by means of a measuring weir (6), which, as a rule, must be calibrated by the volumetric or mass method. Water is discharged into the vessel (3) from which the pump (4) delivers the water into the upper tank (1). The circulation system is ensured in this way. The weir (7) maintains a water level in the tank (1), and through this weir the excess water delivered by the pump is discharged into the vessel (3). Grids (9) and (8) serve to damp and even out the water flow. Power test rigs usually ensure a head of 2 to 6 m.

The quantities measured during the testing are the discharge Q, measured at the height h of the weir; head H, which is taken from the

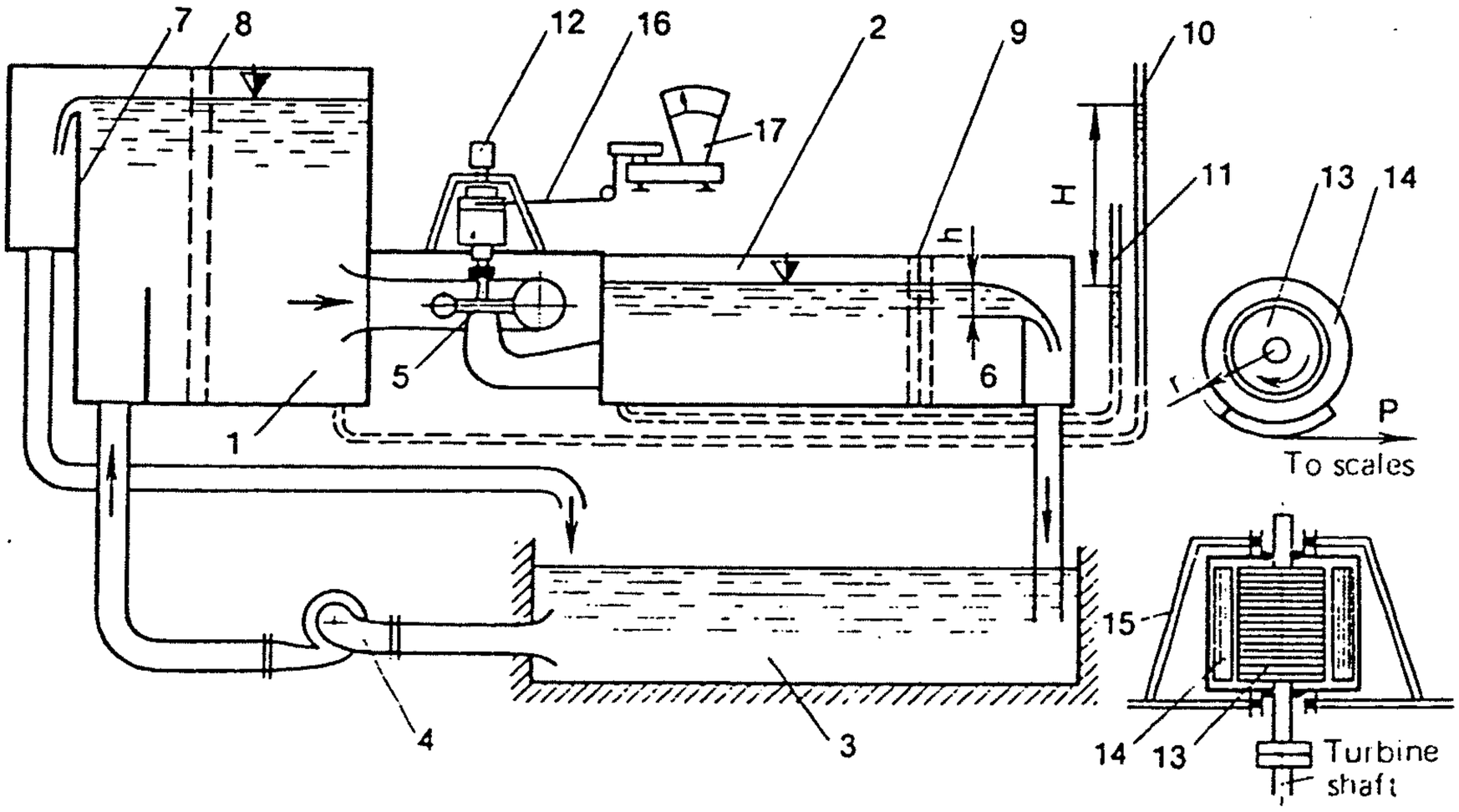


FIGURE 8.5. Turbine power test rig.

readings of piezometers (10) and (11) (losses upstream of the inlet to the spiral case also may be accounted for); the speed n (determined using a tachometer or read-off counter (12)); and the power developed by the turbine N_v. The greatest difficulties are involved in measuring N_v, which is done by means of various brakes (usually electric). The brake rotor (13) is coupled to the model turbine shaft and the stator (14) is secured in bearings on the frame (15). When the rotor rotates, the forces of magnetic interaction (the frictional forces in a mechanical brake) entrain the stator, but it is kept in place by string (16) running to balance (17).

The torque developed by the turbine is determined by the tension of string P and radius r: $T_v = Pr$ (in newton meters) and n is used to determine the power N_v (in kilowatts) for the following formula:

$$N_v = Tn/9550 \tag{8.4}$$

The efficiency of the model is calculated, using test results

$$\eta_m = N_v/9.81QH \tag{8.5}$$

The tests themselves are conducted in the following way. The wicket gate is set with opening a_0 and several points are taken at different speeds, n, varied by means of the brake. The measured quantities are used to calculate the reduced parameters n'_{I} and Q'_{I} by Equations 5.34 and 5.35, and the values of $\eta_m = f_\eta\ (n'_{\mathrm{I}}, Q'_{\mathrm{I}})$ are tabulated for different openings of the wicket gate a_0. These quantities are used to plot a universal characteristic.

In addition to the efficiency, discharge, and power, test results also determine the following quantities: runaway speed, the axial forces acting on the runner, forces acting upon the runner blades and guide vanes, etc.

The cavitation rig (Figure 8.6) is composed of the supply pipeline (1), turbine model (2), closed TW tank (3) (partially filled with water), circulation pipelines (4) and (5), and pump (6). The rig has a closed design and handles a constant volume of water, thereby ensuring a constant TW level.

The following measurements are taken during the tests: discharge Q with the aid of a Venturi flow meter (7) (via the pressure drop Δh shown by a differential pressure gauge), head (crosshead ΔH plus the velocity head in pipeline (1)), power N_v (with the help of brake (8) and balance (9), as is shown in Figure 8.5), and vacuum H_v atop the free surface in tank (3) (vacuum gauge). The vacuum required is ensured by the special vacuum pump (10). To guarantee that no cavitation will originate in pump (6) during the testing, it is installed 10 to 15 m underneath tank (3). While the rig is operating, water heats especially intensely when the flow rate is regulated by the gate upstream of the pump. Water temperature is maintained with the aid of cooling coils (not shown in the rig schematic). Sometimes freshwater is added from the water supply pipeline into tank (3) and water is discharged from the pressure line simultaneously.

Cavitation test rigs are usually operated with a 20 to 30 m head; however, to obtain more reliable data, especially for high-head turbines, cavitation rigs have been elaborated, ensuring a head of 150 to 200 m and higher.

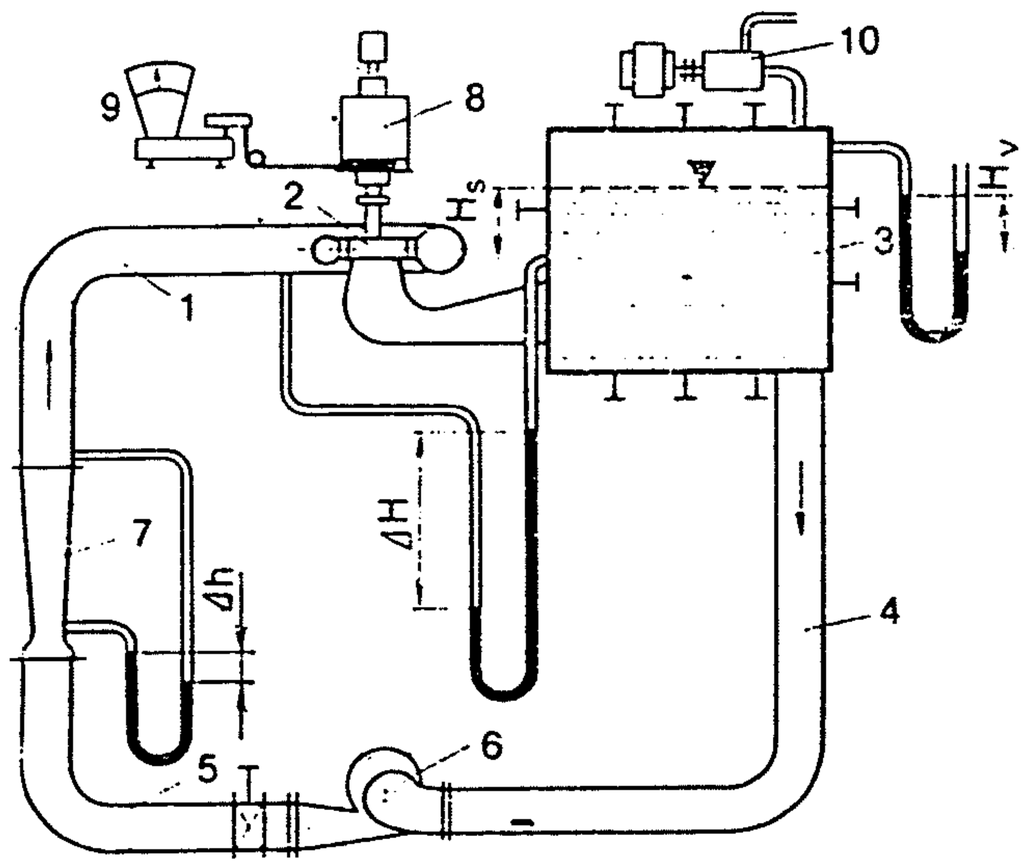


FIGURE 8.6. Cavitation rig for taking turbine characteristics.

The cavitation coefficient is determined on the basis of the general principle described in Chapter 7.1.

The pressure on the free surface in the tank is maintained equal to p_{tw}. Then, for a given operation Equation 7.11 permits determination of the operational coefficient, σ_{op}, which is called the cavitation coefficient for a given installation

$$\sigma_{op} = \frac{\frac{p_{tw}}{\rho g} - H_s - \frac{p_{w.v}}{\rho g}}{H} \tag{8.6}$$

It follows that σ_{op} is in some sense a conditional index.

The cavitation rig test is conducted as follows. The wicket gate is opened arbitrarily at a_0, while head H and speed n (characterizing the mode of operation) are maintained constant. σ_{op} is varied in stages usually at the expense of decreasing p_{tw} (a vacuum is created), and the efficiency η is found for each value of σ_{op}. A graph $\eta = f(\sigma_{op})$ is plotted (see Figure 8.7). With a decreasing mode of operation σ_{op}, η remains constant to some degree and then begins to drop drastically. Because the mode of operation remains unvaried and only the cavitation coefficient changes, it is evidence of the cavitational breakdown as the turbine develops cavitations. (If the model is transparent it is possible to observe them visually.) Additionally, it is easy to record the instant at which cavitation is initiated by observing the abrupt increase in the intensity of ultrasound acoustic oscillations and noise.

At the instant of the curve inflection σ_{op} is the critical cavitation coefficient σ. The values of σ are determined in this way for many operational modes and are plotted for the main universal characteristic in the form of isolines (for instance, lines σ in Figure 8.3).

It should be pointed out that the value of σ, shown in Figure 8.7, is determined to some degree by sight, and the cavitational breakdown, on the basis of which σ is fixed, points to a sufficiently developed cavitation. When σ_{op} slightly exceeds σ the absence of cavitation in the

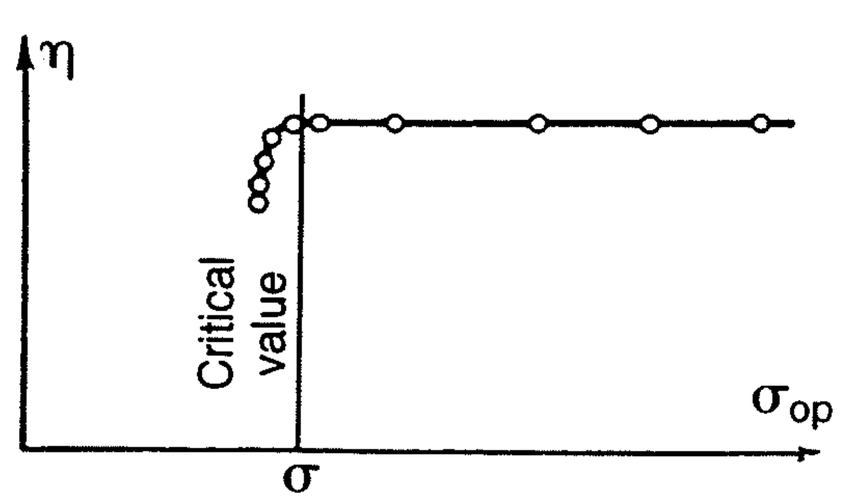


FIGURE 8.7. Efficiency vs. cavitation coefficient.

turbine is not always guaranteed. Therefore, when determining the permissible suction height a safety factor k_σ is taken from Equation 7.14.

8.3. PLOTTING THE CHARACTERISTICS OF THE ADJUSTABLE BLADE TURBINES

Let us consider the flow downstream of the runner in a propeller-type wheel and adjustable blade turbines at a constant speed n and a changing discharge Q. From Figure 8.8a it is obvious that with fixed blades (β_2 = const) discharge variation causes a sharp change in the angle α_2. At low flow rates, the flow is intensively twisted in the direction of runner rotation; at large flow rates the flow is twisted in the opposite direction. It follows that when the discharge Q varies within only a narrow range the conditions downstream of the runner will be close to optimal.

In the case of double-flow regulation (Figure 8.8b) it is possible to preserve the direction of the flow outlet velocity α_2 downstream of the runner in a wide range of discharge Q variation meeting the optimal conditions of flow by changing the blade angle φ. For turbines with double-flow regulation (mixed- and axial-flow) a series (rather than one) of particular universal characteristics are taken for a series of fixed-blade angles φ (so-called partial propeller-type wheel characteristics). A series of such characteristics of an axial flow turbine taken at different angles φ equal to $-15°$, $-10°$, $-5°$, $0°$, $+5°$, $+10°$, and $+15°$ are shown in Figure 8.9. The characteristics of the propeller-type wheel turbines show that discharge Q'_1 increases with increasing angle φ. The characteristic of an adjustable blade turbine is plotted on the basis of partial propeller-type wheel turbine characteristics founded on the

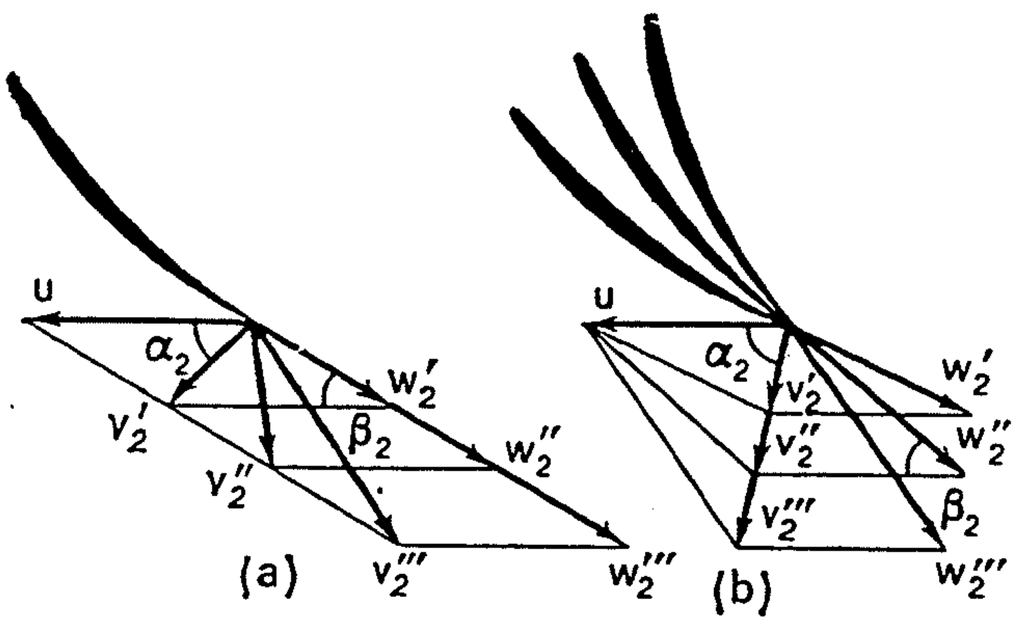


FIGURE 8.8. Outlet velocity parallelograms of propeller-type and adjustable blade turbine wheels (runners).

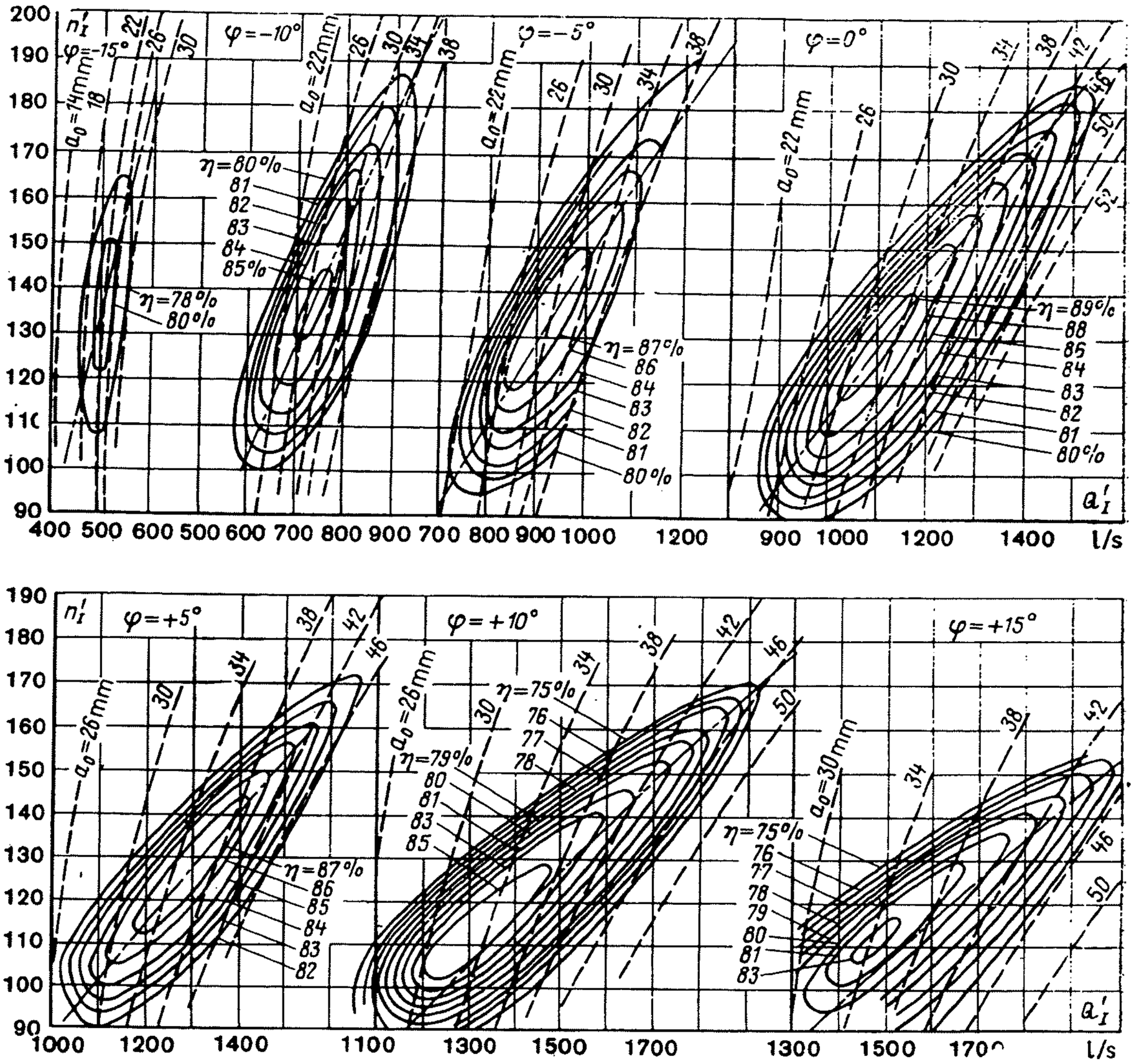


FIGURE 8.9. Partial propeller-type wheel characteristics of axial-flow turbine.

requirement that at any point with coordinates n'_{I} and Q'_{I} the efficiency should be at maximal.

Plotting is usually performed as followings: For a given value of n'_{I} sections of partial propeller-type wheel turbines are plotted that are represented by curves $\eta = f_{\eta}(Q'_{\mathrm{I}})$ and $a_0 = f_a\ (Q'_{\mathrm{I}})$ (shown in Figure 8.10). Each pair of curves complies with a certain blade angle φ. An envelope is plotted over the curves $\eta = f_{\eta}(Q'_{\mathrm{I}})$, and the points at which the envelope touches the particular curves η are plotted on line a_0. Thus, the coordinates n'_{I} and Q'_{I} and also the values of η_r, φ, and a_{0r} are determined. These are regulator points. All found points for a given n'_{I} are plotted and the values of φ, a_{0r} and η_r are inscribed in the field of Q'_{I} and n'_{I}. Points for other values of n'_{I} are plotted similarly. When the number of points is sufficiently great, they may be used to draw the isolines for different equal values of φ, a_{0r}, η_r and to obtain the

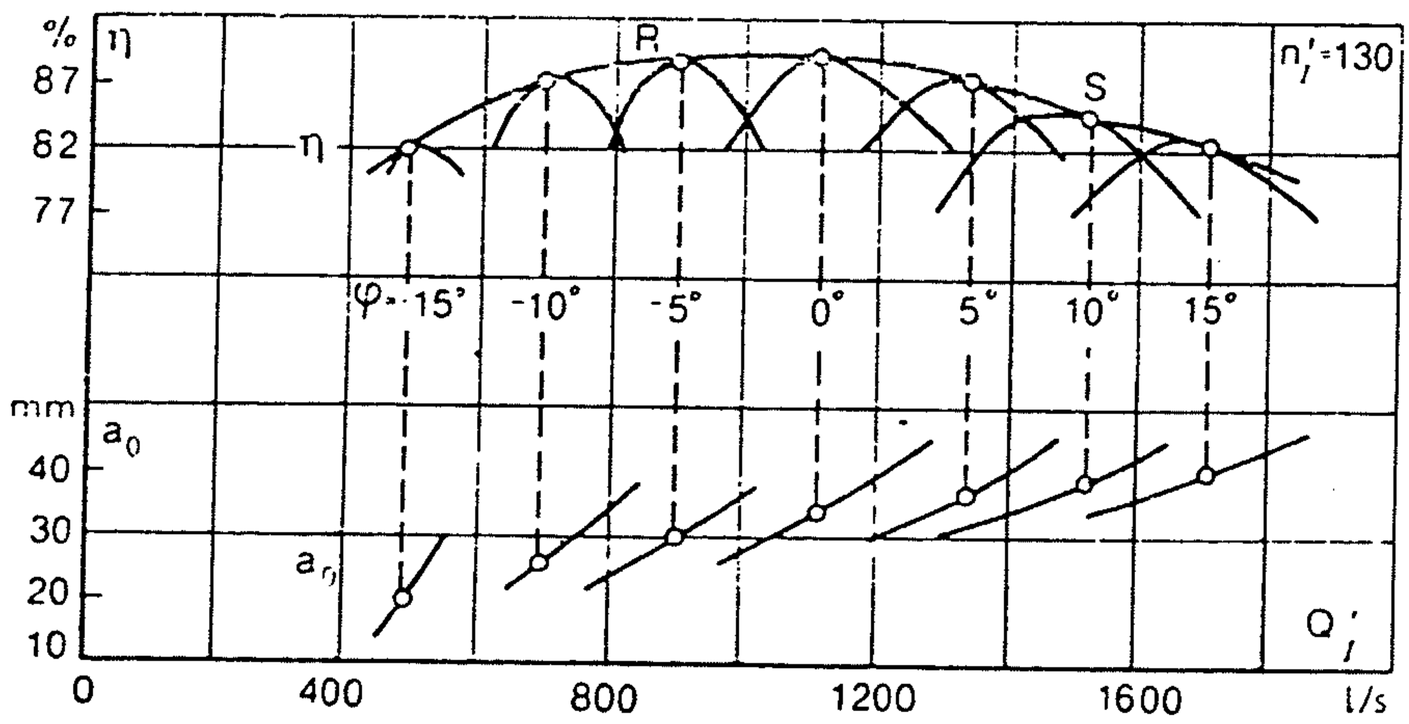


FIGURE 8.10. Determining regulator points at sections of partial propeller-type wheel characteristics.

universal characteristic shown in Figure 8.11 (the index "r" for regulator points is not placed, but it must be kept in mind). To clarify, common points R and S are shown in the section in Figure 8.10 and on the universal characteristic presented in Figure 8.11.

The cavitation coefficients σ are usually determined on a cavitation rig for values of φ, a_{0r}, and n'_1 already discovered on the basis of the combinator characteristics. Then they are plotted on it (dotted lines in Figure 8.11).

The main feature of the characteristics of an adjustable blade turbine is that it is valid only when the angles φ and the openings a_0 are in a strict combinator (or cam) accordance, the accordance being determined by the combinator relationship:

$$\varphi = f_r\,(a_0, n'_1) \tag{8.7}$$

At HEPPs turbines are operated with a constant speed n_{syn} (see Equation 9.1) and in accordance with Equation 5.34

$$n'_1 = n_{syn} D/\sqrt{H} \tag{8.8}$$

It follows that for each head H the proper combinator curve $\varphi = f_r\,(a_0, H)$ exists. Using the universal characteristic, the combinator curves may be plotted in the following manner. Several values H are assumed. For each value H the value of n'_1 is found from Equation 8.8, and a section of the main universal characteristic is made. Then, corresponding values of φ and a_0 are extracted to be used to plot the combinator curves. Figure 8.12 exemplifies the combinator curves, plotted on the characteristic (Figure 8.11) for $n'_1 = 130$ and 150. (For $D_1 = 9.0$ m and $n_{syn} = 60$ rpm it corresponds to a head $H = 17$ and 13 m.)

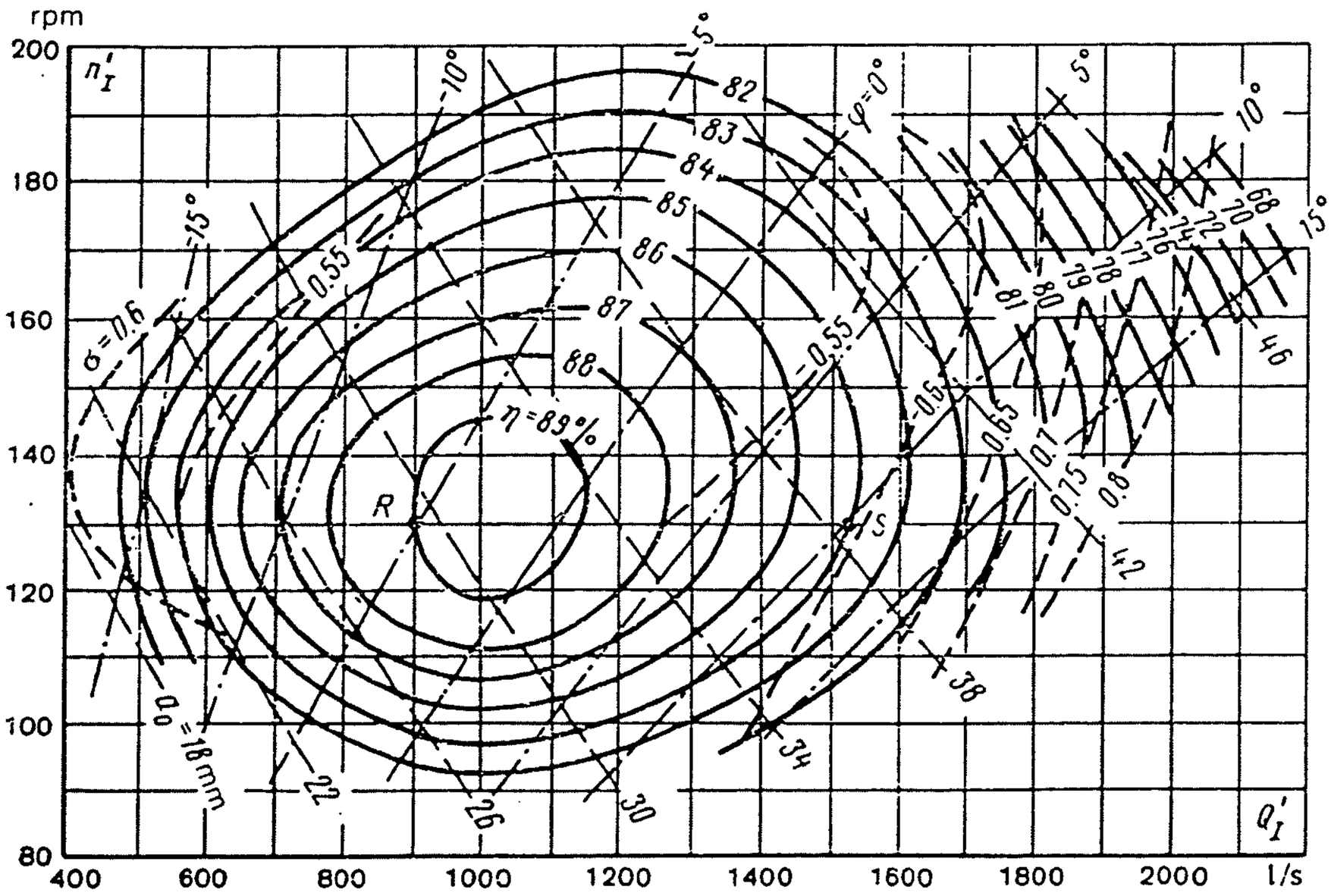


FIGURE 8.11. Universal characteristics of axial-flow adjustable blade turbine (D_m = 460 mm, H = 4 m).

Therefore, in regulating adjustable blade-turbines it is necessary not only to strictly maintain the dependence between φ and a_0, but this relationship must vary with a change of head available at a HEPP.

8.4. CONVERSION OF MODEL PARAMETERS TO FULL-SCALE EQUIPMENT

The universal characteristic plotted in reduced parameters Q'_I and n'_I (Figures 8.3 and 8.11) and representing the properties of turbines of a given type is a model characteristic. (The values of efficiency, wicket gate openings, and some others are given for the model.) The full-scale characteristics that are required in designing HEPPs are received by conversion from the universal characteristic. Their high reliability and accuracy are ensured above all by strict geometric similarity of all elements of the flow passage in the model and full-scale equipment.

The dimensions determining the flow passage of a turbine are obtained by conversion from a model in proportion to the ratio between the diameter of the model D_m and that of the turbine D_t, D_m/D_t. To this end the main dimensions of the flow passage of the model are always given on the universal characteristics. For instance, the opening

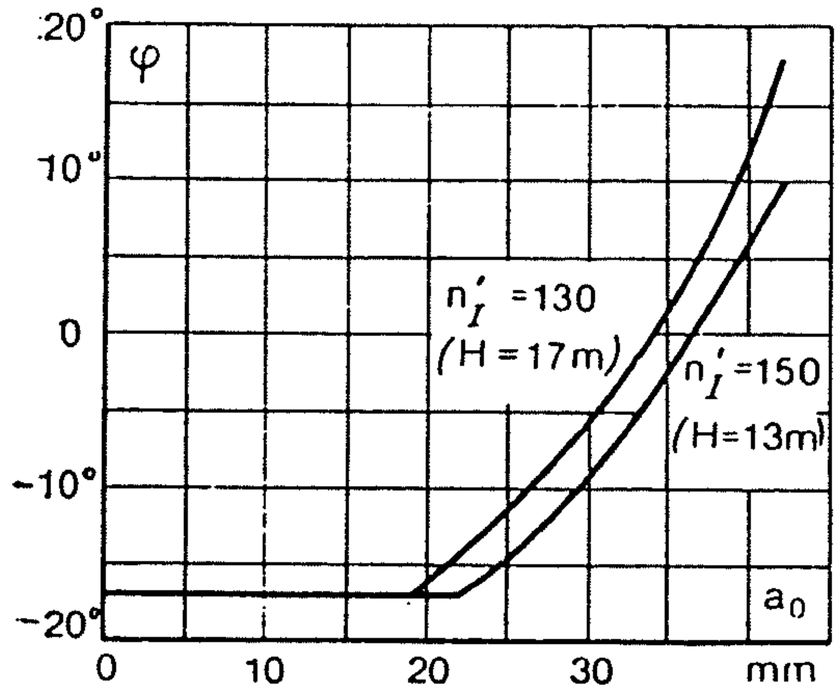


FIGURE 8.12. Combinator relationships of adjustable blade turbine.

of the turbine a_{0t} is calculated by the model

$$a_{0t} = a_0 \frac{D_t}{D_m} \tag{8.9}$$

Then, for similar modes of operation n and Q are converted by Equations 5.36 and 5.37 and the turbine power is calculated from Equation 2.10. However, upon passing to the full-scale conditions some parameters change, the change of efficiency being the parameter of the greatest importance. Bearing this in mind, consider the structure of losses in the turbine and their variation when passing from a model to full-scale equipment.

8.4.1. Losses in Turbine and Balance Characteristics

Losses of energy in a turbine may be represented as three types: hydraulic, mechanical, and volumetric.

The hydraulic losses are due to the flow of water through the turbine at a discharge Q. These losses may be subdivided into: (a) losses caused by friction of the liquid against the walls, h_{fr} (similar to lengthwise losses in water conduits), and (b) vorticity losses, h_v (similar to local losses). Vorticity losses include inlet losses in the blade cascade (Figure 5.7), at the runner outlet (Figure 5.8), and outlet losses (Equation 6.18).

Each type of turbine loss may be represented in terms of loss head. If h_h is the total hydraulic losses (m, mass flow) and the corresponding lost power is N_h, for discharge Q we can write

$$N_h = 9.81 Q h_h$$

and

$$h_h = N_h/9.81Q \tag{8.10}$$

This is the absolute value of hydraulic losses. It is also possible to introduce respective quantity as hydraulic efficiency η_h:

$$\eta_h = \frac{N_l - N_h}{N_l} = \frac{9.81QH - 9.81Qh_h}{9.81QH} = \frac{H - h_h}{H} \tag{8.10a}$$

Here, $N_l = 9.81QH$ is a total available liquid power (see Equation 2.7). As has been noted, the hydraulic losses may be subdivided into the following individual forms: losses in the turbine case stay vanes, wicket gates, and runner—$h_{e.r}$; losses in draft tube (suction)—h_{suc}; and draft tube outlet (exit) losses—h_{out}

$$h_h = h_{er} + h_{suc} + h_{out} \tag{8.11}$$

Volumetric losses due to the leakage flow (discharge q) about the rotating turbine runner blades and through the clearances causes the corresponding lost power N_v, which can be defined by the expression

$$N_v = 9.81qH = 9.81Qh_v$$

It follows that volumetric head loss

$$h_v = qH/Q \tag{8.12}$$

and volumetric efficiency η_{vol} will be

$$\eta_v = \frac{H - H_h - H_v}{H - h_h} \tag{8.12a}$$

Mechanical losses are caused by the friction associated with the rotation of turbine shaft and runner. These losses include losses in bearings and seals, N_{fr}, and so-called disk losses, N_{disk}, resulting from the friction between rotating parts on the liquid, for instance, in clearances between runner rims and the casing (head cover). The power lost on disk friction can be approximately determined by the formulas:

For one side of a disk diameter D	$N_{disk} = P_d n^3 D^5$
coefficient $P_d = (2 - 4) \times 10^{-5}$	
For cylinder diameter D and height b	$N_{disk} = P_c n^3 D^4 b$
coefficient $P_c = (1 - 2) \times 10^{-4}$	

(8.13)

Here, n is the rotation speed (in revolutions per minute) (D and bm) and N_{disc} is measured in watts. The large deviation in P_d and P_c values are due to many factors affecting N_{disk}: clearance dimensions, roughness of walls, temperature, and even peripheral velocity, or nD value. Corresponding mechanical head loss $N_{mech} = N_{fc} + N_{disk}$ can be expressed by the formula

$$h_{mech} = N_{mech}/9.81Q \tag{8.14}$$

Mechanical efficiency with respect to turbine shaft power can be expressed by

$$\eta_{mech} = \frac{H - h_h - h_v - h_{mech}}{H - h_h - h_v} \tag{8.14a}$$

With account taken of the above the total turbine efficiency can be specified by the following expressions:

1. Using absolute losses value

$$\eta = 1 - \frac{1}{H}(h_{e.r} + h_{suc} + h_{out} + h_v + h_{mech}) \tag{8.15}$$

2. Using respective values

$$\eta = N/Ne = \eta_h \eta_v \eta_{mech} \tag{8.16}$$

It is necessary to note that the division of turbine losses practically (discussed above) cannot be exactly fulfilled. For example, volumetric losses in axial- and mixed-flow turbines is very difficult to measure and as a rule they are not given on balance characteristics (Figure 8.13). The different types of mechanical and hydraulic losses can be evaluated also only approximately. Such division is useful, however, for understanding the real factors that affect the turbine efficiency.

8.4.2. Determination of Efficiency of a Full-Scale Turbine

Universal characteristics (for example, Figure 8.3) usually show the hydraulic efficiency of a model $\eta_{h.m}$. Thus, when plotting operating characteristics it is necessary to convert the values of the efficiency obtained on a model into the efficiency of a full-scale turbine and allow for other kinds of losses—mechanical and volumetric. The turbine manufacturer supplies the operating characteristics in which the conver-

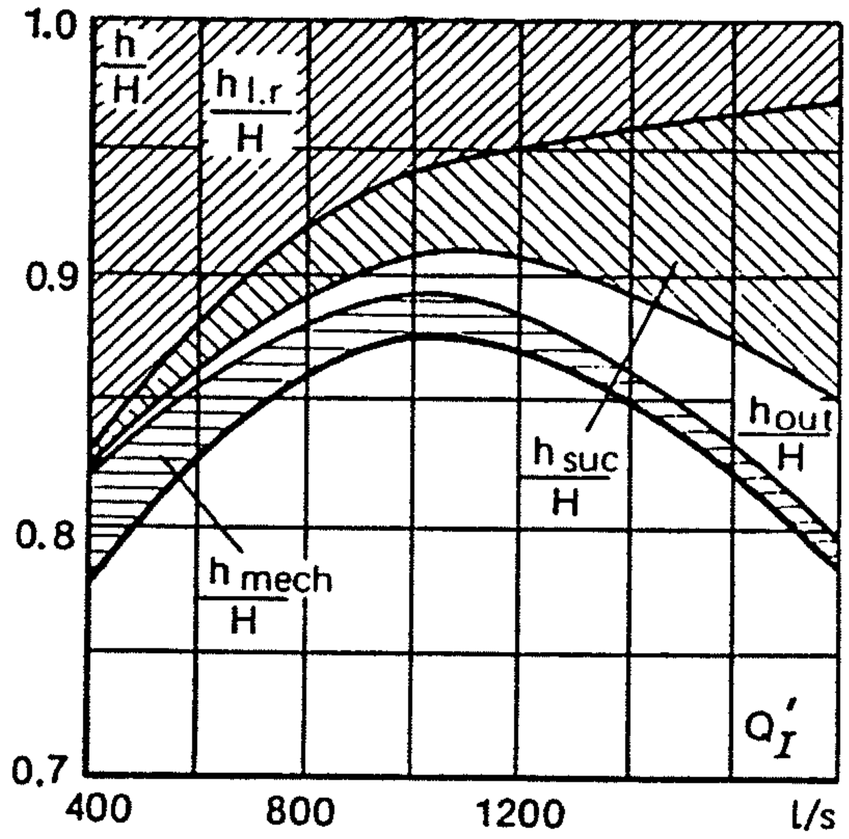


FIGURE 8.13. Balance characteristic of axial-flow adjustable blade turbine.

sion of efficiency is made, taking into account all design features of a given full-scale turbine. Preliminary calculations may be made, however, using the generalized method that consists of the introduction of two corrections: (1) $\Delta\eta_h$—allowing for the change in the hydraulic efficiency, and (2) $\Delta\eta_{m.v}$— allowing for the change in mechanical and volumetric (leakage) losses. As a result the turbine efficiency is expressed via

$$\eta = \eta_{h.m} + \Delta\eta_h - \Delta\eta_{m.v} \tag{8.17}$$

The correction allowing for the mechanical and volumetric (leakage) losses is not great and under normal conditions, we may assume that $\Delta\eta_{m.v} = 0.01$ to 0.02 or 1 to 2%.

The hydraulic efficiency correction is found from a semiempirical formula

$$\Delta\eta_h = (1 - \eta_{h.m})\varepsilon\left(1 - \sqrt[5]{\frac{\nu D_m}{\nu_m D}}\ \sqrt[10]{\frac{H_m}{H}}\right) \tag{8.18}$$

where ε is the ratio of friction losses to all hydraulic losses (for optimal conditions $\varepsilon = 0.75$); D_m and D are the diameters of the model and full-scale turbines, respectively; H_m and H are the heads of the model and full-scale turbines, respectively (the author recommends taking into account the head ratio at $H > 60$ m); and ν and ν_m are coefficients of kinematic viscosity of the liquid in the turbine and in the model. The value of ν depends on the type of liquid and its temperature. $\nu(t)$ quantities are given for water in Table 8.1.

Table 8.1. Kinematic Viscosity of Water

Temperature (°C)	$\nu \times 10^6$ (m^2/s)
0	1.78
5	1.52
10	1.31
15	1.14
20	1.0
30	0.81
40	0.66
50	0.55
60	0.47
70	0.41
80	0.36

In the case of Pelton turbines, $\Delta\eta_h = 0$ (no correction is introduced).

If the characteristic curve represents the values of model total efficiency[1] η_m, rather than of the hydraulic, assume $\eta_{h.m} = \eta_m + \Delta\eta_{m.t}$ when calculating correction $\Delta\eta_h$ from Equation 8.18. It is advisable to calculate $\Delta\eta_h$ from Equation 8.18 only for the optimal conditions and to use the calculated value unchanged for all other operating conditions.

Example 8.1

Determine the efficiency of the turbine with a diameter $D_1 = 5$ m, head $H = 120$ m, water temperature 15°C, according to the characteristic represented in Figure 8.3 for total load $Q'_I = 0.48\ m^3/s$ $n'_I = 70$ rpm (the tests were carried out at 20°C).

Solution

The characteristic is given for model $D_m = 0.46$ m, $H_m = 4$ m. For given Q'_I and n'_I, $\eta_{h.m} = 87\%$. At the optimum point, $\eta_{h.m} = 91.5\%$. Table 8.1 gives $\nu_m = 1 \times 10^{-6}\ m^2/s$ and for the turbine $\nu = 1.14 \times 10^{-6}\ m^2/s$. Using Equation 8.18, find the hydraulic efficiency correction in view of H

$$\Delta\eta_h = (1 - 0.915)0.75\left(1 - \sqrt[5]{\frac{1.14 \times 10^{-6}}{1 \times 10^{-6}}\frac{0.46}{5.0}}\ \sqrt[10]{\frac{4}{120}}\right) = 0.035$$

[1]The international code for model tests of hydraulic turbines permits the use of a simplified method of efficiency correction. The method is based on Moody and Hutton formulas, which are fully similar to Equation 8.18, but deal with values of total efficiency η instead of hydraulic η_h. For axial turbines, $\varepsilon = 0.7$; for Francis turbines, $\varepsilon = 1$.

Assuming $\Delta\eta_{m.v} = 1.5\%$, find the turbine efficiency using Equation 8.17:

$$\eta = 0.87 + 0.035 - 0.015 = 0.89\% \quad \text{(i.e., 89\%)}$$

8.4.3. Theoretical Basis of Hydraulic Efficiency Correction Formula

Flow in a turbine is extremely complex and the regularities involved in the formation of hydraulic losses in the turbine are not quite clear. Therefore, some simplifications are used. Loss coefficient may be regarded as consisting of two parts

$$\zeta_t = \zeta_{loc} + \zeta_f$$

where ζ_{loc} is the loss coefficient similar to local resistance coefficient, and ζ_f is the coefficient of friction losses lengthwise of the surfaces being flown around.

To estimate the variation of ζ_f, consider the behavior of resistance in flowing around a thin plate as an example (Figure 8.14). Resistance force caused by friction P_f is determined by the formula

$$P_f = c_f F \rho \frac{v^2}{2} \tag{8.19}$$

where F is the plate area, v is the oncoming flow velocity, and ρ is the density of fluid.

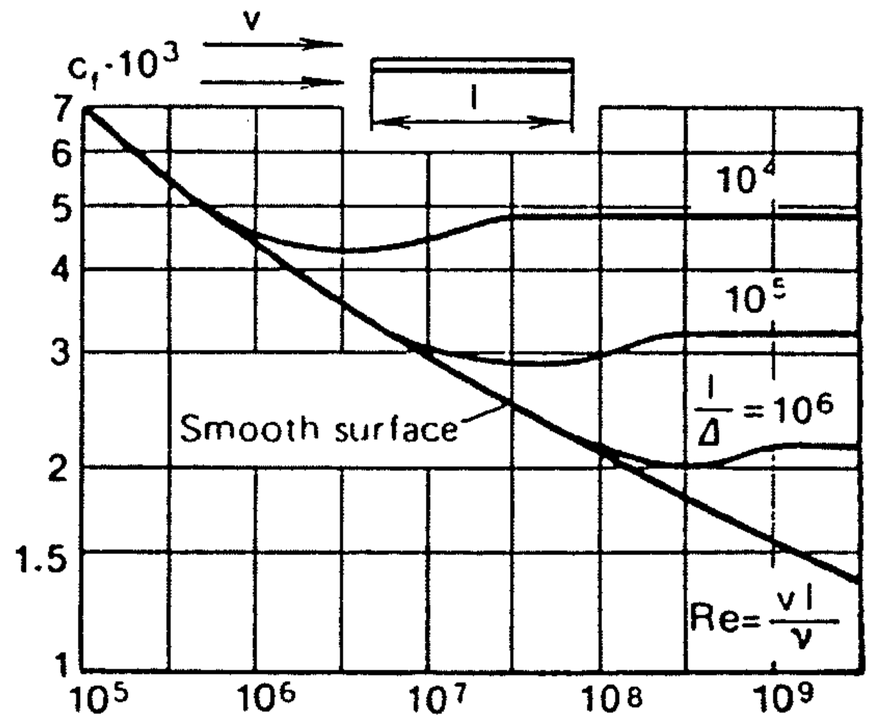


FIGURE 8.14. Plate friction coefficient.

Resistance coefficient c_j depends on relative roughness l/Δ (Δ is the roughness equivalent peak) and the Reynolds number

$$\mathrm{Re} = vl/\nu \tag{8.20}$$

where v is velocity, and ν is kinematic viscosity (Table 8.1).

The relation for a rectangular plate, B wide and l long, is shown in Figure 8.14. The above data show that in the case of a smooth surface coefficient c_j decreases with an increase in Re. According to the von Karman formula for a plate in a turbulent boundary layer

$$c_f = \frac{0.074}{\mathrm{Re}^{0.2}} \tag{8.21}$$

The actual values of Re and l/Δ make it possible to assume that resistance caused by friction changes in turbines approximately the same way as is found on a smooth surface according to Equation 8.21. Obviously, ζ_{fr} is proportional to c_f, and hence we may write

$$\frac{h_{fr.m}}{h_{fr}} = \frac{c_{f.m}v_m^2}{c_f v^2}$$

where $h_{fr.m}$ and h_{fr} are friction losses in the model and full-scale turbines, respectively; v_m and v are the respective velocities.

From Equation 7.7 for similar regimes (modes) it transpires that

$$\frac{v_m^2}{v^2} = \frac{H_m}{H}$$

and hence,

$$h_{fr} = h_{fr.m}\frac{c_f}{c_{f.m}}\frac{H}{H_m}$$

or, in view of Equation 8.21,

$$\frac{h_{fr}}{H} = \frac{h_{fr.m}}{H_m}\left(\frac{\mathrm{Re}_m}{\mathrm{Re}}\right)^{0.2} \tag{8.22}$$

Assume model friction losses to be a certain part of the total hydraulic losses

$$h_{fr.m} = \varepsilon h_{h.m}$$

Thus, if model hydraulic efficiency is $\eta_{h.m}$ relative losses will be as follows:

1. Local (vorticity) losses

$$\frac{h_{loc.m}}{H} = (1 - \varepsilon)\frac{h_{h.m}}{H} = (1 - \varepsilon)(1 - \eta_{h.m})$$

2. Friction losses

$$\frac{h_{fr.m}}{H} = \varepsilon\frac{h_{h.m}}{H} = \varepsilon(1 - \eta_{h.m})$$

Next, refer to hydraulic losses in the full-scale turbine. These losses are also made up of local and friction losses

$$1 - \eta_h = \frac{h_{loc}}{H} + \frac{h_{fr}}{H}$$

For a full-scale turbine, the local relative losses are the same as for the model, while friction losses are represented by 8.22; hence,

$$1 - \eta_h = (1 - \varepsilon)(1 - \eta_{h.m}) + \varepsilon(1 - \eta_{h.m})\left(\frac{\mathrm{Re}_m}{\mathrm{Re}}\right)^{0.2}$$

Allowing for Equation 8.20 and the similarity formulas we present the relationship

$$\frac{\mathrm{Re}_m}{\mathrm{Re}} = \frac{D_m \nu}{D\nu_m}\sqrt{\frac{H_m}{H}}$$

Therefore, the resulting formula for the conversion of hydraulic efficiency will be

$$1 - \eta_h = (1 - \eta_{h.m})\left(1 - \varepsilon + \varepsilon\sqrt[5]{\frac{\nu D_m}{\nu_m D}}\ \sqrt[10]{\frac{H_m}{H}}\right) \qquad (8.23)$$

It is necessary to bear in mind, however, that the formula is valid only for smooth, flowed round surfaces. For the rather high roughness the loss dependence from D and H will differ, and, as seen in Figure 8.14, it can become independent from Re or D and H.

Formula 8.18 based on Formula 8.23 is used for correction of the hydraulic efficiency.

8.5. PLOTTING LINEAR CHARACTERISTICS BASED ON UNIVERSAL CHARACTERISTICS

It is usually necessary to plot a characteristic for a turbine of a given type, which is why the determining parameter is the turbine diameter D_1. The other two parameters that enable us to plot the linear characteristics depend on the kind of linear characteristic. To plot any characteristic it is first necessary to:

1. Find the correction for efficiency $\Delta\eta_h$ from Equation 8.18. The turbine efficiency η is the sum of Equation 8.17.
2. Estimate the margin for the cavitation coefficient k_σ using Equation 7.14. This will make it possible to find the permissible suction height.

Let us consider the methods of plotting some of the more often used characteristics (Figure 8.15a and b).

The linear discharge and power characteristics are a section of the universal characteristic where straight line a–a meets the condition $n'_1 = \text{const}$ (Figure 8.16):

$$n'_{1c} = nD/\sqrt{H} = \text{const}$$

Several points are placed on this line and for each of them the required parameters are calculated: Q, η, N, σ_t, H_s, a_0, and others. The lines $N_{\max}$, $0.95N_{\max}$, and $a_{n.l}$ (no-load run) are essential.

The linear head characteristic (Figure 8.15c) is a section of the universal characteristic where line $a_0 = \text{const}$ (line b–b in Figure 8.16). Several points are placed on this line and for each of them the required parameters are calculated. The head corresponding to any model of

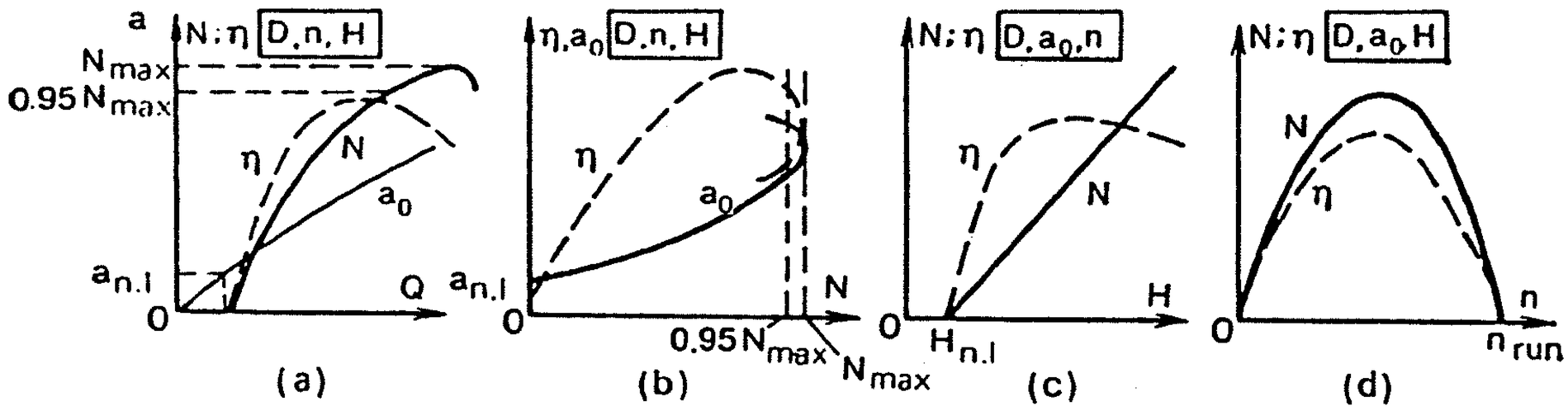


FIGURE 8.15. Linear characteristics of turbine. (a) Discharge; (b) power; (c) head; (d) speed.

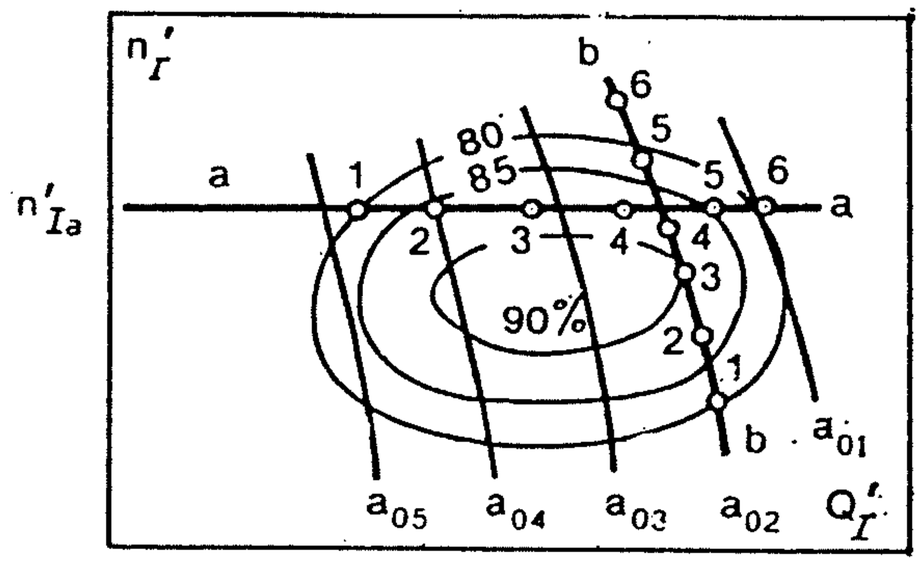


FIGURE 8.16. Plotting linear vs universal characteristics.

operation point is found to be in accordance with points of the similarity formula

$$H = \frac{E}{(n'_{\mathrm{I}})^2}, \quad \text{where} \quad E = (nD_1)^2 \frac{\eta_h}{\eta_{h.m}} \tag{8.24}$$

Here, $\eta_h/\eta_{h.m}$ is the ratio of the optimal hydraulic efficiency of a full-scale turbine to the efficiency of a model. Of interest on this characteristic is the point $H_{n.l}$, the no-load running head. This is the minimum head at which the normal speed is preserved and the overrunning power is zero.

The linear speed characteristic (Figure 8.15d) is also a section of the universal characteristic cut by the line $a_0 = \text{const}$ (line b–b in Figure 8.16). However, here every point determines the rotational frequency rather than the head

$$n = n'_{\mathrm{I}} J, \quad \text{where} \quad J = \frac{\sqrt{H}}{D_1} \sqrt{\frac{\eta_h}{\eta_{h.m}}} \tag{8.25}$$

Of practical interest is point n_{run}, i.e., the maximum speed that the runner may develop in the absence of a load on the shaft. The moment of resistance is equal to zero.

8.6. PLOTTING OPERATION CHARACTERISTICS

The operating characteristics of a turbine differ in that they are plotted on the basis of two parameters: normal speed n_n and a given turbine diameter D_1:

$$n = n_n = \text{const} \qquad D = D_1 = \text{const}$$

Each operating characteristic is a transformation of the domain of universal characteristics in the domain of new coordinates head H and power N (Figure 8.1) or head H and discharge Q (Figure 8.2). Thus, the replotting amounts mainly to a conversion of coordinates from n'_{I} and Q'_{I} into H, N, or H, Q, which is done with the aid of the similarity formulas. The relationships are as follows.

Based on Equation 5.34:

$$H = (nD/n'_{\mathrm{I}})^2 \tag{8.26}$$

Based on Equations 5.35 and 8.26:

$$Q = Q'_{\mathrm{I}} D^2 \sqrt{H} = Q'_{\mathrm{I}} D^2 \frac{nD}{n'_{\mathrm{I}}}$$

$$Q = \frac{Q'_{\mathrm{I}}}{n'_{\mathrm{I}}} nD^3 \tag{8.27}$$

Making use of the power formula

$$N = 9.81QH\eta = 9.81 \frac{Q'_{\mathrm{I}}}{n'_{\mathrm{I}}} nD^3 \left(\frac{nD}{n'_{\mathrm{I}}} \right)^2 \eta$$

we obtain

$$N = 9.81 Q'_{\mathrm{I}} \left(\frac{n}{n'_{\mathrm{I}}} \right)^3 D^5 \eta \tag{8.28}$$

where η is the full efficiency of a given mode of operation (point with coordinates n'_{I} and Q'_{I}).

When plotting operation characteristics, a constant correction is usually introduced in the reduced speed of rotation

$$\Delta n'_{\mathrm{I}} = n'_{\mathrm{I}opt} \left(\sqrt{\frac{\eta_h}{\eta_{h.m}} - 1} \right) \tag{8.29}$$

where η_h and $\eta_{h.m}$ are, respectively, the hydraulic efficiencies of the turbine and model under optimal operating conditions.

Then, for a full-scale turbine:

$$n'_{\mathrm{I}t} = n'_{\mathrm{I}} + \Delta n'_{\mathrm{I}} \tag{8.30}$$

The correction for turbine efficiency is not introduced when calculating the turbine discharge.

Several methods of replotting may be used. For instance, partial linear characteristics are plotted for a number of values of $n'_I - H =$ const and their sections are transferred into field of coordinates H, Q or H, N.

When designing a HEPP and selecting suitable turbines, it is often necessary to tackle the problem of change in the operating characteristics when turbine parameters n and D change. It is convenient to introduce the scale factors

$$k_n = \frac{n_1}{n_2} \qquad k_D = \frac{D_1}{D_2} \qquad k_H = \frac{H_1}{H_2} \qquad k_N = \frac{N_1}{N_2}$$

and find the relationship between $k_H = f_H\ (k_n, k_D)$ and $k_N = f_N\ (k_n, k_D)$. Writing the corresponding relations we obtain

$$k_H = k_n^2 k_D^2 \qquad k_N = k_n^3 k_D^5 \tag{8.31}$$

The relationships (8.31) show that a change of k_n and k_D results in a movement of points of the operating characteristic into the domain of coordinates H and N. Four cases are considered.

1. It is only speed that increases: $k_D = 1$, $k_n > 1$. Note that $k_H > 1$ and $k_N > 1$ and the points of the working zone of the characteristic move upward and to the right (H and N increase). The mode of operation points move along curves $N = PH^{3/2}$, where P is the constant coefficient (the dotted lines in Figure 8.17a).
2. It is only the diameter that increases: $k_n = 1$, $k_D > 1$. Note that $k_H > 1$ and $k_N > 1$, and the points in the working zone of the characteristic also move upward and to the right along the lines $N = RH^{5/2}$, where R is the coefficient (Figure 8.17b, dotted lines).
3. It is necessary to change n and D so that characteristic points move only along the vertical (along the head). To this end, it is necessary to ensure conditions from Equation 8.31: $k_N = 1$ or $k_n^3 k_D^5 = 1$; $k_D = k_n^{-3/5}$. The imposed requirement will be met if n and D are simultaneously changed to adhere to the obtained equality. For instance, if we take $k_n = 1.1$, then $k_D = 0.94$; i.e., the diameter must be decreased. Under these conditions the head will take the form $k_H = k_n^2(k_n^{-3/5})^2 = k_n^{4/5}$. All the mode of operation points move along the vertical (Figure 8.17c).
4. The condition under which the characteristic points will move along a horizontal (i.e., without a change of head) can be expressed on the basis of Equation 8.31 as follows:

$$k_n^2/k_D^2 = 1 \qquad k_n = 1/k_D$$

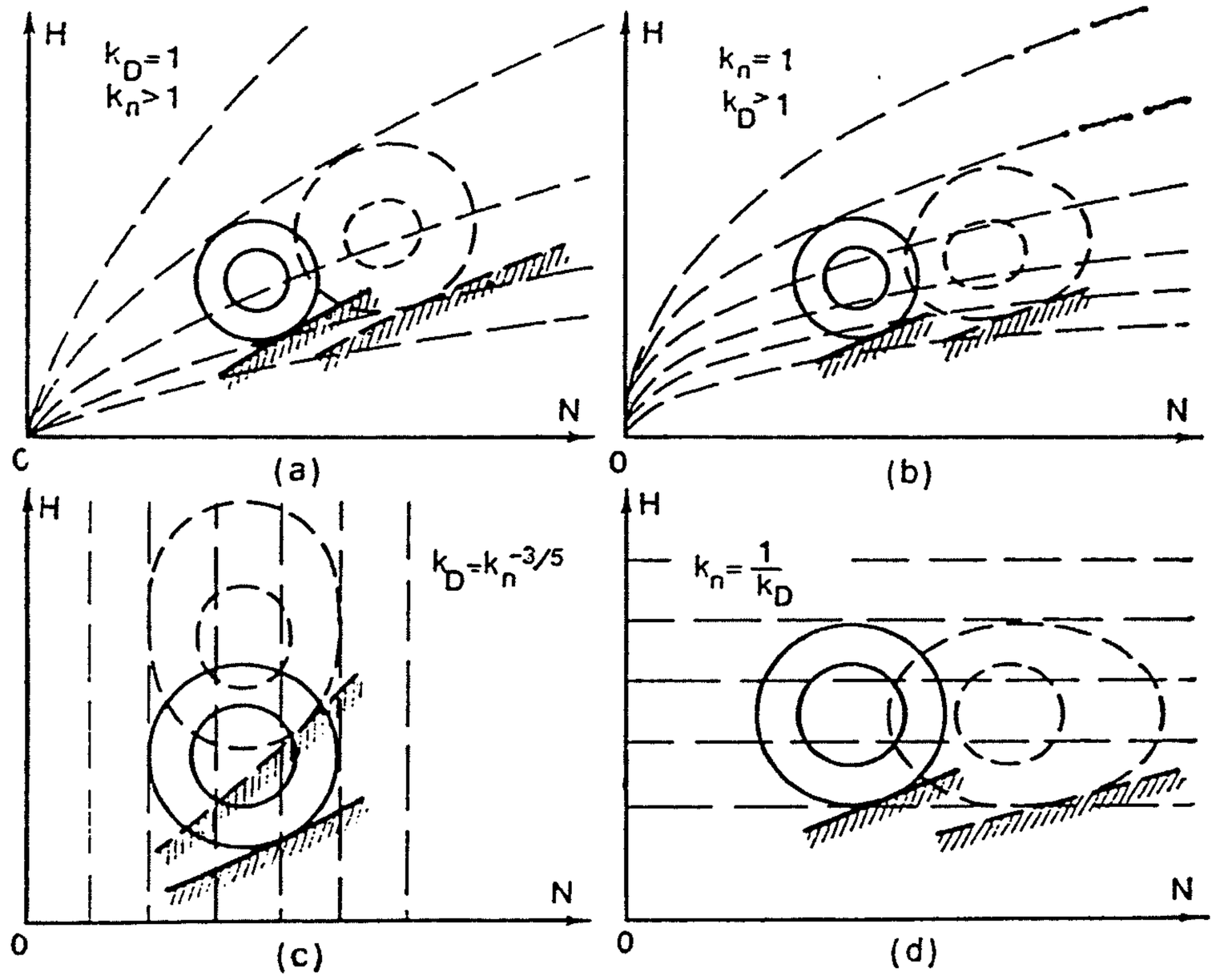


FIGURE 8.17. Displacement of operating characteristic points vs. speed of rotation and diameter of turbine.

Then abscissas of all N points change k_D^2 times (Figure 8.17d).

8.7. RUNAWAY CHARACTERISTICS OF TURBINES

When loaded under normal operating conditions the speed n of a turbine is maintained constant. However, when a loaded hydroelectric set is cut off from the network under emergency conditions, the speed increases rapidly. Further, if the turbine is not closed, the speed may reach the maximum value—the runaway speed. Because this is taken into account when the rotating parts of the hydroelectric set are designed for strength, it is important to define the possible runaway speed. To this end, use is made of the runaway characteristic of the turbine that is taken on the test rig at a braking moment which is equal to zero.

The runaway characteristic of a model is expressed in reduced values of $n'_{\mathrm{I}\,run}$ as a function of the opening of the model $n'_{\mathrm{I}\,run} = f(a_0)$. The runaway characteristic of the radial-axial turbine with an optimal reduced speed $n'_{\mathrm{I}0} = 66$ rpm is shown in Figure 8.18. It shows that $n'_{\mathrm{I}\,run}$ increases as the opening increases, and consequently the most danger-

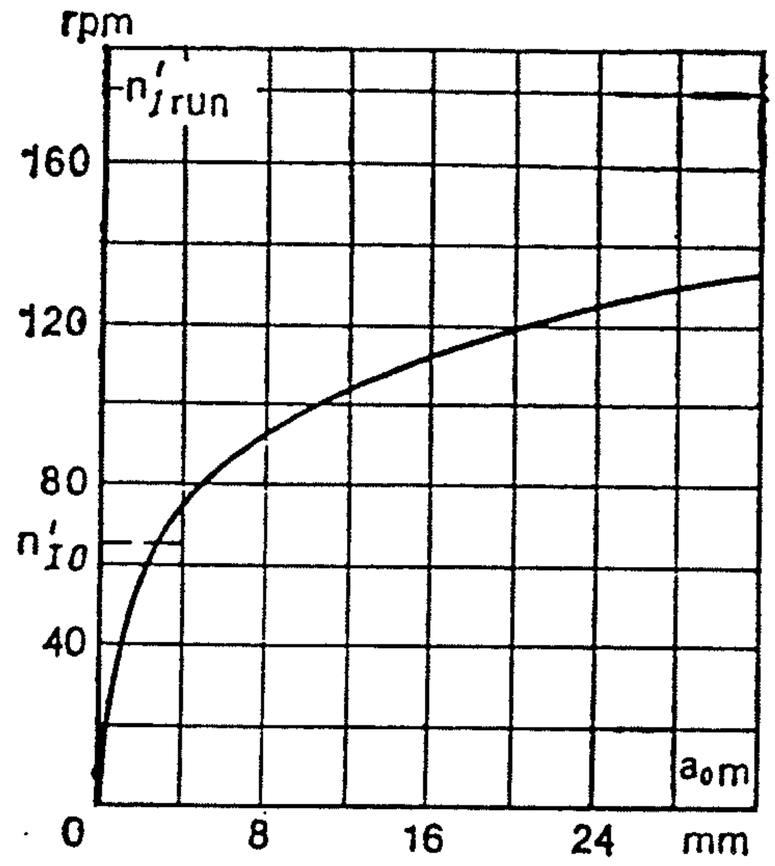


FIGURE 8.18. Runaway characteristic of radial-axial flow turbine ($D_m = 460$ mm).

ous is the runaway at a full opening, with $a_0 = 32$ mm in the case considered.

The runaway coefficient is the ratio

$$k_{run} = \frac{n'_{I\,run}}{n'_{I0}} \tag{8.32}$$

In the case considered $k_{run} = 133/66 = 2.0$; k_{run} for radial-axial turbines varies between 1.6 and 1.7 for low specific speed (high-head) and within 1.9 and 2.1 for high specific speed turbines.

If we know the value of $n'_{I\,run}$, the runaway speed of the turbine is calculated from the similarity formulas of Equation 5.36

$$n_{run} = \frac{n'_{I\,run.t}}{D_1}\sqrt{H} \tag{8.33}$$

with a correction introduced via Equation 8.29:

$$n'_{I\,run.t} = n'_{I\,run} + \Delta n'_I \tag{8.34}$$

The runaway characteristic makes it possible to estimate the no load opening $a_{n.l}$. Therefore, for a given turbine $n'_{I0} = 70$ rpm, then $a_{n.l.m} = 3.5$ mm and for a full-scale turbine $a_{n.l} = 3.5D_1/D_m$.

The runaway characteristics of adjustable blade turbines are more complicated because here $n'_{I\,run} = f(a_0, \varphi)$. Figure 8.19 shows the runaway characteristic of an adjustable blade turbine for which $n'_{I0} = 130$ rpm. The solid lines give propeller relationships at a constant runner blade angle φ. The lines make it clear that $n'_{I\,run}$ increases with

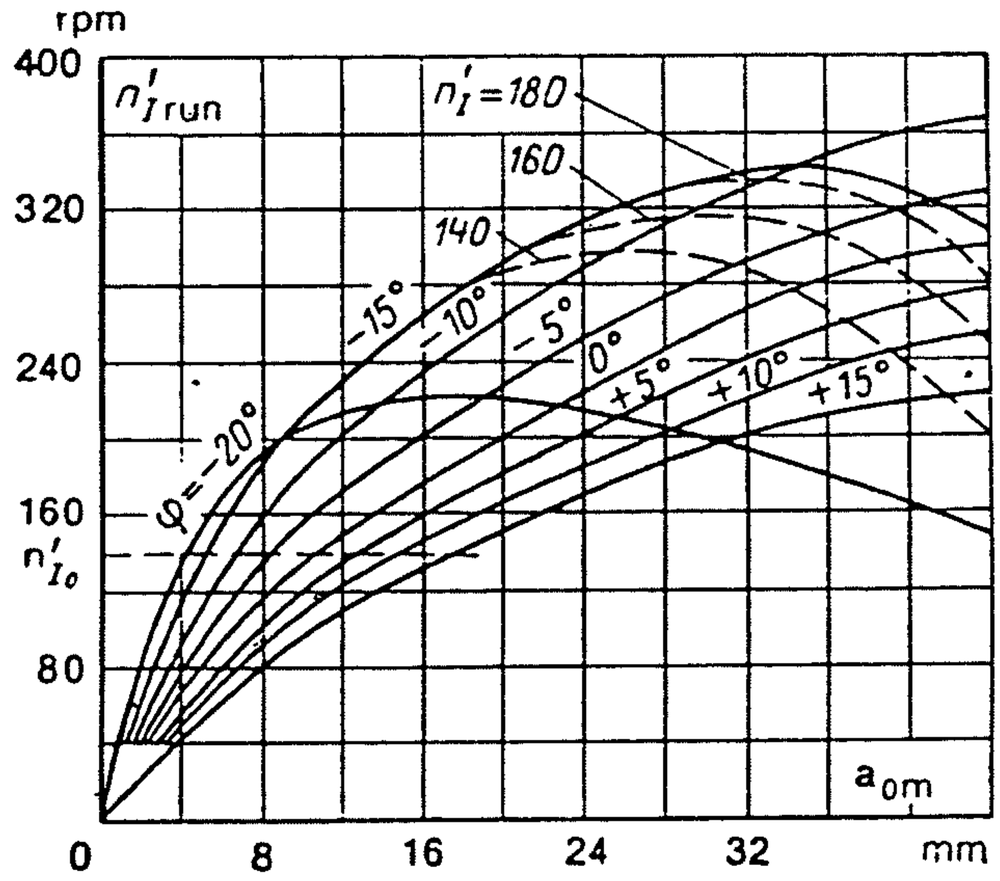


FIGURE 8.19. Runaway characteristic of adjustable blade turbine ($D_m = 460$ mm).

diminishing angle φ and with increasing a_0. Only at very small angles ($\varphi < -15°$) and large openings does the characteristic "tilt" and the runaway speed diminish.

If a very small blade angle ($\varphi = -25°$ to-30°) is set, then $n'_{I\,run}$ drops almost to zero (the average blade incidence angle is close to 90°). Setting the blades to a very large angle, about $\varphi = +60°$, with the average attack angle approaching zero, produces a similar effect. The maximum reduced speed $n'_{I\,run}$ usually corresponds to an angle $\varphi = -5°$ or $-10°$; in this case the runaway coefficient k_{run} is rather high. Thus, for the given turbine at $a_0 = 44$ mm and $\varphi = -10°$, $n'_{I\,run} = 370$ rpm, $k_{run} = 2.85$.

The necessity of calculating the rotating parts of a hydraulic turbine to such a high runaway speed causes a considerable increase in the cost of the generator. However, it must be taken into account that under real conditions the relationships between φ and a_0 are specified by the combinator dependence. As seen in Figure 8.12, at small values of φ, a_0 is also small, and at high values of a_0, φ increases as well. The real relationships between a_0 and φ must be assumed in compliance with the combinator dependence, which is estimated based on the condition $n'_I = \text{const}$.

The several dotted line curves shown in Figure 8.19 correspond to different values of the head. It is of interest to note that the maximum values of $n'_{I\,run}$ occur at comparatively small values of the turbine opening a_0. For instance, at $n'_I = 160$ rpm, $n'_{I\,run.max}$ corresponds to $a_0 = 30$ mm; i.e., to an opening of about 70% of the full opening. Thus, the runaway coefficient reduces considerably (in the case considered $k_{run} = 303/150 = 2.02$).

8.8. AXIAL LOADS ACTING ON THE TURBINE RUNNER

The axial loads acting on the turbine runner and taken up by the axial bearing are composed of axial pressure components acting on the hub, rim, and casing and of the axial component of the water flow's hydrodynamic activity on the runner blades and the weight of the runner. Aiming to diminish the axial force in radial-axial turbines the runner is balanced by placing seals in the crown and band and providing relief holes (Figure 3.15, (20)). It is impossible, however, to balance the runner in axial-flow turbines, and the axial hydrodynamic forces are of great importance to these turbines.

A typical characteristic of reduced hydrodynamic forces P'_1 of an axial adjustable blade turbine are shown in Figure 8.20 for three values of angles $\varphi = -10°$, $0°$, and $+15°$. The axial force for a full-scale adjustable blade axial-flow turbine was converted by the formula

$$P_h = P'_1 D_1^2 H \tag{8.35}$$

The common axial force taken up by the thrust bearing will be equal to the sum of P_h, weight of rotating parts, and of a relative small component, allowing for the pressure in the clearance between the hub and the head cover. For vertical turbines this axial force will be equal to the hydrostatic balancing force (the runner is immersed in water).

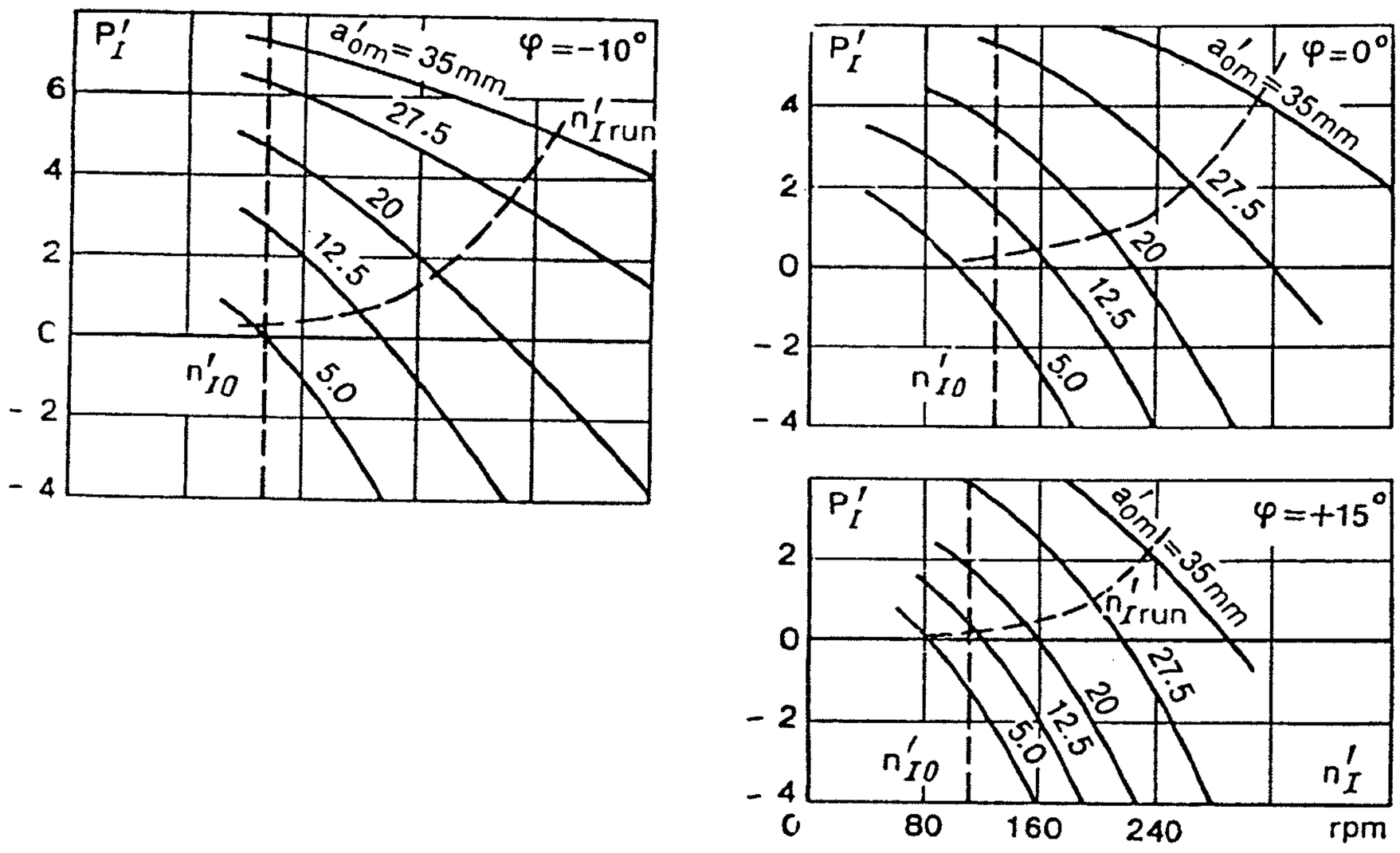


FIGURE 8.20. Axial hydrodynamic forces of runner in an axial-flow adjustable blade turbine.

It is clear from the characteristic that P'_I increases with a diminishing angle φ. Therefore, in the zone of optimal speed $n'_{I\,opt}$ with an opening equal to 27.5 mm for $\varphi = -10°, P'_I = 6.3$ kN, and for $\varphi = +15°$ $P'_I = 4.0$ kN. The hydrodynamic component of the axial force constitutes a rather great load on the bearing. For instance, at $D_1 = 9.0$ m and $H = 25$ m; if $P'_I = 5.0$ kN, $P_h = 5.0 \times 9^2 \times 25 = 10{,}100$ kN.

The axial force P'_I diminishes rapidly with increasing speed n'_I, but at $n'_{I\,run}$ it preserves its positive sign, i.e., is directed along the flow (downward). With a further increase in speed n'_I under braking conditions (the torque on the shaft diminishes), P'_I drops to zero and passes into the negative zone. The negative values of P'_I increase at a particularly high rate at large angles φ and small openings of the wicket gate. This constitutes the danger of a rise of rotating parts when the turbine is rapidly closed because under these conditions the upward acting hydrodynamic axial force may exceed the weight of the rotating parts. Such emergencies have been observed at HEPPs.

8.9. COMPARING TURBINES OF DIFFERENT TYPES VIA THEIR CHARACTERISTICS

At HEPPs the operating conditions for turbines are in a state of flux. The power changes within a wide range depending on the water inflow and the load carried by the power system. Sometimes the head varies considerably with a change in the water basin level, the TW level, and losses in water conduits. In this context, it is very important to know how these changes affect the operation parameters of turbines of different types.

The properties of various turbines can be easily compared using the relative characteristics plotted in dimensionless coordinates. In this case some mode of operation, usually an optimal mode having a maximum efficiency, is selected to serve as a basis and all quantities are determined in relation to the basic ones (with an index 0):

$$\eta_{rel} = \eta/\eta_0 \qquad q = Q/Q_0 \qquad N_{rel} = N/N_0$$

Under these conditions any characteristics of different turbines pass through a common point with coordinates 1, 1 (i.e., coincide), and this makes it possible to obtain a visual idea of their properties. Figure 8.21 demonstrates the relative power (a) and relative discharge (b) characteristics. They show that different turbines respond to a change in load (discharge and power).

The best properties belong to the Pelton and the adjustable blade turbines. If the operating range is limited by a drop in efficiency to 10%, then for these turbines the range of the flow rate q will be from 0.3 to

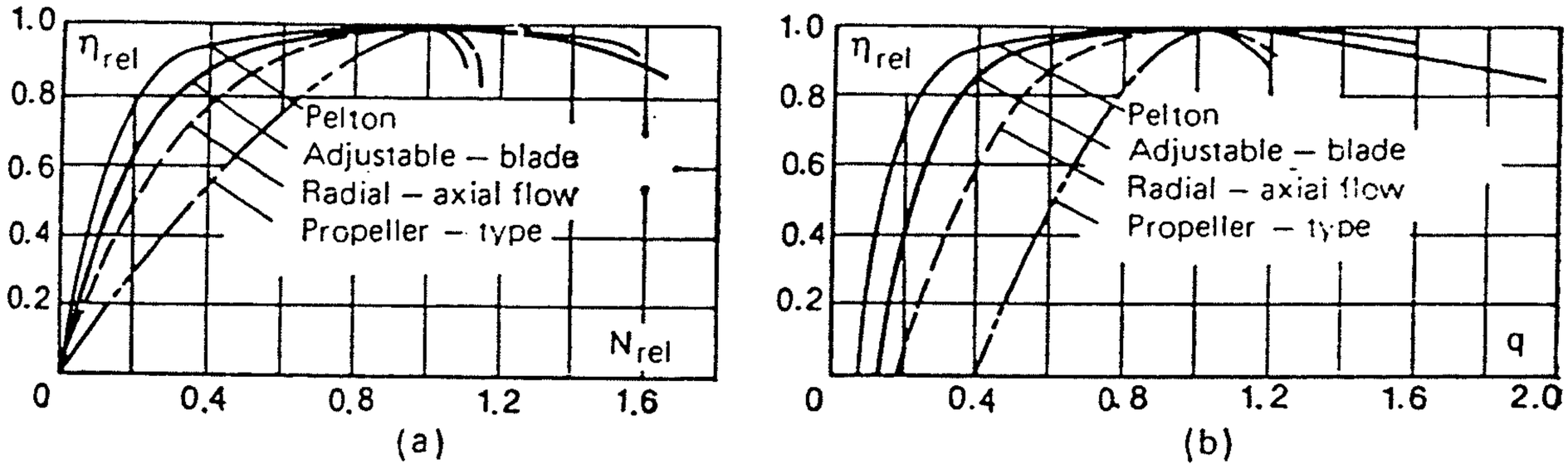


FIGURE 8.21. Power (a) and relative discharge (b) characteristics of turbines.

0.45 to 1.8 and power N_{rel} from 0.25 to 1.6. The point of intersection of the axis q ($\eta_{rel} = 0$) gives a no-load discharge $q_{n.l} = 0.07$ to 0.12 (7 to 12%). Less favorable are characteristics of the radial-axial turbines in which the efficiency changes more rapidly when the load changes. The change is especially abrupt when, increasing above optimum, $q_{n.l} = 0.15$ to 0.2. The operating range of those turbines is considerably smaller, and in terms of power N_{rel} varies from 0.5 to 0.6 to 1.1 to 1.2. The most unfavorable characteristics are of the propeller-type turbines, whose efficiency drops rapidly if the operating conditions deviate from the optimal, i.e., when $q_{n.l}$ reaches 0.4 to 0.45 and the power range is only 0.75 to 1.05.

The noted characteristics are of great practical value. If by the mode of operation of the HEPP turbine power must vary over a sufficiently wide range, then preference must be given to adjustable blade (axial- or mixed-flow) turbines. Under these conditions such turbines reduce the efficiency less than do radial-axial turbines, the factor which ultimately increases the HEPP energy output. This explains the tendency to install adjustable blade turbines that operate under greater heads. Yet, when it is possible to operate with a little varying load of the turbogenerating unit it may be expedient to install simple radial-axial turbines and even propeller-type wheel units.

How the change in head affects turbines operation may be traced by examining the relative head characteristics plotted for a constant speed (Figure 8.22). The relative head $h = H/H_0$, where H_0 is the head corresponding to a maximum efficiency for given n and D. According to Equation 5.34

$$H_0 = (nD/n'_{10})^2$$

These characteristics show that when the head is above H_0 the efficiency of all turbines does not significantly decrease, but, when the head decreases the efficiency drops very rapidly to zero.

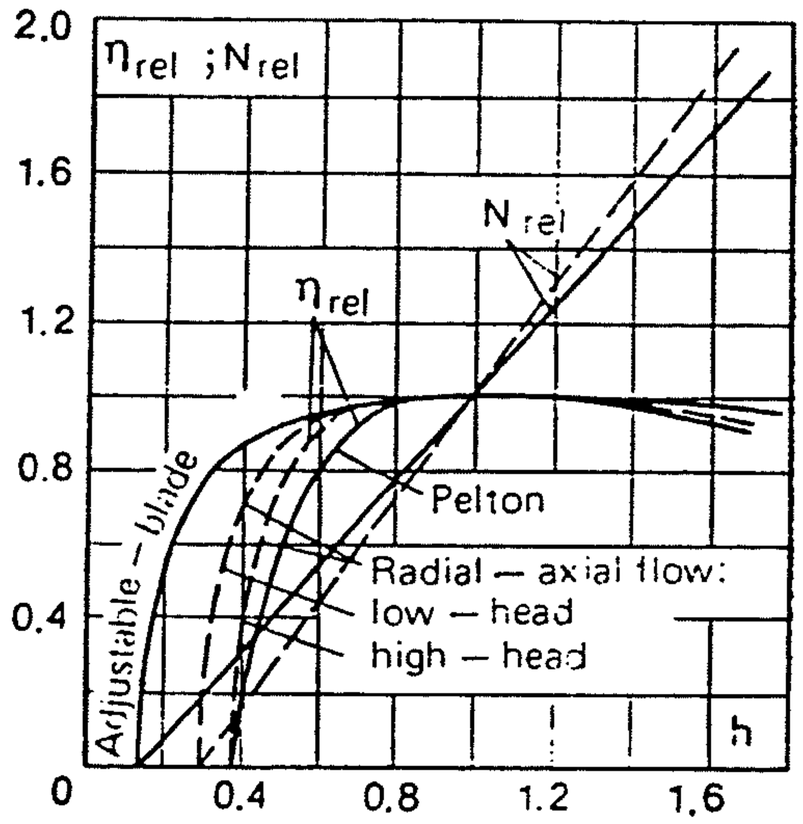


FIGURE 8.22. Relative head characteristics of turbines.

Adjustable blade turbines are the best performers. The efficiency of these turbines is maintained over a wider range of heads, and their power diminishes more slowly with a drop in head. The efficiency and power of Pelton and high-head radial-axial turbines are apt to drop with a diminishing head.

The dependence of power on head $N_{rel} = f(h)$ at $n = \text{const}$ is close to a straight line, and specified rather accurately by the following equation:

$$N_{rel} = \frac{1}{1 - h_{n.l}}(h - 1) + 1 \tag{8.36}$$

where $h_{n.l}$ is the no-load head (points of intersection of the head characteristic with the h axis shown in Figure 8.22).

CHAPTER 9

Selecting Turbines for Hydroelectric Power Plants (HEPPs)

9.1. HYDROELECTRIC UNIT AND POWERHOUSE OF HEPP

Selecting turbines is an essential stage in designing a HEPP. All operating conditions of the turbines (head, power) must be taken into account, especially the layout of the powerhouse, the supply and tailwater (TW) conduits, construction and service conditions, engineering, and cost data. Some elements such as the supply part of the turbine (the spiral case) and the TW conduit (the draft tube) are of such a great size that they almost always prescribe the dimension and layout of the powerhouse of the HEPP. The interrelationship between the turbines and the building structures assumes greater importance due to the fact that the draft tubes, and often the spiral cases, are made from reinforced concrete, and thus the reason they are an integral part of the underwater block of the powerhouse at a HEPP.

A general view of vertical hydroelectric units is shown in Figures 1.2 and 1.4. The horizontal, bulb type is displayed in Figure 1.3. The schematic diagrams of vertical hydroelectric units are depicted in Figure 9.1.

The components of an electric generator are the rotor (1) with poles, which create a rotating magnetic field while in operation, and the stator (2), from whose windings current is transmitted into the power network. The main parts of a turbine are the runner (3), the turbine case (4), the

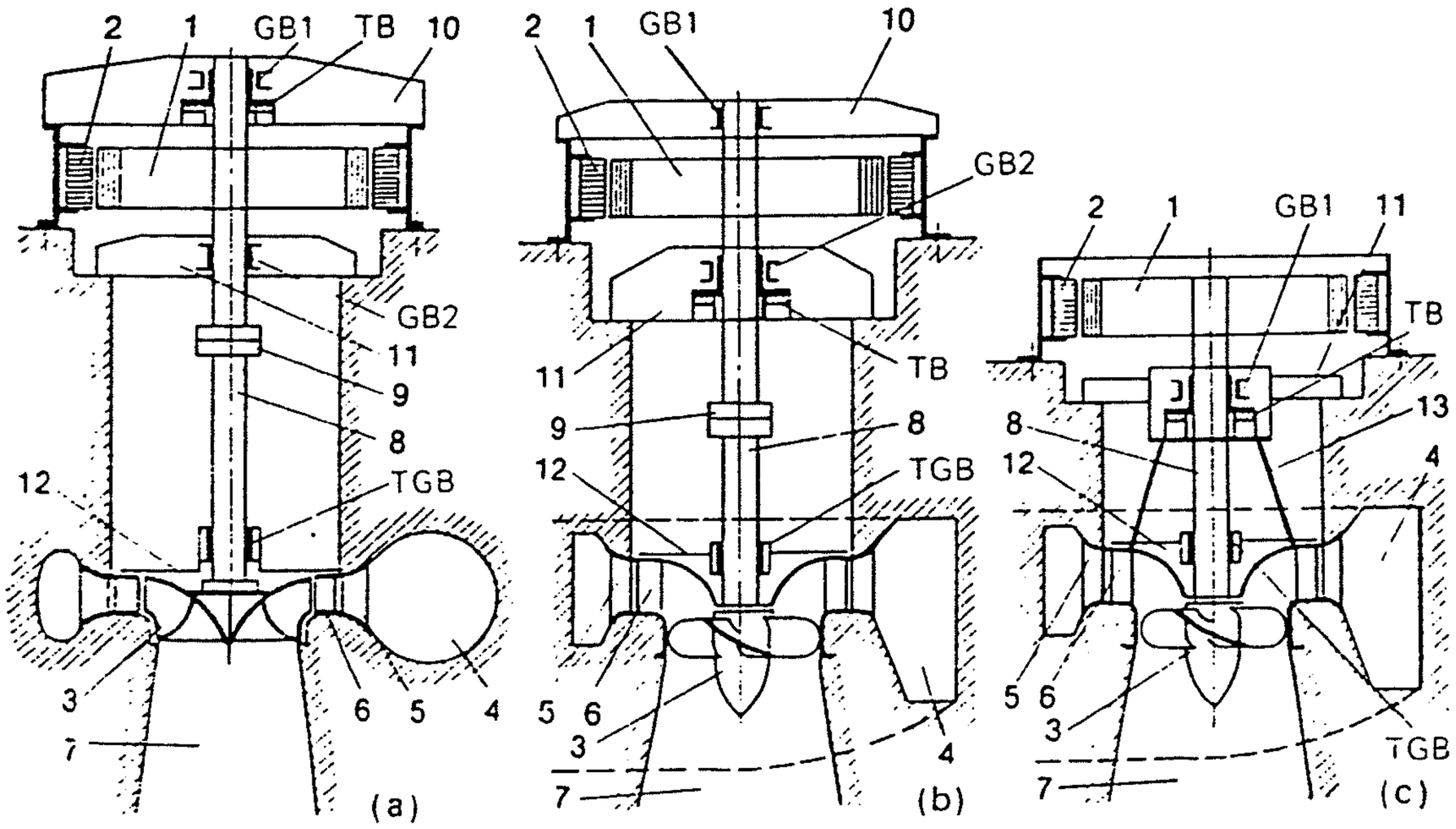


FIGURE 9.1. Vertical hydroelectric units.

stayring (5), the wicket gate (6), and the draft tube (7). The turbine runner and rotor are connected by a common shaft (8) which can have a "built-up" design. The generator and turbine shafts are rigidly connected by flange (9) (Figure 9.1a, b), or may have a solid design (Figure 9.1c). Because the turbine runner and generator rotor are rigidly connected by a common shaft, they rotate with an equal speed. HEPPs presently use ac generators having a standard frequency of 50 Hz; in the United States and other countries, the standard frequency is 60 Hz. When operating with a load, the speed of the generator rotor and that of the turbine runner must be always constant, equal to the synchronous speed of the generator.

Departing from given current frequency, the synchronous speed n_{syn} is determined by two formulas

$$\text{for 50 Hz } n_{syn} = 6000/p$$

$$\text{for 60 Hz } n_{syn} = 7200/p \tag{9.1}$$

where p is the number of generator poles that must be even, and at $p > 24$ it is desirable to be a multiple of four. Thus, a number of n_{syn} values is defined and intermediate values are impossible.

All rotating parts of a hydroelectric (turbine generator) unit, the runner, shaft, and generator rotor, rotate in a common system of

bearings. It is necessary to have two types of bearings: guide bearings, which only prevent radial displacement of the rotating parts, and the thrust bearing, which takes up axial loads. Axial loads in vertical turbine-generator units are defined as the sum of the weight of rotating parts and the axial action of the hydrodynamic flow acting on the runner.

Different schematics show how the rotating parts of the set are arranged to rest. Figure 9.1a shows a suspended generator whose thrust bearing (TB) and the upper guide bearing (GB1) rest on a rigorous upper spider (10) transmitting load on the stator frame that is fastened in the concrete structure. The second guide bearing (GB2) is arranged in the lower spider (11), which is secured in the concrete, and the third turbine guide bearing (TGB) is secured on the turbine head cover (12). Figure 9.1b and c shows the schematics of an umbrella-type generator whose TB is arranged underneath the generator rotor and rests on the rigorous lower spider (11) (Figure 9.1b). It also transmits the load on the turbine head cover (12) through a supporting structure (13) (Figure 9.1c). A very important conclusion follows from the above analysis. Although a hydroelectric unit consists of two machines, a turbine and a generator, they have a common system of bearings.

The layout of the powerhouse, built at a HEPP on the Volga River, having an installed axial-flow turbine (the head varies within 14.7 to 6.5 m, the design head is 9.7 m, the turbine power is 59.3 MW, the flow rate through the turbine amounts to 705 m^3/s, the diameter of the runner measures 10.3 m), is shown in Figure 9.2. This, the world's largest turbine, was manufactured at the Kharkov Turbine Works (KhTW). Figure 9.3 shows a sectional view of the powerhouse of the high-head Nurek Hydro constructed on the Vakhsh River, where radial-axial turbines are installed (fluctuation of heads is from 275 to 207 m, the design head is 223 m, the rated turbine power is 310 MW, and the flow rate is 155 m^3/s, runner turbine diameter measures 4.75 m). The examples show clearly that the turbine and the turbine–generator set determine the dimensions of the submerged portion of the powerhouse and their construction forms are closely connected with the construction part.

9.2. NOMENCLATURE OF REACTION TURBINES

9.2.1. Turbine Type Marks and Range Chart

The turbine nomenclature recommends the types to be used, depending on the head, indicating their main performance parameters, relative

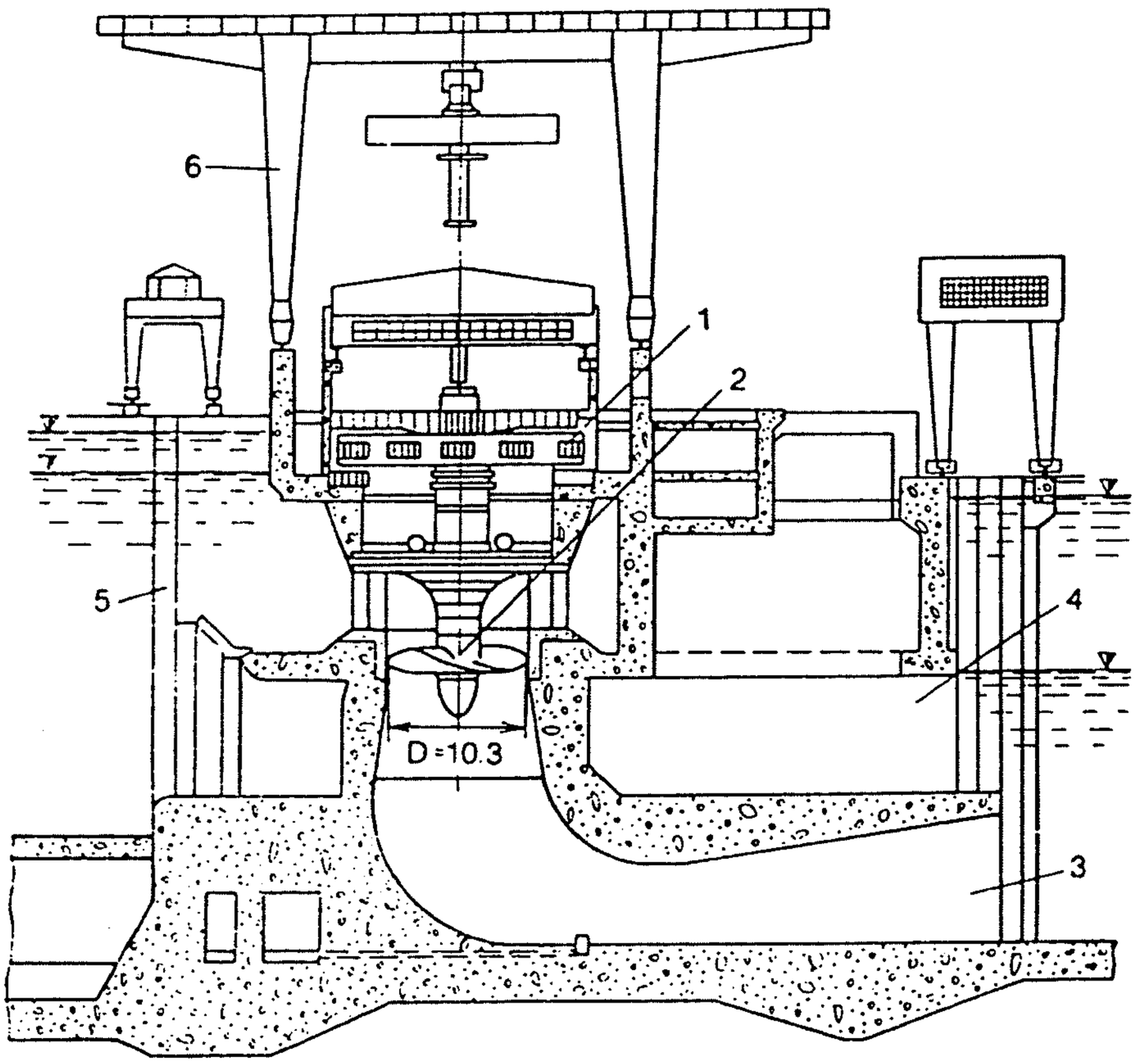


FIGURE 9.2. Powerhouse of Saratov Hydro with axial-flow adjustable blade turbine 1 — Generator; 2 — runner; 3 — draft tube; 4 — spillway; 5 — screen and gate slots; 6 –main crane.

sizes, reduced values of speed n'_I, discharge Q'_I, and cavitation coefficients σ. The nomenclature permits the selection of turbines in designing a hydroelectric station. Each large turbine manufacturing company has its own nomenclature of available types of hydraulic turbines. A nomenclature in the form of range chart usually plotted in coordinates' head and power shows the recommended domain for each type of turbine.

Standard methods for marking the turbine do not exist, as each company uses its own system. Here, and in general, the mark must give basic information such as the kind of turbine, maximum permissible head, and turbine defining dimension.

The turbine mark can be written as follows: K20-800-Kaplan turbine for maximum head up to 20 m, diameter $D = 800$ cm (it can also be written in inches) and F170-500-Francis turbine, for maximum head 170 m, diameter $D_1 = 500$ cm. (It is necessary to note that for the same mark, data can exist for several turbine designs that differ in properties and characteristics. These differences as a rule are insufficient, though sometimes practically important.) The different kinds of turbines can be

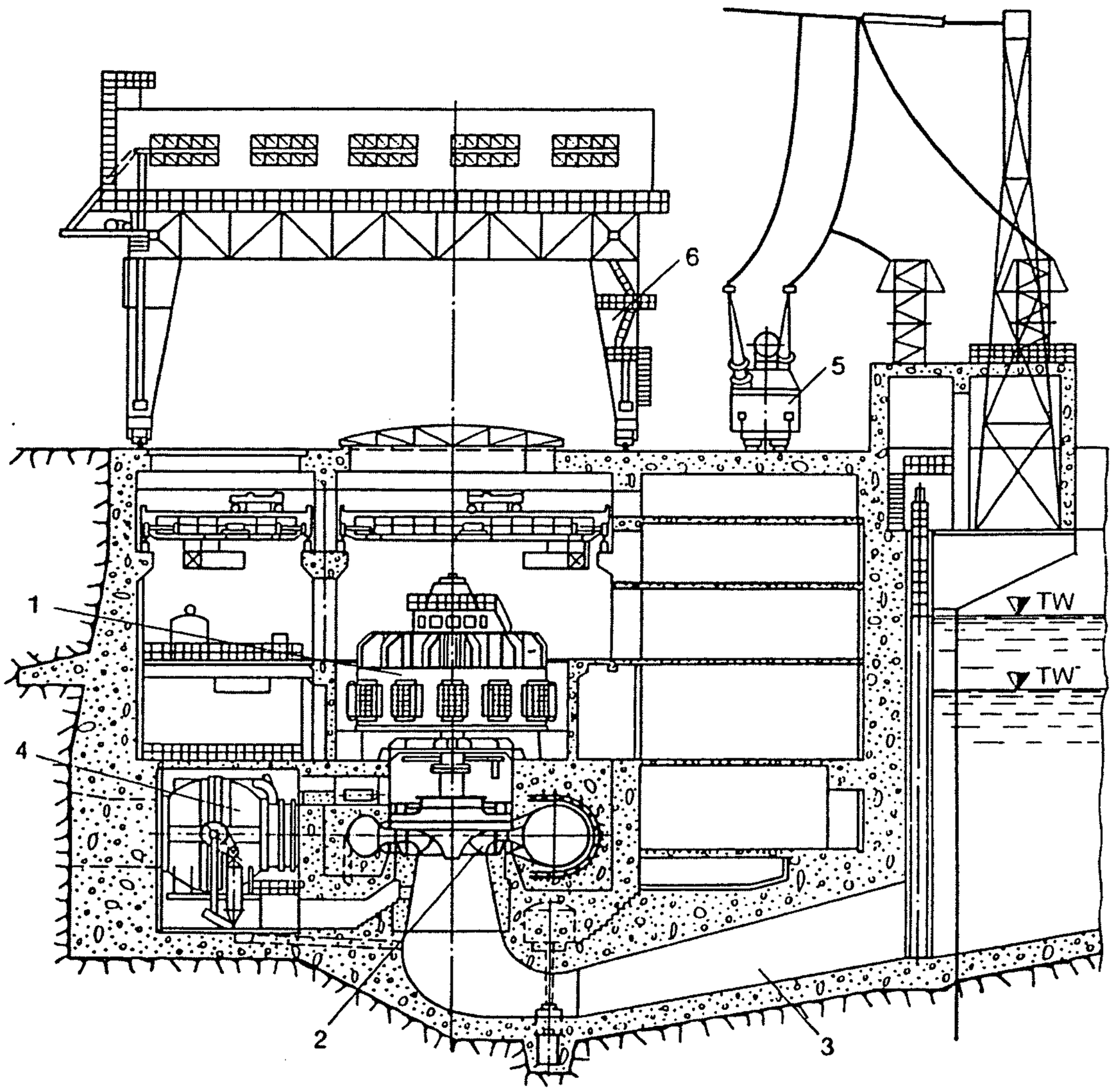


FIGURE 9.3. Powerhouse of Nurek Hydro with radial-axial flow turbine. 1 — Generator; 2 — runner; 3 — draft tube; 4 — ball gate; 5 — transformer; 6 — main crane.

denoted:

Axial, adjustable blade (Kaplan)	K
Axial fixed-blade (propeller)	Pr
Diagonal (mixed-flow)	D
Radial-axial (Francis)	F
Impulse (Pelton)	Pt

The maximum head can be written after the letters defining the type of turbine.

As a turbine defining dimension, the runner entrance diameter D_1 is more often accepted, although sometimes exit diameter D_2 is indicated.

Both methods are principally admittable, but when dealing with turbine characteristics D_2 must be taken into consideration. Nevertheless, the use of D_1 is preferable as it sufficiently affects velocities u_1 and v_1, which, as seen in Equations 5.19 and 5.20 more largely define the turbine operation than u_2 and v_2.

The turbines are divided usually into two groups that are referred to as "large turbines" ($D_1 \geq 200$ cm, axial, and $D_1 \geq 180$ to 125 cm, Francis or $P > 10{,}000$ kW); the less than symbol indicates "small turbines." The practical significance of such division is that large turbines in most cases are designed and manufactured individually, thus more freedom is available when defining their parameters.

A general nomenclature (range chart) of large axial and Francis turbines is given in Figure 9.4. The chart covers a range of heads, from 5 to 700 m, and turbine maximum power from 20,000 to 800,000 kW. The D_1 of the larger turbines are 1100 to 1000 cm for low heads ($H < 30$ m) and up to 500 cm for very high heads ($H > 500$ m). The partial nomenclature of small turbines are shown in Figure 9.5.

The basic dimensions for adjustable blade and radial-axial flow turbines are given in Figures 9.6 and 9.7.

9.2.2. Specific Speed of Turbines

Of great importance is the specific speed of a turbine determined by Equations 5.38 and 5.39 for nominal power using the design values of n'_{I} and Q'_{I}. The tendency is toward the use of high specific speed turbines, since at the same head and rated power of the turbine it is possible to decrease the turbine diameter, i.e., the size of the turbine and that of the powerhouse, to decrease the mass of the turbine and increase the speed of the unit. The field of the actual design specific speeds is shown in Figure 9.8. The recommended values of the design specific speeds, based on current data, are shown by sections of straight lines. The formulas for these straight lines are found in Equations 9.2:

Radial-axial (F) turbines

$$\text{at } H > 200 \text{ m } n_s = \frac{4400}{H^{0.6}}$$

$$\text{at } H < 200 \text{ m } n_s = \frac{2600}{H^{0.5}}$$

Adjustable blade (K or D) turbines (9.2)

$$n_s = \frac{2300}{H^{0.4}}$$

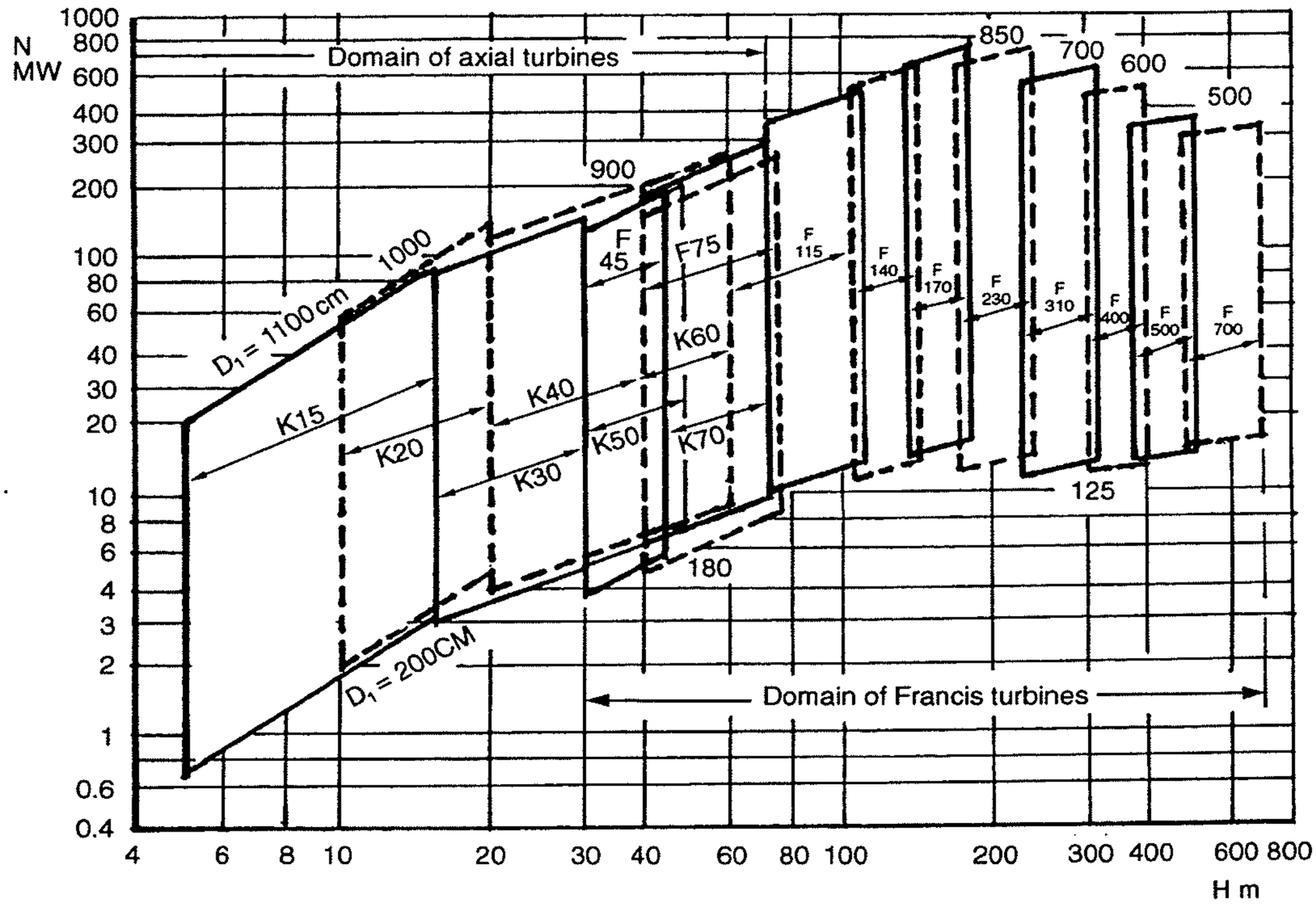


FIGURE 9.4. Nomenclature of axial-flow adjustable blade and radial-axial flow turbines.

Axial flow bulb-type turbines (horizontal)

$$n_s = \frac{2600}{H^{0.4}}$$

The assumed values of the specific speeds may deviate from the given recommendations, but this requires special evidence or substantiation. For instance, lesser specific speeds may be due to the desire to decrease the depth of turbine installation, i.e., to increase the permissible suction height.

Complete data for each type of turbine parameters, dimensions, characteristics can be obtained from the manufacturer. Very useful for the preliminary design stages, analysis, and comparison of different options are generalized dimensions parameters such as reduced speed and discharge ($n'_{\mathrm{I}}, Q'_{\mathrm{I}}$) and cavitation coefficient (σ) for each turbine type. Generalized data are given later in the chapter.

9.2.3. Axial-Flow Adjustable Blade Vertical Turbines

The determining parameters of these turbines are given in Table 9.1. The tabulated design values of $n'_{\mathrm{I}d}$ and $Q'_{\mathrm{I}d}$ are given for the rated power and the design turbine head, which has intermediate values, but closer to minimum. Two corresponding values of $Q'_{\mathrm{I}d}$ and cavitation

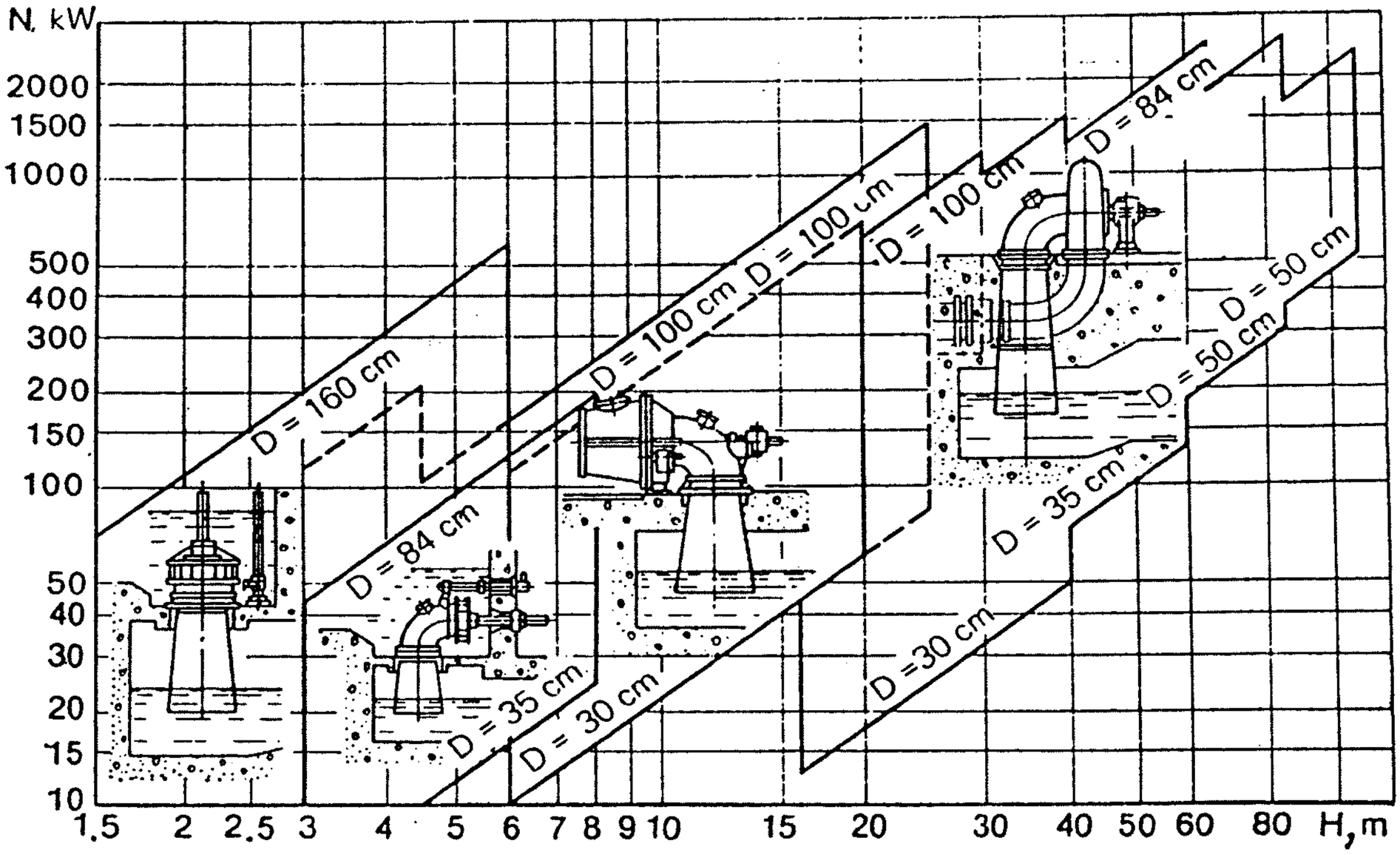


FIGURE 9.5. Nomenclature of small turbines.

coefficients σ are indicated for each turbine. Any values can be taken, including the appropriately interpolated intermediate values. It is seen that Q'_{1d} changes from 2300 to 1000 l/s and σ from 1.4 to 0.28.

The basic dimensions of axial-flow turbines are shown in Figure 9.6a. The dimensions relating to runner diameter D_1, $\bar{b}_0$ and $\bar{d}_{c.s}$, are given in Table 9.1. Other dimensions may be found as follows: $\bar{D}_0 = 1.16$ to 1.25, $\bar{h}_1 = 0.21$; $\bar{h}_3 = 0.09$ to 0.12; $\bar{h}_2 = \bar{d}_{c.s}$; $\bar{d}_c = \bar{d}_{c.s} - 0.05$, and $\bar{D}_c = 0.973 - 0.985$.

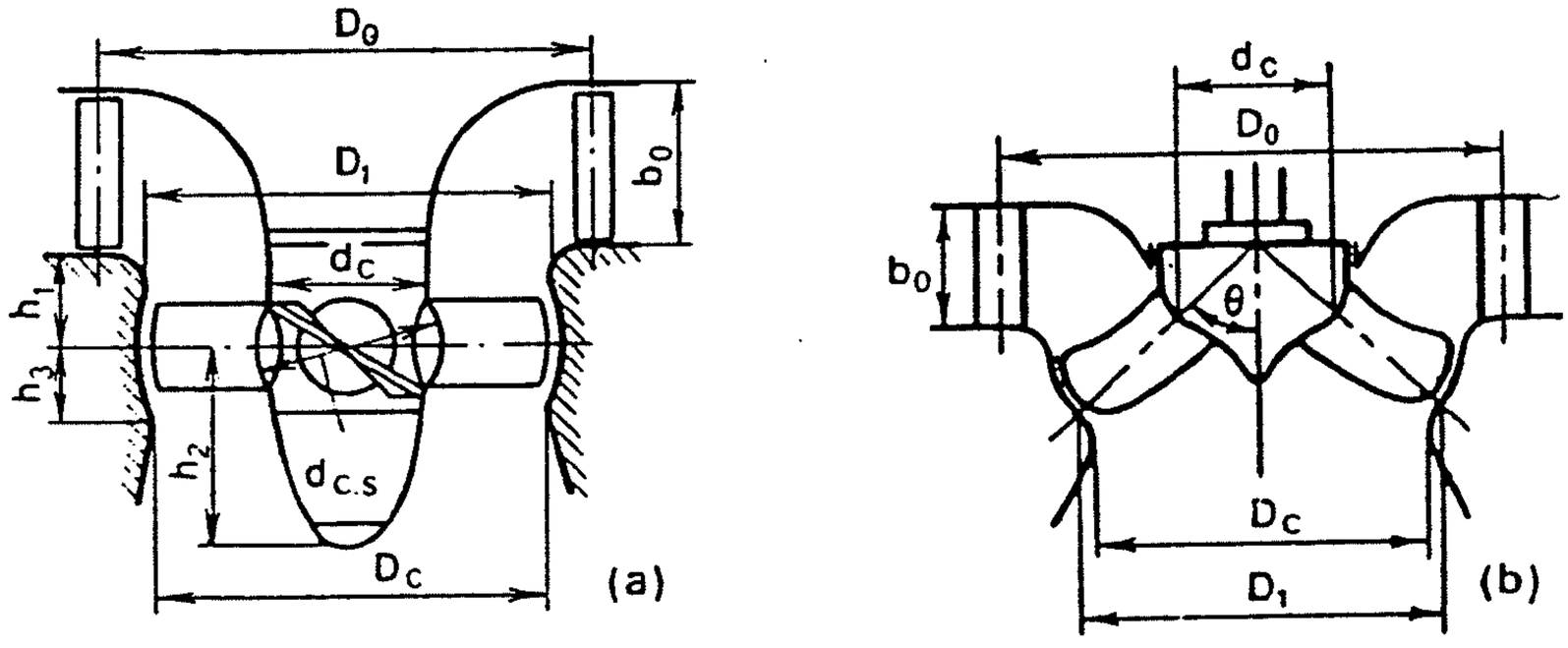


FIGURE 9.6. Basic dimensions of adjustable blade turbines. (a) Axial-flow; (b) mixed-flow.

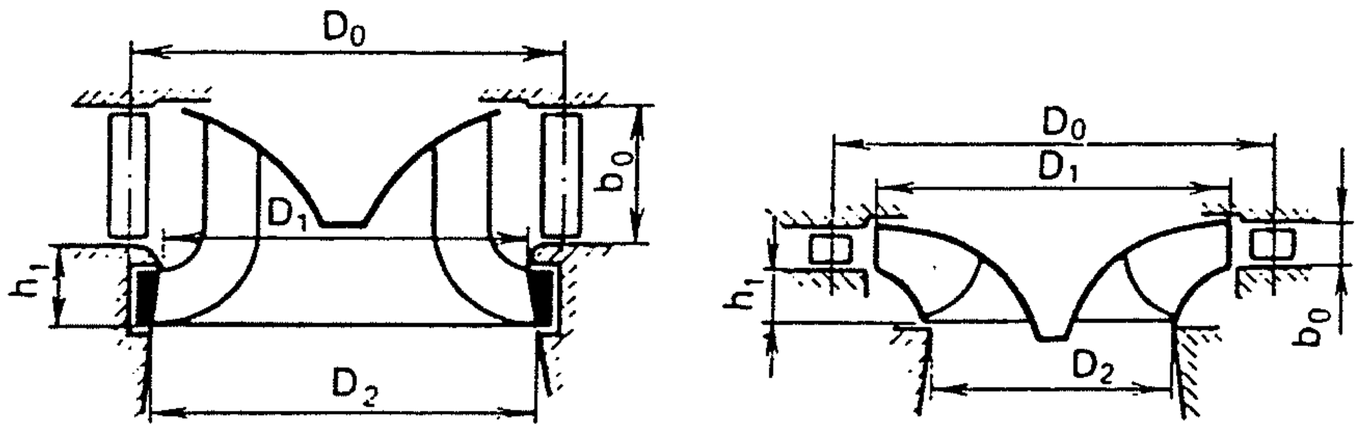


FIGURE 9.7. Basic dimensions of radial-axial flow turbines.

9.2.4. Axial-Flow Adjustable Blade Horizontal Bulb-Type Turbines

The design data of two types of modern axial-flow adjustable blade turbines arranged in horizontal bulb-type units are given in Table 9.2. The K(HB) 10 turbine features a very high specific speed (n_s reaches 1400) and flow rate. These turbines are to be used with the lowest rated heads. The turbines of the K(HB) 16 type are employed at a design head of 6 to 12 m.

9.2.5. Mixed-Flow Adjustable Blade Turbines

These turbines are comparatively new and only a few types have been developed. Therefore, the data of Table 9.3 are tentative, especially

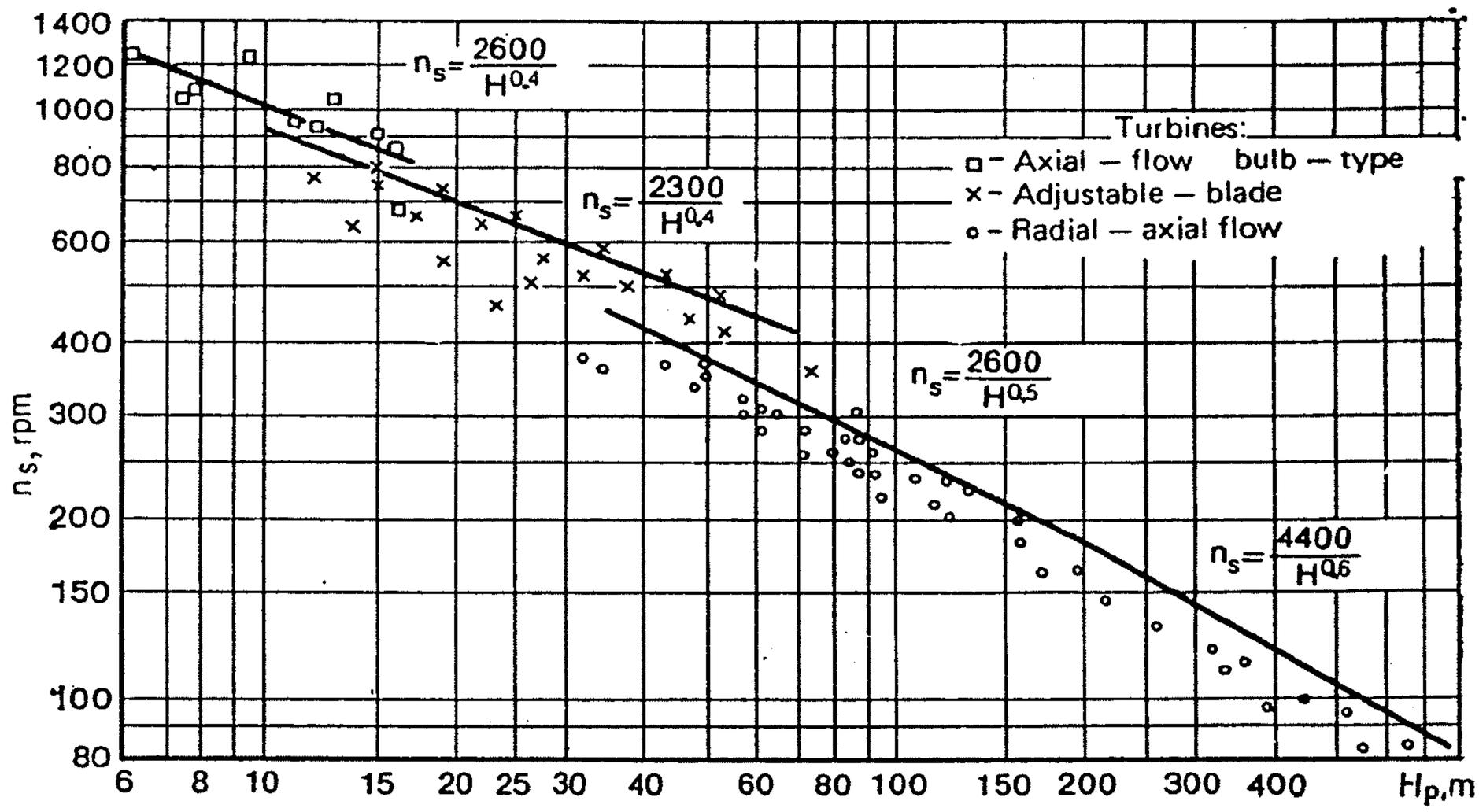


FIGURE 9.8. Reaction turbine design, specific speed.

Table 9.1. Basic Design Data of Adjustable Blade Turbines

Characteristic	Turbine Type						
	K15	K20	K30	K40	K50	K60	K70
Maximum head (m)	15	20	30	40	50	60	70
Reduced speed (rpm)							
Optimal (n'_{1opt})	160	145	125	120	115	110	105
Average design (n'_{1d})	180	155	140	135	125	125	120
Reduced flow rate maximum design flow rate) (Q'_{1d}, L/s)	2300–1900	2200–1750	2000–1500	1700–1300	1500–1200	1300–1100	1250–1000
Cavitation coefficient σ corresponding to Q'_{1d} and n'_{1d}	1.4–0.9	1.3–0.8	1.0–0.65	0.75–0.50	0.55–0.40	0.45–0.30	0.4–0.28
Number of runner blades (z_1)	4	4	5–6	6–7	7–8	8	8
Relative height of wicket gate ($\bar{b}_0$)	0.42	0.4	0.4	0.375	0.375	0.35	0.35
Relative diameter of runner hub (case) ($\bar{d}_{c.s}$)	0.35	0.37	0.41	0.43	0.47	0.51	0.57

Table 9.2. Basic Design Data of Adjustable Blade Bulb-Type Turbines

Characteristic	Turbine Type	
	K(HB)10	K(HB)16
Maximum head (m)	10	16
Reduced speed (rpm)		
Optimal (n'_{1opt})	170	155
Average design(n'_{1d})	210	175
Reduced flow rate (maximum design flow rate) Q'_{1d}, L / s)	4000 –3600	3000 –2400
Cavitation coefficient σ corresponding to Q'_{1d}	3.2 –2.8	2.0 –1.6
Bulb relative diameter ($\bar{D}_{bulb}$)	0.8 –0.95	1.0 –1.25

when applied to the turbine type $D30$. The tabulated range of data for each angle ($\theta = 60°$, $45°$, and $30°$) allows the use of several types of turbines with different water passage shapes. Their basic dimensions are shown in Figure 9.6b. The relative diameter measured at the axes of the guide vanes is $\bar{D}_0 = 1.25$ to 1.30. Nominal diameter d_c of the mixed-flow turbine runner hub is measured at the axes where the blades turn. Runner diameter D_1 is determined similarly. Thus, the maximum size of the hub and the maximum diameter at the leading (inlet) edges of the runner blade will be far greater than d_c and D_1. The draft tube is the same type used with axial-flow turbines; its relative height $\bar{h}$ is equal to 2.3 to 2.5.

Table 9.3. Basic Design Data of Adjustable Blade Mixed-Flow Turbines

Characteristic	Turbine Type		
	D70	D130	D200
Maximum head (m)	70	130	200
Runner blade turn axis angle θ (degrees)	60	45	30
Reduced speed (rpm)			
Optimal (n'_{1opt})	110	90	80
Average design(n'_{1d})	120	100	90
Reduced flow rate (maximum design flow rate) (Q'_{1d}, L / s)	1600 –1300	1200 –950	800 –700
Cavitation coefficient σ corresponding to Q'_{1d}	0.50 –0.4	0.35 –0.26	0.18 –0.12
Number of runner blades (z_1)	8 –9	9 –10	10 –12
Relative diameter of runner hub ($\bar{d}_c$)	0.5 –0.55	0.6 –0.65	0.7 –0.8
Relative diameter of runner case throat ($\bar{D}_c$)	1.0	0.98	0.97
Relative height of wicket gate ($\bar{b}_0$)	0.375	0.25	0.2

9.2.6. Propeller-Type Axial-Flow and Mixed-Flow Turbines

A comparison of the characteristics (see Figure 8.21) reveals that the deviation of load or flow rate from optimal levels causes a more intensive reduction of efficiency in the propeller-type than in the adjustable blade turbines. Thus, powerful propeller-type turbines have not found wide application. However, because multiunit HEPPs allow for the use of this turbine within a narrow operation range approaching optimal conditions, the attitude toward the propeller-type turbines has recently changed. For instance, some powerful propeller-type turbines were developed and manufactured at the KhTW: $D_1 = 6.8$ m, runner blade setting angle $+9°30'$, $N = 115$ MW, $n = 107.1$ rpm. These turbines were installed at the Dneproges II Hydro, put into commission in 1976. Such construction makes it possible to decrease the hub diameter from $\bar{d}_{c.s} = 0.43$ (adjustable blade turbine of corresponding type) to $\bar{d}_c = 0.35$, in order to reduce turbine weight about 10% and (somewhat) to improve cavitation characteristics. The experience gained shows that in some cases the use of propeller type axial-flow and mixed-flow turbines is advantageous.

9.2.7. Radial-Axial Flow Turbines

The parameters of radial-axial flow turbines with a wide range of heads (from 45 to 700 m) are presented in Table 9.4 and their dimensions are shown in Figure 9.7. The relative diameter at guide vane axes is $\bar{D}_0 = 1.16$ to 1.20. The height from the bottom of the runner is $\bar{h}_1 = 0.12$ to 0.15 for heads up to 200 m, and $\bar{h}_1 = 0.18$ to 0.2 for higher heads. There are several types of turbines for each head range and other types can be designed; therefore, the characteristics, particularly Q'_1 and σ, may have intermediate values (i.e., are determined by interpolation).

9.2.8. Turbine Mass or Weight Data

HEPP design often requires the determination of the total weight of the turbine and the weight of its separate components, especially that of the runner. These data are very important because the cost of a given turbine is substantially proportional to its weight, while the runner weight dictates the choice of transportation and erection methods. Accurate weight of the turbine may be determined only on the basis of the manufacturer's design data. It should be borne in mind that turbines of different designs differ in weight, even if their parameters are similar and dimensions (D) are the same due to the varying technical

Table 9.4. Basic Design Data of Radial-Axial Flow Turbines

Characteristic	Turbine Type									
	F45	F75	F115	F140	F170	F230	F310	F400	F500	F700
Maximum head (m)	45	75	115	140	170	230	310	400	500	700
Reduced speed, (n'_{1opt} rpm)	85	80	75	72	70	67	65	60	58	55
Reduced flow rate (Q'_1 corresponding to 5% power margin, L/s)	1400	1250	1050	900	770	570	450	340	250	180
Cavitation coefficient σ	0.22	0.17	0.13	0.11	0.09	0.07	0.055	0.05	0.04	0.035
Wicket gate relative height ($\bar{b}_0$)	0.35	0.3	0.25	0.23	0.2	0.15	0.12	0.1	0.08	0.06
Relative outlet diameter ($\bar{D}_2$)	1.15	1.1	1.0	0.98	0.95	0.88	0.8	0.7	0.65	0.55

solutions involved. Approximate data about turbine mass (weight) can be found using the following practical formulas.

The total weight of axial-flow adjustable blade turbine with a concrete case (Figure 2.2) is as follows:

$$G_T^{a-b} = 0.37(D_1 + 1.6)^{2.7}(H_{\max} + 6)^{0.45} \tag{9.3}$$

where D_1 is the nominal diameter (in meters; for $D_1 \geq 1.8$ m), and $H_{\max}$ is the maximum head (meters).

If the turbine is provided with a steel spiral case, as shown in Figure 3.7, the case weight is

$$G_{s.c}^{a-b} \approx 0.3G_T^{a-b} \tag{9.3a}$$

and the total weight of the turbine is

$$G_T^{a-b} + G_{s.c}^{a-b}$$

The axial-flow turbine runner weight is

$$G_r^{a-b} = (0.17 \text{ to } 0.23)G_T^{a-b} \tag{9.3b}$$

The weight of mixed-flow adjustable blade turbines (Figure 3.12) is 10 to 15% more than the axial-flow units; their runner weight is 25 to 40% greater.

The total weight of radial-axial flow turbines with a steel spiral case (Figure 2.4) is

$$G_T^{r-a} = 2.35(D_1 + 0.8)^{2.5}(H_{\max} + 20.0)^{0.2} \tag{9.4}$$

where D_1 is the nominal diameter (in meters; for $D_1 \geq 1$ m), and $H_{\max}$ is the maximum head.

For a concrete turbine case, weight $G_{s.c}^{r-a}$ should be subtracted from the value obtained from Equation 9.4, approximately,

$$G_{s.c}^{r-a} = 0.25G_T^{r-a} \tag{9.4a}$$

If a portion of the water pressure load is transmitted to reinforced concrete (see Figure 9.3), $G_{s.c}^{r-a}$ should be 25 to 40% less than in Equation 9.4a.

The weight of a radial-axial flow turbine runner is approximately defined by:

$$G_r^{r-a} = (0.55 \text{ to } 0.65)D_1^3 \tag{9.5}$$

The above formulas show that the mass or weight of the turbine increases with increasing maximum head. However, it is important to know the value of turbine specific mass factor $m_{s.t} = G/N$ (kilograms per kilowatts). Such data are given in Figure 9.9 for Kaplan and Francis turbines. They clearly show that with the growing head, the specific mass factor sufficiently diminishes. For $H < 40$ to 50 m Kaplan turbines have less mass than the Francis for equal power. It is interesting to note that turbine dimension D_1 has very little influence on the value of specific mass factor.

9.3. SELECTING REACTION TURBINES USING REDUCED CHARACTERISTIC PARAMETERS

Given: H_d = design head; $H_{\max}$ = maximum head; $H_{\min}$ = minimum head; N_d = required design power of turbine; and ∇ = absolute elevation of TW. Values of n'_{Id}, Q'_{It}, σ, etc. required for calculations may be borrowed from Tables 9.1 to 9.4; however, more complete data are derived from the universal characteristics of turbines of the respective types.

9.3.1. Calculation Procedure

1. The turbine type is chosen mainly by $H_{\max}$.
2. Design flow rate Q_d (maximum) is determined by the assigned power

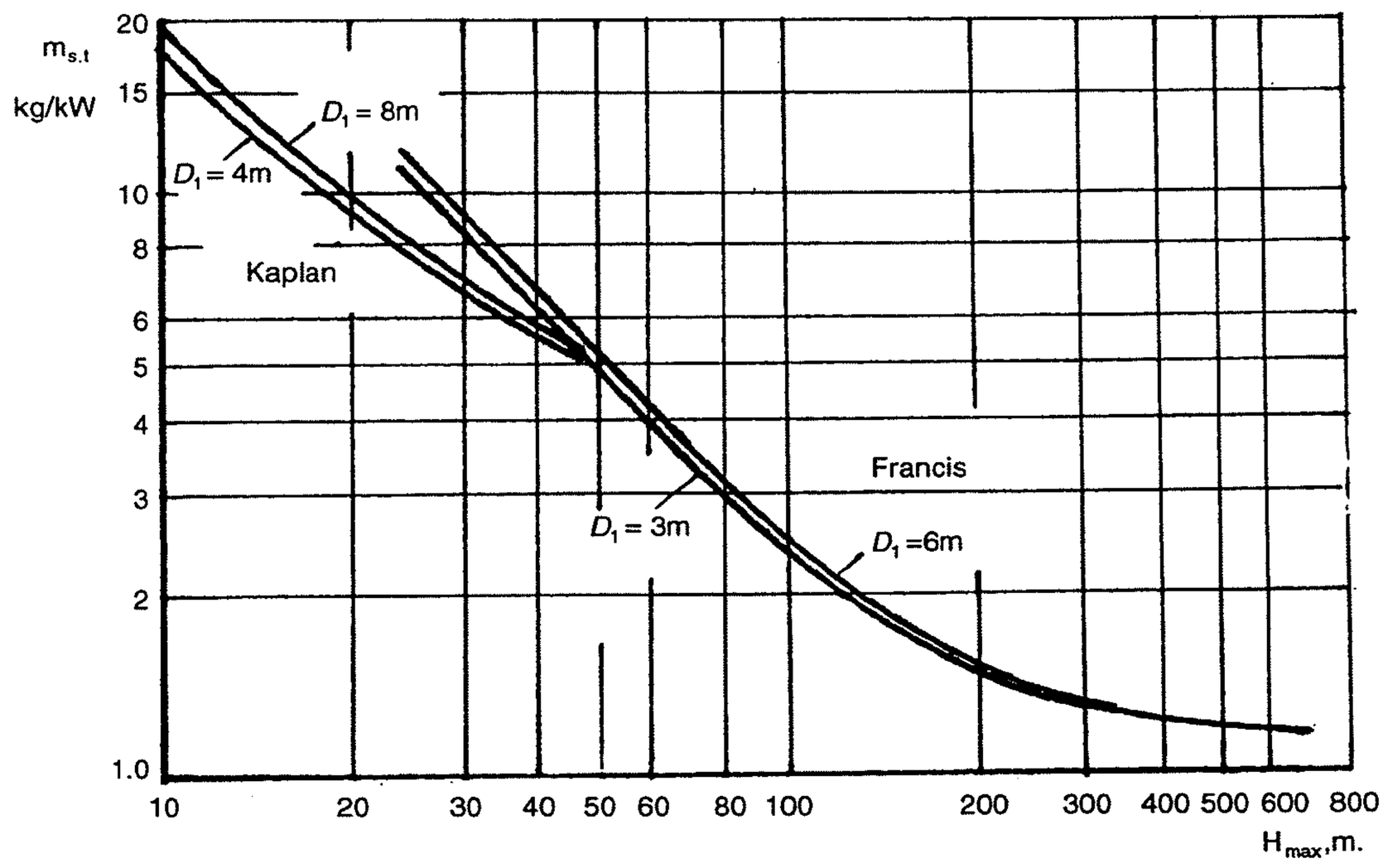


FIGURE 9.9. Turbine specific mass factor dependence from head.

N_d (see Equation 2.10)

$$Q_d = \frac{N_d}{9.81 H_d \eta} \tag{9.6}$$

Because calculations are performed for full opening of the turbine, η is less than optimal. Usually assumed for adjustable blade turbines is $\eta = 0.87$ to 0.9; for radial-axial flow turbines $\eta = 0.9$ to 0.92.

3. Turbine diameter D_1 is found from Equation 5.35:

$$D_1 = \sqrt{\frac{Q_d}{Q'_{Id}\sqrt{H_d}}} \tag{9.7}$$

For radial-axial flow turbines, the design reduced flow rate Q'_{Id} is equal to Q'_I at the line of 5% power reserve ($0.95N_{max}$). In adjustable blade turbines, Q'_{Id} is usually selected depending on the permissible suction lift, i.e., by the maximum value of cavitation coefficient σ. Therefore, Tables 9.1 to 9.3 represent two values of Q'_{Id} with respective values of σ. Maximum Q'_{Id} is always preferable, because it permits decrease of D_1 and the acceptance of higher rotation speed. Intermediate values of Q'_{Id} may also be used; in the latter case σ is found by interpolation.

4. Turbine speed of rotation n is found from the following formula

$$n = \frac{n'_{Id}\sqrt{H_d}}{D_1} \tag{9.8}$$

Design reduced speed n'_{Id} for radial-axial flow turbines is taken close to optimal $n'_{I\,opt}$ (Table 9.4); for adjustable blade and mixed-flow turbines $n'_{Id} > n'_{I\,opt}$ (Tables 9.1 to 9.3). This stems from the fact that most of the time the turbine runs at a head $H > H_d$, so that at the same speed n, the reduced speed n'_I drops down to get into the turbine optimal performance area (see Equation 5.34). After finding n from Equation 9.8, assume the closest synchronous speed n_{syn} whose value is determined from Equation 9.1.

5. Permissible suction lift H_s is calculated from Equation 7.13 by introducing the reserve coefficient from Equation 7.14. It should be borne in mind that the basic universal characteristics and Tables 9.3 to 9.5 indicate values of σ without a reserve.
6. Basic dimensions of the turbine are determined by D_1 against relative dimensions contained in tables, descriptions, and drawings of a given turbine type (see Figures 9.6 and 9.7).
7. Turbine weight is calculated from the approximate formulas of Equations 9.3 to 9.5 or by referring to analogous designs.
8. After selecting the turbine type and determining D_1, n by assigned N_d, and heads H_d, H_{max}, and H_{min}, it is good policy to outline the utilized

area of the universal characteristic. To this end, calculate three values of n'_{I} for all three heads.

$$n'_{\mathrm{I}d} = \frac{nD}{\sqrt{H_d}} \qquad n'_{\mathrm{I}\min} = \frac{nD}{\sqrt{H_{\max}}} \qquad n'_{\mathrm{I}\max} = \frac{nD}{\sqrt{H_{\min}}}$$

For $H_{\max}$, find $Q'_{\mathrm{I}H\max}$. Using Equation 2.10, calculate flow rate $Q_{H_{\max}}$ (value of η is assumed); then

$$Q'_{\mathrm{I}H_{\max}} = \frac{Q_{H_{\max}}}{D_1^2\sqrt{H_{\max}}}$$

Plot the resulting points on the universal characteristic curve as shown in Figure 9.10, thus discriminating the utilized area. This area is defined by lines a, b, c, d, e. The high efficiency region is advantageously located when it is entirely within the utilized area.

Let us consider some numerical examples.

Example 9.1

Select a turbine for the following conditions: $N_d = 70$ MW, $H_d = 95$ m, $H_{\max} = 110$ m, TW elevation = 250 m.

Solution

1. Select a radial-axial turbine PO115 from Table 9.4.
2. Find design flow rate from Equation 9.6 at $\eta = 90\%$

$$Q_d = \frac{70{,}000}{9.81 \times 95 \times 0.9} = 83.5 \text{ m}^3/\text{s}$$

According to Table 9.4, assume $Q'_{\mathrm{I}d} = 1.05$ m^3/s

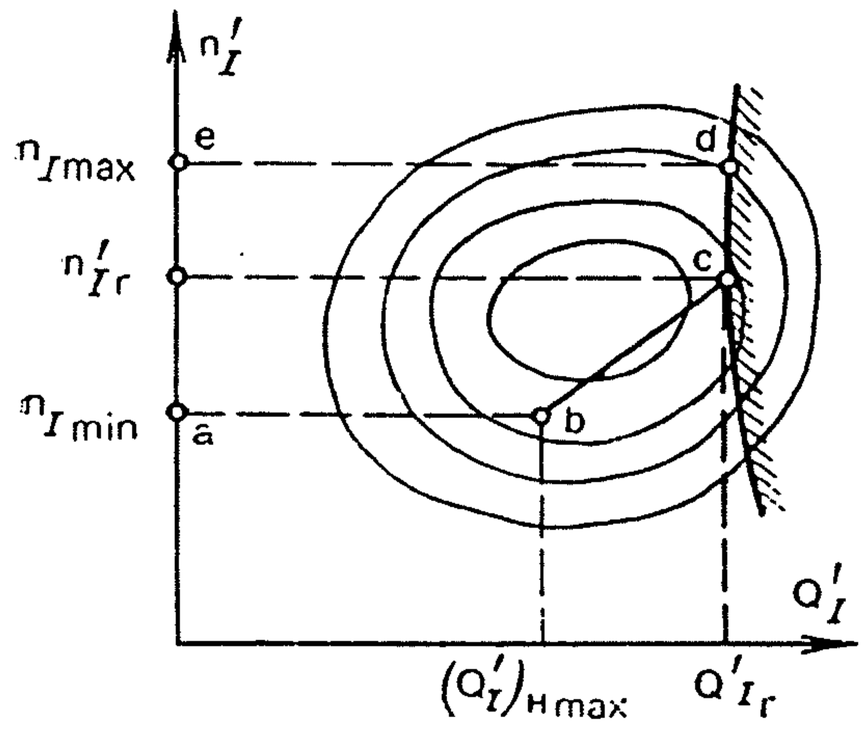


FIGURE 9.10. Utilized area of the turbine characteristic.

3. Find the turbine diameter from Equation 9.7

$$D_1 = \sqrt{\frac{83.5}{1.05\sqrt{95}}} = 2.85 \text{ m}$$

Take diameter $D_1 = 280$ cm.

4. For a radial-axial flow turbine $n'_{1d} = n'_{1\,opt} = 75$ rpm (Table 9.5). From Equation 9.8 determine

$$n = \frac{75\sqrt{95}}{2.8} = 261 \text{ rpm}$$

The closest synchronous speed of rotation according to Equation 9.1 is $n_{syn} = 250$ rpm ($p = 24$). Assume $n = 250$ rpm.

5. Permissible suction lift H_s from Equation 7.13 at $\sigma = 0.13$ (Table 9.4) and $k_\sigma = 1.1$ is

$$H_s = 10 - \frac{250}{900} - 1.1 \times 0.13 \times 95 = -4.3 \text{ m}$$

6. Determine basic dimensions of the turbine from Table 9.4:

- runner outlet diameter $D_2 = 1.0 \times 2.8 = 2.8$ m;
- wicket gate height $b_0 = 0.25 \times 2.8 = 0.67$ m;
- guide vane axis diameter $D_0 = 1.2 \times 2.8 = 3.35$ m; and

7. Find the weight of a turbine with a steel casing from Equation 9.4

$$G_s^{r-a} = 2.35(2.8 + 0.8)^{2.5}(100 + 20)^{0.2} = 153 \text{ t}$$

Find the runner's weight using Equation 9.5

$$G_r^{r-a} = 0.6 \times (2.8)^3 = 13.2 \text{ t}$$

Example 9.2

Select a vertical turbine for the following conditions: $N_d = 45$ MW, $H_d = 10$ m, $H_{\max} = 13$ m, TW elevation 180 m.

Solution

1. Select an adjustable blade turbine (K15) from Table 9.1.
2. Find design flow rate at $\eta = 88\%$ from Equation 9.3:

$$Q_d = \frac{45{,}000}{9.81 \times 10 \times 0.88} = 521 \text{ m}^3/\text{sec}$$

Take $\sigma = 1.2$ for $Q'_{1d} = 2300$ L/sec from Table 9.1. Assume $k_\sigma = 1.15$. For these conditions, find H_s using Equation 7.13:

$$H_s = 10 - \frac{180}{900} - 1.15 \times 1.2 \times 10 = -4.0 \text{ m}$$

Turbine depth is acceptable. If depth is decreased, i.e., lift H_s is to be increased, a lower value of Q'_{1d} may be assumed.

3. Using Equation 9.7, find the turbine diameter:

$$D_1 = \sqrt{\frac{521}{2.3\sqrt{10}}} = 8.46 \text{ m}$$

where diameter $D_1 = 8.5$ m.

4. Find the speed of rotation at $n'_{1d} = 180$ rpm (Table 9.3) from Equation 9.7:

$$n = \frac{180\sqrt{10}}{8.5} = 67.0 \text{ rpm}$$

The closest synchronous speed found using Equation 9.1 is $n_{syn} = 68.2$ rpm ($p = 88$). Accept $n = 68.2$ rpm.

5. We have determined permissible suction lift under item 2 ($H_s = -4$ m).
6. Calculate the basic dimensions of the turbine (refer to Table 9.1 and Figure 9.6a):

- wicket gate height $b_0 = 0.42 \times 8.5 = 3.6$ m;
- guide vane axes diameter $D_0 = 0.973 \times 8.5 = 10.2$ m;
- runner case diameter $D_c = 0.973 \times 8.5 = 8.27$ m;
- runner hub diameter $d_{c.s} = 0.35 \times 8.5 = 2.97$ m;
- runner hub cylindrical portion diameter $d_c = 0.3 \times 8.5 = 2.55$ m;
- blade turn axes height $h_1 = 0.21 \times 8.5 = 1.8$ m; and

7. Find the weight of turbine with a concrete casing (use Equation 9.3):

$$G_t^{a-b} = 0.37(8.5 + 1.6)^{2.7}(13.0 + 6)^{0.45} = 716.6 \text{ t}$$

Find the runner weight from Equation 9.3b:

$$G_r^{a-b} = 0.2 \times 716.6 = 143 \text{ t}$$

Example 9.3

Determine the characteristics if a horizontal bulb-type turbine is used under the conditions of Example 9.2.

Solution

The design flow rate is unchanged, $Q = 521\ \text{m}^3/\text{s}$.

Take an axial-flow adjustable blade bulb-type turbine K(HB)16 and $Q'_{1d} = 3000\ \text{L/s}$ from Table 9.2. Find diameter D_1 using Equation 9.7

$$D_1 = \sqrt{\frac{521}{3.0\sqrt{10}}} = 7.4\ \text{m}$$

According to Table 9.2, $n'_{1d} = 175$ rpm; from Equation 9.8 find

$$n = \frac{175\sqrt{10}}{7.4} = 74.8\ \text{rpm}$$

The closest synchronous speed of rotation according to Equation 9.1 is $n_{syn} = 75$ rpm ($p = 80$).

Find the permissible suction lift (see Table 9.2) at $\sigma = 2.0$ and $k_\sigma = 1.15$ from (see Equation 7.13)

$$H_s = 10 - \frac{180}{900} - 1.15 \times 2.0 \times 10 = -13.2\ \text{m}$$

A comparison of the obtained data with the characteristics of the vertical turbine shows that the diameter has decreased, the speed has risen and the required depth under the TW level has drastically increased. However, the foundation depth is decisive. The draft tube bottom elevation is a determining parameter for a vertical turbine. Assuming the tube height $h = 2.3D_1 = 2.3 \times 8.5 = 19.5$ m (see Figure 6.20) and taking into account that $\bar{h}_1 = 0.21$ and $h_1 = 0.21 \times 85 = 1.8$ m (see Figure 9.6), the minimum elevation of the draft tube relative to the TW for $H_s = -4.0$ m will be as follows:

$$-4.0 - 19.5 + 1.8 = -21.7\ \text{m}$$

The determining parameter for a horizontal turbine is the bottom of the runner (see Figure 6.19c), whose depth under the TW level in view of $H_s = -13.2$ m will be

$$-13.2 - 7.4 = -20.6\ \text{m}$$

i.e., lightly smaller than that for a vertical turbine.

9.4. PECULIARITIES IN SELECTING PELTON TURBINES

In selecting reaction turbines, the initial parameters n'_1, Q'_1, etc., are taken from the experimental curves, while the impulse Pelton turbines may be selected by calculating their basic characteristics to a sufficient accuracy using operating analyses. Jet velocity v_j is explained in Equation 2.11, while the optimal circumferential velocity of the runner without accounting for losses should be 0.5 v_j, and 4 to 6% lower if the losses are taken into account. Thus, the optimal reduced rotational speed of Pelton turbines for $H = 1$ m and $D_1 = 1$ m (see Figure 2.6) is

$$n'_{1\,opt} = \frac{(0.47 \text{ to } 0.48)60\varphi\sqrt{2g}}{\pi} = 39 \text{ to } 40 \text{ rpm}$$

where φ is the nozzle velocity factor equal to 0.98 to 0.99.

We have obtained a very interesting result: $n'_{1\,opt}$ for all Pelton turbines remains substantially constant. Figure 9.11 represents a universal characteristic curve of a Pelton turbine which supports this conclusion. Pelton turbine flow rate is determined by the relation

$$Q = z_j \frac{\pi d_j^2}{4} \varphi\sqrt{2gH} \tag{9.9}$$

where z_j is the number of jets (nozzles), and d_j is the diameter of jet. Multiply and divide the right hand (RH) part of Equation 9.9 by D_1^2 (see Figure 2.6) to obtain

$$Q = z_j \frac{\pi}{4}\left(\frac{d_j}{D_1}\right)^2 D_1^2 \varphi\sqrt{2gH}$$

For reduced parameters $D_1 = 1$ and $H = 1$

$$Q'_1 = \frac{\pi}{4}\varphi\sqrt{2g}\, z_j\left(\frac{d_j}{D_1}\right)^2 = 3.4 z_j\left(\frac{d_j}{D_1}\right)^2 \tag{9.10}$$

Write the reduced flow rate through one nozzle

$$Q'_{1j} = 3.4\left(\frac{d_j}{D_1}\right)^2 \tag{9.10a}$$

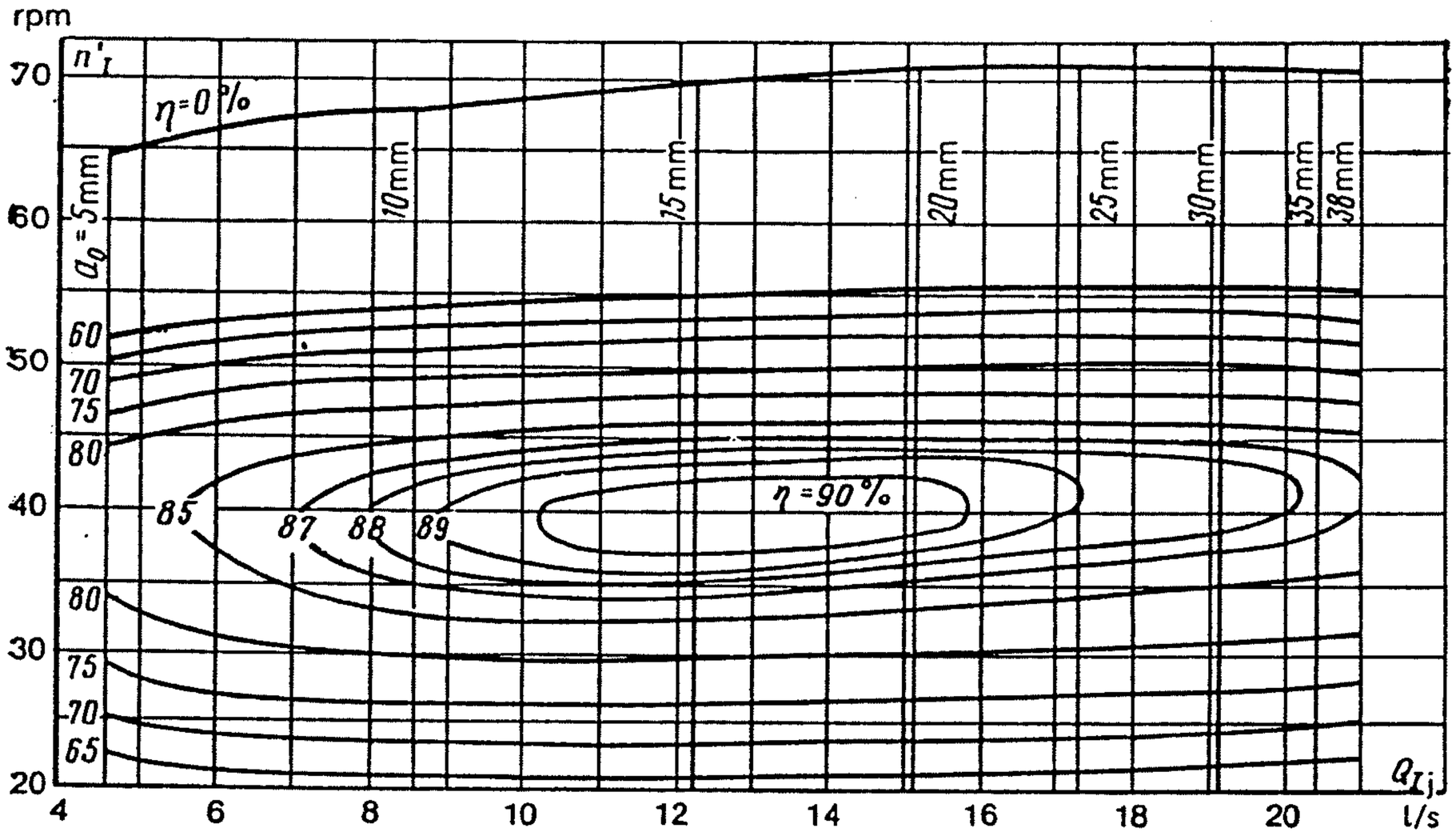


FIGURE 9.11. Universal characteristic of Pelton turbine. (Single-nozzle with 18 runner buckets; model diameter $D = 380$ mm, a_0 = needle shift.)

then for the entire turbine

$$Q'_{\mathrm{I}} = z_j Q'_{\mathrm{I}j} \tag{9.11}$$

Equations 9.10 and 9.11 show that the Pelton turbine capacity Q'_{I} is determined by the number of nozzles (jets) z_j and ratio d_j/D_1 is the maximum capacity corresponding to the full opening of a nozzle. The best energy characteristics are obtained at

$$\frac{d_j}{D_1} = \frac{1}{10} - \frac{1}{18} \tag{9.12}$$

However, greater values (up 1/7 to 1/8) are also tolerable and sometimes when head is very high and power is low, d_j/D_1 may be considerably smaller (say, 1/30 to 1/40), which leads to increasing diameter and reduction speed.

The characteristic curve of Figure 9.11 gives values of $Q'_{\mathrm{I}j}$ for the conditions corresponding to Equation 9.12.

Knowing n'_{I} and Q'_{I}, we can determine the Pelton turbine specific speed by using Equation 5.39

$$n_s = 3.65\ (30 \text{ to } 40)\sqrt{3.4 z_j \left(\frac{d_j}{D_1}\right)\eta}$$

At full opening η may be 88 to 87%. Now,

$$n_s = (245 \text{ to } 253)\sqrt{z_j}\left(\frac{d_j}{D_1}\right) \tag{9.13}$$

Ranges of n_s for most favorable ratios d_j/D_1, according to Equation 9.12, are given in Table 9.5.

In view of the above, the following procedure for selecting Pelton turbines may be recommended.

1. Calculate design flow rate Q_d from Equation 9.6 using the design values of power N_d and head H_d; assume efficiency $\eta = 0.87$ to 0.88.
2. Determine the design value of $Q'_{\mathrm{I}j}$ and runner diameters D_1 for different numbers of nozzles (jets) from the curve of Figure 9.11. Assume $z_j = 1, 2, 3, \ldots$

$$D_1 = \sqrt{\frac{Q_d}{z_j Q'_{\mathrm{I}j}} H_d} \tag{9.14}$$

and for $n'_{\mathrm{I}\,opt}$, find the appropriate speeds of rotation

$$n = \frac{n'_{\mathrm{I}\,opt}\sqrt{H_d}}{D_1} \tag{9.15}$$

Choose the most favorable variant (usually $n \leq 600$ rpm) and take the closest synchronous speed of rotation from Equation 9.1.

As seen from Figure 9.11 Pelton turbine efficiency drops drastically when n'_{I} deviates from the optimal value. Therefore, if synchronous speed of rotation differs from n, change D_1 according to Equation 9.15 in order to preserve $n'_{\mathrm{I}} = n'_{\mathrm{I}\,opt}$.

Table 9.5. Specific Speed of Pelton Turbines

Turbine Type	z_j	n_s
One-nozzle	1	14–23
Two-nozzle	2	20–34
Three-nozzle	3	26–40
Four-nozzle	4	32–47
Six-nozzle	6	38–58

3. Find basic dimensions of the turbine:

- Jet diameter

$$d_j = \sqrt{\frac{4Q_d}{\pi z_j \varphi \sqrt{2gH_d}}} \tag{9.16}$$

- Nozzle diameter

$$d_n \approx 1.3 d_j \tag{9.17}$$

- Runner outer diameter (see Figure 2.6)

$$D_{out} = D_1 + a \tag{9.18}$$

where $a = (2.8 \text{ to } 3.6)d_j$.

4. Select the embodiment of the turbine (see Figure 3.18). It is good policy to refer to analog design drawings.

Example 9.4

Select a Pelton turbine, $N_d = 125$ MW at a design head $H_d = 650$ m.

Solution

1. Determine Q_d at $\eta = 0.88$ from Equation 9.6:

$$Q_d = \frac{125{,}000}{9.81 \times 650 \times 0.88} = 22.3 \text{ m}^3/\text{s}$$

2. For $Q'_1 = 0.022$ m^3/s and $n'_1 = 40$ rpm found from Figure 9.11, determine D_1 and n for different z_j (Table 9.6). Variant with $z_j = 6$ is most favorable as regards the dimensions and value of n. The closest synchronous speed of rotation according to Equation 9.1 is $n_{syn} = 428$ rpm ($p = 14$). Accept $n_{syn} = 428$ rpm.

   To preserve the optimal reduced speed of rotation, decrease the diameter

$$D_1 = 2.57 \times 396.8/428 = 2.4 \text{ m}$$

Table 9.6. Options of the Impulse Turbine

No. of Jets (nozzles, z_j)	1	2	3	4	6
D_1[a]	6.3	4.45	3.63	3.15	2.57
n[b]	161.8	229.2	280.9	323.7	396.8

[a]From Equation 9.14.
[b]From Equation 9.15.

3. Define the basic dimensions of the turbine: (a) jet diameter from Equation 9.16:

$$d_j = \sqrt{\frac{4 \times 22.3}{3.14 \times 6 \times 0.98\sqrt{2 \times 9.81 \times 650}}} = 0.207 \text{ m}$$

ratio $d_j/D_1 = 0.207/2.4 = 1/11.6$ corresponds to Equation 9.12; (b) nozzle diameter from Equation 9.17:

$$d_n \approx 1.3 d_j = 0.27 \text{ m}$$

(c) runner outer diameter from Equation 9.18:

$$a = 3.2 \times 0.27 = 0.66 \text{ m}$$
$$D_{out} = 2.4 + 0.66 = 3.06 \text{ m}$$

4. The design is a vertical turbine with supply case (see Figure 3.21).

Example 9.5

Select a Pelton turbine, $N_d = 1500$ kW at design head $H_d = 700$ m.

Solution

1. Find Q_d at $\eta = 0.88$ from (9.6)

$$Q_d = \frac{1500}{9.81 \times 700 \times 0.88} = 0.25 \text{ m}^3/\text{s}$$

2. Using the characteristic curve of Figure 9.11 for $n'_{\text{I}\,opt} = 40$ rpm and $Q'_{\text{I}j} = 0.02$ m^3/s at $z_j = 1$, we obtain

$$D_1 = \sqrt{\frac{0.25}{0.02\sqrt{700}}} = 0.69 \text{ m} \qquad n = \frac{40\sqrt{700}}{0.69} = 1534 \text{ rpm}$$

The speed is too high. Assume $n = 750$ rpm. Find D_1 from Equation 9.15

$$D_1 = \frac{40\sqrt{700}}{750} = 1.4 \text{ m}$$

In this case

$$Q'_{\text{I}} = \frac{0.25}{1.4^2\sqrt{700}} = 0.0048 \text{ m}^3/\text{s}$$

which is considerably smaller than that according to the curve of Figure 9.11.

3. Find d_j from (9.16)

$$d_j = \sqrt{\frac{4 \times 0.25}{3.14 \times 0.98\sqrt{2 \times 19.6 \times 700}}} = 0.053 \text{ m}$$

In this case $d_j/D_1 = 1/26.6$; i.e., smaller than the value of Equation 9.12, but which is allowable.

4. Design is a one-nozzle horizontal turbine (see Figure 3.18a).

9.5. HYDROELECTRIC POWER PLANT OPERATION CURVES

The basis for selecting the turbines is the HEPP operation curves defining the variation of head and power during the course of operation. The total power of plant turbines, $\sum N_d$, is assigned according to HEPP installed capacity, N_{ins}, which is found from water energy calculations

$$\sum N_d = N_{ins}/\eta_{gen} \tag{9.19}$$

where η_{gen} is the generator efficiency, at 0.97 to 0.98.

According to Equation 2.5, head H depends on two values: static head H_{st} and hydraulic losses h_{loss}, found primarily in HEPP water conduits; therefore, H can be represented by the expression

$$H = z_{hw} - z_{tw} - h_{loss} \tag{9.20}$$

Headwater (HW) elevation z_{hw} is determined by the water reservoir fill and is between the designed full supply level (DFSL) and the dead storage level (DSL). TW elevation z_{tw} depends mainly on discharge Q_{tw} and is represented by the relationship

$$z_{tw} = f(Q_{tw}) \tag{9.21}$$

When Q_{tw} increases, z_{tw} increases as well.

Losses h_{loss} are proportional to square discharge and depend on HEPP water conduit length and cross-sections.

When the discharge rises, i.e., the turbine total power $\sum N$ increases at a given HW elevation z_{hw} according to Equation 9.20, the head drops. The HEPP operation curve is shown in Figure 9.12.

Maximum head $H_{\max}$, minimum head $H_{\min}$, and design head H_d (whereas nominal power of hydraulic units is ensured $\sum N = \sum N_d$ according to Equation 9.19), are important characteristics of the operation curve. Design head H_d is found via water energy calculations. At $H < H_d$ HEPP turbine total power determined by limit power line $1 - m$ is less than $\sum N_d$; under such conditions HEPP capacity will be less than N_{ins}.

9.6. TOTAL CHARACTERISTICS OF HEPP TURBINES OPERATING IN PARALLEL

HEPP capacity is equal to the sum of the powers of the operating units

$$N_{\text{HEPP}} = \sum_{1}^{m} N_a = \sum_{1}^{m} N\eta_{gen} \tag{9.22}$$

where N is turbine power, and η_{gen} is generator efficiency. Load may be distributed between separate units in different ways. Optimal distribution of load occurs when the total discharge of all the turbines is minimal, or average efficiency is maximal.

The common characteristic for power regulation conditions is derivative:

$$\chi = \partial Q / \partial N \tag{9.23}$$

χ is referred to as the relative increment. Optimal distribution of load between units corresponds to equal relative increments of all the units.

The generator efficiency varies only slightly; therefore, turbine performance is of decided importance (water conduit losses also exert the effect). *In the case of turbines with identical characteristics optimal conditions correspond to uniform distribution of load between the operating turbines*. This rule makes it possible to plot a total characteristic curve of all turbines at parallel operation of the units, while comparing this curve with the HEPP operation curves allows determination of the turbine operation range at a given HEPP.

A linear total characteristic is most easy to plot when the head is constant. Knowing the turbine type, D_1 and n, we plot turbine linear power characteristic $\eta = f_\eta\ (N)$ for H_d (see Section 8.5, Figure 8.15b). This characteristic is represented by curve (1) in Figure 9.13. According

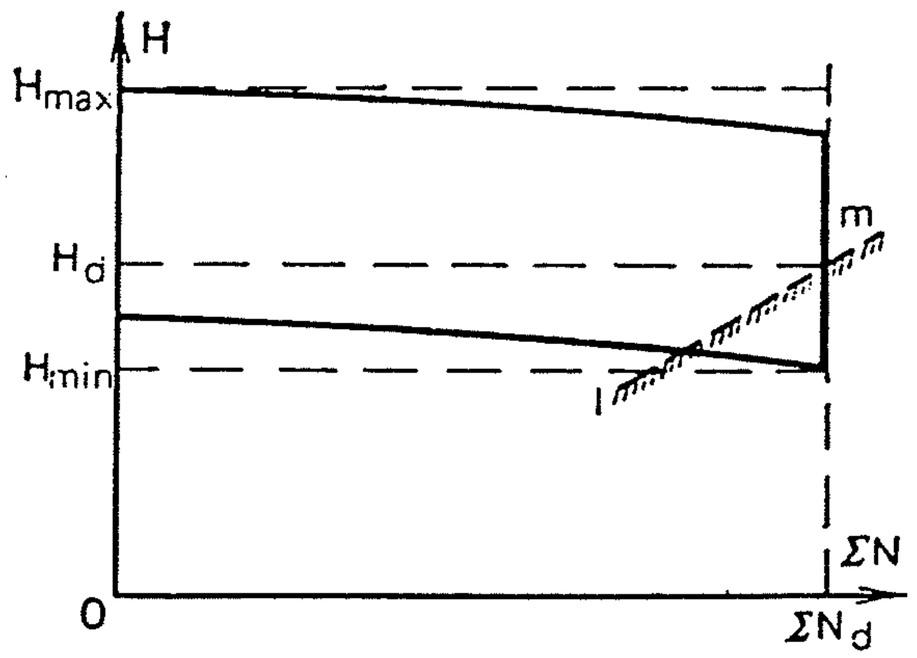


FIGURE 9.12. HEPP turbine operation curve.

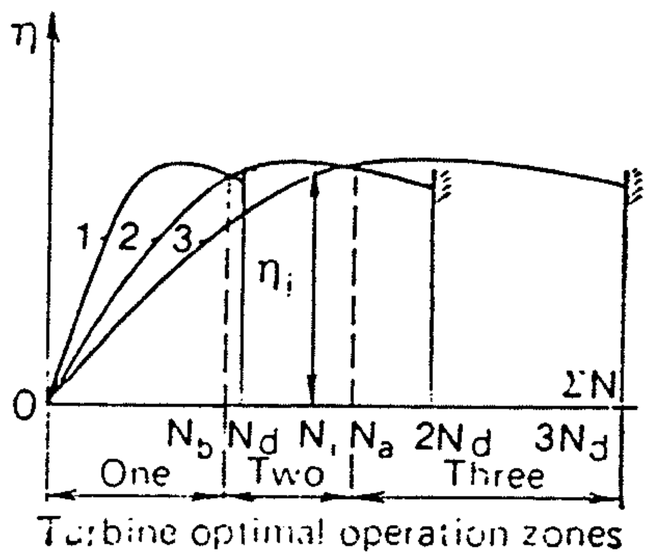


FIGURE 9.13. Total linear operating characteristic of turbines.

to the rule derived above, the load must be uniformly distributed among the turbines of equal type operating in parallel. Thus, to plot a curve representing the operation of two turbines, the abscissas of all the points on curve (1) should be increased twofold. Next, we obtain curve (2) illustrating variations in the efficiency of two turbines operating in parallel. By increasing the abscissas of curve (1) threefold we can obtain the characteristics of three parallel turbines (line (3)), and so on.

The total characteristic makes it possible to draw conclusions that are very important for the proper operation of a HEPP. First, it helps to determine the optimal switching conditions, i.e., the conditions under which the number of turbines for parallel operation is selected. For instance, when total power drops to $2N_d$ (N_d is the design power of one turbine), it is possible to shut down the third unit and run only two units. However, the characteristic curve of Figure 9.13 shows that keeping three units operating to N_a is more expedient for higher efficiency, while two units are operated to N_b. Thus, the optimal operation zones are established for one, two, etc. turbines.

If HEPP load curve $\Sigma N = f(t)$ is known (Figure 9.14), the total characteristic will allow the determination of average efficiency from

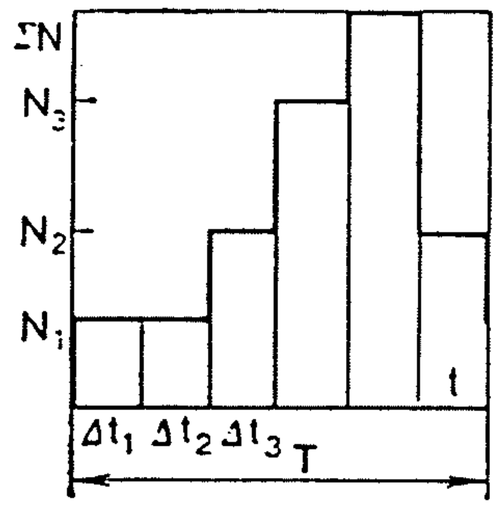


FIGURE 9.14. HEPP load curve.

the formula

$$\eta_{av} = \frac{\sum_T (\sum N_i)\,\Delta t_i}{\sum_T \dfrac{(\sum N_i)\,\Delta t_i}{\eta_i}} \tag{9.24}$$

where $\sum N_i$ is the total power of HEPP turbines within time period Δt_i; η_i is efficiency found from the total characteristic of Figure 9.13, which corresponds to power $\sum N_i$; and T is the total time. With η_{av} calculated, we may compare different variants of turbine equipment, say, with the different number of turbines.

The linear total characteristic is of help when HEPP head variations do not exceed 10 to 15%.

If head variations are considerable, the total operation characteristic of parallel turbines is to be plotted. It is based on the operation head–power (see Figure 8.1) or head–discharge (see Figure 8.2) characteristic with given D and n. The technique of plotting such a curve against the main universal characteristic is described in Section 8.6.

The characteristic of one turbine within the system of coordinates H and $\sum N$ (Figure 9.15) occupies the area defined by two curves: curve (1), determining the limit power of the turbine, and curve (1′), restricting turbine power according to the nominal power of the generator. The curves of equal efficiencies η and H_s (the latter are omitted not to complicate the drawing) are found within this area.

The total characteristic for two, three, etc. parallel turbines is determined by increasing the abscissas of all the points of a given operation mode twofold, threefold, etc., as taught by the load equality rule. For instance, point A' with $\eta = 92\%$ will shift to A'' if two turbines are used, or to A''' when three turbines operate in parallel. As a result, the total characteristic of two turbines will be limited by curves (2-2′), that of three turbines by curve (3-3′). Note that the curve shape changes in

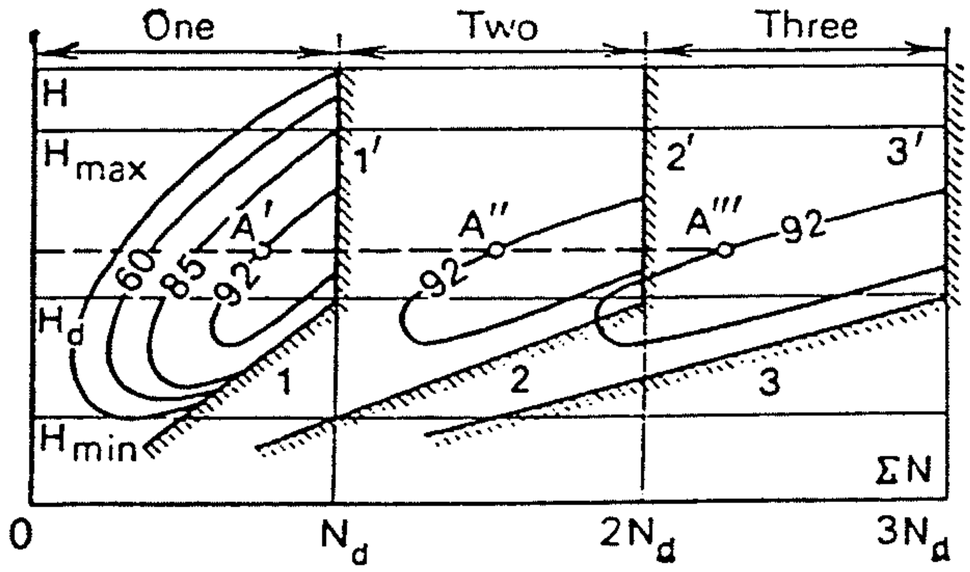


FIGURE 9.15. Plotting total operating characteristic.

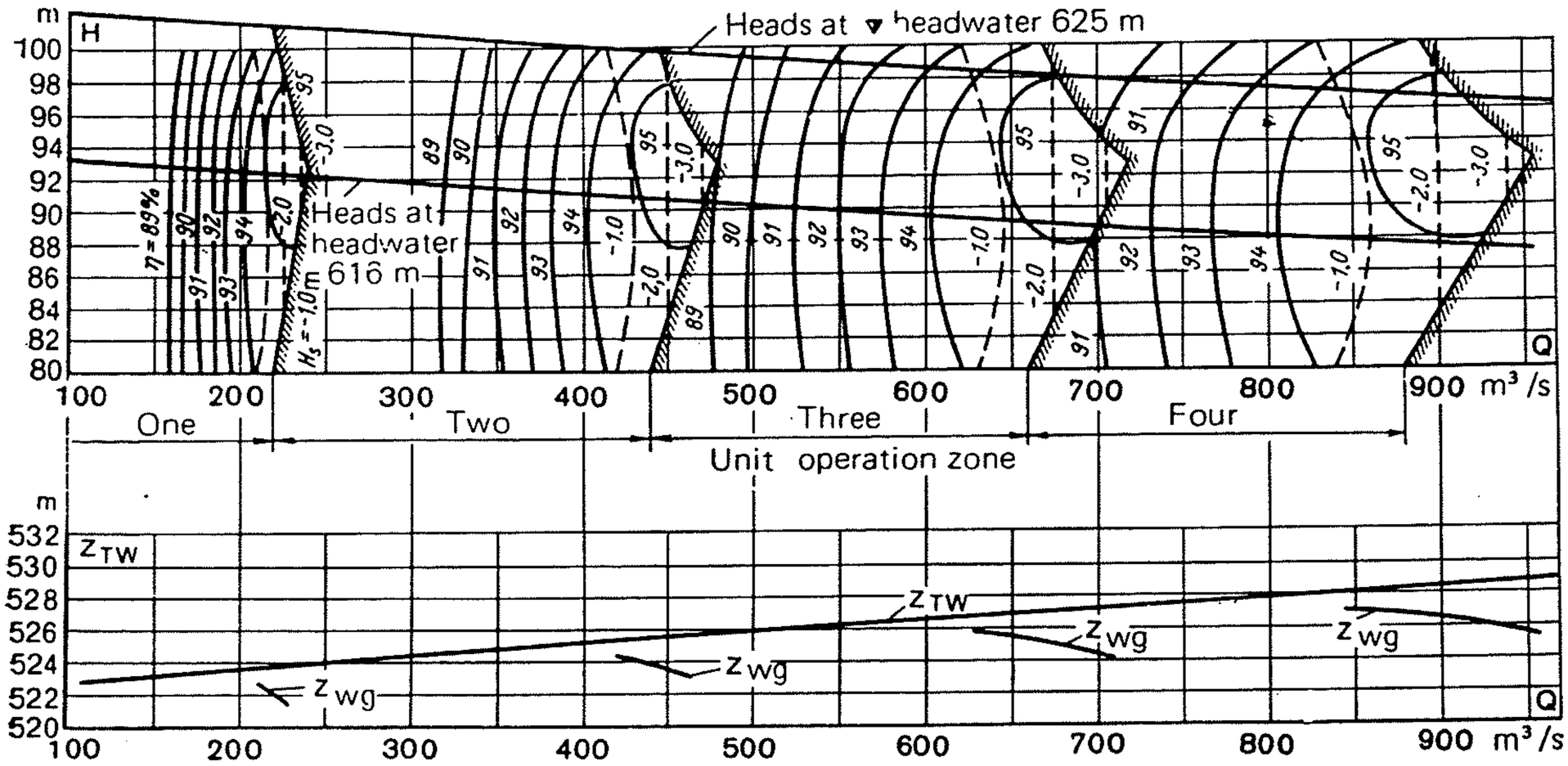


FIGURE 9.16. Operating head–discharge characteristic of HEPP turbine.

this case, which is illustrated by line $\eta = 92\%$ given for two and three turbines.

Figure 9.16 exemplifies a total operation head–discharge characteristic for four radial-axial flow turbines ($D_1 = 5.0$ m, $n = 136.4$ rpm, head $H_d = 92.8$ m, $N_d = 206$ MW, $Q_d = 239$ m^3/sec) aligned with the HEPP operation curve. The characteristic represents curves of efficiency and permissible suction lift H_s. Also illustrated are the TW level curves (z_{tw}) and the curves determining the maximum permissible elevation of the turbine wicket gate axis z_{wg} obtained from the equation

$$z_{wg} = z_{tw} + H_s$$

These curves provide the basis for selecting the turbine elevation.

CHAPTER 10

Automation, Installation, and Operation of Turbines

10.1. TURBINE AUTOMATIC CONTROL SYSTEMS

HEPP operation involves starting and shutting down the unit, and varying its power according to the load, discharge, or head. All these operations are carried out with the aid of a turbine automatic control system which ensures, at normal operation of the unit under load, maintenance of the required speed of rotation and optimal distribution of load between operating turbines, and which allows quick shutdown of the turbine in emergency cases (bearings overheating, failure of lubrication system, etc.).

In discussing turbine design (Chapter 3), we noted that opening the wicket gate, varying the runner blade angle in the adjustable blade turbines, and displacing the needle and baffle in Pelton turbines are carried out by hydraulic servomotors, actuated by high-pressure oil. Thus, apart from servomotors, the turbine automatic control system should include a means of feeding and distributing oil at the required pressure.

A schematic diagram of a single-loop automatic control system for radial-axial flow and propeller-type turbines is shown in Figure 10.1. The system includes three main parts: the oil pumping unit (OPU), for supply of oil under pressure; the control cabinet (CC), accommodating all control and distribution elements; and servomotors, which are linked

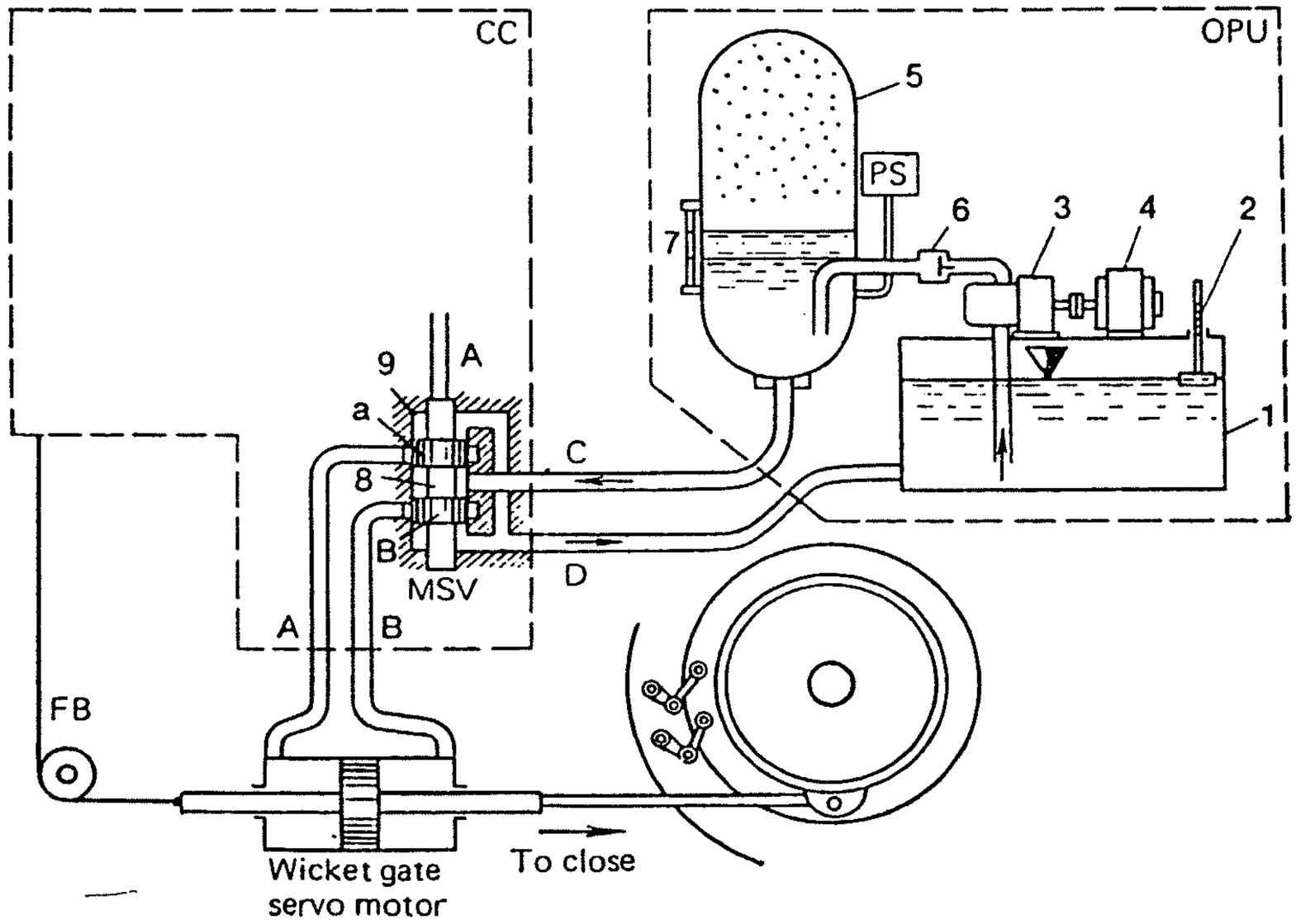


FIGURE 10.1. Turbine automatic control system.

to the wicket gate vane operating mechanism. These three parts are interconnected as follows: OPU and CC by oil lines C and D, CC and servomotors by oil lines A and B, and by a feedback tie (FB).

10.1.1. Oil Pumping Unit

The OPU (Figure 10.1) is comprised of a return tank (1) filled with oil to a level indicated by a float-type indicator (2), positive-displacement (usually screw-type) oil pumps (3) with electric motors (4), and an air-loaded accumulator (pressure tank) (5), which is filled with compressed air for about two thirds and with oil for one third.

During operation of the automatic control system pressurized oil from the accumulator (5) is fed via the pipe C, while the same amount of oil is returned via the pipe D to the return tank (1). Oil in the accumulator is replenished by the pump which transfers it from the return tank to the accumulator; the oil level in the accumulator is checked against a glass gauge (7).

The pump usually operates intermittently with a pressure differential of 0.2 to 0.3 MPa: when the accumulator oil level minimizes and the pressure drops by 0.2 to 0.3 MPa from the nominal value of 2.5 to 4.0 or 6.3 MPa, the pressure switch (PS) cuts on the electric motor and the pump feeds oil to the accumulator to restore the level at which the pressure is again nominal (preset). Now the pressure switch turns the

pump off. The nonreturn valve (6) closes, thus relieving the pump of oil pressure.

Provision is also made for continuous operation of the pump through a bypass valve that connects the delivery pipeline to the return line when the pressure in the accumulator reaches its maximum. The air-loaded accumulator improves reliability of the turbine automatic control system and decreases the required capacity of the pumps.

The designation of the OPU is determined by its basic specifications: accumulator volume, number of accumulators, and the nominal pressure. For instance, OPU 8-1/40 is an OPU with one air-loaded accumulator, 8 m^3 in capacity having a nominal pressure of 4 MPa (40 kg_f/cm^2); OPU 20-2/40 is an OPU with two accumulators having a total capacity of 20 m^3 and the same nominal pressure.

Because the pumping unit is a vital component of the automatic control system, it is provided with two pumps: a main pump and a standby pump; some large installations include a third low-capacity pump to compensate for oil leakage in the turbine control system.

The industry manufactures pumping units with a rated (nominal) pressure of 4 MPa (40 kg_f/cm^2) comprising one or two accumulators of the following capacities (in cubic meters):

With one accumulator —1.6, 2.5, 4.0, 5.6, 8.0, 10.0, 12.5
With two accumulators — 16.0, 20.0, 25.0, 32.0, 36.0

Some pumping units are designed for a pressure of 6.3 MPa.

10.1.2. Control Cabinet

The CC is a fairly complex assembly accommodating control, distribution, and adjustment elements. The main oil distribution element (Figure 10.1) is a master slide valve (MSV) comprising a slide valve (8) with two isolating cylinders (a) and (b) of a body (9) in which a slide valve moves. The slide valve is installed with small clearances. Provided in the body are two grooves somewhat smaller in height than the isolating cylinders. Oil is fed to the middle space of the slide valve from the pumping unit accumulator via a pipe (C); the upper and lower spaces are connected by a pipe (D) to the return tank, while the grooves in the MSV body are connected by pipes (A) and (B) to the servomotors. Because the end face areas of the slide valve are equal, the latter is hydraulically balanced at any pressure in pipes (C) and (D), so that a relatively light force is needed to displace it.

When the slide valve is in the neutral position, both grooves are sealed off, and pressures in pipes (A) and (B) and in respective spaces of the servomotors are equal (small amounts of oil penetrate through

clearances from the middle space to the return ones); the pistons are stationary. If the slide valve is shifted upward from neutral, the pipe and space (A) of the servomotors get connected to pipe (C) and the pressure in it rises, while the pipe and space (B) become connected to pipe (D) and the pressure within drops.

The pressure differential moves the piston with the rod to the right to turn the adjustment ring and close the wicket gate. When the slide valve is displaced downward, the wicket gate will open. The greater the slide valve displacement, the higher the rate of servomotor piston movement, and the less the time of turbine opening or closing.

It is often necessary to limit the maximum opening and closing rates of the servomotor. This is achieved by limiting displacement of the slide valve (8) from neutral with the aid of adjustable stops.

The automatic control equipment and control cabinets differ widely in embodiment and operating principles. These may be divided into two principal groups: hydromechanical, using mechanical elements, and electrohydraulic, base don electric devices. The electrohydraulic control equipment has found the widest application.

Figure 10.2 illustrates generally an electrohydraulic control unit comprising an electric cabinet and a hydromechanical CC. These units can be arranged at a considerable distance from each other.

The automatic controller must meet very stringent accuracy and sensitivity requirements; for example, the permissible sensitivity error is up to 0.05% as regards frequency.

The designation of a CC, or controller, is determined by its construction (e.g., hydromechanical or electrohydraulic) and by its characteristic size. The characteristic size for controllers of large turbines is the diameter of the master slide valve (usually equal to the diameter of the oil lines). The CC is unified (Figure 10.2), and only the MSV is replaceable. The controllers come with the following MSV diameters: 60, 100, 150, 200, and 250 mm.

10.1.3. Design Features of Automatic Controllers for Adjustable Blade Turbines

The adjustable blade axial-flow and mixed-flow turbines, in addition to wicket gate control devices which are similar to Figure 10.1, are provided with runner blade controllers. These controllers are intended to automatically implement the combinatorial relationship $\varphi = f_r\,(a_0 H)$ in compliance with Figure 8.12.

The schematic diagram of runner blade control is given in Figure 10.3. The runner slide valve (RSV) is an oil distribution element which includes a slide valve (1) and a body (2). Pressurized oil is fed to the middle space from the OPU accumulator, while the upper and lower

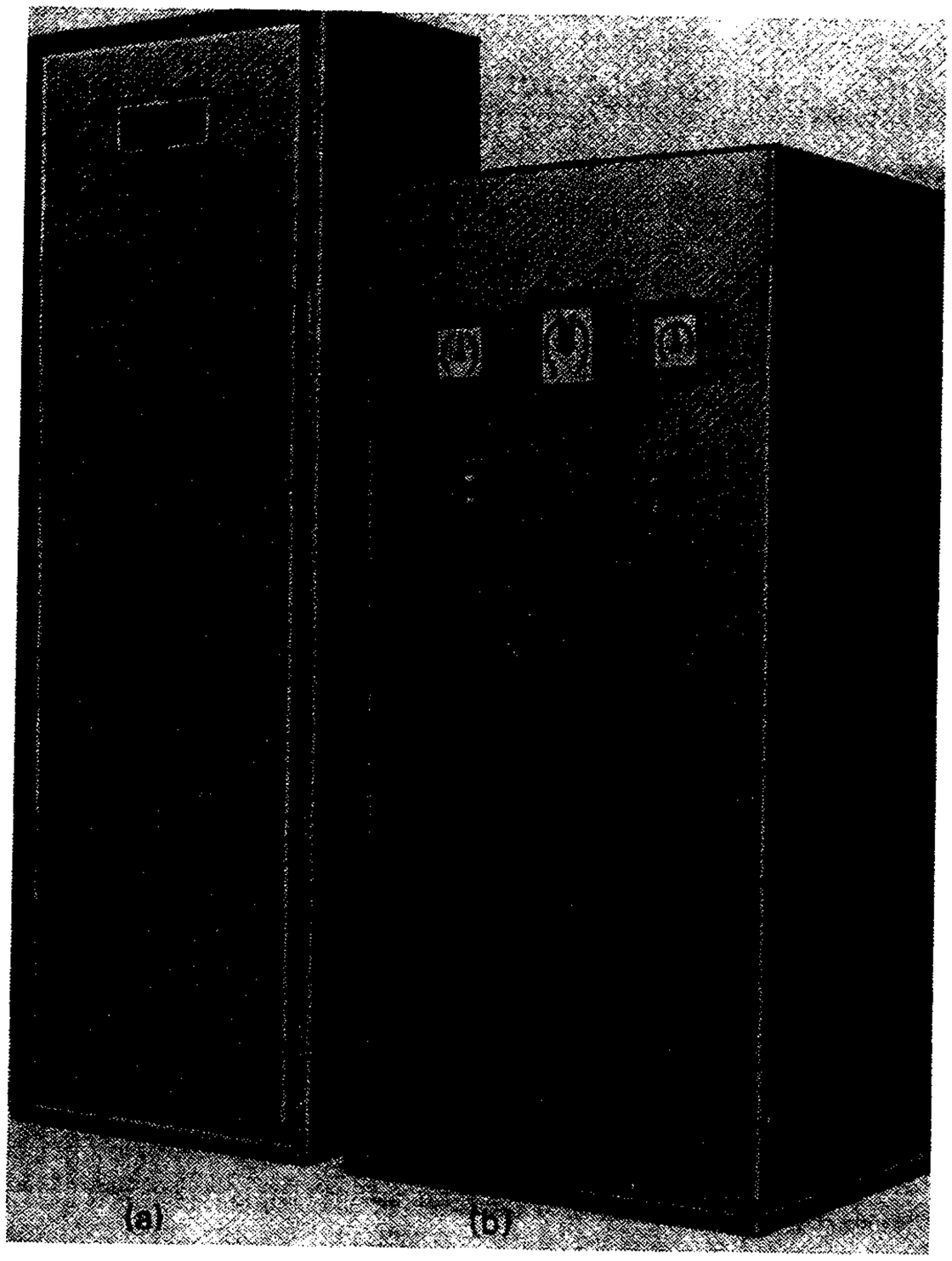


FIGURE 10.2. CC (a) and electric equipment cabinet (b) of a regulator.

spaces are connected to the return pipeline leading to the OPU tank. Two pipelines (A_c and B_c) supply oil from RSV to the oil receiver (3), usually disposed over the generator. Oil then flows through two coaxial pipes (A_c and B_c) arranged inside the shaft and rotating within it. Oil flowing through pipe A_c gets into the space above the piston (4) of the runner servomotor, and through pipe B_c, rigidly coupled with the piston (4), it gets under the piston (see Figures 4.6 and 4.7).

The slide valve (1) is suspended from a lever (5) having one end coupled with the FB cable of the runner feedback cable (RFC) and the other end (carrying a roller) is pressed by a spring against a curvilinear cam of the combinator. The cam is fitted to the FB shaft (6) to turn with the latter. The cam profile is shown in Detail CC. Cable RFC is attached to pipe B_c and its displacement is equal to that of the runner servomotor piston.

When the system is balanced, as shown in Figure 10.3, RSV is near its netural position. When the wicket gate servomotor is shifted for closing, the shaft (6) turns clockwise together with the curvilinear cam, which lowers the end of the lever (5), with the roller owing to its profile.

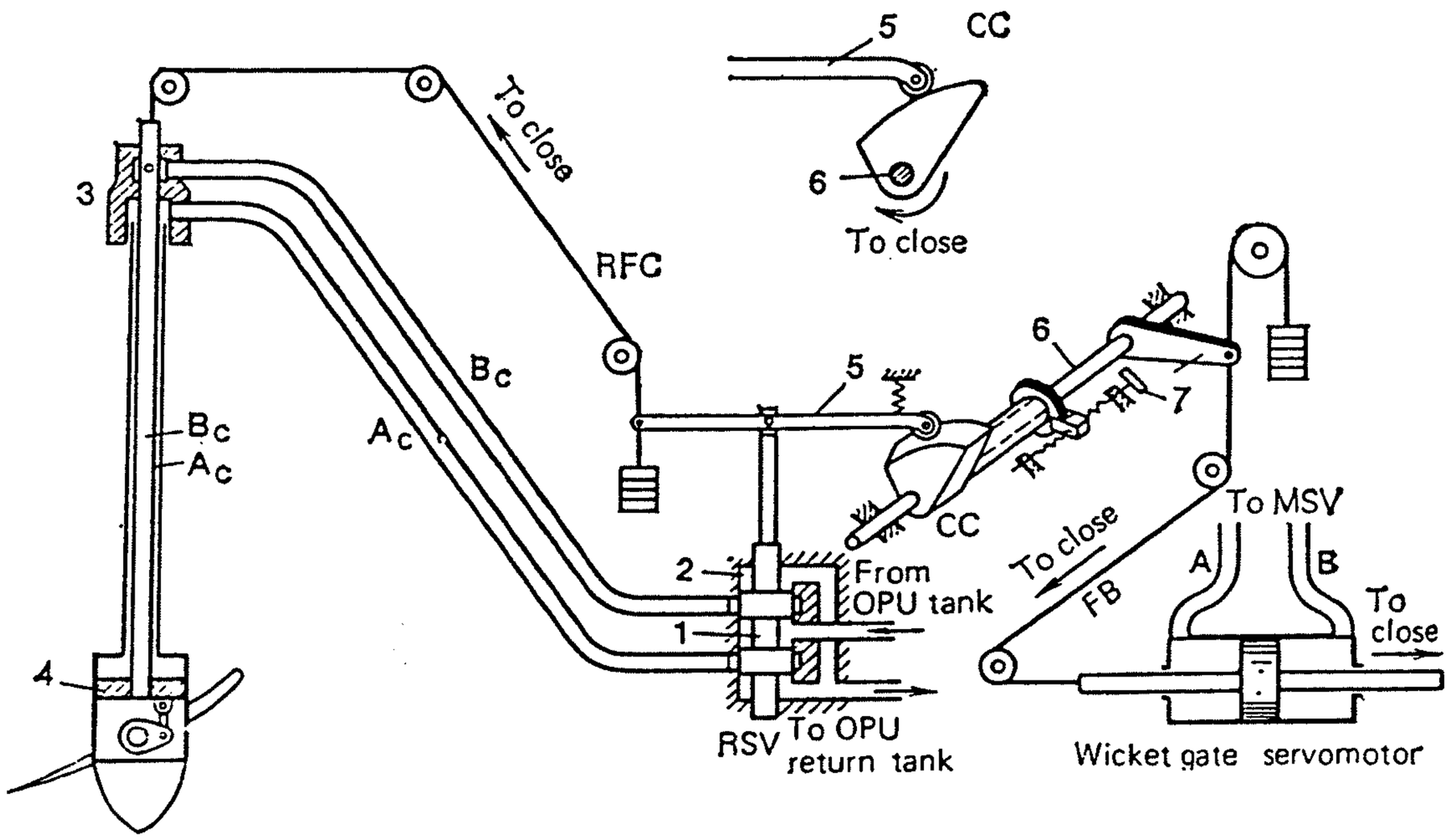


FIGURE 10.3. An adjustable blade turbine control system.

The slide valve (1) also moves down. Pressurized oil from the pumping unit accumulator gets into pipe A_c, and pipe B_c is connected to the return line; the piston (4) moves down, turning all the runner blades for closing (decreasing angle φ). Movement of the piston is accompanied by displacement of pipe B_c, which lifts the end of the lever (5) through cable RFC to return the slide valve (1) to neutral. Thus, each position of the wicket gate servomotor corresponds to a particular position of the runner servomotor. The required combinatorial relationship is ensured by the combinator cam profile.

In addition to the above it is necessary that the combinatorial relationship be changed according to the head employed. For this purpose, the combinator cam surface supporting the roller of the lever (5) is so shaped that when the curvilinear cam is displaced along the shaft (6) by a screw (7), the combinatorial relationship curve will also change ("spatial cam"). Adjusting curvilinear cam vs. head may be automated by using a device that measures HEPP head and actuates an electric drive coupled to the screw 7.

The adjustable blade turbines use electrohydraulic or hydromechanical CCs.

10.1.4. Peculiarities of Automatic Control in Pelton Turbines

The rapid reduction in power that is developed by Pelton turbines is effected by displacing the baffle (jet deflector or shut-off element) while the needle is closed slowly to diminish the water hammer in the delivery

conduit. Opening the needle may be accomplished at a far greater rate. The most common Pelton turbine control system is schematically illustrated in Figure 10.4. The MSV coupled with a sensing element responsive to rotational speed deviations controls a servomotor of a shut-off device (1) in conjunction with a FB to a shaft (2). The needle is controlled by a hydraulic follow-up circuit using a servomotor (3), needle slide valve (NSV) (4) with flow restrictors (5 and 6), combinator (NC), and lever (7). The system operates in a way similar to the runner blade control devices of the adjustable blade turbines.

10.1.5. Turbine with Pressure Regulator

When water is fed to the turbine through long conduits, a provision should be made for quick closing of the wicket gate without a considerable water hammer. Because the water hammer is proportional to discharge variation rate dQ/dt, the discharge through the pipeline should be varied more slowly than the turbine opening in order to decrease it. This may be achieved by providing a pressure regulator or surge relief valve.

A pressure regulator (Figure 10.5) comprises a scroll or power conduit duct (1) and a valve (2) having a diameter $D_{n.l}$ secured to a rod (3) with relief piston (4). The valve is displaced by a hydraulic servomotor (5) with the aid of a slide valve (6) to which pipelines (7, 8, and 9) from the oil pumping unit are connected. The valve is controlled by a rod (10), which is connected to the adjustment ring of the turbine wicket gate. When the wicket gate closes, the pressure regulator valve is moved for opening. Water is discharged through the pipe (11) to the tailwater (TW) reservoir.

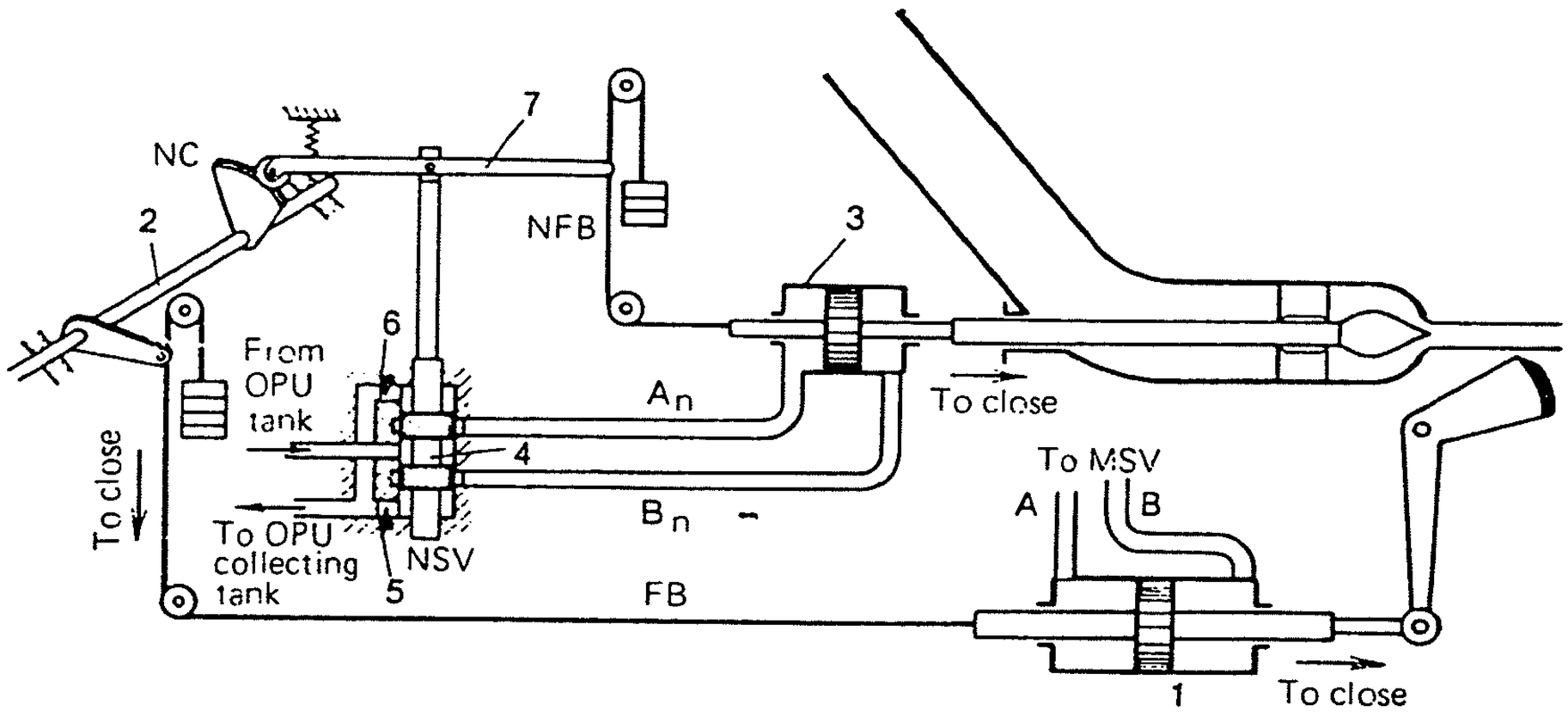


FIGURE 10.4. Pelton turbine control system.

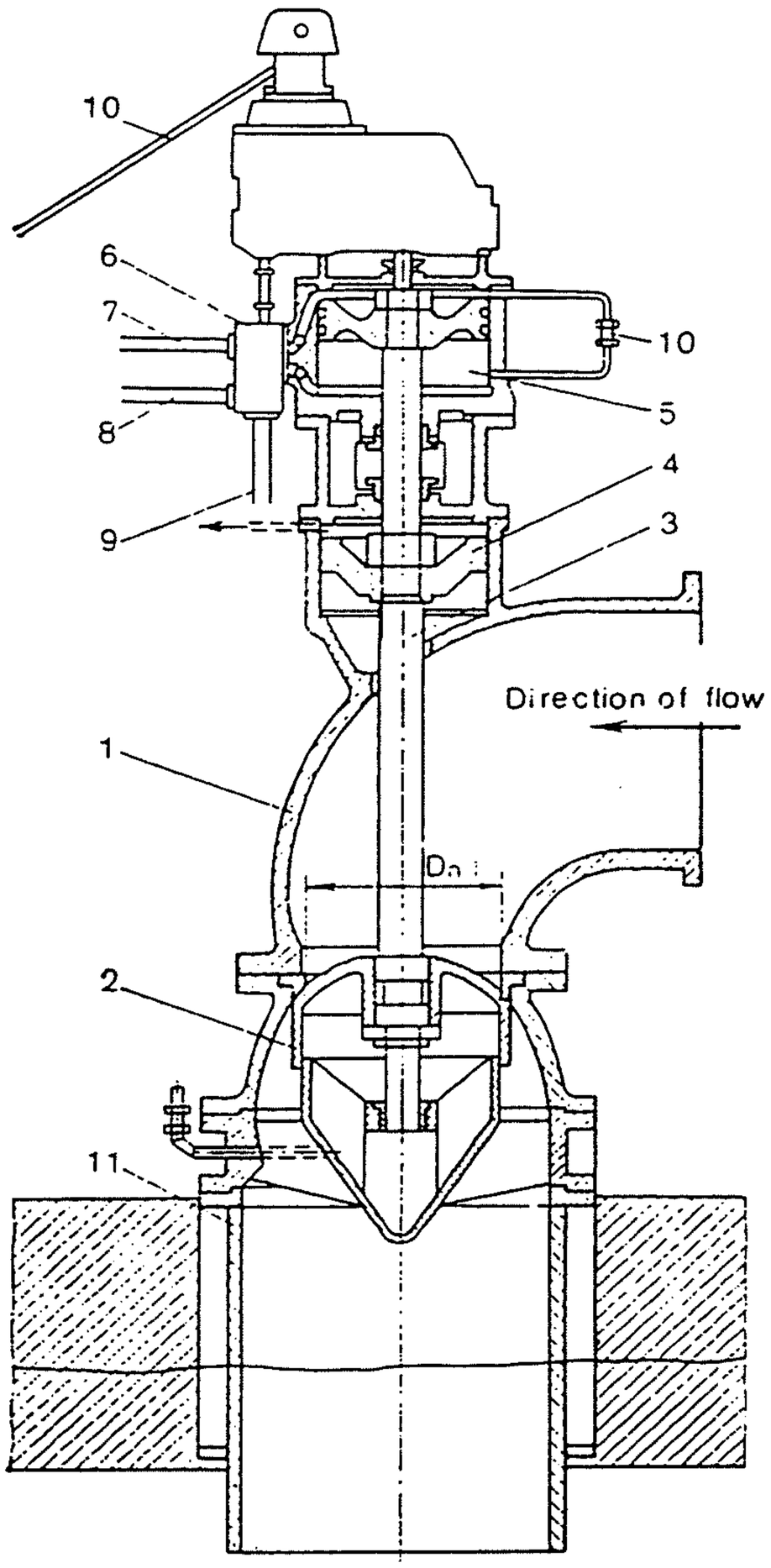


FIGURE 10.5. Turbine pressure regulator.

The system operates as follows (Figure 10.6): When the turbine load is constant, the valve is closed. As the load drops down during closing of the wicket gate (s_{wg} decreases), the valve opens ($s_{n.l}$ increases), and a portion of the water is discharged, by passing the turbine. After the turbine closure is discontinued, the valve slowly starts returning to the initial position ($s_{n.l}$ decreases), and becomes fully closed after $T_{n.l}$. The pressure regulator ensures that the conduit discharge changes according to curve (1), i.e., much more slowly than if no such facility were provided (curve (2)). This decreases dQ/dt accordingly, and hence, water hammer. Obviously, the pressure regulator valve should open only when the turbine is being closed. Thus, the greater the travel of the wicket gate servomotor rod, the greater the opening of the valve should

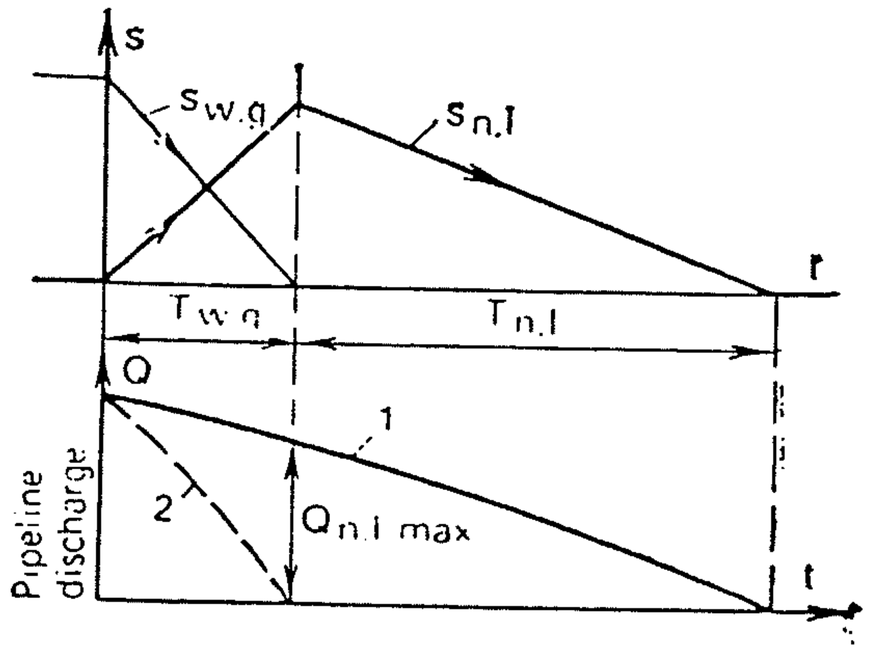


FIGURE 10.6. Operation of pressure regulator.

be. The valve remains closed when the turbine is being opened, so the pressure regulator acts only for turbine closing.

A characteristic size of the pressure regulator is its diameter $D_{n.l}$ (Figure 10.5).

10.2. INSTALLATION OF THE TURBINES

Installation of large turbines should meet particular requirements. First, the large turbines are always designed and manufactured individually with a view to particular conditions of the HEPP, and may include a plurality of specific design features that require appropriate approaches to installation. On the other hand, large turbines are only partially assembled by the manufacturer so that their installation at HEPP becomes the completion stage of their manufacturing process.

Another factor of vital importance is that turbine installation work is always closely linked with powerhouse erection operations. To maximize labor productivity and reduce the time required for the commissioning of HEPP units, an integrated plan is elaborated for organizing the building and installation work. As proved by experience, the utmost efficiency is obtained at parallel accomplishment of building and installation operations. Turbines are mounted in large components assembled at the assembly sites, while the required building work is carried out around the unit. Flow-line mounting operations are organized at several units with the appropriate time shift. When elaborating such a plan, great attention should be paid to load handling equipment, especially to cranes. As a rule, construction cranes are used at the initial stages of installation, while the main crane of the turbine room is employed in the final stages.

All turbine parts to be installed can be divided into two groups: insert parts, which are embedded in concrete after installation and are not

subject to disassembly, and removable parts, which are attached by bolts or studs and can be removed for repair.

The insert parts include the draft tube cone lining, stayring (stayring blades and support bands), runner cases of adjustable blade and mixed-flow turbines, and steel scroll. After concrete is laid at the lower elevation of the draft tube cone, the steel lining is installed, aligned, and secured, as shown in Figure 10.7. Then, concrete placement continues, and the steel lining doubles as a form. This method ensures reliable embedding of the lining in concrete.

Most insert parts are installed and secured in toothings, the cavities and hollows left in the concrete. The toothings are visible in Figures 3.1, 3.7, and 3.17. The stayring blades, support rings, and the runner case lining are installed in toothings on special pads. The runner case lining installed in toothings is braced by turnbuckles (elongated frames with one left hand (LH) and one right hand (RH) thread screw) and is supported by jacks and wedges. It is very important to ensure proper positioning relative to the unit axis, correct shape and dimensions (diametrical deviations should be within the specified allowances), elevation and horizontal alignment (for example, that of the lower and upper stayrings), and reliable attachment of all the parts installed. Then, the surface of the previously placed concrete is carefully scored and cleaned, and the metal surfaces are cleaned of paint and rust, only then can placement of concrete be started. These operations are to be accomplished with care to ensure reliable embedding of the insert parts.

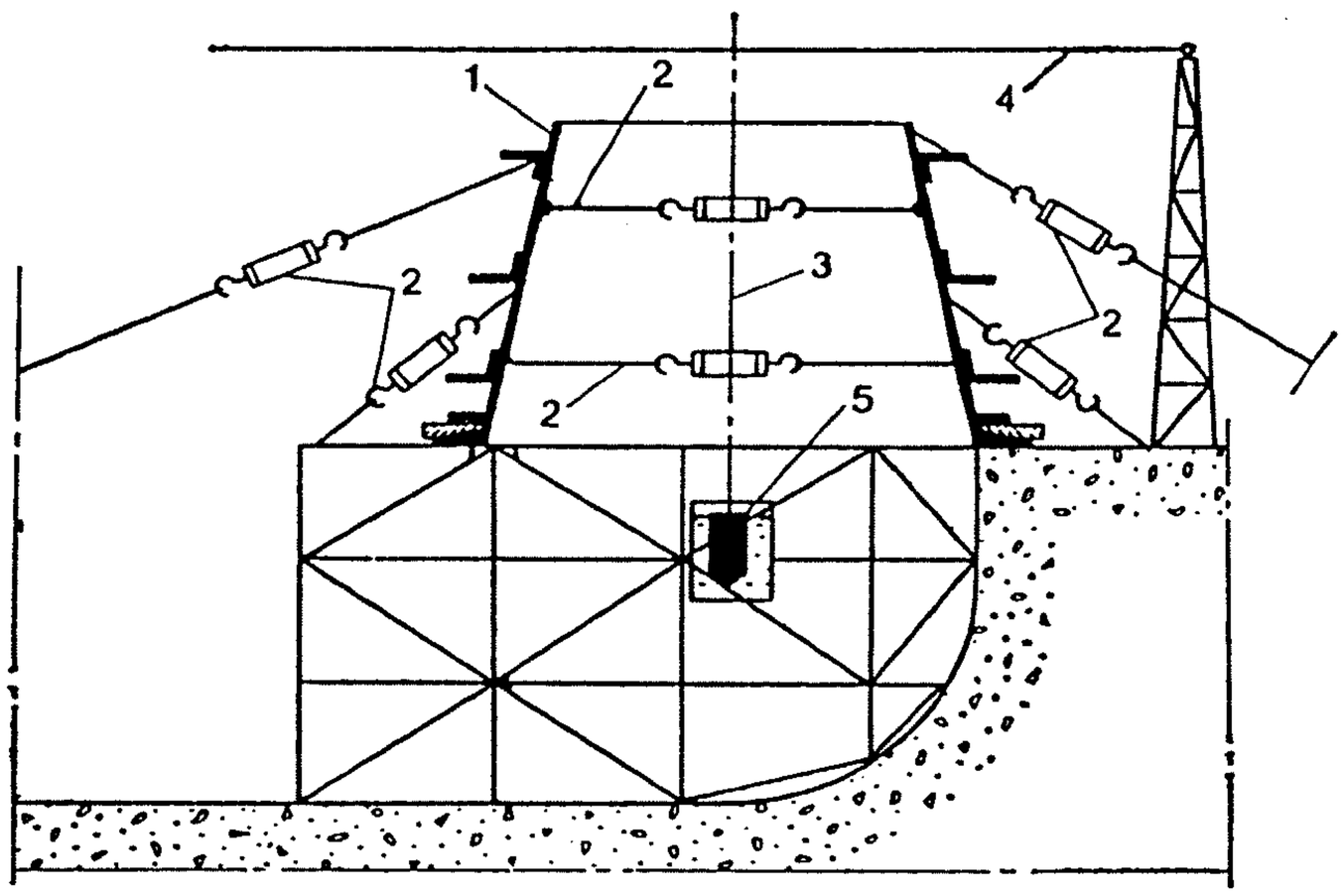


FIGURE 10.7. Installation of draft tube cone lining. 1 — steel lining; 2 — brace with turnbuckles; 3 — plumb line; 4 — axial line; 5 — plumb bob in tank with oil.

The assembly of steel scrolls is a most important operation. At the HEPP construction site, they usually receive separate sections of the shell made from sheet steel; the manufacturer performs only a check assembly of the shell, but not for all the turbines. The scroll is assembled in two stages: assembly of sections by tack welding and by final welding. Usually, the scroll is assembled either from the collar or from the inlet section. Joint is accomplished on the middle section where all the errors are eliminated (see Figure 6.4).

Special attention is paid to the quality of the welding, the strength of the welds, absence of local deformation, and weakening of metal that may stem from heating. High quality welds are achieved by appropriately preparing the edges to be butt welded (V-preparation for sheets up to 20-mm thick, and double V-preparation for sheets $>$ 20-mm thick), employment of high-quality electrodes and strict observation of welding conditions, and employment of skilled welders (only those welders who hold special certificates are admitted for welding steel scrolls). Special measures should be taken when welding high-strength low-alloyed steels used in scrolls of high dimensions and heads (special conditions, austenite welding electrodes, etc.).

Welds are checked by X-ray inspection, γ-ray inspection (a cobalt radioactive isotope is used; this method requires special care), and ultrasonic inspection. Alongside these modern methods an old, but sufficiently reliable technique can be used of checking welds by kerosene: The inner surface of the weld is coated with chalk and after the latter dries, rags soaked with kerosene are placed on the outer surface. The surface is inspected after 2 or 3 hr. If kerosene stains are detected, the weld is leaky; it is chiseled away and rewelded.

After completing welding operations the scroll is concreted; sometimes the upper half is covered with special yielding material to avoid transfer of load to the concrete (see Figure 6.6a).

The removable parts of a turbine include a wicket gate, a runner, shaft and cover of the turbine with guide bearing, and a wicket gate operating mechanism. By the time installation of these parts begins, the inserts are already installed, the powerhouse is elevated, and the main cranes of the turbine room are mounted; this allows the installation of the turbine in large-size components.

How the installation proceeds depends on the turbine design. If the lower ring does not interfere with lowering the runner, as shown in Figures 3.7, 3.15, and 3.17, assembly starts by installing the guide blade pivots into the bushings of the lower ring. Then, the intermediate support ring is installed to secure the bearings of the guide blade pivots. However, in many cases no intermediate ring is used, so the guide blade pivot bearings are attached directly to the turbine cover (see Figures 3.7, 3.15, and 3.17). If this is the case, the runner is lowered into the

case, and the turbine cover is installed by passing the guide vane upper pivots through the cover holes.

The runners of radial-axial flow turbines are usually delivered to the HEPP construction site as a single piece so that preliminary assembly is confined to cone attachment (ref. no. 18 in Figure 3.15). When the large dimensions of the runner preclude railway shipment, the runner comes in two, four, or even more parts (see Figure 3.16). On such an occasion, a very complex and important turbine runner assembly is accomplished at HEPPs. Such assembly involves fitting the bands with preheating, special welding, and machining.

The runners of adjustable blade and mixed-flow turbines are always delivered to HEPPs in separate parts (blades, body parts, servomotor piston, levers, shackles, cone, etc.); therefore, the runner is preassembled on the installation site and is checked for smooth and easy movement of the blade operating mechanism by supplying oil at the low pressure of 0.2 to 0.3 MPa.

To check the joints and seals of blades for leakage, the assembled runners are subject to a compulsory hydraulic pressure test with oil for 24 hr. Taking into account today's requirements for environmental control, external leakage of oil cannot be tolerated.

The dimensions of the crane and structures are the factors that determine the choice of installation method. The runner may be installed in the turbine case with the shaft or separately; thus, the latter case the runner is connected to the shaft in the chamber. The flange joint bolts are tightened and their elongation accurately check i.e., to a strictly definite torque.

The turbine cover is usually installed fully assembled, but its final attachment is accomplished after alignment of the runner. Therefore, the runner is adjusted first with respect to the clearance between the blades and the case in the adjustable blade and mixed-flow turbines or the clearances in the seals of the radial-axial flow turbines.

The next step is a very important operation: vertical alignment of the shaft. This operation requires an extreme amount of accuracy. Permissible vertical misalignment should not exceed 0.02 mm/m of the shaft length. Then, the cover is attached, and the guide bearing and the wicket gate vane operating mechanism are installed. The mounting operations are completed by filling in service logs, which are important documents for acceptance of the turbine and unit. In particular, the service logs are filled in for measuring runner clearances, shaft vertical alignment, guide vane end gaps, and opening at different travel of the servomotor rod, runner blade setting angle.

After installation of the turbine and generator is completed, the unit is subjected to a 72-hr preoperational test to check the unit for operability and correspondence to basic specifications.

10.3. OPERATION OF THE TURBINES

The task involved in the operation of the turbines is the most effective utilization of their capabilities at a hydro, and includes maintenance, routine and major repairs for ensuring a high reliability, and longevity of the units.

Effective utilization of turbines is mainly characterized by achieving the maximum average efficiency of the plant (optimal distribution of load between units), which is represented in the form of total characteristics of turbines (see Figure 9.16). When plotting such characteristics at HEPPs, it is recommended that corrections be introduced against the full-scale test data of the turbine. This makes possible the refinement of the combinator curves of the adjustable blade turbines, taking into account deviations in characteristics of the separate turbines, and sometimes the difference in hydraulic losses of the water conduits of the different turbines of the plant (such loss difference may stem from different lengths of the conduits or from conduit branching).

Reliability is a very important characteristic of the turbine and includes a series of indices. The most significant of these indices follow:

1. Operability is the operating state of the turbine corresponding to the specified power, efficiency, vibration, noise, leaks, and other characteristics.
2. Trouble is a loss of operability that manifests itself in that either the unit is rendered inoperable, complete failure (for instance, the guide bearing or the blade operating mechanism of the adjustable blade turbine has failed) or that some parameter falls outside the permissible limits; (for instance, a drop in efficiency or an increase in vibration level). In the latter case the turbine may be operated but it cannot be regarded to be in good repair.
3. Durability is the period of time during which the turbine remains operable under the operating conditions specified in the technical documents.
4. Probability of failure-free operation is the capacity of a unit to operate with a certain probability of absence of failures within a specified period of time.

Quantitative indexes of reliability also exist. The so-called availability factor K_{av} is used widely with HEPPs. This factor for turbines is determined as follows:

$$K_{av} = \frac{\sum_T t_{op}}{\sum_T (t_{op} + t_{rep})} \tag{10.1}$$

where

$$\sum_T t_{op} = \sum_T (t_{turb} + t_{comp} + t_{stby})$$

where t_{turb}, t_{comp} are, respectively, the time periods of turbine and compensation operation; t_{stby} is the time of standby (complete availability); and t_{rep} is the time of repair (shut-down) (additional time spent for repair of other parts of the unit, say of the thrust bearing). The sum is taken for a sufficiently long time period T (at least 1 year).

Hydraulic turbines are simple to operate and fairly reliable machines whose availability factor under favorable conditions may be 0.96 to 0.97 and even higher; however, in cases of intensive cavitation and abrasive wear the factor may drop below 0.9. Turbine wear stems from cavitation or abrasive action of sediments suspended in water or from both.

Axial-flow adjustable blade turbines suffer from cavitation more intensely. As illustrated in Figure 10.8, cavitation erosion develops at the rear ("vacuum") of the runner blades, and the zone (1) near the leading edge is formed by local stalling at high angles of attack. Zone (2) near the trailing edge is the greatest, as it expands toward the periphery. The runner case (3) under the blade pivot and the end surfaces of the blade airfoil (the so-called slit cavitation) are sometimes subject to the intense erosion.

In radial-axial flow turbines the runner blade ("vacuum") part adjacent to the trailing edge and the inner part of the lower rim suffer from the most intense cavitation erosion.

The intensity of cavitation erosion can be very high to reach a depth of 5 to 10 mm/year. It depends on turbine design features, service conditions (operation TW elevation, H_s; increasing H_s above the permissible limits is particularly dangerous) and materials used (see Chapter 7).

Turbine parts subjected to intensive cavitation action often are made from cavitation-stable materials such as stainless steel (Table 7.1). To solve the problem less expensively, some parts such as blades can be

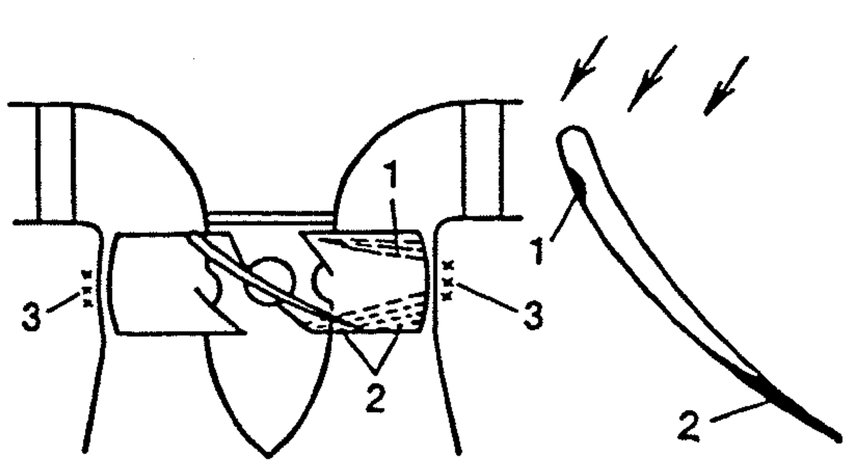


FIGURE 10.8. Points of cavitation erosion of axial-flow turbines.

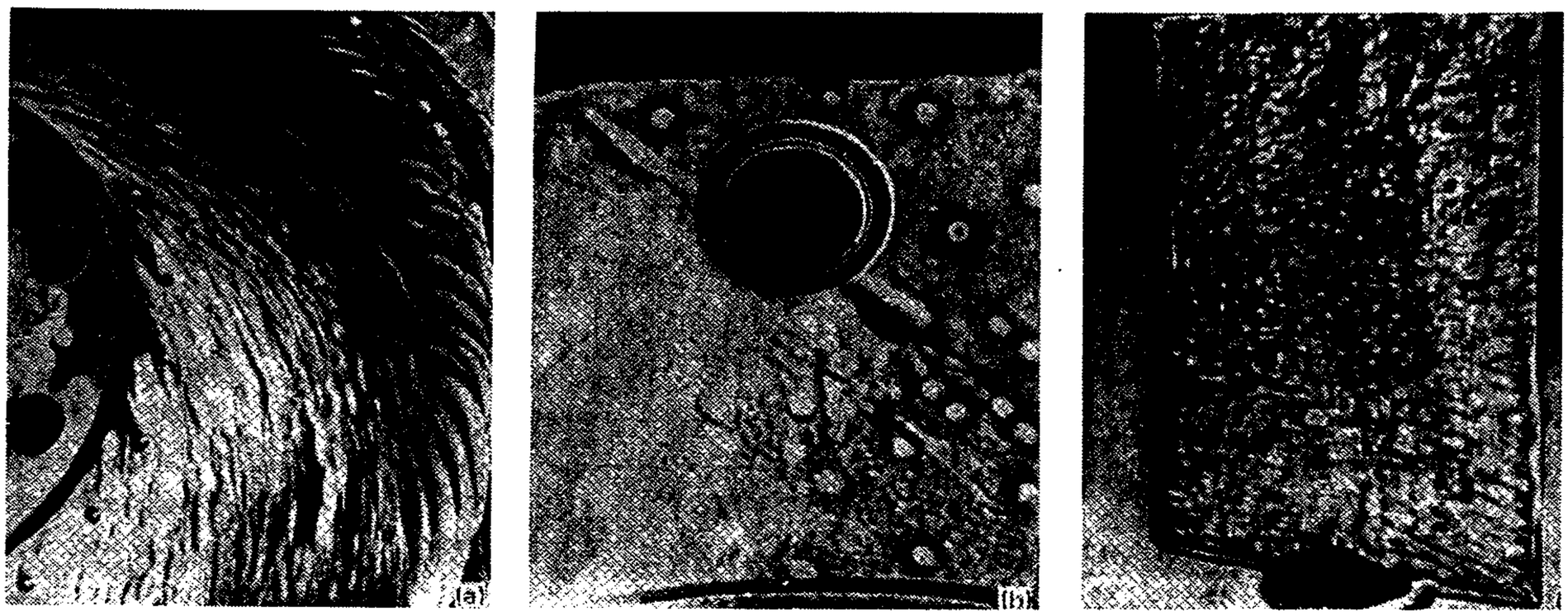
made from ordinal steel that have a protective lining made from thin plates of stainless steel. Special technologies have been developed to create this type of cover, including blowup welding.

The abrasive action of sediments contained in water, particularly quartz particles, causes very intense wear on turbines. This phenomenon is most common with HEPPs erected on mountain rivers.

The abrasive wear of structures, including hydraulic machines, is very complex. Despite the investigations into this situation, many problems are still unsolved. According to the existing concepts abrasive wear stems from particles striking and scratching the surfaces. Abrasive wear is dictated mainly by the content of suspended sediments in water (turbidity), the quantity of hazardous fractions (diameter $D > 0.1$ to 0.15 mm), grainy material (most dangerous is quartz with sharp edges), relative velocity, and resistance of the surfaces of the turbine that are in contact with water flow (see Section 17.4 for more detail).

Subject to abrasive wear in turbines are guide vanes (Figure 10.9c illustrates scaly surface), the support ring (Figure 10.9b shows traces of wear with a distinct recess formed at the location at which the guide vane end rests for a protracted period), and the runners (Figure 10.9a depicts the abraded surface of the upper rim of the runner facing the cover). The radial-axial flow turbine runners (particularly their rim), blade trailing and leading edges, and upper and lower seals also suffer from intense abrasive wear. Sediment penetration into the guide bearing is particularly dangerous as the bearing is rapidly worn in this fashion.

Turbine wear deteriorates their energy characteristics, decreases efficiency and sometimes power, and may lead to increased vibration



(a) (b) (c)

FIGURE 10.9. Abrasive wear of parts in radial-axial flow turbine.

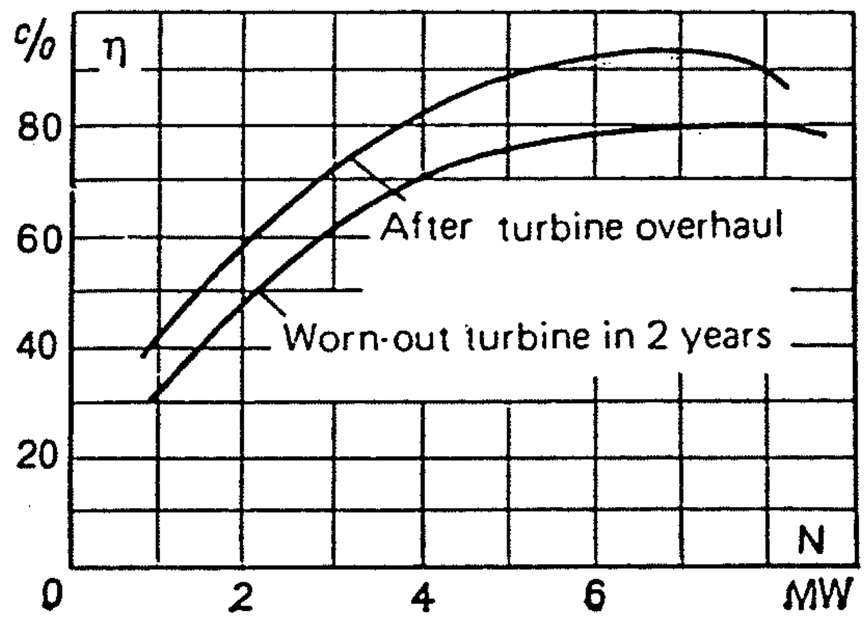


FIGURE 10.10. Effect of wear on radial-axial flow turbine characteristic.

and noise and increased losses of water at shut-down periods because of leakage through the wicket gate. As illustrated in Figure 10.10, after 2 years of operation turbine wear has led to a 10 to 12% decrease in efficiency, though power has not changed owing to increased throughput capacity. This occurs due to the shortened trailing edges that result from abrasive wear.

Intensive wear necessitates shut-down of the turbine for repair by surfacing or dressing worn out areas or by replacing worn out parts.

All these factors decrease HEPP efficiency and increase operation costs.

To exclude intensive abrasive wear of turbines the most reliable solution is to construct a special settling basin.

Establishing an optimal time between overhauls is an important factor. For regular conditions, when abrasive content in water is normal, the time between overhauls may be from 25,000 to 30,000 hr of turbine operation, or at least 4 years with $\lesssim$ 25,000 operating hours. The total service life of the turbine should be $\lesssim$ 30 years.

SECTION 3

Pumps

CHAPTER 11

Basic Characteristics of Pump Installations and Types of Pumps

11.1. HEADS OF PUMP INSTALLATION

A schematic diagram of a pump installation (Figure 1.1b) illustrates that a pump converts the energy delivered to it via a drive into the hydraulic energy of a liquid being transferred. Consider a hydraulic diagram of a pump installation (Figure 11.1a), applicable to any type of pump. The principal elements of the installation are a pump having two branch pipes, an inlet (suction) pipe (section 1–1) and an outlet (delivery) pipe (section 2–2); suction pipeline S; and delivery (pressure) pipeline H.

The following characteristics of a pump installation also may be distinguished.

Static or elevation head H_{st} (measured in meters) is the difference between elevations of upper and lower reservoirs (headwater, HW, and tailwater, TW, elevation difference) z_{hw} and z_{tw}, respectively; i.e., the height to which liquid is lifted

$$H_{st} = z_{hw} - z_{tw} \tag{11.1}$$

If liquid is supplied to a reservoir where excessive pressure p (measured in Pascals) is maintained, as shown in Figure 11.1b, static head is

$$H_{st} = z_{hw} - z_{tw} + \frac{p}{\rho g} \tag{11.1a}$$

where ρ is density of liquid being transferred (measured in kilograms per cubic meter), and g is the free fall acceleration (measured in meters per second square).

Suction lift H_s is elevation of the pump over the lower reservoir level (Figure 11.1a).

For inlet pressure, write Bernoulli's equation (see Equation 1.8) for a flow between two sections: (1) liquid surface in the lower reservoir, section TW, and (2) section 1–1 in the inlet pipe. Arrange datum plane 0–0 at elevation TW. For these conditions, assuming zero is an excessive pressure on surface TW $p_{tw}/\rho g = 0$, $z_{tw} = 0$ and $v_{tw} = 0$, and $\alpha_1 = \alpha_2 = 1$, we obtain

$$0 = \frac{p_1}{\rho g} + H_s + \frac{v_1^2}{2g} + h_{suc}$$

where $p_1/\rho g$ is a hydraulic lift corresponding to pressure in inlet section 1–1, and h_{suc} are hydraulic losses in the suction pipeline. Then

$$\frac{p_1}{\rho g} = -\left(H_s + \frac{v_1^2}{2g} + h_{suc}\right) \tag{11.2}$$

Thus, $p_1/\rho g < 0$. This indicates vacuum in section 1–1 (Figure 1.6b), H_v, which is called vacuum suction lift

$$H_v = H_s + \frac{v_1^2}{2g} + h_{suc} \tag{11.3}$$

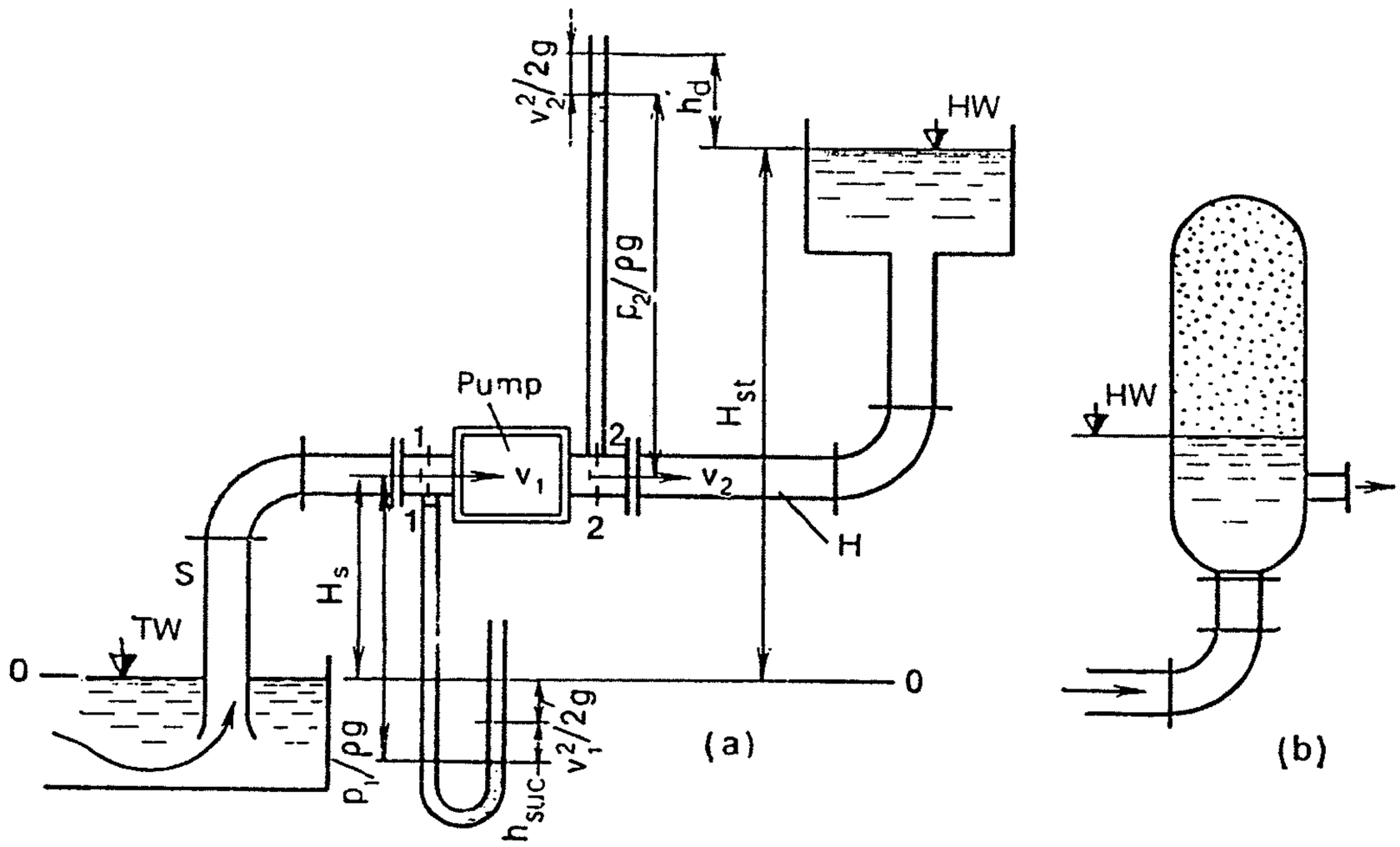


FIGURE 11.1. Pump installation.

Absolute pressure in liquid cannot be negative in essence ($p_a > 0$), otherwise stream discontinuity will result. Therefore, according to Equation 1.3:

$$H_v < p_{atm}/\rho g$$

At sea level $p_{atm} \approx 0.1$ MPa, i.e., for cold clean water flow $H_v < 10$ m. By substituting this value in Equation 11.3, we shall see that the pump suction lift should be limited to $H_s < 10$ m, which is a very important practical conclusion (more details about H_s in Chapter 14).

For outlet (delivery) pipe pressure, write Bernoulli's equation for the flow between sections 2–2 and the free surface in the upper reservoir HW. Datum plane 0–0 will remain at elevation TW. Taking into account the characteristics shown in the diagram of Figure 11.1 $p_{hw}/\rho g = 0$, $v_{hw} = 0$, we obtain

$$\frac{p_2}{\rho g} + H_s + \frac{v_2^2}{2g} = H_{st} + h_d$$

where h_d are hydraulic losses in the delivery pipeline. Therefore, the pressure sought is

$$\frac{p_2}{\rho g} = H_{st} - H_s - \frac{v_2^2}{2g} + h_d \qquad (11.4)$$

Figure 11.1a represents the geometric values of hydraulic lift $p_1/\rho g$ and $p_2/\rho g$.

Pump head H is equal to the difference of specific energy of liquid in outlet pipe e_2 and in inlet pipe e_1

$$H = e_2 - e_1 \qquad (11.5)$$

According to Equation 11.5, the definition of specific energy of liquid given in Section 1.1 determines that head H (meters) is a numerical value of energy (Joules) received by a mass of flowing liquid corresponding to weight force of 1 N, which passes through the pump and is delivered to the outlet pipe (delivery pipeline).

Using specific energy Equation 1.4 and assuming $z_1 = z_2 = H_s$ according to Figure 11.1, we obtain the following relations for e_1 and e_2 at $\alpha = 1$:

$$e_2 = \frac{p_2}{\rho g} + H_s + \frac{v_2^2}{2g} \qquad e_1 = \frac{p_1}{\rho g} + H_s + \frac{v_1^2}{2g} \qquad (11.5a)$$

By substituting $p_1/\rho g$ values from Equation 11.2 and $p_2/\rho g$ from Equation 11.4 in Equation 11.5a, we obtain

$$e_1 = -\left(H_s + \frac{v_1^2}{2g} + h_{suc}\right) + H_s + \frac{v_1^2}{2g}$$

$$e_2 = \left(H_{st} - H_s - \frac{v_2^2}{2g} + h_d\right) + H_s + \frac{v_2^2}{2g}$$

Finding their difference from Equation 11.5, we determine the head

$$H = H_{st} + h_{loss} \tag{11.6}$$

where $h_{loss} = h_{suc} + h_d$ are total hydraulic losses both lengthwise and local or minor in the suction and delivery pipelines. Thus, pump head is equal to the sum of static head and hydraulic losses in the system or pipelines. The same result can be obtained directly from the Bernoulli equation (Equation 1.8), written for sections 1–1 and 2–2, if we denote $H = h_{ex}$ using the minus sign and accept $h_{1+2} = 0$. It helps to reveal the energetic essence of pump head notion.

Hydraulic theory tells us that lengthwise and minor losses

$$h_i = \zeta_{li}\frac{v_i^2}{2g}$$

and

$$v_i = Q/F_i$$

where v_i is the average velocity of flow, Q is the flow rate (delivery), and F_i is the pipeline area; therefore, h_{loss} in Equation 11.6 may be represented through Q

$$h_{loss} = \left(\sum \frac{\zeta_i}{2gF_i^2}\right)Q^2$$

or

$$h_{loss} = K_r Q^2$$

As seen in the above relationship, K_r is a coefficient of resistance (or drag) of the pipeline (system), which depends only on the pipeline geometry (length and diameter) and types of additional flow restrictors installed (elbows, reducers, valves, etc.). As a result, we obtain another

expression for the head required to ensure flow rate Q through a given system (therefore designated H_r)

$$H_r = H_{st} + K_r Q^2 \tag{11.6a}$$

The relationships in Equations 11.6 and 11.6a are called system characteristic relationships.

Pump head is measured by a pressure gauge (PG) connected to the outlet pipe and by a vacuum gauge (VG) installed on the inlet pipe (IP) (Figure 11.2). Prior to measuring, these two gauges are blown by opening the three-way cocks. As a result, the pipe leading to the pressure gauge will be filled with liquid, while that leading to the vacuum gauge will contain air. Thus, the vacuum gauge indicates rarefaction at the pipeline point at which it is connected, and the pressure gauge with the pressure corrected to its installation height z_{pg}. The readings corrected to the height are used to find the piezometric differential created by the pump

$$\frac{p_2}{\rho g} - \frac{p_1}{\rho g} = h_p + H_v + z_{pg}$$

where h_p and H_v are readings of the pressure gauge and the vacuum gauge corrected to a lift of liquid being transferred. Pump head, according to Equations 11.5 and 11.5a is equal to

$$H = h_p + H_v + z_{pg} + \frac{v_2^2 - v_1^2}{2g} \tag{11.7}$$

i.e., it is slightly different from the piezometric differential.

If a pump is installed with submergence (see Figure 17.1) and excessive pressure exists in its inlet pipe, the pump head is determined

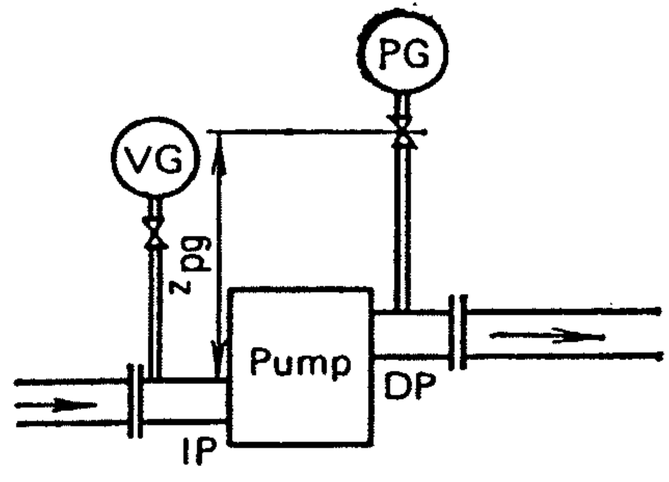


FIGURE 11.2. Measurement of pump head.

from readings of the two pressure gauges

$$H = h_{p2} - h_{p1} + z_{1-2} + \frac{v_2^2 - v_1^2}{2g} \tag{11.7a}$$

where h_{p1} and h_{p2} are readings of the pressure gauges connected to the inlet and outlet pipes intended for the lift value of liquid to be transferred, and z_{1-2} is the difference in pressure gauge elevations.

Pump pressure P (Figure 11.1) is determined from the formula

$$P = p_2 - p_1 + \rho\frac{v_2^2 - v_1^2}{2} + \rho g z_{1-2} \tag{11.8}$$

where p_1 and p_2 are pressures at the inlet and outlet pipes (Equations 11.2 and 11.4), and v_1 and v_2 are respective velocities. When pump pressure is known, its head according to Equation 11.7 is determined by the relationship

$$H = P/\rho g \tag{11.8a}$$

11.2. PUMP CAPACITY

An important characteristic of pump operation is liquid delivery (discharge) Q, i.e., volume of liquid delivered by the pump to the pressure pipe per unit time. Delivery Q is measured in liters per second, cubic meters per second, or cubic meters per hour.

According to the above definition, head H is specific energy in joules per newton. Thus, the gross useful power transferred by the pump to the liquid being pumped N_{liq} (measured in watts) is

$$N_{liq} = \rho g Q H \tag{11.9}$$

where ρ is the density of liquid being transferred (kilograms per cubic meter), g is the freefall acceleration (meters per second square), and Q is the volumetric delivery of the pump (cubic meters per second).

A certain portion of energy N received by the pump is not transmitted to the liquid because of energy losses, which are accounted for by the efficiency η

$$\eta = \frac{N_{liq}}{N} \tag{11.10}$$

Using Equations 11.9 and 11.10, we find the formula to define power N (kilowatts), required for driving the pump

$$N = \frac{\rho g Q H}{1000\eta} \tag{11.11}$$

For clean water $\rho = 1000$ kg/m^3, $g = 9.81$ m/s^2, and the power formula takes the following form:

$$N = \frac{9.81 Q H}{\eta} \tag{11.11a}$$

Example 11.1

Determine the pump capacity (drive power) for the following conditions: delivery $Q = 20$ L/s of clean water, head $H = 45$ m, $\eta = 75\%$.

Solution

Find capacity for $Q = 0.02$ m^3/s from Equation 11.11a

$$N = \frac{9.81 \times 0.02 \times 45}{0.75} = 11.8 \text{ kW}$$

Example 11.2

Determine the pump capacity for transferring pulp (water with soil) with the following conditions: pulp density $\rho = 1200$ kg/m^3, delivery $Q = 1100$ L/s, head $H = 60$ m, $\eta = 70\%$.

Solution

From Equation 11.11, find

$$N = \frac{1200 \times 9.81 \times 1.1 \times 60}{1000 \times 0.7} = 1110 \text{ kW}$$

11.3. TYPES OF PUMPS

A general analysis of pump operating conditions shows that they should exchange energy between the liquid and a moving working member to which energy is supplied. There is a wide diversity of types and designs of pumps, but as regards their operating principle all can be divided into two classes: positive displacement and rotodynamic units.

11.3.1. Positive Displacement Pumps

The positive displacement pumps transfer liquid by periodically changing the volume of the chamber filled with the liquid and alternately connected to the inlet and outlet branch pipes. This is a general principle, which is explained below by way of examples.

A plunger pump (Figure 11.3) comprises of housing (1), a plunger (2) with diameter d reciprocating (stroke s) from an external drive and two valves: a suction valve (3) and a pressure valve (4). The plunger may be driven by an electric motor through a crank mechanism. When the plunger moves to the right, the volume of the chamber C increases with a drop in pressure, and liquid is sucked from the lower reservoir. The suction valve is opened by water flow. As soon as the plunger movement direction reverses and it begins moving to the left, the volume of chamber C decreases, the suction valve closes, and the liquid is expelled from the chamber through the pressure valve. A volume of liquid equal to $\pi d^2 s/4$ is fed to the pressure pipe during each cycle. Thus, if the number of cycles per minute is n_c, the average theoretical delivery rate of such a pump is

$$Q_{av\cdot theor\cdot} = \frac{\pi d^2}{4} s \frac{n_c}{60} \tag{11.12}$$

A particular feature of this pump is that delivery is affected by pulses and Q_{max} is well above Q_{av} (Figure 11.3).

A double-acting piston pump (Figure 11.4) comprises a cylinder (1) with a diameter d accommodating a piston (2) with a rod (3) which reciprocates within the cylinder. The cylinder has two groups of valves:

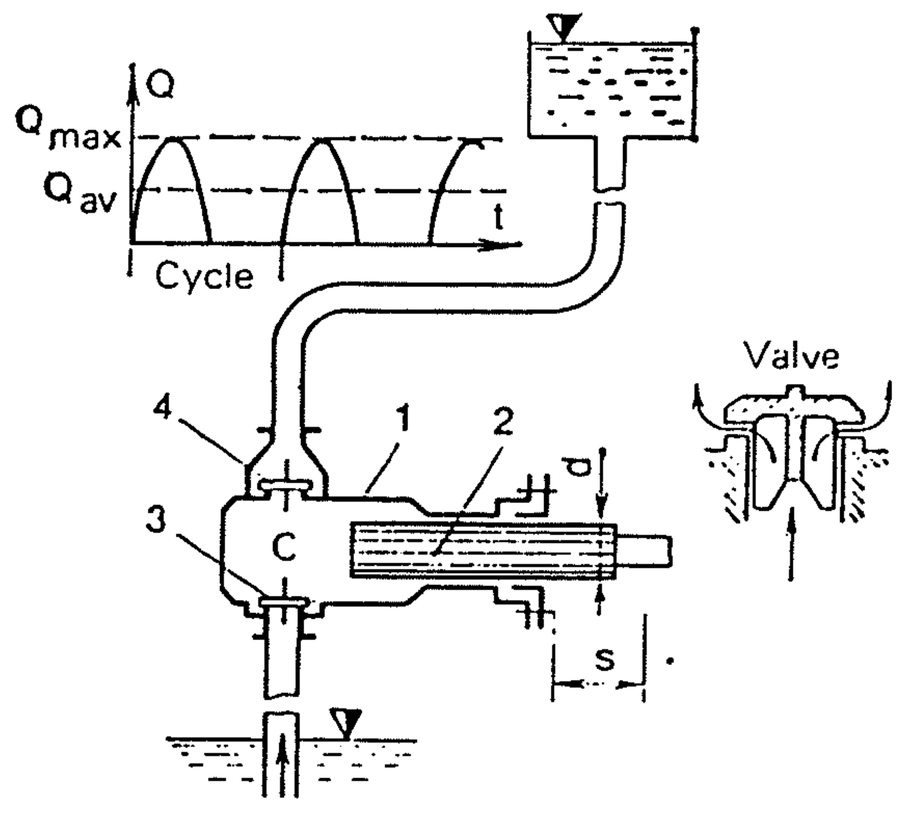


FIGURE 11.3. Plunger pump.

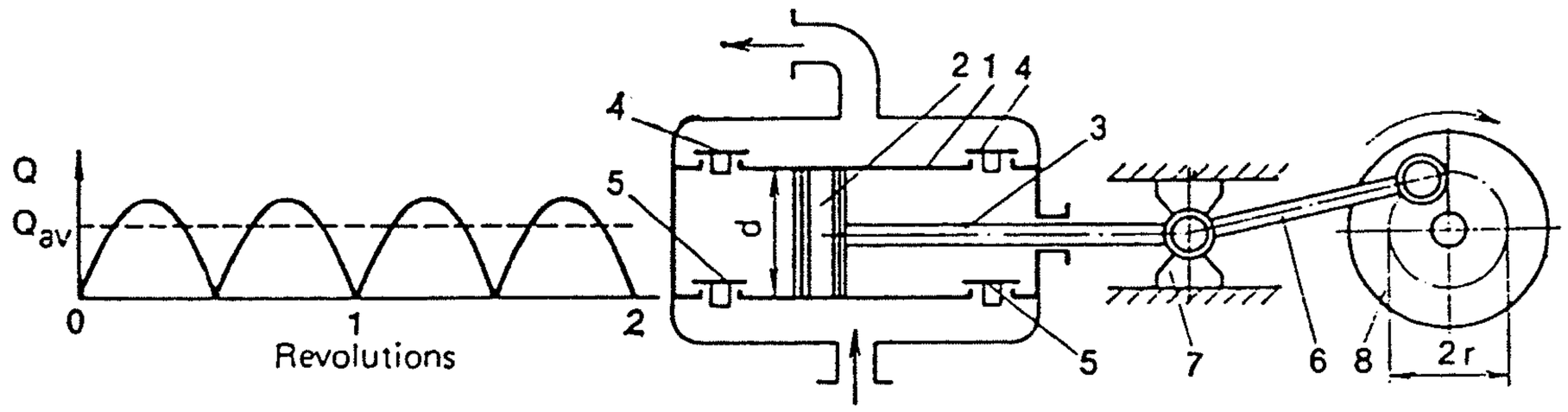


FIGURE 11.4. Double-action piston pump.

delivery valves (4) and suction valves (5). The piston is actuated by a crank mechanism, including a connecting rod (6), slide (7), and flywheel (8) with a driving pin arranged at radius r. Each revolution of the flywheel (8) makes the piston perform double stroke through $2r$.

The piston pump operates as follows. When the rod (3) and piston (2) move to the right, the LH suction valve (5) and the RH delivery valve (4) open. Water from the suction pipeline fills the LH space and it is expelled from the RH space to the delivery pipeline. During a reverse motion water is expelled from the LH space and is sucked into the RH space. Thus, two batches of water are fed to the delivery pipeline during each revolution, as illustrated in the graph. Delivery is also carried out in pulses, but the intervals between them are shorter than in the single-acting pump shown in Figure 11.3. The average delivery rate, if ignoring the area of the rod (3), is as follows:

$$Q_{av} = 2\frac{\pi d^2}{4}2r\frac{n}{60} \tag{11.12a}$$

where n is the speed of rotation (in revolutions per minute).

A diaphragm-type pump (Figure 11.5) differs in that it comprises a flexible diaphragm (1) made from rubber or rubberized fabric which is deformed through stroke s owing to reciprocations of the rod, thus changing the volume of chamber C having a suction valve (2) and a delivery valve (3).

Working members of the gear pump (Figure 11.6) are two gears (1 and 2) arranged in a housing (3) with small radial and end clearances. As illustrated in the drawing, rotation of the gears will make a liquid move from the LH pipeline (4) to the RH pipeline (5). Such pumps are widely used in lubrication systems. The so-called lobe pumps operate similarly, but instead of gears they have two or three lobe elements.

The screw pump (Figure 11.7) has three screws (a three-screw design) as its working members: a central driving screw (1) and side driven screws (2) and (3) disposed in a housing (4). The bore (section A–A) is

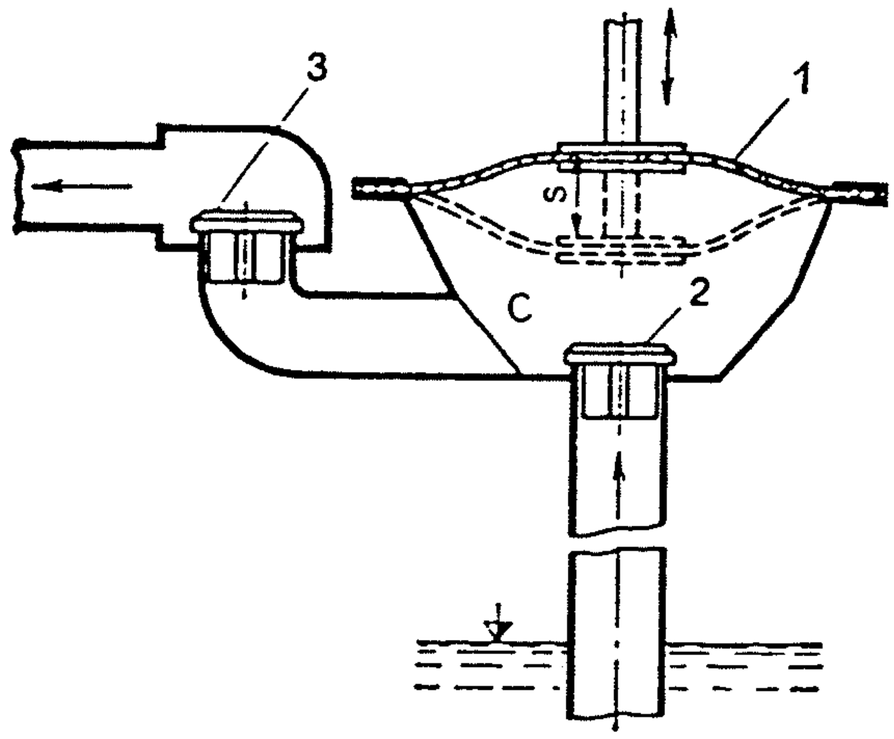


FIGURE 11.5. Diaphragm pump.

embodied so as to minimize the clearance between the housing and the external surface. The screws have a special shape thread (Detail A) that ensure continuous contact between mating surfaces. As a result, three groups of closed spaces are formed between the screw thread apices and the housing a, a, . . . ; b, b, . . . ; c, c, . . . displacing during rotation of the screws along the arrow from left to right. Liquid from the inlet pipe (IP) gets to the screws through passages in the housing, fills spaces a, b, and c, is brought to the RH part and fed to the delivery pipe (DP).

Screw pumps can create high pressure and ensure uniform delivery, but are used mainly to transfer lubricants. Such pumps are installed, for example, in OPUs (see Figure 10.1). The pumps may include two screws; these are simpler in design and may be used for the transfer of nonlubricants.

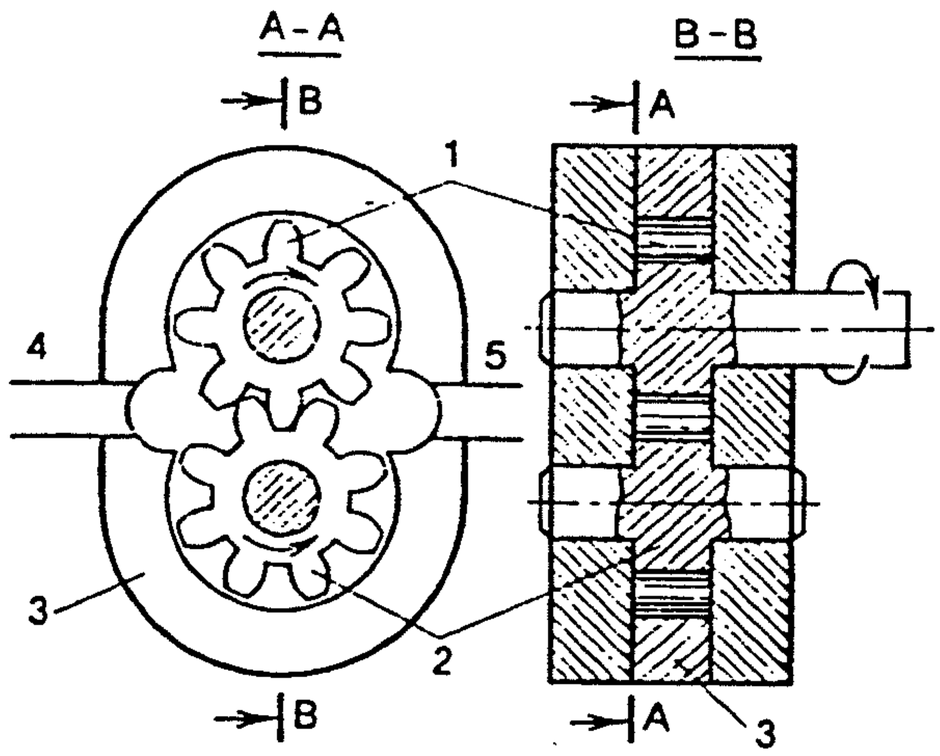


FIGURE 11.6. Gear pump.

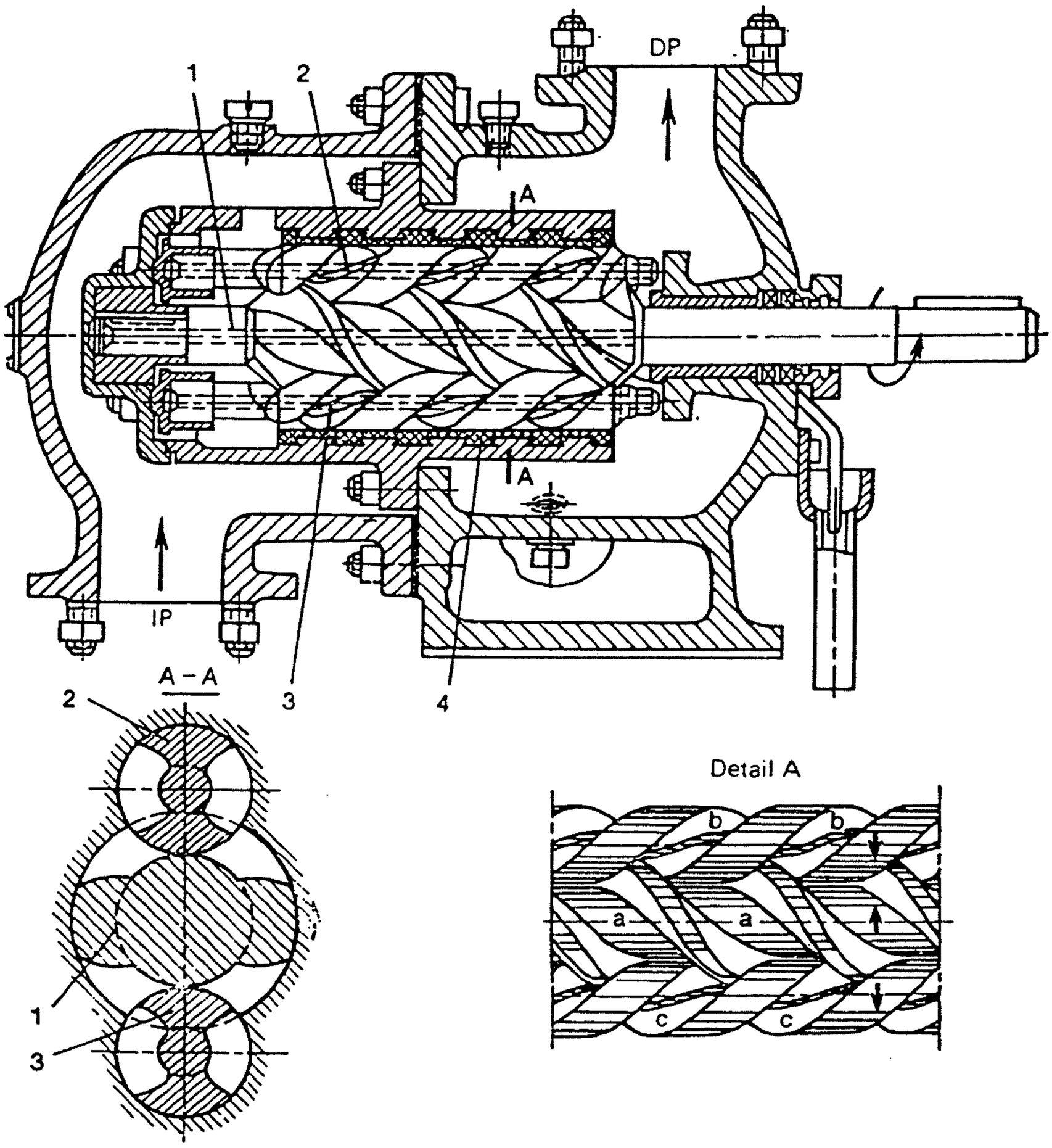


FIGURE 11.7. Screw pump.

The examples given above vividly illustrate the construction of displacement pumps. Head developed by the positive displacement pumps is theoretically unlimited. It depends on the force that might be created at the working member, and on component strength. Therefore, *never shut down the delivery pipeline valve during operation of the positive displacement pump*. The plunger and piston pumps, as mentioned above, feature nonuniform pulsating delivery which is a shortcoming. To eliminate pulsing, special air chambers are often used.

All positive displacement pumps can be divided into two groups: (1) the working element has a reciprocating movement (Figures 11.3 to 11.5) and (2) the working elements rotate—rotary pumps. The property common to all displacement pumps is that their inlet and outlet branches are disconnected by valves or by working elements.

11.3.2. Rotodynamic Pumps

In rotodynamic pumps liquid moves under the force created in the chamber which is in constant communication with the inlet and outlet pipes. The rotodynamic group includes a variety of impeller pumps that have found wide application, as well as peripheral pumps, jet pumps, etc. A discussion of their schematics follows.

The impeller pumps convert energy owing to the dynamic interaction between the liquid flow and blades of the rotating impeller, which is the working member of the pump. The impeller pumps include centrifugal, axial-flow, and mixed-flow units.

A centrifugal pump (Figure 11.8) comprises an impeller (1) with curved blades fitted to a shaft (2) and a chamber (3) accommodating the impeller. Water enters the pump through the inlet branch pipe (IP) (4) to the central part of the impeller and is ejected from the impeller to the spiral case (3) which transforms into a short diffuser (delivery pipe, DP).

The impeller rotates in direction n, the liquid is carried by the blades, and is ejected toward the periphery (thus, the pump was called centrifugal). Dynamic action of the blades upon the flow results in the pressure in the DP being higher than in the inlet (suction) pipe (IP); i.e., the pump creates a head that is obviously dependent on the impeller speed of rotation. The higher the speed, the higher the head. The pump can be driven directly from an electric motor shaft, which is very convenient.

An axial-flow pump (Figure 11.9) comprises an impeller (1) with a hub (a) mounting several blades (b) (from four to six blades). The shaft (2) rotates in bearings (3) and (4), the lower bearing resting on radially extending vanes (strainer), the so-called straightening vane assembly (5).

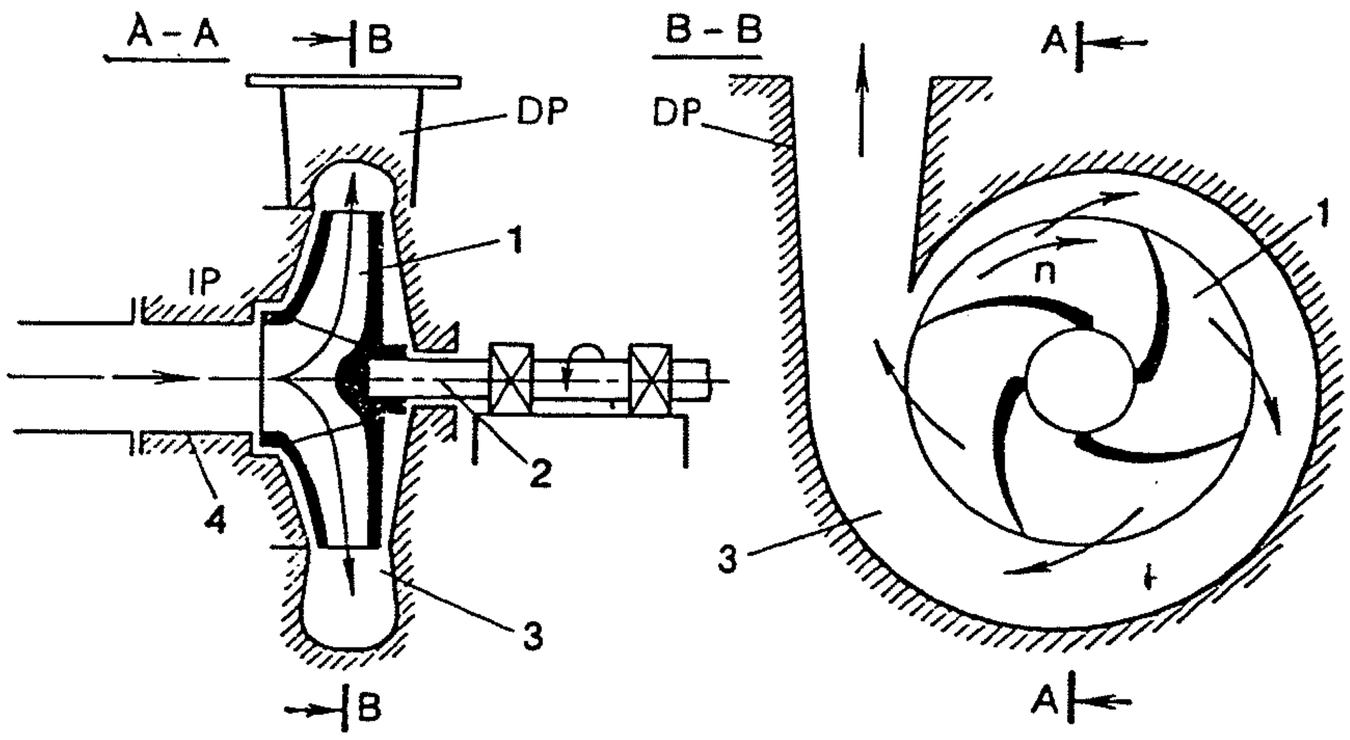


FIGURE 11.8. Centrifugal pump.

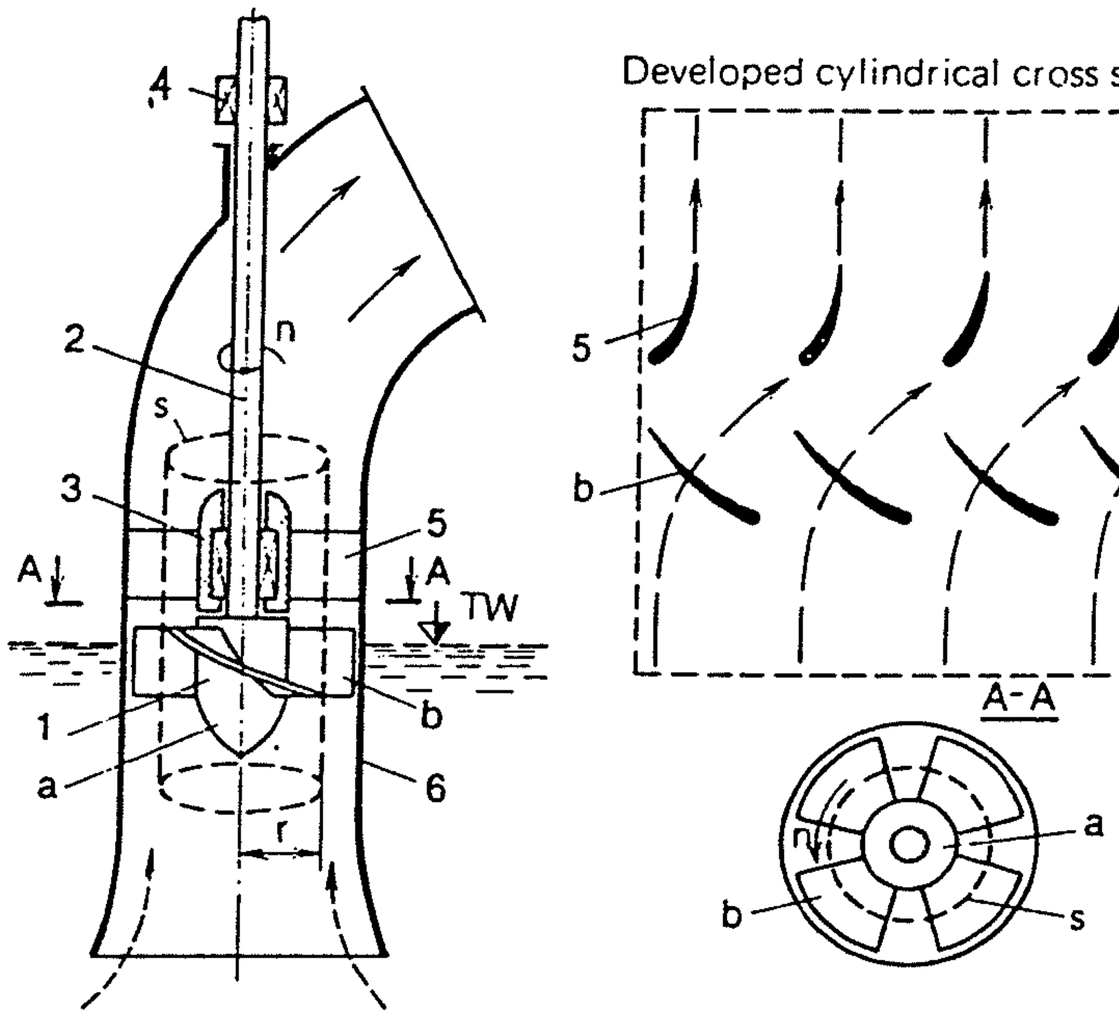


FIGURE 11.9. Axial-flow pump.

The impeller and the straightening vane assembly are arranged in a tubular casing (6) which receives and ejects water transferred by the pump.

In axial-flow pumps, the impeller blade and straightening vane shapes, like the water flow pattern, are conveniently represented as cylindrical sections. Such a section of radius r is shown in Figure 11.9. The developed view of the section is also represented in this figure. Blades (b) move in direction n. Water entrained by them reaches the blade leading edges near their center lines (dotted lines with arrows) and is ejected from the trailing edges obliquely (it moves along helical lines). On passing the straightening vanes (5) the water regains a substantially axial direction, which decreases hydraulic losses and increases the head developed by the pump.

A peripheral side channel or vortex pump (Figure 11.10) comprises an impeller (1) and a casing (2) with an annular channel having a partition (3). Short, straight blades of the impeller partially overlap the cylindrical channel. During rotation of the blades the fluid is entrained by them and is swirled by centrifugal forces as illustrated in section A–A. Thus, a twin vortex moves along the annular chamber, making the liquid adhere to the impeller and move from the inlet to the outlet.

A jet pump (Figure 11.11) differs from all pumps considered above by the absence of moving parts and its working member is liquid per se. The pump includes a pipeline (1) through which liquid under pressure is supplied, a nozzle (2), mixing chambers (3 and 4), and a diffuser (5).

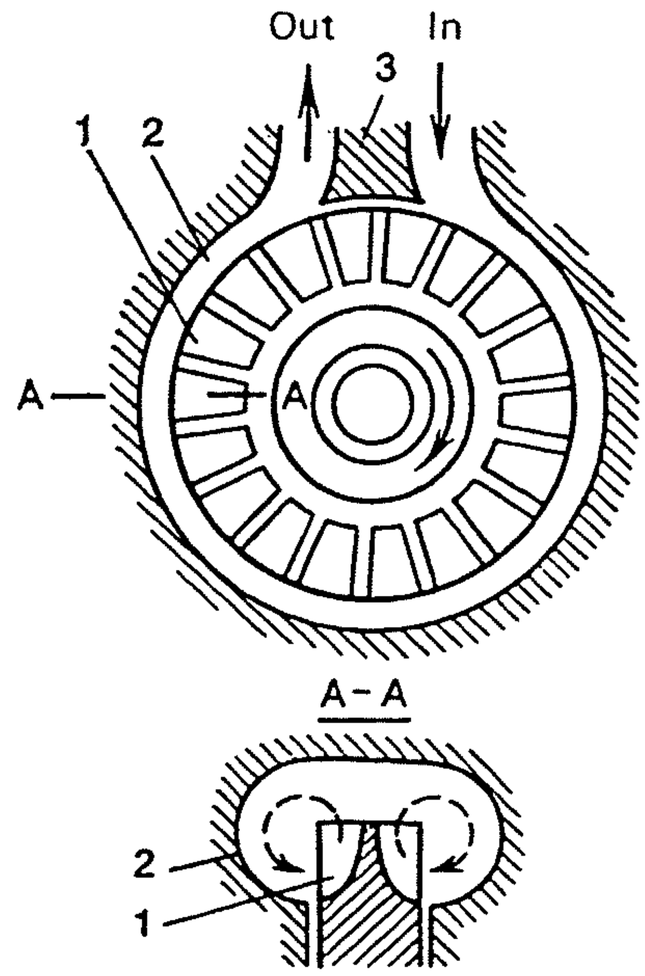


FIGURE 11.10. Peripheral or side channel pump.

Liquid is ejected from the nozzle (2) at high velocity into the mixing chamber (4) and entrains liquid sucked into it, imparting some of its energy to the latter. The discharge of liquid being transferred is marked by Q, that of head developing liquid is Q_n. The liquids may be different —Q_n is clear water, Q is contaminated water. Jet pumps may be used for pumping air through the vacuum created in chamber (3) with a water jet.

11.3.3. Classification of Pumps

The general classification of pumps regarding the operating principle, kind of action upon liquid, motion of working members, and form of working members, is shown in Figure 11.12. Centrifugal pumps include cradle-mounted, double-entry, multistage, etc. units. The mixed-flow impeller pumps differ from the axial-flow pumps in inclined axes of

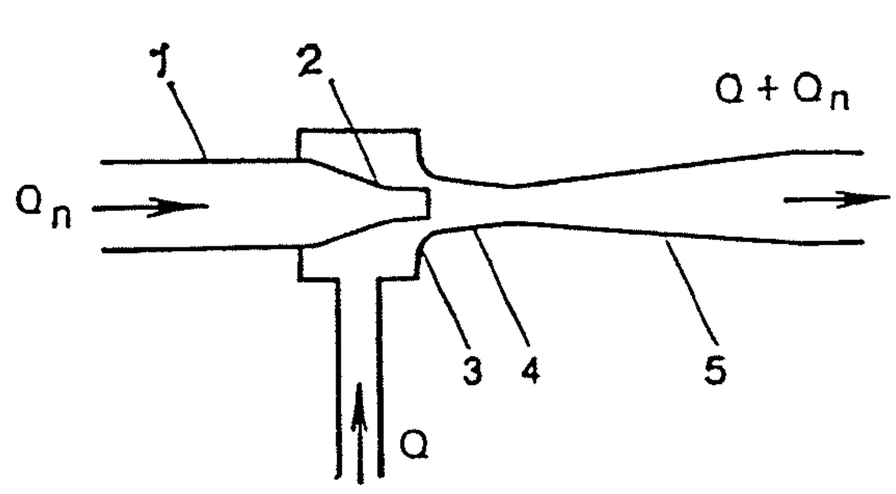


FIGURE 11.11. Jet pump (ejector).

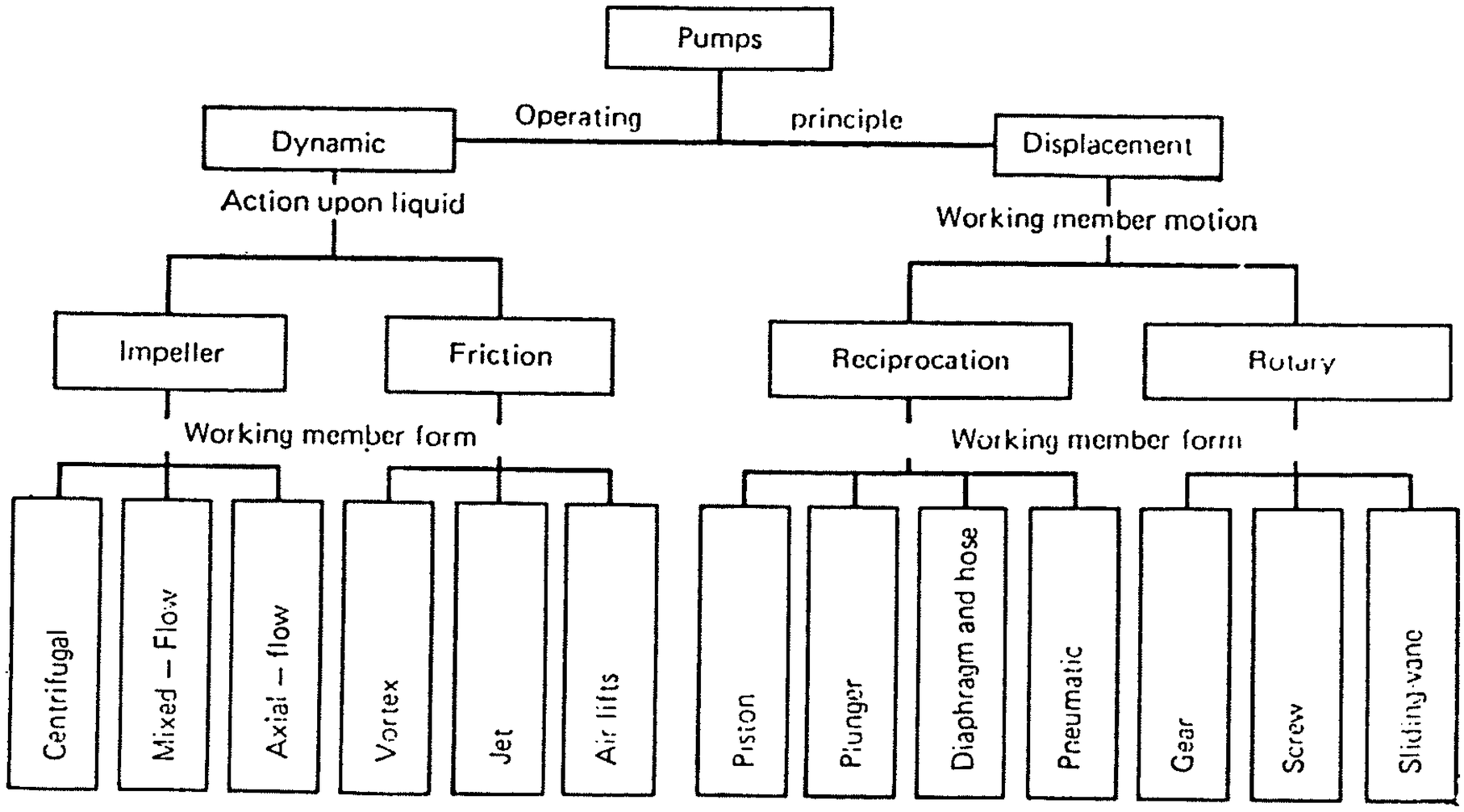


FIGURE 11.12. Classification of pumps.

impeller blade setting (Figure 13.10). The air-lift pumps raise water through a pipe by admitting compressed air (see Figure 18.19). The diaphragm and hose-type pumps employ flexible (rubber) elements that are particularly important when pumping liquids with sand, or even cement or lime solutions. In pneumatic pumps liquid is expelled from the chamber by compressed air. The working member of guided-vane pumps is a cylindrical drum with slots receiving sliding vanes, which together with the eccentric casing, form the variable-displacement chambers during rotation of the drum.

In addition, pumps may be classed according to fluid being transferred, type of drive, etc.

CHAPTER 12

Working Process of Impeller Pumps

12.1. KINEMATICS OF FLOW

The schematics of impeller pumps show that their main function, energy conversion, occurs by passing a liquid flow through the rotating blade setting of the impeller. Thus, a principal factor characterizing the work done by these pumps is a flow structure which is determined by the interaction between the liquid and the impeller blades. Also of great importance are kinematic characteristics such as magnitudes and vectors of velocities, acceleration, and trajectories of flow (flow lines).

The motion of liquid within a rotating impeller can be regarded as a sum of two motions: transportation motion (rotation) and relative motion (displacement relative to the impeller per se). By substituting **u** and **w** for vectors of the respective velocities, we obtain an absolute velocity vector

$$\mathbf{v} = \mathbf{u} + \mathbf{w} \tag{12.1}$$

Thus, flow kinematics within a pump impeller may be based on velocity parallelograms. To plot the velocity parallelogram, it is necessary to know the shape and dimensions of the impeller and its separate parts within the flow part (geometry of the impeller flow part); the pump operating conditions also should be given. Let us consider some principal variants.

Centrifugal pumps (see Figure 11.8): The liquid motion in the impeller is nearly planar. All the dimensions defining the flow part of the

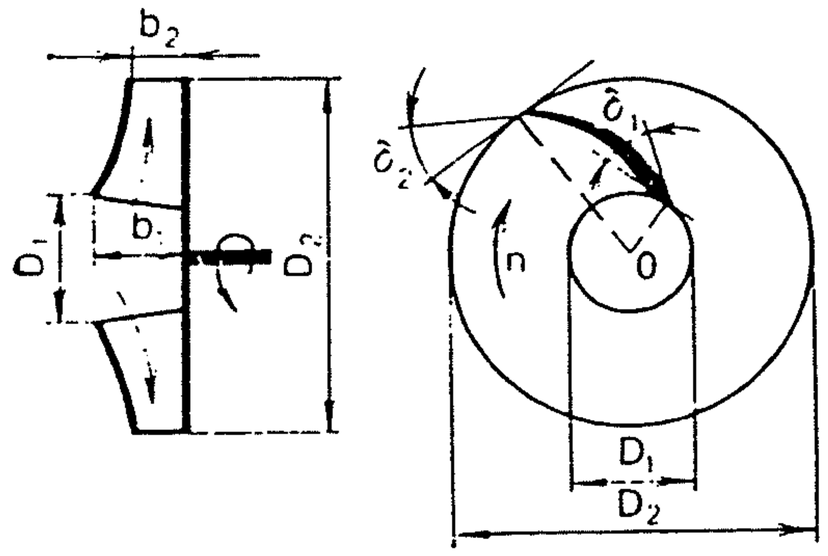


FIGURE 12.1. Geometry of centrifugal pump impeller.

impeller are known; the values relating to the leading edge of the blades have index 1, to trailing edges, index 2 (Figure 12.1).

The direction of the impeller blade setting is determined by angle δ between a tangent to the blade traced downstream of the fluid and a straight line perpendicular to the radius. The impeller blade width is determined by values b_1 and b_2.

The pump operating conditions are set by two characteristics: delivery Q and impeller speed of rotation n (in revolutions per minute).

The direction of velocity at inlet to the impeller depends on the conditions of inlet. In pumps with axial inlet at the entry to the impeller, it may be assumed that absolute velocity $\mathbf{v}_1$ is directed along the radius, i.e., $\alpha_1 = 90°$ (Figure 12.2).

Now, average velocity[1] is

$$v_1 = \frac{Q}{\pi D_1 b_1 \psi_1} \tag{12.2}$$

where coefficient $\psi_1 < 1$ allows for constriction caused by the blade. Leading edge peripheral velocity u_1 depends on D_1 and n

$$u_1 = \pi D_1 n/60 \tag{12.3}$$

Having two vectors $\mathbf{v}_1$ and $\mathbf{u}_1$, we can plot the inlet velocity parallelogram and find $\mathbf{w}_1$ (Figure 12.2). Use is frequently made of a velocity triangle also shown in Figure 12.2.

---

[1] The following symbols are used here: vectors **v**, **u**, **w** and their respective moduli, v, u, w.

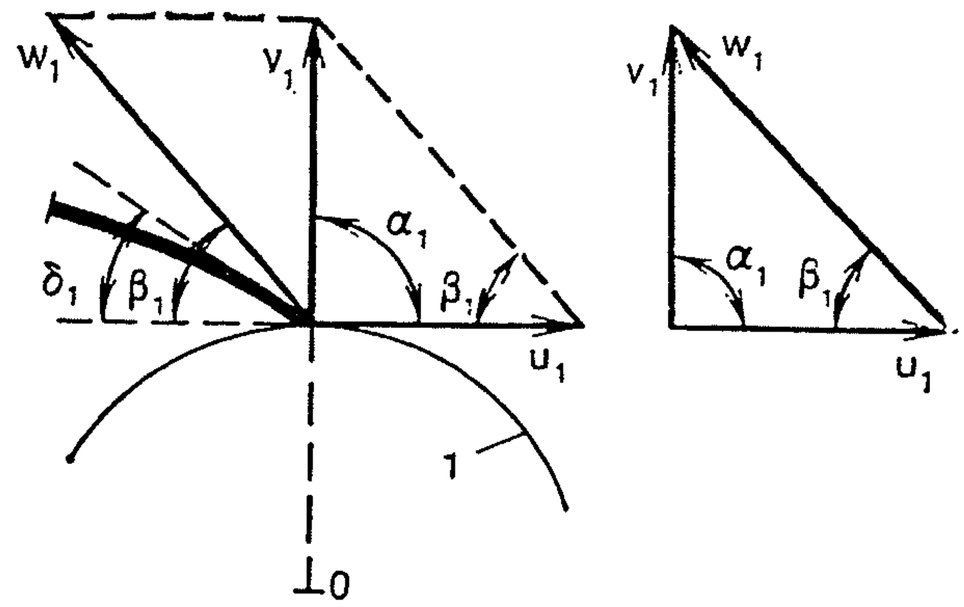


FIGURE 12.2. Velocity parallelograms and triangles for leading edge of centrifugal pump impeller.

Transportation velocity u_2 in the outlet section of the impeller (see Figure 12.3) is found from the formula

$$u_2 = \pi D_2 n/60 \tag{12.3a}$$

Relative velocity w_2 can be found, provided its direction is known. In this case, as seen from Figures 12.1 and 12.3

$$w_2 = \frac{Q}{\pi D_2 b_2 \psi_2 \sin \beta_2} \tag{12.4}$$

In the first approximation, assume $\beta_2 = \delta_2$, i.e., the direction of w_2 is aligned with the direction of the blade trailing edge. (In fact, there is some angle deviation $\Delta\beta_2$ which is taken into account in designing.) Knowing two vectors $\mathbf{u}_2$ and $\mathbf{w}_2$, we can plot a parallelogram or triangle of outlet velocities and find vector $\mathbf{v}_2$ and angle α_2.

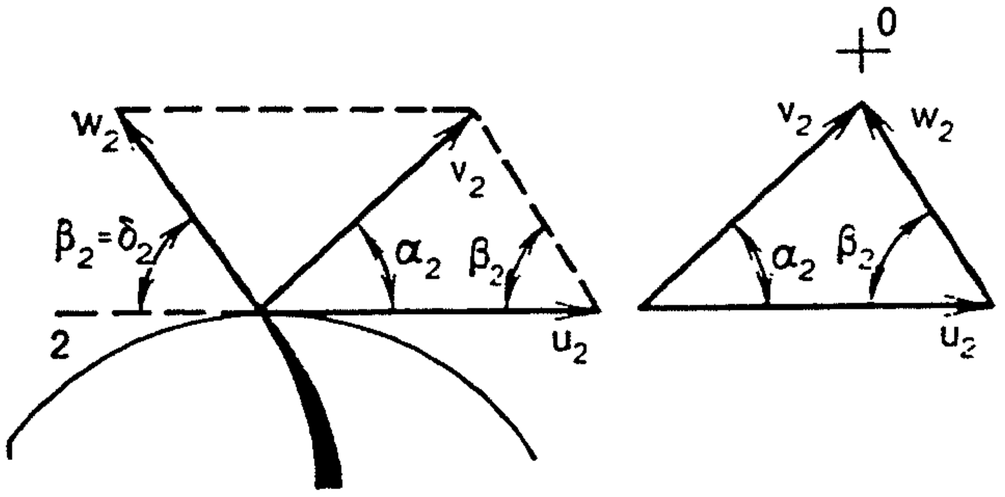


FIGURE 12.3. Velocity parallelograms and triangles for trailing edge of centrifugal pump impeller.

Knowing the impeller dimensions and blade shape for given operating conditions Q and n, we can determine velocity triangles for intermediate sections, thereby finding vectors **v**, and trace the liquid absolute motion trajectory by reference to the latter. The form of the absolute motion trajectories is shown in Figure 12.4. As seen in the figure, the pump impeller swirls the liquid flow passing through it. Flow swirl is characterized by circulation Γ (Equation 5.2) which may be represented as

$$\Gamma = \pi D v \cos \alpha \tag{12.5}$$

Taking into account the form of the velocity triangles in Figures 12.2 and 12.3, $\Gamma_1 = 0$ and $\Gamma_2 > 0$. Thus, circulation of the liquid increases as it flows through the impeller.

Axial-flow pumps (see Figure 11.9) differ in that the liquid moves substantially axially within the impeller. Flow kinematics are analyzed, as shown in Figure 11.9, for separate cylindrical sections of radius r.

When plotting axial-flow pump velocity parallelograms or triangles bear in mind:

1. Peripheral velocities of all points of the impeller blades at a given cylindrical section are equal and determined by speed of rotation n and section radius r

$$u_1 = u_2 = u = 2\pi rn/60 \tag{12.6}$$

2. Axial components of vectors of absolute and relative velocities of flow should be equal at all the points of a given cylindrical section

$$v_1 \sin \alpha_1 = w_1 \sin \beta_1 = v_2 \sin \alpha_2 = w_2 \sin \beta_2$$

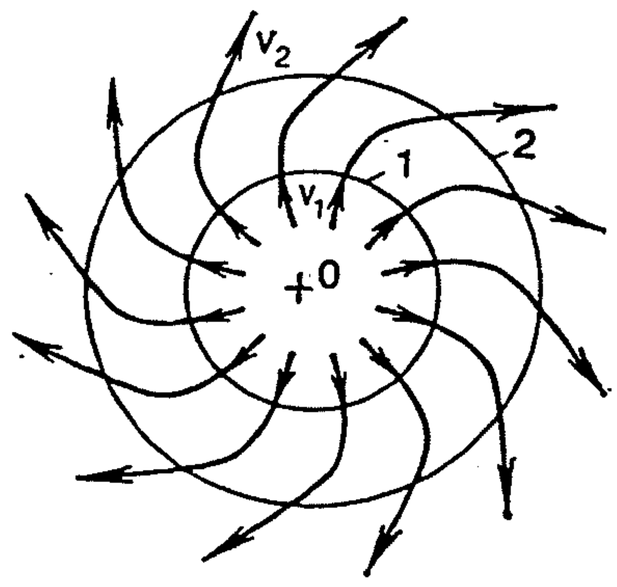


FIGURE 12.4. Trajectory of liquid absolute motion in centrifugal pump impeller.

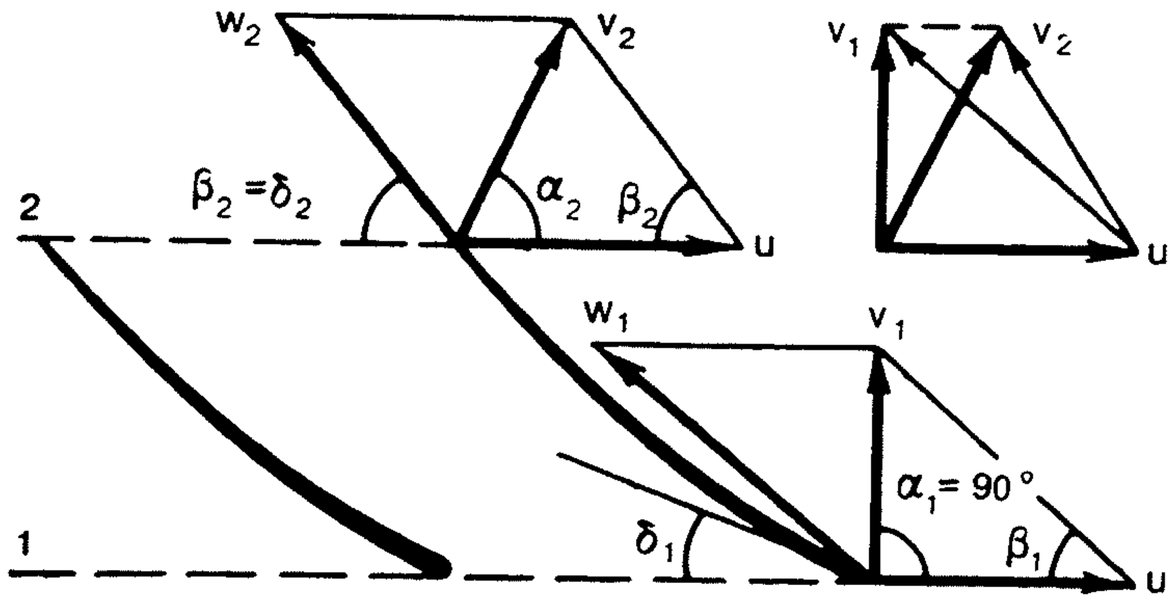


FIGURE 12.5. Velocity parallelograms and triangles for axial-flow pump impeller.

If we assume that the distribution of axial components of velocities over the section is uniform, then

$$v_i \sin \alpha_i = w_i \sin \beta_i = \frac{4Q}{\pi(D^2 - d_h^2)\psi} \tag{12.7}$$

where D is the impeller diameter, d_h is the hub diameter, and ψ is the blade constriction coefficient, $\psi < 1$.

Plotting parallelograms and triangles of velocities in an axial-flow pump impeller is shown in Figure 12.5. Velocity u at the leading edge (1) is found from Equation 12.6. Assuming the inlet flow is not swirled, $\Gamma_1 = 0$ and $\alpha_1 = 90°$; from Equation 12.7 we obtain

$$v_1 = \frac{4Q}{\pi(D_1^2 - d_h^2)\psi} \tag{12.8}$$

Using u and v_1, plot the parallelogram and find w_1 and β_1. Assuming $\beta_2 = \delta_2$, determine w_2 from Equation 12.7 for the trailing edge (2) and plot the parallelogram against u and w_2.

Knowing the impeller geometry and values of n and Q, we can plot a trajectory of water absolute motion for each of the cylindrical sections shown in Figure 11.9.

12.2. MAIN ENERGY EQUATION

We have just considered the relations that characterize the kinematics of flow in the impeller. A discussion of dynamic and energy characteristics follows.

To find the power interaction between impeller blades and flowing liquid, use the law of angular momentum in the form of Equation 5.14 for a volume of liquid defined by the impeller rims, and reference surfaces (1) and (2) lying on the leading and trailing edges of the blades (Figure 12.6). In Equation 5.14 Q is the pump delivery and ρ is the density of liquid being transferred; by taking averaged values of velocities, we obtain

$$v_{1u}r_1 = 0.5D_1v_1 \cos \alpha_1$$

$$v_{2u}r_2 = 0.5D_2v_2 \cos \alpha_2$$

moments of external forces relative to axis 0–0 acting upon the defined volume of liquid are a sum of the moment M imparted by the pump blades and the friction moment which we neglect. Pressure forces normal to the defining surfaces develop no moment relative to axis 0–0, as they are either directed to the center (surfaces (1) and (2) or lie in the meridional plane (rim surfaces). Thus, the sum of the moments of external forces acting upon the defined volume of liquid is confined to torque M imparted to the liquid by the impeller blades

$$M = \rho Q(0.5D_2v_2 \cos \alpha_2 - 0.5D_1v_1 \cos \alpha_1) \qquad (12.9)$$

Using Equation 12.5 for liquid circulation, we have at the impeller inlet $\Gamma_1 = \pi D_1v_1 \cos \alpha_1$ and at the impeller outlet $\Gamma_2 = \pi D_2v_2 \cos \alpha_2$; now Equation 12.9 may be written as

$$M = \frac{\rho Q}{2\pi}(\Gamma_2 - \Gamma_1) \qquad (12.9a)$$

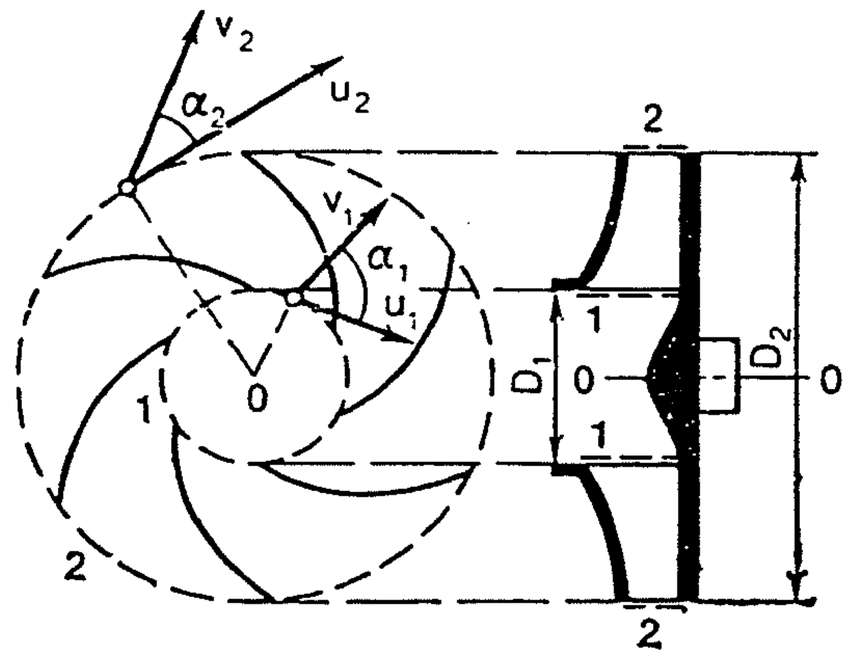


FIGURE 12.6. Deriving the basic equation of the impeller pump.

The result shows that the moment developed by the impeller is proportional to mass discharge and to variation in liquid circulation or its velocity moment.

Knowing the moment M (measured in newton meters), developed by the impeller, and angular velocity ω, 1/s ($\omega = 2\pi n/60$), we find energy per second, i.e., power developed by the impeller acting upon the liquid, which is determined by the product $[M\omega] = \text{Nm/s} = \text{J/s} = \text{W}$. If we assume that the energy imparted by the impeller to the mass corresponding to force of 1 N of the liquid flowing through it is equal to H_T, then power received by the liquid according to Equation 11.9 is $\rho g Q H_T$ (measured in watts). By equating both powers, and using Equation 12.9, we obtain

$$M\omega = \omega\rho Q(0.5D_2 v_2 \cos \alpha_2 - 0.5D_1 v_1 \cos \alpha_1) = \rho g Q H_T$$

Because $0.5D\omega = u$ is the peripheral, i.e., transportation velocity, we derive the expression for theoretical head of the pump H_T

$$H_T = \frac{1}{g}(u_2 v_2 \cos \alpha_2 - u_1 v_1 \cos \alpha_1) \tag{12.10}$$

or according to Equation 12.9a:

$$H_T = \frac{\omega}{g2\pi}(\Gamma_2 - \Gamma_1) \tag{12.10a}$$

These formula's, being the main equation of pumps or the Euler equation, are applicable to impeller pumps of any type. They are of great practical importance for establishing relationships between theoretical head and kinematic characteristics of liquid flow through the impeller.

Using the Bernoulli equation for relative motion (Equation 5.21) it is possible to arrive at a different formula for impeller pump theoretical head. Adding and subtracting in the left hand (LH) part of the equation $v_1^2/2g$ and in the right hand (RH) part $v_2^2/2g$ we have

$$\frac{p_1}{\rho g} + z_1 + \frac{v_1^2}{2g} - \frac{v_1^2}{2g} + \frac{w_1^2}{2g} - \frac{u_1^2}{2g}$$

$$= \frac{p_2}{\rho g} + z_2 + \frac{v_2^2}{2g} - \frac{v_2^2}{2g} + \frac{w_2^2}{2g} - \frac{u_2^2}{2g} + h_{loss}$$

In accordance with Equation 1.4, assuming $\alpha = 1$

$$\frac{p_1}{\rho g} + z_1 + \frac{v_1^2}{2g} = e_1 \qquad \frac{p_2}{\rho g} + z_2 + \frac{v_2^2}{2g} = e_2$$

Taking into account that $H = e_2 - e_1$ and assuming for this case $h_{loss} = 0$ we have

$$H_T = \frac{v_2^2 - v_1^2}{2g} + \frac{u_2^2 - u_1^2}{2g} + \frac{w_1^2 - w_2^2}{2g} \qquad (12.10b)$$

Equations 12.10 make it possible to reach several important conclusions:

1. It was mentioned above that angle α_1 is usually near 90°, i.e., $\Gamma_2 = 0$, or its value is very small. Therefore, the impeller theoretical head for given ω (measured per second) or n (measured in revolutions per minute) determined by exit circulation Γ_2.
2. Deviation of α_1 from 90° or existence of flow rotation at the impeller entrance affects the theoretical impeller head. It demands an appropriate design of pump delivery constructions (sumps).
3. In axial pumps $u_2 = u_1$ (see Equation 12.6). Thus, according to Equation 12.10b only v and w define the developed head. However, they cannot be too large due to hydraulic losses. The result is that axial pumps are effective only for small heads up to 15 to 25 m.
4. Equation 12.10b shows that the best way to increase the impeller head is to increase the value of $u_2^2 - u_1^2$. From Equations 12.3 and 12.3a it follows that for given n it can be achieved by increasing the ratio D_2/D_1. This is a characteristic dimension of the centrifugal pump (Figure 12.1).

Actual head H developed by the pump will be less than the theoretical head because of hydraulic losses in the impeller and casing. If pump hydraulic losses are h_p, then $H = H_T - h_p$. By introducing the notion of hydraulic efficiency

$$\eta_h = \frac{H}{H_T} \qquad (12.11)$$

we obtain

$$H = H_T \eta_h \qquad (12.12)$$

Equation 12.12 used with the Euler equations (12.10) makes it possible to find the equation for actual head of the pump

$$\frac{H}{\eta_h} = \frac{1}{g}(u_2 v_2 \cos \alpha_2 - u_1 v_1 \cos \alpha_1) \tag{12.13}$$

or

$$\frac{H}{\eta_h} = \frac{\omega}{g 2\pi}(\Gamma_2 - \Gamma_1) \tag{12.13a}$$

The hydraulic efficiency of pumps is $\eta_h = 0.75$ to 0.93 (lower values correspond to smaller pumps).

12.3. PUMP OPERATION AND OPERATION SIMILARITY CONDITIONS

Pump operation conditions can be set by two parameters: delivery (discharge) Q and rotational speed n. Figure 12.7 illustrates variations in the velocity parallelograms in relation to delivery Q with n being constant; *a*, for a centrifugal pump, and *b*, for an axial-flow pump, for leading (1) and trailing (2) edges of the impeller. With n being constant, the most common condition for pumps operation, vector **u** retains its value. Delivery is characterized by vectors $\mathbf{v}_1$, which, as seen from Equations 12.2 and 12.8, are proportional to Q; index «′» corresponds to low Q, index «‴» to high Q.

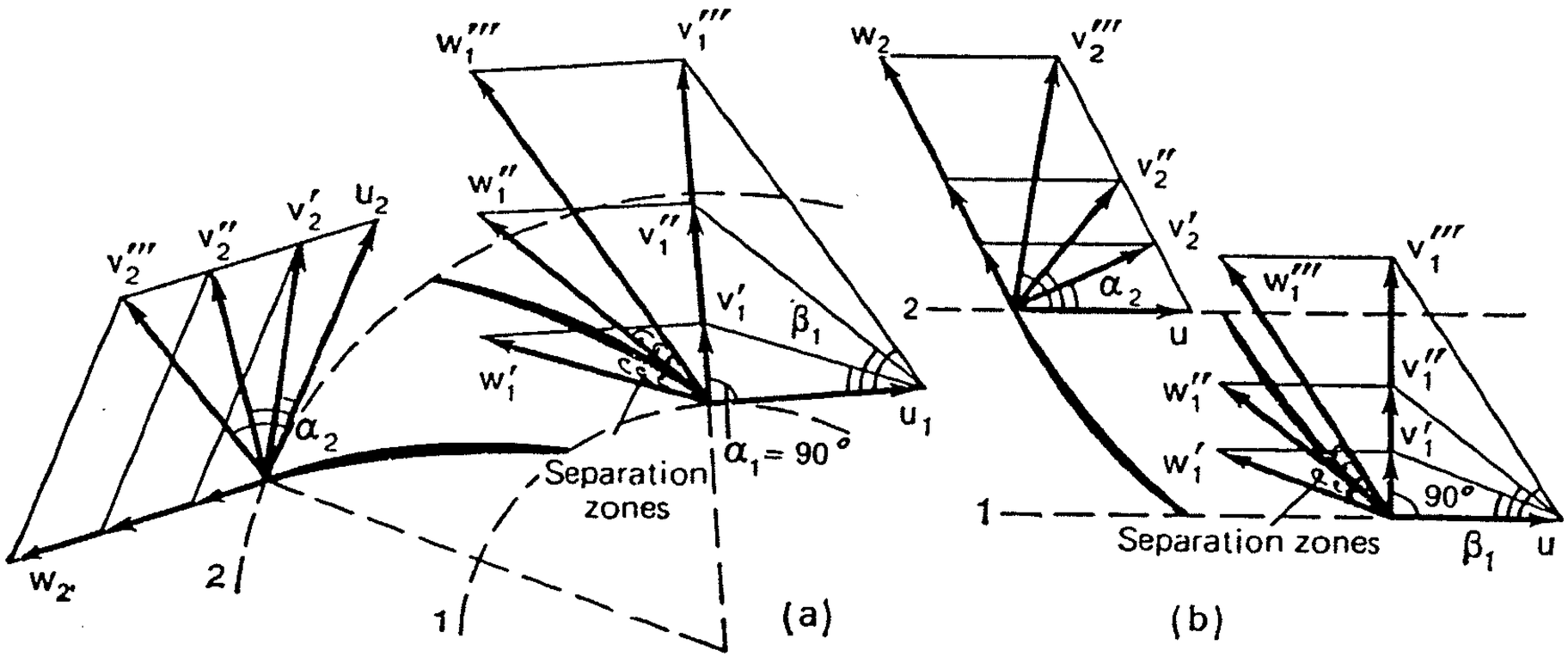


FIGURE 12.7. Pump operation vs delivery rate at constant speed of rotation.

Variation of Q at the inlet to the impeller causes a variation of vector $\mathbf{w}_1$ and its direction β_1. As Q increases, angle β_1 increases as well. When angle β_1 is small (conditions «′») and when it is large (conditions «‴»), the water enters at a certain angle to the blade leading edge, which causes local separation of flow (creation of a vorticity zone) and increases hydraulic losses. At low discharges the separation zone is arranged on the back of the blade, at high discharges on the working side. Losses at inlet will be minimal if $\beta_1 \approx \delta_1$; i.e., if angle β_1 approaches the blade leading edge angle (Figure 12.1) which approximately corresponds to $\mathbf{v}''$. The conditions where in $\beta_1 = \delta_1$ and losses at inlet to the impeller are minimal are called shockless entry conditions.

At the exit from the impeller as the discharge decreases, angle α_2 of vector $\mathbf{v}_2$ also decreases. As seen from the velocity parallelograms, this leads to an increase in peripheral velocity $\mathbf{v}_2 \cos \alpha_2$ and in outlet circulation Γ_2; hence, this influences the losses and head of the pump.

The analysis performed shows that the impeller pump operating modes (regimes) are determined primarily by the angles of the velocity parallelograms, i.e., values of α and β. If angles α and β remain unchanged, the operating conditions are regarded as kinematically similar. Such conditions are sometimes called isogonal. This definition makes it possible to represent the pump operation similarity conditions mathematically in the form of two ratios:

1. The ratio between the velocities at respective points i should be constant

$$\frac{v_{i1}}{v_{i2}} = \frac{u_{i1}}{u_{i2}} = \frac{w_{i1}}{w_{i2}} = \text{const} \tag{12.14}$$

2. Respective angles of the velocity parallelograms should be equal

$$\alpha_{i1} = \alpha_{i2} \qquad \beta_{i1} = \beta_{i2} \tag{12.15}$$

Hence, the kinematic conditions for pump operation similarity can be derived. As we have already pointed out, the pump operating conditions can be set in the form of values of delivery Q and rotational speed n. Using Equations 12.2 and 12.3, we obtain

$$\frac{v_{11}}{v_{12}} = \frac{Q_1}{\pi D_1 b_1 \psi_1} \frac{\pi D_1 b_1 \psi_1}{Q_2} = \frac{Q_1}{Q_2}$$

$$\frac{u_{11}}{u_{12}} = \frac{\pi D_1 n_1}{60} \frac{60}{\pi D_1 n_2} = \frac{n_1}{n_2}$$

Taking into account Equation 12.14, we conclude:

$$\frac{v_{11}}{v_{12}} = \frac{u_{11}}{u_{12}} \qquad \frac{Q_1}{Q_2} = \frac{n_1}{n_2}$$

which gives the final condition for the kinematic similarity of operations for a given pump

$$Q/n = \text{const} \tag{12.16}$$

The impeller pump type is determined by the form (geometry) of its flow part, primarily of its impeller. The pumps with geometrically similar flow parts belong to one type characterized by the following relations (Figure 12.1):

1. The relation between appropriate dimensions should be constant

$$\frac{D_{i1}}{D_{i2}} = \frac{b_{i1}}{b_{i2}} = \cdots = \text{const} \tag{12.17}$$

2. All respective angles should be equal

$$\delta_{i1} = \delta_{i2} \tag{12.18}$$

Assume two pumps have geometrically similar flow parts (i.e., of the same type), but with different values of D_1 and D_2 (we assume here the respective diameters, say, impeller exit diameter) with delivery rates of Q_1 and Q_2 and speeds of rotation n_1 and n_2. Using Equations 12.2 and 12.3 for these, we obtain

$$\frac{v_{11}}{v_{12}} = \frac{Q_1}{\pi D_1 b_1} \frac{\pi D_2 b_2}{Q_2} = \frac{Q_1}{Q_2}\left(\frac{D_2}{D_1}\right)^2$$

$$\frac{u_{11}}{u_{12}} = \frac{\pi D_1 n_1}{60} \frac{60}{\pi D_2 n_2} = \frac{D_1 n_1}{D_2 n_2}$$

According to Equation 12.7, if the operating conditions are similar, both relations should be equal

$$\frac{Q_1}{Q_2}\left(\frac{D_2}{D_1}\right)^2 = \frac{D_1 n_1}{D_2 n_2} \qquad \frac{Q_1}{n_2 D_1^3} = \frac{Q_2}{n_2 D_2^3}$$

As a result, we get the general formula of kinematic similarity of pumps operating mode (regime)

$$\frac{Q}{nD^3} = \text{const} \tag{12.19}$$

If the geometry of the pump flow part is changeable, as is the case with axial-flow pumps, wherein the impeller blade angle can be altered, Equation 12.19 is true only for equal angles.

The similarity kinematic conditions Equation 12.14 do not include vital characteristics such as head. To allow for it, consider some energy relations.

Euler's equation for some operating conditions of the pump determined by characteristics n_1, Q_1, and D_1 may be written, using Equation 12.13, as:

$$H_1 = \frac{1}{g}(u_{21}v_{21}\cos\alpha_{21} - u_{11}v_{11}\cos\alpha_{11})\eta_{h1} \tag{12.20}$$

Let the characteristics change for n_2, Q_2, and D_2 (the same type of pump), but preserve operation similarity. For new values of the characteristics Euler's equation takes the form

$$H_2 = \frac{1}{g}(u_{22}v_{22}\cos\alpha_{22} - u_{21}v_{21}\cos\alpha_{21})\eta_{h2} \tag{12.21}$$

Because the operating conditions are similar, conditions 12.14 and 12.15 should be met

$$\alpha_{22} = \alpha_{21} \qquad \alpha_{12} = \alpha_{11}$$

$$\frac{u_{22}}{u_{21}} = \frac{v_{22}}{v_{21}} = \frac{u_{12}}{u_{11}} = \frac{v_{12}}{v_{11}} = \frac{n_2 D_2}{n_1 D_1} \tag{12.22}$$

Using Equation 12.22, we may rewrite Equation 12.21 as follows:

$$H_2 = \frac{1}{g}\left(\frac{n_2 D_2}{n_1 D_1}\right)^2 (u_{21}v_{21}\cos\alpha_{21} - u_{11}v_{11}\cos\alpha_{11})\eta_{h2} \tag{12.23}$$

Relating Equation 12.20 to 12.23 and assuming that hydraulic efficiency is preserved under such conditions, i.e., $\eta_{h2} = \eta_{h1}$, we obtain

$$\frac{H_1}{H_2} = \left(\frac{n_1 D_1}{n_2 D_2}\right)^2 \tag{12.24}$$

The relationship between heads, rotational speeds, and impeller diameters (Equation 12.24) in view of kinematic similarity (Equation 12.19) makes it possible to derive the general similarity formulas of pump operation

$$\frac{H_1}{H_2} = \left(\frac{n_1}{n_2}\right)^2 \left(\frac{D_1}{D_2}\right)^2 \tag{12.25}$$

$$\frac{Q_1}{Q_2} = \left(\frac{n_1}{n_2}\right) \left(\frac{D_1}{D_2}\right)^3 \tag{12.26}$$

Furthermore, using Equation 11.11 and assuming $\eta_1 = \eta_2$, we obtain

$$\frac{N_1}{N_2} = \left(\frac{n_1}{n_2}\right)^3 \left(\frac{D_1}{D_2}\right)^5 \tag{12.27}$$

The similarity formulas (Equations 12.25 and 12.26) are of great practical importance as they allow conversion of the parameters that determine pump operation, their characteristics for various rotational speeds n, as well as uncovering model pump characteristics for full-scale conditions, which is particularly vital for large pumps.

Example 12.1

The pump that is at disposal has high efficiency regime parameters $H = 15$ m, $Q = 20$ L/s with electric motor 4 kW, 1450 rpm. It is necessary to obtain higher head and discharge H and Q. What can be gained if we use an electric motor, $n = 2900$ rpm?

Solution

The solution is based on similarity lows. As pump is the same, $D_2 = D_1$; and Equation 12.25 gives

$$H_2 = H_1 \left(\frac{n_2}{n_1}\right)^2 = 15 \left(\frac{2900}{1450}\right)^2 = 60 \text{ m}$$

Equation 12.26 gives

$$Q_2 = Q_1\left(\frac{n_2}{n_1}\right) = 20\left(\frac{2900}{1450}\right) = 40 \text{ L/s}$$

According to Equation 12.27, the power of the new motor, therefore, is

$$N_2 = N_1\left(\frac{n_2}{n_1}\right)^3 = 4\left(\frac{2900}{1450}\right)^3 = 32 \text{ kW}$$

The head and the power will increase sufficiently. The efficiency will be preserved.

12.4. SPECIFIC SPEED

As has been noted, pumps of the given type (geometrically similar pumps) can be of different sizes and operate within a wide range of rotational speeds, delivery rates, heads, and capacities. Therefore, the characterization of pump type requires criteria reduced to uniform, standard conditions. One such criterion, widely used for impeller pumps, is the specific speed. Specific speed n_s of a given pump is the speed of rotation of a geometrically similar pump of such a size that it ensures a delivery of 75 L/s at head $H = 1$ m (the origin of this value is the capacity 1 hp).

Let D, H, n, and Q be known for a given pump. The decisive factor here is the delivery corresponding to optimal operation at maximum efficiency. Determine the pump specific speed which according to the above definition corresponds to the following characteristics: n_s, D_s (impeller diameter), $H = 1$ m, $Q = 75$ L/s $= 0.075$ m^3/s. From Equation 12.25, we obtain the first equation:

$$\frac{H}{1} = \left(\frac{n}{n_s}\right)^2\left(\frac{D_1}{D_s}\right)^2$$

and from Equation 12.26, the second equation:

$$\frac{Q}{0.075} = \frac{n}{n_s}\left(\frac{D}{D_s}\right)^3$$

To eliminate D_s, raise the first equation to the 3/2 power:

$$\frac{H^{3/2}}{1} = \left(\frac{n}{n_s}\right)^3 \left(\frac{D}{D_s}\right)^3$$

Dividing the second equation by the one above, we obtain

$$\frac{Q}{0.075H^{3/2}} = \left(\frac{n_s}{n}\right)^2$$

Determine specific speed n_s, bearing in mind that $1/\sqrt{0.075} = 3.65$:

$$n_s = 3.65\frac{n\sqrt{Q}}{H^{3/4}} \tag{12.28}$$

Pump designers often use another specific speed form, usually marked by n_{s1}, and determined from the formula

$$n_{s1} = \frac{n\sqrt{Q}}{H^{3/4}} \tag{12.28a}$$

Obviously n_{s1} differs from n_s only in that the pump characteristics are reduced to conditions of $H = 1$ m and delivery of $Q = 1\ \text{m}^3/\text{s}$. Accordingly, values of n_{s1} are 3.65 times smaller than those of n_s. In Equations 12.28 and 12.28a Q is in cubic meters per second, H is in meters, and n is in revolutions per minute.

Because the specific speed determined from the above formulas is a dimensional parameter, its absolute value depends on units of measure. For instance, if head is given in feet and delivery in gal/min (U.S.), the relation takes the following form:

$$\frac{\text{rpm}\sqrt{\text{gal/min}}}{(\text{ft})^{3/4}} = 51.64\frac{\text{rpm}\sqrt{\text{m}^3/\text{s}}}{\text{m}^{3/4}}$$

Specific speed may have a dimensionless form, n_{s0}. If the reference values are $Q_s = 1\ \text{m}^3/\text{s}$, and specific energy e_m (according to Equation 1.4) is joules per kilogram (mass), and speed of rotation (1/s)

$$n_{s0} = \frac{n\sqrt{Q}}{(gH)^{3/4}} \tag{12.28b}$$

It is clear that straight proportion exists between n_{s0} and n_{s1}

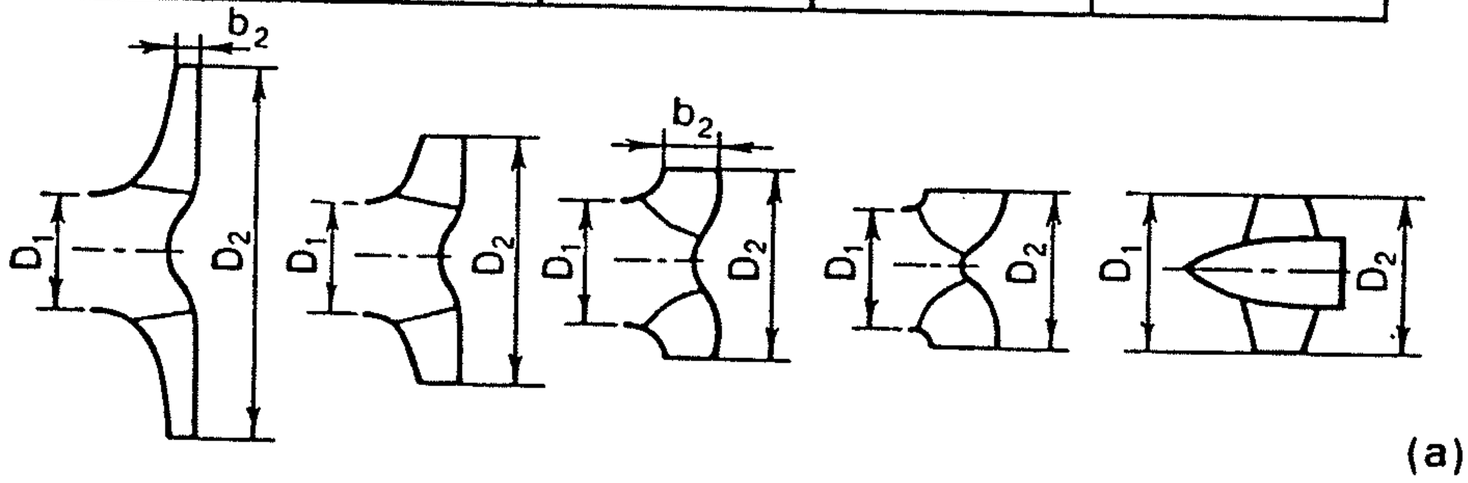
$$n_{s1} = 60 \times 9.81^{3/4} \times n_{s1} = 332.6\, n_{s0}$$

The essence of all the forms of specific speed is the same and differ only by constant coefficient.

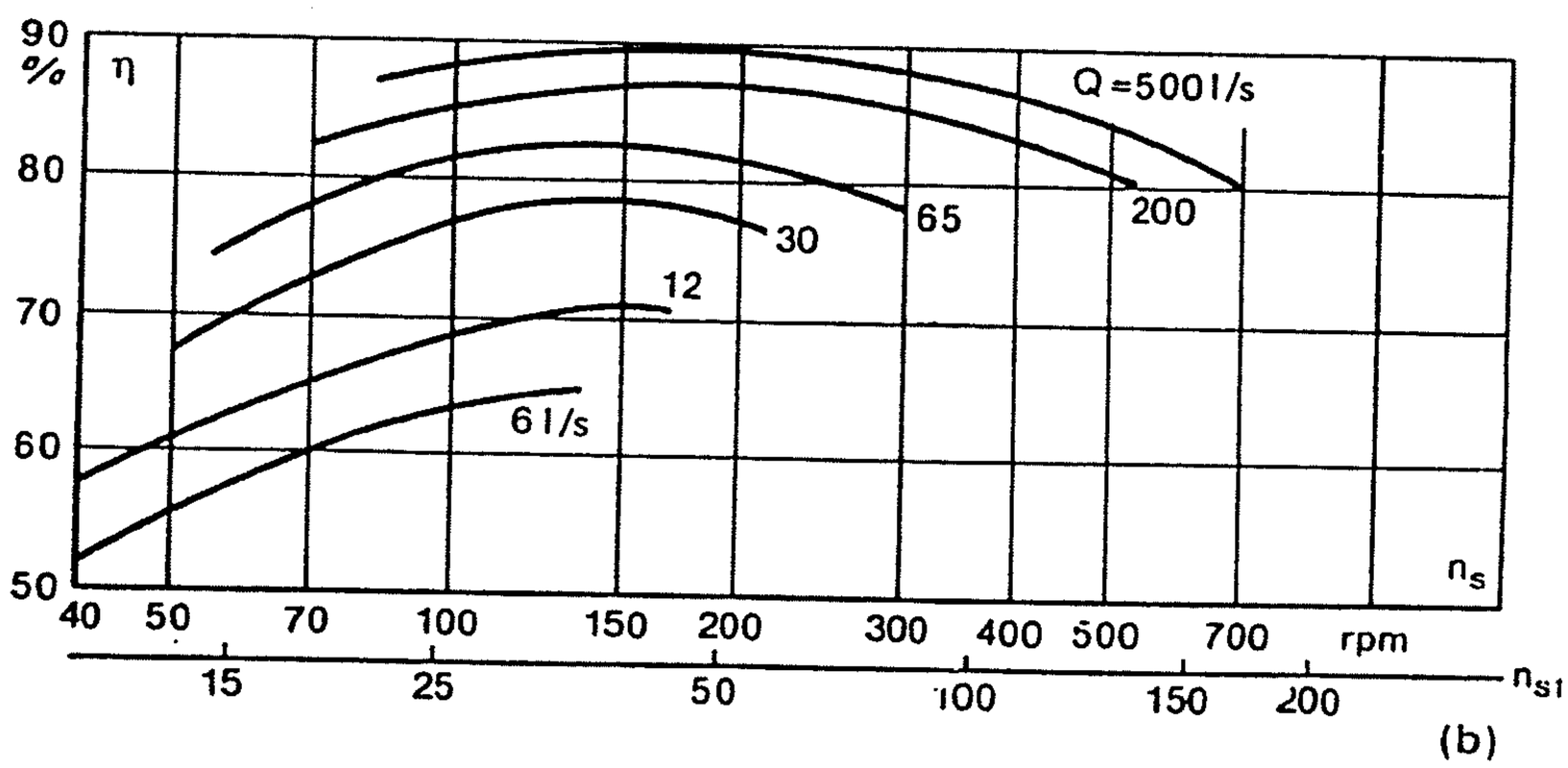
Specific speed n_s is an important characteristic that is widely used for describing the pump type. This characteristic is complex because it is based on the three most important characteristics of the pump: rotational speed, delivery, and head. Therefore, the specific speed characterizes the pump type to a sufficiently large extent. For instance, some pumps differing in type, geometry, and design but having close values of n_s will have many other similar features. For instance, low specific speed pumps (n_s = 60 to 100 rpm, n_{s1} = 16 to 28 rpm) are always used at high heads; on the contrary, high specific speed pumps (n_s = 400 to 800 rpm, n_{s1} = 110 to 220 rpm) at low heads.

Specific speed n_s largely determines the form of the impeller (Figure 12.8a). Low specific speed impellers (n_s = 60 to 80 rpm) are character-

n_s	60 -80	80 -120	120 -240	240 -350	400-800
D_2/D_1	3.0 -2.4	2.4 -1.8	1.8 -1.3	1.3 -1.1	1.0



(a)



(b)

FIGURE 12.8. Specific speed vs impeller shape and pump efficiency.

ized in that the exit diameter is far greater than the inlet diameter and that width b_2 is relatively small. As the specific speed increases, this difference decreases; the width increases so that finally the impeller becomes a mixed-flow and axial-flow wheel.

Specific speed also influences the pump efficiency. The general forms of this relation are shown by the curves in Figure 12.8b. As seen in these curves, maximum efficiencies correspond to the range of $n_s = 140$ to 220 rpm, the influence of delivery Q, i.e., pump size, being very great. Increasing Q gives rise to efficiency.

Various dimensionless coefficients are also used to characterize the pump. Of these, ψ and φ are the most popular; they are found from the formula

$$\psi = \frac{H}{u_2^2/2g} \qquad \varphi = \frac{4Q}{\pi D_2^2 u_2} \tag{12.29}$$

where u_2 is peripheral velocity of the impeller outlet edge (Equation 12.3a). Here, ψ is head coefficient, φ is delivery coefficient proportional to v_{m2}/u_2, and $v_{m2} = v_2 \sin \alpha_2$ is a meridional component of velocity (Figures 12.3 and 12.5). It is important that ψ and φ remain constant for a given impeller under similar conditions.

The same property has a dimensionless head and discharge coefficients C_H and C_Q:

$$C_H = \frac{gH}{n^2D^2} \qquad C_Q = \frac{Q}{nD^3} \qquad C_N = \frac{N}{\rho n^3 D^5} \tag{12.29a}$$

Here, ρ is fluid density (measured in kilograms per cubic meter), and n is per second.

It is easy to establish the straight connection between ψ, φ, and C_H and C_Q:

$$\psi = \frac{2gH}{u_2^2} = \frac{2 \times 60}{\pi^2} \frac{gH}{n^2D^2} = 12.16C_H$$

$$\varphi = \frac{4.Q60}{\pi D^2 \pi Dn} = \frac{4 \times 50}{\pi^2} \frac{Q}{nD^3} = 24.3C_Q$$

If pump characteristics are found in coordinates ψ, φ, or C_H and C_Q they can be transformed from one to anther simply by changing the scales of appropriate coordinates.

A rather stable relation exists between ψ and specific speed of the pump (see Figure 19.2).

Example 12.2

What specific speed has the pump with parameters given in Example 12.1 and what maximum efficiency can be expected?

Solution

1. Using Equation 12.28

$$n_s = 3.65\frac{1450\sqrt{0.02}}{15^{3/4}} = 98$$

or using Equation 12.28a

$$n_{s1} = \frac{1450\sqrt{0.02}}{15^{3/4}} = 26.9$$

For dimensionless form (Equation 12.28b)

$$n_{s0} = \frac{24.17\sqrt{0.02}}{(9.81 \times 15)^{3/4}} = 0.081$$

2. From Figure 12.8 for given values of n_s or n_{s1} and $Q = 20$ L/s the efficiency is about 75%.

12.5. STRUCTURE OF FLOW

The peculiarities of motion in the moving setting of blades at its power interaction with liquid flow were considered in Section 5.9. It was shown that the power interaction between liquid and the blade is possible only in the presence of circulation along the blade (Γ_b). Thus, nonuniform distribution of velocities and pressures should exist within the blade space of the impeller because circulation motion is imparted to the averaged flow at this point.

An approximate structure of flow in a centrifugal pump impeller is shown in Figure 12.9, in which (a) is the direction of blade circulation Γ_b and distribution of pressure on the blade; (b) is the distribution of relative velocities in the blade spaces; and (c) is the distribution of pressures at a certain radial section. The blade circulation decreases relative velocity on the working side of the blade and increases it at the back side, in the opposite direction of rotation. This forms a pressure differential which is overcome by the torque developed by the drive.

Nonuniform distribution of pressures and, in particular, additional reduction of pressure relative to average inlet pressure, which is found

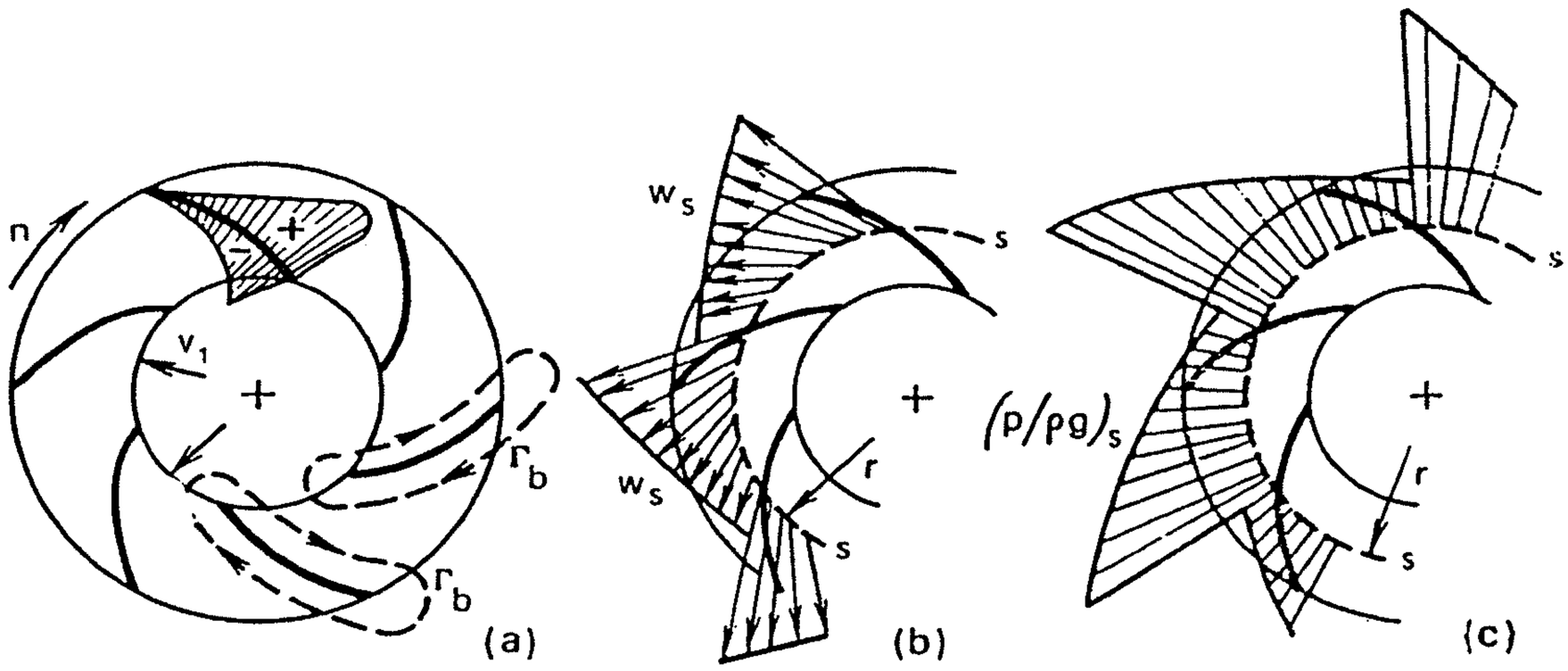


FIGURE 12.9. Structure of flow in centrifugal pump impeller.

at the back side of the blade (especially at the inlet portion), and is important for pump operation.

12.6. PUMP ENERGY LOSSES

While the pump efficiency coefficient (Equation 11.10) takes into account the overall losses, it is important to discover the nature of energy losses and their mutual relation. Even from the simplest of the impeller pump schemes (Figures 11.8 and 11.9) it is easy to see that there must be three types of losses:

1. Mechanical losses caused by friction on bearings and shaft packings and liquid friction in the gaps between rotating parts of the impeller and casing. This lost energy (power) can be designated ΔN_{mech}.
2. Hydraulic flow head loss on Δh_h inside the pump and impeller with blades. The lost power $\Delta N_h = \rho g(Q + q)\,\Delta h_h$. Here, Q is pump delivery and q is inside leakage through the seal clearances between high pressure outlet casing (chamber) and low pressure inlet nozzle.
3. So-called volumetric losses. It is q that is equivalent to the lost power $\Delta N_v = \rho g H q$ (H is the pump head).

It is worthwhile to introduce dimensionless parameters such as the efficiency coefficient. If the pump capacity or consumed power in accordance with Equation 11.11 is N, we can introduce:

- Mechanical efficiency

$$\eta_{mech} = \frac{N - \Delta N_{mech}}{N}$$

- Hydraulic efficiency

$$\eta_h = \frac{N - \Delta N_{mech} - \Delta N_h}{N - \Delta N_{mech}}$$

- Volumetric efficiency

$$\eta_v = \frac{N - \Delta N_{mech} - \Delta N_n - \Delta N_v}{N - \Delta N_{mech} - \Delta N_h}$$

Because the overall efficiency is

$$\eta = \frac{N - \Delta N_{mech} - \Delta N_h - \Delta N_v}{N}$$

it follows that

$$\eta = \eta_{mech}\, \eta_h\, \eta_v \tag{12.30}$$

The relation in Equation 12.30 is rather important for practice.

Example 12.3

For a new pump maximum efficiency was 84% ($\eta = 0.84$) and approximately $\eta_v = 0.96$. After a period of operation it was revealed that impeller wear rings (Figure 13.19a) deteriorate and their clearance increased approximately 2 $\times$. What change of overall pump efficiency can be expected?

Solution

Prior volumetric losses were $1 - 0.96 = 0.04$. As clearance increased approximately twice, so did leakage q, and volumetric losses will be 0.08 or $\eta_v = 0.92$. According to Equation 12.13, new pump efficiency η_1 will be

$$\eta_1 = 0.84 \times 0.92/0.96 = 0.805 \quad (80.5\%)$$

or 3.5% lower.

CHAPTER 13

Construction of Impeller Pumps

13.1. TYPES

To consider the numerous types of impeller pumps manufactured by the industry, let us divide them into two groups: general purpose and special purpose pumps.

General purpose pumps are intended to transfer clear water (a small amount of inert impurities is allowed; water temperature should not exceed 70° to 100°C). These pumps are manufactured in series and have the following characteristics: delivery from 1.5 to 5000 L/s, head from 5 to 700 to 800 m, and capacity from 0.5 to 1500 kW. Pumps of this type include cradle-mounted, double-entry, vertical axial-flow, mixed-flow, and multistage units. The latter are used to produce high head exceeding 100 to 120 m.

Special pumps may differ in liquid handled, method of installation, or characteristics; e.g., suction dredges intended to transfer slurries with a large content of abrasive particles (soil, sand, ash, slug, and crushed ore), sanitary pumps for transfer of feces and other contaminated liquids, acid pumps for handling chemically active liquids, etc. Special pumps also include units intended for removing water from wells and mines—oil well and submersible electric pumps.

The pumps having characteristics outside the limits specified for general purpose pumps may also be regarded as special: pumps of large irrigation installations, pumped-storage plants, or circulation systems of large thermal power stations. These pumps may be of a very high

capacity, say, 5 to 100 MW and more, and as a rule are manufactured individually.

Feedwater pumps intended to supply water to steam boilers are rated for a very high head (up to 2000 to 3500 m) and water temperature of 160°C and higher. Condensate pumps intended to pump out condensate operate under high vacuum and handle water heated to 120°C.

13.2. CRADLE-MOUNTED PUMPS

The schematic diagram of a cradle-mounted impeller pump is shown in Figure 11.8. As regards the shaft position, this is a horizontal pump whose working members are arranged on the cantilever portion of the shaft. Figure 13.1 illustrates the longitudinal cross-section of the cradle-mounted pump, type K; its external view is shown in Figure 13.2. An impeller (1) is secured by a nut and key on the end of the shaft (2). A one-piece cast spiral casing (3) with a delivery pipe (DP) is bolted to a support frame or cradle (4) (hence the name of the pump). The annular boring whose diameter somewhat exceeds that of the wheel is closed with a cover (5) cast integral with inlet pipe (IP). Whenever necessary, the runner or impeller (1) can be removed after detaching the cover (5) without complete disassembly of the pump. The pump shaft (2) is secured in ball bearings (6 and 7) arranged in bores of the cradle whose part forms an oil-filled reservoir. Fitted to the shaft end is a half-coupling (8) which is mated with a half-coupling (9) installed on the electric motor shaft.

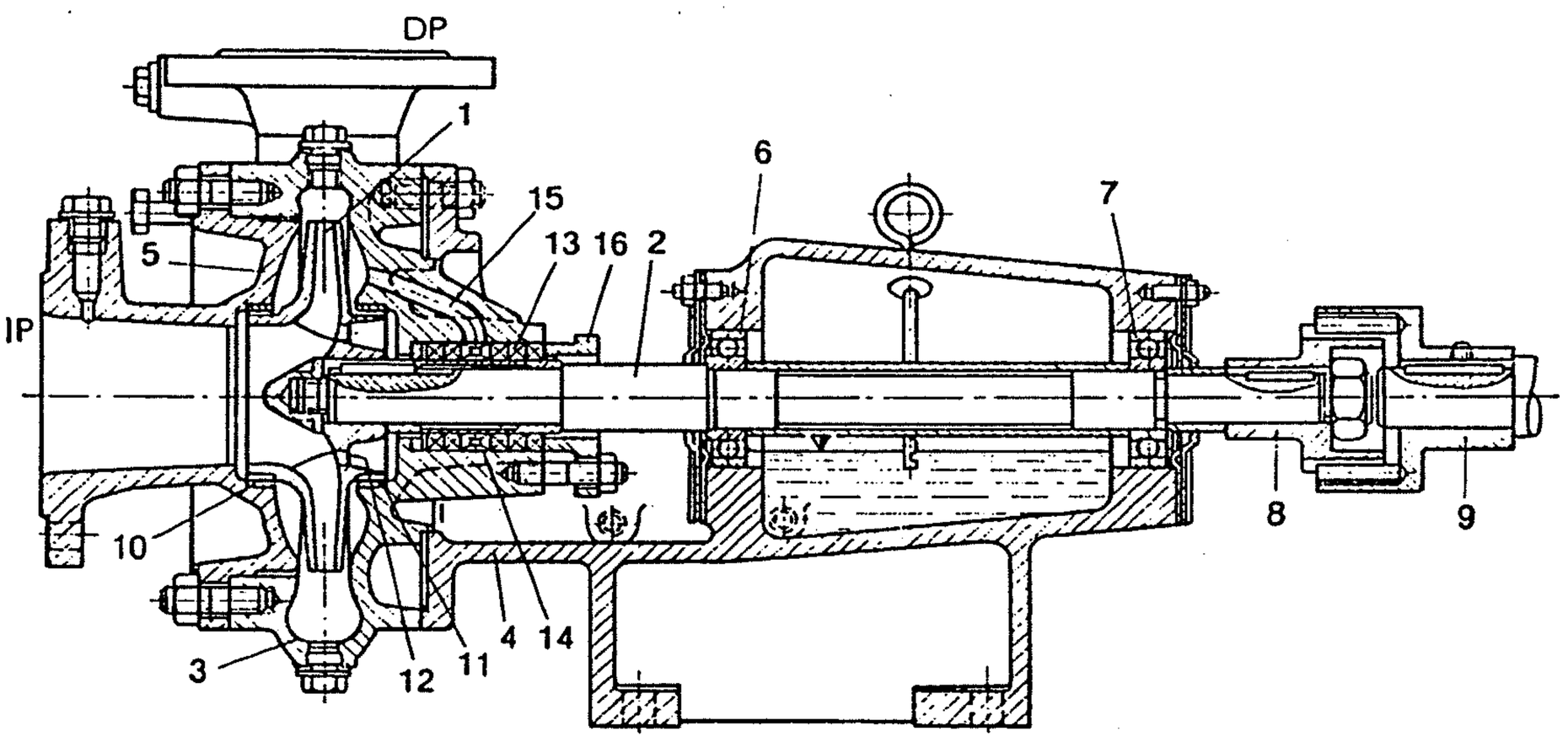


FIGURE 13.1. Cradle-mounted centrifugal pump, type K.

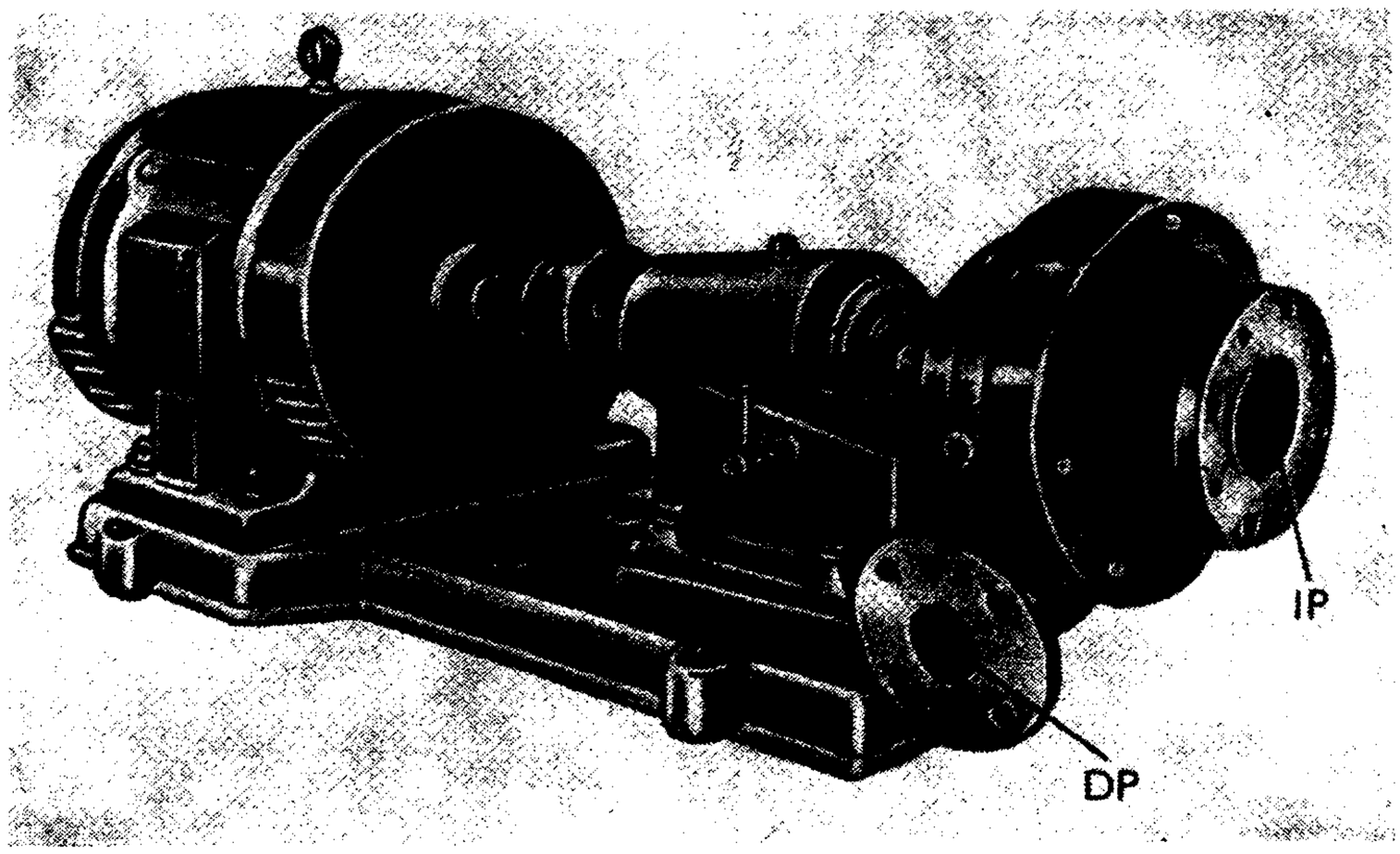


FIGURE 13.2. Cradle-mounted pump with electric motor.

To decrease leakage from the spiral casing (3) into the inlet pipe (IP), use is made of an annular seal (10). A second annular seal (11) and relief ports (12) are provided to balance the wheel, i.e., to decrease axial forces applied to it.

The packing gland sealing the hole through which the shaft extends is a vital element of the pump. Pump operation is sometimes accompanied by high vacuum created in the suction pipe. Ports (12) provide for a similar vacuum to be formed near the wheel hub on the shaft side. Therefore, if the shaft seal is not tight enough, air will enter the suction pipe during pump operation, which may disturb normal functioning ("surge"). To increase reliability of the seal, the packing gland is provided with water seals. The packing (13) (comprised of hemp twine boiled in tallow with graphite powder or special collars) is separated with a metal spacing ring (14) to which water under pressure is fed from the spiral casing via a passage (15) (in many instances water is delivered through an external pipe). This precludes the ingress of air to the wheel chamber. The packing gland is tightened by pressure cover (16) with bolts. As the packing wears and the seal becomes leaky, the cover (16) is tightened.

Cradle-mounted pumps are usually delivered in set with an electric motor mounted on a common cast frame (Figure 13.2). The DP with spiral casing is turnable through 90° and can be set to any of the four positions in mounting (two horizontal and two vertical).

Being used increasingly are monoblock pumps (Figure 13.3). Here, the impeller (1) is attached directly to the shaft (2) of the flange-mounted

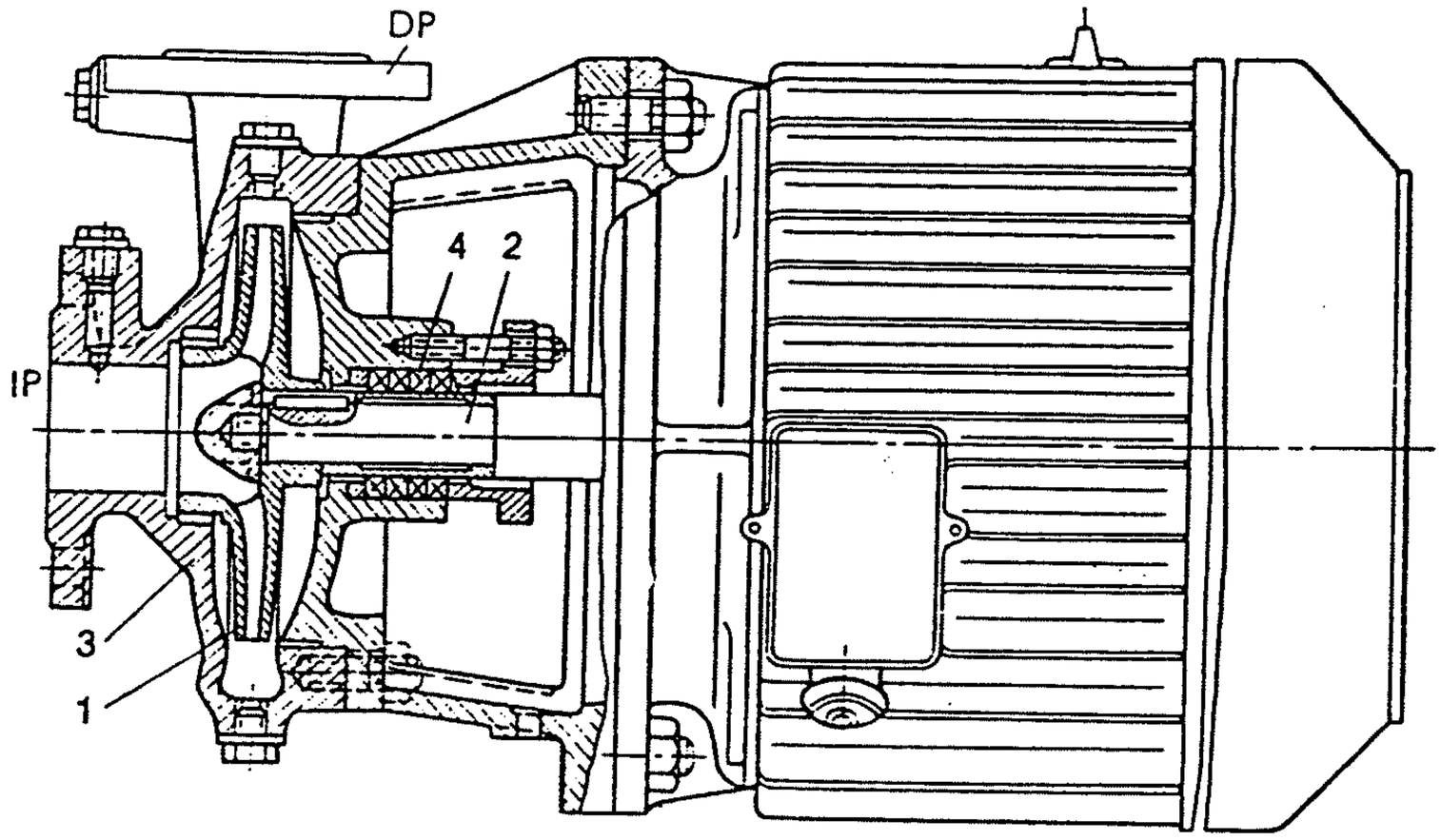


FIGURE 13.3. Monoblock pump, type KM.

motor. This obviates the need for pump bearings and coupling and decreases dimensions and weight. The wheel of this pump is not unloaded (there are no ports in the hub or second sealing ring). Therefore, it uses a simple packing gland (4) without a water seal. The spiral casing (3) is cast integral with IP and DP. The monoblock pumps are manufactured with both horizontal and vertical arrangement of the shaft.

13.3 DOUBLE-ENTRY PUMPS

The external view of a double-entry, double-suction (inlet), or horizontal split case pump, type D, is shown in Figure 13.4. The IP and DP are cast integral with the casing (1) and lugs (2 and 3). Thus, the suction and delivery pipelines are connected to the pump in the horizontal plane. The pump cover (4) is secured to the casing by bolts (axial joint). The sectional view of the type D pump along the axis of rotation is represented in Figure 13.5. Here, (1) is the pump casing; (2) and (3) are lugs; (4) is a detachable cover (the joint is screened by the shaft). The runner (5) is fitted on a horizontal shaft (6). Passages (b) are connected to the IP and water is fed to the runner from two sides (hence the name "double-entry"). The impeller ejects the water into the spiral case (7) and then to the DP. The shaft rests on bearings (11) and has a coupling (12) on one end for connection to the electric motor shaft. Because packing glands (8) seal the spaces (b) where fairly high vacuum can occur, they are provided with a water seal. Water is fed to the packing

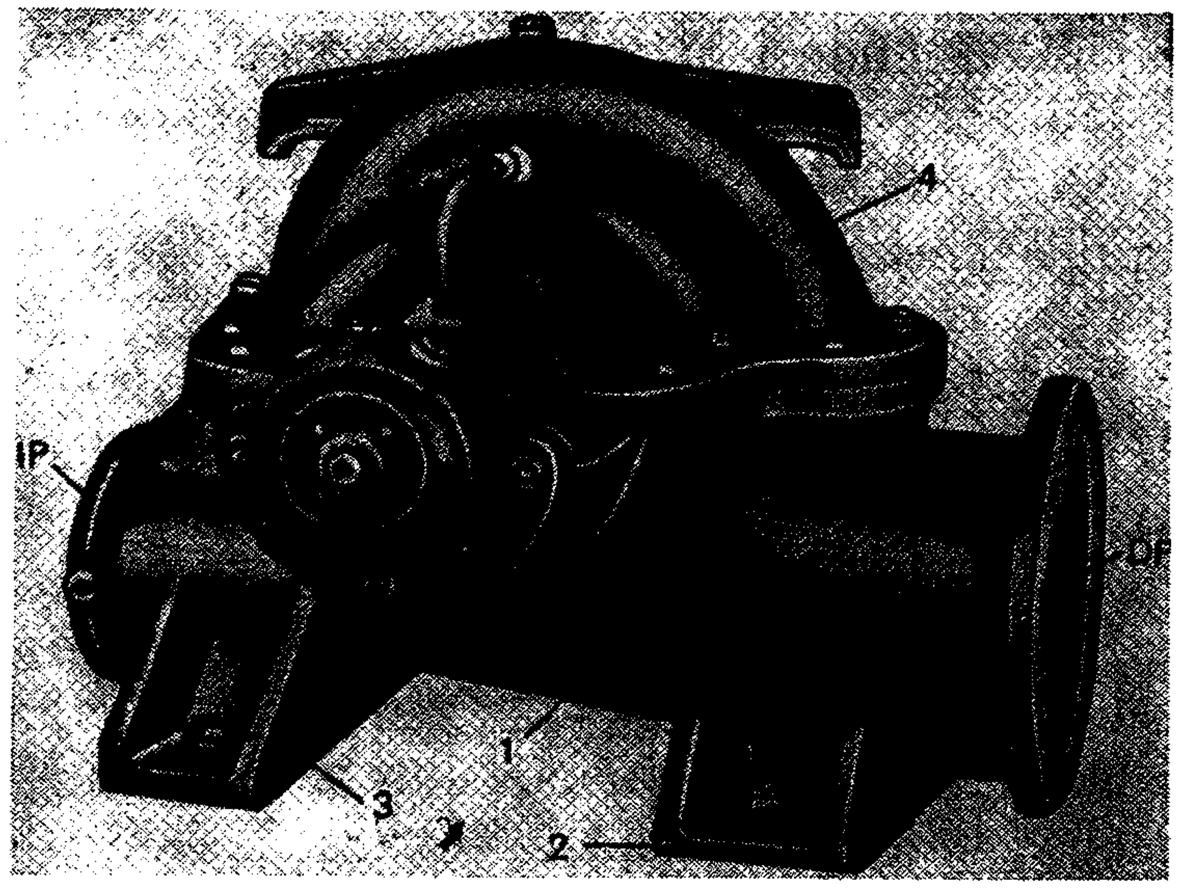


FIGURE 13.4. Double-entry pump, type D.

glands from the increased pressure space via the pipes (9). Annular seals (10) are provided on the wheel rims.

If compared to a cradle-mounted pump impeller, the double-entry pump runner can be regarded as a twin wheel. Therefore, when calculating the specific speed of a type D pump using Equations 12.28, take $0.5Q$ rather than full delivery.

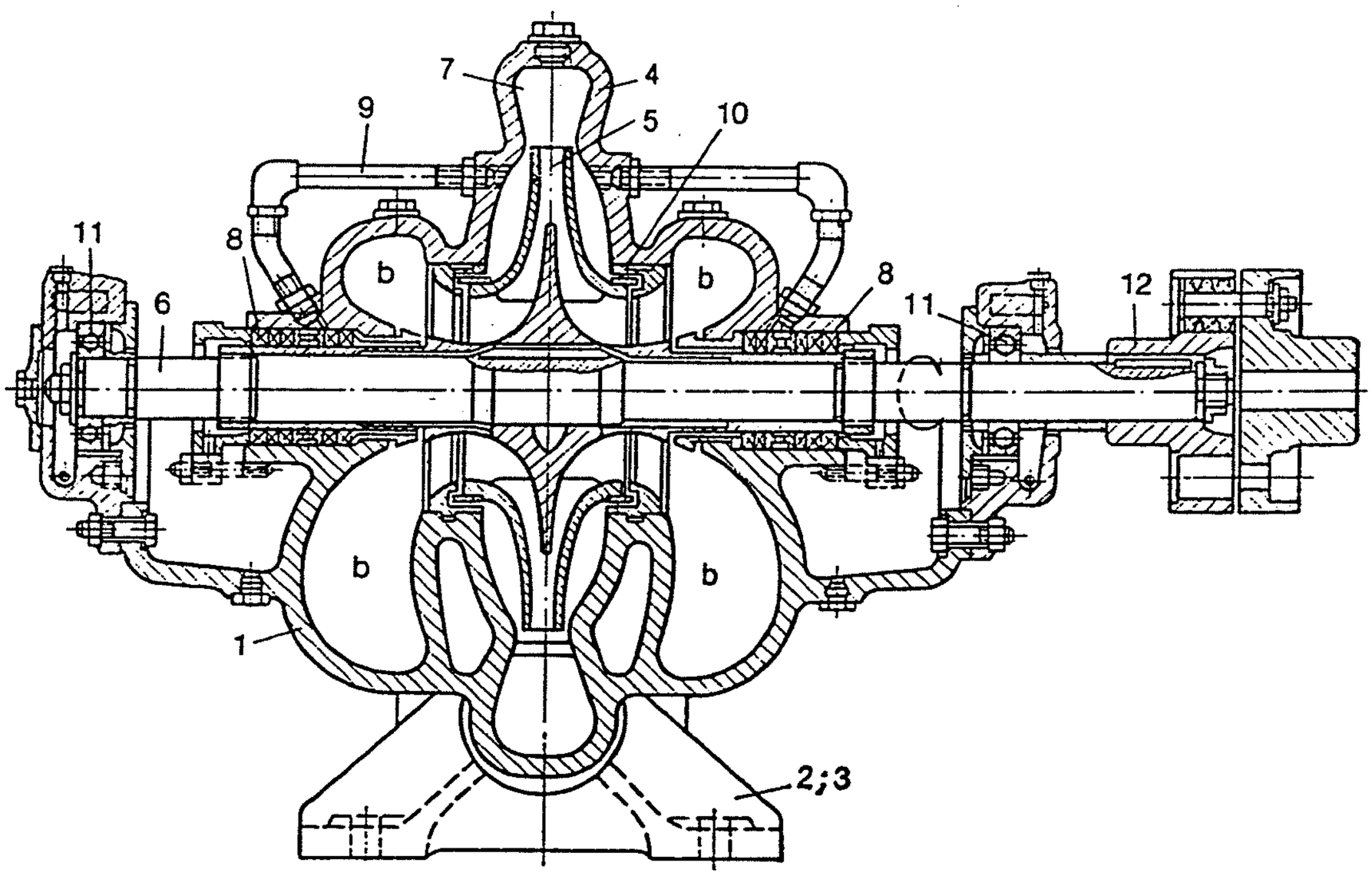


FIGURE 13.5. Double-entry pump, type D, sectional view.

The properties of type D pumps have almost twice as high delivery as the cradle-mounted pumps at the same diameter of the impeller, balanced axial loads of the runner, which simplifies operation of the bearings and the possibility of withdrawing the wheel and shaft without disconnecting the pipelines running to the pump.

13.4. AXIAL-FLOW PUMPS

The schematic diagram of an axial-flow pump is shown in Figure 11.9. Its main components are represented in Figure 13.6, while the vertical cross-section is illustrated in Figure 13.7. The wheel of the pump consists of a hub (1), blades (2) (from four to eight in all), and a cone (3). The wheel is bolted to the lower flange of the shaft (4) whose position is fixed by two bearings: a lower guide bearing (6) arranged in the hub of the straightening vane assembly (5) (the vanes (5) are shown in the cylindrical cross-section of Figure 11.9) and an upper bearing (7). Axial force is taken up by the electric motor bearings. The casing comprises a lower support ring (8) mated with a suction pipe, an impeller chamber (9), a straightening vane assembly shroud (10), and a discharge elbow (11) to which the DP is connected.

The lower guide bearing uses, as a rule, water lubrication, and has laminated wood plastic shells; the upper bearing may be either water- or oil-lubricated. In the latter case, it is arranged outside the casing. The point of shaft protrusion from the casing is sealed with a packing gland (12). The flange (13) is used to couple the pump shaft with the shaft of the motor.

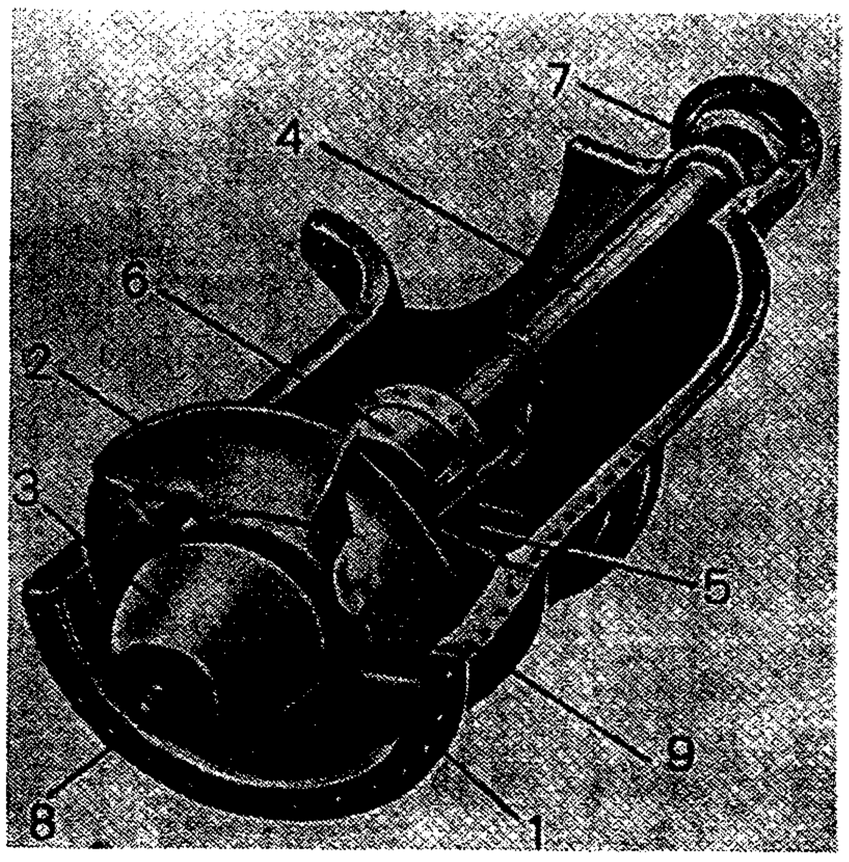


FIGURE 13.6. Axial-flow pump.

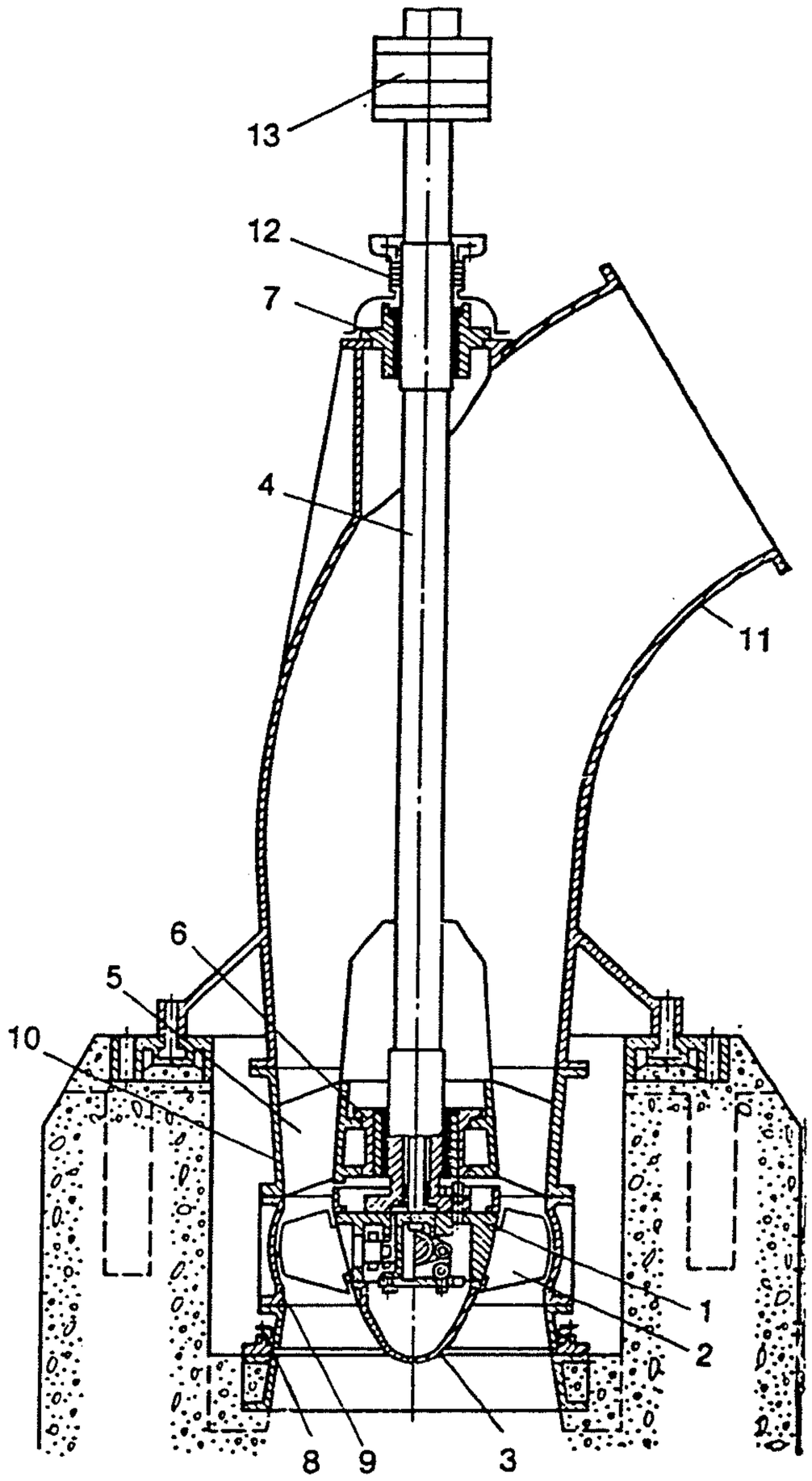


FIGURE 13.7. Axial flow pump, type VAB.

The impeller blade angle may be different depending on the required delivery and head. There are two types of impeller pumps as regards construction: vertical axial with fixed blades, or VAF (propeller type), and vertical axial with adjustable blades, or VAB (vertical, axial, blades adjusted type), wherein the vane angle can be adjusted in the course of the work. The adjustment is carried out either manually after stopping the pump, or with the aid of oil servomotors or an electric actuator while the pump is running. The rod to the wheel vane operating mechanisms arranged inside the hub (1) passes through the hollow in the shaft.

Axial-flow pumps are used with relatively low head (15 to 25 m) and high delivery. These pumps also come with a horizontally arranged

shaft. Horizontal axial pumps also may have a fixed blade or vane impeller, type HAF, or adjusted blade type HAB.

Figure 13.8 illustrates a horizontal pump. Here, (1) is a wheel, 220 cm in diameter; (2) is a guide vane assembly; (3) is an S-shaped suction pipe with a metal part (4) which passes a shaft resting on a bearing (5) and has an end coupling (6) for connection to the shaft of a horizontal electric motor (7). Pump discharge is adjusted by turning the wheel vanes by a hydraulic (oil) servomotor. Such pumps are used with heads of 7 to 10 m. In some pump installations the shaft is inclined, yet in this case the shaft and the electric motor are arranged on the side of the delivery conduit.

Some axial-flow pumps are embodied as horizontal bulb-type units. These are particularly efficient at very high deliveries, say, 100 to 250 m^3/s and heads of 10 to 12 m. These pump units may be used in the system to divert part of a river flow to other regions. Figure 13.9 is the design of a pump plant with a bulb-type unit comprising a wheel (1),

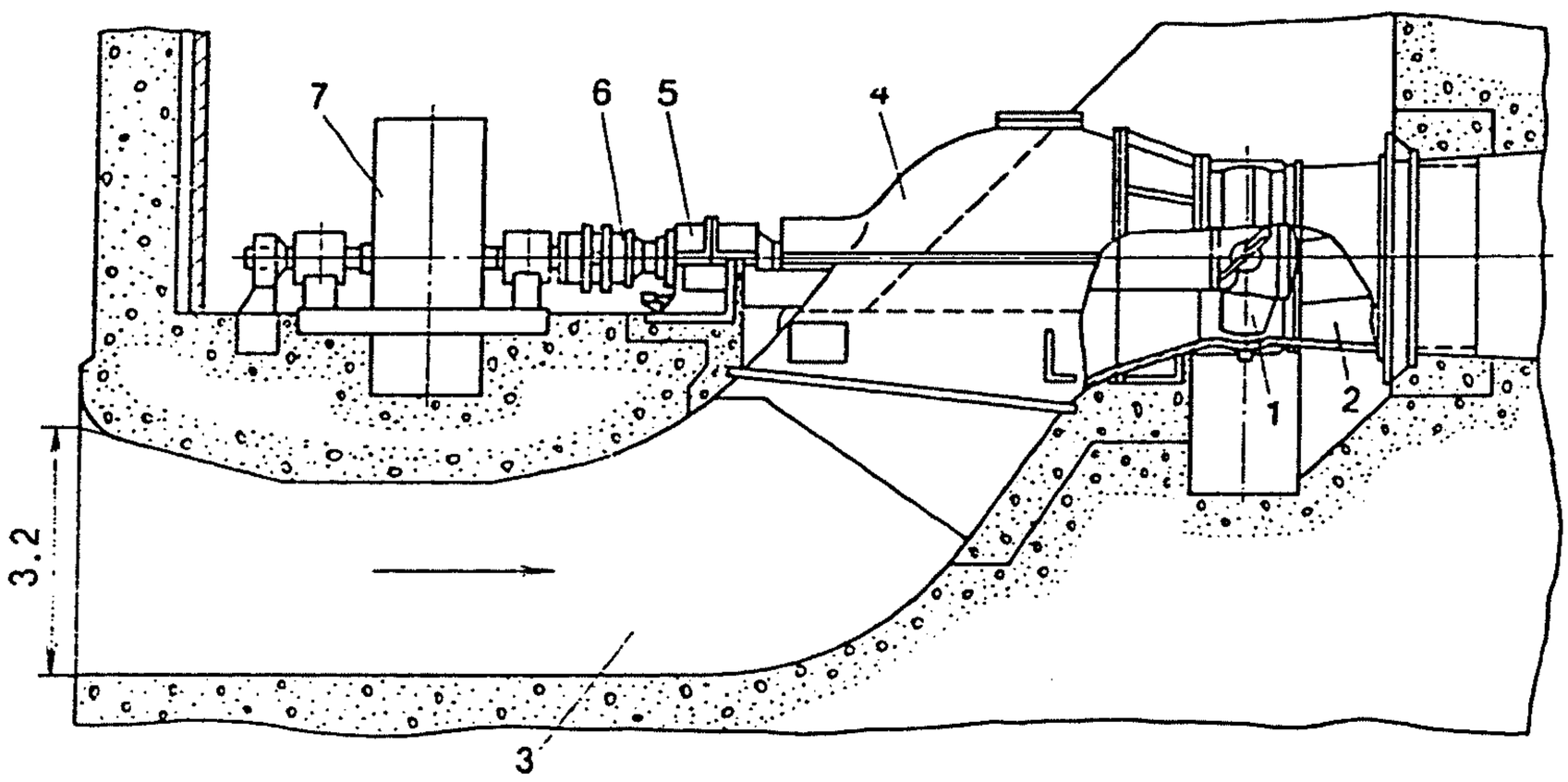


FIGURE 13.8. Horizontal axial-flow pump.

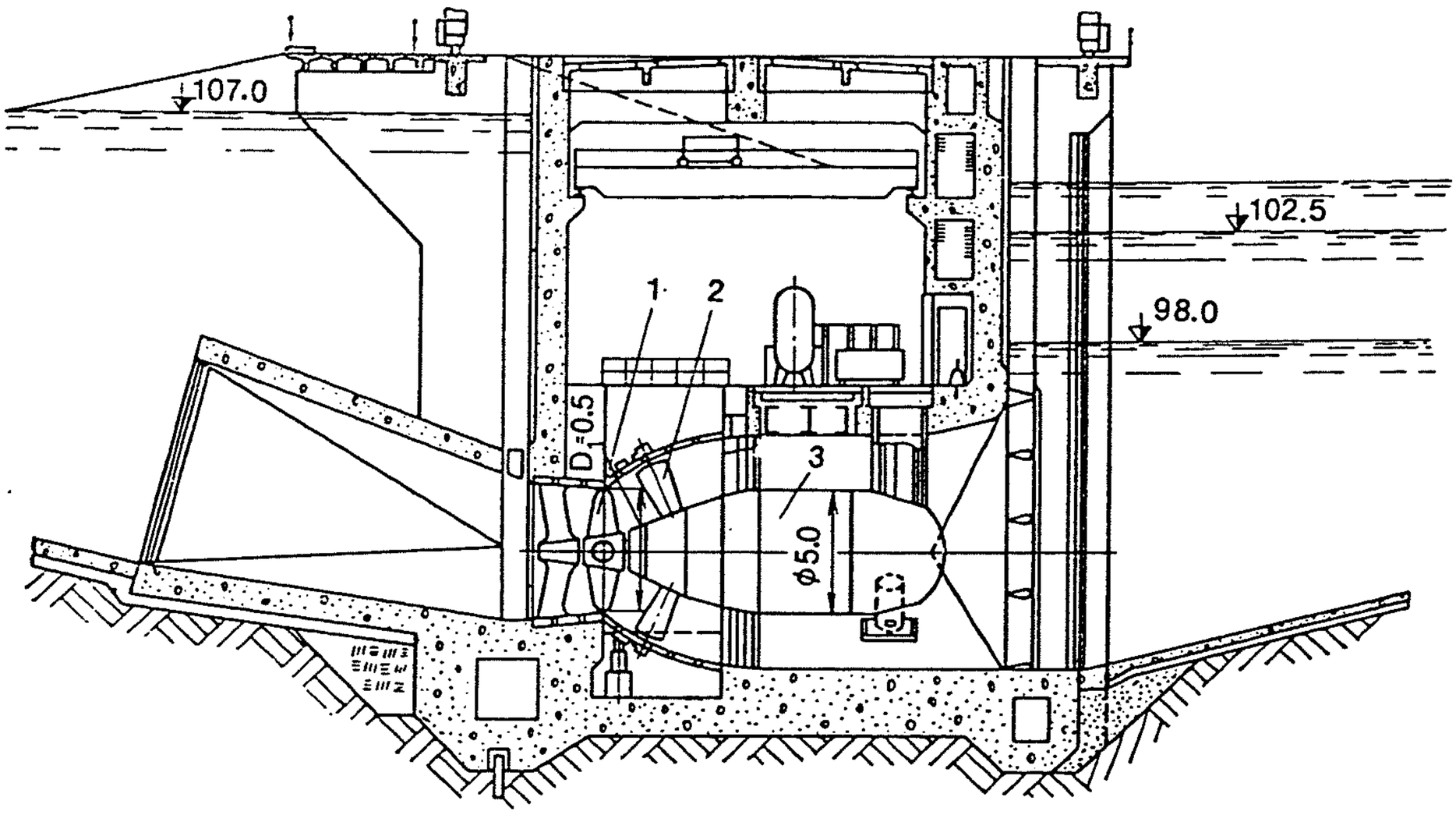


FIGURE 13.9. Horizontal bulb-type unit with axial flow pump.

5.0 m in diameter, a guide vane assembly (2), and a bulb (3) floating around in the water and accommodating an electric motor.

As seen from Equation 12.10a, if the guide vanes create before the wheel circulation Γ_1 in a direction opposite of the wheel rotation, the pump will be operable also when $\Gamma_2 \approx 0$, i.e., when the flow is close to axial downstream of the wheel. In this case no large straightening vane assembly is needed.

13.5. MIXED-FLOW PUMPS

Figure 13.10 illustrates a mixed-flow adjustable-blade pump with a wheel diameter of 2.0 m, designed for a head of 30 m. The main components of the pump are a wheel consisting of an impeller with blades (1) secured to a hub (2), a shaft (3), a guide bearing (4) housed inside a cone (5), which rests on a casing (6) through straightening vanes (7). Water is supplied through an elbow (8) connected to the delivery pipeline. Arranged in the upper portion of the unit are a packing gland (9) and a bearing assembly (10). Large mixed-flow pumps include six to nine vanes, and the small ones ($D < 100$ cm) have fewer vanes. Mixed-flow pumps, particularly small ones, also may be with fixed blades (propeller-type pumps).

Figure 13.10 shows that the mixed-flow pumps are similar to axial-flow units in the layout; the only difference resides in the wheel shape.

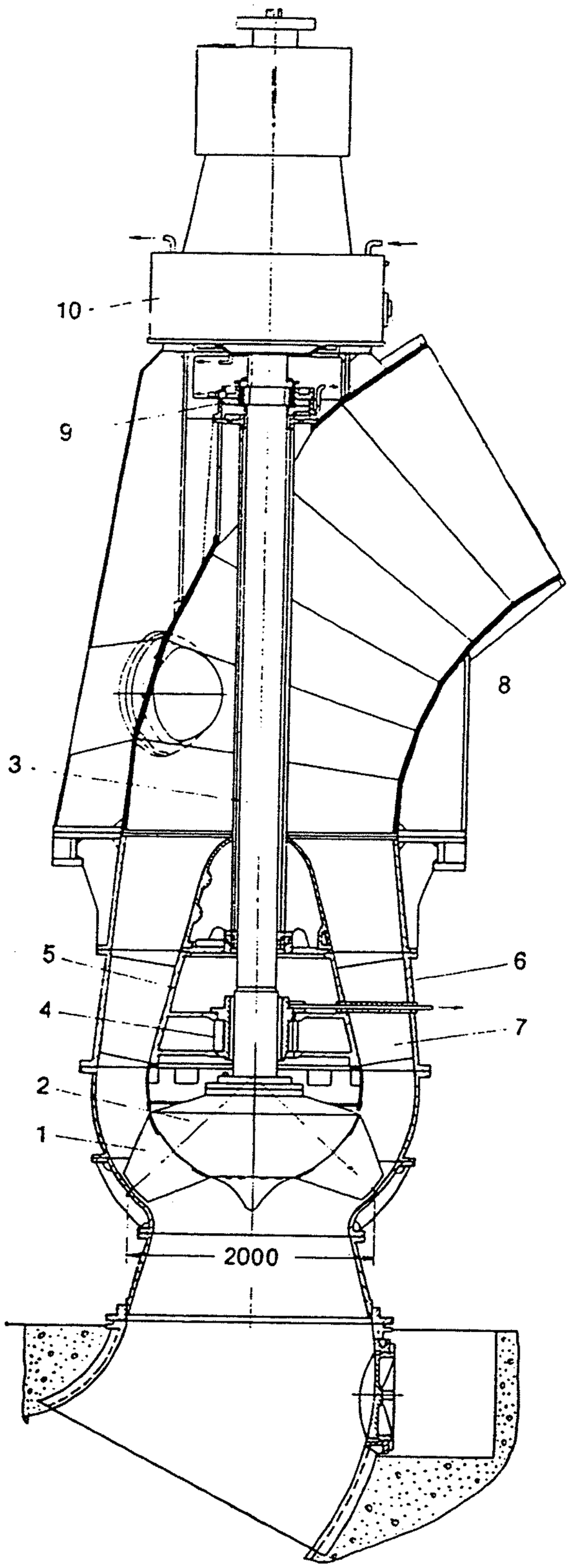


FIGURE 13.10. Mixed-flow pump.

13.6. VERTICAL CENTRIFUGAL PUMPS

The principal advantages of the vertical centrifugal pumps are the smaller floor area required for installation and convenient layout in certain pump houses. These advantages are particularly significant for large pumps. Figure 13.11 presents a cross-section of a large, type B vertical pump. The wheel diameter is 2.09 m, and the inlet diameter is 1.25 m. Water from the wheel (1) is ejected into a one-piece cast spiral casing (2), which is transformed into a DP. Because the spiral cross-section is open, internal pressure causes considerable bending moments which are taken up by strong stiffening ribs (3). To decrease bending moments, the spiral is sometimes provided with closing piles (stayring; see Figure 18.11).

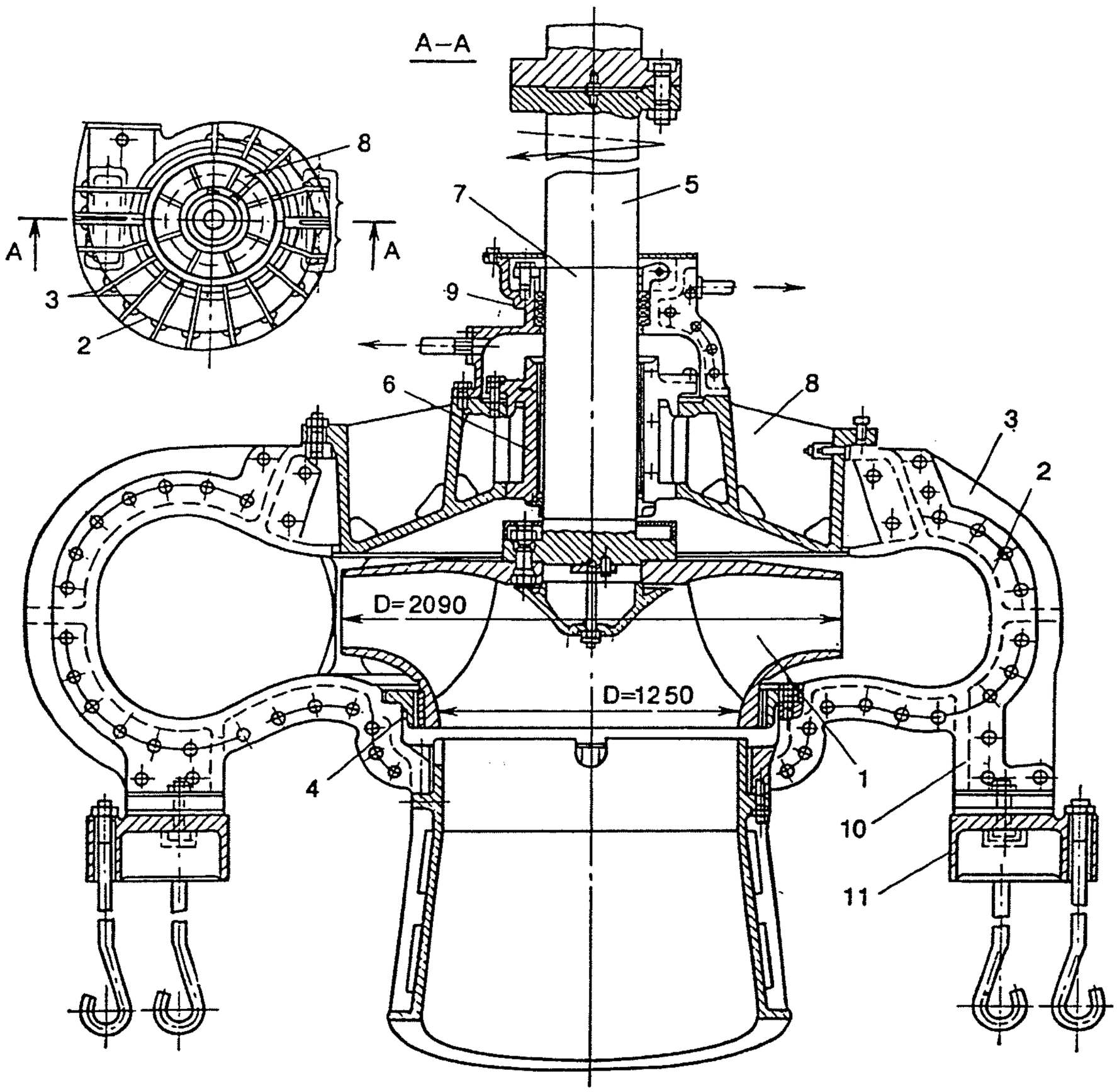


FIGURE 13.11. Vertical centrifugal pump, type B.

The cast casing of the pump consists of two halves bolted to each other (see the top view in Figure 13.11). A groove seal (4) (clearance 0.8 to 1.2 mm) is provided at the lower rim of the wheel. The wheel is secured to the lower flange of the shaft (5) which is fixed by a guide bearing (6) with laminated wood plastic or rubber shells that are lubricated by water (a protective stainless steel jacket (7) is fitted to the shaft at the bearing location). The bearing is attached to cast pump cover (8). A packing gland (9) is arranged over the bearing.

The upper flange of the shaft is coupled to the flange on the electric motor shaft. In this case wheel axial forces are not balanced, leading to high axial loads that are determined by different top and bottom pressures applied to the wheel rims. The pump is secured to the substructure by foundation bolts using lugs (10) and pads (11).

13.7. MULTISTAGE PUMPS

In multistage pumps the liquid being transferred is passed successively through several wheels or stages. If each stage develops head H_i, the head developed by z stages of the pump is $H = \sum_1^z H_i$, or if all the wheels are identical $H = zH_1$.

When determining specific speed n_s using Equations 12.28 for a multistage pump, use H/z (if the wheels are identical) or H_1, the first stage head, rather than the total head of the pump. In construction phases, all multistage pumps can be divided into two types: stage-chamber pumps having a casing with end-face joints and pumps having a common casing consisting of two halves with an axial joint (split-case pump).

A multistage chamber pump is shown in Figure 13.12; its longitudinal section is represented in Figure 13.13. The pump has four wheels or

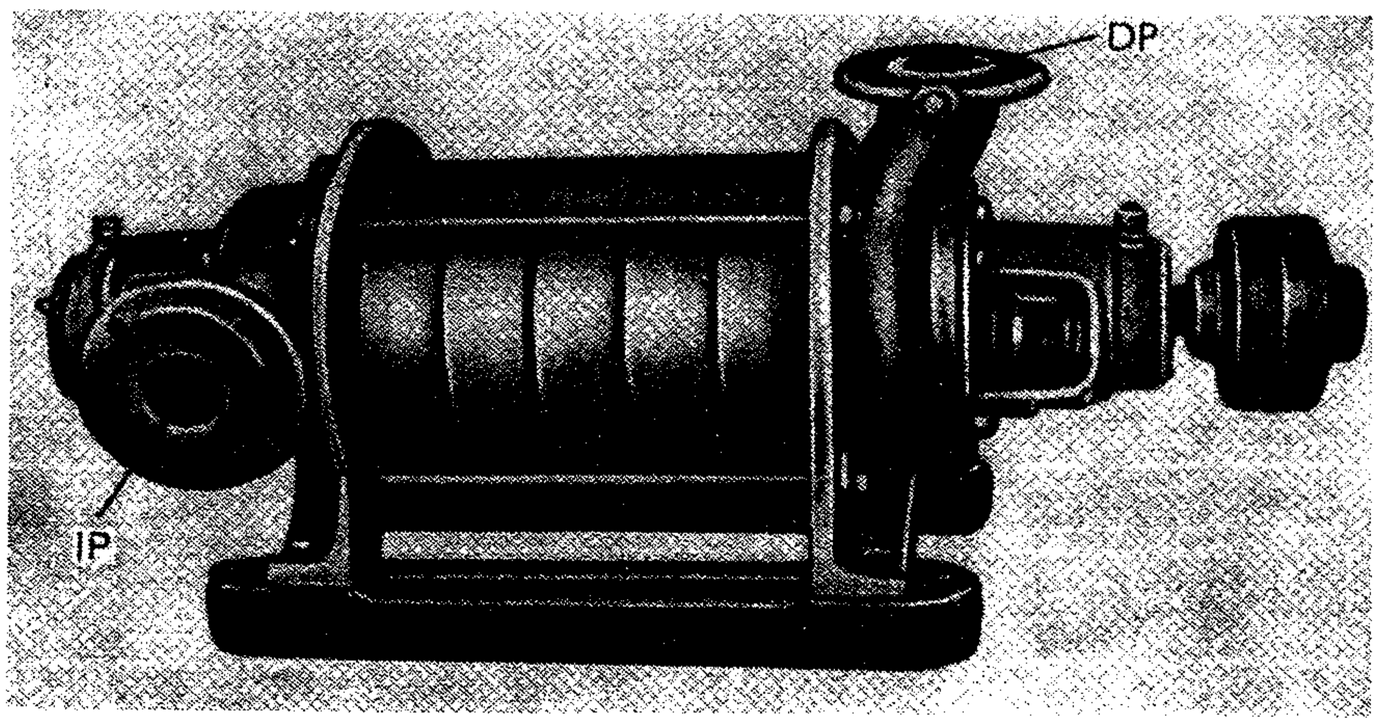


FIGURE 13.12. Multistage chamber pump.

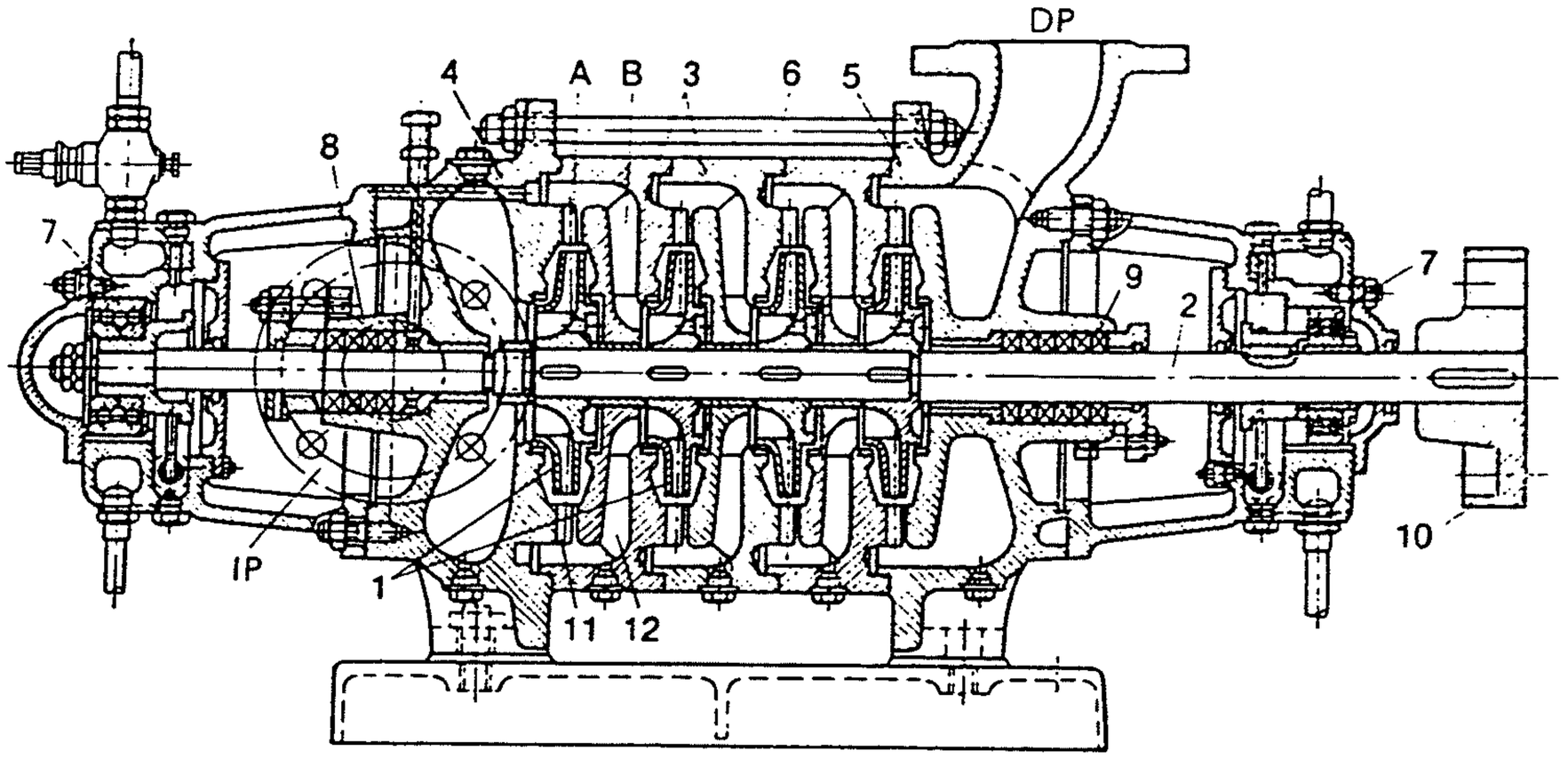


FIGURE 13.13. Multistage chamber pump.

rotors (1) fitted to a common shaft (2) (a four-stage pump). It consists of three identical sections (3) and two end sections: an inlet section (4) with an IP and an outlet section (5) with a DP. The end sections, coupled by bolts (6), accommodate packing glands (a suction packing gland (8) with a water seal and a delivery packing gland (9) and bearings (7)). The shaft is connected to the electric motor shaft by a coupling (10). Axial forces on each wheel of the pump are balanced (there are two seals and relief ports for each wheel).

Some stage-chamber pumps are equipped with unbalanced wheels, which decrease leaks and simplify the construction. In such pumps axial force is hydraulically balanced by a special thrust disk fitted onto the shaft.

An important element of a multistage chamber pump is a guide vane assembly which passes water to the inlet of the next-stage wheel. The assembly is intended to minimize hydraulic losses and ensure axial entry of the flow to the wheel (without swirling). The assembly is comprised of two sets of vanes: guide vanes (11) arranged immediately after the wheel (section A–A in Figures 13.13 and 13.14) and backward curved vanes (12) (section B–B).

Multistage pumps with an axial joint that have a split cast casing are embodied in different ways. An external view is shown in Figure 13.15, a longitudinal section in Figure 13.16. Its shaft (1) carries four wheels (2) (four-stage pump), but contrary to the stage-chamber pump their inlets face in opposite directions. Liquid from the IP enters space b and the inlet of the first-stage wheel. Then the liquid is ejected to the spiral and is transferred via passage K1 in the casing cover to the inlet of the second-stage wheel. The third stage wheel is the rightmost wheel, and the fluid is fed to it via an external (bypass) pipe (EP) (see Figure 13.15)

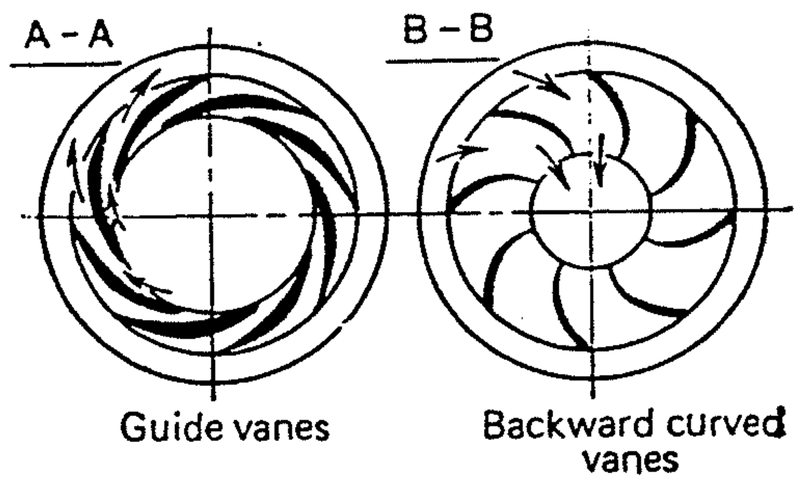


FIGURE 13.14. Vaned diffuser of multistage pump (sections *A–A* and *B–B* are shown also in Figure 13.13).

and then via passage K2 to the fourth-stage wheel, whose spiral transforms into a DP. The liquid flow path is shown in Figure 13.17. The main advantage of such a wheel arrangement is in that with the even number of stages it produces a balanced system wherein the axial component of the hydrodynamic load is small, and this facilitates operation of the bearings (3) (Figure 13.16). The pump casing consists of two halves: a bottom part (4) and a top part (5) inter-connected by bolts. The pump includes a suction packing gland (6) with a water seal and a delivery packing gland (7). The electric motor is connected by means of a coupling (8). High-head 6- to 15-stage feed boiler pumps of this design have two external transfer pipes and are capable of developing heads over 2000 m at 2950 rpm.

All the wheels of the multistage pumps considered above are similar in design. However, in some cases the first-stage wheel has a different shape, for example, with double entry. The main purpose is to improve cavitation characteristics and increase permissible suction lift of the pump.

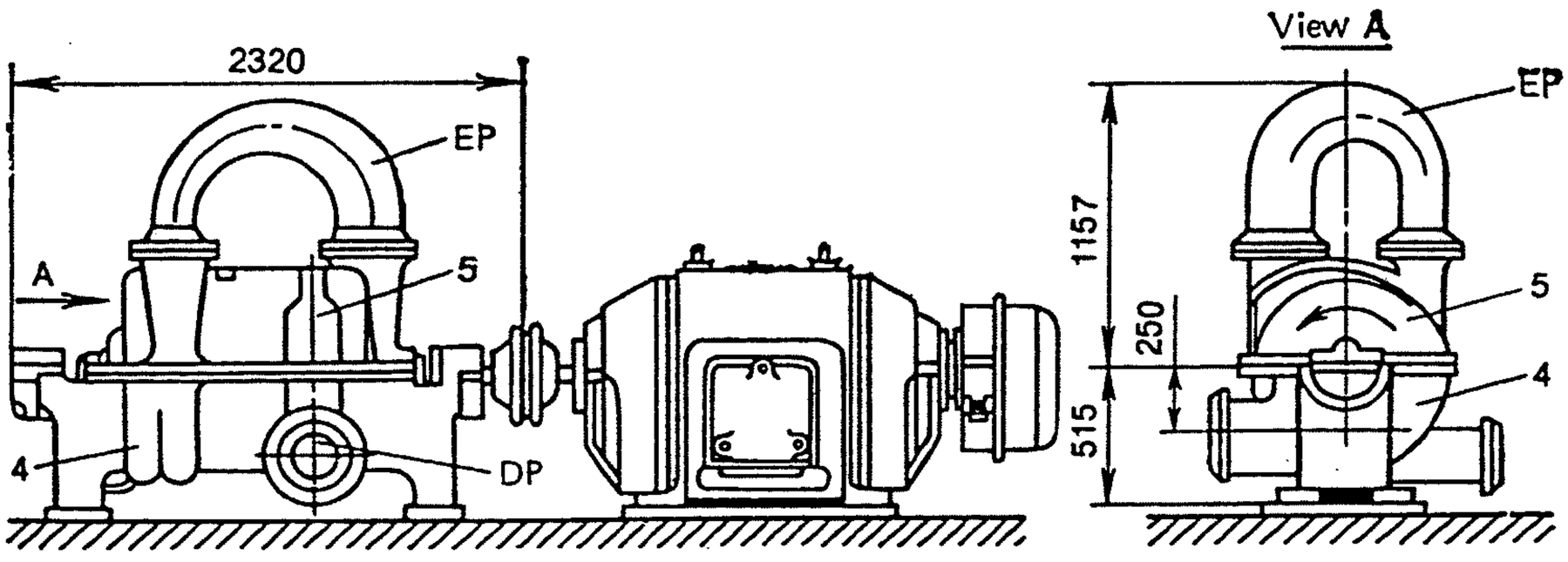


FIGURE 13.15. Multistage pump with axial joint. External view of installation.

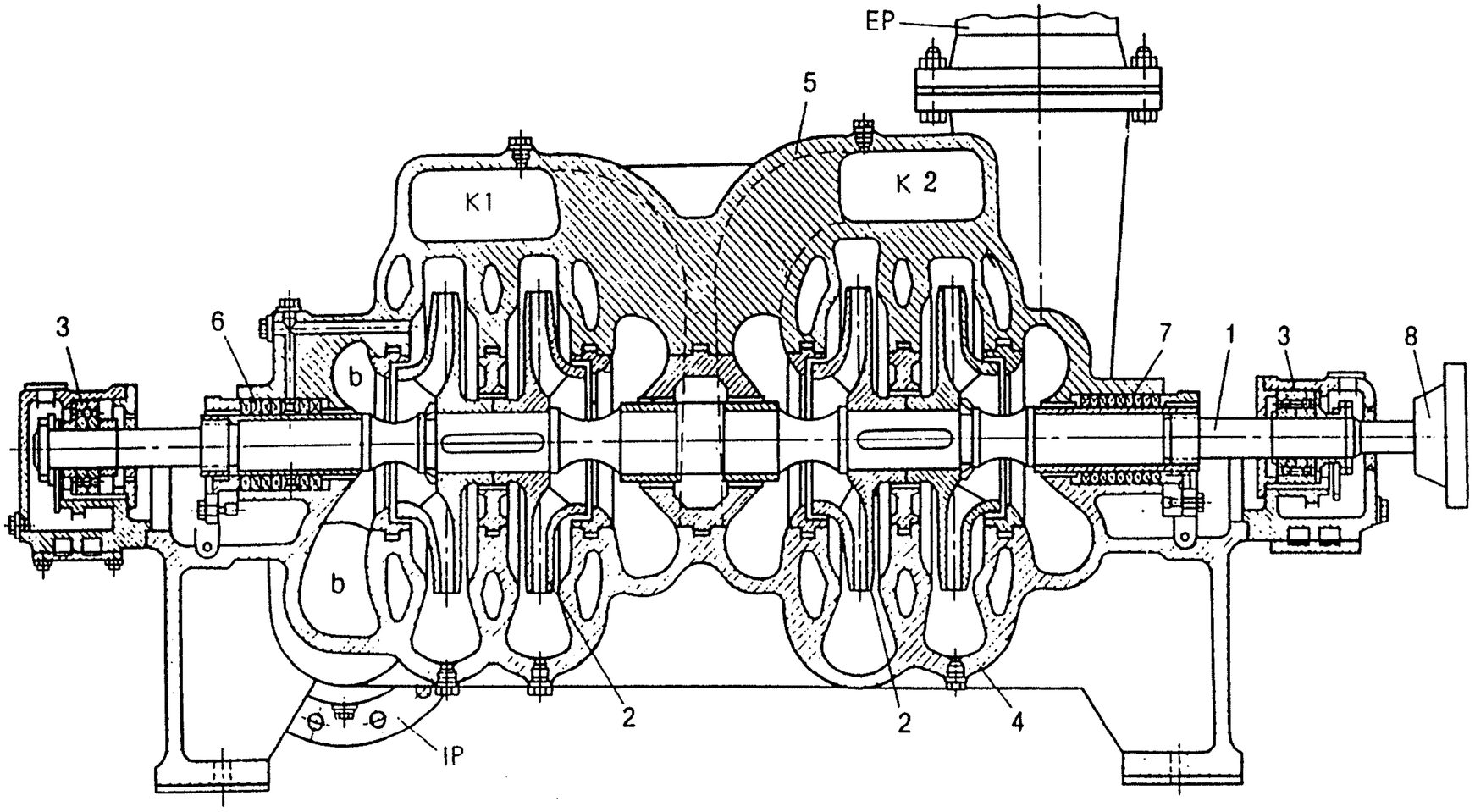


FIGURE 13.16. Multistage split case pump.

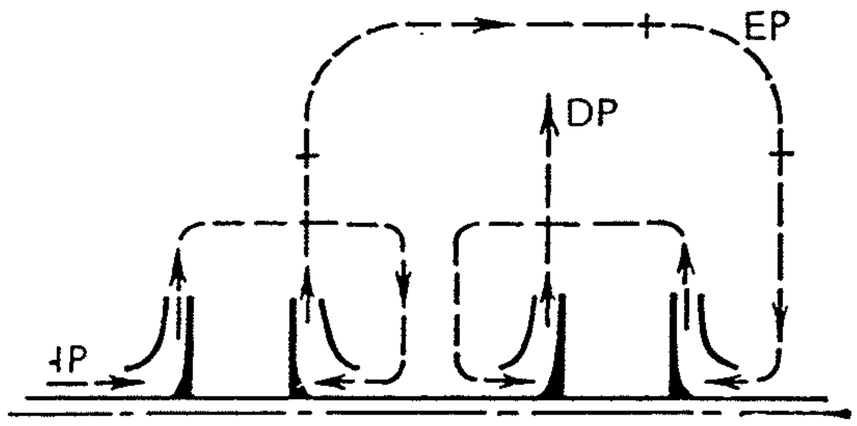


FIGURE 13.17. Flow path in multistage pump (see Figures 13.15 and 13.16).

13.8. SOME ELEMENTS OF IMPELLER PUMP CONSTRUCTION

The **wheel** or **impeller** is the main element of the pump which converts energy imparted by the motor into the energy of the fluid being transferred. The wheel shape depends on specific speed n_s and varies in compliance with Figure 12.8a. The axial-flow pump wheels usually have detachable vanes; the centrifugal pump impellers, one-piece cast vanes (bronze, cast iron, or steel). Because the relative velocity of the liquid flowing around the wheel is fairly high, the wheels should be carefully machined and have a smooth surface in order to decrease hydraulic losses and increase the efficiency.

The shape and dimensions of the wheel vanes are determined by hydromechanical calculations and experiments.

The pressure in the space between the wheel and the casing (Figure 13.18a) greatly influences the pump operation. The pressure at point A is equal to that in the outlet chamber, but the pressure in the space will drop down toward point B due to centrifugal forces caused by rotation of the liquid in the gap. This rotation stems from entrainment of the liquid by the impeller walls.

Let peripheral velocity of liquid rotation at radius r (Figure 13.18b) be equal to v_u. As is known from mechanics, such a motion develops centripetal acceleration a determined by the formula

$$a = \frac{v_u^2}{r} \tag{13.1}$$

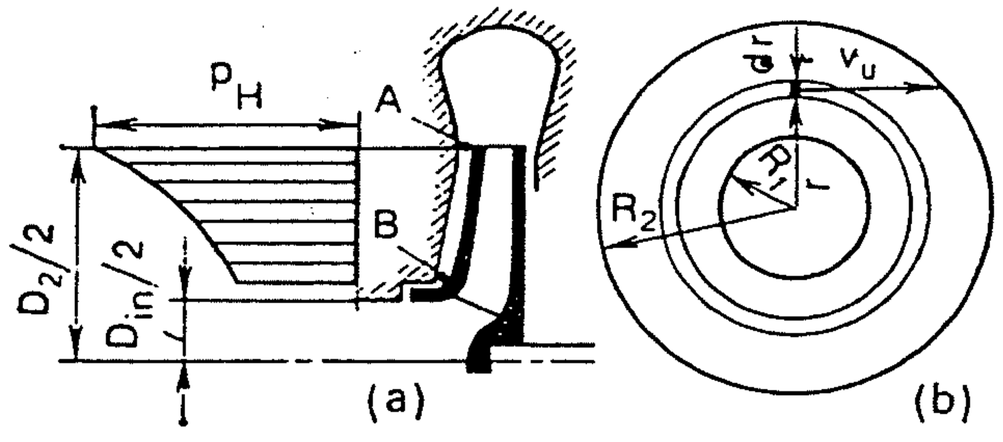


FIGURE 13.18. Pressure in the space between the rotating wheel and the casing.

If a circle of radius r is discriminated in the rotating liquid, pressure variation dp at layer dr in view of Equation 13.1 is

$$dp = \rho \frac{v_u^2}{r} dr \tag{13.2}$$

where ρ is the density of liquid. By integrating Equation 13.2, we obtain the pressure drop from radius R_1 to radius R_2

$$p_2 - p_1 = \rho \int_{R_1}^{R_2} \frac{v_u^2}{r} dr \tag{13.3}$$

As seen from Equation 13.3, pressure drop depends on the peripheral velocity curve $v_u(r)$. If we assume the liquid rotates as a solid with a constant angular velocity ω_{lq} then

$$v_u = \omega_{lq} r \tag{13.4}$$

Substituting v_u from Equation 13.4 in Equation 13.3, we obtain the pressure drop caused by the rotation of liquid

$$\Delta H_{rev} = \frac{p_2 - p_1}{\rho g} = \frac{\omega_{lq}^2}{2g}(R_2^2 - R_1^2) \tag{13.5}$$

For the gap having smooth end surfaces of the wheel, it is usually assumed that

$$\omega_{lq} = 0.5\omega \tag{13.6}$$

where $\omega = 2\pi n/60$ is the wheel angular velocity.

As transpires from Equation 13.5, the pressure curve for the gap is a paraboloid of revolution (Figure 13.18a).

The pressure difference between point B (Figure 13.18a) and the inlet section is less than head H developed by the wheel for ΔH_{rev}, according to Equation 13.5, but it is still fairly high.

Estimate the difference quantitatively. Let $D_2 = 270$ mm and $D_{in} = 100$ mm, head $H = 60$ m, suction lift $H_s = 5.0$ m, inlet vacuum $H_v = 6.2$ m (Equation 11.3), and $n = 2900$ rpm. This gives $\omega = 304$ 1/s. Assuming $\omega_{lq} = 152$ 1/s (Equation 13.6), we obtain from Equation 13.5

$$\Delta H_{rev} = \frac{152^2}{2 \times 9.81}(0.135^2 - 0.05^2) = 18.5 \text{ m}$$

Thus, the difference ΔH between point B and the inlet is

$$\Delta H = 60 - 18.5 - 5.0 + 6.2 = 42.7 \text{ m}$$

Under these conditions sealing the rotating wheel-to-casing joint becomes a challenge.

The **wheel seals** are always of the groove type (i.e., without direct friction between solid sealing elements), but the section and shape of the gaps are selected so as to minimize leaks from the delivery space to the suction pipe, which determines the volumetric efficiency of the pump.

Figure 13.19 illustrates different types of seals with wear rings. The minimum sealing clearance is always radial (0.25 to 0.8 mm, depends from diameter), while the axial gap s_1 should be much larger. The annular seals (Figure 13.19a and b) installed in the pumps shown in Figures 13.1 and 13.11 are the simplest. High resistance, hence lower leakage, are ensured by labyrinth seals (Figure 13.19 c to e), but they are more complicated in design. For instance, the seals shown in Figure 13.19c are used in the pumps of Figure 13.5. It is worth noting that the seal rings are subject to rather intense wear. Gaps increase owing to the rapid flow of liquid, especially if the latter contains even small amounts of abrasive particles. Therefore, the seals are usually made with replaceable rings.

Packing glands are a vital element of the pump and require the utmost attention in the course of operation and maintenance. When considering the constructions of pumps we classed the packing glands as regular, in which pressure in the sealing space exceeds the atmospheric pressure, and vacuum type, in which rarefaction forms in the sealing space. In the latter case packing glands with water seals are used (see Figures 13.1 and 13.5).

The shaft journal within the gland is squeezed by the gland stuffing and is subjected to local wear. If water contains abrasive particles, wear becomes intense. To facilitate repair of the shaft and decrease its wear in the packing gland, a stainless steel protective sleeve is fitted over the shaft. This method is used in the pumps shown in Figures 13.1 and 13.5. The stainless steel sleeve is usually installed on the shaft at the packing

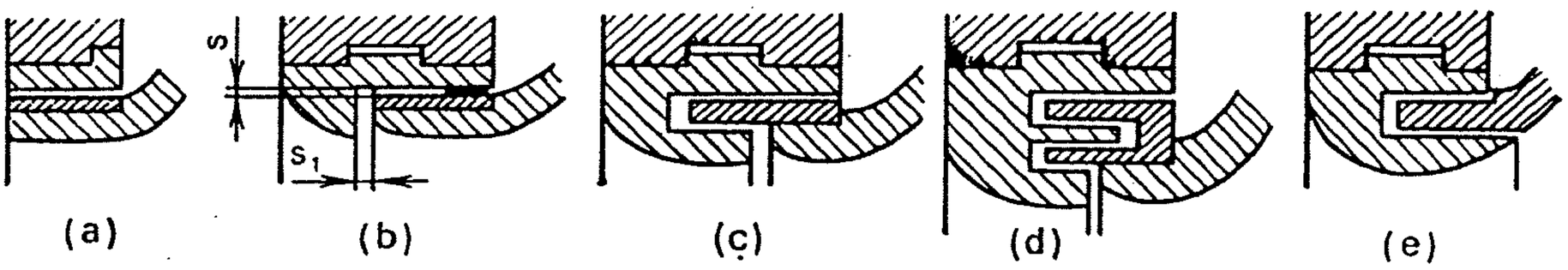


FIGURE 13.19. Types of impeller seals with wearing rings.

gland location at which the shaft rests against a water-lubricated sliding bearing in axial flow (Figure 13.7) and vertical (Figure 13.11) pumps.

Pump outlets receive water ejected by the wheel and supply it to the DP or to the wheel of the next-stage in multistage pumps. The liquid is ejected from the wheel at a high velocity, $v_2 = 20$ to 30 m/s; i.e., its kinetic energy is very high. It is important to utilize this energy and convert it to pressure. This problem is solved when designing outlets.

As pointed out earlier, when treating the constructions of pumps, there are two types of outlets: a spiral outlet or volute, and an outlet with a straightening vane assembly. The spiral outlet is shown in Figure 13.20. The cross-sectional dimensions are selected so that the average velocity of liquid in the outlet is substantially constant. The part of the outlet between sections (7) and (8) is a diffuser. The flow average velocity decreases lengthwise to the diffuser so that an additional part of kinetic energy is converted into pressure.

Outlet width b_3 is usually greater than wheel width b_2 (see also Figures 13.1, 13.5, and 13.11).

In vaned outlets (see Figure 13.14) water from the wheel enters the diffusion expanding channels, which smoothly decelerate the flow, thus converting kinetic energy into pressure.

Radial force acting on the impeller is transmitted to the bearings, which affects pump operation conditions. In centrifugal pumps with spiral outlet (Figure 13.20) for an optimal regime ($\eta = \eta_{max}$), the radial force is approximately equal to zero, but rises in regimes that deviate from optimal. If $Q < Q_{opt}$ spiral case works as a diffuser, the pressure in entering sections 2 and 3 is less than in exit sections 6 and 7. It creates a radial force F_r acting in the direction of sections 2 to 3 (its direction is about 100°C to the exit diffuser axis). $Q > Q_{opt}$ spiral case

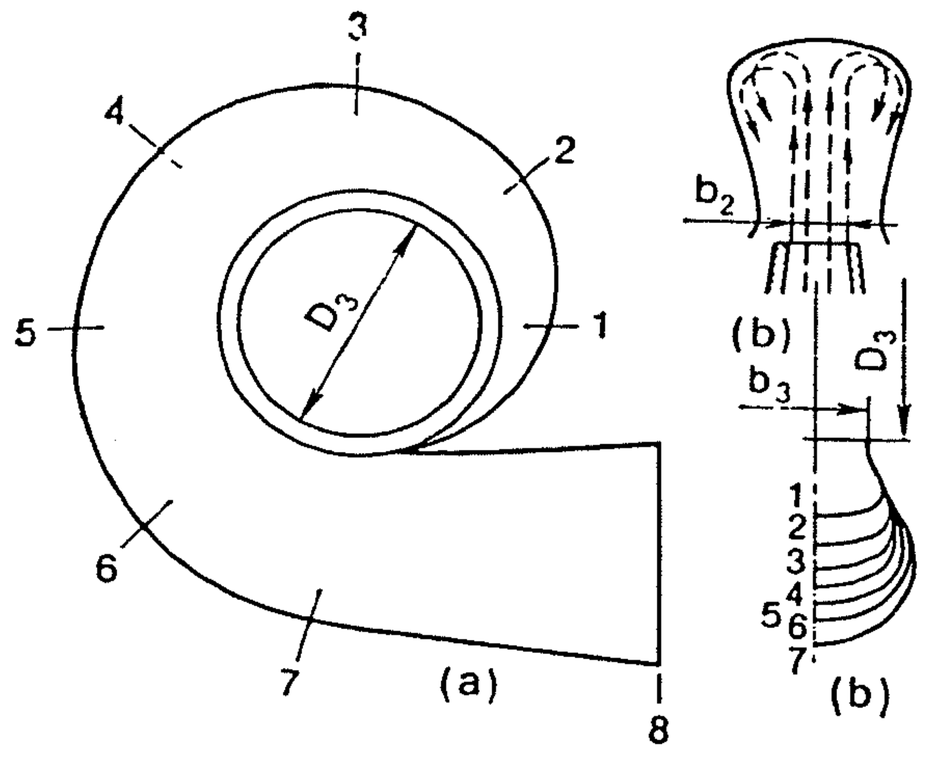


FIGURE 13.20. Centrifugal pump spiral outlet. (a) Longitudinal section; (b) cross-section.

works as contraction and pressure in sections 2 to 3 is larger than in sections 6 and 7. In this case radial force F_2 is directed to sections 6 and 7 (about 300°C to exit diffuser axis).

The value of radial force $F_r(N)$ can be determined approximately by the formula

$$F_r = K_r \left| 1 - \left(\frac{Q}{Q_{opt}} \right)^2 \right| \rho g H D_2 b'_2 \tag{13.7}$$

Here, K_r is the experimental coefficient (for centrifugal pumps, $K_r = 0.36$), ρ is the liquid density (in kilograms per cubic meter), H is head (meters), D_2 is diameter (meters) (Figure 13.18), b'_2 is the impeller height, $b'_2 = b_2 + 2\delta$ (b_2, see Figure 13.20, δ is the impeller disk thickness).

The radial force can also arise if there is misalignment occurs between impeller and casing sealing rings.

Example 13.1

Determine the radial force in the centrifugal pump (Figure 13.11): $D_2 = 2090$ mm, $b_2 = 300$ mm, $\delta_2 = 30$ mm, $H = 100$ m for water for two conditions, $Q/Q_{opt} = 0.6$ and $Q/Q_{opt} = 1.3$.

Solution

$$b'_2 = 0.03 + 2 \times 0.03 = 0.36 \text{ m}$$

From Equation 13.7,

$$F_r = 0.36 \mid 1 - 0.6^2 \mid 1000 \times 9.81 \times 100 \times 2.09 \times 0.36$$

$$= 170{,}060\ N \quad \text{or about 17 t}$$

$$F_r = 0.36 \mid 1 - 1.3^2 \mid 1000 \times 9.81 \times 100 \times 2.09 \times 0.36$$

$$= 183{,}345\ N \quad \text{or about 18 t}$$

From this it is understood that the radial forces are rather large.

The **axial force** of a pump impeller is created by hydrodynamic pressure acting on vanes, rims, and a hub. This force is of sufficient importance because it is transmitted through the shaft to axial bearings, thus affecting pump operation.

The value of axial force for centrifugal wheel (Figure 13.18) can be approximately determined as a difference between LH and RH rim paraboloids of pressure (Equation 13.5). For axial-flow pumps, axial

force P_{ax} due to flow action approximately equals

$$P_{ax} = K_{ax}\rho g H \frac{\pi D^2}{4} \tag{13.7a}$$

where H is pump head, D is impeller diameter, and coefficient K_{ax} is equal to 0.85 to 0.95.

There are different design solutions concerning wheel axial force. The simplest is not to provide any special measures and transmit the total acting axial force to the bearings. Examples of such design are given for centrifugal pumps in Figures 13.3 and 13.11, and for axial flow and mixed flow pumps in Figures 13.7 and 13.10.

Impellers of centrifugal pumps are often hydraulically balanced by providing additional sealing rings. This design is shown in Figures 13.1 and 13.13. In this case the pressure curves for the RH and LH sides are almost similar, and the axial force is substantially zero. This facilitates operation of the bearings but complicates the construction of the pump. What is most important, however, is that leaks from the delivery space to the inlet space increase almost twofold, i.e., volumetric losses increase.

An effective method to obtain a fully balanced pump rotor is to place on one shaft the identical wheels in pairs that move in the opposite direction. These are the double-entry pump (Figure 13.5) and the multistage pump (Figure 13.16).

For high head multistage sectional pumps, such as feed boiler pumps, in which axial force can reach tens of tons, a special arrangement to balance this force, shown in Figure 13.21 is used. It is comprised of an unloading disk (1) fixed on the pump shaft (2). The disk with pump casing (3) creates a chamber, which by narrow annular aperture δ_1 is connected with the outlet chamber of the last stage wheel (4) and by aperture δ_2 with the free flow cavity. Pressure p_1 depends on the pump head and pressure p_2 depends on the ratio of δ_1 and δ_2, hydraulic resistance. The dimension of δ_1 is constant, but δ_2 can vary in its

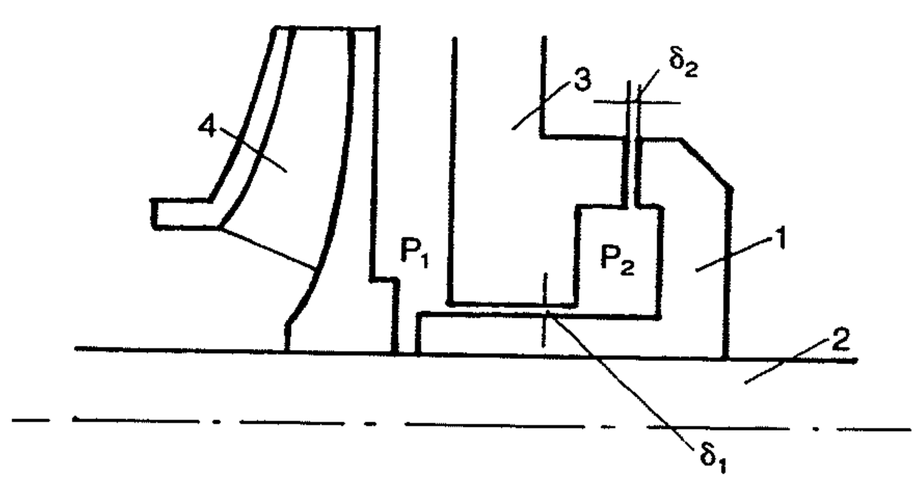


FIGURE 13.21. Multistage pump axial force balancing disk.

dependence on the shaft and the whole pump rotor axial displacement. Therefore, the pressure p_2 will automatically create the needed balancing force on the disk. This arrangement also serves as a high-pressure shaft sealing. It is clear that the system's operation is based on the flow through both apertures, which causes some additional energy losses.

CHAPTER 14

Cavitation in Pumps

14.1. CAVITATION AND PERMISSIBLE SUCTION LIFT

As outlined in Section 11.1, when a pump unit is running, the pump inlet pressure may be low, and high vacuum is frequently formed in the inlet pipe. The pressure is additionally decreased on the back of the impeller vanes (see Section 12.5). As a result, the absolute pressure in a certain part of the wheel, primarily in the inlet part, may decrease to the pressure of the saturated vapor of the liquid, at which cavitation takes place.

The physical nature of cavitation linked with the flow pressure drop to the pressure of saturated vapor $p_a \leq p_{s.v}$ and the formation of discontinuities (cavities) in the flow was considered in Chapter 7. The most important effects of cavitation (increased hydraulic losses, noise and vibration, intensive wear of surfaces) require that cavitation not be permitted to ensure normal pump operation. The no-cavitation condition according to Equation 7.2 is that the absolute pressure within the flow part exceeds the pressure of saturated vapour

$$p_{ai} > p_{s.v}$$

The difficulty in using this "straight" criteria is the absence of the reliable data concerning pressure distribution in pump flow. Taking this into account a "practical" dimensionless criterion, σ, the cavitation coefficient, was derived (Equations 7.2b and c), which could be used for

pump installations. In pump design practice, however, preference is given to the dimensional criterions net positive suction head (NPSH) or permissible vacuum suction lift, which as a rule are given in pump operation characteristics.

14.1.1. Permissible Vacuum Suction Lift

Let us conduct the following experiment. Reduce pressure in the pump inlet pipe (IP) in steps, i.e., increase H_v and maintain delivery Q and rotational speed n constant (the test procedures are outlined in Section 15.3). Measured head H, required power N, and efficiency η at each H_v (Equation 11.3).

Plot the curves for these values vs H_v (Figure 14.1). Points H, N, and η will be on the horizontal line up to a certain value of H_v, which indicates that the latter has no effect. However, after certain values of H_v, the deviations become implicit either in the form of a sharp surge (Figure 14.1a) or smooth changes prior to surge (Figure 14.1b).

Surge and variation in characteristics stem from cavitation appearing in the pump (it also may be proved by such symptoms as specific noise "cracking", increased vibration, and intensive ultrasonic oscillations). This allows us to determine the value of critical vacuum suction lift H_v^{cr}, above which the cavitation in the pump appears. Introducing a certain reserve (15 to 25%), we determine the permissible suction lift H_v^{per}.

With H_v^{per} being known, the no-cavitation condition in the pump may be represented by

$$H_v \leq H_v^{per} \tag{14.1}$$

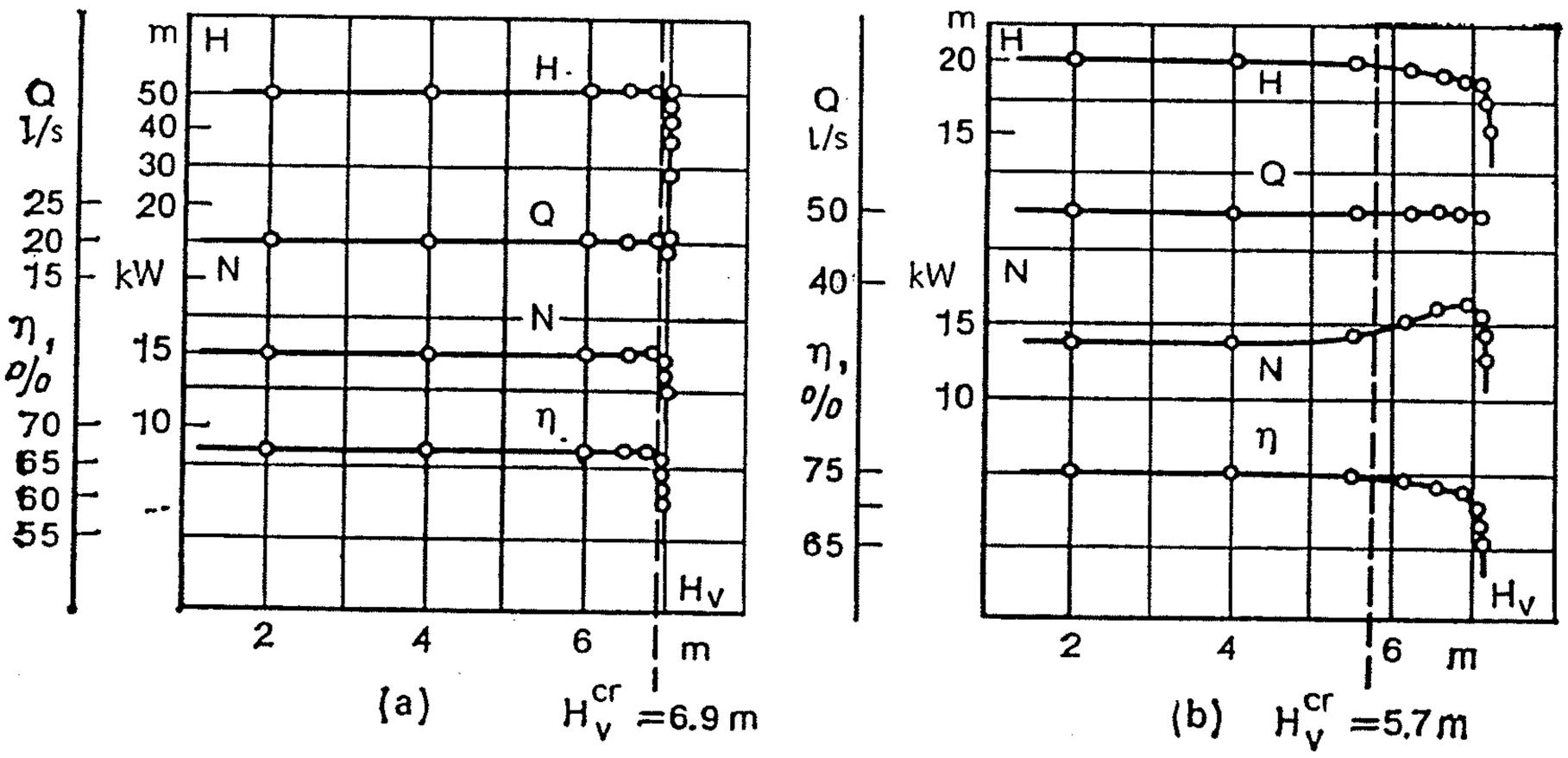


FIGURE 14.1. Determining pump critical vacuum lift.

According to Equation 14.1, the pump will exhibit no cavitation if the suction lift does not exceed its maximum permissible value. Using Equation 11.3 for the vacuum suction lift H_v we may proceed to geometric (static) suction lift H_s (see Figure 11.1)

$$H_v = H_s + \frac{v^2}{2g} + h_{suc} \leq H_v^{per} \tag{14.2}$$

Hence,

$$H_s \leq H_v^{per} - \frac{v_1^2}{2g} - h_{suc} \tag{14.3}$$

Thus, to preclude cavitation in the pump, the suction lift should be limited according to Equation 14.3.

H_v^{per} is usually given for normal atmospheric pressure at sea level and for cold water $\leq 35°C$. As the terrain elevation increases, atmospheric pressure drops by Δp_{atm}, according to Figure 1.5. It may be assumed approximately that (Equation 1.2)

$$\frac{\Delta p_{atm}}{\rho g} = \frac{\nabla}{900}$$

where ∇ is absolute elevation (meters) of the lower reservoir (tailwater, TW; above sea level $\nabla > 0$, below sea level $\nabla < 0$). If heated fluid is to be transferred, its saturated vapour pressure $p_{s.v}$ should be additionally taken into account (for water, $p_{w.v} = f(t)$; Figure 7.1).

More generally, the suction lift in view of the elevation and fluid temperature can be found from the formula

$$H_s \leq H_v^{per} - \frac{v_1^2}{2g} - h_{suc} - \frac{\Delta p_{atm}}{\rho g} - \frac{p_{s.v}}{\rho g} \tag{14.4}$$

Example 14.1

Determine permissible suction lift for a cradle-mounted pump in which $H_v^{per} = 8.0$ m at $Q = 48$ L/s (see Figure 15.1). Cold water and water at 70°C are being pumped. Absolute elevation of the lower reservoir (TW) $\nabla = 0$. For $Q = 48$ L/s and $v_1 = 3.0$ m/s, $h_{suc} = 1.5$ m.

Solution

1. From Equation 14.3:

$$H_s \leq 8.0 - \frac{3.0^2}{2 \times 9.8} - 1.5 = 6.1 \text{ m}$$

2. According to Figure 7.1, for water at 70°C, $p_{s.v} = 30$ kPa. Hence,

$$\frac{p_{s.v}}{\rho g} = \frac{30 \times 10^3}{1000 \times 9.81} = 3.05 \text{ m}$$

From Equation 14.4:

$$H_s \leq 7.0 - \frac{30^2}{19.6} - 1.5 - 3.05 = 3.05 \text{ m}$$

The result obtained shows that with increasing water temperature the permissible suction lift decreases. Should the absolute elevation of TW be higher, say +400 m, according to Equation 14.4, the permissible suction lift would decrease by $400/900 = 0.45$ m.

14.1.2. Net Positive Suction Head

To estimate the pump cavitation characteristics, use is made of NPSH, which indicates a surplus of absolute specific energy of liquid in the IP relative to specific energy determined by the pressure of liquid saturated vapor

$$\text{NPSH} = \left(\frac{p_{a1}}{\rho g} + \frac{v_1^2}{2g}\right) - \frac{p_{s.v}}{\rho g} \tag{14.5}$$

where $p_{a1}/\rho g$ is the absolute pressure head in the pump IP.

The critical value of $(\text{NPSH})_{cr}$ when incipient cavitation arises is determined experimentally in a special testing set (described in Section 15.3). The curves for $n = \text{const}$ and $Q = \text{const}$ of H, N, and η are plotted as functions of NPSH value. The critical point is determined at the point of abrupt or gradual but distinct change of the curves, similar to that shown in Figure 14.1 for determining H_v^{cr}.

It is interesting to note that a straight connection exists between NPSH and H_v. From Equations 11.2 and 11.3 it follows that $p_{a1}/\rho g = p_{at}/\rho g - H_v$. Substituting into Equation 14.5,

$$(\text{NPSH}) = \frac{p_{atm}}{\rho g} - H_v + \frac{v_1^2}{2g} - \frac{p_{sv}}{\rho g} \tag{14.5a}$$

Thus, both parameters are changing in opposite directions, and the coefficient of connection equals -1. Take as an example Figure 14.1b. For this centrifugal pump $H_v^{cr} = 5.7$, $v_1 = 3.8$ m/s, $p_{sv}/\rho g = 0.3$ m,

$p_{atm}/\rho g = 10.3$ m. Thus, $(\text{NPSH})_{cr} = 10.3 - 5.7 + 3.842/19.6 - 0.3 = 5.0$ m.

Using these curves we can find $(\text{NPSH})_{cr}$ as the critical value and by introducing a safety coefficient of 1.1 to 1.3, determine permissible NPSH which are given for pump operation characteristics. Knowing the NPSH the no-cavitation condition in the pump may be represented by the relation

$$(\text{NPSH})_{op} > \text{NPSH} \tag{14.6}$$

According to Equation 14.6, no-cavitation pump operation is ensured if operation or available $(\text{NPSH})_{op}$ will be greater than the permissible NPSH value.

Relate NPSH to suction lift H_s. According to Equation 1.3:

$$\frac{p_{a1}}{\rho g} = \frac{p_{atm}}{\rho g} + \frac{p_1}{\rho g}$$

Taking into account $p_1/\rho g$ from Equation 11.2, we obtain

$$\frac{p_{a1}}{\rho g} = \frac{p_{atm}}{\rho g} - \left(H_s + \frac{v_1^2}{2g} + h_{suc} \right)$$

Hence, according to Equation 14.5

$$(\text{NPSH})_{op} = \frac{p_{atm}}{\rho g} - H_s - h_{suc} - \frac{p_{s.v}}{\rho g} \tag{14.7}$$

Taking into account Equation 14.6 we obtain

$$\frac{p_{atm}}{\rho g} - H_s - h_{suc} - \frac{p_{s.v}}{\rho g} \geq \text{NPSH}$$

from which suction lift

$$H_s \leq \frac{p_{atm}}{\rho g} - \text{NPSH} - h_{suc} - \frac{p_{s.v}}{\rho g} \tag{14.8}$$

This is a general form of the formula accounting for atmospheric pressure, temperature, and properties of the liquid being transferred.

Example 14.2

Determine the permissible suction lift for an axial-flow pump according to the curve of Figure 15.2 (cold water) at delivery $Q = 5.2$ m^3/s, head = 15 m having NPSH = 12.0 m. Absolute elevation is TW = +300 m, $h_{suc} = 0.5$ m.

Solution

Find H_s from Equation 14.8

$$\frac{p_{atm}}{\rho g} = 10.3 - \frac{300}{900} = 10.0 \text{ m} \qquad \frac{p_{s.v}}{\rho g} = 0.3 \text{ m}$$

$$H_s \leq 10.0 - 12.0 - 0.5 - 0.3 = -2.8 \text{ m}$$

The pump should be installed so that the axis of the impeller vanes is 2.8 m below TW (with submersion).

It is possible to introduce for pumps the notion of the dimensionless cavitation coefficient in accordance with Equation 7.26. For this purpose let us accept that reference pressure $p_a = p_{a1} + \rho v^2/2$, where p_{a1} is absolute pressure and v_1 is velocity in pump entry cross-section 1–1 (Figure 11.1). Therefore, p_a is the flow volume specific energy J/m^3 (e_v). The denominator in Equation 7.2b $\rho v^2/2 = P_{pump}$ is pump pressure. In this case,

$$\sigma = \frac{(p_{a1} + \rho v_1^2/2) - p_{s.v}}{P_{pump}}$$

Here, $p_{s.v}$ is liquid saturated vapor pressure (for water, $p_{w.v}$). Accepting that $P_{pump} = \rho g H$, where H is pump head we gain

$$\sigma = \left(\frac{p_{a1}}{\rho g} + \frac{v_1^2}{2g} - \frac{p_{s.v}}{\rho g} \right) \Big/ H = \frac{\text{NPSH}}{H}$$

Using cavitation coefficient σ the suction lift H_s for a pump can be determined by

$$H_s \leq \frac{p_{atm}}{\rho g} - h_{suc} - \sigma H - \frac{p_{s.v}}{\rho g} \qquad (14.8a)$$

The last item is added if liquid temperature is higher than 20° to 30°C.

14.2. CONVERTING CAVITATION CHARACTERISTICS vs CHANGES IN PUMP ROTATIONAL SPEED

14.2.1. Vacuum Suction Lift

Assume vacuum suction lift H_v^{cr} is known for a certain n. Then,

$$\frac{\Delta p}{\rho g} = \frac{p_{atm}}{\rho g} - H_v^{cr} - \frac{p_{s.v}}{\rho g} \qquad (14.9)$$

is an additional dynamic drop of pressure over a portion from the IP to the wheel area, where the pressure is minimal and cavitation takes place. The dynamic action of flow is obviously proportional to the square of its velocity v. If we preserve the conditions of similarity according to Equation 12.14 and in view of Equation 12.3, then for a given pump

$$\frac{v}{v_1} = \frac{n}{n_1}$$

For new rotational speed n_1 we may write

$$\left(\frac{\Delta p}{\rho g}\right)_1 = \frac{\Delta p}{\rho g}\left(\frac{n_1}{n}\right)^2 \tag{14.10}$$

A new pressure differential will correspond to another value of H_{v1}^{cr}, which can be determined from Equations 14.9 and 14.10

$$\left(\frac{p_{atm}}{\rho g} - H_v^{cr} - \frac{p_{s.v}}{\rho g}\right)\left(\frac{n_1}{n}\right)^2 = \frac{p_{atm}}{\rho g} - H_{v1}^{cr} - \frac{p_{s.v}}{\rho g}$$

Hence,

$$H_{v1}^{cr} = \frac{p_{atm}}{\rho g} - \left(\frac{p_{atm}}{\rho g} - H_v^{cr} - \frac{p_{s.v}}{\rho g}\right)\left(\frac{n_1}{n}\right)^2 - \frac{p_{s.v}}{\rho g} \tag{14.11}$$

For normal atmospheric pressure $p_{atm}/\rho g = 10.3$ and cold water $< 35°C$ $p_{s.v}/\rho g = 0.3$ m. As a result, from Equation 14.10 we obtain

$$H_{v1}^{cr} = 10 - (10 - H_v^{cr})\left(\frac{n_1}{n}\right)^2$$

This ratio is also adopted for the permissible vacuum suction lift. Then,

$$H_{v1}^{per} = 10 - (10 - H_v^{per})\left(\frac{n_1}{n}\right)^2 \tag{14.12}$$

14.2.2. Net Positive Suction Head

Determine variation of the NPSH as a function of rotation speed. According to Equation 14.5, write

$$(\text{NPSH})_{cr} = \left(\frac{p_{a1}}{\rho g} - \frac{p_{s.v}}{\rho g}\right) + \frac{v_1^2}{2g} = \frac{\Delta p_{cr}}{\rho g} + \frac{v_1^2}{2g}$$

where $\Delta p_{cr}/\rho g$ is the critical pressure drop ΔH, and v_1 is velocity in the pump IP. However, because head ΔH, hence, v^2 are proportional to the square of the rotational speed under similar operating conditions (according to Equation 12.25), for new speed of rotation n_1 we obtain

$$(\text{NPSH})_{cr1} = (\text{NPSH})_{cr}\left(\frac{n_1}{n}\right)^2 \tag{14.13}$$

Applying this relation to the permissible values, we obtain

$$\text{NPSH}_1 = \text{NPSH}\left(\frac{n_1}{n}\right)^2 \tag{14.14}$$

Equations 14.12 and 14.14 point out that the cavitation characteristics of the pump—permissible vacuum suction lift H_v^{per} and permissible NPSH—change, even if the operating conditions or regime are similar. This is a shortcoming of these characteristics when compared with the coefficient of cavitation.

Example 14.3

The axial pump parameters determined in Example 14.2 were for $n = 485$ rpm (Figure 15.2). It is necessary to find the characteristics of the same pump, but with motor $n = 580$ rpm.

Solution

New discharge (Equation 12.26):

$$Q_1 = Q\frac{n_1}{n} = 5.2\frac{580}{485} = 6.2\ \text{m}^2/\text{s}$$

The suction losses will be larger:

$$h_{suc1} = h_{suc}\left(\frac{Q_1}{Q}\right)^2 = 0.5\left(\frac{6.2}{5.2}\right)^2 = 0.7\ \text{m}$$

The cavitation parameter, according to Equation 14.14:

$$\text{NPSH}_1 = \text{NPSH} \times \left(\frac{n_1}{n}\right)^2 = 12\left(\frac{580}{485}\right)^2 = 17.2\ \text{m}$$

New permissible suction lift (Equation 14.8):

$$\frac{P_{atm}}{\rho g} = 10 \text{ m} \qquad \frac{P_{sv}}{\rho g} = 0.3 \text{ m}$$

$$H_{s1} = 10 - 17.2 - 0.7 - 0.3 = -8.2 \text{ m}$$

The results show that increasing n leads to the sufficient growth of NPSH and diminishing permissible suction lift. In this case, the needed additional pump submergence is $H_{s1} - H_s = -8.2 + 2.8 = -5.4$ m.

14.3. PUMP SPECIFIC SPEED CAVITATION COEFFICIENT

One of the peculiarities of specific speed n_s according to Equations 12.28 is that it does not change under similar conditions for pumps of a given type. This property can be used to calculate the cavitation characteristic.

Critical cavitation margin $(\text{NPSH})_{cr}$ according to Equations 14.5 is a certain head created by the wheel which is proportional to the pump head. In fact, according to Equation 14.13, in view of the similarity formula (Equation 12.25), we have

$$\frac{(\text{NPSH})_{cr1}}{(\text{NPSH})_{cr2}} = \left(\frac{n_1}{n_2}\right)^2 = \frac{H_1}{H_2}$$

Hence,

$$(\text{NPSH})_{cr} = kH$$

For similar conditions k is constant. Thus, substituting $(\text{NPSH})_{cr}$ for H in Equations 12.28, we obtain the coefficient which will also be constant under similar operating conditions.

$$C = \frac{n\sqrt{Q}}{(\text{NPSH}_{cr})^{3/4}} \tag{14.15}$$

This is called the specific speed cavitation coefficient. When determining C for a double-entry wheel (Figure 13.15) half delivery is taken (0.5 Q).

Coefficient C offers a number of important advantages. First, it is constant for similar mode conditions, as mentioned above. Second, C varies slightly for impeller pumps of different types. For instance, under near-optimal conditions pumps with good cavitation characteristics have

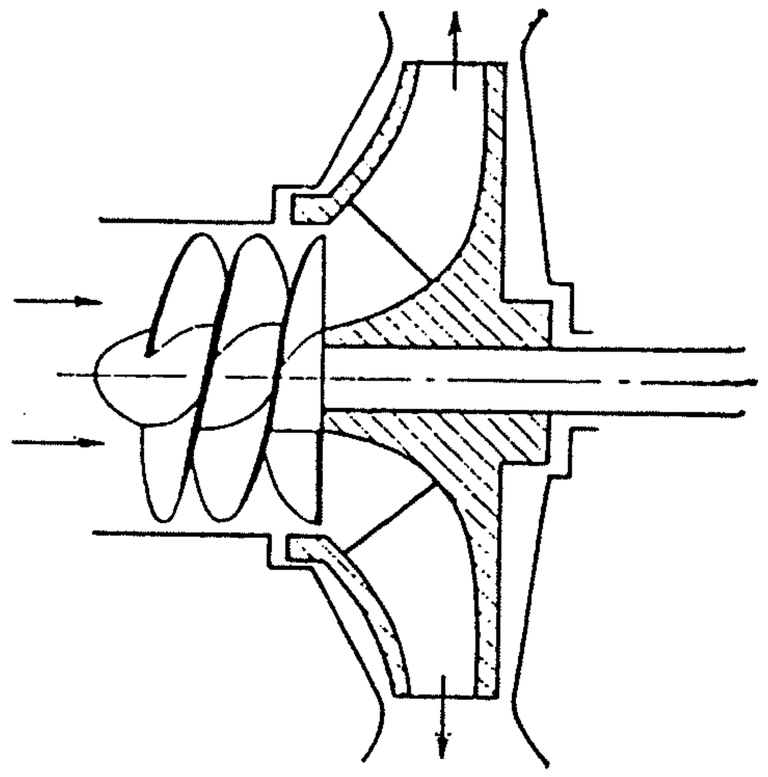


FIGURE 14.2. Centrifugal pump impeller with upstream auger.

$C = 160$ to 200, while for pumps with best cavitation properties it reaches 230 to 265. Thus, the specific speed cavitation coefficient makes it possible both to determine $(\text{HPSH})_{cr}$ and to estimate the cavitation characteristics of a pump.

To improve cavitation characteristics, increase permissible vacuum suction lift, and decrease permissible NPSH, the flow portion and (primarily) the impeller are subject to the appropriate treatment, which includes widening passages, decreasing flow velocity and curvature of stream lines. In other words, various measures are taken to increase pressure in the flow portion. Special devices are sometimes used for this purpose, for example, a centrifugal pump impeller with upstream auger (Figure 14.2) rigidly coupled with the impeller and rotating at the same angular velocity. The auger is a two- or three-thread screw which increases the pressure at the inlet to the wheel and increases the critical speed cavitation coefficient, according to Equation 14.15, to $C = 530$ to 900.

CHAPTER 15

Characteristics of Impeller Pumps

15.1. KINDS

An important stage in designing pumping stations or installations is the choice of pumps—the determination of their types, dimensions, basic parameters, required power of motors, and solution of problems involved in pump installation, the conditions of which are greatly dependent on the permissible suction lift. In the course of maintenance it is necessary to determine the most feasible operating modes of the pumps with respect to energy consumption, reliability, durability, operating conditions, and costs. To solve these problems, the designer should have fairly complete data on pump properties under different operating conditions. These data are represented in the form of pump characteristic curves.

In considering the impeller pump operating conditions, Chapter 12 states that the basic characteristics such as head, delivery, efficiency, etc. Depend on the shape and dimensions of the flow part (impeller) and operating conditions.

Specific relations of pump parameters vs operating conditions usually graphically represented are called pump characteristics. The characteristics, or performance curves, are provided for a pump of a given type (definite shape and dimensions of the flow part) at a constant rotation speed.

Figure 15.1 exemplifies a characteristic curve of a centrifugal cradle-mounted pump with an inlet diameter of 150 mm at $n = 1450$ rpm, an

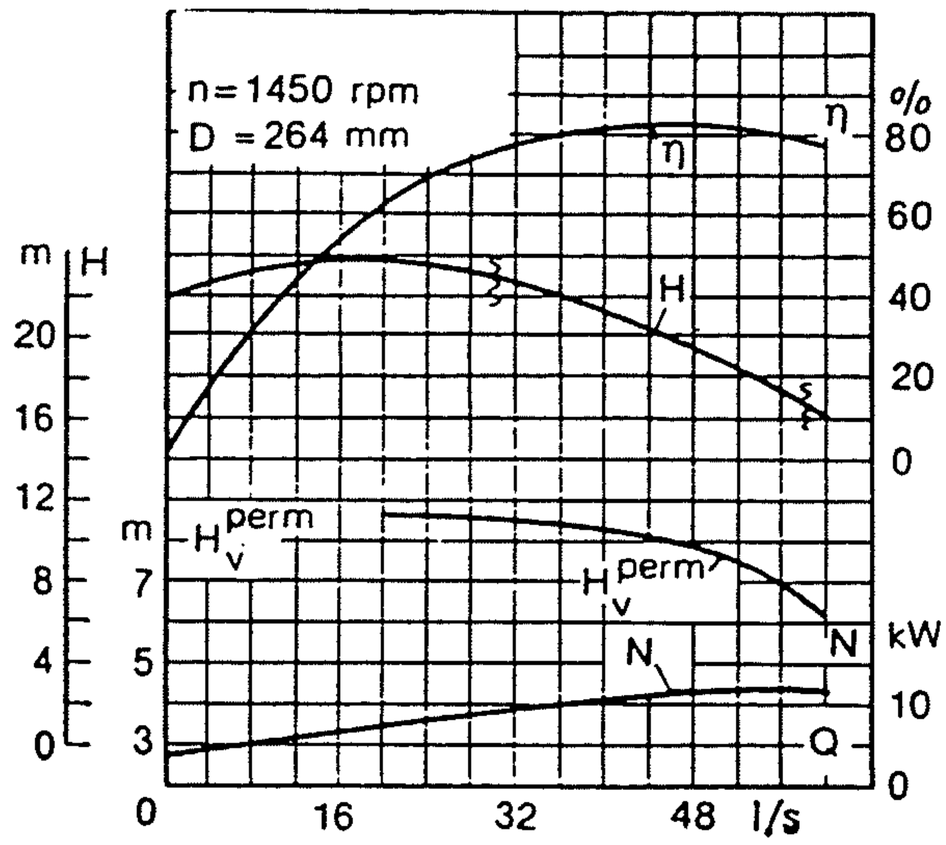


FIGURE 15.1. Characteristics of type K centrifugal pump.

external wheel diameter $D = 264$ mm, and specific speed $n_s = 120$ rpm (for regime with maximum efficiency). The characteristic curve represents the variation of all vital parameters H, η, N, and H_v^{per} vs delivery Q. The recommended range of operation of the pump, which is indicated on curve H, is between delivery values of 30 and 58 L/s. Here, H_v^{per} changes from 8.5 to 6.6 m. The required power at $Q = 0$ is 4 kW and at $Q = 58$ L/s it increases to 13 kW. Maximum efficiency under optimal conditions is 81%; within the recommended area of operation it decreases to 75 to 77%. Usually this area is selected so that the reduction of efficiency from η_{max} does not exceed 5 to 8%.

In Figure 15.1a the same characteristic as Figure 15.1 is represented in dimensionless form, using Equation 12.29a for calculation of the

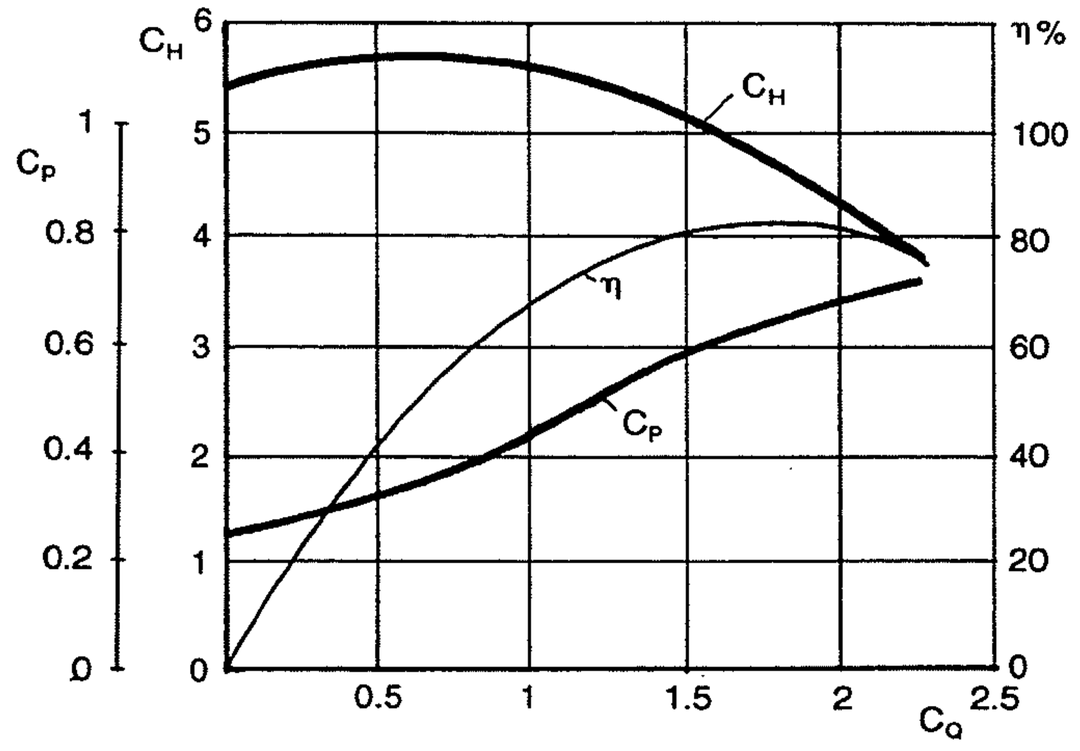


FIGURE 15.1a. Dimensionless characteristic of type K centrifugal pump.

coefficients C_Q, C_H, and C_p. This dimensionless form is more generalized, but for practical purposes ordinary dimensional characteristics are more convenient, and they are widely used.

Figure 15.2 illustrates a general characteristic of the adjustable blade axial-flow pump, type VAB at $n = 485$ rpm. The curves for different blade setting angles from $\varphi = -10°$ to $\varphi = +2°$ are traced in the field of coordinates Q, H. (Angle $\varphi = 0$ is assumed to be the impeller design angle, therefore, this angle curve usually passes near the maximum efficiency curve.) A peculiarity in these curves needs emphasis: with $Q = 0$, the head developed by the pump is 30 to 32 m; as delivery Q increases, the head drops rapidly and curves $H = f_H(Q)$ approach straight lines, but at portion $Q = 1.6$ to 3.2 m^3/s, they shoot upward, and the higher the φ goes, the greater the displacement. Furthermore, with increasing Q, the head lowers. This zone represents a working part of the curve (it is common practice to give only the working zone rather

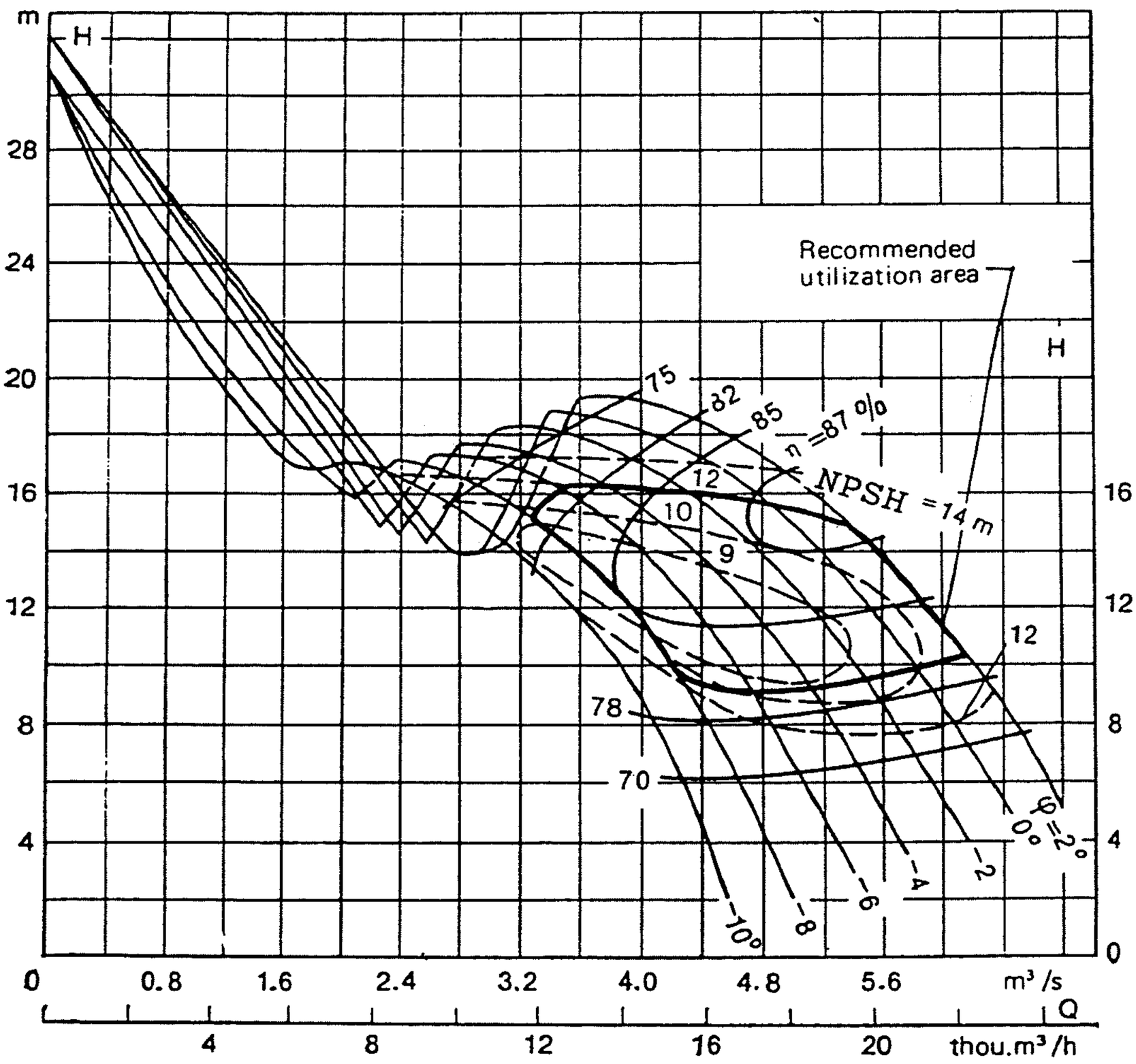


FIGURE 15.2. Characteristic of axial-flow adjustable blade pump, type VAB ($n = 485$ rpm, $D = 1100$ mm).

than the entire characteristic curve). The graph also includes the efficiency curves; in the optimal operation zone the efficiency is 87%. The recommended area of pump operation indicated by a thick line is located within angles from $\varphi = +2°$ to $\varphi = -8°$. The dotted-line curves of Figure 15.2 represent NPSH values. Note that the minimum value of NPSH is 9 m, which rises rapidly to reach 12 to 14 m. Thus, according to Equation 14.8, suction lift $H_s < 0$ indicates that the impeller should be submerged beneath the lower reservoir level tailwater (TW) (see Example 14.2).

The pump required power is not shown, but if H, Q, and η are known, it can be calculated for each curve point by using Equation 11.11.

15.2. THEORETICAL CHARACTERISTICS

Using Euler's equation and triangles of velocities, it is possible to determine the approximate relations that characterize variations in pump performance.

Assume that the flow at inlet to the wheel is axial ($\Gamma_1 = 0$, $\alpha_1 = 90°$). Then, using Equation 12.10, the theoretical head of a pump

$$H_t = \frac{u_2 v_2 \cos \alpha_2}{g}$$

The triangle of outlet velocities is shown in Figure 15.3a. The peripheral component of absolute velocity $v_2 \cos \alpha_2 = v_{2u}$ depends on

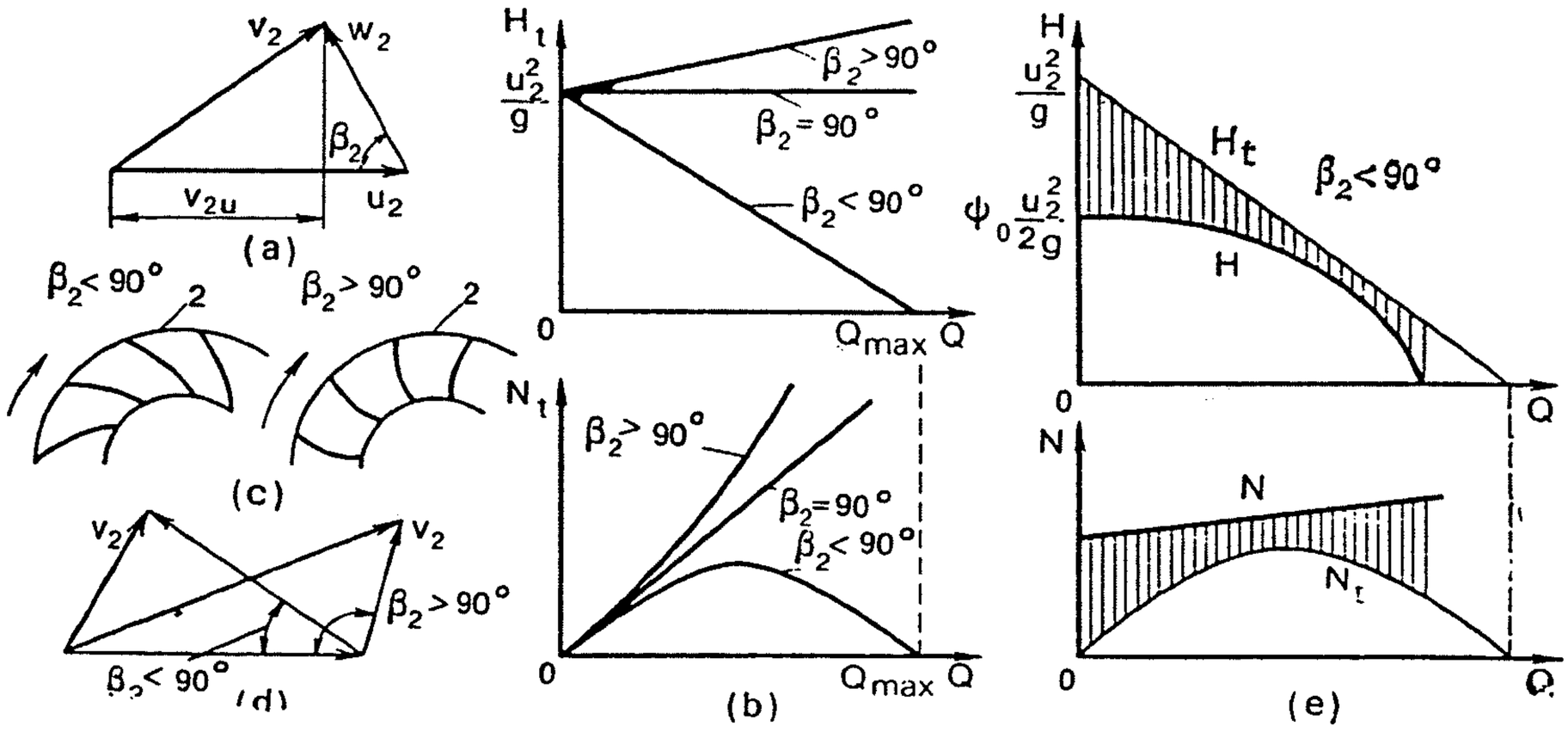


FIGURE 15.3. Theoretical characteristics of the impeller pump.

delivery Q and exit angle β_2, which for the sake of simplicity may be assumed to be equal to vane outlet angle δ_2. From Equation 12.4,

$$w_2 = \frac{Q}{\pi D_2 b_2 \psi_2 \sin \beta_2}$$

and from the triangle of velocities

$$v_{2u} = u_2 - w_2 \cos \beta_2 = u_2 - \frac{Q}{\pi D_2 b_2 \psi_2} \cot \beta_2$$

Substitute the values obtained in the initial relation to find

$$H_t = \frac{u_2^2}{g} - \frac{Q}{\pi D_2 b_2 \psi_2} \frac{u_2}{g} \cot \beta_2 \qquad (15.1)$$

Equation 15.1 is the sought-after theoretical head characteristic of the pump. It shows that the head is linearly dependent on delivery Q (Figure 15.3b). If $\beta_2 < 90°$ (the vane is deflected backward, Figure 15.3c), increasing Q decreases head H_t if $\beta_2 = 90°$, $\cot \beta_2 = 0$ and $H_t = u_2^2/g = \text{const}$. Finally, if $\beta_2 > 90°$ (the vane is deflected forward), increasing Q increases head H_t. This seems to allow an increase in the pump head, but as seen from the respective triangles of velocities (Figure 15.3d), increasing β_2 gives rise to v_2; i.e., the growth of kinetic energy at the impeller exit involves increases in hydraulic losses. Besides, an increase of β_2 may lead to an unstable operation. Therefore, β_2 in centrifugal pumps is usually between 20° and 35°.

Knowing H_t and Q, and again using Equation 11.9, determine the pump required power. Assuming it to be theoretical, write

$$N_t = \rho g Q H_t = \rho g Q \frac{1}{g} \left(u_2^2 - \frac{Q u_2}{\pi D_2 b_2 \psi_2} \cot \beta_2 \right)$$

After conversions, we obtain

$$N_t = \rho \left(u_2^2 Q - \frac{Q^2}{\pi D_2 b_2 \psi_2} u_2 \cot \beta_2 \right) \qquad (15.2)$$

Equation 15.2 is the theoretical power characteristic of the pump. It shows that power N_t changes along the parabola as a function of Q, and if $\beta_2 < 90°$, the maximum is at point $0.5Q_{max}$ (Figure 15.3b).

The theoretical characteristics do not allow for losses; therefore, they should differ from the actual characteristics. For comparison, Figure

15.3e represents theoretical head H_t and power N_t characteristics in relation to actual H and N at a constant rotational speed. Difference $H_t - H$ indicates hydraulic losses; difference $N - N_t$ indicates energy losses. Of interest are the values of heads for both characteristics at zero discharge $Q = 0$. Equation 15.1 gives

$$H_{t0} = u_2^2/g$$

while according to the actual curve

$$H_0 = \psi_0 u_2^2/2g \tag{15.3}$$

and for centrifugal pumps ψ_0 approaches 1. Thus, for $Q = 0$ the theoretical head is about twice the actual head.

15.3. EXPERIMENTAL DETERMINATION OF PUMP CHARACTERISTICS

Pump characteristics are obtained by testing separate full-scale samples, or if their dimensions and required power are too high, by testing geometrically similar models. In the latter case the model characteristics are converted to the full-scale values using similarity formulas 12.25 and 12.26.

A schematic diagram of a test set for getting characteristics of pumps is shown in Figure 15.4. Here, (1) is a pump, (2) is a delivery pipeline, (3) is a sealed tank partially filled with water (water level is checked against gauge glases (9)), and (4) is a suction pipeline. These components form a closed system operating with a constant volume of water. The pump is driven from a variable-torque motor (5). The stator of this motor rests on bearings and is free to rotate. Attached to the stator by bracket b is a pan for weights (c). The stator is balanced by counterweight d. When energized, the rotor tends to turn the stator in the direction opposite to the direction of load P (newtons). Torque T is calculated from the formula

$$T = Pr \tag{15.4}$$

where r is the arm (meters). To provide for varying rotational speed, use is often made of a dc motor. Rotational speed n is measured by a tachometer or counter, while required power N, with T and n being known, is found from the formula

$$N = T\omega/1000$$

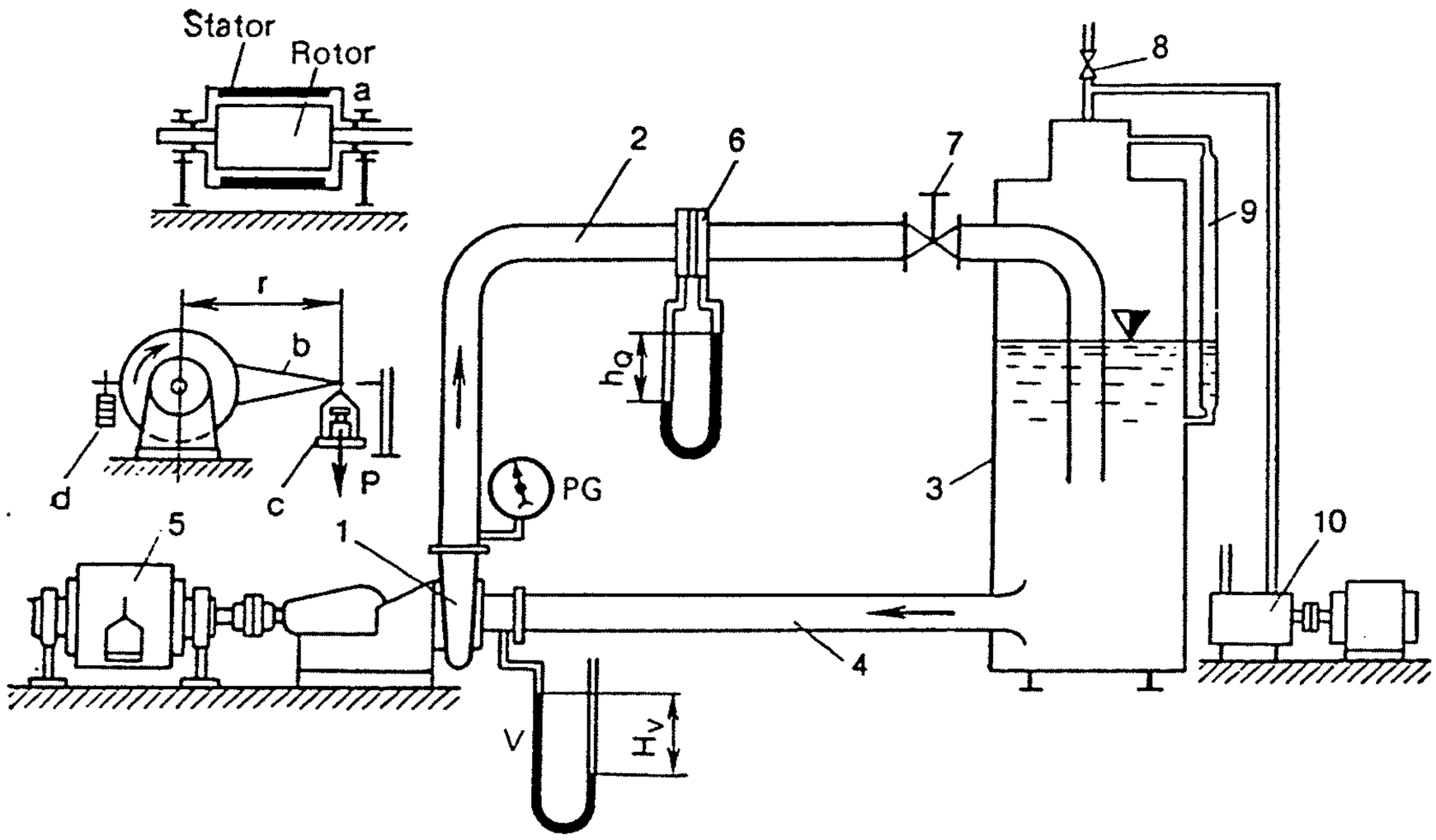


FIGURE 15.4. Test set for getting pump characteristics.

where $\omega = 2\pi n/60$, N in kilowatts T in newton meters, and ω is measured per second.

The head developed by the pump is determined against readings of pressure gauge h_p and vacuum gauge H_v (see Equation 11.7). Delivery Q is measured by a diaphragm (6), measuring nozzles, or Venturi meters. Pressure difference h_Q is measured using a differential pressure gauge and the flow rate is calculated from the formula

$$Q = C\sqrt{h_Q}$$

where C is the flowmeter coefficient. (Normal diaphragms and nozzles can be used without calibration, provided they are in line with appropriate rules.)

The discharge characteristic is usually taken at atmospheric pressure in the tank above water level (valve (8) is open). The pump rotational speed is maintained constant and operation is regulated by gate valve (7), whereby the discharge can be varied from zero to a certain maximum value (complete opening). The values of Q, N, H, and η are determined at each position of the gate valve. Efficiency for clean water is calculated from

$$\eta = 9.81QH/N \tag{15.5}$$

If it is impossible to maintain constant rotational speed during the test, the values obtained are recalculated for the required rotational speed according to the similarity formulas given in Chapter 12.

The cavitation characteristic of the pump is taken at the same test set in compliance with the principle mentioned in Chapter 14. After setting arbitrary operating conditions and closing the valve (8), curve points should be successively checked while vacuum is increased in the tank (3) above water level. Vacuum is formed by a special vacuum pump (10). Vacuum near the suction pipe H_v is measured by a vacuum gauge V. The discharge is maintained constant throughout the test by a gate valve (7). The measurements of each operation mode are used to plot the characteristic variation curve shown in Figure 14.1, and critical value H_v^{cr} or the critical value of NPSH is found from it.

15.4. DEPENDENCE OF PUMP CHARACTERISTICS ON SPECIFIC SPEED

The theoretical analysis carried out in Section 15.2 shows that the pump characteristic form is largely dependent on the shape of the wheel and other components of the flow part, and should change as a function of specific speed n_s. The wheel shape vs n_s graph is shown in Figure 12.8, while Figure 15.5 represents the form of respective characteristics H, η, and N as a function of delivery Q. We see that increasing the specific speed makes the H–Q curve lower more rapidly, and in high-speed pumps it displays an inflection point. The efficiency curves do not change as sharply. In the case of low-speed pumps, the efficiency curves are more convex and the high efficiency zone occupies a greater area of Q. As the specific speed increases, variations in efficiency with Q become more pronounced and the optimal efficiency zone becomes more narrow. The variation of H and η manifests itself in the form of power curves N. In low-speed pumps, the required power continuously increases with Q, and is minimum if $Q = 0$. In medium-speed pumps, an increase in Q decreases the variation of power, and at high Q it may

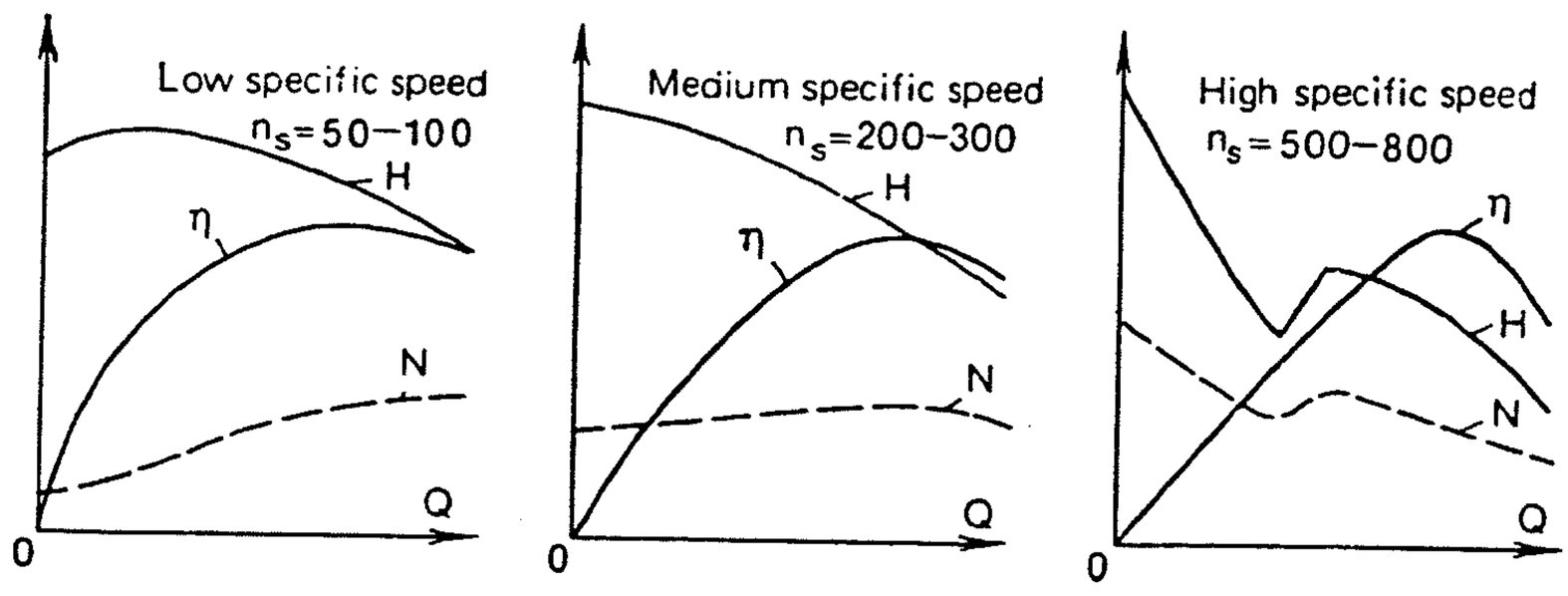


FIGURE 15.5. Characteristics of pumps of different specific speeds.

even drop, which may account for a more rapid decrease in the head. In high-speed pumps an increase in Q continuously decreases power in all sections except that of the H–Q curve inflection.

15.5. CONVERTING PUMP CHARACTERISTICS

Pump characteristics are given for a constant speed of rotation; however, in practice it is often necessary to determine the pump operating conditions for other speeds of rotation, i.e., to convert the pump characteristic from n to a new speed of rotation n_1. Conversion is performed using Equations 12.25 and 12.26, and because the diameter does not change, $D_1/D_2 = 1$. As a result, we obtain new values of head H_1 and delivery Q_1

$$H_1 = H(n_1/n)^2 \qquad Q_1 = Q(n_1/n) \tag{15.6}$$

According to Equation 15.6, when the rotational speed varies each point of the H–Q curve moves along a parabola (Figure 15.6, points A and A_1). Because the similarity conditions are not infringed upon, efficiency does not change, and it may be assumed for points A and A_1 that $\eta_1 = \eta$. Power N_1 is determined from Equation 11.11 and may be calculated from Equation 12.27. Finally,

$$N_1 = N(n_1/n)^3 \tag{15.7}$$

The values that characterize the cavitation properties of the pump are determined for new rotational speed n_1 from Equation 14.12 for H_v^{per} and from Equation 14.14 for NPSH.

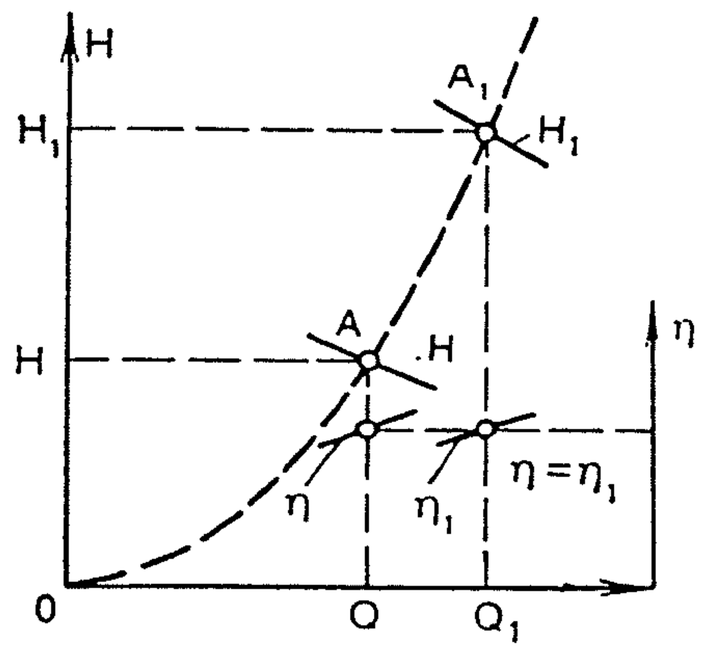


FIGURE 15.6. Displacement of characteristic point vs increase in pump speed.

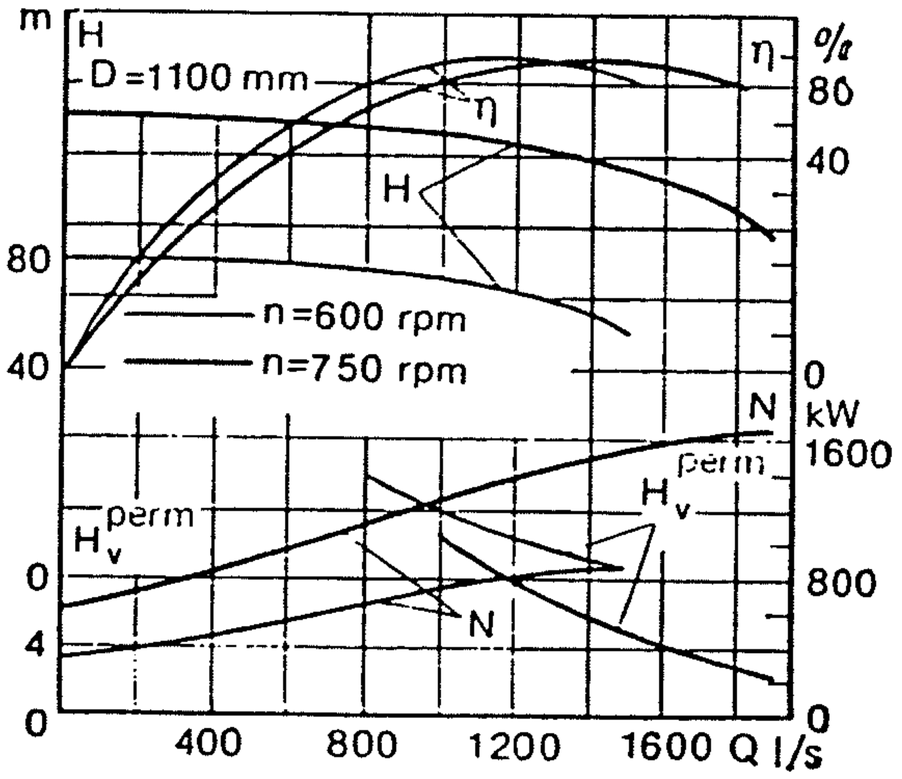


FIGURE 15.7. Centrifugal pump characteristics at $n = 600$ and 750 rpm.

Figure 15.7 illustrates the variation of the curve vs rotational speed when the characteristic of a type B vertical centrifugal pump, $n_s = 120$, is converted from $n = 600$ rpm to $n = 750$ rpm. It is worth to note that H_v^{per} decreases intensively (NPSH increases) in the high delivery zone.

In some special cases, for example, when the pump model characteristic is used, it is necessary to convert the characteristic when both n and D are changed. In principle, the procedure is the same as that described above, but in Equations 12.25 and 12.26 the ratios n_1/n_2 and D_1/D_2 are not equal to the unit. In this case, particularly if the difference between D_1 and D_2 is large, it is recommended that amendment $\Delta\eta$ be introduced into efficiency value. This can be done using the method developed from turbines (Equations 8.18 and 8.23), but for pumps the respective friction losses coefficient ε is less and it can be accepted that $\varepsilon = 0.5$. This may partially explain why for the same pump type (i.e. for the same specific speed n_s or n_{s1}) the efficiency increases for pumps with larger delivery Q (see Figure 12.8).

CHAPTER 16

Pump Selection

16.1. PUMP UNITS OF PUMP PLANTS AND INSTALLATIONS

As mentioned on several occasions in this volume, an important stage in designing pump plants and installations is the choice of *pump unit*, defined as a set consisting of a pump and an electric motor. The pump unit, to a considerable extent, determines the layout and dimensions of the building, particularly in large pump plants, as well as its construction, foundation depth, etc. This is illustrated in the following examples.

Figure 16.1 represents a pump plant with type VAB vertical axial-flow adjustable blade pumps (wheel diameter, 260 cm). Here, the wheel axis elevation is 0.0 m, the minimum elevation of the tailwater (TW) is +4.6 m, and the suction lift H_s is −4.6 m. Water is fed to the pump via a converging conduit (*1*) whose lower elevation is −6.0 m, which determines the substructure elevation of −8.0 m. The pump outlet pipe is connected to an inclined pipeline (*2*), diameter 3.5 m, by a tapered (diffusor) adapter. The pump casing is embedded in concrete to preclude vibration. Twenty-two similar pumping plants with axial pumps (D = 180 cm, total capacity, 350 MW) were constructed on the Irtysh–Karaganda (Russia) water supply canal (450 km long), which delivers about 2×10^9 m^3 of water per annum to a height of 420 m (the pump heads are 16 to 26 m).

Figure 16.2 illustrates a low-head pump plant with horizontal adjustable blade pumps, type HAB (wheel diameter, 220 cm). In this case, the unit axis elevation is 6.7 m and the minimum elevation of TW is 8.8

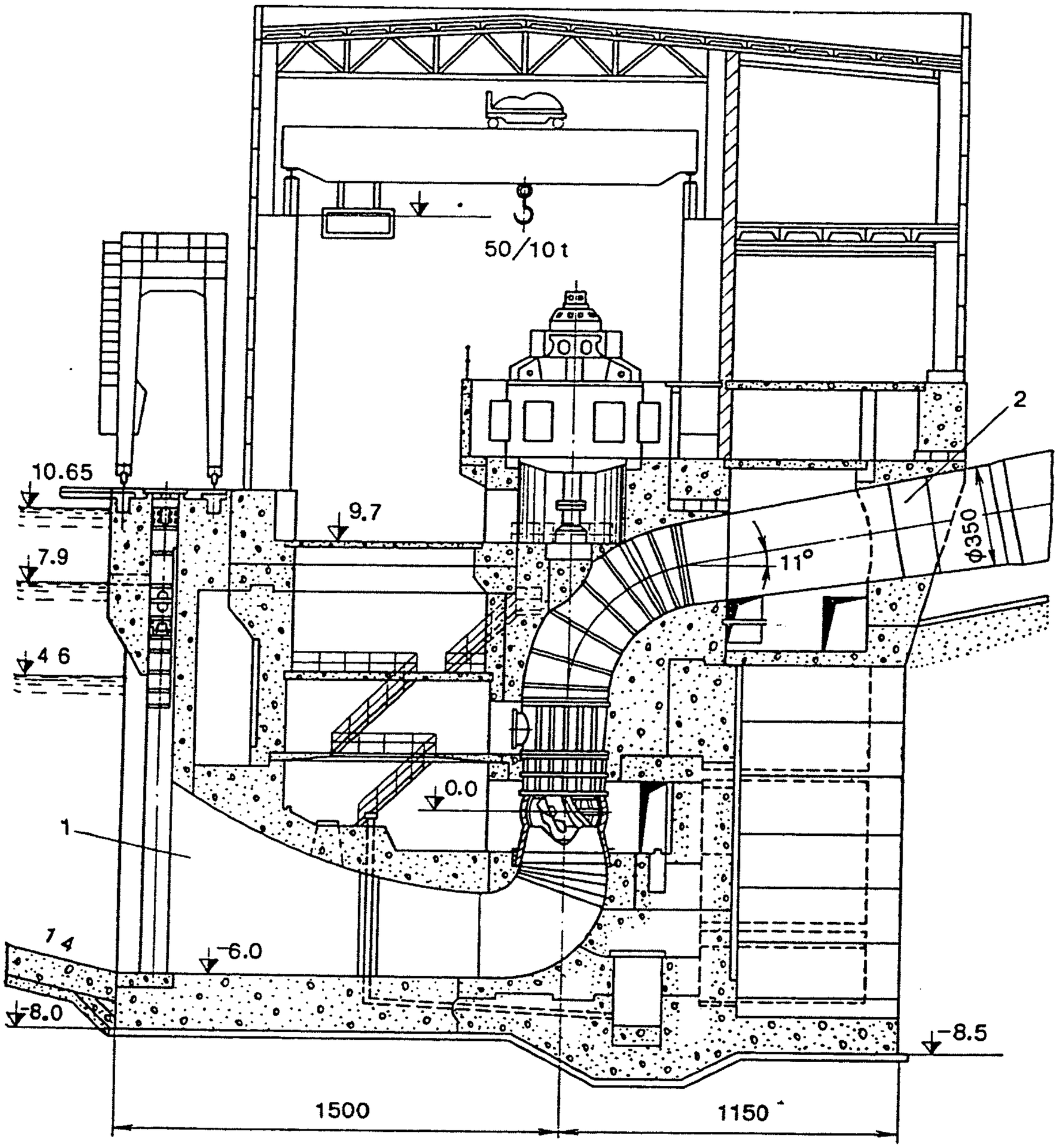


FIGURE 16.1. Pump plant with vertical axial-flow pumps.

m. Thus, the design suction lift to the axis is -2 m (to the wheel top $H_s = -0.9$ m). The pump plant extends 13.7 m along the unit axis, which is determined mainly by the dimensions of the inlet and delivery conduits and the top chamber with a radial gate. The low-head pump plant with a bulb-type pump unit is shown in Figure 13.9.

Figure 16.3 represents a high-head pump plant with vertical centrifugal pumps, type B. Here, the pump elevation is 0.0 m and the minimum elevation of TW is 2.7 m. The suction lift (-2.7 m) determines the elevation of the inlet conduit bottom (-2.6 m) and the depth of the pump plant substructure. The electric motor is arranged above the

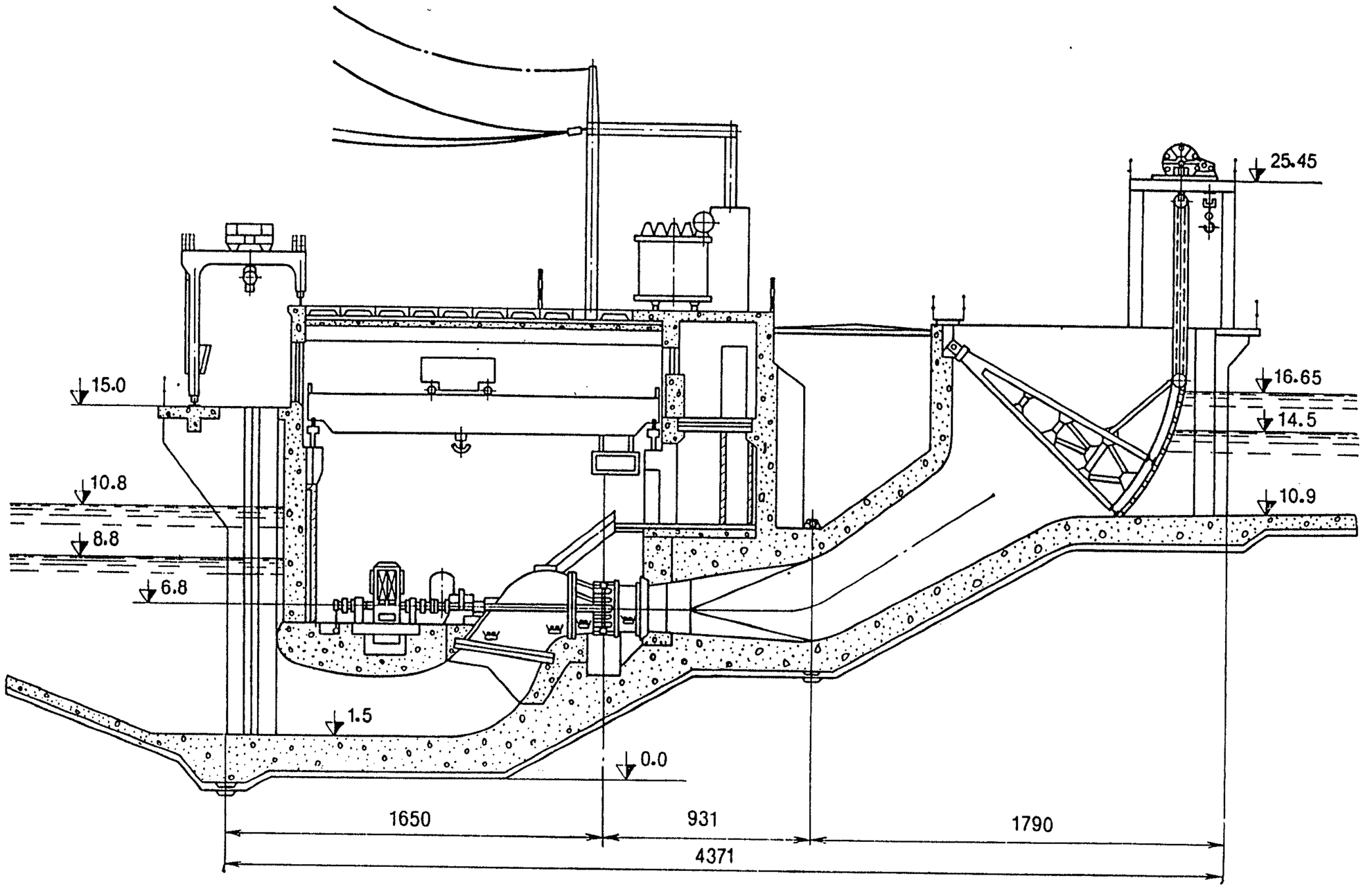


FIGURE 16.2. Pump plant with horizontal axial-flow pumps.

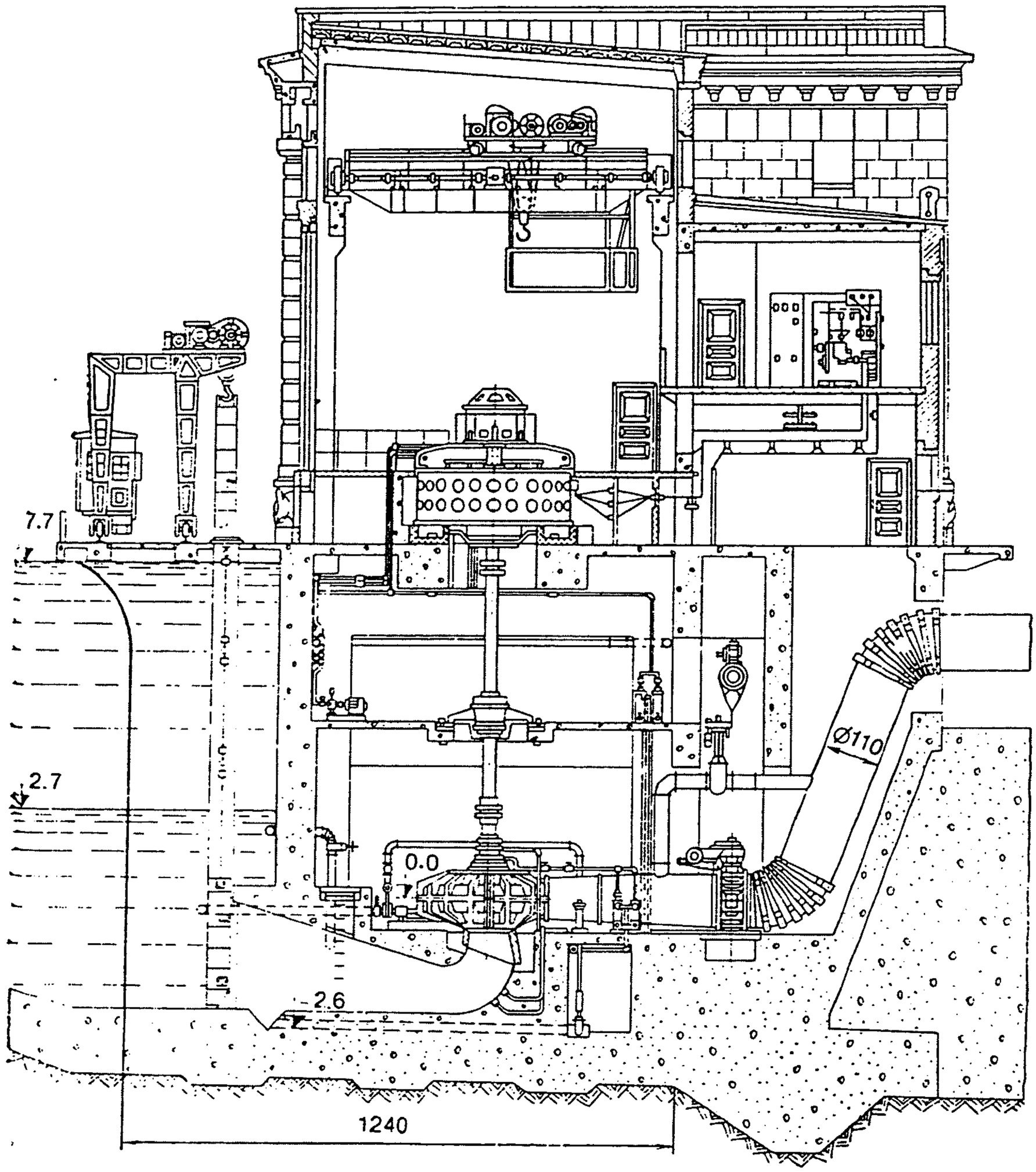


FIGURE 16.3. Pump plant with vertical centrifugal pumps.

maximum level elevation of the taylwater (TW), which has resulted in a considerable length shaft and has required installation of an intermediate bearing. The pump outlet pipe is connected via a conical adapter to the delivery pipeline, diameter 1.1 m, and is provided with a disk gate (the pump is started with the gate closed).

The pump installations, say for HEPP process water supply systems, draining, fire extinguishing facilities, etc., employ smaller pump units that do not greatly influence the building; nevertheless, in this case it is also important to select the most suitable types of pump and to properly assign methods of installation (elevation) and optimal operating conditions.

The basic initial data necessary for selecting the pumps are the required total discharge (delivery) and head. The object is to find the optimal option of the pumping unit (standard sizes and number) that will meet the service conditions and minimize outlays and operation costs.

16.2. CHARACTERISTIC OF WATER SYSTEM AND ACTUAL DELIVERY OF PUMP

As a result of analyzing the operation of a pump unit (see Section 11.1), we have found the expression for required head in the form (Equation 11.6a) of a characteristic of the water system, or pipeline, which is represented in the field of coordinates Q, H as a parabola originating from point $Q = 0$ and $H_r = H_{st}$, where H_{st} is static head at $Q = 0$ (Figure 16.4a). Coefficient K_r (dimensional s^2/m^5) for a given pipeline remains constant, and for the pipelines without branches it can be found using the formula

$$K_r = \frac{16}{\pi^2 2g}\left(\sum \lambda_i \frac{l_i}{d_i^5} + \sum \zeta_i \frac{1}{d_i^4}\right) \tag{16.1}$$

where l_i and d_i are the length and diameter of pipeline sections, respectively, and λ_i and ζ_i are coefficients of lengthwise and local friction losses.

The water system characteristic may take different forms. It may be represented by a steep parabola starting almost from the coordinate point of origin, when head H_{st} is low and the main head is spent for overcoming losses (Figure 16.4b, curve H_{r1}); it may be very flat when the pipeline is short, or its section is large and losses are small while the main head is spent for lifting water (Figure 16.4b, curve H_{r2}).

In considering the theoretical (see Figure 15.3) and experimental (see Figures 15.1 and 15.2) characteristics of pumps, clearly prove that the

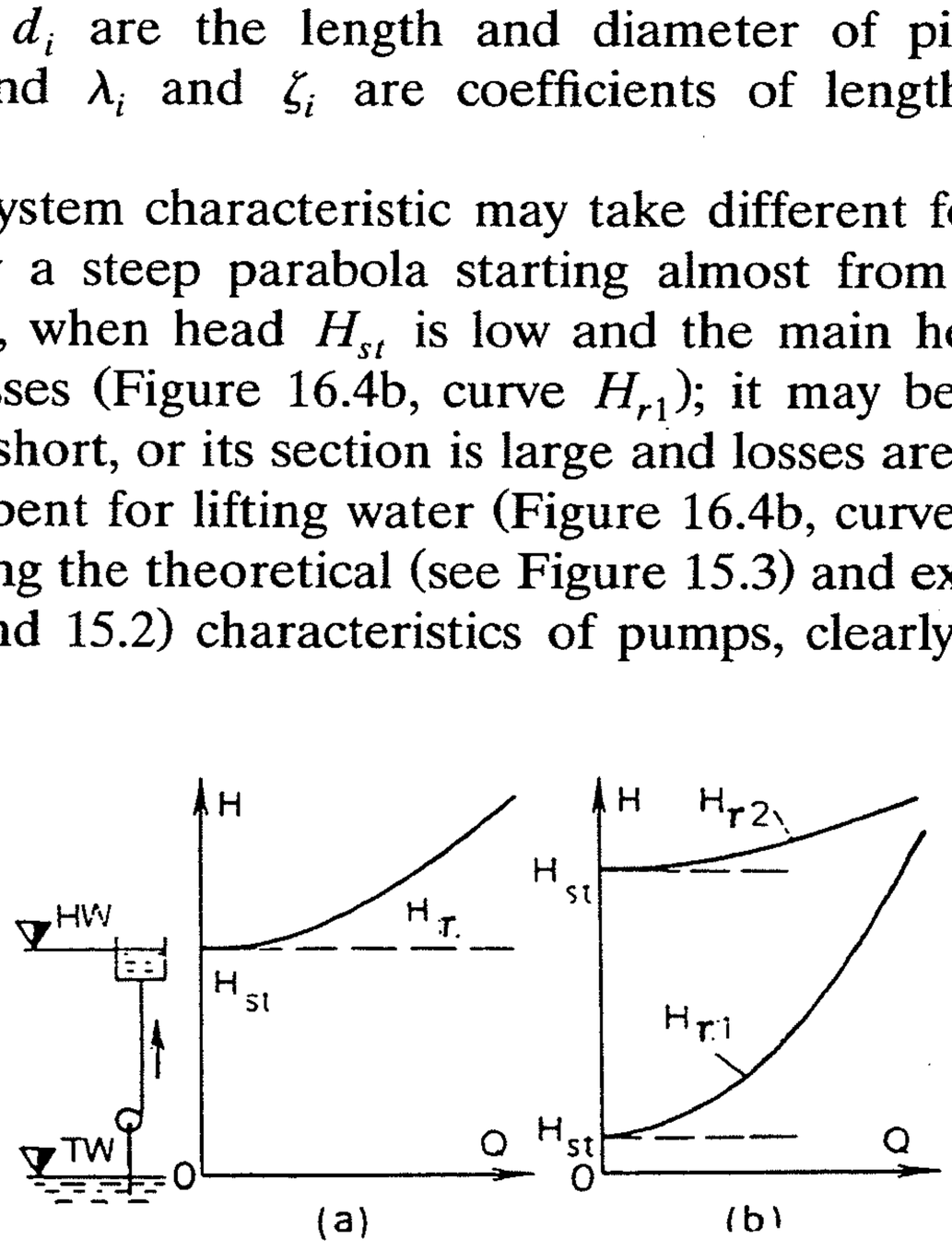


FIGURE 16.4. Characteristics of water supply system (pipelines).

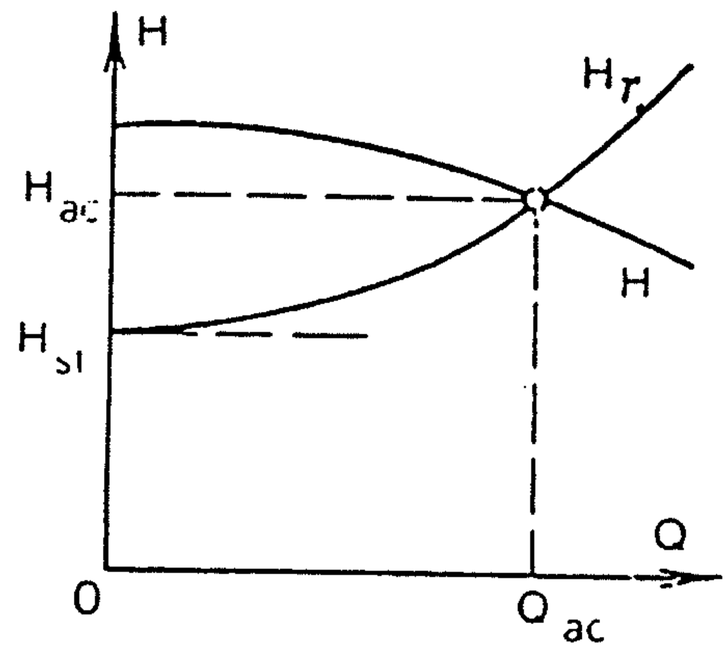


FIGURE 16.5. Determining actual operational mode of pump.

head developed by the impeller pump is greatly dependent on the delivery. Therefore, even when the pump characteristic is known, it is impossible to predict the actual delivery when operating with a given pipeline. The actual delivery Q_{ac} may be determined only by combining two characteristics, $H-Q$ curve of the pump and H_r-Q of the network, and the operating conditions will be determined by their intersection point (Figure 16.5). This point makes it possible to find actual head H_{ac}, efficiency, H_{υ}^{per}, and the required power. It is obvious that variation of the network characteristic, for instance, because of changes in the pipeline length or H_{st}, will change actual delivery Q_{ac}, while excessive increase of H_{st} may zero the delivery (if $H_{st} > H_{Q-0}$).

16.3. NOMENCLATURE OF PUMPS

The pumps of each type are manufactured in a wide variety of standard sizes corresponding to the required range of characteristics, which forms the nomenclature of pumps or range charts. Establishing the nomenclature is a technico-economical problem that is solved with due regard for production and operation costs, including expenditures on electricity. To optimize the solution, designers strive to widen the sphere of application of each standard size pump. This is achieved by several methods:

1. Widening the sphere of operation as regards Q; i.e., allowing considerable deviations from optimal conditions may be advisable within certain limits, but excessive deviations lead to such an intense drop in efficiency that the cost of excessive energy consumption exceeds the economy in production costs.
2. Changing the blade setting angle in the axial-flow and mixed-flow pumps makes it possible to use each standard size for a fairly wide

range of deliveries and heads. For instance, the adjustable blade pump VAB, with blade setting angles of from $+2°$ to $-8°$ (see Figure 15.2), may be advantageously used with deliveries from 4.0 to 6.0 m^3/s and heads from 10 to 16 m at the same speed of rotation.

3. In type K, D and B centrifugal pumps (see Figures 13.1, 13.5, and 13.11), to additionally displace the characteristic (primarily the head curve), the wheel with vanes is turned over the diameter to decrease D. Decreasing the diameter by a maximum of 15 to 20% does not involve great drops in efficiency (1 to 2% maximum).

Because according to Equation 15.1 the head is proportional to squared peripheral velocity, the following approximate relation may be used to find H_{turn}

$$H_{turn} = H(D_{turn}/D)^2 \tag{16.2}$$

When turning the wheel of a low specific speed pump, the delivery decreases approximately in line with the diameter ratio

$$Q_{turn} = QD_{turn}/D \tag{16.3}$$

It should be borne in mind that the wheel is turned by the manufacturer and is indicated in the specifications and nomenclatures of the appropriate standard sizes of the pumps. For instance, a characteristic of a centrifugal double-entry pump, type D, with a turned wheel (types a and b) is shown in Figure 16.6. Here, the normal wheel exit diameter is 432 mm; the turned wheel diameters are 395 mm (a) and 355 mm (b). The head H and power N decrease accordingly and rather intensely. The efficiency and delivery displacements are small. The permissible vacuum suction lift H_v^{per} and NPSH at the same delivery do not change. This is attributed to the fact that the conditions of entry to the wheels do not change after turning.

In view of the wheel turning, each standard size of the pump includes two or three head–delivery curves displaced heightwise. In reference to the recommended areas of operation alone, it may be assumed that each standard size of pump in the field of Q, H covers a certain region defined by a curvilinear rectangle, as that shown in Figure 16.7 for a given pump, type D, $n = 1450$ rpm. The areas of employment of the axial-flow and mixed-flow pumps in view of the vane angle φ variation range (see Figure 15.2) have similar shapes.

16.3.1. Pump Designation

Each manufacturer uses its own system for designating pumps; however, on most occasions, the designation (representation) of the

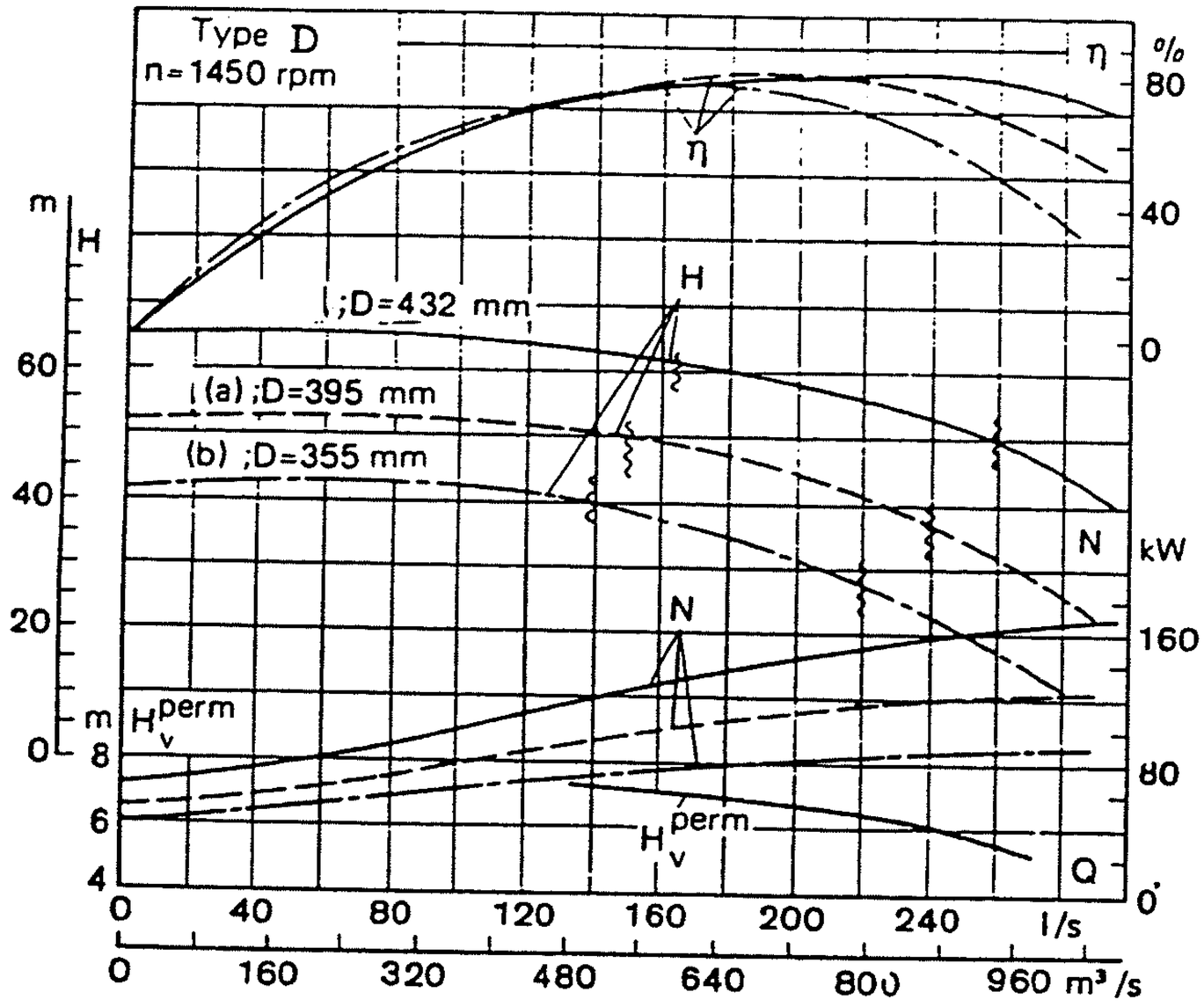


FIGURE 16.6. Characteristic of centrifugal pump with turned wheel.

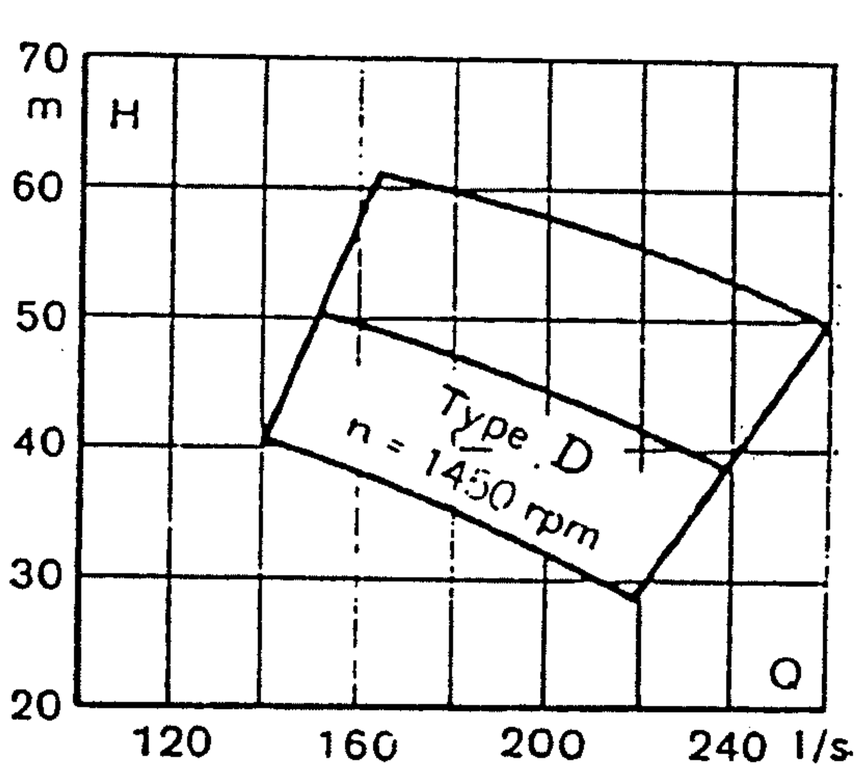


FIGURE 16.7. Type D pump application area.

standard size includes the following data:

1. Pump type can be marked by the letters K, cradle mounted; KM, cradle-mounted mono-block; D, double-entry; B, centrifugal vertical; VAF, vertical axial-flow with rigidly secured blades; VAB, vertical axial-flow adjustable-blade; HAB, axial-flow adjustable blade horizontal.
2. Design delivery, m^3/hr (or for very large pumps m^3/sec), corresponding to the maximum diameter of the wheel under near-optimal conditions (maximum efficiency).

3. Design head, meters, of the column of liquid being transferred, for conditions set forth in item 2.
4. Characteristic size (optional). This is either the delivery pipe diameter (B type pumps), or the wheel diameter (axial-flow pumps).

In addition, the wheel diameter D_w is indicated, which is particularly important if the pump comes with a wheel that can be turned to different diameters, as is rotational speed n (revolutions per minute).

16.3.2. Nomenclature of Impeller Pumps

The nomenclatures of pumps in the form of the Q, H field showing the areas of employment of all standard sizes of a given pump, are represented in appropriate catalogs and reference books which usually set forth the characteristics and required dimensions of the pumps. The pump nomenclatures are used in selecting the pumps and designing pump plants and installations. Examples of the nomenclatures of the impeller pumps are presented below.

16.3.2.1. Centrifugal Cradle-Mounted Pump

This pump, used for water, is shown in Figure 16.8. These pumps can be used within the delivery range of 5 to 300 m^3/h (1.5 to 90 L/s) and

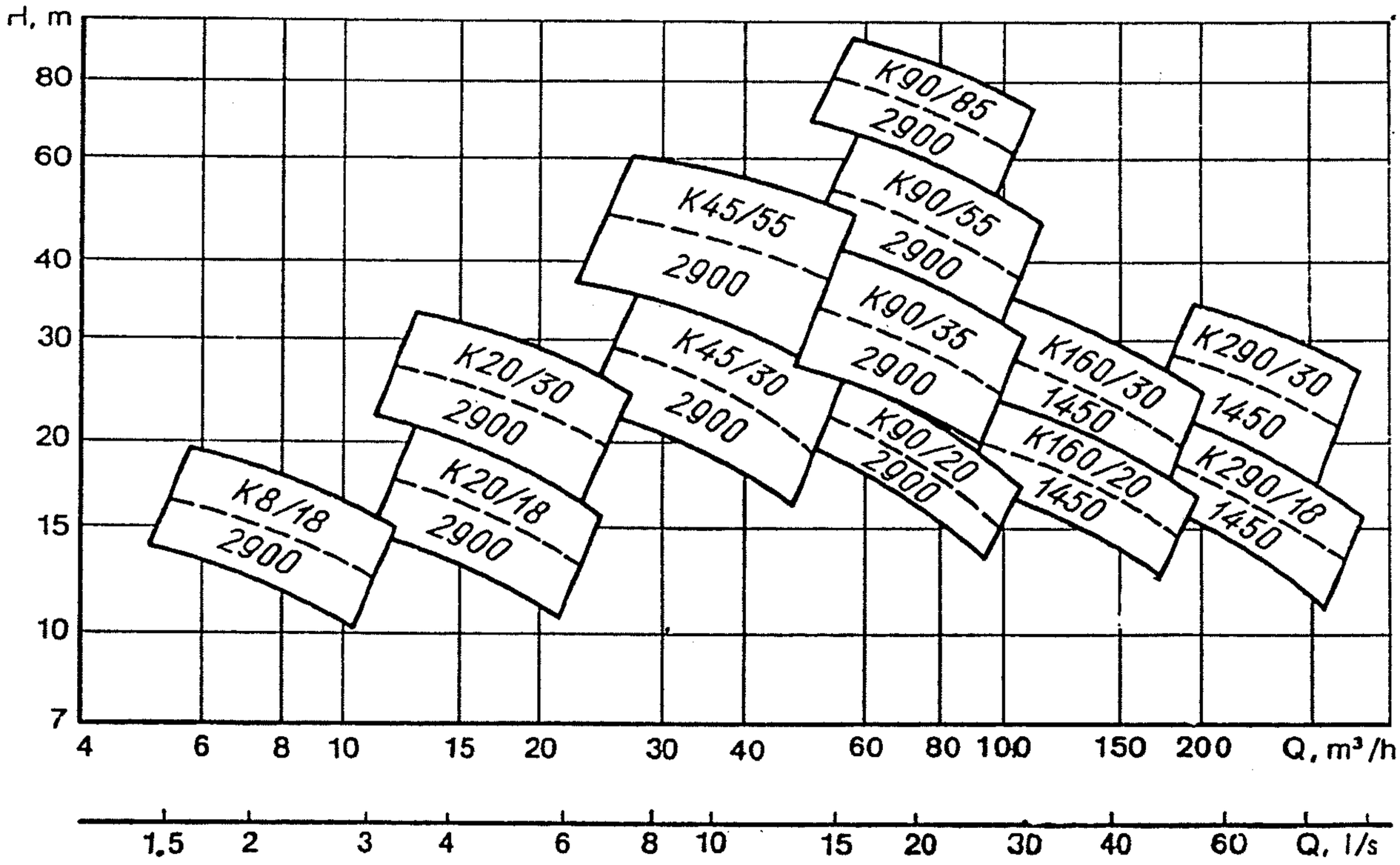


FIGURE 16.8. Nomenclature of types K and KM centrifugal pumps.

heads of 30 to 60 m. The pumps come with a separate cradle (type K; see Figure 13.2) and integrated with an electric motor (monoblock, type KM, see Figure 13.3).

16.3.2.2. Centrifugal Double-Entry Pump, Type D

This pump, used for water, is shown in Figure 16.9. The pump to be used within the delivery range of 200 to 12,500 m^3/s (5 to 3500 L/s) and heads from 15 to 120 m. To reduce the variety of standard sizes some pumps are delivered with decreased speed motors. In this case the actual delivery and head are lower than those that are rated, included in the designation. An example is the type D pump 3200-75 (730 rpm).

16.3.2.3. Centrifugal Vertical Pump, Type B

This pump (see also Figure 13.11) is shown in Figure 16.10. This pump, with an entry mouth diameter of 600 to 2400 mm, is intended to be used within the delivery range of 1.2 to 25 m^3/s and heads from 30 to 100 m.

16.3.2.4. Vertical Axial-Flow Pump, Types VAF and VAB

These pumps have fixed impeller vanes. The vertical adjustable blade, type VAB is shown in Figure 16.11 (see also Figure 13.7) (in the

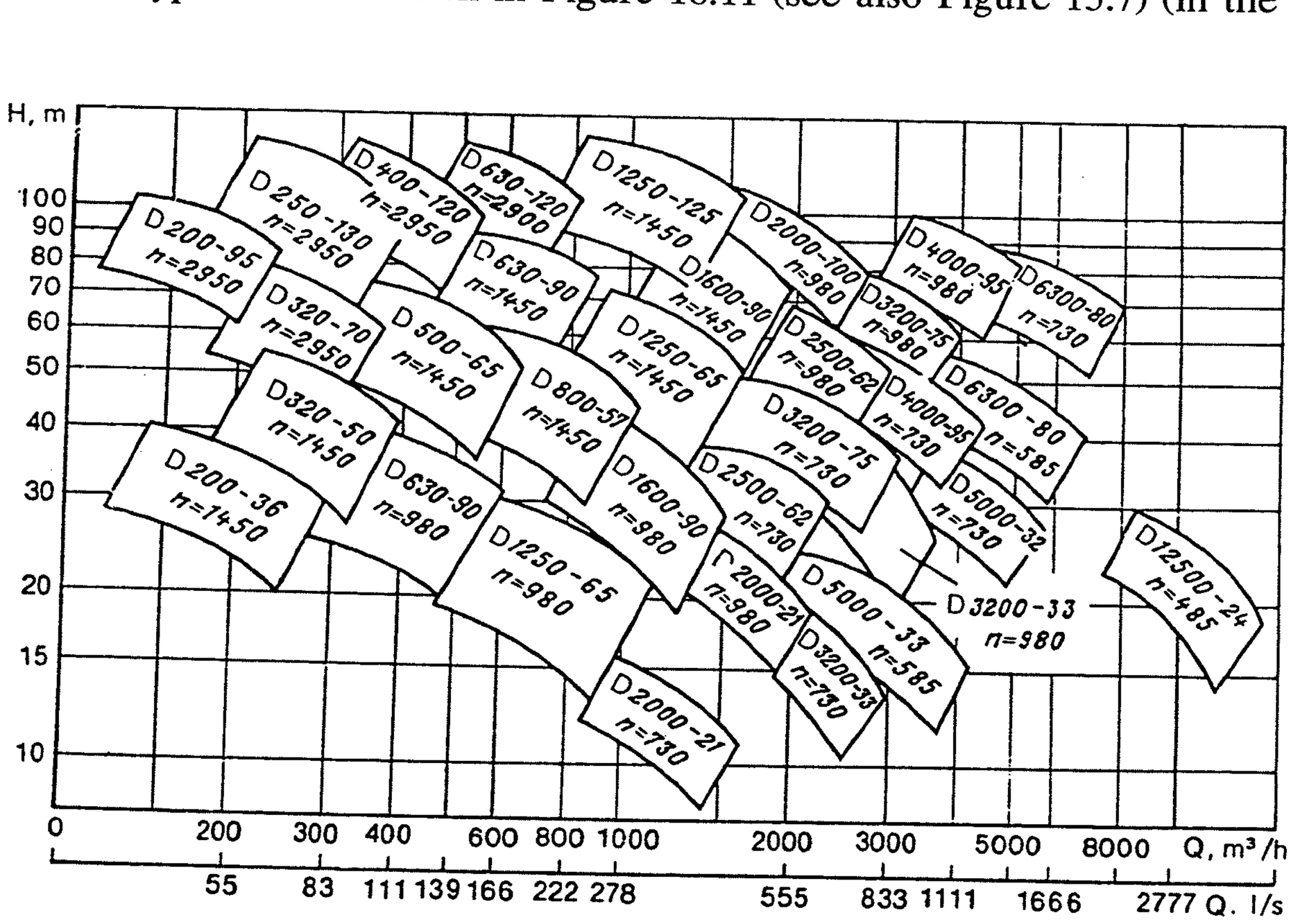


FIGURE 16.9. Nomenclature of type D centrifugal pumps.

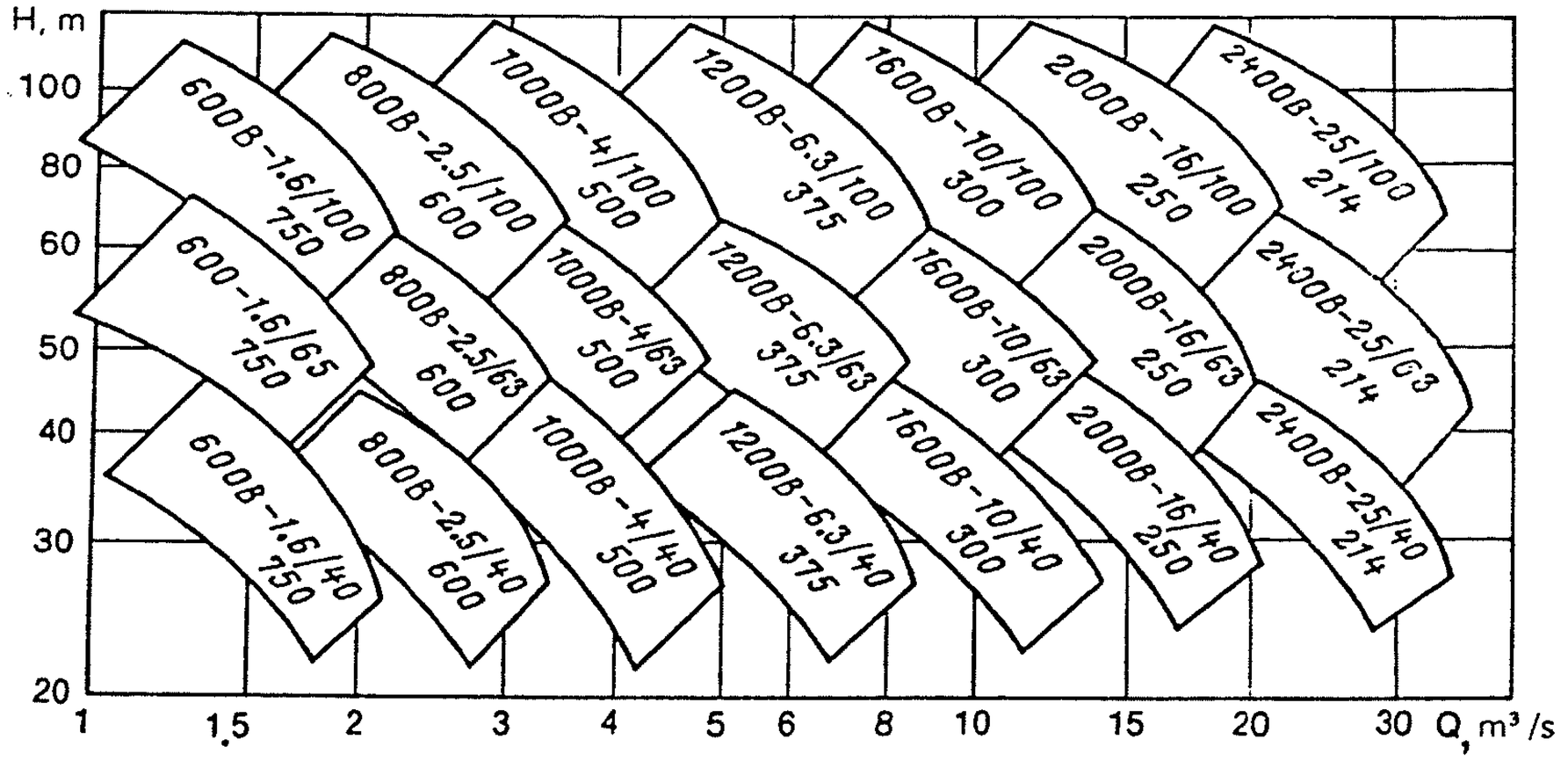


FIGURE 16.10. Nomenclature of type B vertical centrifugal pumps.

figure the first mark indicates the type number, then wheel diameter, and then n (revolutions per minute)). The nomenclature includes axial-flow vertical pumps with wheel diameters from 47 to 260 cm that operate within the delivery range of 0.6 to 40 m^3/s and a head range of 3 to 15 to 25 m.

16.3.2.5. Horizontal Axial-Flow Pump, Type HAF

This type also has fixed impeller vanes and is shown in Figure 16.12. These pumps, which have wheel diameters of 15 to 70 cm, are operable

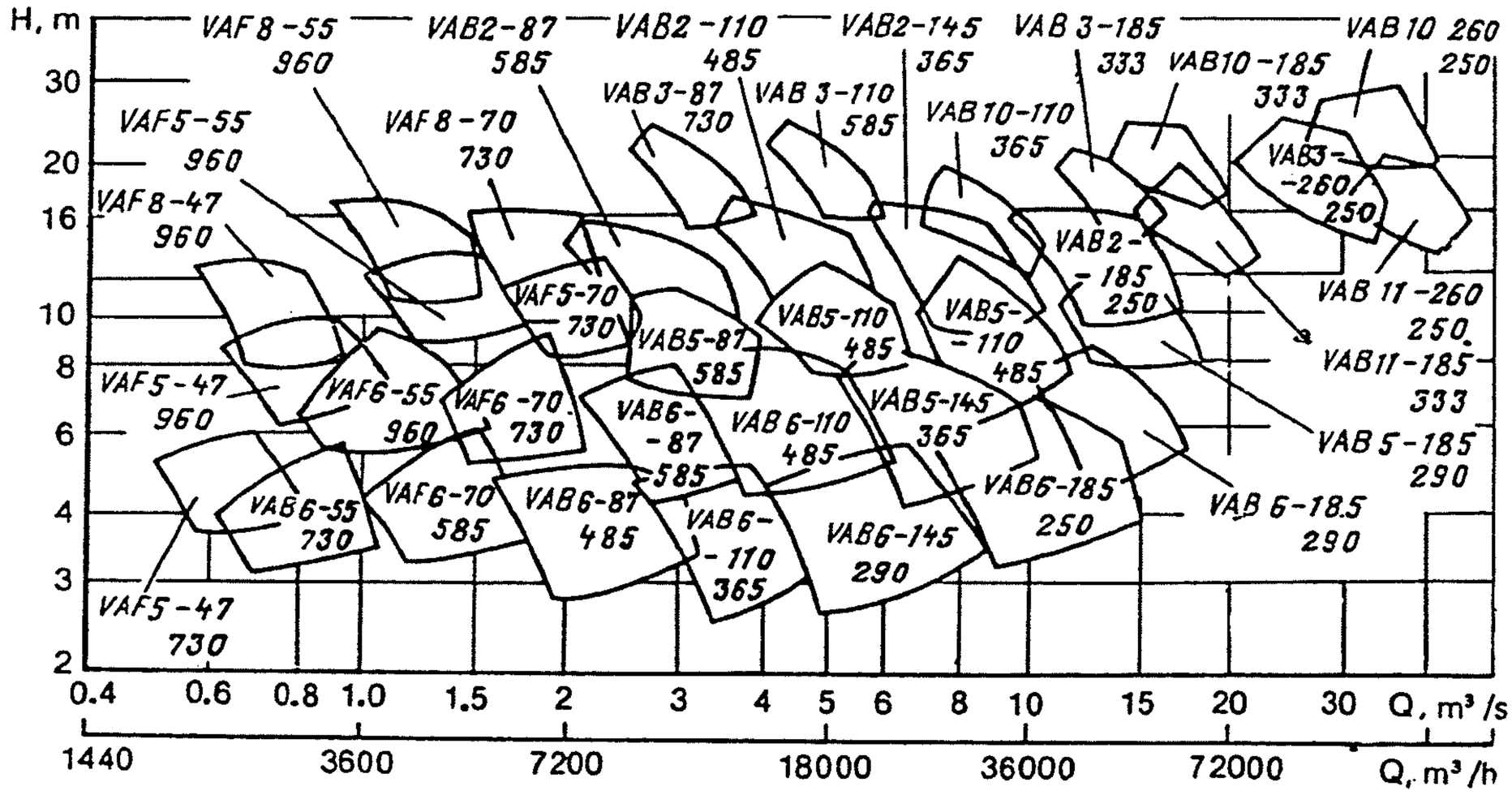


FIGURE 16.11. Nomenclature of types VAF and VAB vertical axial-flow pumps.

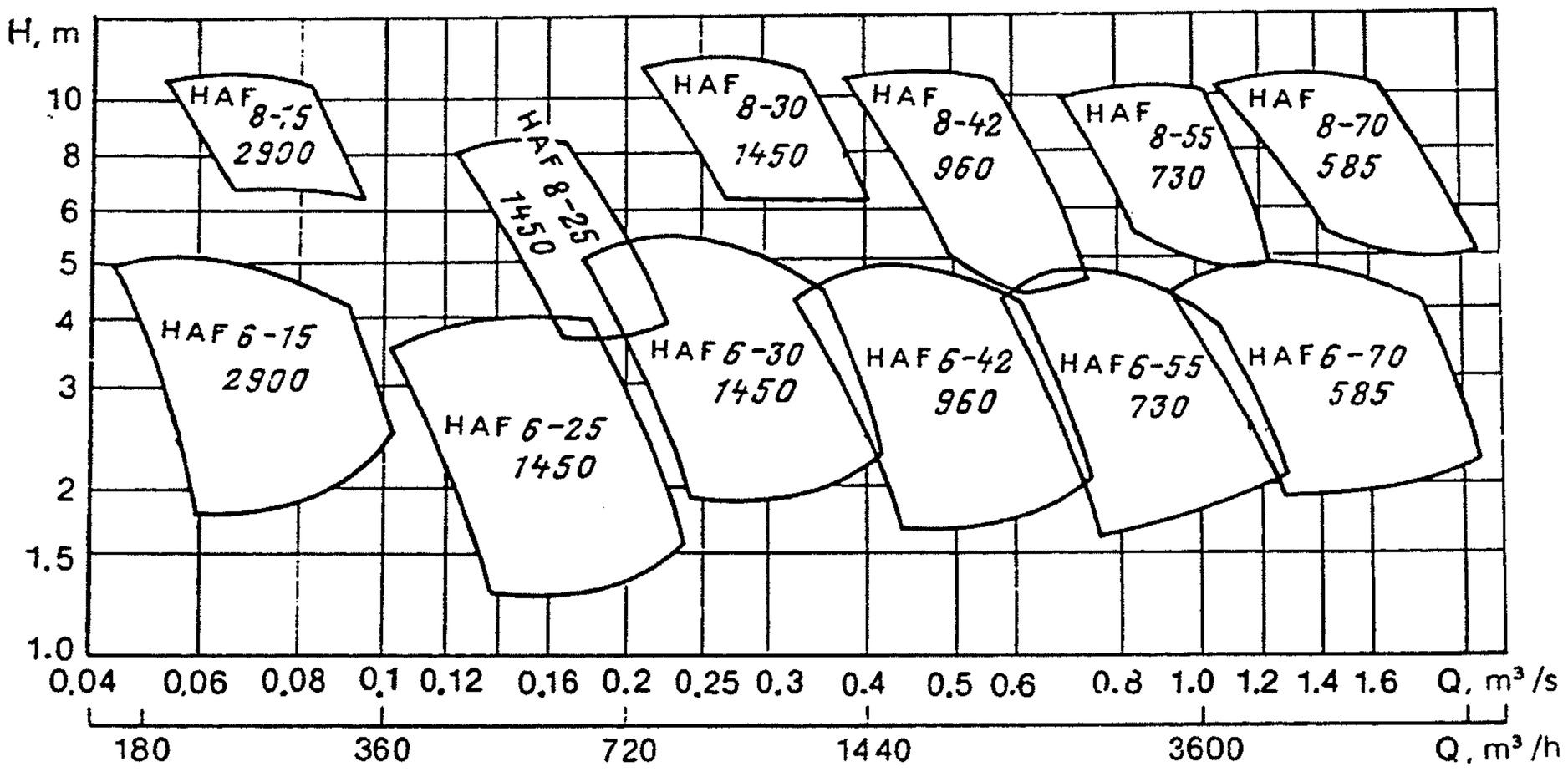


FIGURE 16.12. Nomenclature of type HAF horizontal axial-flow pumps.

at deliveries from 0.05 to 2 m^3/s (180 to 7200 m^3/h) and heads from 2 to 12 m. Horizontal adjustable blade pumps are also manufactured.

16.4. PARALLEL CONNECTION OF PUMPS TO A COMMON PIPELINE

If several pumps are connected in parallel to one line (Figure 16.13a), the line delivery is equal to the sum of the deliveries of all parallel pumps, and the heads developed by all the pumps will be practically equal. This condition makes it possible to plot a total characteristic for the entire group of pumps operating in parallel.

Figure 16.13b illustrates a simple case in which two similar pumps H_1 are connected in parallel. The total characteristic H_{1+2} is plotted by doubling the abscissas (deliveries) of one curve. The efficiency line η_{1+2}

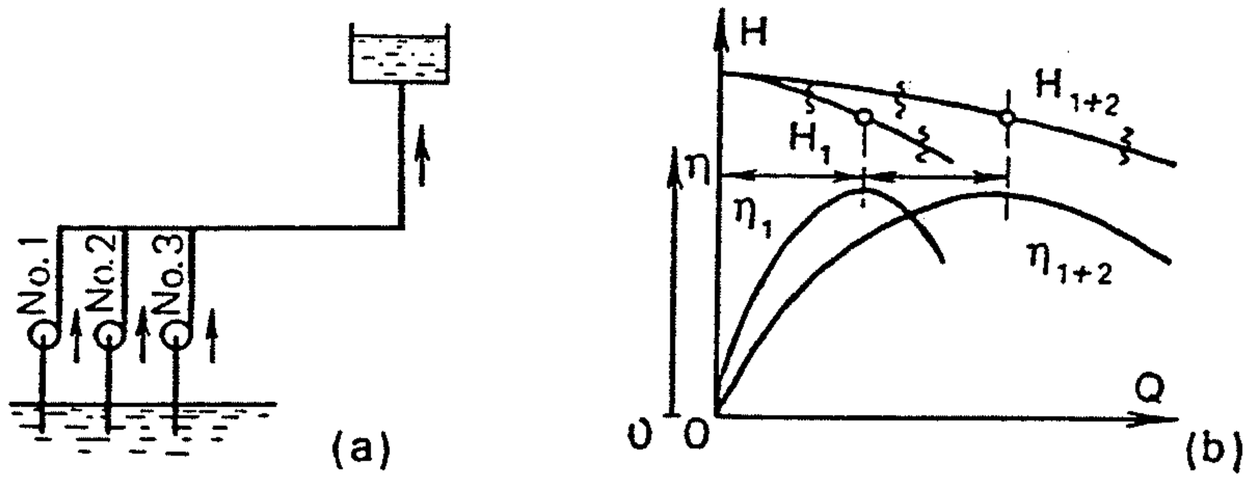


FIGURE 16.13. Parallel connection of pumps to a common pipeline.

is shaped similarly. It should be noted that the recommended area of employment for two pumps H_{1+2} is widened with respect to Q.

Consider the variation of actual delivery in the pipeline with the pumps run in parallel. Given is the water system characteristic $H_r = f(Q)$ (Figure 16.14a). All pumps are identical. With one pump operating, delivery is Q_1, two pumps Q_{1+2}, and three pumps Q_{1+2+3}. When plotting the total characteristic of the group the delivery of one pump is increased two- and threefold, but the actual total delivery in view of the network characteristic will increase less intensively: $Q_{1+2} < 2Q_1$. This is quite clear and is explained by the curvature of the line characteristic. Obviously the steeper the line characteristic, the higher the losses and the less the delivery increment at parallel connection of additional pumps.

In some cases, one or two pumps cannot be used in parallel and a larger group is used. For instance, under the conditions shown in Figure 16.14b, only with three pumps operating in parallel does the operation point get into the recommended area of employment, while with two pumps and, more to the point, with one pump running, the operation points are shifted considerably to the right of the recommended area, which is detrimental both from energy and cavitation considerations (low efficiency and rapid drop of H_v^{per} or increase of NPSH). The reader is referred to the notion of parallel operation of different pumps. To begin with, we shall consider one particular aspect.

Assume that the upper tank level gradually increases (Figure 16.15). Under such conditions, pump delivery decreases and $Q = 0$ at $H_{st} = H_{Q=0}$. The tank level cannot be further increased by the action of the pump. If water is fed to the tank from another source, the level may exceed $H_{Q=0}$, but though the pump is operating the water will flow through it in the reverse direction, i.e., the pump will operate with countercurrent flow. The values of H and Q_r are determined from the pump characteristic curve of Figure 16.15. Let pumps with different heads H_1 and H_2 be connected in parallel (Figure 16.16). Obviously, the total characteristic H_{1+2} for heads $H < H_{1Q=0}$ is determined by

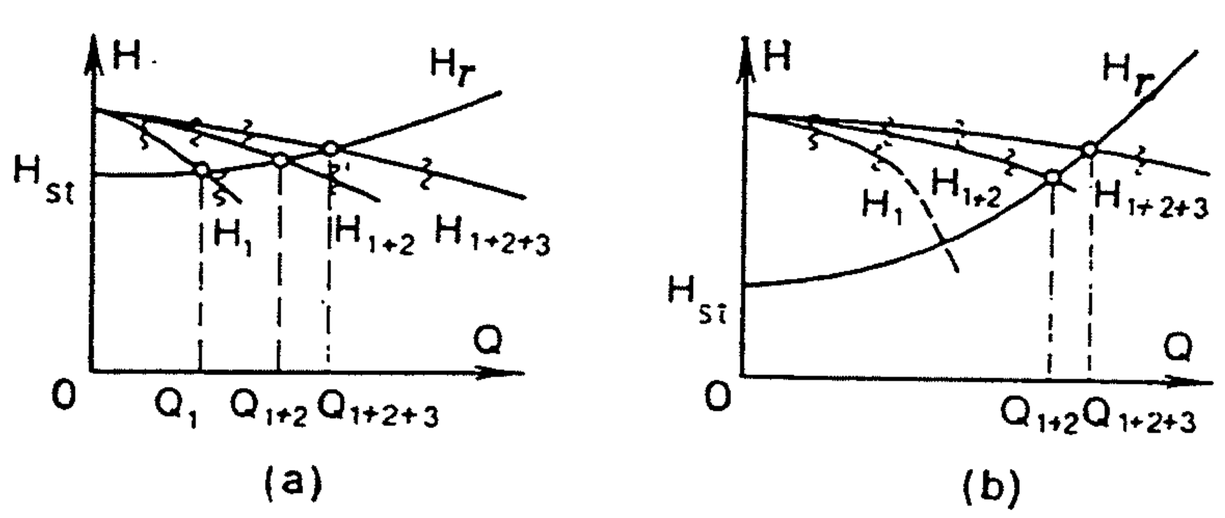


FIGURE 16.14. Delivery rate in pipeline at parallel operation of pumps.

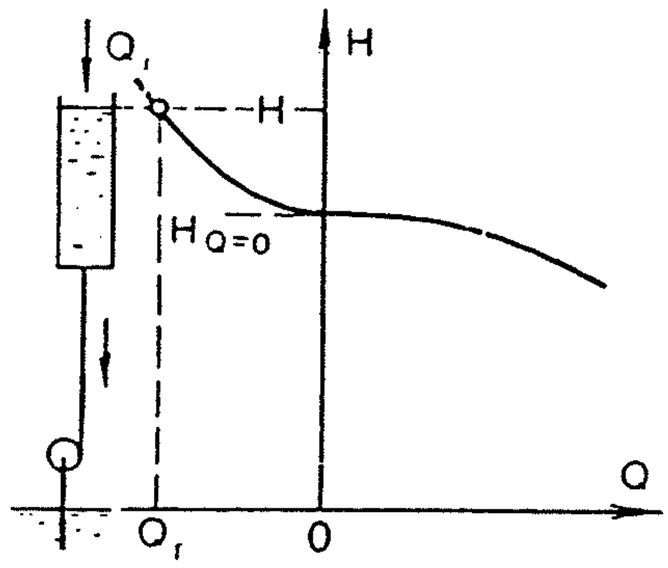


FIGURE 16.15. Counterflow operation of pump.

summing up the deliveries of each pump (abscissas) at a given head. However, at portion $H > H_{1Q=0}$ (left of point A), pump 1 will operate with countercurrent flow. As a result, the total delivery curve will be to the left of H_2 (the total delivery will be less than the delivery of the no. 2 pump). It is quite obvious that operating two pumps within this portion is unadvisable, and pump 1 should be eliminated. Thus, we have arrived at an important practical conclusion: *only pumps with close heads* (dimensions or deliveries are of no consequence) *should be connected for parallel operation.*

The average efficiency of a group of different pumps operating in parallel is found from the ratio, which is the total capacity of each pump and of the entire group according to Equation 11.11

$$\frac{\rho g H \sum_m Q_i}{1000\eta_{av}} = \sum_m \frac{\rho g H Q_i}{1000\eta_i}$$

where m is the number of operating pumps. Hence,

$$\eta_{av} = \frac{\sum_m Q_i}{\sum_m (Q_i/\eta_i)} \tag{16.4}$$

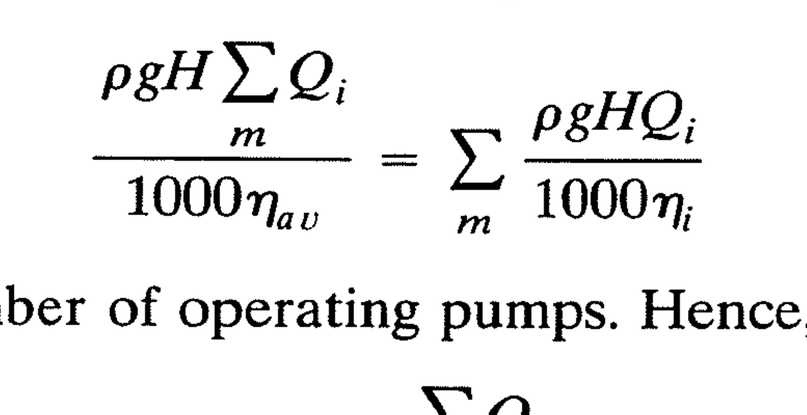


FIGURE 16.16. Parallel connection of different pumps.

If identical pumps are connected in parallel, the efficiency does not change, while delivery becomes $\Sigma_m Q_i = mQ$, where m is the number of pumps.

16.5. SERIES CONNECTION OF PUMPS TO A COMMON PIPELINE

In series connection the delivery pipe (DP) of the first pump (first stage) is coupled to the intake pipe (IP) of the second pump (second stage), etc. as shown in Figure 16.17. Thus, *with the series connection the deliveries of the pumps are equal to each other while the head is the sum of the heads of each pump* (stages). This rule makes it possible to plot the characteristic of the entire group of series-connected pumps using the characteristics of separate pumps.

Figure 16.18 illustrates the characteristics of two pumps, H_1, η_1 and H_2, η_2, and total head curve H_{1+2} corresponding to the series connection. Accordingly, the average efficiency η_{av} for the entire groups of pumps can be determined on the basis of the capacity equation (11.11)

$$\frac{\rho g Q(H_1 + H_2)}{1000\eta_{av}} = \frac{\rho g Q H_1}{1000\eta_1} + \frac{\rho g Q H_2}{1000\eta_2}$$

and thus,

$$\eta_{av} = \frac{H_1 + H_2}{H_1/\eta_1 + H_2/\eta_2} \tag{16.5}$$

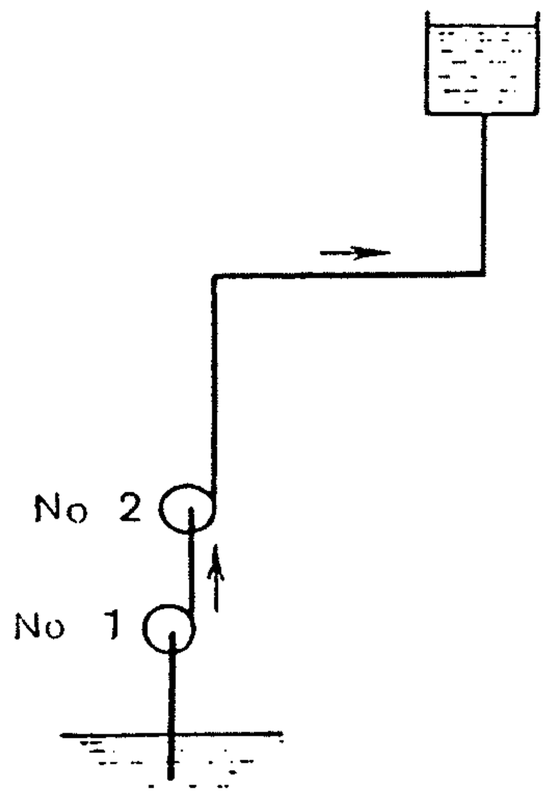


FIGURE 16.17. Series connection of pumps.

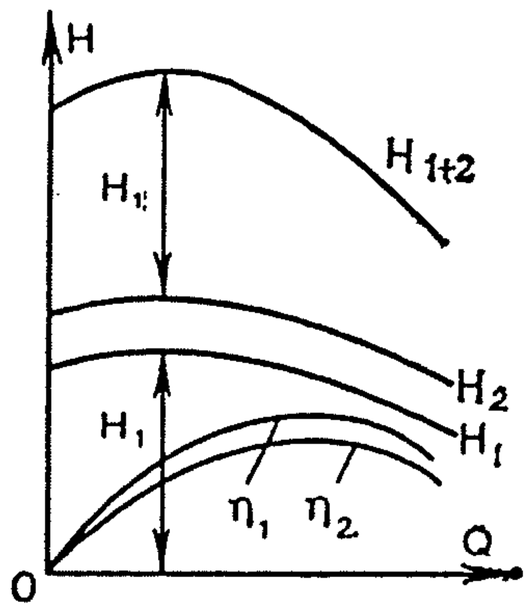


FIGURE 16.18. Total characteristics of pumps at series connection.

If several identical pumps are connected in series, the efficiency does not change, while total head becomes $H_m = mH$, where m is the number of the pumps and H is the pump head.

Series connection of pumps is used when a high head is required, which cannot be attained by one pump, or when the pump unit is to have an adjustable head. However, it should be borne in mind that housings and other parts of the pumps are designed for a particular pressure. The pump catalogs usually specify the maximum permissible pressure in the intake pipe, which determines the possibility of series connection of the pumps. Note that pumps of different heads can be run in series, but because the flow rates are identical, the pumps should have close design deliveries, i.e., they should have close inlet or outlet nozzle dimensions.

It appears that to put several pumps in series into operation, it is theoretically possible to develop any head that is necessary to do so. In practice, however, there are limitations. The higher the head, the larger the internal pressure in the pump, and each pump is designed with a definite maximum pressure. Therefore, connecting pumps in a series requires that permissible internal pressure be checked. This is given in the pump characteristic. Generally speaking, no more than two identical pumps can be connected in series. If a need exists to have such a high head that it cannot be developed by one-stage pumps, the multistage pump must be used.

16.6. SELECTION OF PUMPS

The initial data for selecting a pump include the design delivery of a pump unit or pump plant Q_{pp}, its layout (including dimensions of IP and DP), static head H_{st}, and design delivery of pump Q_d. The pumps are selected in two stages: (1) selecting the type and standard size of the

pump, and (2) determining actual performance of the pump unit on the basis of its characteristics.

The type and standard size of the pump are selected with the aid of the nomenclature zones or range charts.

First, determine the design head H_d. To this end, calculate the coefficient K_r (for nonbranched pipeline from Equation 16.1) on the basis of the assigned dimensions and pipeline scheme and find design losses $h_{d\cdot l}$ from the formula

$$h_{d\cdot l} = K_r Q_d^2$$

The design head is represented by the formula (according to Equation 11.6)

$$H_d = H_{st} + h_{d\cdot l}$$

The type and standard size of the pump are determined with the aid of the respective nomenclature zones by reference to the "design point" with coordinates of Q_d and H_d. The design point should be within the operation region of any standard size. If the point is outside the operation region, change the layout of the pump unit or pump plant; e.g., change the number of pumps (i.e., Q_d).

Often, in pump characteristics the recommended zone of employments is not shown. In such cases the pump user must decide up to what point or in what regime it is acceptable to use the pump. The most decisive factors are efficiency and cavitation conditions.

Determining the actual performance of the pump unit involves matching characteristics of the pump from a relevant catalog with the characteristics of the mains (pipeline) according to Figure 16.5. As a result, find the impeller diameter for the centrifugal pump or blade angle for the axial- or mixed-flow pump, provided actual delivery Q_{ac} is close to design delivery Q_d; determine actual head H_{ac}, efficiency, required power of the motor (against the graph or from Equations 11.11 and 11.11a, permissible vacuum suction lift H_v^{per} or permissible NPSH; and calculate permissible suction lift H_s using Equations 14.3 or 14.8.

All necessary overall and mounting dimensions as well as weight data are given in pump catalogs.

Example 16.1

Select pumps for a pump plant of the type shown in Figure 16.3: discharge $Q_{pp} = 14\ \text{m}^3/\text{s}$, number of pump unit 4 with steel pipelines, diameter 1.1 m, 1250-m long, static head $H_{st} = 40.0$ m, design delivery $Q_d = 3.5\ \text{m}^3/\text{s}$, TW absolute elevation 630 m.

Solution

1. Select the pump type and standard size.

- Determine design losses. For pipe, $d = 1.1$ m, with roughness coefficient $n = 0.012$, $\lambda = 0.0165$ (from any hydraulic handbook for example see Bibliography number 17). Ignoring local losses, find from Equation 16.1

$$K_r = \frac{16 \times 0.0165 \times 1250}{\pi^2 2g \times 1.1^5} = 1.06$$

hence, design losses

$$h_{d\cdot l} = K_s Q_d^2 = 1.06 \times 3.5^2 = 13.0 \text{ m}$$

- Design head of the pump

$$H_d = H_{st} + h_{d\cdot l} = 40 + 13.0 = 53.0 \text{ m}$$

- According to the nomenclature (Figure 16.10) design point $Q_d = 3.5$ m^3/s and $H_d = 53.0$ m gets into the operating area of pump 1000 B-4/63, $n = 500$ rpm. Therefore, we select this pump.

2. Determine the actual characteristics of the pump.

- Calculate the system characteristics using Equation 11.6a, $K_r = 1.06$

$$H_r = H_{st} + 1.06Q^2$$

Q (m^3/s)	0	1.0	2.0	3.0	3.5	4.0
h_{loss} (m)	0	1.1	4.4	9.9	13.0	17.0
H_r (m)	40.0	41.1	44.4	49.9	53.0	57.0

- Determine the actual operation conditions for the pump. Take the characteristic of the pump corresponding to that selected from the catalog of type B pumps, and plot the system characteristic according to the above equation on the pump curve, as shown in Figure 16.19. Point $Q_d = 3.5$ m^3/s lies between the curves for $D = 1360$ and 1320 mm. Take $D = 1360$ mm to provide some reserve.
- The actual characteristics determined by the point of intersection between the pump and network curves are as follows: delivery $Q_{ac} = 3.8$ m^3/s, head $H_{ac} = 55$ m, efficiency $\eta = 84\%$, cavitation parameter NPSH = 11.5 m of water column, required motor power 2500 kW. Checking by Equation 11.11a yields

$$N = \frac{9.81 \times 3.8 \times 55.0}{0.84} = 2440 \text{ kW}$$

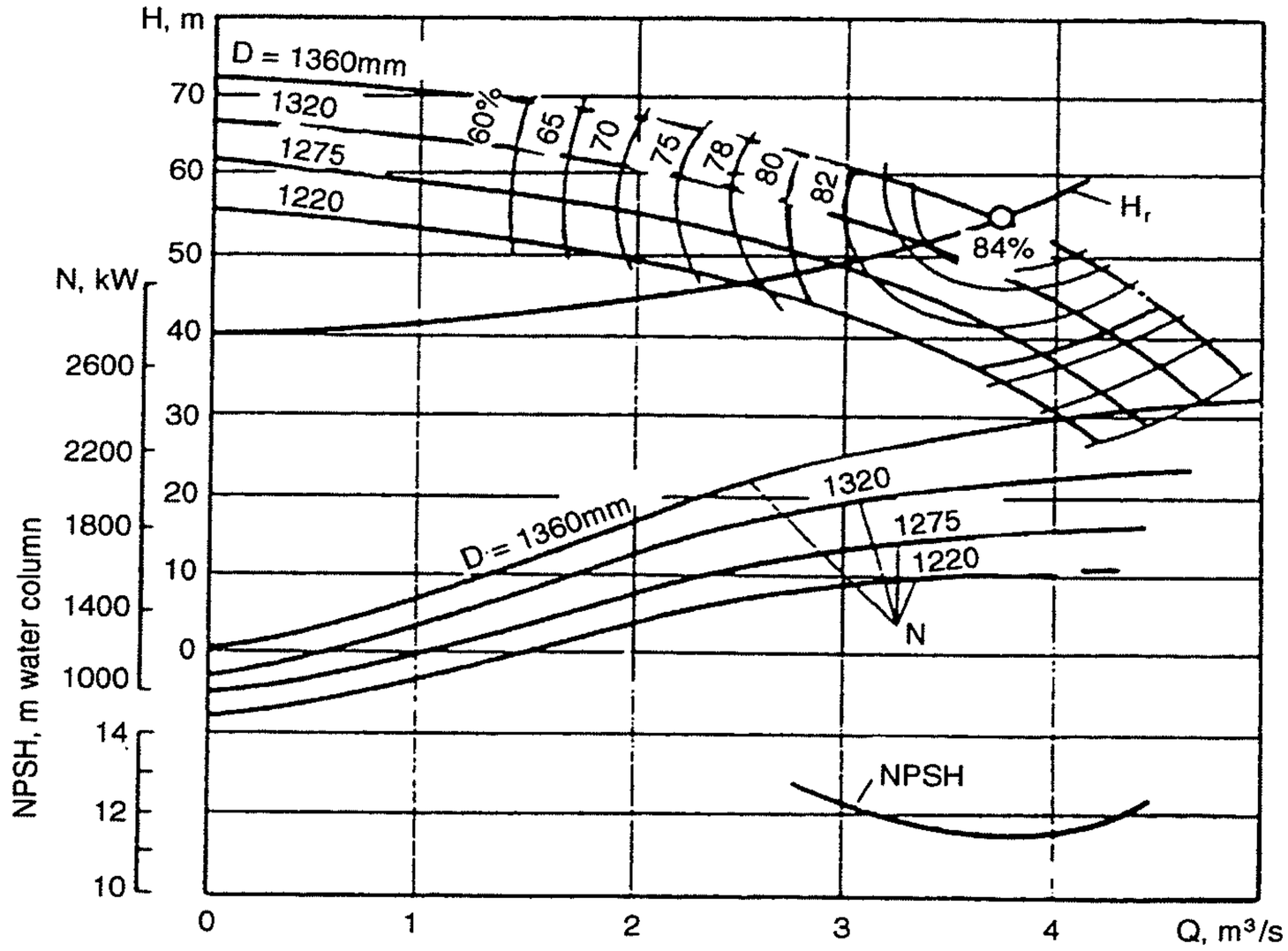


FIGURE 16.19. Characteristic of pump and network.

Using Equation 14.8, find the permissible suction lift. According to Equation 1.2:

$$\frac{\Delta p_{atm}}{\rho g} = \frac{\nabla}{900} = \frac{630}{900} = 0.7 \text{ m}$$

For the suction pipe of the type shown in Figure 16.3 we may assume $h_{suc} = 0.5$ m. For cold water, $p_{s\cdot v}/\rho g = 0.3$ m. From Equation 14.8:

$$H_s = 10.3 - 0.7 - 11.5 - 0.5 - 0.3 = -2.7 \text{ m}$$

Pump installation is shown in Figure 16.3.

CHAPTER 17

Operation of Impeller Pumps

17.1 STARTING

A pump impeller rotating in air creates a head equal to H, meters of air column. If calculated for water, this head will be very small. For instance, if according to the characteristics, $H = 24$ to 64 m the head will be only 0.03 to 0.08 m of water column, because air density is about 800 times less than of water. Thus, if the casing and suction line of the pump are filled with air, after the electric motor is turned on the pump will suck water into the suction line only by 3 to 8 cm. H_s is usually greater, therefore, water will not fill the casing or the impeller and will not reach the delivery pipe (DP). The pump will not start. This leads to a very important conclusion: *to start an impeller pump and make it supply liquid to the delivery line, its suction line, casing, and impeller should be filled with liquid.* All methods of starting impeller pumps are restricted to this basic requirement. The starting methods below are used most frequently.

Installing the pump with submergence (backwater installation): i.e., below the tailwater (TW) level (in this case $H_s < 0$) as shown in Figures 16.1 to 16.3 and 17.1. In this case, the suction line and the impeller casing are always filled with water, so no prestarting operations are needed. However, such arrangement of the pump is not always possible. In the case of axial-flow pumps, it may be also determined by the cavitation conditions, because they often have $H_s < 0$ (see Example 14.2).

Priming the suction line and impeller casing before starting (Figure 17.2): An intake or foot valve (IV) is arranged at the end of the suction pipeline. Prior to starting the pump, the suction pipeline and the casing is filled with water through the DP (point B) or through the hole in the scroll (point A). The small pumps, especially mobile units at construction sites, for example, are sometimes primed manually through a funnel installed in hole A. When priming, ensure the release of air from all the points of the suction line and casing (for instance, if filling through point B, open the cock at point A and continue priming until water flows out from the cock). If air bags are left somewhere in the line, the pump will often fail to supply water to the delivery line after starting the motor. Such air bags after cause multiple restarts of the pump.

Trouble-free starting of the pump also depends on the tightness of the intake valve. If it leaks excessively, it is difficult to evacuate all air from the suction line of the pump, which impedes starting and may even preclude priming the pump. To prevent clogging and damage to the valve, a protective strainer or perforated hood *S* is arranged before it. The intake valves differ in the design. The simplest version is a hinged valve made from metal or rubber (clapper) (Figure 17.2a); the seat (Figure 17.2b) and ball (Figure 17.2c) valves are more complex.

Starting with priming is a sufficiently simple method which is widely used in small pumps. Its disadvantage is the need for an intake valve which operates under rather adverse conditions and is hard to reach for inspection and repair. The intake valve creates additional resistance, which necessitates a reduction in suction lift H_s. Therefore, such a method is not advisable for large pumps (it is regarded acceptable for pump units with suction pipe diameters < 200 mm).

Using vacuum pumps. Prior to starting a pump (Figure 17.3), the gate valve (GV) on the delivery pipeline is closed, the valve (V) is opened, and the vacuum pump (VP) connected to the top point of the scroll is turned on. As air is evacuated, vacuum in the space increases and water moves upward along the suction line. As soon as the entire scroll space

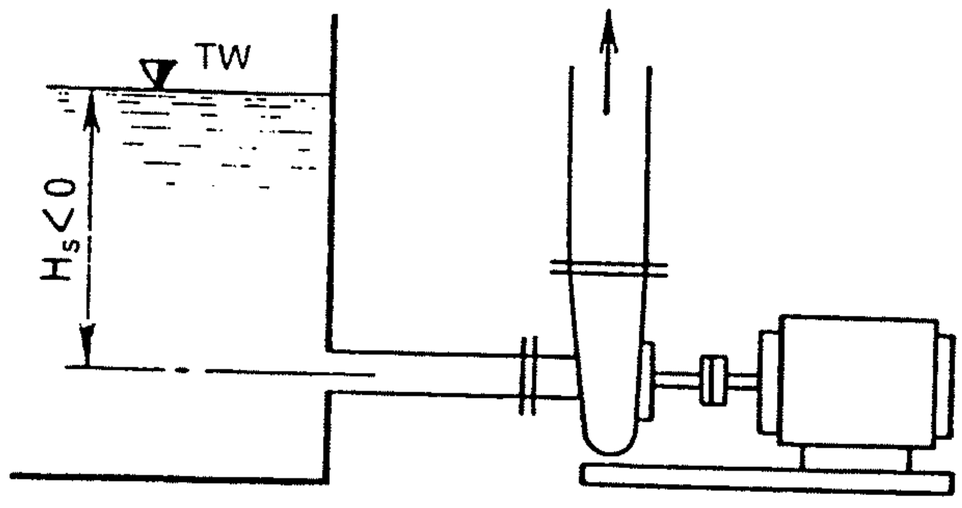


FIGURE 17.1. Backwater installation of pump.

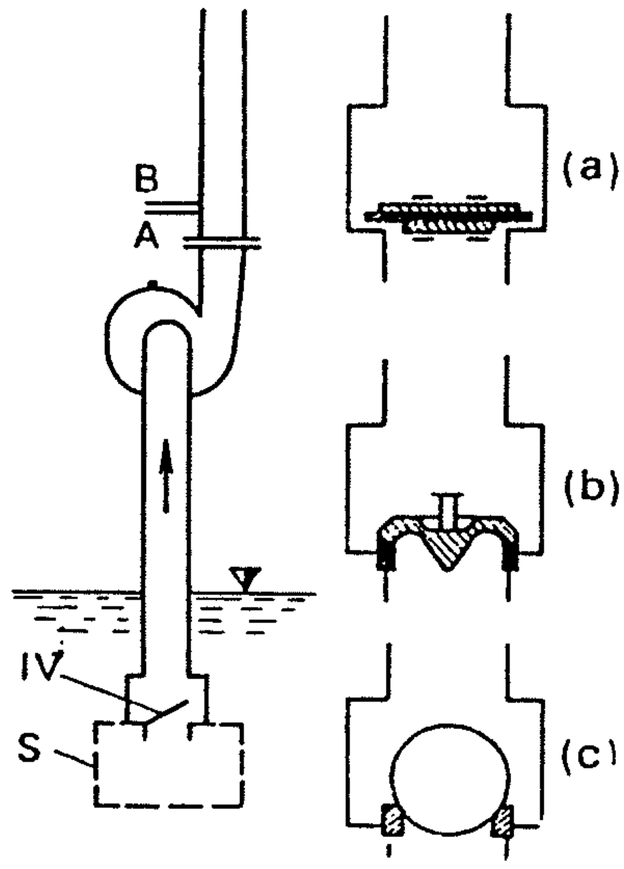


FIGURE 17.2. Pump foot valves.

is filled with water, the VP begins ejecting water instead of air. Now the electric motor can be turned on and the GV can be opened. The pump will supply water to the delivery pipeline. The V is closed and the VP is turned off. The starting process is fairly simple, but the entire system should be pressure-tight. The time of starting (priming) is determined by the volume of the suction line and capacity of the vacuum pump.

Only special vacuum pumps admitting the ingress of water can be used for priming the pumps. Liquid-packed vacuum pumps and ejectors have found wide application in this field.

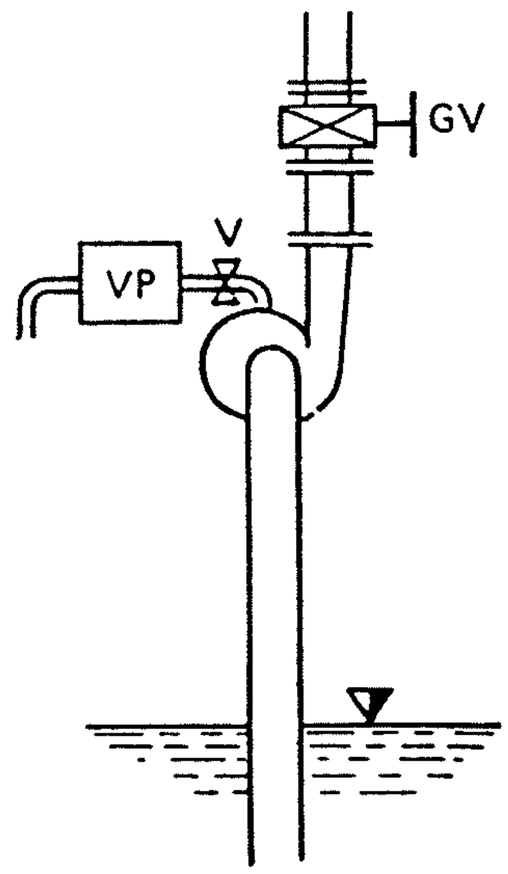


FIGURE 17.3. Pump unit with priming vacuum pump.

The liquid-ring vacuum pump, or wet vacuum pump (Figure 17.4), comprises a cylindrical casing (1) with flat sidewalls accommodating an eccentrically rotating drum (2) with vanes (3). The height of the drum and vanes is almost equal to the height of the cylindrical casing (1), so that the end face clearances are minimized. The sidewall has two grooves (shown in black) that communicate with pipes (4) and (5).

Prior to starting, little water is filled in the vacuum pump casing. When drum (2) rotates, its vanes entrap water and centrifugal force creates a rotating water ring whose center coincides with the axis of the stationary cylinder of casing (1); the inner radius of the rotating ring is determined by the position of the grooves.

The vacuum pump operates on the following principle: The eccentric position of the drum with vanes in the cylindrical casing ensures that during their rotation volume W of a closed space defined by the vanes and water surface changes. At the top where the vanes are deeply immersed in the water ring the space is minimum, while at the bottom where the vanes are mostly out of the water, the space is maximum. While moving along the arrow, space W advancing along the groove of pipe (4) increases in volume and is filled with air. Its further motion along the groove of pipe (5) space W decreases in volume, air pressure rises, and the air is ejected into pipe (5). Thus, the liquid-packed vacuum pump operates on the principle of the positive-displacement pump.

The liquid-packed vacuum pump is very simple in design. It includes no valves and creates a vacuum sufficient for lifting water to a level of 8 to 9 m; it does not cause trouble if water penetrates the suction pipe (4); i.e., it is quite suitable for starting impeller pumps. Its sole shortcoming is that it can operate only in clean water (contains no abrasive inclusions (sand)). The same requirement covers the water transferred by its parent pump, because it will inevitably enter the vacuum pump during starting.

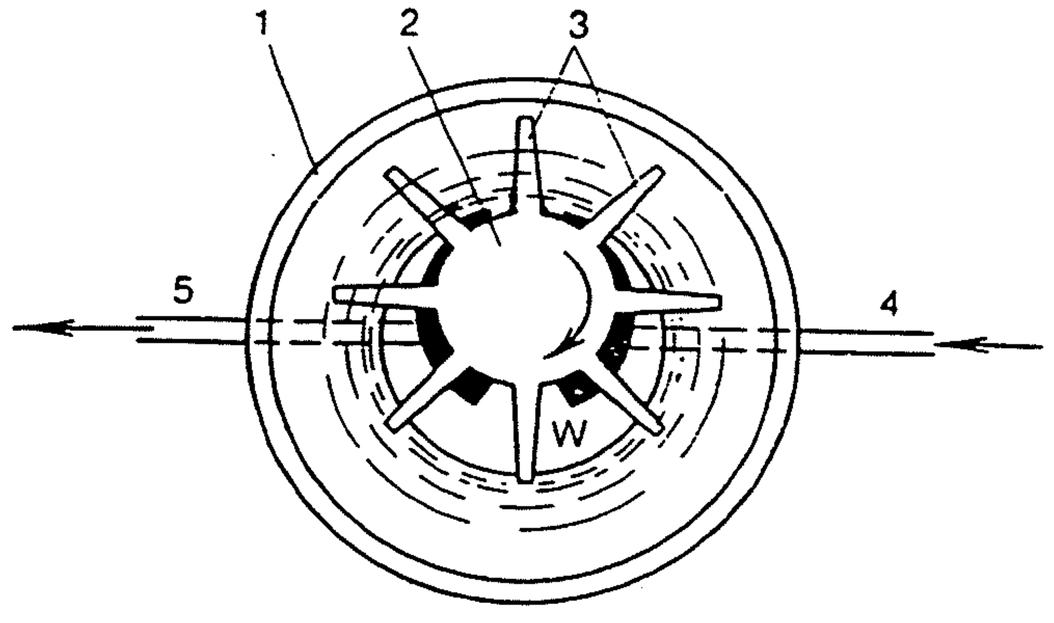


FIGURE 17.4. Liquid-ring vacuum pump.

The jet-type pump (ejector), whose diagram is shown in Figure 11.11, can be also used for creating a vacuum which is needed to prime the suction pipeline and the impeller casing. When water at a sufficient head (over 20 to 30 m) is fed to the nozzle, the jet entraps air in the supply duct and acts as a vacuum pump. The ejector is obviously very convenient for starting impeller pumps. It has no moving parts, and water or sand cannot harm it, which is of primary importance for slurry pumps and regular pump units used to transfer dirty water.

Self-priming centrifugal pumps are provided with devices that allow water to be suctioned from the lower reservoir and supplied to the delivery pipeline when the drive (electric motor) is turned on. According to these priming devices, the pumps can be divided into three groups:

1. Those for which the impeller of a liquid-packed pump (Figure 17.4) is fitted on the shaft parallel to the centrifugal impeller. Such a pump can handle only clear water without suspensions. The additional impeller decreases the pump efficiency.
2. The pumps that have special additional reservoirs that remain filled with water after the pump is turned off. When the pump is started, water from the spaces is ejected into the delivery pipeline by the impeller, and this "piston effect" suctions water from the lower reservoir. These pumps can be used with dirty liquids, but they are bulkier and heavier.
3. The recirculation-type pumps have a space filled with water and an ejecting device on the suction pipe (similar to Figure 11.11); the ejecting device is operated by the head created by the impeller.

The self-priming pumps are designed for relatively small delivery rates and are used primarily with mobile units.

To select the method of starting a pump, it is necessary to determine if it can be started with closed gate valve. The power variation curve form is of primary importance in this case. As seen in Figure 15.5, the pumps of low and medium specific speed feature an power increase as the delivery rate increases from zero. Such pumps may be started with a closed gate valve or a nonreturn valve, which are sometimes installed on the delivery pipeline. In case of high-speed axial-flow or mixed-flow pumps, power at $Q = 0$ may far exceed that required for service. Besides, the delivery curve of such pumps has a break of nonsteady operation. Therefore, such pumps are usually started with the pipeline empty and at the initial moment head $H_0 = 0$. As the speed of rotation increases and the pipeline is filled the head rises to the required value, after which the gate valve is opened or the siphon water outlet is engaged at the water conduit top. Thus, starting axial-flow and mixed-flow pumps involves a number of particular problems.

17.2. DELIVERY CONTROL OF THE IMPELLER PUMP

The pump or a group of pumps is usually selected with a view toward ensuring maximum required delivery. However, it may become necessary to decrease the delivery rate, i.e., to vary or adjust the pump delivery within a fairly wide range. Actual delivery is known to be determined by the point of intersection of the head–discharge characteristic of the pump with the characteristic of the system (see Figures 16.5 and 16.14). Thus, we can change delivery by changing either the pump or system characteristic. There are several practical methods of delivery control.

17.2.1. Control by Gate Valve or by Throttling

This is one of the most popular methods of impeller pump delivery control. It decreases the gate valve opening on the delivery line to create additional resistance in order to change the system characteristics. In view of this, coefficient K_r (included in Equation 16.1) may be represented by sum $K_r = K_p + K_{gv}$, where K_p is the coefficient accounting for pipeline losses, and K_{gv} are the additional losses created by the gate valve. Now the system characteristic is determined by the formula

$$H_r = H_{st} + K_p Q^2 + K_{gv} Q^2 \tag{17.1}$$

Coefficient K_{gv} increases as the valve opening is decreased. Variation (in percent) of the system characteristic and pump delivery vs opening s of the gate valve is illustrated by points 0 to 4 in Figure 17.5. The same figure presents curve $Q_a = f(s)$ which shows the actual flow rate in the delivery pipeline as a function of opening s of the gate valve. As seen in the figure, the delivery rate can be smoothly adjusted from Q_{max} to 0 by varying the opening of the gate valve.

It is necessary to keep in mind that pump operation at reduced delivery can lead to increased heat in the pumping liquid and the pump itself. The real danger arises if the pump operates for a rather long time with a fully closed valve ($Q = 0$). The evaluation can be made using a formula for temperature rise derived with the assumption that no heat transfer occurs through ambient air.

$$\Delta t = \frac{14.3 N_0}{Mc}$$

Here, Δt is the temperature rise (degrees Celsius per minute), N_0 is power (kilowatts) at $Q = 0$, M is the mass of liquid in the pump (kilograms), and c is its thermic capacity (for water, $c = 1$).

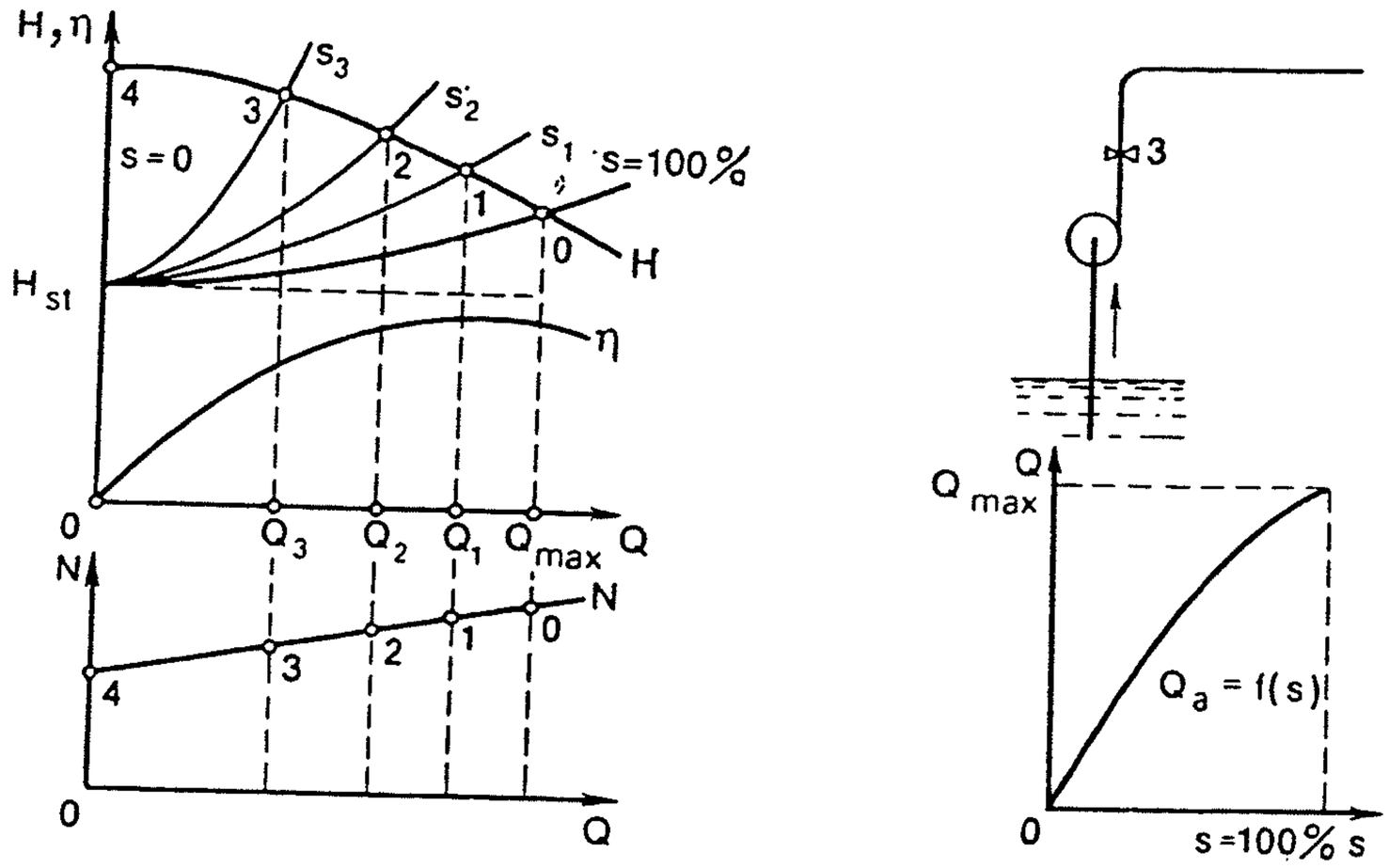


FIGURE 17.5. Delivery control by throttling valve.

The concept delivery control by means of a gate valve is very simple. The shortcomings of the method include increased consumption of energy, mainly for overcoming additional resistance, $K_{gv}Q^2$. The gate valves are used for varying delivery in centrifugal pumps, in which reduction of Q decreases required power N (see Figure 17.5).

17.2.2. Control by Varying Pump Speed of Rotation

If at a certain design speed of rotation n_0 the pump has characteristic H_{n0} and delivery Q_{max}, reducing the speed to 0.9 n_0, 0.8 n_0, etc., will depress the characteristics according to Equations 12.25 and 12.26 and decrease the delivery (Figure 17.6). As a result, a smooth variation of the rotational speed allows a smooth variation of delivery $Q_a = f(n)$ within a wide range. This rather efficient method of delivery control is difficult to realize because the pumps are usually driven by asynchronous motors which run at substantially constant speed.

There are several ways to use adjustable speed electric engines. One is the wound rotor induction motor, with variable resistance, variable voltage drive, variable frequency drive, etc. These motors are not only more complicated and expensive, but also have a lower efficiency at decreased speed (for 70 to 75% of normal speed, the efficiency drops up to 55 to 75%). This can be improved by increasing pump efficiency. The best are direct current motors, but their use is acceptable only in special cases.

Hydraulic or fluid coupling between pump and electric motor is used in the form of a hydrodynamic speed convertor, the scheme of which is

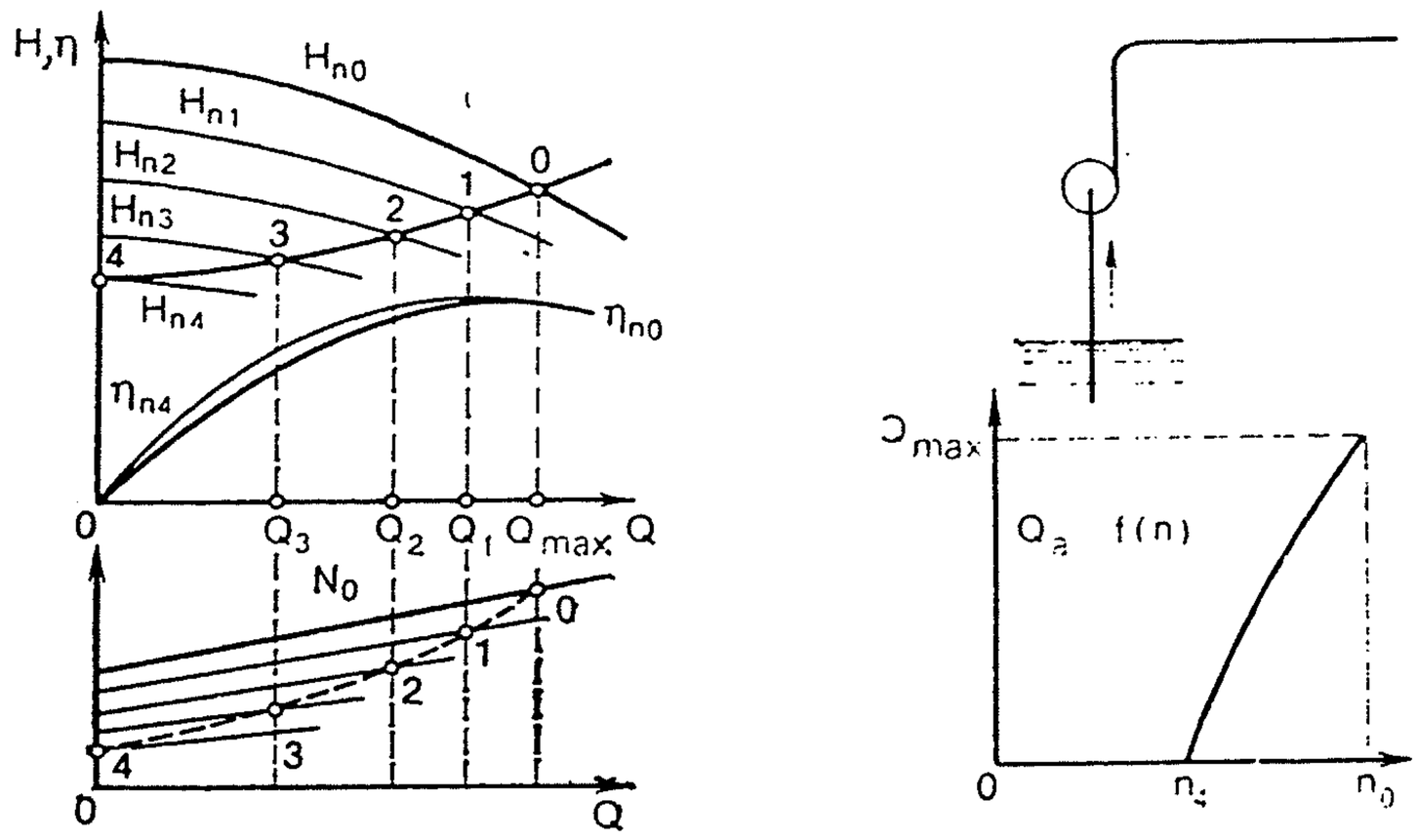


FIGURE 17.6. Delivery control by varying pump rotation speed.

given in Figure 17.6a. It comprises the drive portion with shaft (1) on which pumping wheel (2) with cover (3) is rigidly fixed, and running part with shaft (4) is rigidly connected to turbine runner (5). The both parts are supported and centred by bearings. The pump wheel and turbine runner have straight vanes. The interior of the convertor is filled with liquid (low viscous oil). Sealing (6) prevents its leakage. The working condition of the convertor is determined by the slip factor s:

$$s = \frac{n_1 - n_2}{n_1} \qquad \frac{n_2}{n_1} = 1 - s$$

where n_1 and n_2 are drive and running speed of rotation. The efficiency of hydraulic coupling $\eta = n_2/n_1 = 1 - s$. At the optimal operation conditions the slip $s = 0.02$ to 0.04 or $\eta = 96$ to 98%. If the convertor is

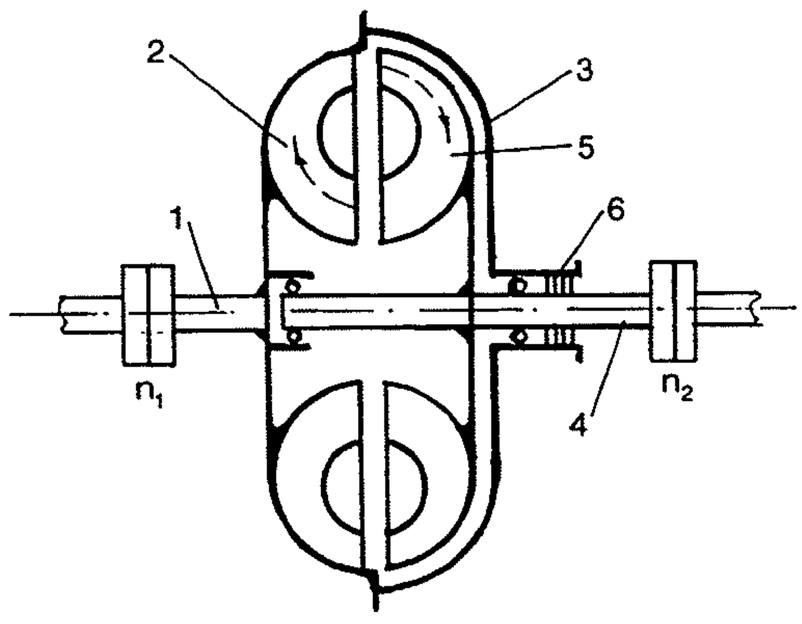


FIGURE 17.6a. Hydraulic speed convertor.

arranged in such a way to change the volume of its liquid fill, the slip can be changed and can be used to change the rotation speed of the runner shaft n_2. However, the larger the slip, the less the efficiency. Nevertheless, hydraulic coupling has applications especially in cases with difficult starting conditions.

The energy characteristics of both delivery control methods can be compared by referring to the power during flow restriction (Figure 17.5) and to the variation of rotation speed (Figure 17.6). In the first case the power changes along line N; in the second case it decreases with reduction of Q far more rapidly owing to the displacement of line N according to Equation 12.27, points 0 to 4.

17.2.3. Control via Bypassing (Figure 17.7)

This is carried out by changing the opening of the GV installed on the bypass pipe connecting the delivery pipeline with the suction pipeline. Increasing the opening of this valve decreases delivery Q_A in the delivery pipeline. Such a method is energetically advisable only for high specific speed pumps whose power decreases with an increase in delivery. However, bear in mind that opening the GV increases the actual delivery of the pump and the latter begins operating with adverse cavitation characteristics. This method is used very seldom, sometimes when starting the pumps.

17.2.4. Control by Changing the Impeller Blade Angle

This can be effected only in axial and mixed-flow adjustable blade pumps having special means for changing the blade setting angle of the rotating impeller. As is illustrated by the curve of Figure 15.2, this

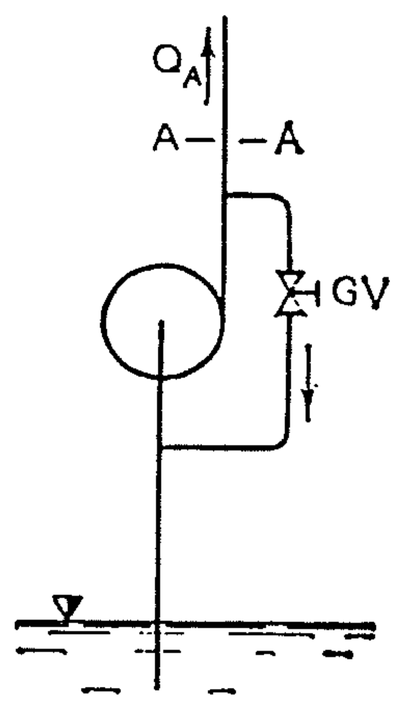


FIGURE 17.7. Delivery control via by-passing.

method provides for a smooth change of delivery, but within a narrow range.

17.2.5. Control by Changing the Circulation of Flow Before the Entrance to the Impeller

Euler's equation (12.10a) shows that changing inlet circulation Γ_1 should change the head developed by the pump. This property can be used to control the pump delivery. Figure 17.8 represents a mixed-flow pump in which an axial turnable guide vane assembly is arranged in front of the impeller (1). The assembly vanes (2) are driven by adjustment ring (3). By turning ring (3) it is possible to change the delivery by about 30% without considerably impairing the efficiency.

17.2.6. Control by Changing the Number of Pumps

In cases of parallel connection of several pumps, delivery can be controlled by changing the number of pumps (in stopped pumps the gate valves on the delivery lines should be closed). Variation of delivery in this case is illustrated in Figure 16.14.

This a method is convenient and widely used in pumping plants, but cannot ensure a smooth variation of delivery. Using it jointly with flow restriction may improve energy delivery.

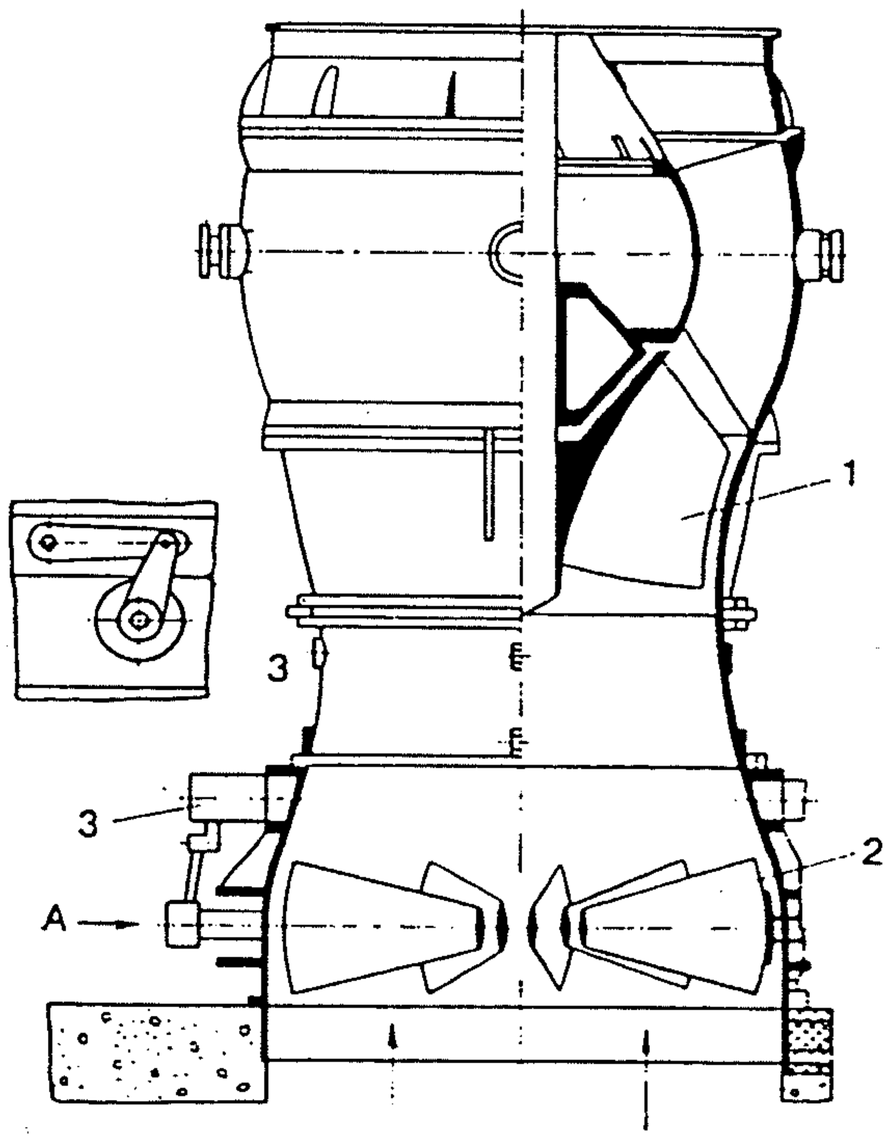


FIGURE 17.8. Delivery control by varying inlet circulation.

Sometimes large pumps in pump plants are complemented by smaller units, which are engaged when low delivery is needed.

17.3. INSTALLATION OF IMPELLER PUMPS

When designing pump plants and pump units (even temporary pump units), it is necessary to take into account a number of requirements that dictate their reliable operation. This primarily applies to the choice of standard size and number of pumps in compliance with the required deliveries and heads; special attention should be pair to the hydraulic losses involved.

The pump elevation relative to the lower reservoir water level (H_s determined from Equations 14.3 or 14.8) is of primary importance. Values of H_v^{per} and NSPH are found using the pump characteristic curve for the most adverse operating conditions.

As seen from the above-mentioned formulas, H_s depends on suction line losses h_{suc}. Therefore, to increase H_s and diminish cavitation hazard, the suction pipeline losses should be minimized. To this end, the pipeline should be made as short as possible (which also facilitates starting the pumps because the volume to be primed is decreased), velocity in the suction pipeline should be less than in the delivery pipeline, i.e., the diameter of the suction pipeline should be somewhat greater. The suction pipeline should have the minimum possible number of turns to preclude additional local losses. If a foot valve is installed for the purpose of priming the pump (see Figure 17.2), hydraulic losses in the valve and in the strainer are taken into account when determining h_{suc}. The valve size should exceed that of the pipeline.

Reliable operation and easy start of a pump are greatly dependent on the quality of the suction pipeline mounting. The suction pipeline should be fully pressure tight, since deep vacuum formed in the course of operation will suck air through leaky joints, which may lead to a decrease in delivery and even eliminate vacuum, i.e., may result in complete cessation of delivery to the delivery pipeline.

The suction pipeline shape should preclude the formation of air pockets. The pipe contraction and suction pipeline should be made as illustrated in Figure 17.9a . If it is constructed as shown in Figure 17.9b, an air space will form in the upper part during priming. This space will expand as the impeller begins rotating, and will shut off the entire cross-section, thus precluding starting the pump. If this pump is started with the aid of a vacuum pump, air liberated from water during the operation will accumulate here, which may result in disruption or cessation of delivery.

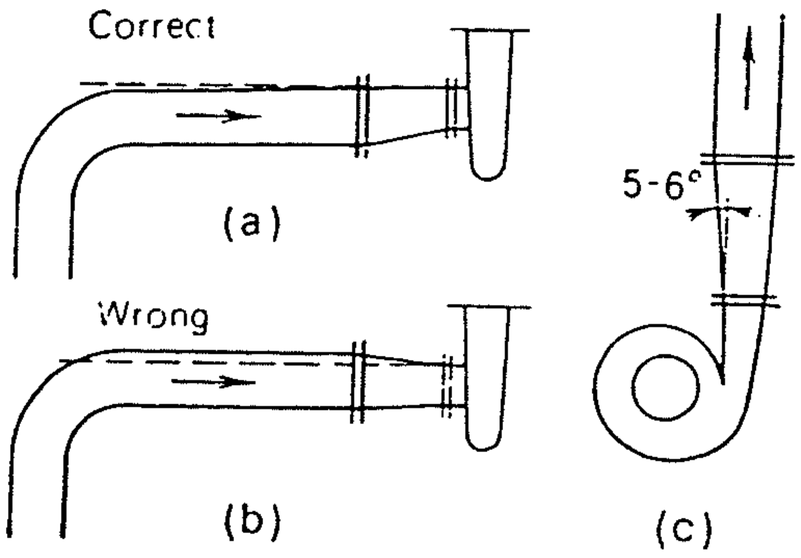


FIGURE 17.9. Laying suction pipeline and connecting delivery pipeline to pump.

The delivery pipeline is far less responsible for pump operation. However, because actual delivery depends on the amount of losses, the diameter of the delivery pipeline should be appropriately chosen. Average velocity in the pump inlet nozzle reaches 6 to 7 m/s, while in the delivery pipeline it usually reaches from 1.5 to 3. To decrease losses, it is good policy to arrange a conical diffuser with a central angle of no more than 10° to 12° near the DP (Figure 17.9c).

17.4. CAVITATION AND ABRASIVE WEAR OF PUMPS

Impeller pumps are fairly durable machines which can operate under normal conditions for 15 to 20 years and more. However, in practice pumps sometimes wear out far more rapidly and need to be overhauled every 1 or 2 years. This intense wear is usually caused by cavitation and the abrasive effect of solid impurities contained in liquid being transferred or both.

Cavitation wear. Though the height of pump installation is determined on the basis of no-cavitation conditions, intense cavitation wear can be sometimes detected after prolonged operation. The wear may stem from two groups of factors: those determined by operating conditions and those linked with the pump manufacturing quality. Operation factors of cavitation wear include all the causes that result in the actual vacuum in the suction line (Equation 11.3) being greater or the actual $(NPSH)_{op}$ (Equation 14.5) being less than the respective permissible values. This is usually the result of increased hydraulic losses in the suction pipeline as compared to design values (partial clogging of the intake strainer, increased resistance of the valve, trouble localized in the suction line) or of the actual value of suction head H_s exceeding the permissible value (e.g., the lower reservoir level is under the specified limit). These can be detected easily by measuring the vacuum in the

pump suction pipe and comparing it to the permissible value for the same delivery.

Cavitation wear factors determined by pump quality are that the cavitation characteristics H_v^{per} and NPSH specified in the pump certificate fail to eliminate cavitation. Critical values of H_v and $(NPSH)_{cr}$ have been found during bed tests at intensive cavitation, and are determined by the separation point (see Figure 14.1). However, cavitation may appear earlier at some points and cause accelerated local wear without affecting efficiency and other characteristics of the pump. Intense cavitation wear can also stem from some manufacturing and mounting defects (surface irregularities, misalignment, increased clearances, etc.).

The areas with the highest vacuum are the most liable to cavitation wear. In centrifugal pumps (Figure 17.10) these include the leading portions of the impeller blades on their back (A), the inner surface of the entrance rim (B) and the sealing clearance (C). A particular form of cavitation, "slit cavitation," develops in the gap. This cavitation is caused by local contraction of the flow and an additional pressure drop occurs.

Axial-flow pumps (Figure 17.11) feature cavitation erosion on the blade leading edge (back A), on airfoil types (B), on the lower portion of the impeller spherical chamber (C), at the blade tips (slit cavitation; D), and on the surface of the hub (E). To decrease slit cavitation, the author recommends rounding the tip edges of the blades (part II) or provide a tip rib (part I).

Another very important factor is the quality of materials used for manufacturing which are subjected to cavitation pump elements. The data of Table 7.1 show that the most cavitation-stable materials are cast aluminum bronze and stainless steel. They are used for impeller sealing (wearing) rings (Figure 13.19) and sometimes even for wheels.

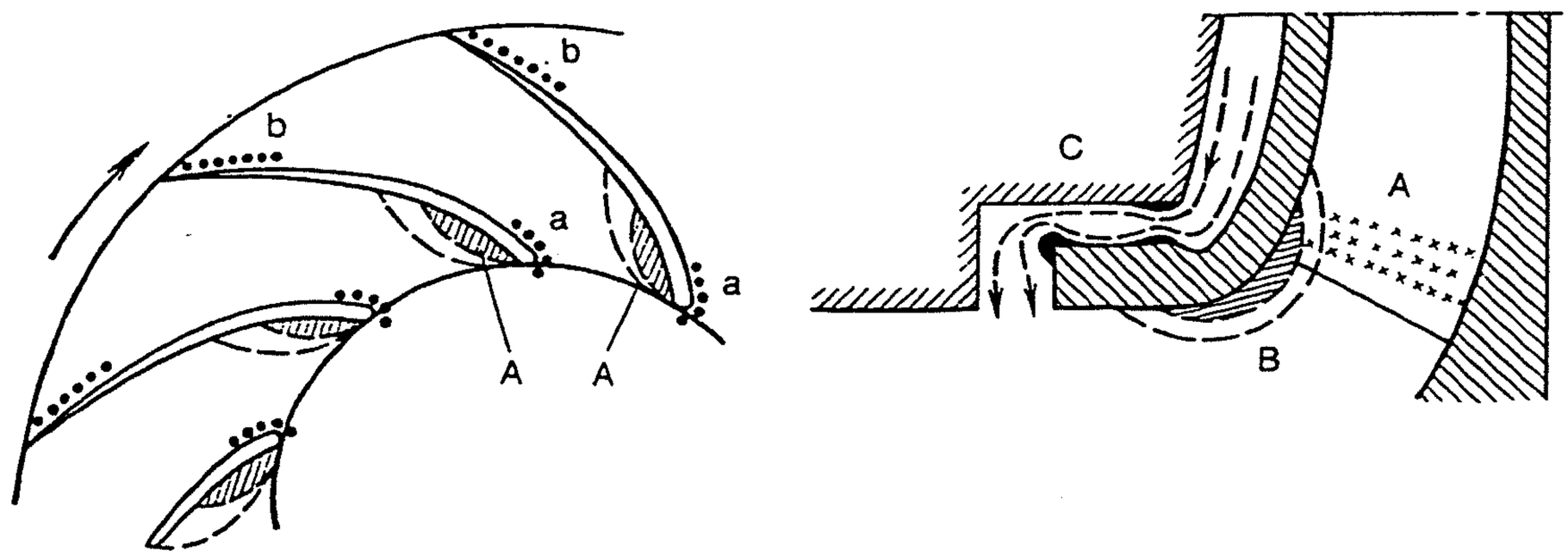


FIGURE 17.10. Points of most intensive wear in centrifugal pumps. A, B, C — Cavitation wear; a, b — abrasive wear.

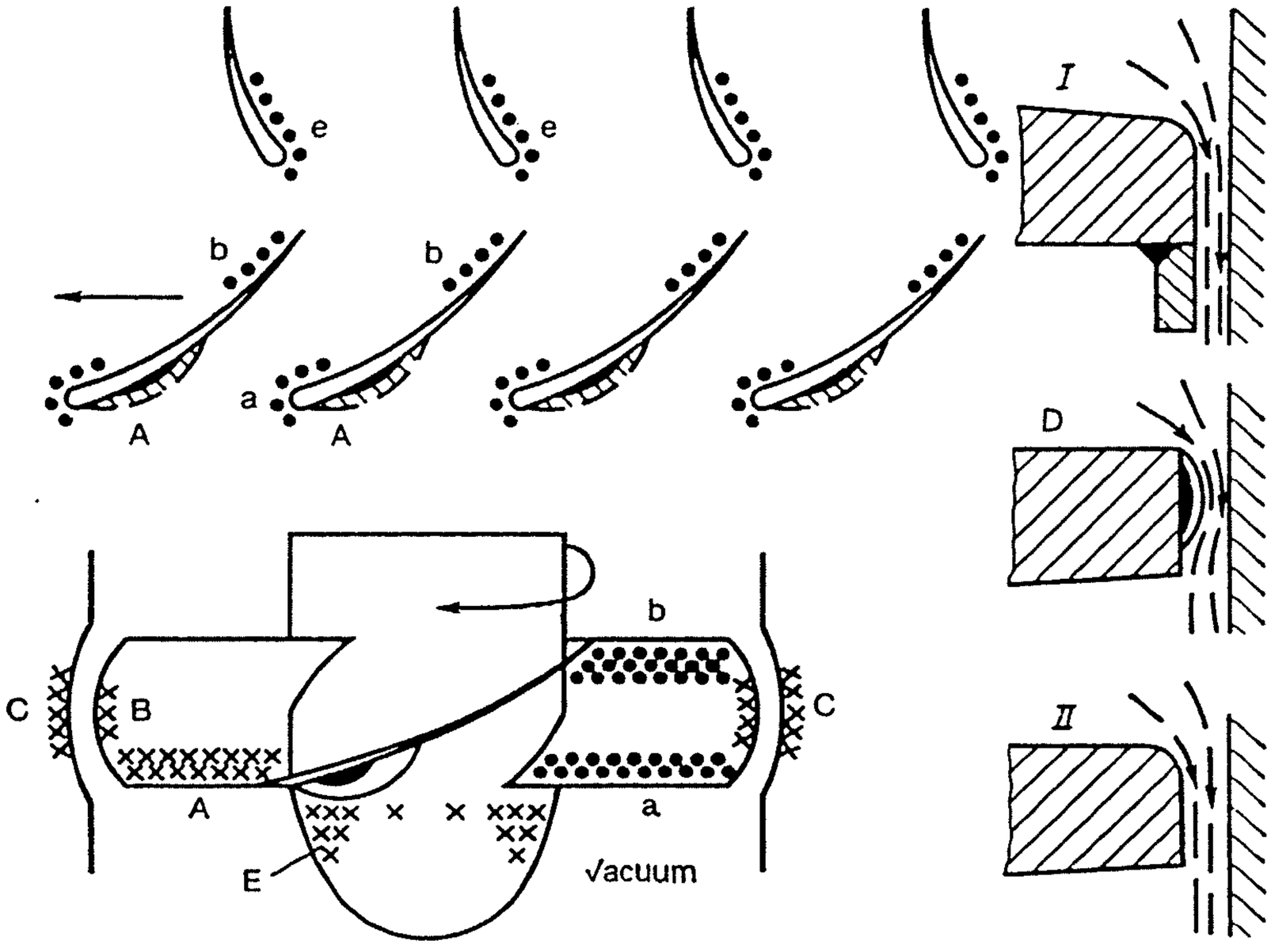


FIGURE 17.11. Points of most intense wear in axial-flow pumps. A, B, C, D, E — Cavitation erosion; a, b, e — abrasive wear.

Abrasive wear. Section 13.1 explains that the general purpose pumps are intended for delivering clean water, but in some cases they are used for pumping water from rivers or from pits that contain a quantity of solids, such as sediments or ground particles. Nevertheless, that the water has only a small quantity of solids (e.g., river water can contain suspended sediments 0.5 to 3 kg/m^3), they are able to inflict intense abrasive damage on the pump. Abrasive wear is determined mainly by the concentration of solids in water, relative velocity of flow in the pump, and abrasive resistance of the material.

The process of solids abrasive action is very complicated and the confines of this chapter allow only the reporting of the most important factors. Due to a greater density of solid particles their trajectories differ from trajectories of liquid. The larger the acceleration of the flow the greater the deviation of the trajectories. When the flow meets a surface that changes its direction, the solid particles strike and scratch this surface. The greater the kinetic energy (KE) of the particle, the stronger its abrasive action on the surface. So the first factor is KE of the particle.

$$\mathrm{KE} = m\frac{w^2}{2} = \rho_s\left(\frac{\pi d_s^3}{6}\right)\left(\frac{w^2}{2}\right)$$

where d_s is diameter of the particle, ρ_s is its density, and w is the relative velocity. The second factor is the quantity of particles acting on the unit surface area during unit time QT

$$QT = KC_s w$$

where K is the coefficient, and C_s is the solid particles content (kilograms per cubic meter). The third factor is the quality of solids, their hardness, edge sharpness, abrasive ability (AA) (the most dangerous are quartz solids). The fourth factor is the abrasive resistance (R) of the material of the element that is flowing around.

Summarizing all the factors, the general relationship determining abrasive intensity (AI), e.g., the loss of mass of some element (kilograms per hour) can be expressed in the form

$$AI = SC_s(k_{AA}/k_R)d_s^3 w^3 \tag{17.2}$$

where S is any coefficient, and k_{AA} and k_R are the generalized appropriate factor parameters.

As revealed by experience with the operation of centrifugal pumps (Figure 17.10), the impeller blades near leading edge a and on trailing portion b on the working side suffer the most intense wear. The solid particles that get into seals rapidly increase clearances. In axial-flow pumps (Figure 17.11) leading edges a and trailing portions b of the impeller blade working side and the vanes of straightening vane assembly e are subjected to the heaviest abrasive wear. The pump operation experience (Figures 17.10 and 17.11) shows that cavitation and abrasive zones do not coincide on impeller blades, but in clearances both act together.

Solid particles carried by the liquid cause abrasive wear of one additional type: while entering packing glands and bearings they accelerate local wear of the shaft. To simplify the repair process, a special replaceable sleeve (jacket) is often fitted on the respective portions of the shaft. For the same purpose replaceable sealing rings (see Figures 13.1 and 13.5) are employed.

In conclusion it is usefull to note that cavitation wear can be diminished by different methods, including operation measures aimed at minimizing the time of cavitation-hazardous operation and increasing the cavitation margin to the maximum possible extent (decreasing vacuum in the suction pipe). This can be achieved by decreasing H_s, which reduces losses in the suction pipeline.

The material used for manufacturing pump components also plays an important role. Cast iron offers the lowest resistance; stainless steel is the best; some plastics and rubber display fairly good cavitation and abrasive strength. The latter materials can be used for protecting steel

parts. There are a number of methods for applying protective polymer coatings: putty applied in a layer several millimeters thick, or paint. The most challenging problem here is to ensure reliable adhesion of the coating to the base metal. The adhesion depends on the coating composition and method of its application, and on the surface finish of the part to be coated.

With high concentrations of abrasive particles in water, special slurry pumps are used.

17.5. UNSTABLE OPERATION OF PUMP

To ensure normal operation of pumps and pump units, the operation of the pump–pipeline system should be stable. This implies that normal operating conditions should be restored after any inadvertent disturbances that may be brought about by different causes (temporal variation in discharge rate, resistance, etc.).

Let us consider the operation of a pump and pipeline at a constant static head (water is delivered to a large reservoir) and check whether operating conditions P determining actual delivery Q_{ac} (Figure 17.12a) are stable. Let the discharge be increased temporarily by ΔQ. H_{sys} will

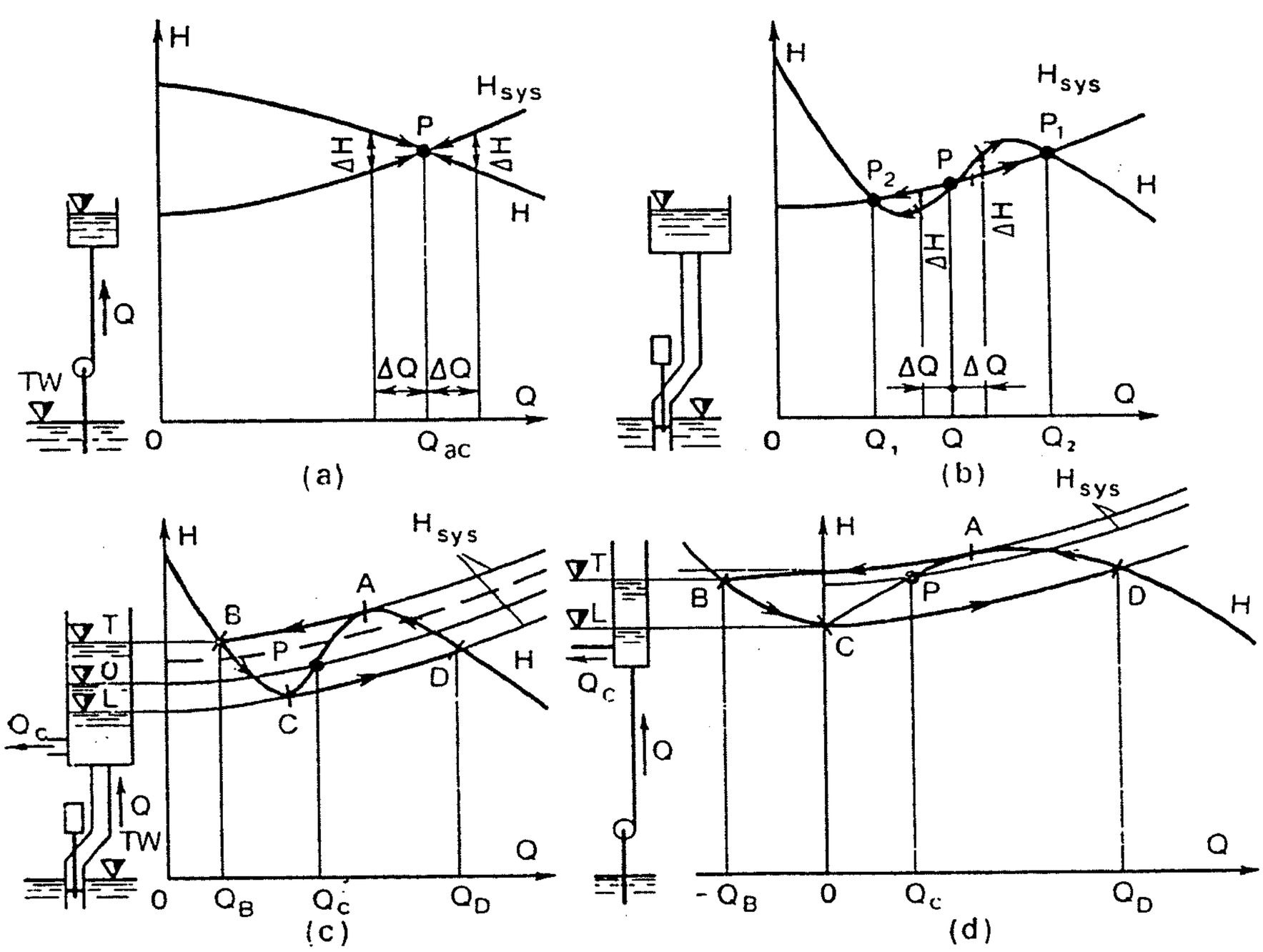


FIGURE 17.12. Stable and unstable pump operating conditions.

rise, pump head H will drop, resulting in head difference ΔH opposite to water flow. The head difference will decrease the water flow rate and make the condition return to the initial point P, as indicated by the arrows. If discharge is temporarily decreased by ΔQ, ΔH will be directed downstream of the flow, thus increasing the discharge, i.e., returning to initial point P as shown by the arrows. Thus, operating conditions P determining actual delivery in Figure 17.12a are steady.

Next, take a high specific speed pump whose curve has an inflection (see Figure 15.5) and apply it to the same conditions in order to check the stability conditions of point P shown in Figure 17.12b. Increase the discharge by ΔQ. Head H developed by the pump will rise more intensively than H_{sys}, and the resulting difference ΔH will be directed down the liquid flow and will cause a still greater increase in the discharge. The conditions will not return to the initial state and, as illustrated by the arrows, will deflect from it until it reaches point P_1 lying on the intersection between curves H and H_{sys}. If discharge is decreased by ΔQ, the resulting difference ΔH will be directed opposite to the liquid flow to point P_2. The analysis shows that conditions P shown in Figure 17.12b are not stable and can inadvertently displace either to P_1 or to P_2. That is known as static instability.

We can define the condition stability criterion, which is linked with the inclination of the tangents to curves H and H_{sys}. The conditions will be stable, provided the following is observed at the intersection between pump curve H and system curve H_{sys}:

$$\frac{\partial H}{\partial Q} < \frac{\partial H_{sys}}{\partial Q} \tag{17.3}$$

Let us consider more complex conditions, in which the system also has a certain volume (Figure 17.12c). Discharge from the upper reservoir is constant, Q_c, while reservoir level and static head can change depending on the ratio between pump delivery Q and discharge Q_c. Let discharge Q_c reach the curve inflection zone (point P). Assume the delivery has somewhat increased. The level in the reservoir will rise and line H_{sys} will move upward; the delivery will continue to increase, which in turn will increase the level in the reservoir. This occurs until curve H_{sys} reaches point A. At this point delivery $Q > Q_c$ and the reservoir level goes on increasing, curve H_{sys} rises, but separates from the pump characteristic curve and the conditions change over from point A to point B, where pump delivery $Q < Q_c$ (inertia forces also take part in this). Now the reservoir level goes down and the condition point moves along pump curve H to point C. Here, the conditions are again disrupted and change over to point D where $Q > Q_c$. This causes an increase in the reservoir level and displacement of the condition point

from D to A. The process then repeats. Thus, the condition point continuously moves along the sections of curve $DACB$, $BCAD$ passing through unstable point P. The reservoir level changes from ∇L to ∇T and the delivery from Q_B to Q_D.

The phenomenon described above is called surging and is a form of self-oscillation which is very detrimental for both the pump and the entire system. Surging may be also found in centrifugal pump units. Assume a system is shown in Figure 17.12d and discharge Q_c is such that condition point P is on the back drop zone $\partial H/\partial Q > 0$ of pump curve H. This point is not stable because here, $\partial H/\partial Q > \partial H_{sys}/\partial Q$, i.e., condition (17.3) is not met. Assume the conditions move to the right. This involves an increase in pump delivery Q and in the reservoir level. Line H_{sys} rises, reaches point A and then the condition disrupts and changes over to point B located in the LH quadrant of the curve (see Figure 16.15). Now, discharge Q moves in an opposite direction, and the reservoir level drops rapidly. The condition point displaces from B to C. Here again, a changeover from C to D takes place, after which the reservoir level rises, thus shifting the condition from D to A. Then the process repeats. Thus, the self-oscillating process is started and the pump delivery changes from Q_B to Q_D, and the reservoir level from ∇T to ∇L. The oscillation period in surging depends on the pump characteristic H, system characteristic H_{sys}, and reservoir area.

The surges in the above described pumping systems with free volume have a low frequency. But similar conditions in the system of a pump with rather long pipeline instability can arise due to water hammer action. This will be high frequency pulsations that are much more dangerous.

A specific type of instability can arise if pumps that have head characteristics with back drop zone are connected for parallel operation on a common pipe system. Let us analyze the most simple case of two identical pumps (Figure 17.13). Here, $H_{1,2}$ is the head curve of each pump, H_{1+2} is the curve of both pumps in parallel ADE, which is plotted as usual by doubling the abscissas of the ABC curve. For given conditions, however H_{1+2} also can be plotted by adding abscissas AB for one pump to BG for the other. This will give DG curve for parallel work. The possibility also exists to add abscissas ABG to the abscissas of the AF part. It will also give a curve ALG for parallel operation. Therefore, in zone $H_{Q=0} \le H \le H_{\max}$ three possible curves exist for parallel work. If pipeline system characteristic H_{sys} intersects all of them, as shown in Figure 17.13 (points P_1, P_2, P_3), three regimes are possible. The interchange between them creates the possibility of surges and pulsations.

To preclude instability, surging, and pulsation it is advisable to avoid pumps operation in the region $H_{Q=0} \le H \le H_{\max}$, which sometimes is called the unstable zone of the pump characteristic.

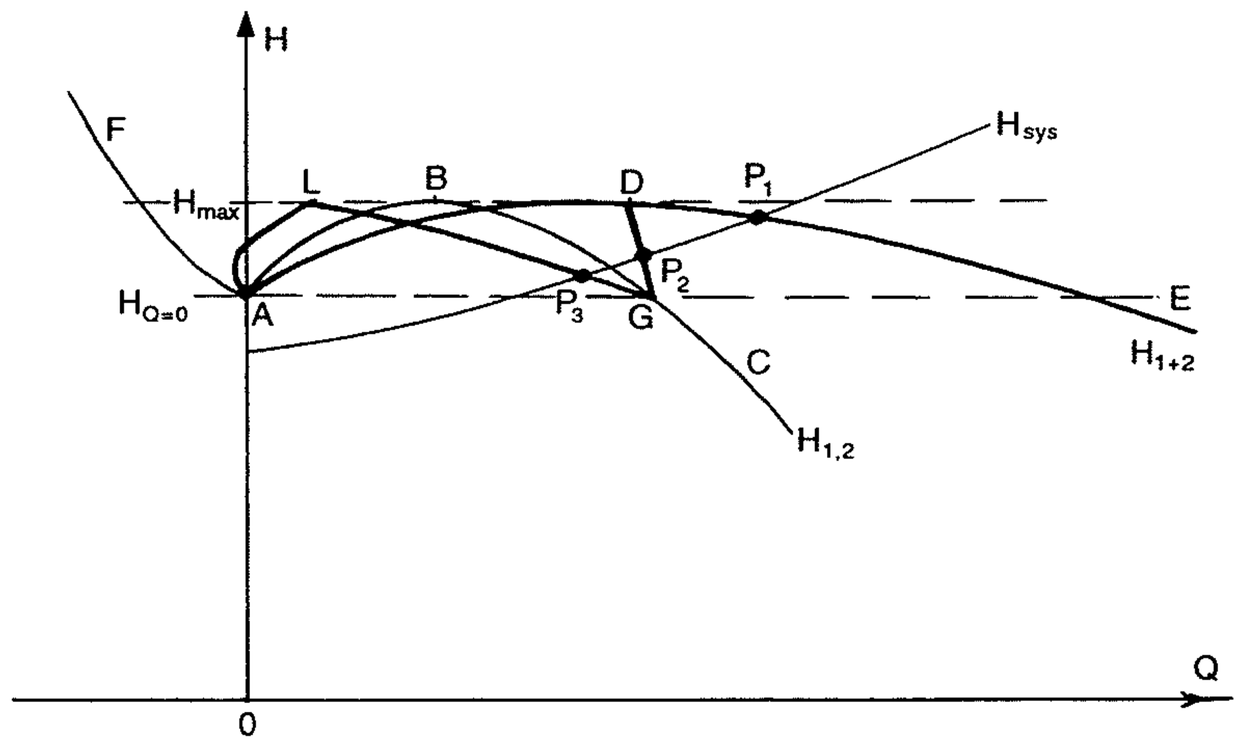


FIGURE 17.13. Pump instability in parallel operation.

17.6. PUMP SUMPS

The purpose of the sump is to deliver water from tailrace to the pump inlet branch. The principal demands made on the sumps, partially discussed earlier in connection with suction pipes, are to warrant low hydraulic losses which affect permissible suction lift, exclude air sucking through joints or creation of air bags, and air entrainment through free surface vortices. It is necessary to bear in mind that admission in pump suction, even 1% of air, can diminish the delivery up to 5 to 10% and if air discharge will be 10 to 15% the delivery can drop to zero.

The sump design must be such that velocity distribution before the inlet nozzle is rather uniform (can be checked by α value, Equation 5.1, $\alpha \leq 1.1$) and that the overall circulation (prerotation) here will be low. It is most important for low-head high specific speed axial pumps, for which (as it is clear from Equation 12.13a) Γ_1 can have a sufficient influence on pump head. The accepted permissible value is

$$\frac{1}{Q}\int_0^{0.5D_0}\Gamma_1\, dr \leq 0.05$$

where Q is the pump discharge, and D_0 is the impeller eye or inlet diameter.

There are two types of sumps. For large pumps $Q > 1.5$ to 2 m^3/s each pump has an intake in the form of a curvilinear duct with a gradually decreasing cross-sectional area as shown in Figure 16.1 and 16.3. The entrance cross-section, in which trashracks and gates are located, is such that the mean velocity here is 0.8 to 1.3 m/s. The form of the duct usually is given by the pump manufacturer; it is constructed from concrete.

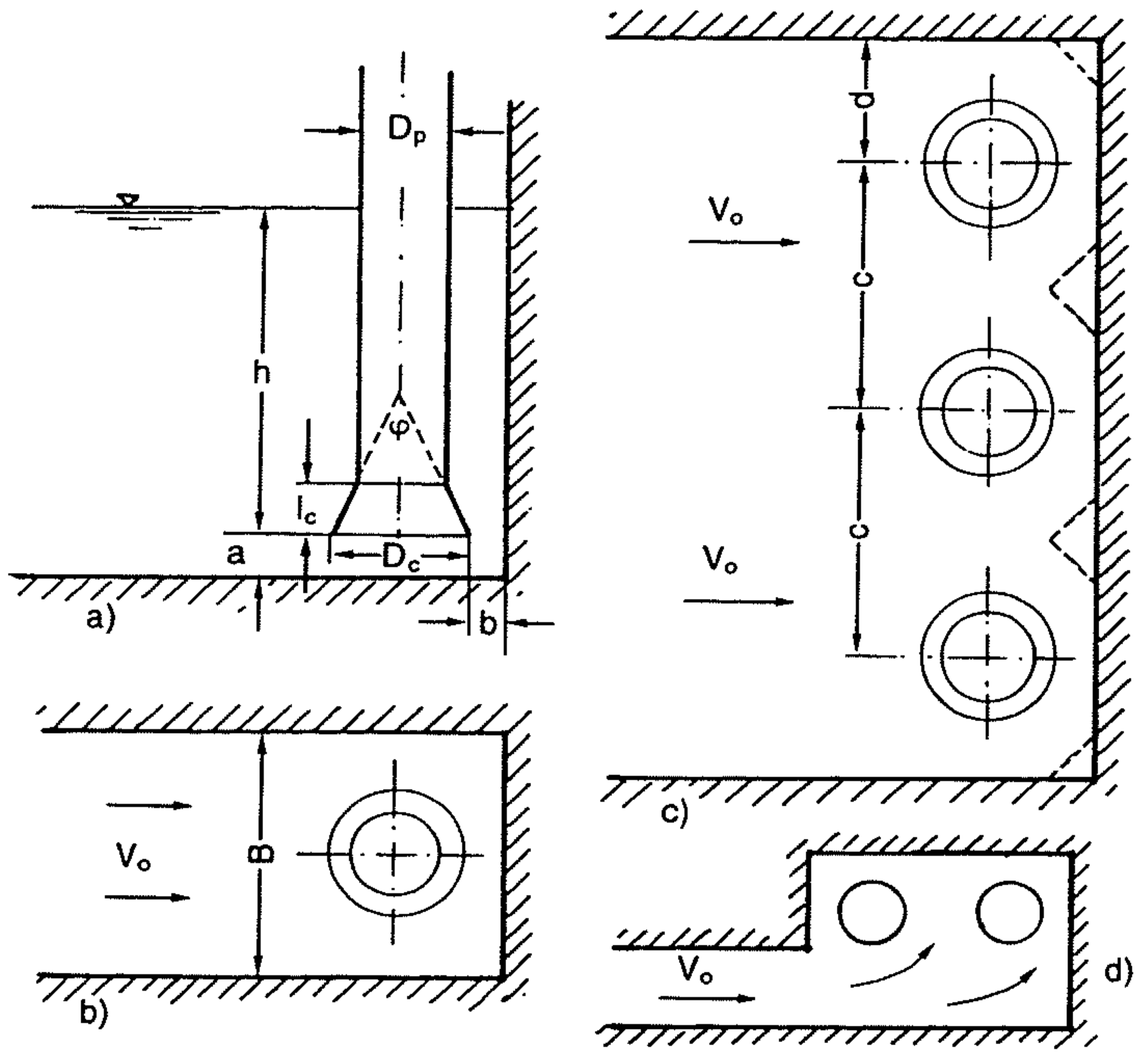


FIGURE 17.14. Free flow pump sumps.

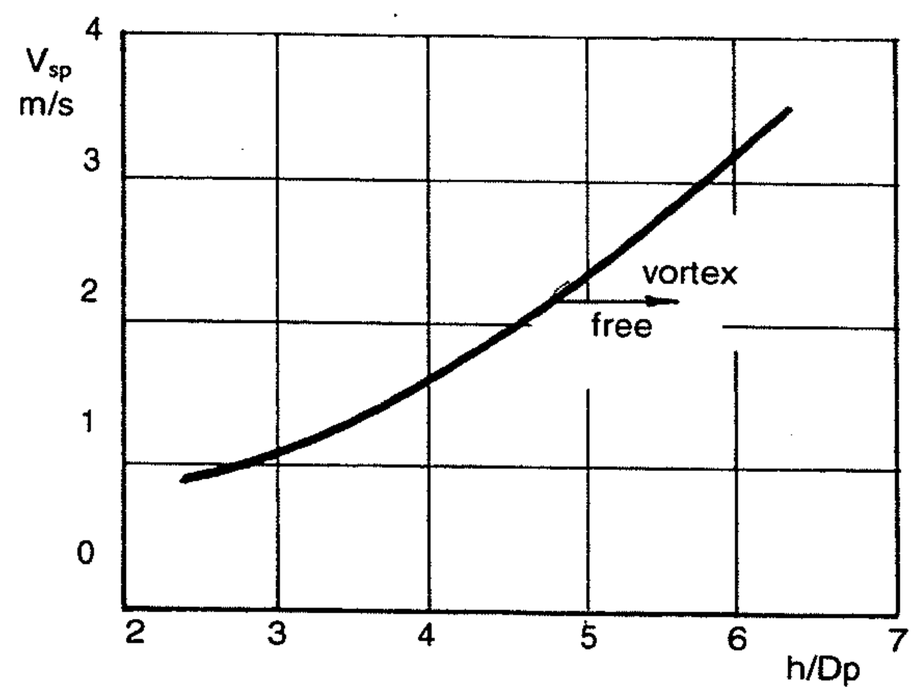


FIGURE 17.15. Suction pipe submergence and air entrainment.

To prevent air entrainment through the vortices on the free surface the upper edge of the intake section must be submerged no less than 1.2 to 2 m (depends on entrance velocity) under minimum TW level.

For smaller pumps, the chamber or free-flow open sumps are often used (Figure 17.14). Their basic dimensions are D_p, diameter of suction pipe accepted that takes into account that rated velocity V_{sp} is about 0.8 m/sec for $D_p \leq 0.25$ m and 2.5 m/s for $D_p \geq 0.6$ m. To decrease pipe entry losses a cone $\varphi = 35°$ to 45°, l_c is $(0.8 - 0.6)D_p$ and $D_c = 1.5D_p$ is arranged. The distance between cone and floor $a = (0.4 - 0.6)D_p$

and no more than 0.8 D_p. For this condition the entry resistance coefficient $\zeta_c = 0.15$ to 0.2 with regard to pipe velocity.

For one suction pipe the width of sump $b \geq 3D_p$ and the distance to the back wall $b \geq 0.4D_p$. If several suction pipes are found in one sump chamber (Figure 17.14c) their mutual influence must be avoided. The distance between the pipes must be $c \geq 3D_p$ and $d \geq 1.5D_p$. Contour with triangle ledges shown by the dotted line is useful. Where the approach velocity v_p has momentum toward suction pipes the sump design similar to Figure 17.14d cannot be recommended because it stimulates the creation of circular flow in suction pipes.

To prevent entrainment of air through free surface vortices, the lower edge of the suction cone must be sufficiently submerged under minimum free surface level. Its value can be determined by the graph in Figure 17.15, where h/D_p is given as a function of maximum suction pipe velocity v_{sp}.

CHAPTER 18

Special Pumps

18.1 DREDGE PUMPS

Dredge pumps transfer slurry (soil-water mixture) and are used in making pits and open casts in mining, erecting dams and embankments in hydraulic engineering, conveying soil and minerals (ore, coal), bottom deepening (coastal engineering, river transports), removing ash at thermal power plants, etc.

Dredge pump design features are dictated by a high concentration of solid particles in the water being transferred, which cause intensive abrasive wear, and by the need to pass rather large inclusions (pebbles, stones) that may enter the pump with the slurry.

A light-duty dredge pump is shown in Figure 18.1. Its general layout is similar to that of a regular cradle-mounted pump (see Figure 13.1), and the particular design features are entirely determined by the aforementioned requirements to be met. Impeller (1) has a relatively large width b and only three or four blades to ensure a sufficient flow area. A solid casing (2) forms a large intake chamber with a substantially constant flow area with is then transformed into a delivery pipe (DP). Attached to the casing is a cover (3) with an intake pipe (IP), while the casing is secured via a plate (4) to a bed (5). The casing and the bed are bolted to the foundation. Protective disks (6) and (7) made from wear-resistant steel are disposed between the impeller and the casing components. Fitted to a shaft (9) near a packing gland (8) is a protective sleeve which is replaced in case of wear. To diminish the

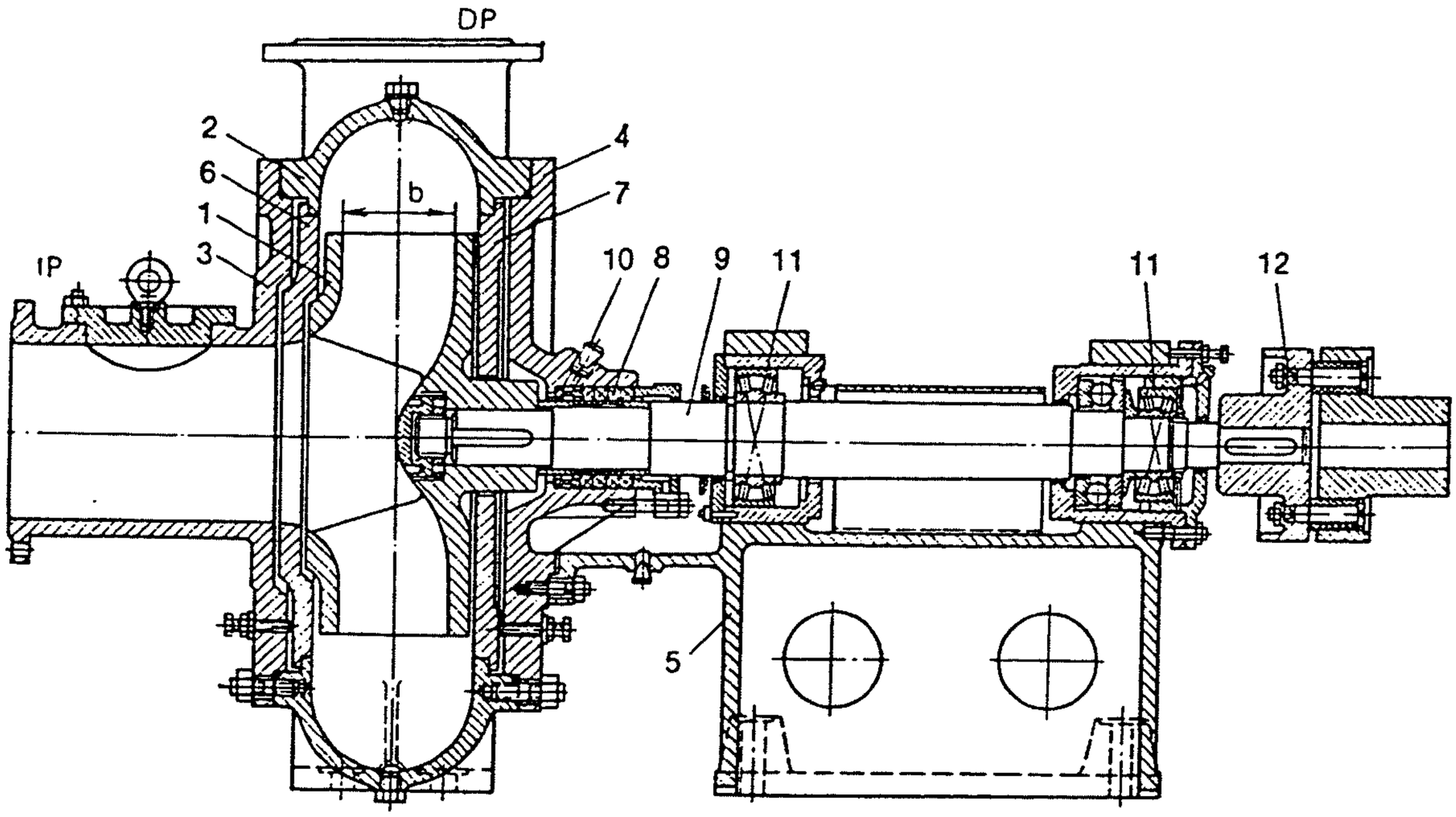


FIGURE 18.1. Light-duty dredge pump.

ingress of solid particles into the cavity between rotating and stationary parts, clean water is supplied through connection (10). The shaft is mounted on roller bearings (11) and has a thrust ball bearing that takes up axial loads (the impeller axial forces are not balanced). A resilient coupling (12) connects the pump shaft to the electric motor.

A heavy-duty dredge pump (Figure 18.2) includes substantially the same parts as the light-duty pump, but differs in that it is more reliably protected because of a double casing. Arranged inside its load-carrying casing (2) is an additional protective casing (13) which tightly adjoins to protective disks (6) and (7). Thus, impeller (1) rotates in a continuous protective shell made from wear-resistant steel.

Despite various protection measures, the dredge pump working parts wear rather rapidly, especially in heavy-duty service. Therefore, their construction allows easy disassembly and replacement of high-mortality components.

The dredge pump type designation (Figure 18.3) shows design delivery (cubic meters per hour); head (meters); and speed of rotation (revolutions per minute).

The dredge pump nomenclature (Figure 18.3) includes pumps with regular flow area (Figure 18.1) and with increased flow area. Several types of dredge pumps fit various operating conditions with regard to intensity of abrasive effect: single-casing light-duty, medium-duty lined with rubber or abrasive material with organic binder, and heavy-duty double-casing (Figure 18.2). The available standard sizes of dredge

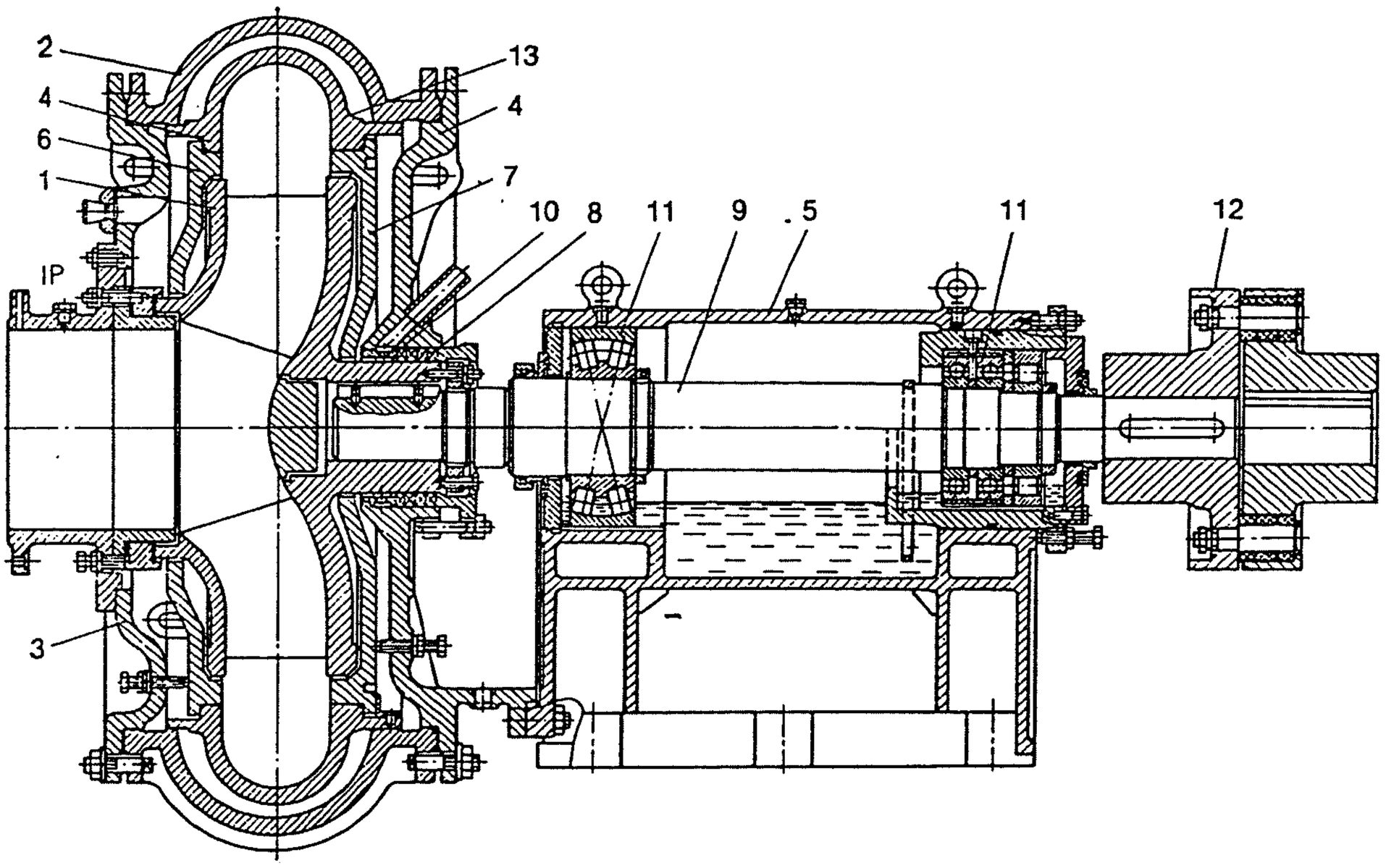


FIGURE 18.2. Heavy-duty dredge pump.

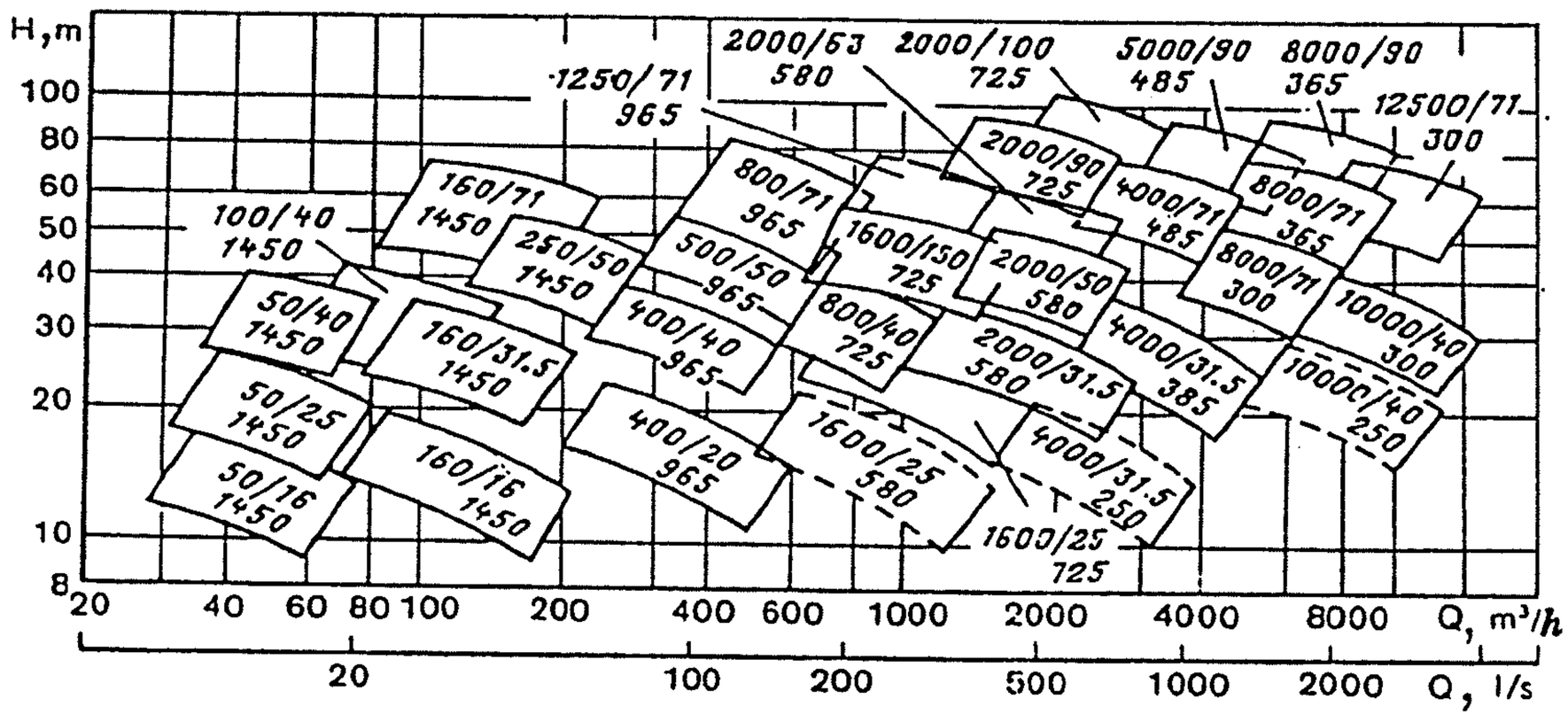


FIGURE 18.3. Nomenclature of dredge pump.

pumps cover a delivery range of 40 to 12,500 m^3/h and a head range of 10 to 15 and 70 to 100 m.

To transfer slurries containing fine particles (sand, crushed ore or slag, ash particles, etc.), use is made of sand pumps. These are structurally similar to the light-duty dredge pumps, but smaller in size and have easy-to-disassemble casings. The sand pump nomenclature indicat-

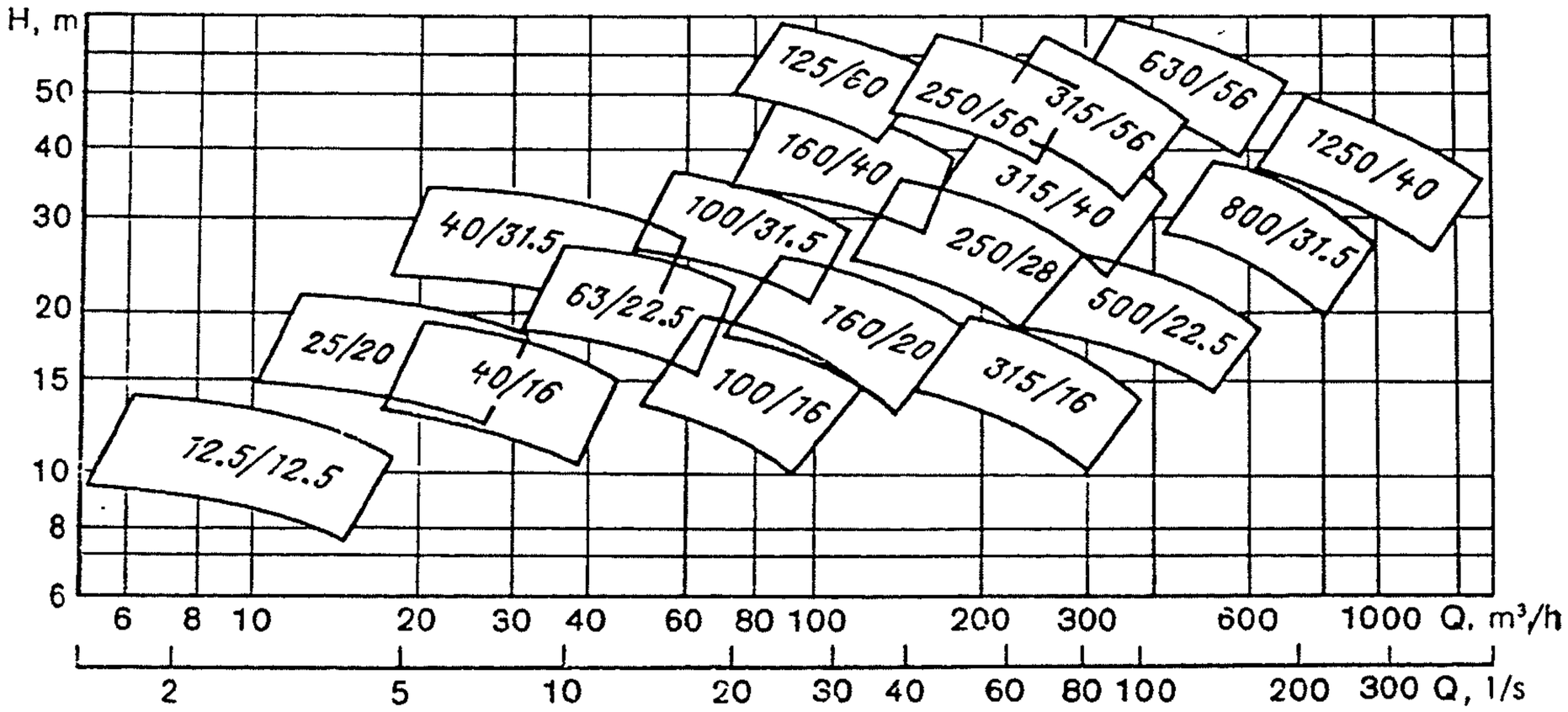


FIGURE 18.4. Nomenclature of sand pump.

ing design deliveries (cubic meters per hour) and heads (meters), is shown in Figure 18.4. These are mainly small pumps with delivery ranging from 6 to 1200 m^3/h and heads from 10 to 60 m.

The dredge and sand pump characteristics are always given for clean water. Figure 18.5 exemplifies a characteristic curve of dredge pump 4000/71 with an impeller of two sizes (regular diameter of 1390 mm and reduced diameter of 1250 mm). The figure presents the curves of head H, power N, efficiency η and permissible vacuum suction lift H_v^{per}. Note that despite considerable dimensions, the efficiency of this pump is relatively low, slightly above 60%, which is explained by hydraulically unfavorable forms of the flow passage which cannot be avoided.

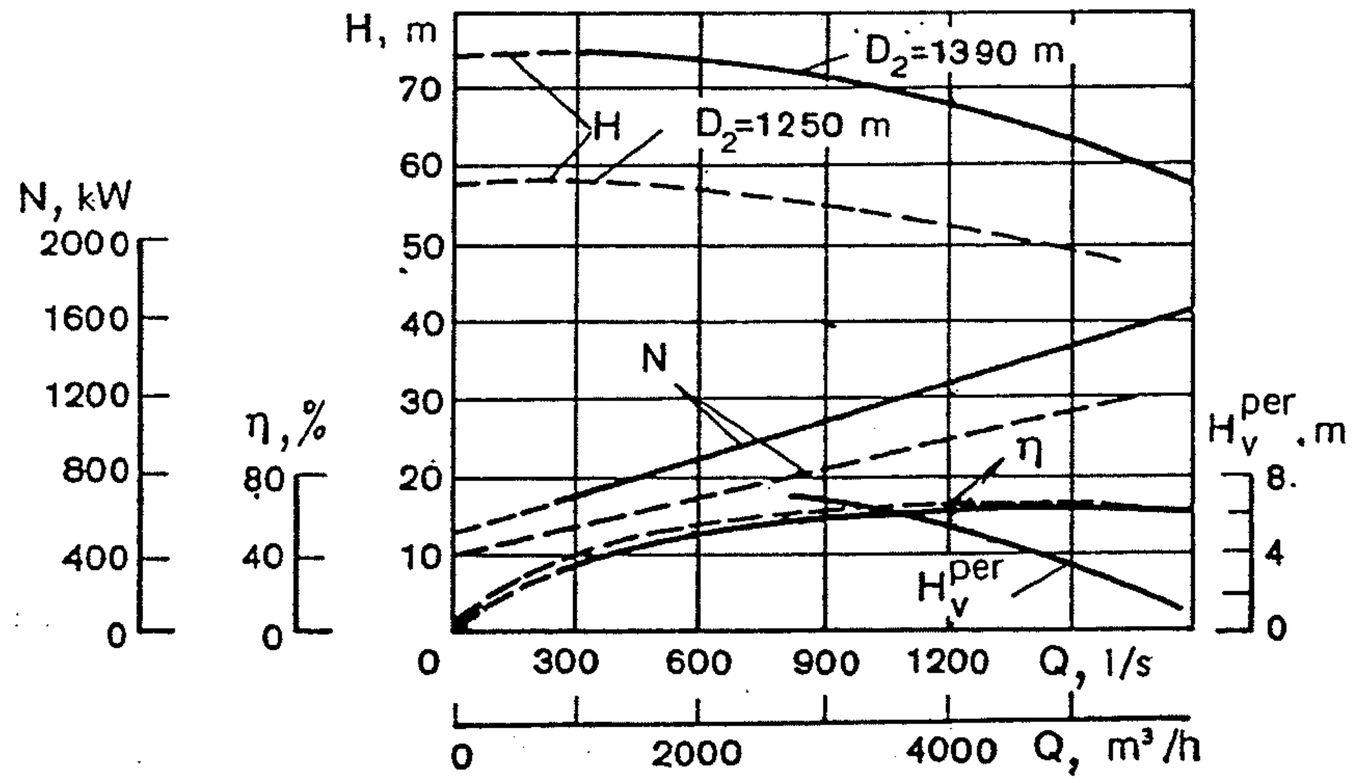


FIGURE 18.5. Characteristics of dredge pump 4000 / 71, $n = 485$ rpm.

When recalculating the dredge pump characteristics for transferring slurry, it is assumed that slurry average density $\rho_{sl.av}$ depends on the relative volume concentration of solid fractions

$$\varepsilon_{sl} = W_s / W_{sl} \tag{18.1}$$

where W_s is the volume of all solid particles contained, and W_{sl} is the total volume of slurry.

Because water density $\rho_w = 1$ t/m^3,

$$\rho_{sl.av} = \varepsilon_s(\rho_s - 1) + 1 \tag{18.2}$$

where ρ_s is the solid particle density that is about 2.5 t/m^3 for soil. The average density of slurry is $\rho_{sl.av} = 1.15$ to 1.20 t/m^3 (limit value up to 1.3 t/m^3).

When discussing dredge pump operating conditions, slurry is usually regarded as a heavy, homogeneous liquid. Therefore, when changing over from water to slurry, pressure H_{sl} and power N_{sl} should change proportionally to the $\rho_{sl.av}/\rho_w$ ratio, and slurry delivery Q_{sl} should not change. However, slurry may be considered a homogeneous liquid only by assumption, and thus corresponding corrections are introduced:

$$H_{sl} = k_H \frac{\rho_{sl.av}}{\rho_w} H$$

$$Q_{sl} = Q$$

$$N_{sl} = \frac{k_H}{k_\eta} \frac{\rho_{sl.av}}{\rho_w} N \tag{18.3}$$

where ρ_w is the density of water, and k_H and k_η are the corrections for head and efficiency. These corrections are needed because the acceleration of slurry results in the additional motion of heavy solid particles relative to liquid. This changes the action of forces and creates additional losses, and results in a drop in head and a rise in losses. The correction values depend on a number of factors, of which the particle size is most vital. For fine soil $d < 3$ mm, it may be assumed that $k_H = 1$ and $k_\eta = 1$; for coarse gravel, $k_H = 0.85$ and $k_\eta = 0.95$. Accordingly, system characteristic $H_{s.sl}$ (meters) is also corrected for slurry

$$H_{s.sl} = \frac{\rho_{sl.av}}{\rho_w} H_{st} + h_{sl} \tag{18.4}$$

where H_{st} is the geometric head (elevation difference; meters), and h_{sl} is the losses involved in slurry motion along the pipeline (meters of water column).

The actual delivery is determined by the point of intersection of the dredge pump H_{sl} curve displaced according to Equation 18.3 with the system $H_{s.sl}$ curve displaced according to Equation 18.4.

The proper determination of the permissible suction lift (geometrical) H_s^{per} should receive special attention. The dredge pump characteristics include line H_v^{per} obtained by water tests, i.e., at $\rho_w = 1\ \text{t/m}^3$. If density ρ of liquid increases, the dynamic pressure drop should increase, and hence, permissible suction lift $H_{v.sl}^{per}$ for slurry should decrease.

When the pump starts cavitating in transferring water the dynamic pressure drop in the impeller relative to the intake pipe pressure is

$$\Delta H_d = \frac{p_{atm}}{\rho g} - H_v^{cr} - \frac{p_{s.v}}{\rho g}$$

For normal atmospheric pressure and cold water, we may assume

$$\frac{p_{atm}}{\rho g} - \frac{p_{s.v}}{\rho g} \approx 10$$

and

$$\Delta H_d = 10 - H_v^{cr}$$

When transferring slurry, a heavy liquid with an average density $\rho_{sl.av}$, we obtain in meters of water column

$$\Delta H_{d.sl} = \frac{\rho_{sl.av}}{\rho_w}(10 - H_v^{cr})$$

and hence,

$$H_v^{cr} = 10 - \Delta H_d$$

For slurry, we obtain, in meters of water column

$$H_{v.sl}^{cr} = 10 - \frac{\rho_{sl.av}}{\rho_w}(10 - H_v^{cr})$$

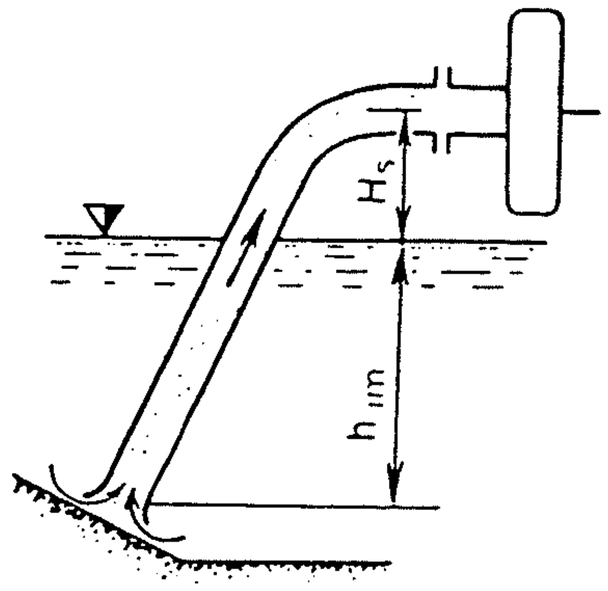


FIGURE 18.6. Determining permissible suction lift of the dredge pump.

Applying this to permissible suction lift, we obtain a conversion formula (meters of water column)

$$H_{v.sl}^{per} = 10 - \frac{\rho_{sl.av}}{\rho_w}(10 - H_v^{per}) \tag{18.5}$$

When converting dredge pump characteristics for slurry, a new line $H_{v.sl}^{per}$ is plotted according to Equation 18.5.

A suction lift $H_{v.sl}$ of a dredge pump transferring slurry contrary to Equation 11.3 also depends on the immersion of the suction pipeline under the liquid level h_{im} (Figure 18.6). Expressing $H_{v.sl}$ in meters of water column, we obtain

$$H_{v.sl} = \frac{\rho_{sl.av}}{\rho_w} H_s + h_{im} \frac{\rho_{sl.av} - \rho_w}{\rho_w} + \frac{v_1^2}{2g} + h_{suc} \tag{18.6}$$

Here, h_{suc} are the hydraulic losses in the suction pipeline (meters of water column), including the intake pressure difference needed to suck soil in.

Permissible suction lift H_s^{per} is found from Equation 18.6:

$$H_s^{per} = \frac{\rho_w}{\rho_{sl.av}} \left(H_{v.sl}^{per} - h_{im} \frac{\rho_{sl.av} - \rho_w}{\rho_w} - \frac{v_1^2}{2g} - h_{suc} \right) \tag{18.7}$$

To preclude cavitation, the following condition should be observed in a dredge pump

$$H_s \leq H_s^{per}$$

The results obtained show that the dredge pump installation permissible suction lift is substantially decreased when soil is sucked from a great depth. Therefore, various methods are used to increase pressure in the suction pipeline. These methods include special ejectors installed at the dredge intake end of the suction pipeline (see Figure 18.17c). Submerged installation of a dredge pump (below water level) is an efficient way of precluding cavitation.

18.2. WELL PUMPS

The pumps designed for delivering water from wells or shafts are called well or submersed pumps and are used for water supply, reduction of groundwater level, pit unwatering, and drainage. There are two popular types of well impeller pumps: pumps with a transmission shaft (formerly referred to as an artesian well pump) and pumps with an immersion motor.

18.2.1. Well Pumps with Transmission Shaft

These pumps are composed of three main units (Figure 18.7a): *I*—the pump per se (centrifugal, multistage) which is embodied so that it can be immersed into the well; *II*—a support structure with electric motor located on the surface; and *III*—a delivery pipeline and a transmission shaft passing inside the tube and resting on intermediate guide bearings. The pump is driven via this long shaft. The pump with intake strainer *IV* is submersed into water in the well.

Figure 18.7b illustrates the construction of a three-stage pump. Each stage comprises a centrifugal impeller (1) fitted to a vertical shaft (2), a casing (3) accommodating a diffuser (4) with an insert passing the shaft. Arranged between the casing and the diffuser are the vanes of the guide vane assembly (5). The form of the vanes is similar to that shown in Figure 13.14. These vanes zero the circulation of flow created by the wheel double as spacers between casing (3) and diffuser (4). The stages are interconnected by bolts and studs. Intake cone (6) is arranged in front of the first stage. A guide bearing is located in the center of the cone. An intake strainer (7) is secured to the cone. Sections of delivery line (8) 2 to 3.5 m long are secured by flanges over the last stage. The upper part of each stage accommodates a water-lubricated guide bearing (9). To preclude the ingress of sand into the bearings, clean water is supplied to them via a pipe (10). The main components of the upper support structure (Figure 18.7c) are the outlet elbow, whose vertical part is coupled with the last section of the delivery pipeline, and the

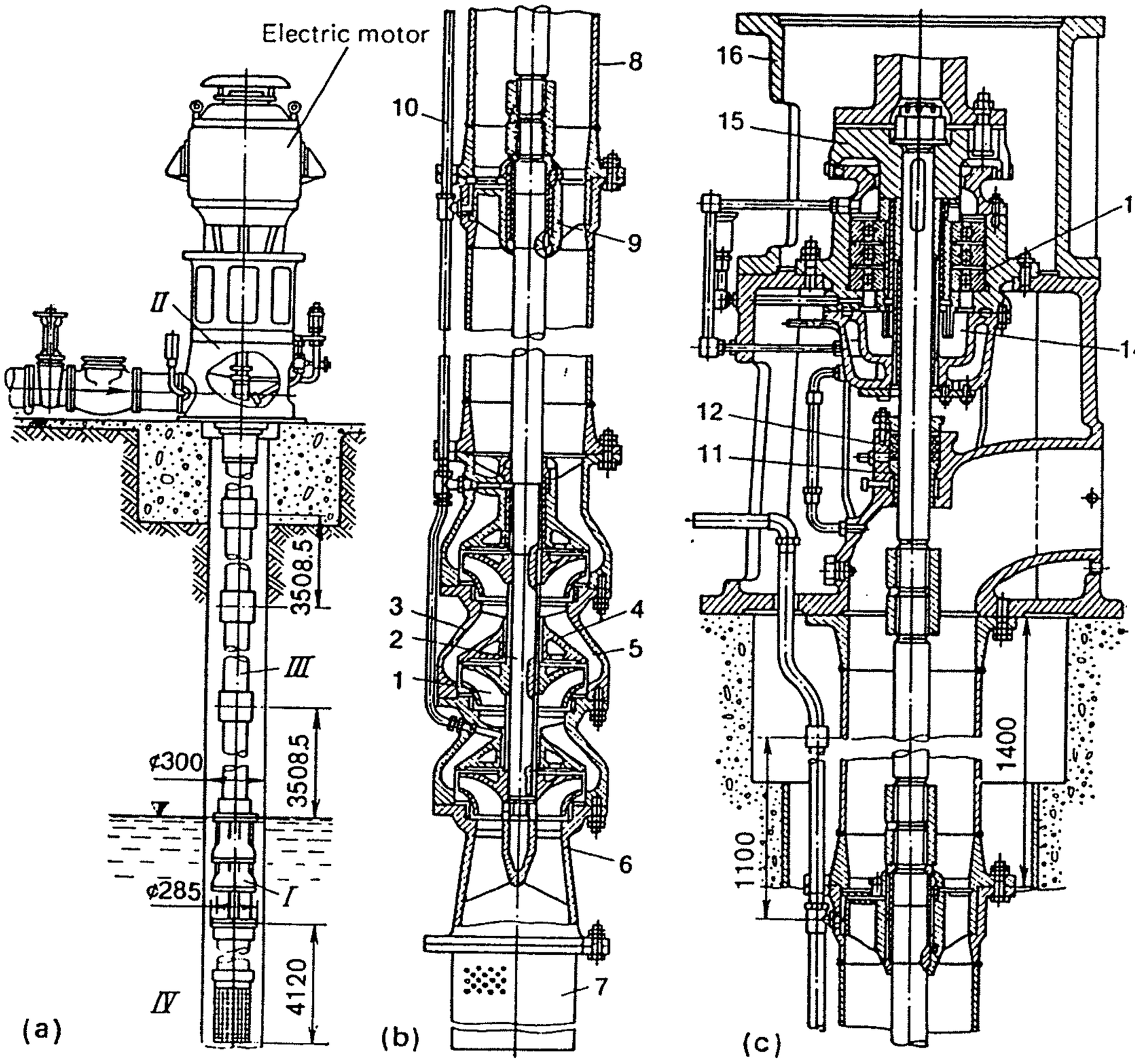


FIGURE 18.7. Well pump with transmission shaft.

horizontal part with the transfer pipeline, a guide bearing (11), a packing gland (12), and a very powerful thrust bearing (13) with an oil bath (14), which takes up the weight of all rotating parts of the pump and the total hydraulic axial force. Attached to the upper end of the shaft is a coupling 15 for connection with the shaft of a vertically mounted electric motor which is attached to a flange 16.

Centrifugal well pumps with a transmission shaft, type are intended to transfer clean cold water containing up to 0.1% mechanical impurities. There are special pumps for corrosive water and for elevated temperature. The generalized nomenclature of centrifugal well pumps with a transmission shaft is shown in Figure 18.8. Each pump type is designated by three parameters: dimension (diameter of well tube in inches), optimum delivery (cubic meters per hour), and head (meters). The available range of the pumps are the well diameters, from 6 to 20 in. (150 to 500 mm), delivery from 25 to 1000 m^3/h and heads at 25 m

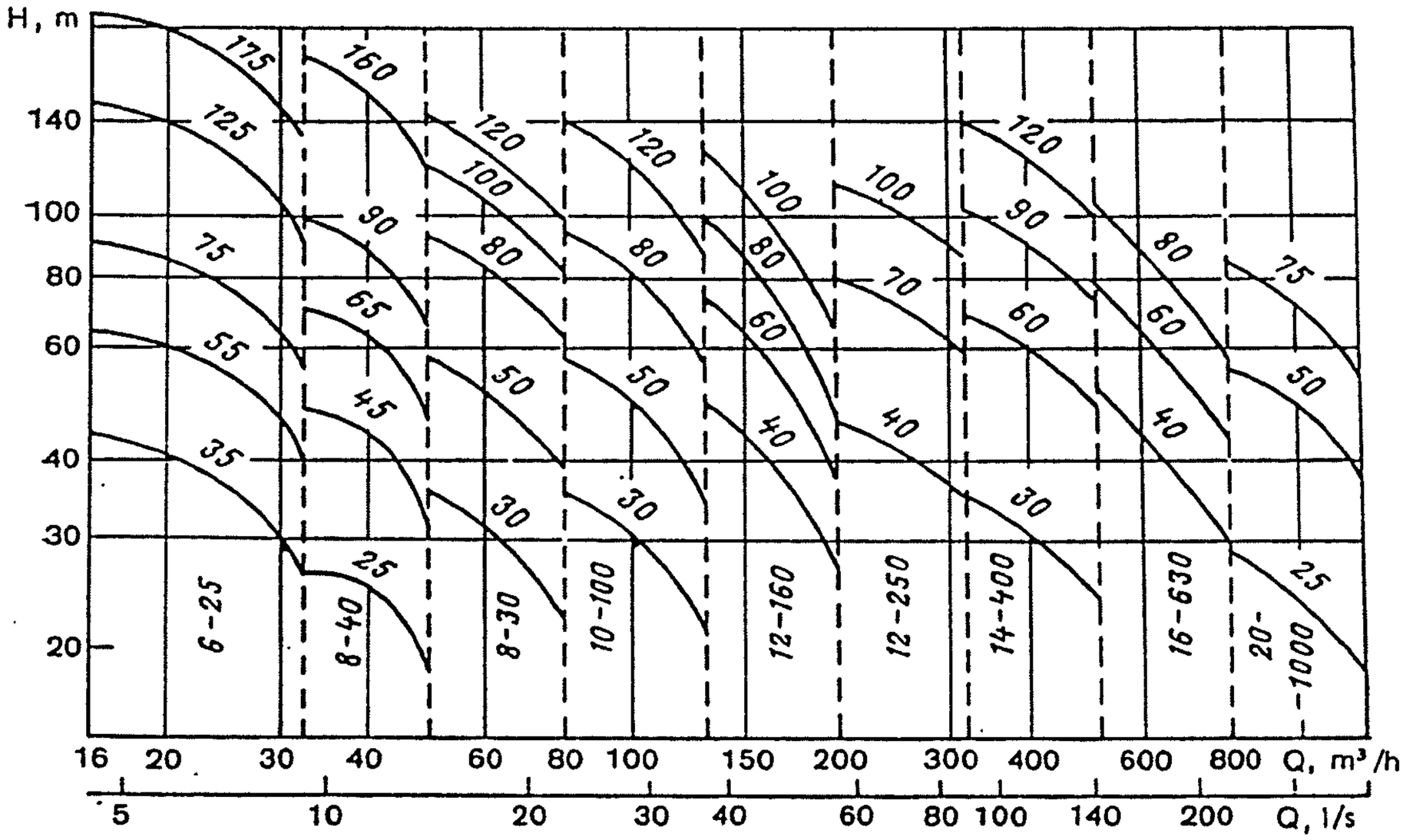


FIGURE 18.8. Nomenclature of well pumps with transmission shaft.

and up to 120 to 160 m. The transmission shafts are rather complex and require careful installation (pipe axis bends, displacements, etc., are intolerable). The installation depth should be accurately determined by the number of standard sections.

18.2.2. Immersion Motor Well Pumps

These pumps are characterized by their being driven from an electric motor submerged in water. The pump unit shown in Figure 18.9a comprises a multistage centrifugal pump (1), an intake strainer (2), an immersion motor (3), a delivery pipeline (4), and an electric cable (5). The two-stage pump is shown in Figure 18.9b. It includes impellers (1), guide vanes (2), and an upper flange (3) for coupling the delivery pipeline. An induction motor has a stator winding (4) with plastic insulation. The winding terminals are connected to power cable (5), and the joint is reliably sealed. The squirrel-cage rotor (6) rotates in water. The motor and the pump have rigidly coupled shafts with a coupling (7), water-lubricated guide bearings, and a thrust bearing (8) which takes up axial forces.

To ensure the durability of this unit, suspended abrasive particles should be kept off the electric motor. To this end, the electric motor is filled with clean water which is separated from the water being transferred by a collar (9). Oil-filled motors are also used.

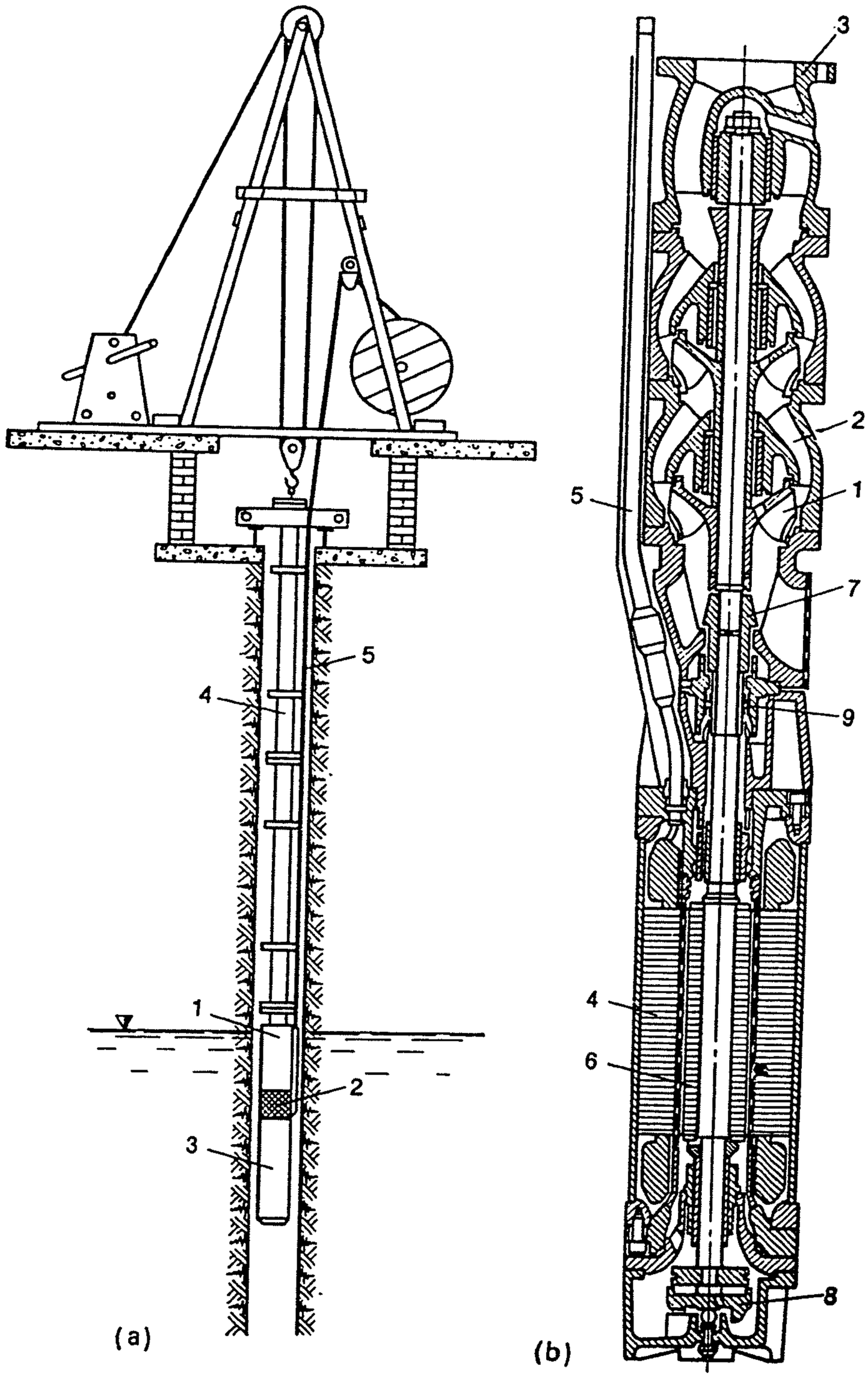


FIGURE 18.9. Well pump with immersion electric motor.

Well pumps with immersion motors are designed to transfer clean cold water, but there are modifications adapted to handle chemically active water with an increased content of solid particles.

The generalized nomenclature of centrifugal well pumps with immersion motors is presented in Figure 18.10. Here, each type is designated

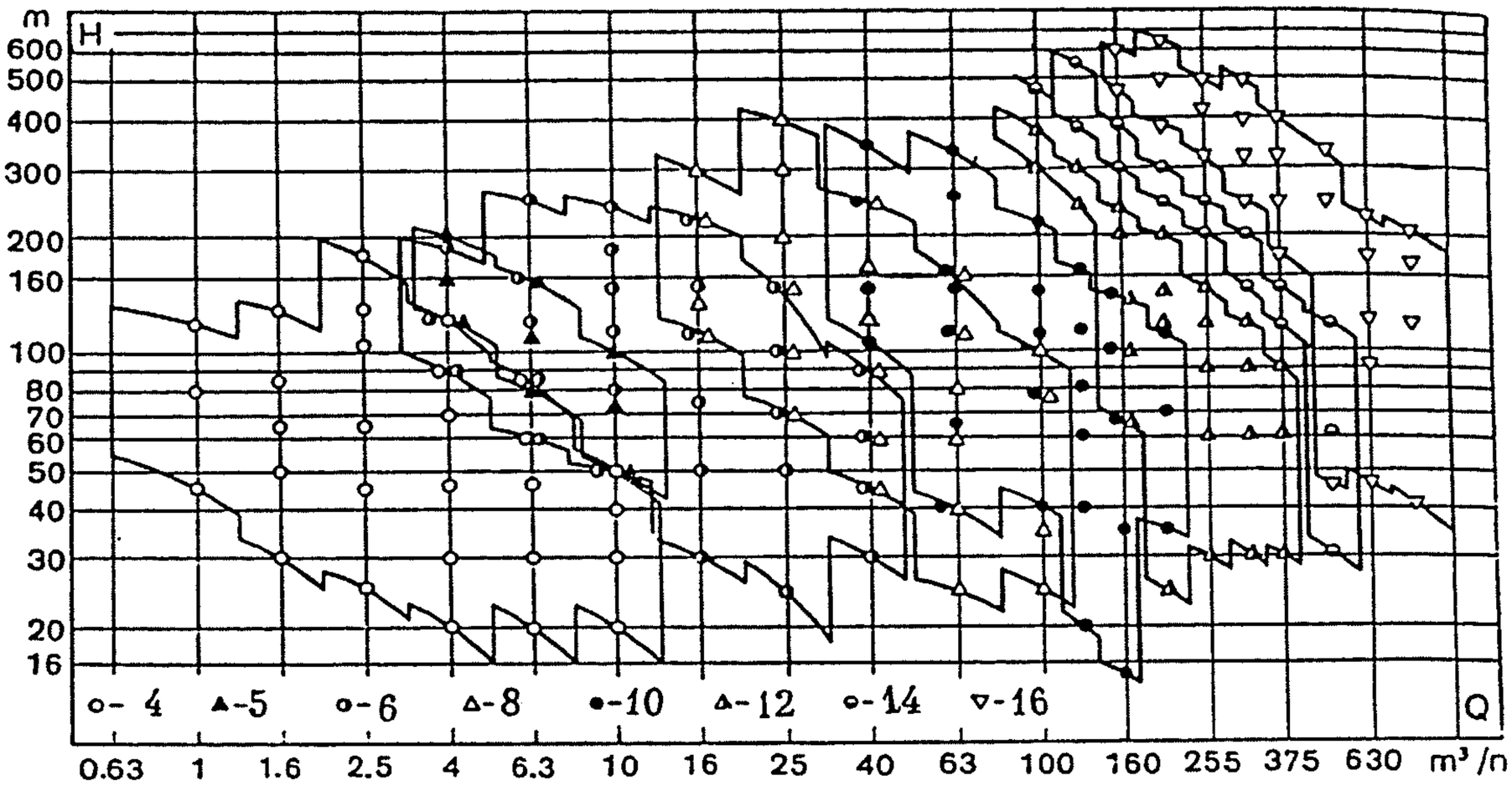


FIGURE 18.10. Nomenclature of well pumps with immersion electric motor.

only by its dimension, diameter of the well. It includes pumps from 4 to 16 in. (100 to 400 mm), but the larger diameters are also available if necessary. Each "type," as seen from the nomenclature, can be used in 2 wide range of discharges and heads. For example "type" 10 (250 mm), acceptable for deliveries from 40 to 200 m^3/h and for heads from 20 to 300 m. The head difference is achieved by accepting different numbers of stages.

The general range of this pump is for delivery from 1 to 1000 m^3/h and heads from 20 up to 300 to 500 m.

18.3. HYDRAULIC PUMPED-STORAGE PLANTS PUMPS

Hydraulic pumped-storage plants (HPSP) are intended to balance the power grid load curves. The pumped storage plants operate as follows. At night, when electricity consumption drops, the pumps are turned on and water is transferred from the lower to the upper reservoir. During the daytime load peak periods the turbines are engaged to use water from the upper reservoir. Thus, HPSP consumes electricity at night and generates it in the daytime.

HPSP may be equipped with pumps of very high power input and head. The desire for higher heads is explained by that they allow reduction of the volumes of water to be transferred and stored. Because the HPSP pumps have unique characteristics, they are designed and manufactured individually, and thus similar to large turbines.

Special scaled models are used to study the pumps and to get their characteristics; the results obtained (efficiency, etc.) are recalculated for full-scale conditions by the similarity formulas. The parameters, types, and constructions of HPSP pumps are very diverse.

Figure 18.11 illustrates a vertical pump of the Waldeck II HPSP in Germany, manufactured by Foith Co. The pump, with a 4110-mm wheel, has the following characteristics: head 330 m, delivery 65.5 m^3/s, speed of rotation, 375 rpm and power 230 MW. The pump shaft runs in a guide bearing (1) secured in a strong cover on which rests a thrust bearing (2) transmitting axial load through the support cone to the

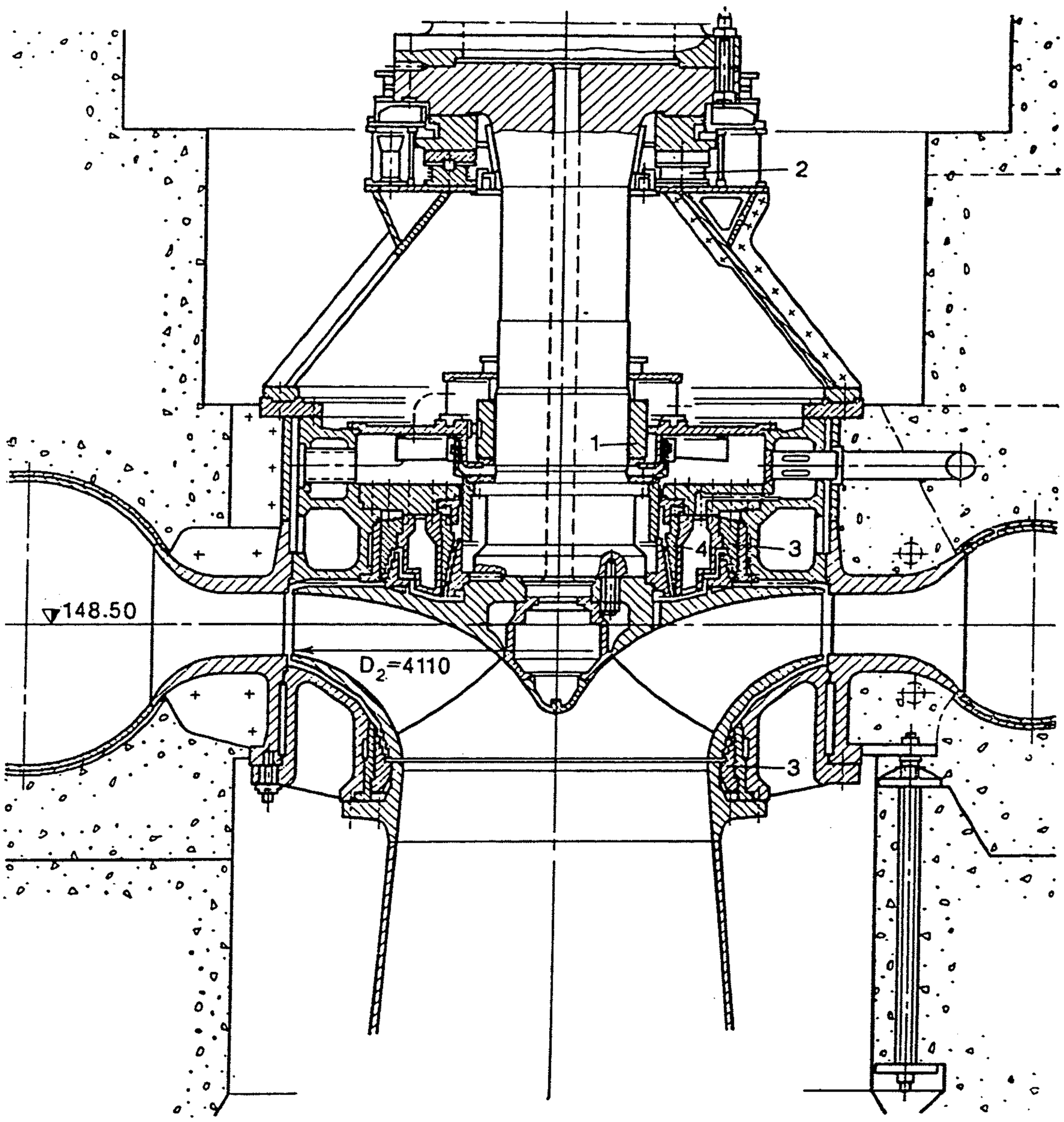


FIGURE 18.11. Vertical pump of Waldeck II HPSP.

stator. The pump has an intricate sealing system, including rings (3) and (4), which are axially displaceable for precluding damage to them in the generator mode, when water is forced out from the wheel space by compressed air.

The Vianden HPSP (Luxembourg) is equipped with two-stage double-entry pumps manufactured by Escher Wyss Co. (Figure 18.12) rated for 69 MW with speed of rotation 428 rpm, head 268 to 282 m, and delivery 23 to 20.7 m^3/s. Disposed after the first stage wheels (1) and guide vane assemblies (2) supply water to second-stage double-entry wheel (3). A scroll (4) has stayring vanes. A clutch (5) has a small Pelton turbine that spins the unloaded wheel of the pump up to synchronous speed before engaging the clutch.

This pump, designed for a head of 268 to 282 m, uses two stages, while the pump shown in Figure 18.11 has only one stage, which develops a head of 330 m. According to Equation 15.3 the head is mainly dependent on circumferential velocity of the wheel. In the first case $D = 2.32$ m

$$u_2 = \frac{\pi 2.32 \times 428}{60} = 52 \text{ m/s}$$

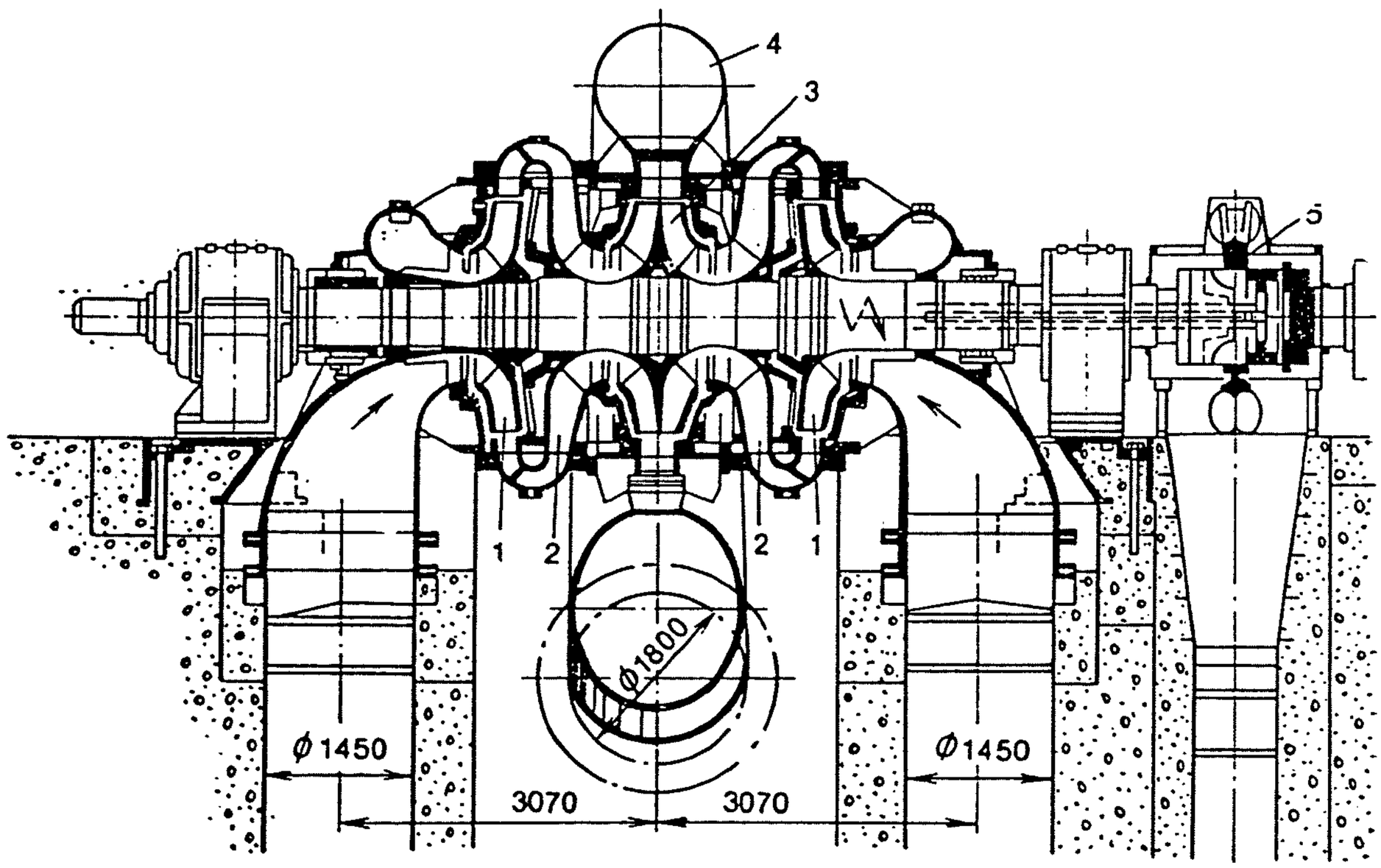


FIGURE 18.12. Horizontal two-stage pump of Vianden HPSP.

assuming $k_H = 1$, we obtain

$$\frac{u_2^2}{2g} = \frac{52^2}{2g} = 138 \text{ m}$$

Thus, two stages are needed to ensure the required head. In the second case (Figure 18.11)

$$u_2 = \frac{\pi 4.11 \times 375}{60} = 80.7 \text{ m/s} \qquad \frac{u_2^2}{2g} = \frac{80.7^2}{2} = 333 \text{ m}$$

which corresponds to the required head.

Figure 18.13 illustrates a two-stage vertical pump manufactured by CKD-Blansko for the Černé Vag HPSP (Czechoslovakia). The 2.6-m wheel pump has the following characteristics: head, 439 to 415 m; delivery, 20 m^3/s; power, 97.2 MW; speed of rotation, 500 rpm. Forward curved guide vanes (1) and backward curved guide vanes (2) (see Figure 13.14) are disposed between the first and second stage wheels. There are two guide bearings and a thrust bearing (3) mounted on a concrete support. Arranged on the upper end of the shaft is a gear clutch (4) which allows the pump to be disengaged when the unit is driven from a turbine.

Figure 18.14 shows a vertical five-stage pump manufactured by CKD-Blansko for the Belmeken HPSP (Bulgaria). The pump wheel diameter is 2090 mm, the head is 748 to 680 m, delivery is 5.7 to 6.9 m^3/s, power is 52 MW, and speed of rotation is 500 rpm. The cast and welded casing consists of two parts with borings accommodating the components of each stage, such as wheels (1), guide vanes (2), and backward curved vanes (3). A thrust bearing (4) taking up axial force is arranged at the bottom on a concrete support. The upper end of the shaft has a special gear clutch (5) for coupling with the motor-generator for disengaging the pump when the unit operates in the generator mode. The inner rim engagement rod passes through the shaft axial bore.

18.4. JET PUMPS

The schematic diagram of a jet pump (ejector) was described in Section 11.3 (see Figure 11.11). Consider the operating process of such a pump and find the relations that dictate its characteristics (Figure 18.15). The main component at which liquid energy conversion takes place is the mixing chamber (area $F_{m.ch}$, length $l_{m.ch}$). The velocities of

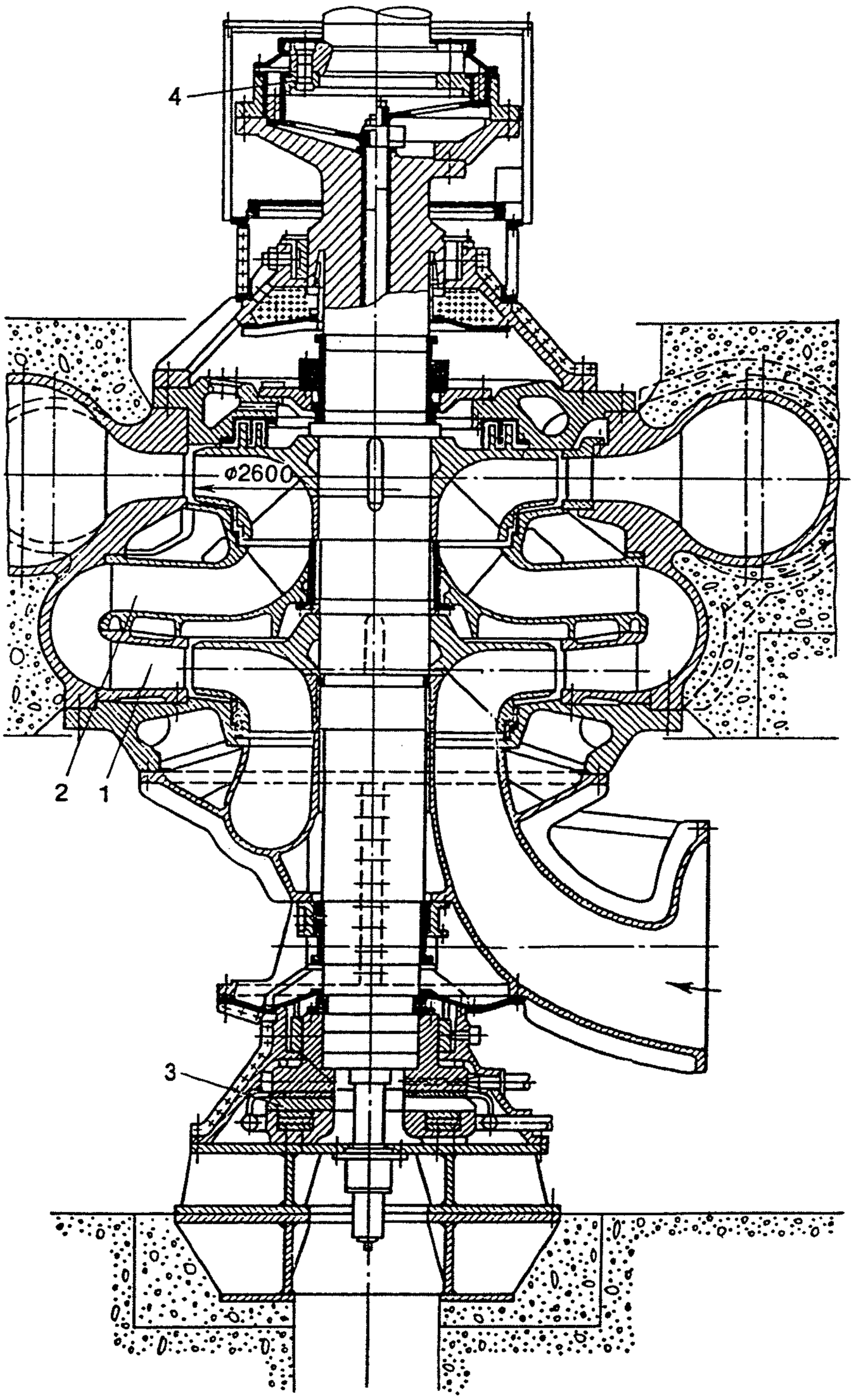


FIGURE 18.13. Vertical two-stage pump of Černé Vag HPSP.

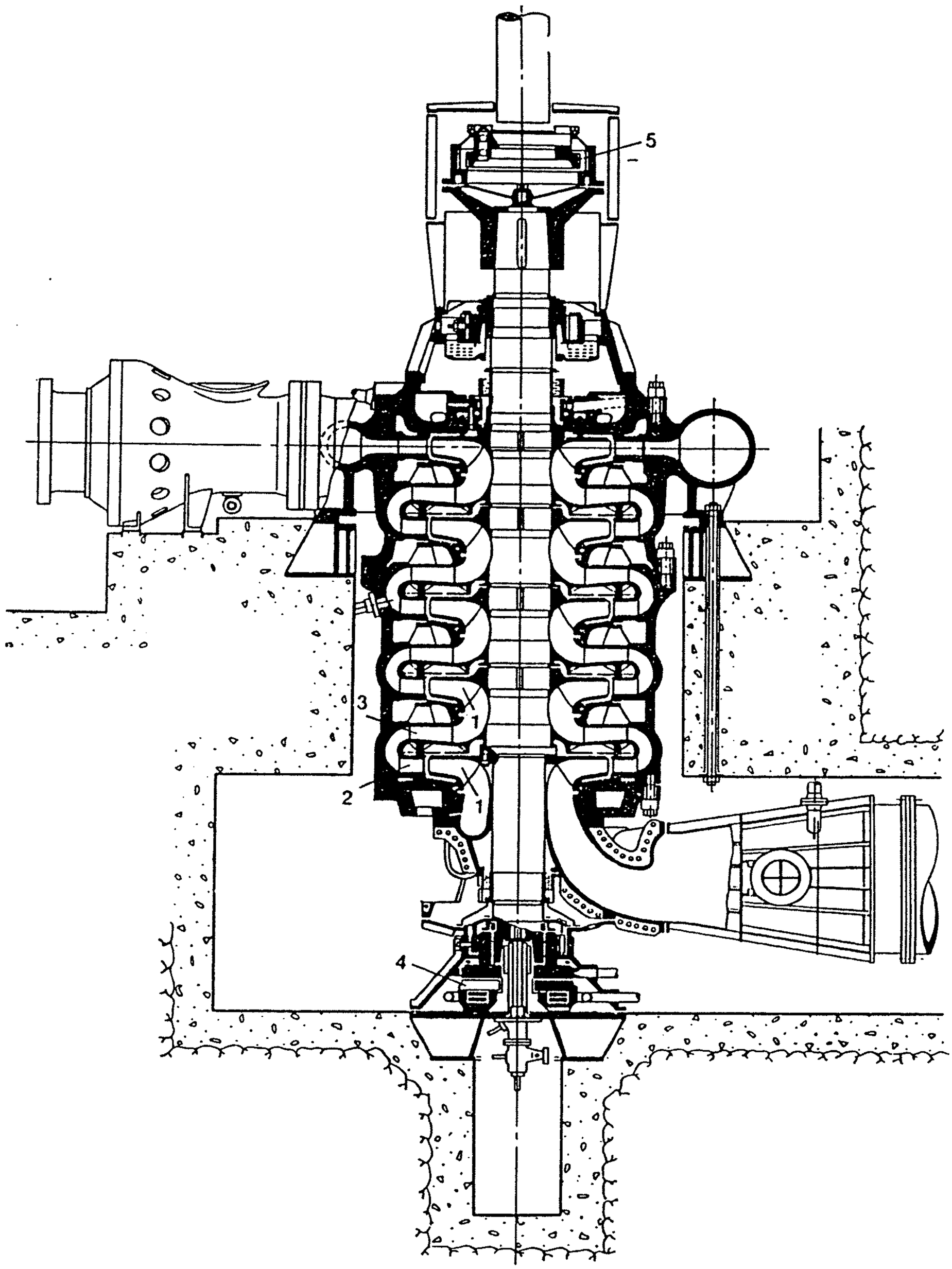


FIGURE 18.14. Vertical five-stage pump of Belmeken HPSP.

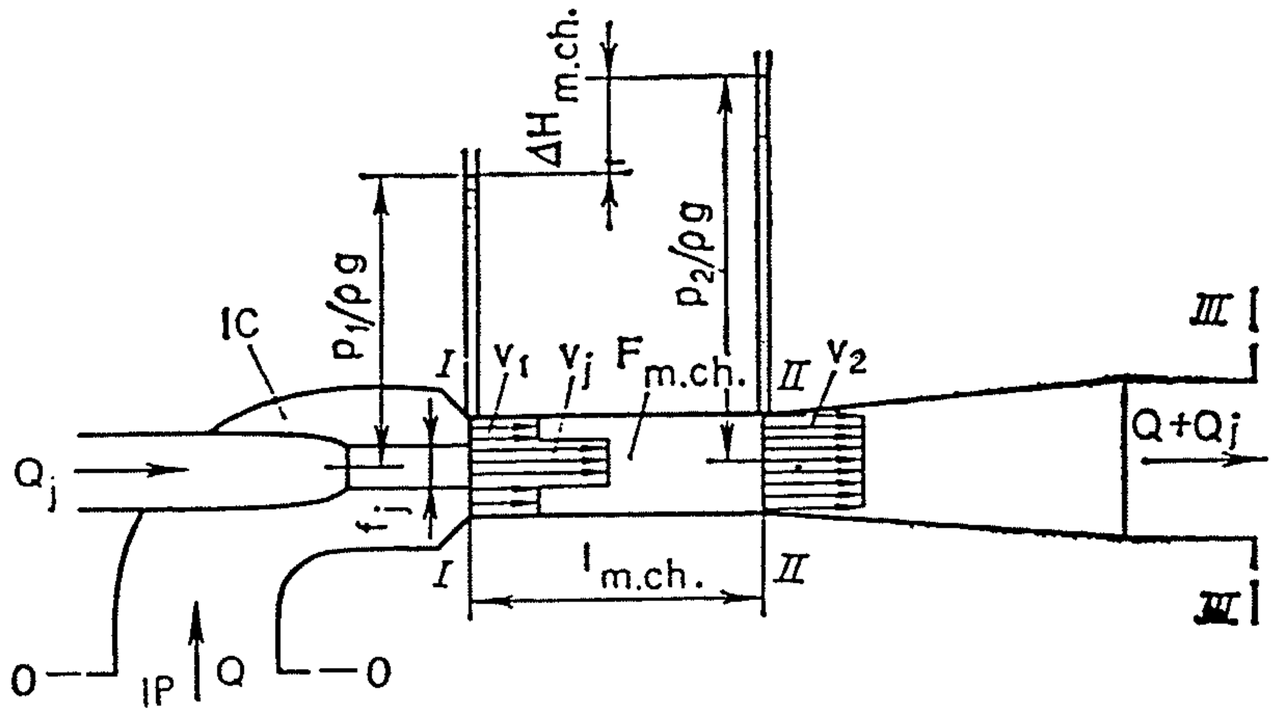


FIGURE 18.15. Hydraulic diagram of jet pump.

two jet (Q_j, nozzle (jet) discharge and Q, delivery to intake chamber, IC, through IP) are fully equalized between cross-sections I–I and II–II. The velocity curve in cross section I–I consists of two sections

$$v_j = \frac{Q_j}{f_j} \qquad v_1 = \frac{Q}{F_{m.ch} - f_j}$$

where f_j is the nozzle (jet) area. The velocity is equalized in section II–II

$$v_2 = \frac{Q + Q_j}{F_{m.ch}}$$

Next, determine certain relations. Find the pressure difference within the mixing chamber

$$\Delta H_{m.ch} = \frac{p_2}{\rho g} - \frac{p_1}{\rho g} \tag{18.8}$$

by using the momentum equation written for the mixing chamber portion between sections I–I and II–II. The mass flow rate of liquid per second is

$$m = \rho(Q_j + Q) \tag{18.9}$$

(assume liquid densities Q_j and Q to be equal). If the axial components of interaction between the liquid and the chamber wall are ignored (the

chamber is cylindrical; friction forces are neglected), using momentum equation, we obtain

$$\rho Q_j v_j + \rho Q v_1 - \rho(Q_j + Q)v_2 = F_{m.ch}(p_2 - p_1)$$

Substituting the expressions for velocities and solving the equation for the pressure difference (Equation 18.8), we find

$$\Delta H_{m.ch} = \frac{Q_j^2}{2gf_j^2}\frac{2f_j}{F_{m.ch}} \times \left[1 - \frac{1}{(F_{m.ch} - f_j)/(f_j)}\left(\frac{Q}{Q_j}\right)^2 - \frac{f_j}{F_{m.ch}}\left(1 + \frac{Q}{Q_j}\right)^2\right] \tag{18.10}$$

To obtain a more general solution, introduce two dimensionless parameters:

- Geometric parameter s determined by the ratio of areas

$$s = F_{m.ch}/f_j \tag{18.11}$$

  where s is always > 1;
- Operation parameter q being the ratio of discharges

$$q = Q/Q_j \tag{18.12}$$

Taking into account that $v_j = Q_j/f_j$ and substituting dimensionless parameters s and q in Equation 18.10, we obtain

$$\Delta H_{m.ch} = \frac{v_j^2}{2g}\frac{2}{s}\left[1 + \frac{1}{s-1}q^2 - \frac{1}{s}(1+q)^2\right] \tag{18.13}$$

The head developed by the jet pump according to Equation 11.5 is the difference in specific energies in the outlet section III–III and in entrance section 0–0 for discharge Q of the liquid being transferred. However, if losses are neglected and ideal head H_{id} is determined, the latter will be equal to the difference of specific energies e_2 in section II–II and e_1 in section I–I of the mixing chamber. The value of H_{id} can

be found from Equation 18.13 by adding the difference of velocity heads in sections II–II and I–I to the RH part of the equation

$$H_{id} = \frac{v_j^2}{2g}\left[\frac{2}{s} + \frac{s-2}{(s-1)^2 s}q^2 - \frac{1}{s^2}(1+q)^2\right] \qquad (18.14)$$

The jet pump actual head $H_{j.p}$ will be, of course, lower than the ideal head determined from Equation 18.14 because intake chamber losses $h_{i.ch}$, mixing chamber losses $h_{m.ch}$, and diffuser losses h_d are subtracted from the latter

$$H_{j.p} = H_{id} - h_{i.ch} - h_{m.ch} - h_d \qquad (18.15)$$

Equation 18.14 makes possible an analysis of jet pump characteristics. First, it shows that the head developed by the jet pump is proportional to $v_j^2/2g$; i.e., to head H_n, at which water is supplied to the nozzle because $v = \varphi\sqrt{2gH_n}$. Head $H_{j.p}$ depends on geometric parameter s and relative discharge q.

Figure 18.16a represents characteristics for $s = 1.5$, 2.5, and 4, which show that increasing s decreases the head developed by the jet pump, but increases relative discharge.

Jet pump efficiency is determined by the ratio of liquid useful energy to energy input, and if losses are neglected, it is expressed by the formula

$$\eta_{id} = q\left[\frac{2}{s} + \frac{s-2}{(s-1)^2 s}q^2 - \frac{1}{s^2}(1+q)^2\right] \qquad (18.16)$$

To estimate absolute values, curves η_{id} for $s = 1.5$, 2.5, and 4 are plotted in Figure 18.6b. The curves show that maximum efficiency is in

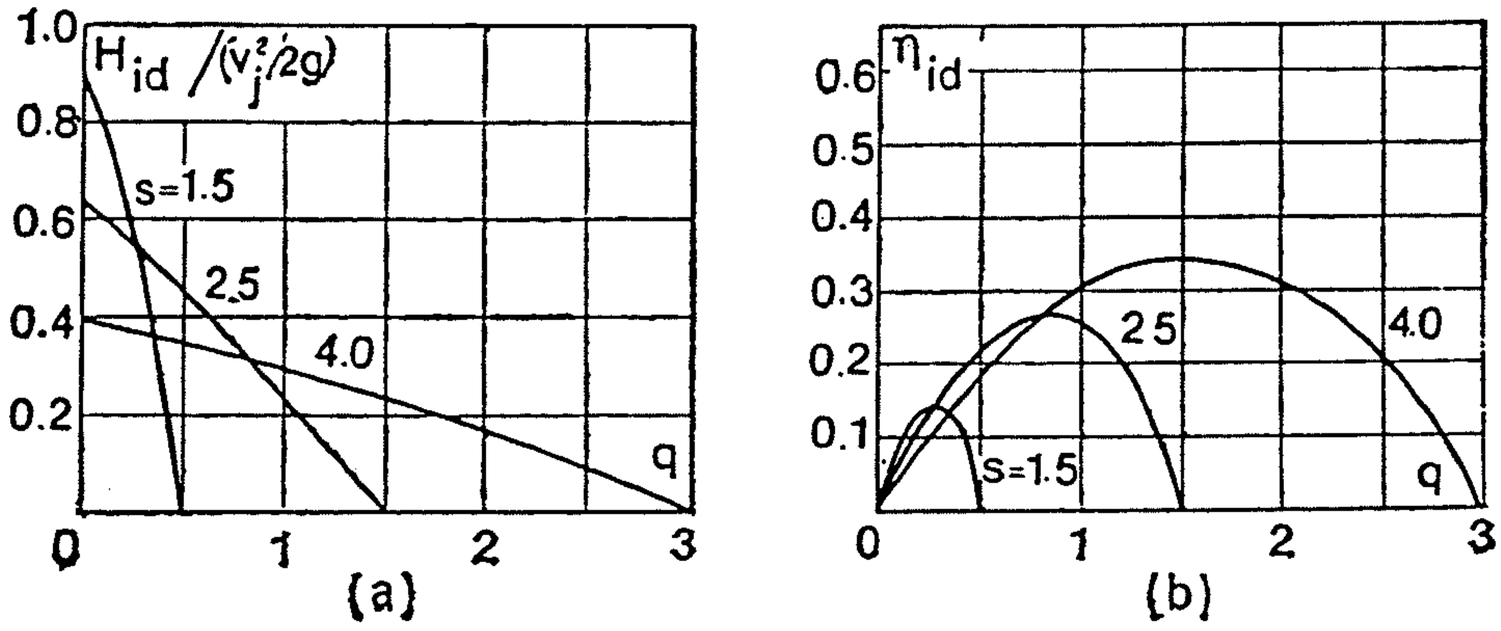


FIGURE 18.16. Theoretical characteristics of jet pump.

the middle of the characteristics and is not too high. For $s = 2.5$ and 4, $\eta_{max} = 0.27$ to 0.35. These efficiency values take into account only the losses involved in mixing flows with different velocities (impact losses). If a jet pump is used for water supply or cooling, useful discharge is the sum of discharges $Q + Q_j$ in section III–III and the efficiency is higher.

The design of the jet pump is very simple and can be readily made at any shop. However, to ensure proper operation, it needs to be accurately dimensioned and carefully manufactured. The shape of the nozzle, distance between the nozzle and the mixing chamber, and the shape of the intake chamber and the diffuser are of great importance.

Figure 18.17a shows a jet pump for a service water system of a large-capacity hydraulic unit. Water is collected from the tailwater (TW) and fed to the nozzle via a pipeline, diameter 100 mm, from a scroll with a head of 90 to 100 m.

Figure 18.17b illustrates a hydraulic elevator intended to dewater mine shafts. Such elevators can be also used for suctioning slurry from pits, shafts, and working fine soils for caissons.

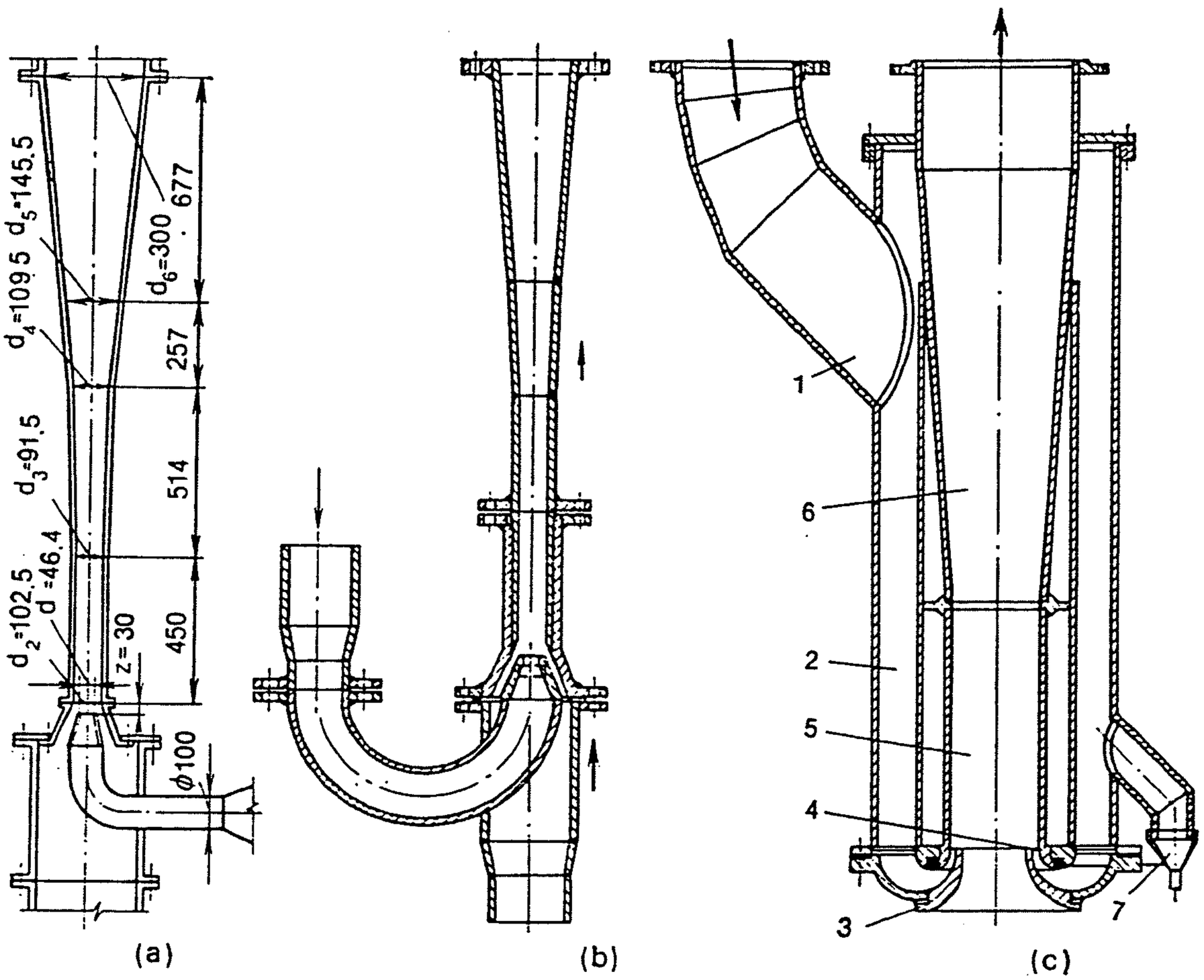


FIGURE 18.17. Designs of jet pumps (ejectors).

Figure 18.17c represents an ejector-type intake of a suction-tube dredger. Water under pressure is fed through duct (1) and annular space (2) to an annular slit (4) and exerts an ejection effect upon the flow fed through head (3) to mixing chamber (5) and then to diffuser (6). The nozzle (7) increases operational efficiency by lossening the soil.

The ejection devices used on suction pipelines of installations with dredge and regular pumps decrease vacuum in the intake pipe, thus precluding cavitation and providing for increased permissible suction lifts.

18.5. VACUUM GROUNDWATER LOWERING INSTALLATIONS

To lower the groundwater level, primarily in construction, and to supply groundwater for various applications, use is made of vacuum lowering installations. These installations (Figure 18.18a) consist of wellpoints (steel pipes perforated and protected with a strainer at the lower end, which are immersed in the ground under the groundwater level), a manifold to which the wellpoints are connected by hoses, and a water vacuum pump unit (PU). When the PU operates, vacuum is formed in the manifold which suctions water through the wellpoints and supplies it to the manifold. Water collected in the manifold is drained

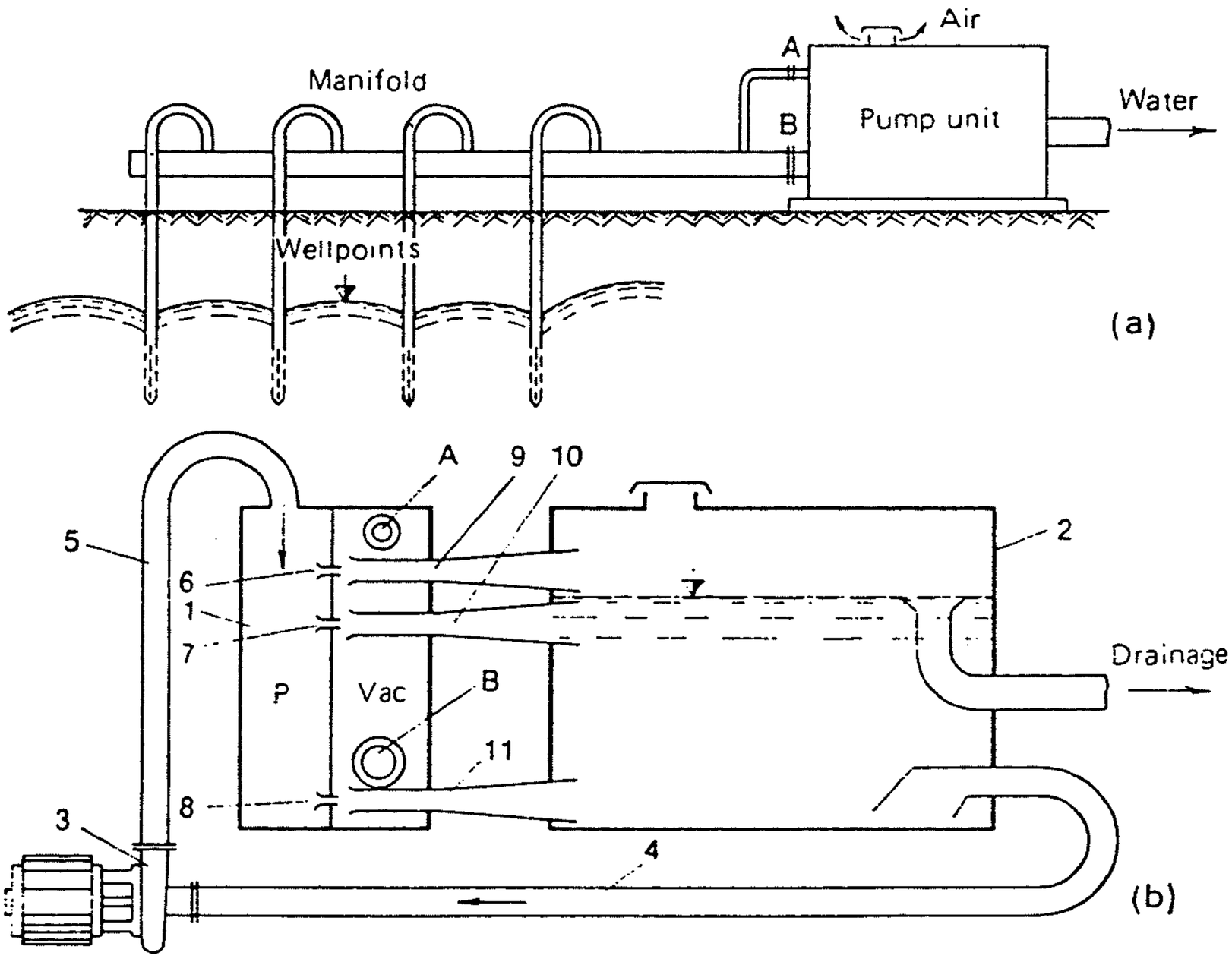


FIGURE 18.18. Vacuum water lowering installation.

or directed to the delivery pipeline. The water vacuum pump unit (Figure 18.18b) consists of pressure-vacuum chamber (1), circulation tank (2), and circulation centrifugal pump (3). The unit operates as follows. The circulation tank is filled with water to the level of the drain funnel. The pump transfers water from the circulation tank via pipes (4) and (5) to the pressure-vacuum chamber separated by partition (6) into a pressure compartment P and vacuum compartment Vac. The water from the pressure compartment is ejected through nozzles (6 to 8) to the vacuum compartment Vac and enters the mixing chambers (9 to 11) with tapered diffusers protruding into the circulation chamber. The nozzles with mixing chambers and diffusers operate as jet pumps (see Section 18.4) and create the ejecting effect. Upper ejector 6 to 9 operates mainly on a water–air mixture, the lower one 8 to 11 on a water–water mixture. Provided in the vacuum compartment Vac are two flanges; the manifold is coupled to the lower flange B and the vent pipe from the manifold is connected to the upper flange A. Water fed from the manifold is ejected by ejectors 8 to 11 and 7 to 10 into the circulation tank and is drained through the drain funnel.

The vacuum dewatering system is simple and mobile, but its water lift does not exceed 7 to 8 m. There are installations designed for the delivery of 45 m^3/h (12.5 L/s), maximum vacuum of 0.075 MPa (suction lift of 7.5 m) with a circulation pump of 15 kW.

18.6. AIR LIFT

The air lift (Figure 18.19) consists of a vertical water-elevating pipe (1), air supply pipe (2) with air release holes at the end, air separator (3), and water collecting tank (4). The water-elevating pipe is lowered to the immersion depth H_{im} below the water level. Compressed air flowing from a compressor is supplied via the pipe (2) and is ejected through perforations at the end. As a result, a water–air emulsion is formed in the water-elevating pipe. The density of emulsion ρ_{em} is lower than that of water ρ, which ensures that it moves upward through height H to the air separator.

Water pressure in the lower intake section of pipe (1) is $\rho g H_{im}$, while the emulsion column pressure is $\rho_{em.av} g(H_{im} + H)$, where $\rho_{em.av}$ is the average density of emulsion. Obviously the emulsion will ascend along pipe (1); i.e., water will be supplied to the upper outlet end of pipe (1) if

$$\rho H_{im} > \rho_{em.av}(H_{im} + H)$$

Hence, the air lift head is

$$H = H_{im}\left(\frac{\rho}{\rho_{em.av}} - 1\right) - h_{loss} \tag{18.17}$$

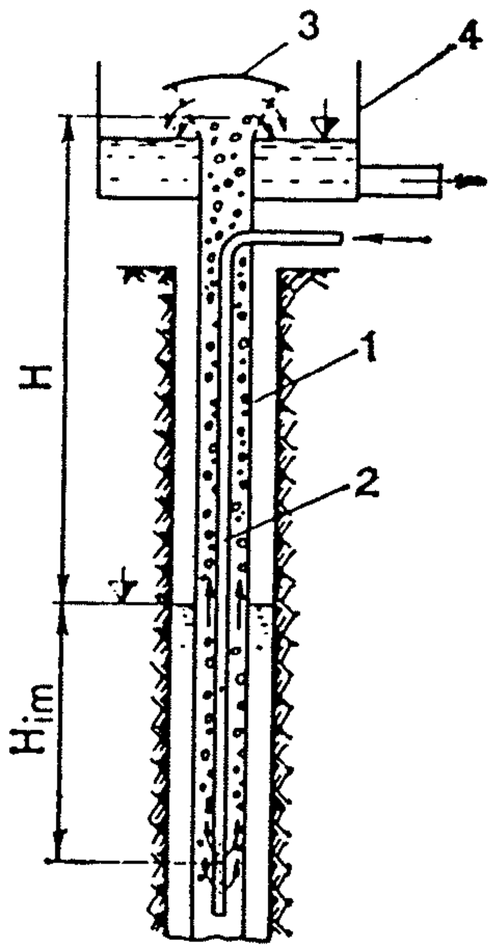


FIGURE 18.19. Air lift.

where h_{loss} are hydraulic losses in the pipe. The formula (18.17) shows that as the required head of the air lift or the required water elevation height increases, it is necessary to increase the immersion of the intake inlet under the water level because the emulsion density cannot be too low to ensure satisfactory operating conditions.

Air pressure p_{air} depends on H_{im} and is determined by the formula

$$p_{air} = \rho g H_{im} + \Delta p \tag{18.18}$$

where Δp is the compressor pipeline losses and aerator losses.

The experience shows that the optimal operating conditions of the air lift, characterized by relative immersion depth H_{im}/H and relative air flow rate $Q_{a.p}/Q$, where $Q_{a.p}$ is air flow rate at atmospheric pressure, depend mainly on the head

H (m)	H_{im}/H	$Q_{a.p}/Q$
Up to 20	3 –2.5	1.5 –2
40	2.0	3.5 –2
60	1.5	5 –5.5
80	1.2	6.5 –7
100	1.0	8 –9

The air lift is built simply. It has no movable parts and is not affected by suspended particles. It is particularly advantageous for the elevation of water from small-diameter wells. It can be easily assembled at the construction site. Air is supplied from a mobile compressor. The short-

comings of the air lift include the need for deep immersion of the pipe under the water level, and comparatively low efficiency, which is usually not above 40 to 50% with regard to the energy of the compressed air supplied, and amounts to only 15 to 25%, as regards power consumption, including compressors losses.

18.7. HYDRAULIC RAM

A special arrangement for pumping water called hydraulic ram (Figure 18.20) comprises a driving pipe (1) (length L_{dr} and available head H_{dr}), accelerating valve (2), air pressure tank (3), with delivery valve (4) and delivery pipeline (5) (head H) $H > H_{dr}$. In the standing still position all valves are closed, the valve (2) is closed by pressure inside the driving pipe and valve (4) is closed by the action of the pressure difference $H - H_{dr}$. To start the system it is necessary to displace (open, immerse) the valve (2). After that, water in the driving pipe will flow with acceleration due to H_{dr} action, the velocity v_{dr} will increase. When v_{dr} reaches a critical value the hydrodynamic draft acting on the valve (2) body will instantly close it. This creates a sharp increase of pressure inside the driving pipe–water hammer and the head under delivery valve (4) becomes greater than H; it opens and water moves in the pressure tank (3). During this time the water in the driving pipe flows with retardation and velocity v_{dr} decreases up to zero. The delivery valve closes and the negative water hammer arises in the driving pipe. The inside pressure at valve (2) drops so that inside head becomes less than H_{dr} and forces it to open. After that, the process repeats.

The ram works in three cycles: water acceleration in driving pipe, water delivery in the air tank and water retardation in the driving pipe,

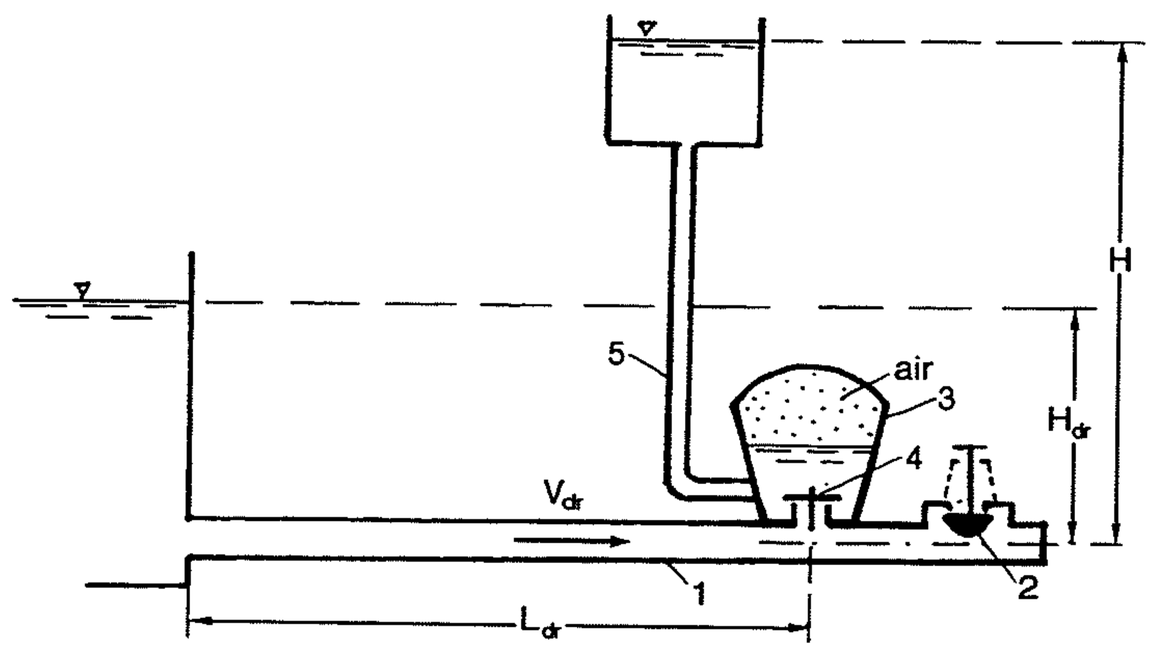


FIGURE 18.20. Hydraulic ram.

and arising negative water hammer and opening of accelerating valve.

As seen the hydraulic ram is a self-operating device that does not require a motor, but it pumps water using available H_{dr} energy. According to theory and existing practice for stable ram operation it is necessary to have $H/H_{dr} > 2$. The shortcoming of the ram is that its operation is accompanied by rather high noise in the form of regular, strong shocks.

SECTION 4

Reversible Hydraulic Machines (Pump-Turbines)

CHAPTER 19

Characteristics of Reversible Hydraulic Machines

19.1. APPLICATION

Hydraulic pumped-storage plants (HPSP) operations comprise two main cycles: a pumping cycle, in which water from the lower reservoir is transferred to the upper reservoir, and a generator cycle, in which the accumulated water is used to generate electricity.

HPSP can be based on different equipment schemes. According to the so-called four-machine scheme, separate pump and turbine units are installed. The "three-machine scheme" includes separate pumps and turbines that are connected to one motor–generator. The "two-machine scheme" is the most popular; it comprises a motor-generator and a reversible hydraulic machine (pump-turbine) adapted to operate both in the pump and in the turbine mode. The two-machine scheme is compact and inexpensive with regards to equipment and construction costs.

The turbine mode head is always lower than the pump mode head because in the turbine mode, the water conduit losses are subtracted from the static head (Equation 2.5). In the pump mode, they are added to the static head (Equation 11.6). Thus, the design heads of these modes will be different. HPSP usually operates so that in the pump mode, the maximum delivery is lower than the discharge of the turbine mode. However, in half-peak HPSPs, the duration of the generator mode can reach 8 to 12 h, so that the relationship will be reversed (the

total delivery of the units in the pump mode should exceed the total discharge in the turbine mode). The power values differ accordingly. The upper and lower reservoir water level elevations change during one HPSP cycle, which leads to varying head and suction lift H_s of the reversible hydraulic machines.

19.2. REVERSIBILITY OF HYDRAULIC MACHINES AND PRINCIPAL CHARACTERISTICS OF PUMP AND TURBINE MODES

Figure 19.1 details the radial-axial flow hydraulic machine, including a guide vane cascade and wheel blades (edges 1 and 2) with angles δ_1 and δ_2. Because the flow changes its direction in the reversible machine, the edges cannot be referred to as "leading" and "trailing." Let us denote them by indexes 1 and 2, and 1 will always correspond to the leading edge in the turbine mode. The operating conditions will be optimal, if water enters shockless in the pump mode on edges 2, and exits normally in the turbine mode. The corresponding velocity triangles for equal circumferential velocities and discharges are shown in Figure 19.1. The same figure illustrates velocity triangles for edges 1, where shockless entrance should be ensured in the turbine mode, while in the pump mode the outlet velocity vector should coincide with the guide vane setting angle (shockless entrance to the vanes). As seen in the

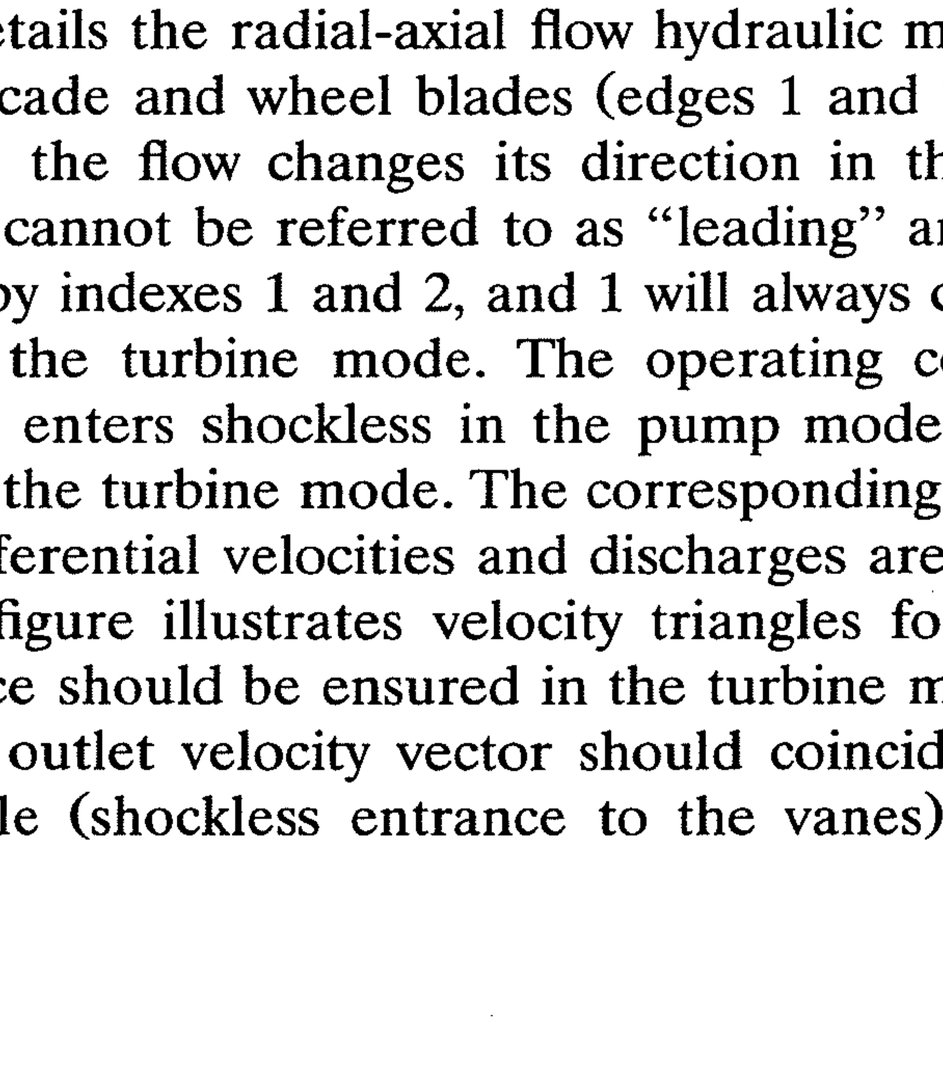


FIGURE 19.1. Velocity triangles of radial-axial flow reversible hydraulic machine.

figure, the required optimum conditions can be met in the first approximation upon reversing wheel rotation and flow direction while preserving rotational speed.

Determine the head ratios for both modes. To this end write Euler's equation (Equation 5.19) for the turbine mode

$$H_t\eta_t = \frac{1}{g}(u_1v_1 \cos \alpha_2 - u_2v_2 \cos \alpha_2)$$

and, according to Equation 12.13 for the pump mode,

$$\frac{H_p}{\eta_p} = \frac{1}{g}(u_1v_1 \cos \alpha_1 - u_2v_2 \cos \alpha_2)$$

Here, η_t and η_p are the efficiencies of the turbine and pump modes. For the assumed conditions, the expressions in brackets are equal. Then we find

$$H_p/H_t = \eta_t\eta_p \tag{19.1}$$

This relation shows that when rotational direction and water flow changes, a fixed-blade hydraulic machine is reversible, but the head developed in the pump mode is lower than in the turbine mode (if assuming efficiency to be about 90% on the average, $H_p/H_t = 0.8$). On the other hand, as mentioned above, during HPSP operation the head in the pump mode should exceed that in the turbine mode. Therefore, when *selecting a reversible pump-turbine, the designer should proceed from the head required for pump mode operation.*

Analysis of the working process of the impeller pumps and Equation 15.1 show that the head developed depends on a number of factors: shape and size of the wheel, including blade setting angles; shape and size of the entire flow passage; and operating conditions, i.e., n and Q. However, one of the main factors is wheel circumferential velocity u_1 (in accordance with Figure 19.1). In view of this, the head developed by the impeller machine under optimal conditions can be approximately expressed by

$$H_p = \psi u_1^2/2g \tag{19.2}$$

Here, ψ is the head coefficient dependent on specific speed $n_{s.p}$ in the pump mode determined for optimal conditions (maximum efficiency) via Equations 12.28. The values of ψ are given for pumps and for some reversible hydraulic machines (pump-turbines) in Figure 19.2. The data show that the pumps and reversible pump-turbines are similar as

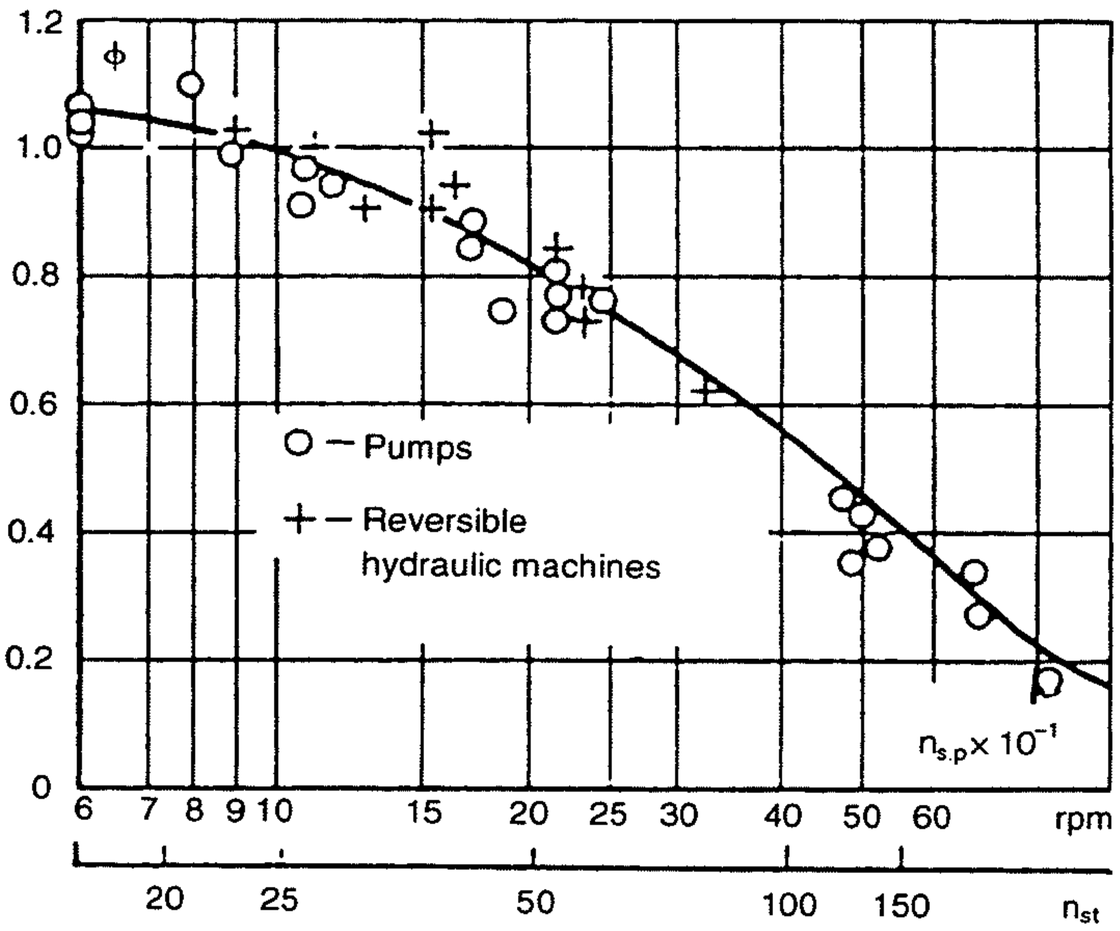


FIGURE 19.2. Head coefficient vs specific speed in pump mode.

regards coefficient ψ. As $n_{s.p}$ increases, the head coefficient decreases in compliance with a particular law. Despite the spread of points, which obviously reflects the effects of other factors ignored in Equation 19.2, said law is sufficiently vivid and may be expressed by an approximate empirical formula

$$\psi = 1.2e^{-n_{s.p}/500} \tag{19.3}$$

applicable to a fairly wide range of $n_{s.p}$.

Referring to the reduced speed of rotation n'_{1p} from Equation 5.34 for $H_p = 1$ m and for $D_1 = 1$ m, and using Equation 19.2, we obtain for reversible pump-turbines

$$n'_{1p} = \frac{nD_1}{\sqrt{H_p}} = \frac{nD_1}{\sqrt{\psi\left(\dfrac{\pi nD_1}{60}\right)^2 \dfrac{1}{2g}}}$$

or

$$n'_{1p} = \frac{84.6}{\sqrt{\psi}} \tag{19.4}$$

Thus, to ensure the required head in the pump mode, an impeller-type hydraulic machine should have a sufficiently high reduced speed of rotation $n'_{\mathrm{I}p}$.[1]

An intrinsic feature of a turbine mode of a reversible pump-turbine is specific speed $n_{s.t}$ determined from Equations 5.38 or 5.39 for the rated power and design head. Figure 19.3 shows the field of H, $n_{s.t}$ with points corresponding to reversible machines of several modern HPSPs. The data prove that decreasing the head increases $n_{s.t}$, and this regularity is vividly manifested despite a particular spread of points. If aiming at higher values of $n_{s.t}$ used, the relation between $n_{s.t}$ and head may be presented as follows

$$\text{At } H \leq 300 \text{ m } n_{s.t} = \frac{1550}{H^{0.4}}$$

$$\text{At } H > 300 \text{ m } n_{s.tL} = \frac{15000}{H^{0.8}} \tag{19.5}$$

Specific speed in the pump mode, $n_{s.p}$, is usually equal to

$$n_{s.p} = (0.9 - 1.05)n_{s.t} \tag{19.5a}$$

The cavitation coefficient for the turbine modes of reversible hydraulic machines is close to the values of σ for turbines of the same specific speed and corresponds to the data of the graph in Figure 7.8. The pump modes are decidedly important when determining permissible suction lift H_s, which dictates the reversible machine elevation. For

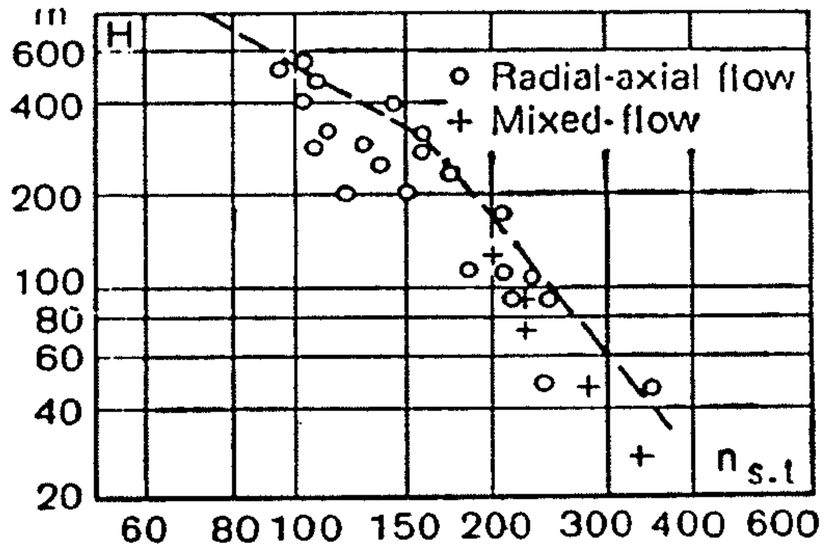


FIGURE 19.3. Specific speed vs head in modern reversible hydraulic machines.

[1] In using Equation 19.4 for mixed-flow machines, relate n'_{I} to the wheel outer diameter rather than to D_1, according to Figure 96.b.

such conditions the cavitation characteristics can be estimated from the following. Write the equation used to determine suction lift H_s for critical conditions according to Equation 14.8

$$H_s = \frac{p_{atm}}{\rho g} - (\text{NPSH})_{cr} - h_{suc} - \frac{p_{s.v}}{\rho g}$$

and according to Equation 14.8a

$$H_s = \frac{p_{atm}}{\rho g} - h_{suc} - \sigma_{cr} H - \frac{p_{s.v}}{\rho g}$$

Equating the RH parts to each other, find the relation between $(\text{NPSH})_{cr}$ and σ_{cr}

$$\sigma_{cr} = \frac{(\text{NPSH})_{cr}}{H} \tag{19.6}$$

Using Equation 14.15 it is possible to express $(\text{NPSH})_{cr}/H$ through cavitation specific speed C

$$\frac{(\text{NPSH})_{cr}}{H} = \frac{\left(n\sqrt{Q}\right)^{4/3}}{C^{4/3}H}$$

or, in view of Equations 12.28 for pump specific speed,

$$\frac{(\text{NPSH})_{cr}}{H} = \frac{1}{3.65^{4/3}}\left(\frac{n_{s.p}}{C}\right)^{4/3} = \frac{n_{s.p}^{4/3}}{5.6C^{4/3}} \tag{19.7}$$

In view of the results of Equation 19.6, obtain the formula for σ_{cr}

$$\sigma_{cr} = \frac{n_{s.p}^{4/3}}{5.6C^{4/3}} \tag{19.8}$$

wherein

$$n_{s.p} = 3.65\frac{n\sqrt{Q}}{H^{3/4}} \tag{19.9}$$

Because good cavitation characteristics of the pump correspond to C of about 200, derive the formula

$$\sigma_p = \frac{n_{s.p}^{4/3}}{6400} \tag{19.10}$$

which makes it possible to estimate the cavitation coefficient in the pump mode. When determining the permissible suction lift, find the design cavitation coefficient $\sigma_{p.d}$, similar to Equation 7.14, and $k_\sigma = 1.2$ to 1.3; for high-head hydraulic machines ($H > 400$ m), however, the margin is increased to 1.5 to 2.0. Now, we obtain

$$\sigma_{p.d} = k_\sigma \sigma_p \tag{19.11}$$

For designing HPSP the experimental pump-turbine characteristics, representing all necessary data including reduced parameters Q'_I, n'_I, efficiency η and cavitation coefficient σ for turbine and pump mode of operation are used. In this case generalized formulas 19.3–19.10 are not necessary. But they can be very useful on preliminary design stages for analysis, for finding out possible options, for checking the recommended parameters.

19.3. DETERMINING THE PARAMETERS OF REVERSIBLE PUMP-TURBINES VIA GENERALIZED CHARACTERISTICS

The following data are preset when selecting HPSP equipment: design head in turbine mode $H_{t.m}$, maximum head in pump mode $H_{p.\max}$, minimum head in pump mode $H_{p.\min}$, unit power in turbine mode $N_{u.t}$, and lower reservoir elevations. Using these data in view of the generalized characteristics given in the previous section, it is possible to determine the pump-turbine parameters. The calculation procedure is as follows:

1. Referring to $H_{t.m}$, find design discharge in the turbine mode

$$Q_{t.m} = \frac{N_{u.t}}{9.81 H_{t.m} \eta_t \eta_e} \tag{19.12}$$

   where $\eta_t = 0.9$ to 0.92, an overall turbine efficiency for rated regime, and motor–generator efficiency $\eta_e = 0.97$ to 0.98.
2. According to $H_{t.m}$, find specific speed $n_{s.t}$ from Equation 19.5 and determine $n_{s.p}$ from Equation 19.5a.
3. Determine the design value of the reduced rotational speed in the pump mode $n'_{\mathrm{I}p}$ from Equation 19.4, calculating coefficient ψ from Equation 19.3 by $n_{s.p}$ found prior.
4. Knowing $n_{s.t}$ and assuming $n'_{\mathrm{I}t} = n'_{\mathrm{I}p}$ (the turbine and pump mode rotational speeds are equal; head difference is neglected), find the reduced discharge in the turbine mode $Q'_{\mathrm{I}t}$

$$Q'_{\mathrm{I}t} = \left(\frac{n_{s.t}}{3.65 n'_{\mathrm{I}t}}\right)^2 \frac{1}{\eta_t} \tag{19.13}$$

5. Knowing $Q_{t.m}$ from Equation 19.12 and Q'_{1t} from Equation 9.7 find wheel diameter D_1.
6. Determine the rotational speed of the machine from Equation 9.8 and take the nearest value corresponding to the synchronous rotational speed from Equation 9.1.
7. Using $n_{s.p}$ (item 2) and n'_{1p} (item 3), find the reduced discharge in the pump mode Q'_{1p} and actual delivery $Q_{p.ac}$

$$Q'_{1p} = \left(\frac{n_{s.p}}{3.65n'_{1p}}\right)^2 \tag{19.14}$$

$$Q_{p.av} = Q'_{1p} D_1^2 \sqrt{H_{p.av}} \tag{19.15}$$

where $H_{p.av} = 0.5\ (H_{p.\max} + H_{p.\min})$.

8. Examine whether the reversible hydraulic machine covers the required range of heads in the pump mode $\Delta H_p = H_{p.\max} - H_{p.\min}$. The permissible value of the $\Delta H_p / H_{p.av}$ ratio depends on the hydraulic machine type and $n_{s.p}$ determined for average head. This relation can be approximately presented for the Francis turbine type by:

$$\frac{\Delta H_p}{H_{p.av}} \leq 0.07 n_{s.p}^{0.25} \tag{19.16}$$

If the required range is wider, use a machine of another type, say, the adjustable blade pump-turbine or, if possible, decrease the amplitude of the head fluctuations at HPSP.

9. Determine permissible suction lift H_s. For the pump mode find the approximate value of suction pipe losses h_{suc} for $Q_{p.av}$ and σ_p from Equation 19.10. Take the design cavitation coefficient $\sigma_{p.d}$ from Equation 19.11 and calculate H_s:

$$H_s = 10 - \frac{\nabla}{900} - \sigma_{p.d} H_{p.av} - h_{suc} \tag{19.17}$$

Determine H_s in compliance with Figure 7.9.

The calculation procedure discussed above allows the analysis of the effect of an increase or a decrease of specific speed $n_{s.t}$ and hydraulic machine parameters, according to Equation 19.5. It is necessary to note that most reliable data obtained when calculating parameters of the reversible pump-turbines were taken from their experimental characteristics, as described below. However, the data obtained by the generalized characteristics as well as analogs available may be very useful for preliminary conceptual designs, when experimental characteristics have not yet been taken.

Example 19.1

Determine the parameters of a reversible pump-turbine under the following conditions: design head in turbine mode $H_{t.m} = 100$ m, maximum head in pump mode $H_{p.\max} = 116$ m, minimum head in pump mode $H_{p.\min} = 94$ m; rated power in turbine mode $N_{r.t} = 200$ MW, lower reservoir elevation $+200$ m.

Solution

1. Find discharge using Equation 19.12:

$$Q_{t.m} = \frac{200{,}000}{9.81 \times 100 \times 0.92 \times 0.98} = 226.1 \text{ m}^3/\text{s}$$

2. Find specific speed using Equation 19.5:

$$n_{s.t} = \frac{1550}{100^{0.4}} = 245.6 \text{ rpm}$$

and from Equation 19.5a:

$$n_{s.p} = 0.9 \times 245.6 = 221.0 \text{ rpm}$$

3. Find reduced rotational speed using Equation 19.3:

$$\psi = 1.2e^{-221/500} = 0.8$$

and from Equation 19.4:

$$n'_{1p} = 84.8/\sqrt{0.8} = 94.7 \text{ rpm}$$

4. Find reduced discharge in the turbine mode from Equation 19.13:

$$Q'_{1t} = \left(\frac{245.6}{3.65 \times 94.7}\right)^2 \frac{1}{0.92} = 0.549 \text{ m}^3/\text{s}$$

5. Find wheel diameter from Equation 9.7:

$$D_1 = \sqrt{\frac{226.1}{0.549\sqrt{100}}} = 6.4 \text{ m}$$

6. Find rotational speed using Equation 9.8:

$$n = \frac{94.7\sqrt{100}}{6.4} = 148 \text{ rpm}$$

Take the closest synchronous speed according to Equation 9.1 $n = 150$ rpm ($p = 40$).

7. Find the delivery in the pump mode from using Equations 19.14 and 19.15:

$$Q'_{1p} = \left(\frac{221.1}{3.65 \times 94.7}\right)^2 = 0.409 \text{ m}^3/\text{s}$$

Average head $H_{p.av} = 0.5\ (116 + 94) = 105$ m.

$$Q_{p.av} = 0.409 \times 6.4^2\sqrt{105} = 171.7 \text{ m}^3/\text{s}$$

8. Check the required head range in the pump mode using Equation 19.15:

$$\frac{\Delta H_p}{H_{p.av}} \leq 0.07 \times 221^{0.25} = 0.269$$

Head difference $\Delta H_p = 116 - 94 = 22$ m. The actual value of the ratio is

$$\frac{\Delta H_p}{H_{p.av}} = \frac{22}{105} = 0.209 < 0.269$$

The required range head is ensured.

9. Find suction lift H_s. For discharge of 171.7 m^3/s, suction pipe losses h_{suc} are assumed to be 0.7 m:

From Equation 19.10

$$\sigma_p = \frac{(221.1)^{4/3}}{6400} = 0.209$$

From Equation 19.11 for

$$k_\sigma = 1.2$$

$$\sigma_{p.d} = 0.209 \times 1.2 = 0.25$$

and from Equation 19.17:

$$H_s = 10 - \frac{200}{900} - 0.25 \times 105 - 0.7 = -17.2 \text{ m}$$

Should it result that the suction lift (machine elevation) is to be increased, take a specific speed less than that given by Equations 19.5.

19.4. CIRCULAR CHARACTERISTIC OF THE IMPELLER HYDRAULIC MACHINE

As seen from the above, the reversible hydraulic machines operate within a wide range of conditions. However, regular pumps also may

encounter a wide range of conditions; for instance, if the electric motor is turned off inadvertently, the head brings the pump to the counterflow mode, then changes the direction of rotation and changes the pump over to the turbine mode. Thus, the study of operation of a hydraulic machine within a wide range of conditions is an important practical task.

The probable operating conditions of a hydraulic machine are most fully presented by the so-called circular characteristic shown in Figure 19.4. It is plotted in the coordinates of n (speed of rotation) and Q (discharge of a radial-axial flow machine of a given diameter at a constant opening of the wicket gate). The similarity condition is represented by the ratio

$$Q/n = \text{const}$$

and, hence, each beam passing through the coordinate origin characterizes its respective conditions (for instance, efficiency is preserved on each beam).

The characteristic shows variation of efficiency η and head H in all four quadrants (I to IV). The following groups of modes are distin-

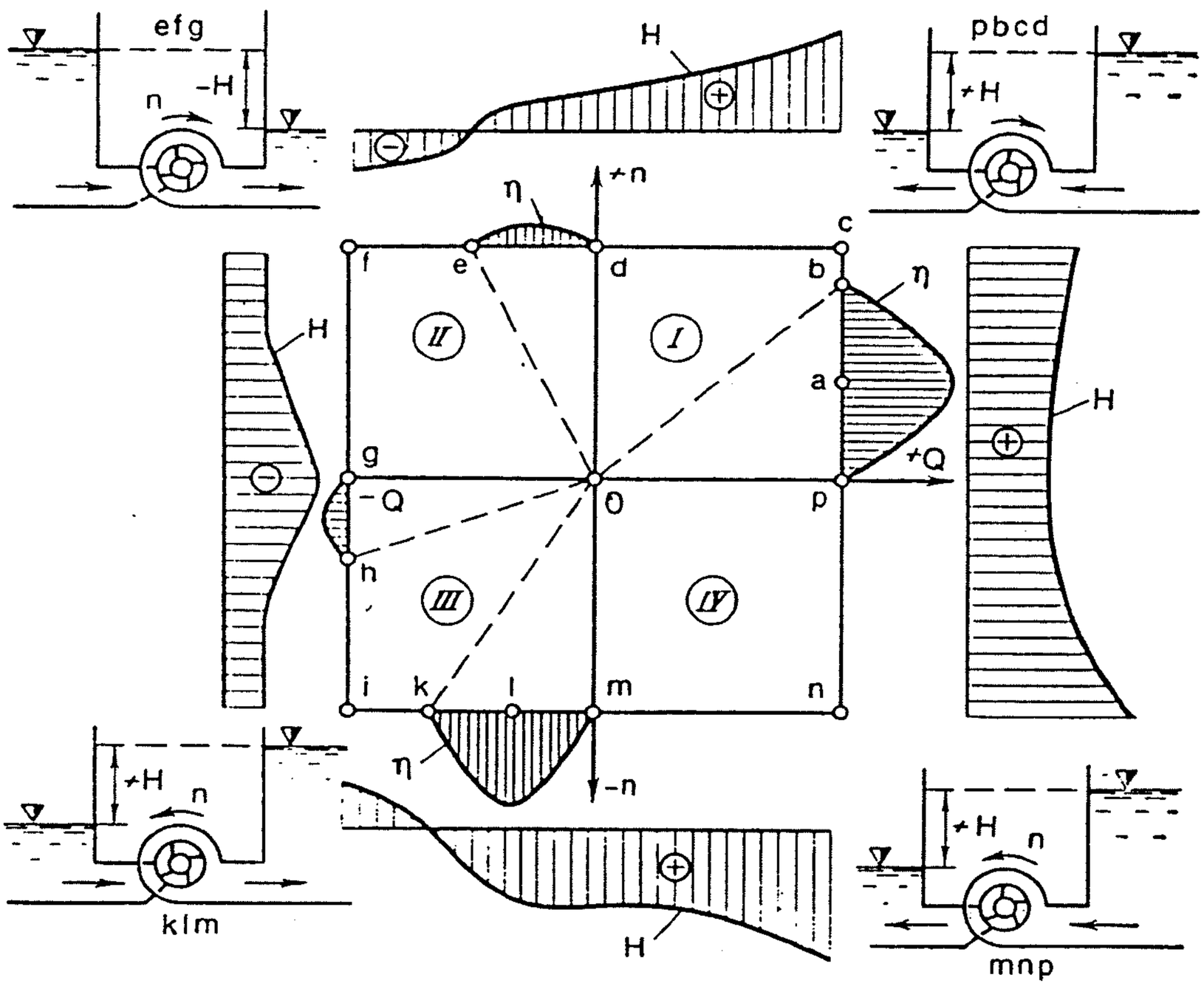


FIGURE 19.4. Circular characteristics of a radial-axial flow hydraulic machine.

guished: turbine direct (quadrant I—portion p to b, point a—turbine optimal; pump direct (quadrant III—portion k to m, point l—pump optimal; pump reverse (quadrant II)—portion d to e (operates as a pump, but with reverse rotation of the wheel); and turbine reverse (quadrant III)—portion g to h. Between these four "working" modes there are four braking modes: energy is consumed but no useful work is produced (quadrant I portion bcd, quadrant II portion efg, quadrant III portion nik and quadrant IV full, portion mnp).

All eight modes can be found only in installations in which the head can reverse its direction, say, in tidal power plants. In HPSP, in which the upper reservoir elevation is always above that of the lower reservoir (i.e. the head is positive), only one turbine mode, two pump modes, and one braking mode (quadrant IV) are possible.

19.5. TYPES OF REVERSIBLE PUMP-TURBINES AND THEIR UNIVERSAL CHARACTERISTICS

Radial-axial flow reversible pump-turbines are being used increasingly at HPSPs. There are some HPSPs with mixed-flow adjustable blade reversible machines. Axial-flow reversible machines can be also employed.

As seen from Figure 19.3, the radial-axial flow reversible machines are used within a head range of 60 to 700 m, the mixed-flow adjustable blade units are employed for heads < 80 to 100 m, while the axial-flow machines, in particular bulb-type pump-turbines, can be used at low heads of 5 to 20 m.

The modern HPSPs with heads above 600 to 700 m are equipped with three-machine units consisting of Pelton turbines (impulse turbines) and multistage pumps. However, the reversible hydraulic machines persistently advance to the higher head areas. Such a process can take different forms. One way is to increase the head of the radial-axial flow reversible machine. As transpires when employing Equation 19.2, an increase of the head raises the wheel circumferential velocity. For instance, to obtain $H_p = 1000$ m, the circumferential velocity should be 135 to 150 m/s. Rising u_1 rapidly intensifies stress in the runner and increases relative velocity of flow, causing dynamic effects and cavitation. Another way to increase the head in reversible hydraulic machines is to use multistage units (see Figure 20.6). Both methods are employed currently.

Let us consider universal characteristics of reversible pump-turbines by referring to a radial-axial flow unit with $n_{s.t} = 250$ rpm, rated for heads from 95 to 115 m (Figure 19.5). The characteristic is given in reduced parameters n'_{I} and Q'_{I} for all four quadrants. Applied in the graph are the lines of the guide vane opening (for a model, diameter

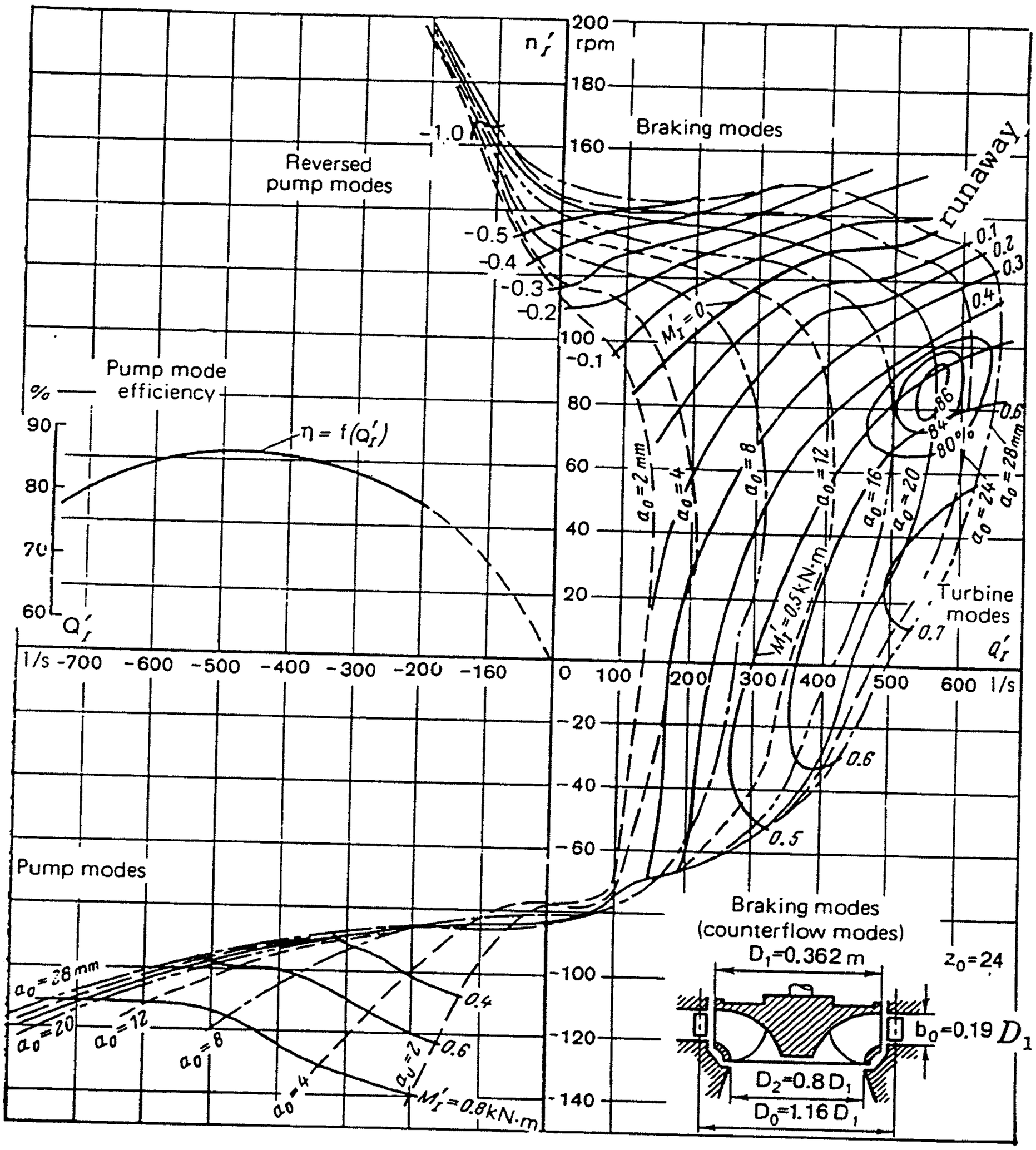


FIGURE 19.5. Universal characteristic of a radial-axial flow reversible pump-turbine.

362 mm), the lines of reduced shaft moments M'_I, and some lines of efficiency.

Knowing the relation between power N (kilowatts) rotational speed n (revolutions per minute), and shaft moment M (kilonewton meters),

$$N = Mn/9.55$$

Using power formulas, we can determine the ratios between the reduced parameters.

- For the turbine mode

$$N'_{\mathrm{I}} = 9.81 Q'_{\mathrm{I}} \eta_t \qquad M'_{\mathrm{I}} = \frac{9.55 N'_{\mathrm{I}}}{n'_{\mathrm{I}}} = \frac{9.55 \times 9.81 Q'_{\mathrm{I}} \eta_t}{n'_{\mathrm{I}}}$$

hence

$$M'_{\mathrm{I}t} = 93.7 \frac{Q'_{\mathrm{I}}}{n'_{\mathrm{I}}} \eta_t \tag{19.18}$$

- For the pump mode

$$N'_{\mathrm{I}} = \frac{9.81 Q'_p}{\eta_p} \qquad M'_{\mathrm{I}} = \frac{9.55 N'_{\mathrm{I}}}{n'_{\mathrm{I}}} = \frac{9.55 \times 9.81 Q'_{\mathrm{I}}}{n'_{\mathrm{I}} \eta_p}$$

hence

$$M'_{\mathrm{I}p} = 93.7 \frac{Q'_{\mathrm{I}}}{n'_{\mathrm{I}} \eta_p} \tag{19.18a}$$

Equation 19.18 and 19.18a allow determination of the relation between M'_{I} and efficiency by the operation point coordinates Q'_{I} and n'_{I}. The efficiency isolines are shown on the characteristic for a narrow zone of "working" turbine modes. Presenting the variation of efficiency in the form of isolines for pump modes is inconvenient because of the tight arrangement of opening lines a_0. Therefore, the efficiency variation here is given as a separate graph $\eta = f(Q'_{\mathrm{I}})$ corresponding to optimal openings of the wicket gate.

The coordinates of the optimal turbine mode approach $n'_{\mathrm{I}\ opt} = 90$ rpm and $Q'_{\mathrm{I}} = 560$ L/s. Discharge Q'_{I} is dependent mainly on the opening of the wicket gate and is substantially proportional to a_0. However, with increasing $n'_{\mathrm{I}} > n'_{\mathrm{I}\ opt}$, lines a_0 get curved and Q'_{I} drops drastically. This is an important feature of radial-axial flow reversible hydraulic machines. M'_{I} simultaneously decreases. Line $M'_{\mathrm{I}} = 0$ characterizes the runaway mode of operation ($\eta = 0$). Then, at $n'_{\mathrm{I}} > n'_{\mathrm{I}\ \mathrm{runaway}}$, when $M'_{\mathrm{I}} < 0$, the braking (quadrant I) and reverse pump (quadrant II) modes are initiated.

With a reduction in $n'_{\mathrm{I}} < n'_{\mathrm{I}\ opt}$ in the turbine mode area, the reduced discharge changes slightly, up to $n'_{\mathrm{I}} = 0$. Further, as the rotation is reversed $n'_{\mathrm{I}} < 0$ for the pump mode, the sign of discharge Q'_{I} does not change. All the braking modes or the so-called counterflow modes (the wheel rotates in the pump direction, while the discharge occurs in the turbine direction, i.e., from the upper reservoir to the

lower reservoir) are located in quadrant IV. Approaching $n'_I = -80$ to 85 rpm, the lines of all openings a_0, converge, the discharge rapidly drops to zero: $Q'_I = 0$. As n'_I increases in the same direction, the hydraulic machine changes over to the pump mode (direct, normal), which also features some peculiarities. Lines of openings $a_0 = 28$ to 16 mm pass close to each other and only after $a_0 = 12$ mm (i.e., $< 45\%$ of full opening) does Q'_I start decreasing noticeably. Thus, the wicket gate opening in the pump mode only slightly affects the delivery (discharge) and power of the radial-axial reversible hydraulic machine.

In the pump mode, the maximum efficiency $Q'_I = 500$ L/s and $n'_I = 97$ rpm.

For better clarity, Figure 19.6 presents curves for one opening only $a_0 = \text{const}$. Here, relations $Q'_I = f(n'_I)$ and $M'_I = f_1(n'_I)$ are shown on a common ordinate axis n'_I. It is helpful to highlight two points: $n'_{I\ opt}$, optimal reduced speed of the turbine mode, and $n'_{I\ \text{runaway}}$ runaway speed of rotation. The relation

$$k_{\text{runaway}} = \frac{n'_{I\ \text{runaway}}}{n'_{I\ opt}} \tag{19.19}$$

giving the runaway coefficient is an important characteristic. In the case of a radial-axial flow reversible hydraulic machine k_{ac} depends on specific speed, and for $n_{s.t} = 140$ to 250 rpm, $k_{ac} = 1.5$ to 1.7, i.e., far lower than for the turbines of the corresponding specific speed.

As n'_I decreases from $n'_{I\ \text{runaway}}$ in the turbine mode region, reduced moment M'_I continuously increases and starts decreasing only at relatively low values of n'_I. After changing over to the counterflow conditions, M'_I decreases rather intensely to reach its minimum at point, where line a_0 intersects vertical $Q'_I = 0$.

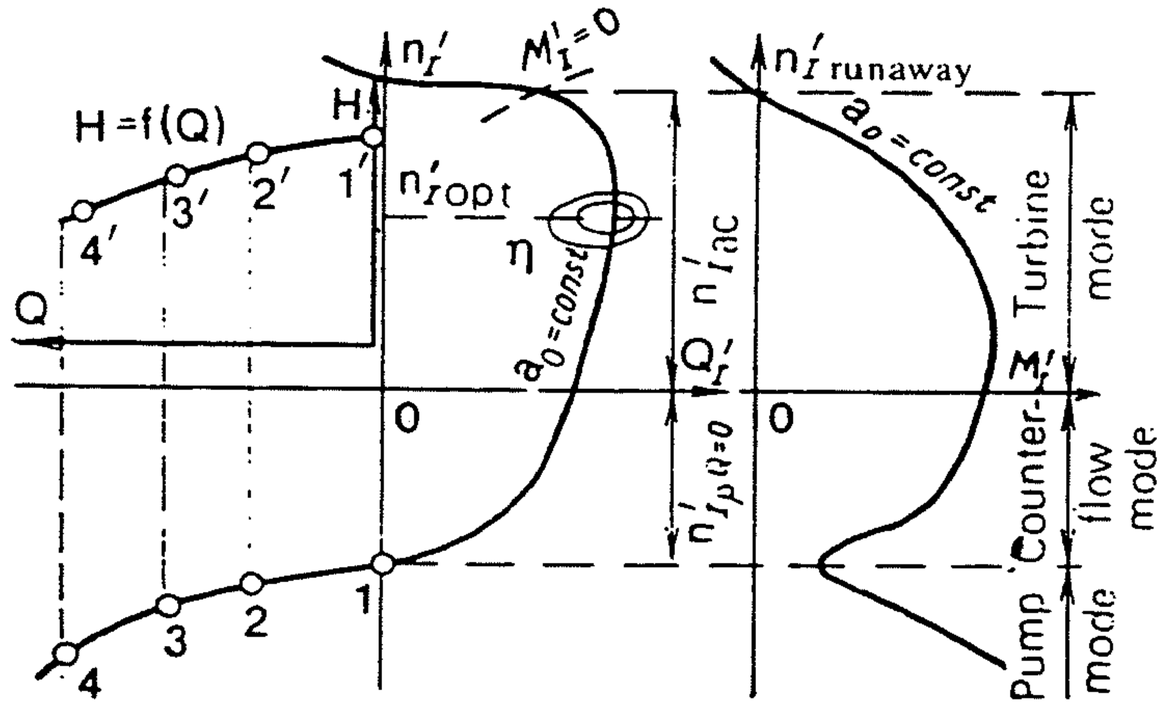


FIGURE 19.6. Discharge, moment, and head characteristics of radial-axial flow reversible hydraulic machine.

It is inconvenient to choose reversible machines and determine actual delivery, efficiency, and power in the pump mode using the reduced characteristic. Therefore, it is necessary to plot the operation discharge characteristic for the adopted speed of rotation n and diameter D. The reduced parameters are converted with the aid of similarity formulas (Equations 5.34 and 5.35). As a result, we obtain

$$H = \left(\frac{nD}{n'_{\mathrm{I}}}\right)^2$$

$$Q = Q'_{\mathrm{I}} D^2 \sqrt{H} = Q'_{\mathrm{I}} D^2 \frac{nD}{n'_{\mathrm{I}}} \tag{19.20}$$

and hence,

$$Q = \frac{Q'_{\mathrm{I}}}{n'_{\mathrm{I}}} nD^3 \tag{19.21}$$

Figure 19.6 illustrates the replotted head–discharge curve, where the scale of axis Q is related to Q'_{I} by coefficient nD^3. For clarity, points 1 to 4 are applied to line a_0 in the pump mode region and appropriate points 1′, 2′, to 4′, to line Q–H. Displacement of these points relative to the initial point is caused by the increase of n'_{I} in Equation 19.21.

Consider some peculiarities in selecting the reversible hydraulic machines. As seen on the characteristic of Figure 19.5, lines a_0 are flat in the pump mode zone, which indicates that changing n'_{I} causes an abrupt change in Q'_{I}. Thus, at any rate, n'_{I} should never be lower than is required for the pump mode, say, 92 to 100 rpm for a given characteristic.

Taking into account that

$$n'_{\mathrm{I}p} = \frac{n_p D_1}{\sqrt{H_p}}$$

and in the turbine mode

$$n'_{\mathrm{I}t} = \frac{n_t D_1}{\sqrt{H_t}}$$

where n_p and n_t are the speeds of rotation and H_t and H_p are the heads in the turbine and pump modes, we find

$$n'_{It} = n'_{Ip} \frac{n_t}{n_p} \sqrt{\frac{H_p}{H_t}} \tag{19.22}$$

If the rotation speeds are equal ($n_p = n_t$) and it is assumed that $H_p/H_t = 1.06$, the range of n'_{It} for the given characteristic is from 95 to 103 rpm. This range is above the optimum for the turbine mode, which decreases the efficiency. This is a particular feature of the characteristics of radial-axial flow pump-turbine units.

Optimal efficiencies in the pump and turbine modes can be matched (see Equation 19.22) by using motor–generators with different speeds of rotation $n_t < n_p$. Such two-speed motor–generators are installed at several HPSPs (for instance, at the Ava-Spin HPSP in Switzerland, $n_p = 500$ rpm, $n_t = 375$ rpm). However, these units are bulky, expensive, offer worse energy characteristics, and are, therefore, used rather seldom. The speeds of rotation are usually equal in both modes ($n_p = n_t$), and the designers try to optimize the operating conditions by imparting an appropriate shape to the flow passage of the machine.

CHAPTER 20

Constructions of Reversible Hydraulic Machines (Pump-Turbines)

20.1. RADIAL-AXIAL FLOW PUMP-TURBINES

The 1200-MW Zagorsk HPSP uses reversible radial-axial flow hydraulic machines with a capacity of 206 MW at a design head of 95 m. These machines were designed and manufactured at the St. Petersburg Metal Works (Figure 20.1). There embodiment is generally similar to that of the radial-axial flow turbines (see Figures 3.15 and 3.17). A wicket (1), $D_1 = 6.3$ m, with seven blades is made from stainless steel. A wicket gate has height $b_0 = 1.15$ m, relative height $\bar{b}_0 = 0.18$, with adjustable guide vanes (2). Hydraulic machine shaft (3) rests on oil guide bearing (4) secured in a strong cover (5). The guide vanes are actuated by individual servomotors (6) (see Figure 4.4) or by two servomotors (Figure 4.2).

Figure 20.2 illustrates a reversible hydraulic machine of the Rodund-II HPSP manufactured by Voith Co. (Germany) and having the following characteristics: head, 354 m; turbine power, 270 MW; turbine discharge, 85 m^3/s; pump power, 256 MW; delivery, 67 m^3/s; and speed of rotation, 375 rpm. Wheel (1) has an outer diameter $D_1 \approx 4.4$ m and an inner diameter $D_2 \approx 2.4$ m ($D_2/D_1 = 0.55$). The wicket gate (2) relative height $\bar{b}_0 = 0.108$. Oil-lubricated guide bearing (4) is secured on a strong cover (3). The guide vanes are actuated by individual cylindrical servomotors (5). Thrust bearing (6) rests on a strong steel cone (7) transmitting load to the cover. Provided under the wheel rim is

Centralna tehnična knjižnica UNIVERZA V LJUBLJANI

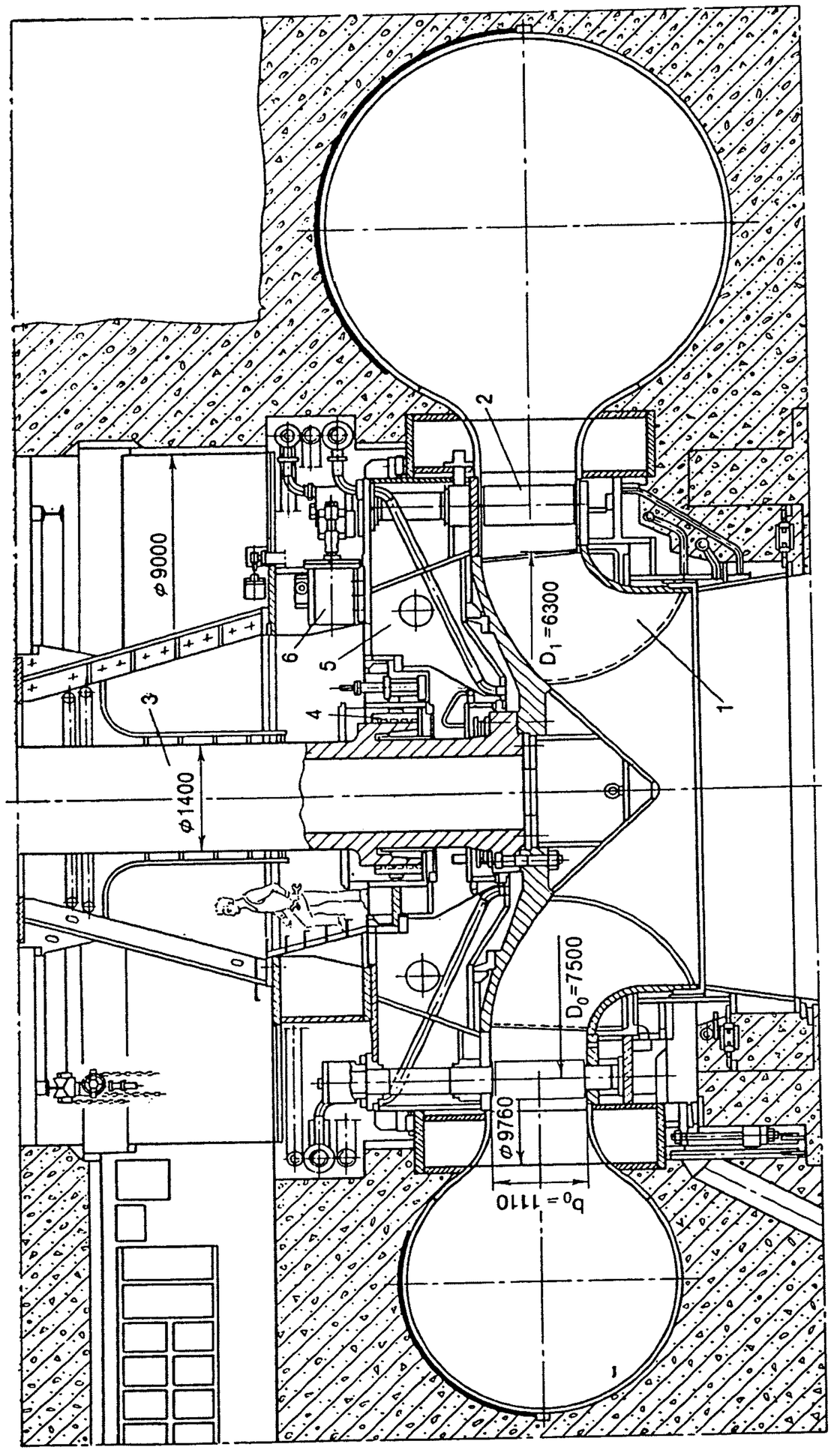


FIGURE 20.1. Zagorsk HPSP radial-axial flow reversible hydraulic machine.

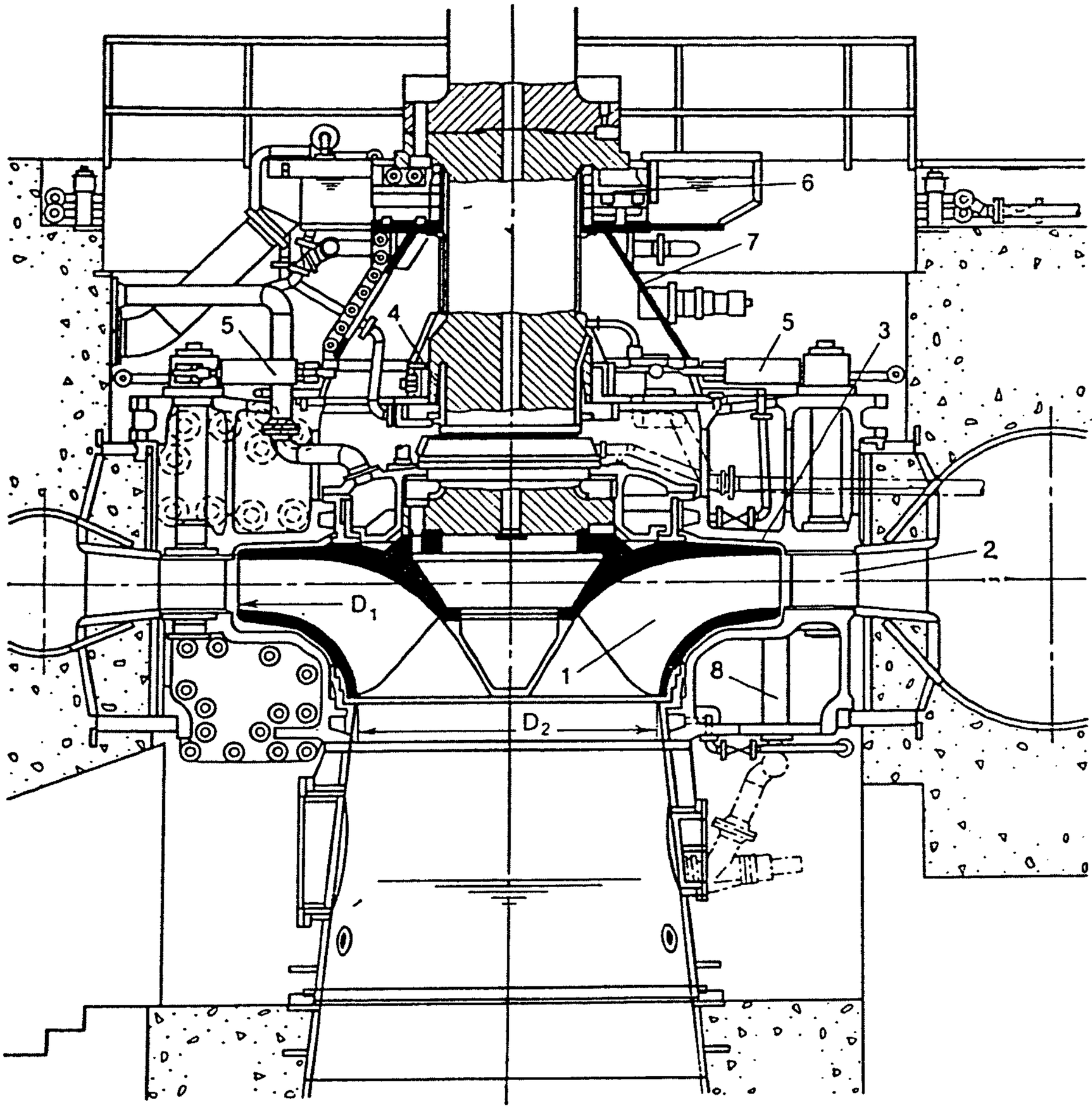


FIGURE 20.2. Rodund-II HPSP radial-axial flow reversible hydraulic machine.

a roomy space for collecting water that penetrates through leaks in the wicket gate in the compensator mode; the water is drained through release pipes (8). The steel scroll is coupled with very strong stayrings.

Table 20.1 presents data on some radial-axial flow reversible pump-turbines. The Bajina Basta HPSP was the leader in head, while the Ladington HPSP was the leader in wheel diameter and power.

20.2. MIXED-FLOW REVERSIBLE PUMP-TURBINES

The first mixed-flow reversible pump-turbines (Deriaz) were commissioned in 1957 at the Adam-Back HPSP in Canada (head from 27 to

Table 20.1. Basic Specifications of Radial-Axial Flow Reversible Hydraulic Machines

HPSP	Country	Year	Wheel Diameter (m)	Speed n (rpm)	Turbine Mode H_{max} (m)	Turbine Mode H_{min} (m)	Turbine Mode N (MW)	Pump Mode H_{max} (m)	Pump Mode H_{min} (m)	Pump Mode Q (m^3/s)	H_s (m)
Zagorsk	Russia	1989	6.3	150	108	93	206	112	97	170	−15
Numappara	Japan	1974	5.0	375	500	422	230	528	428	50	−50
Ladington	United States	1973	8.4	112.5	108	87	343	114	93	314	−7.6
Bajina Basta	Yugoslavia	1983	4.8	428.6	600.3	497.3	294	621.3	531.7	36.7 / 50.8	−54.0
Dinorwic	United Kingdom	1984	4.0	500	536		317	545		50	—

Table 20.2. Basic Specifications of Mixed-Flow Reversible Hydraulic Machines

				Turbine Mode			Pump Mode		
HPSP	Country	Year	Speed n (rpm)	H_{max} (m)	H_{min} (m)	N (MW)	H_{max} (m)	H_{min} (m)	Q (m^3/s)
Valdecanas	Spain	1964	150	74	49	82	72	51	96
Takane I	Japan	1969	277	136	—	87	138	—	60
Kagedeira	Japan	1969	240	90	—	48	94	—	24
Guio de Grandilla (bulb-type unit)	Spain	1980	88.2	25	18	25.5	25	18	25.5

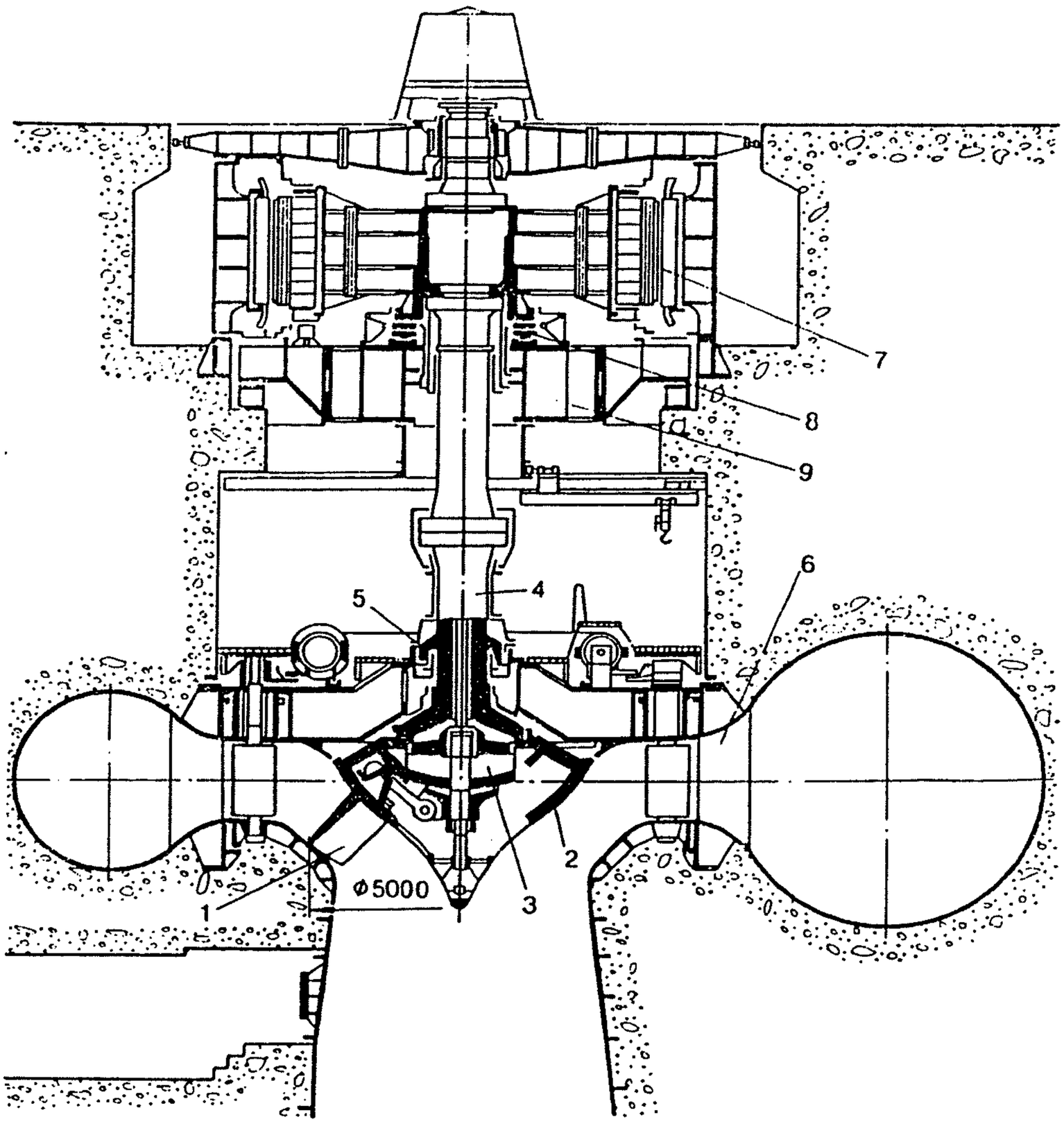


FIGURE 20.3. Liptovska Mara HPSP mixed-flow reversible hydraulic machine.

18 m; power, 34 MW; speed of rotation, 92.4 rpm). Such units are used fairly extensively today (Table 20.2).

Figure 20.3 exemplifies a pump-turbine unit with a mixed-flow reversible hydraulic machine manufactured by CKD-Blansko for the Liptovska Mara HPSP in 1975. The hydraulic machine has a head from 48 to 30 m; speed of rotation, 136.5 rpm, turbine power, 50.3 MW; and delivery, 107 m^3/s. Wheel 1, diameter 5 m, has eight adjustable blades arranged at 45° to the axis of rotation. Disposed inside hub (2) is servomotor (3), diameter 1.7 m, by which the blade angle is adjusted. The oil lines are arranged inside shaft (4). The cover carries guide bearing (5) with oil lubricant. The radial-type wicket gate has a height of 1.35 m ($\bar{b}_0 = 0.27$). The circular-cross-section scroll has a steel shell welded to stayring (6). Suction lift $H_s = -9.2$ m. A synchronous motor–generator (7) is arranged at the top. It has a thrust bearing (8) resting on a load-bearing cross piece (9). Appropriate combinator

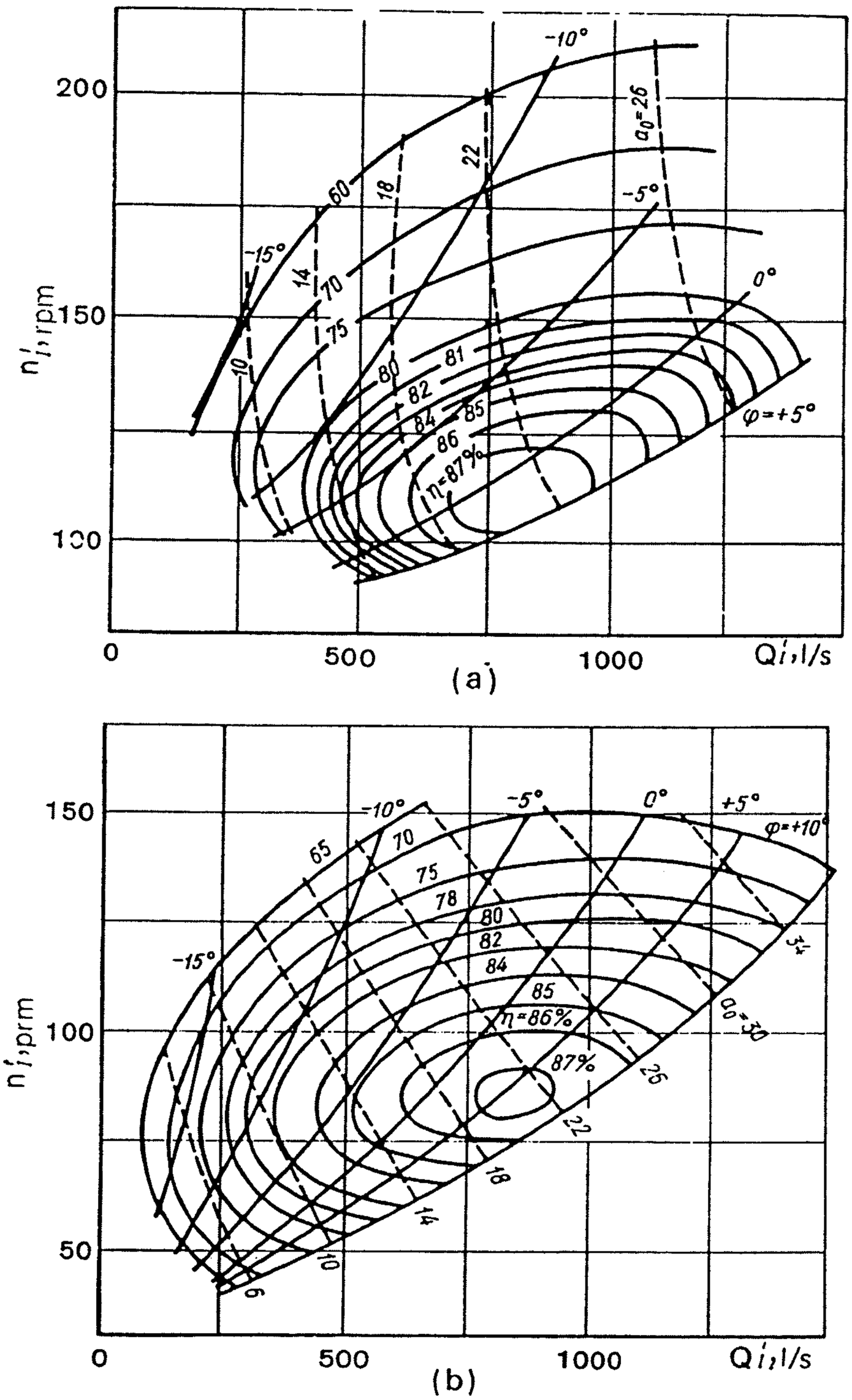


FIGURE 20.4. Characteristics of a mixed-flow reversible hydraulic machine. (a) Pump mode; (b) turbine mode.

relationships determining the optimum ratio between the wheel blade angle and the opening of the wicket gate vanes should be maintained in both the turbine and pump modes.

A reduced characteristic of a mixed-flow reversible hydraulic machine (model $D_1 = 300$ mm) with a specific speed of about 360 rpm in the turbine mode is shown in Figure 20.4. As seen in the figure, n'_1 should be about 110 rpm for the pump mode (Figure 20.4a). In this case, the turbine mode efficiency (Figure 20.4b) decreases to 84%. This is inherent only to this particular shape of the flow passage.

20.3. MULTISTAGE REVERSIBLE PUMP-TURBINES

Single-stage pump-turbines may develop a head of up to 600 to 700 m. If the head is higher, it is necessary either to use a three-machine scheme or to use multistage reversible units.

Figure 20.5 exemplifies a two-stage reversible machine manufactured in Neyrpic, France for the Rudlin HPSP. The machine has a head of

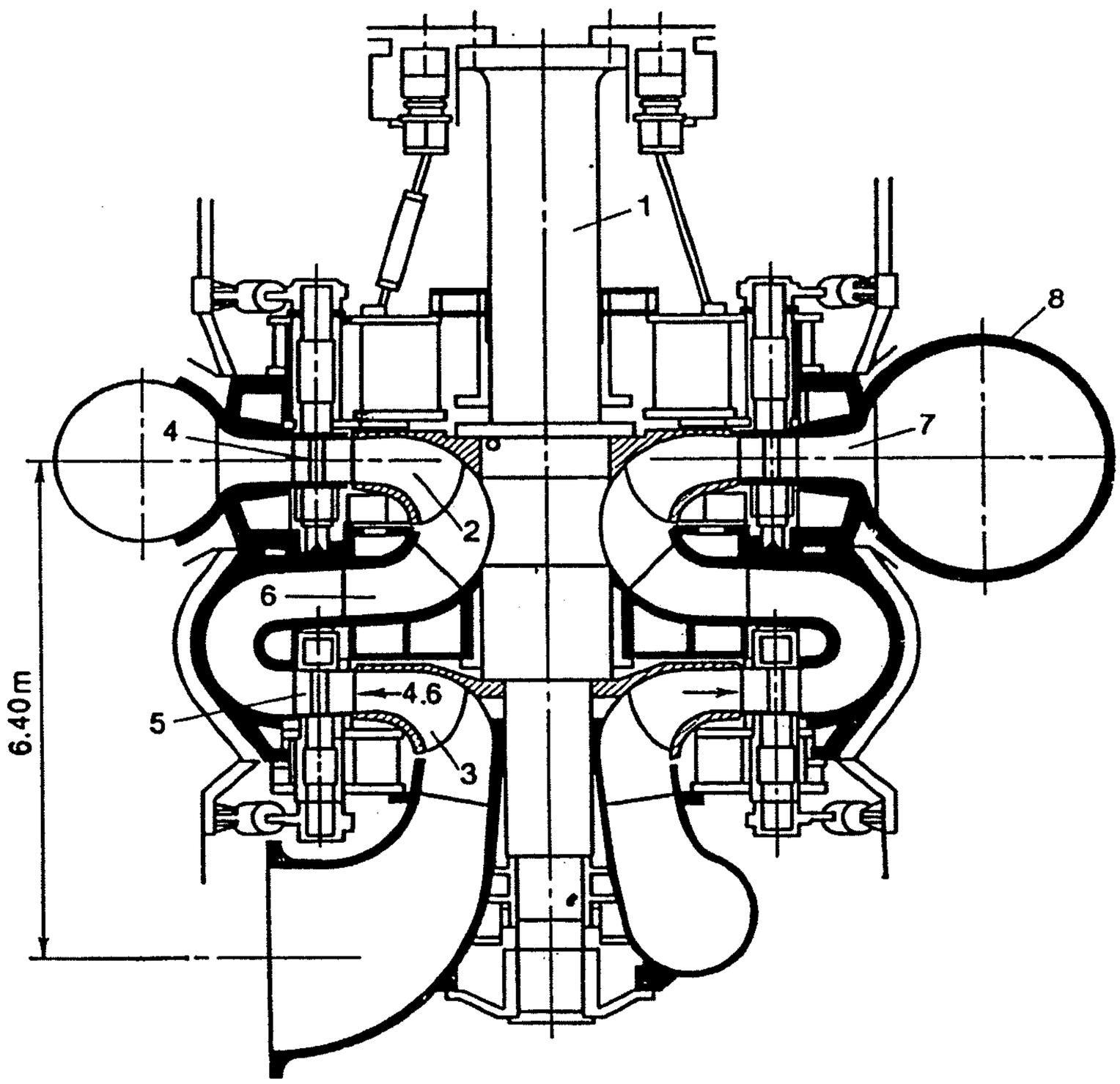


FIGURE 20.5. Two-stage reversible hydraulic machine.

600 m, a speed of rotation of 333 rpm, and power of 400 MW. Two wheels (2 and 3), diameter 4.6 m, are fitted to shaft (1). There are two rows of guide vanes (4 and 5). Disposed between the wheels are straightening guide vanes (6) which eliminate the circulation formed at the exit from the first-stage wheel (3) in the pump mode and at the entrance to the second-stage wheel (2). The adjustment ring of wicket gate (4) is arranged at the top and ring (5) at the bottom. Adjoining stayring (7) is a circular scroll (8) connected to the delivery pipeline.

Two-stage units are installed at the Le Clou HPSP (four units, 320 MW each; head, 1050 m; speed of rotation, 600 rpm) and at some other pumped-storage plants.

If a greater number of stages (3 to 5) is needed, power adjustment must be abandoned so that the unit is started and stopped with the use of a gate.

Multistage reversible hydraulic machines are now used increasingly. The Chiotas HPSP, Italy, is equipped with eight reversible four-stage machines, 150 MW each, having a wheel diameter of 2.3 m, a head of 1047 to 1070 m, and speed of 600 rpm. The Edolo HPSP uses five-stage reversible units with heads of 1256 to 1287 m.

Multistage reversible hydraulic machines (pump-turbine units) are installed at some high-head HPSPs in France. For instance, the Grand Maison HPSP has eight four-stage pump-turbine units (turbine mode: heads, 775 to 930 m; power, 109 to 152 MW; pump mode: heads, 827 to 972 m; power, 157 to 146 MW; speed of rotation, 600 rpm; wheel diameter, 2.2 m).

It is very important that using two-stage and multistage reversible hydraulic machines ensures a high head and decreases the immersion required for precluding cavitation.

20.4. DOUBLE-WHEEL REVERSIBLE PUMP-TURBINES

Creating a reversible hydraulic machine with one wheel operating in both the turbine and pump mode involves many problems pertaining to both the optimal shape of the flow passage and the need for reversing the wheel to change over from one mode to the other. These problems can be solved if a reversible machine is used with two separate wheels: a pump wheel and a turbine wheel. Strictly speaking, this is a three-machine scheme rather than a reversible unit, but it is embodied as a single reversible hydraulic machine. An example of such a two-wheel reversible machine is HONE, proposed by Hosnedel and Nekhleba in Czechoslovakia (Figure 20.6). A semisphere (2), accommodating a larger diameter pump wheel (4) and a turbine wheel (5) on axle (3), is attached to shaft (1). The wicket gate has two rows: lower row (6), including

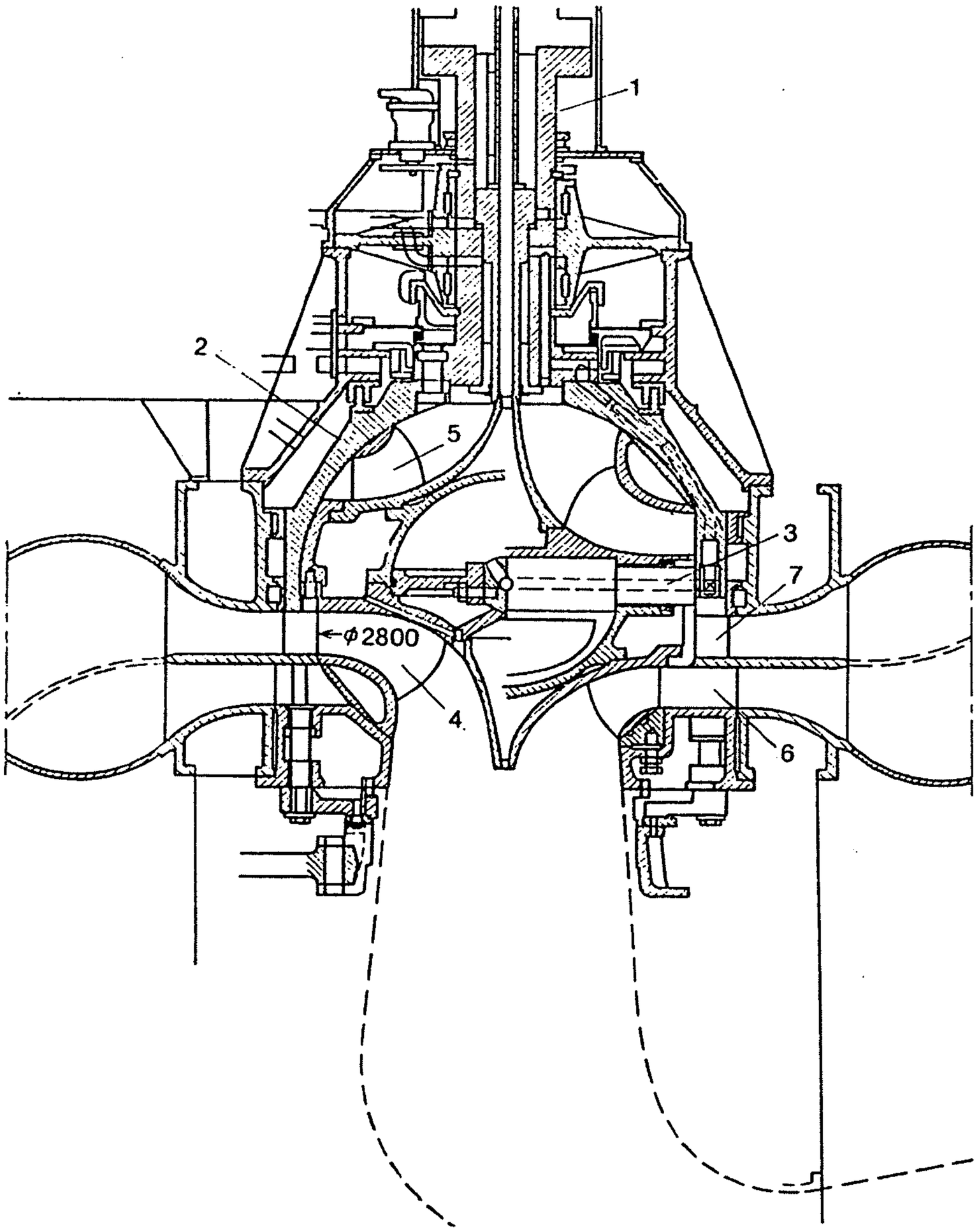


FIGURE 20.6. Reversible hydraulic machine HONE.

adjustable blades for the turbine wheel, and upper row (7), including stationary blades for the pump wheel. In operation the required wheel is set opposite the respective wicket gate by turning on shaft (3). The HONE construction is rather complex. To decrease hydraulic losses, it is necessary to force out water from the space between the cover and the semisphere.

A two-wheel reversible hydraulic machine—"isogir"—was developed by Atelier-de-Charmilles. The prototype, having a head of 395 m and power of 10 MW, passed operating tests at the Robiey HPSP in 1968. As a result, isogirs have been developed for various HPSPs.

Figure 20.7 illustrates an isogir for the Haut-Chute HPSP rated for heads of 610 to 500 m, speed of rotation of 428 rpm, power of 300 to

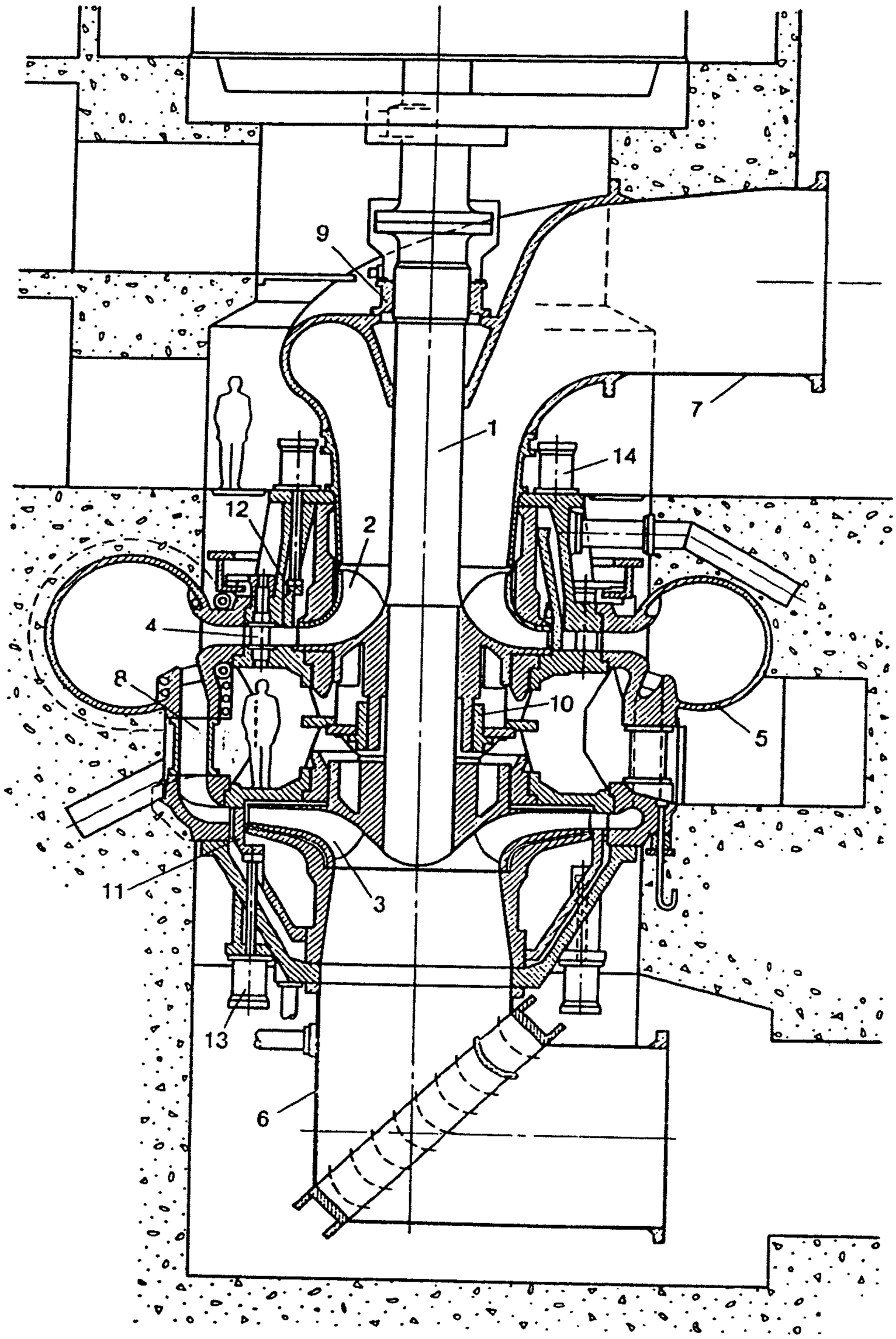


FIGURE 20.7. Reversible two-wheel hydraulic machine.

250 MW, and delivery of 42.4 to 53.5 m^3/s. The basic components include a shaft (1) with turbine wheel (2), and pump wheel (3), and a wicket gate with adjustable blades (4) and scroll (5). Water is fed to pump wheel (3) via suction pipe (6) and is withdrawn from the turbine wheel through draft tube (7). Water is supplied from the pump wheel to the scroll via passages (8). Shaft (1) has two bearings (9 and 10). Wheels

(2 and 3) are rigidly fitted to the shaft and rotate jointly with it. To engage or disengage a wheel, use is made of cylindrical gates (11 and 12), which are able to be displaced by servomotors (13 and 14). When the unit operates in the turbine mode, gate (11) is closed and gate 12 is open (the LH side view); in the pump mode, gate (12) is closed and gate (11) is open (the RH side view). The construction is rather complex.

Main Symbols

a_0, α_0	Wicket gate opening
B, b	Width or height
b_0	Wicket gate height
C, c	Coefficients
C	Cavitation specific speed
D, d	Diameter
E, e	Flow specific energy
F	Area
E_r	Radial (lateral) runner force
G	Mass or weight
g	Gravity acceleration
H	Head
H_{st}	Static head
H_v	Vacuum hight
H_s	Suction height (lift)
H_v^{per}	Permissible vacuum suction lift
h	Head difference
h_{loss}	Head loss
HEPP	Hydroelectric power plant
HPSP	Hydaulic pumped-storage plant
K, k	Parameters, factors
k_σ	Cavitation safety factor
L	Length
M	Moment, torque
m	Mass flow
N	Power
n	Speed of rotation
n'_{I}	Reduced (unitary) rotation speed
n_s, n_{s0}, n_{s1}	Specific speed (different forms)
NPSH	Net positive suction head
P, p	Pressure
p_a	Absolute pressure
p_{atm}	Atmospheric pressure
p_v	Vapor pressure
P	Axial force, thrust
Q	Discharge
Q'_{I}	Reduced (unitary) discharge
q	Leakage discharge, relative discharge
R, r	Radius

s	Relative aria, shift
T, t	Time
T	Torque
u	Peripheral rotation velocity
v	Flow velocity
w	Relative velocity
z	Elevation over datum level, number of blades, jets, etc.
α	Coefficient of kinematic energy, angle
β	Angle
δ	Angle
Γ	Circulation
ε	Relative friction losses, relative volume
ζ	Coefficient of local (minor) losses
η	Efficiency
λ	Coefficient of pipe friction losses
ν	Kinematic viscosity
ρ	Density
σ	Cavitation coefficient
τ	Tangential stress
φ	Discharge coefficient of hydraulic machine, blade setting angle, spiral case angle
ψ	Head coefficient of hydraulic machine, coefficient of constriction
ω	Angular velocity

APPENDICES

Measuring Units and Their Conversion

Table A. 1. International System of Units (SI)

Type	Units	Name	Notation	Formula
Basic	Length	Meter	m	—
	Mass	Gram	g	—
	Time	Second	s	—
Derived	Force	Newton	N	$kg \times m/s^2$
	Pressure	Pascal	Pa	N/m^2
	Energy	Joule	J	$N \times m$
	Power	Watt	W	J/s

Table A. 2. Decimal Units Values

Unit	$\times 10^{-3}$	$\times 10^{-2}$	$\times 10^{-1}$	$\times 10^{3}$	$\times 10^{6}$	$\times 10^{9}$	$\times 10^{12}$
Name	Milli-	Centi-	Deci-	Kilo-	Mega-	Giga-	Tera-
Symbol	m	c	d	k	M	G	T

Table A.3. Conversion of Measuring Units

Length	Meter (m)	Inch (in.)	Foot (ft)
1 m	1	39.37	3.28
1 in.	0.0254	1	1 / 12
1 ft	0.3048	12	1

Area	Square meter (m^2)	Square inch ($in.^2$)	Square foot (ft^2)
1 m	1	1550	10.76
1 $in.^2$	6.45×10^{-4}	1	1 / 144
1 ft^2	0.0929	144	1

Volume	Cubic meter (m^3)	Liter (L)	Cubic inch ($in.^3$)	Cubic foot (ft^3)	U.K. gallon (imperial gal)	U.S. gallon (gal)
1 m^3	1	10^3	6.1×10^4	35.31	220	264.2
1 L	10^{-3}	1	61	0.0353	0.22	0.264
1 $in.^3$	1.64×10^{-5}	0.0164	1	5.79×10^{-4}	3.6×10^{-3}	4.33×10^{-3}
1 ft^3	0.0283	28.3	1728	1	6.23	7.48
1 imperial gal	4.546×10^{-3}	4.546	277.4	0.16	1	0.833
1 U.S. gal	3.79×10^{-3}	3.79	231	0.134	1.2	1

Force	Newton (N)	Kilopond (kp)	Pound force lb_f
1 N	1	0.102	0.2248
1 kp	9.81	1	2.205
1 lb_f	4.45	0.454	1

Table A.3. (continued)

Pressure	Pascal (pa)	Bar	kp / cm²	Pounds per square inch lb_f / in.²	m of water (height mwh)	Torr (mm Hg)
1 Pa	1	10^{-5}	1.02×10^{-5}	14.5×10^{-5}	1.02×10^{-4}	7.5×10^{-3}
1 Bar	10^5	1	1.02	14.5	10.2	750
1 kp / cm²	98.066	0.981	1	14.2	10	736
1 lb_f / in.²	6895	0.069	0.0703	1	0.703	51.7
1 mwh	9810	0.0981	0.1	1.42	1	73.5
1 torr	133	1.33×10^{-3}	1.36×10^{-3}	0.0193	0.0136	1

Density (specific mass)	kg / m³	kp × s² / m⁴
1 kg / m³	1	0.102
1 kp / s² / m⁴	9.81	1

Energy	Joules (J)	Kilowatt Hours (kWh)	Kilocalories (kcal)	Kiloponds per Meter (kpm)
1 J	1	2.78×10^{-7}	2.39×10^{-4}	0.102
1 kWh	3.6×10^6	1	860	3.67×10^5
1 kcal	4187	1.16×10^{-3}	1	427
1 kpm	9.81	2.72×10^{-6}	2.34×10^{-3}	1

Power	Watt (W)	Kilowatts (kW)	Horsepower (hp)
1 W	1	10^{-3}	1.34×10^{-3}
1 kW	1000	1	1.34
1 hp	746	0.746	1

Temperature (t°)	Celsius (t°C)	Fahrenheit (t°F)	Absolute Kelvin (t K)
t°C	1	5 (t°F − 32) / 9	t K − 273.15
t°F	(9 / 5) × t°C + 32	1	(9 / 5) × t K − 459.72
t K	t°C + 273.15	(5 / 9) × t°F + 255.4	1

Bibliography

Addison, H. *Centrifugal and Other Rotodynamic Pumps* (London: Chapman & Hall, 1966).

Dickenson, C. *Pumping Manual* (London: The Trade and Technical Press, 1988).

Frick, P. A., and Alexander, G. C. *Cost and Control of Small Hydroelectric Plants or River Systems* (Washington, DC: U.S. Department of Energy, 1979).

Hicks, T. G., and Edwards, T. W. *Pumps Application Engineering* (New York: McGraw-Hill, 1971).

International Electrotechnical Commission, *International Code for Model Acceptance Tests of Hydraulic Turbines* (Geneva: Bureau Central, 1965).

Karassik, I. J., Krutzsch, W. C., Fraser, W. H., and Messina, J. P. *Pump Handbook* (New York: McGraw-Hill, 1986).

Knapp, R. T., Daily, J. W., and Hammit, F. G. *Cavitation* (Iowa City: Institute of Hydraulic Research, 1979).

Kovalev, N. N. *Hydraulic Turbines* (Jerusalem: Institute for Scientific Translations, 1965).

Moniton, L., Nir, M. L., and Roux, J. *Micro Hydroelectric Power Stations* (New York: John Wiley & Sons, 1984).

Nechleba, M. *Hydraulic Turbines* (Prague: Artia, 1957).

Pfleiderer, G., and Potermann, H. *Stromungmaschinen* (Berlin: Springler-Verlag, 1964).

Pollak, F. *Pumps Users Handbook* (London: Trade and Technical Press, 1980).

Raabe, J. *Grundlagen der Hydraulischen Stromungmaschinen*, Teil 2, *Wasserturbinen*, Teil 3, *Pumpen* (Dusseldorf: VDI-Verlag, 1970).

Robertson, J. A., and Crowe, C. T. *Engineering Fluid Mechanics* (Boston: Houghton Mifflin, 1985).

Siminons, Ch. *Hydro-Power* (Oxford: Pergamon Press, 1980).

Stepanoff, A. J. *Centrifugal and Axial Flow Pumps* (New York: John Wiley & Sons, 1957).

Sulzer Brothers Ltd., *Sulzer Centrifugal Pump Handbook* (New York: Elsevier Applied Science, 1989).

Warnick, C. C. *Hydropower Engineering* (Englewood Cliffs, NJ: Prentice-Hall, 1984).

Webb, D. E. *Pump Turbine Schemes* (New York: American Society of Mechanical Engineers, 1979).

Index

active turbines, *see* Pelton turbines
adjustable blade turbines, *see* axial-flow turbines
afterbay, *see* tailwater
air lift, 361–363
atmospheric pressure, 9
  vs excessive pressure, 9
axial-flow pumps, *see* impeller pumps
axial-flow turbines, 5, 6, 22–24; *see also* individual hydroelectric power plants
  absolute motion in, 72
    trajectories of, 77
  application of, 29–30
  blade profile, 69
  casing of, 22
    concrete vs steel, 22
  cover of, 24
  draft tubes, 24, 114–123
    diffuser of, 26
    efficiency of, 117
    hydraulic characteristics of, 115
    performance of, 115–118
      outlet losses, 116
    elbow-type, 119–123
    straight type, 118–119
  efficiency of, 170
  energy equation of, 79–84
    angular momentum equation, 79
    Bernoulli's equation, 82
    circulation, 80, 84
    Euler equation, 81, 83–84
    leading edge of runner blade, velocities at, 79, 80
    torque, of runner, 80
    trailing edge of runner blade, velocities at, 79, 80
  flow in, 28
  horizontal turbines, 39–43
    straight-flow unit, 42–43
    TPP, 43
  hydrodynamic forces, reduced, 167
  nomenclature, 173–185
    horizontal turbines, 179, 181
    mass or weight, 182, 184, 185
    propeller-type turbines, 182
    range chart, 176–178
    specific speed, 176–177, 179
      adjustable blade turbines, 176
      axial-flow bulb-type turbines, 177
    turbine type marks, 173–176
    vertical turbines, 177–180
  propeller turbines, 37
  regime of, 77–79
    absolute velocity, 78
    inlet flow, 78
    normal outflow, 79
    optimal mode, of operation, 79
    outlet flow, 78
    relative velocity, 77
    shock-free entrance, 79
    velocity parallelogram, 77
    vorticity regions, 78
  relative motion in, 72
  runaway characteristics of, 165–166
  runner of, 22
  runner blade operating gear, 64–67
    casing, 65
    servomotors, 65–66
  stayring vanes of, 23
  transportation motion in, 72
  velocity parallelogram (triangle), 73–77
  wicket gate of, 23, 24
    guide vanes of, 23

water flow created by, 69–72
angular-momentum equation, 71
circulation, 70–71
law of conservation of velocity momentum, 72

babbit, 58
Bernoulli's equation, 12, 13, 17–18, 220, 221

cavitation
in pumps, 277–286, 328–330
coefficient, 282, 284
of pump specific speed, 285–286
NPSH, 278, 280–282
permissible vacuum suction lift, 278–280
geometric (static) suction lift, 279
pump rotational speed, changes in, 282–285
NPSH, 283–285
vacuum suction lift, 282–283
in turbines, 125–132
coefficient, 131, 133, 134
Bernoulli's equation, 132–133
determination of, 135–138
vs specific speed, 136
erosion of, 128
resistance factors of, 132
formation of, 126–127
local, 129
permissible suction height, value of, 135
profile, 129
bubble, 129, 130
separating, 129, 130
sheet, 129, 130
supercavitation, 129, 130
zonal, 129, 130
rig, 144, 146–148
saturated water vapor vs temperature, 126
similarity formula, 133
slotted, 129
suction head, allowable, 137–138
suction lift, 137
Thoma equation, 134
turbulent flow, 127
Cimego Hydro (Italy), 52
combinator dependence, 37
Coriolis factor, 11–12, 116
cross-flow Banki turbines, 55

Deriaz, contribution to turbine design by, 60, 387
discharge elements, *see* specific elements
Djerdap-Iron Gate hydroelectric power plant (Danube River), 33, 34
dredge pumps, 339–346
actual delivery, 344
cavitation in, precluding, 345
characteristics of, 342–343
design features of, 339
heavy-duty, 340
light-duty, 339–340
nomenclature of, 340–341
operating conditions of, 343
permissible suction lift, 344–346
sand pumps, 341–342
slurry, 339, 341, 343, 344

energy, specific, 10–13
averaging, achievement of, 11
components of, 10
tailwater, relation to, 18
Euler, contribution to turbine design by, 59–60
excessive (gauge) pressure, 9
piezometric height, association with, 9, 10
vs atmospheric pressure, 9

Fink, contribution to turbine design by, 60
forebay, *see* headwater
Fourneyron, contribution to turbine design by, 60

Francis, contribution to turbine design by, 60
Francis turbines, *see* radial-axial turbines
free-jet turbines, *see* Pelton turbines

Grand Coulee Hydro (Washington State), 48–49
gross head, 19
guide vanes
  cascade, 69
  operating gear, 61–64
    regulating ring, 61
    servomotors, 61–64

HAB, *see* horizontal axial-flow pump, adjustable blade
HAF, *see* horizontal axial-flow pump, fixed blade
Haut-Chute hydroelectric power plant, 394–396
headwater (HW), 3, 8, 17
  specific energy of, 17–18
HEPP, *see* hydroelectric power plants
high-head turbines, 7; *see also* Pelton turbines
horizontal axial-flow pump, adjustable blade (HAB), 262–263
horizontal axial-flow pump, fixed blade (HAF), 262–263
HPSP, *see* pumped-storage plant pumps
HW, *see* headwater
hydraulic losses, 18–20, 25
hydraulic ram, 363–364
hydroelectric power plants (HEPP), 3; *see also* specific power plants
bulb-type units, 39–42, 60
  bearings, 40–41
  components, 40, 41
  draft tubes of, 119
  water flow, 40
turbines
  installation of, 17, 18
  selection of for, *see* turbine selection
  service at, 3
  static head of, 17

impeller pumps
  abrasive wear in, 330–332
    most resistant materials, 331–332
  axial-flow pumps, 238–239
    velocity parallelograms, 239
    velocity triangles, 239
  cavitation wear in, 328–331
    most resistant materials, 331–332
  centrifugal pumps, 235–237
    flow kinematics
      absolute velocity, 235, 238
      leading edge velocity, 236, 237
      relative velocity, 237
      trailing edge velocity, 237
      transportation velocity, 237
      velocity parallelograms, 235
    flow structure, 252–253
    geometry, 236
    with upstream auger, 286
  characteristics of, 287–296
    blade setting angles, 289
    conversion of, 295–296
    dimensionless pump, 288–289
    experimental determination of, 292–294
      cavitation, 294
      test set, 292–293
    NPSH values, 290
    pump characteristic curves, 287
    specific speed, dependence on, 294–295
    theoretical, 290–292
      head, 290–292
      velocity triangles, 291
    for VAB, 289
  circular characteristic of, 376–378
  construction of, 255–276
    axial-flow pumps, 231, 260–263
      HAB, 262–263
      HAF, 262–263
      VAB, 261
      VAF, 261

axial force, 274–275
centrifugal pumps, vertical, 265–266
cradle-mounted pumps, 230, 256–258
monoblock pump, 257–258
double-entry pumps, 258–260
feedwater pumps, 256
general purpose pumps, 255
mixed-flow pumps, 263–264
multistage pumps, 266–270
packing glands, 272–273
pressure, 271–272
pump outlets, 273
pump rotor, 275, 276
radial force, 273–274
special purpose pumps, 255–256
wheel, 270
wheel seals, 272
delivery control of, 322–327
by bypass pipe, 325
by changing blade angle, 325–326
by changing circulation, 326
by changing number of pumps, 326–327
by gate (throttling) valve, 322–323
by varying rotation speed, 323–325
hydrodynamic speed converter, 323–325
slip factor, 324
energy losses, 253–254
hydraulic, 253
hydraulic efficiency, 254
mechanical, 253
mechanical efficiency, 254
overall efficiency, 254
volumetric, 253
volumetric efficiency, 254
installation of, 327–328
suction pipeline, 327, 328
main energy equation, 239–243
Bernoulli's equation, 241
circulation, 240
Euler equation, 241
hydraulic efficiency, 242–243
law of angular momentum, 240
theoretical pump head, 241
torque, 240
regime, 243–248
delivery, 243
isogonal, 244
rotational speed, 243
kinematic similarity, 244–248
velocity parallelograms, 244
specific speed, 248–252
delivery coefficient, 251
head coefficient, 251
pump efficiency, influence on, 251
starting, 317–321
backwater installation, 317
closed gate valve, 321
priming, 318, 319
air bags, 318
valve tightness, 318
self-priming, 321
vacuum pumps, use of, 318–321
jet-type pump (ejector), 321
liquid-ring, 320
sumps, 335–337
air entrainment, 336, 337
free flow, 336–337
prerotation, 335
unstable vs stable operation of, 332–335
stability criterion, 333
surging, 333–334
impulse turbines, *see* Pelton turbines
inclined-jet Turgo turbines, 55
Inguri Hydro (Georgia), 49–50

jet pump (ejector), 353, 356–360
cavitation in, precluding of, 360
designs of, 359–360
theoretical characteristics, 358

Kaplan, contribution to turbine design by, 60
Kaplan turbines, *see* axial-flow turbines
Kiev Hydro (Dnepr River), 40

kinetic energy, 10
correction factor for, 11–12; *see also* Coriolis factor
Kremenchug hydroelectric power plant (Dnepr River), 31–39
heads, 37
relationship to runner, 37
runner, 35–39
blades, 35–39
angle of, 36–37, 39
combinator dependence, 37
casing, 38, 39
turbine cover, 39
turbine stayring, 31, 33
wicket gate, 31–34
axial, 35
conical, 33, 35
radial, 33
Kviatkovski, contribution to turbine design by, 60

Liptovska Mara hydroelectric power plant, 390, 392
liquid (flowing) power, absolute, 12–13
low-head turbines
axial-flow, *see* axial-flow turbines
horizontal type, 6
vertical type, 4–5

medium-head turbines, *see* radial-axial turbines
mixed-flow turbines, 24, 43–45
application of, 29–30
runner blade operating gear, 66
Murray, Sidney A., Jr. Hydropower-station (Mississippi River), 41

net head, 19
no-cavitation
in pumps, 277–279, 281
in turbines, 129–132
permissible suction height, value of, 135
power test rig, 144
NPSH, *see* cavitation, net positive suction head
Nurek Hydro (Vakhsh River), 173, 174

Pelton turbines, 26–28, 50–54
application of, 29–30
buckets, 50–51
capacity, regulation of, 27
deflectors, 51–52
horizontal, 50
nozzle of, 26
pipeline of, 26
regime of, 85–86
jet velocity, 85
relative velocity, 86
torque, of runner, 86
regulating needle of, 66–68
runner of, 26, 51
buckets of, 26–28
kinetic energy of, 28
shaft of, 26
vertical, 50
positive displacement pumps, 226–229
diaphragm, 227, 228
gear, 227, 228
piston, 226–227
plunger, 226
reciprocating movement, 229
rotary, 229
screw, 227–229
potential energy, 10
pressure energy, 10
pump capacity, 224–225
pump classification, 232–233
pumped-storage plant pumps (HPSP), 8, 350–353, 367
day vs night usage, 8, 350
five-stage vertical pump, 353, 355
"four-machine scheme," 367
"three-machine scheme," 367, 392
"two-machine scheme," 367
two-stage double-entry pump (horizontal), 352–353
two-stage vertical pump, 353, 354
vertical pump, 351–352
pump installation, heads of, 219–224
absolute pressure in liquid, 221

coefficient of resistance, 222
elevation, *see* static head
flow rate created by, 223
hydraulic losses, 222
inlet pressure, 220
measurement, 223
outlet pressure, 221
pump pressure, 224
static head, 219
vacuum suction lift, 220
pump selection, 297–315
design delivery, 312
design head, 313
design losses, 314
nomenclature, 302–308
application of pumps, widening scope, 302–304
of impeller pumps, 305–308
centrifugal cradle-mounted pumps, 305–306
centrifugal double-entry pump, 306
centrifugal vertical pump, 306, 307
horizontal axial-flow pump, 307–308
vertical axial-flow pumps, 306–307
pump designation, 303–305
range charts, 302
wheel, turning, 303, 304
parallel connection, 308–311
average efficiency, 310
counterflow operation, 310
delivery rate, 309
plant
HAB, 297, 299
VAB, 297, 298
vertical centrifugal pumps, 298, 300
series connection, 311–312
average efficiency, 311
head required, 312
suction lift, 298
unit, 297, 301
pump installations, 300
water system characteristics, 301–302
actual delivery, 302
head required, 301, 302
network characteristic, 302
pump-turbines, *see* reversible hydraulic machines

radial-axial-flow turbines, 24–26, 45–50
absolute motion in, 72, 75, 76
trajectories of, 77
application of, 29–30
blade profile, 69
cover of, 26, 47
draft tubes, 114–123
diffuser of, 26
efficiency of, 117
elbow-type, 119–123
hydraulic characteristics of, 115
performance of, 115–118
outlet losses, 116
straight type, 118–119
energy equation of, 79–84
angular momentum equation, 79
Bernoulli's equation, 82
circulation, 80, 84
Euler equation, 81, 83–84
leading edge of runner blade, velocities at, 79, 80
torque, of runner, 80
trailing edge of runner blade, velocities at, 79, 80
flow in, 28
meridional plane, 73, 75
flow in, 74
nomenclature, 173–185
mass or weight, 182, 184, 185
radial-axial-flow turbines, 182, 183
range chart, 176–178
specific speed, 176–177, 179
radial-axial turbines, 176
turbine type marks, 173–176
regime of, 77–79
absolute velocity, 78
inlet flow, 78
normal outflow, 79

optimal mode, of operation, 79
outlet flow, 78
relative velocity, 77
shock-free entrance, 79
velocity parallelogram, 77
vorticity regions, 78
relative motion in, 72
runaway characteristics of, 164–165
runner of, 24, 46, 47, 74
labyrinth seals, 49
servomotors, 47, 64
slot seals, 46–48
spiral casing of, 25, 46
stayring vanes of, 25, 46
transportation motion in, 72
velocity parallelogram (triangle), 73–77
wicket gate of, 25
water flow created by, 69–72
angular-momentum equation, 71
circulation, 70–71
law of conservation of velocity momentum, 72
reaction turbines, *see* axial-flow turbines; radial-axial turbines
recovery drop, 19–20
reduced parameters, 90–93
discharge coefficients, 92
head coefficients, 92
reversible hydraulic machines, 8, 367–383; *see also* specific power plants
design head, 367
double-wheel machines, 393–396
HONE, 393–394
"isogir," 394–396
impeller pump, circular characteristics of, 376–378
modes of, 377–378
mixed-flow machines, 387, 389–392
characteristics, 391, 392
multistage machines, 392–393
parameters, determination of, 373–376
radial-axial flow machines, 385–388
reversibility, 368–373
cavitation coefficient, 371–373
Euler's equations, 369
head coefficient, 369–370
rotation speed, reduced, 370–371
specific speed, 371
velocity triangles, 368
selecting, 382
universal characteristics of, 378–383
braking modes, 379, 380
pump modes, 379–383
runaway coefficient, 381
runaway mode, 380
turbine modes, 380, 382
Rodund-II hydroelectric power plant, 385, 387
rotodynamic pumps, 230–232
axial-flow, 230–231
centrifugal, 230
impeller, 230
jet, 231–232
vortex, 231, 232
Rudlin hydroelectric power plant, 392–393

Safanov, contribution to turbine design by, 60
Saratov Hydro (Volga River), 173, 174
Sayano-Shushenskoye hydroelectric power plant (Yenisey River), 45–48, 105
Sestrimo Hydro (Bulgaria), 52, 53
slurry, 339, 341, 343, 344
small hydroelectric power plants, 54–55
cross-flow Banki turbines, 55
inclined-jet Turgo turbines, 55
specific speed, 93–97
head, effect of on, 95
reduced parameters, effect of on, 96
universal form, 94, 95
Straflo, 42, 43
submersed pumps, *see* well pumps

suction lift, 10
supply elements, *see* specific elements

tailwater (TW), 3, 8, 17, 114
  specific energy of, 18–19
tidal power plants (TPP), 43, 378
TPP, *see* tidal power plants
turbine automation, 201–209
  for adjustable blade turbines, design features of, 204–206
  control cabinet, 203–204
    master slide valve, 203, 204
  oil pumping unit, 202–203
    accumulator, 202
    pumps, 202
  for Pelton turbines, design features of, 206–207
    jet deflectors, 206
  pressure regulator, 207–209
  servomotors, 203–204
turbine bearings, 56
  lateral (radial) force, 58–59
  oil-lubricated, 57–58
  water-lubricated, 56–58
turbine capacity (power), 21–23
  discharge of, 21
  efficiency of, 21, 22
turbine cases, 101–114
  design of, 102–114
    average velocities, design of, 109–112
    concrete cases, 106–107
    coverage angle, 106
      erection of, 103, 104
      shell of, 103
      two-pipeline case, 105
    stayring, dimensions of, 108
    steel spiral (scroll), 102–105
    uniform water flow, 108
    velocity direction, 112–114
    width of, 108
  requirements of, 101
  types, 101–102
turbine characteristics, 139–170
  of adjustable blade turbines, 148–151
    balance, 155
    double flow regulation, 148
    outlet velocity parallelograms, 148
    plotting, 149–150
      combinator curve, 150
      combinator relationship, 150, 152
  axial loads acting on runner, 167–169
  comparison of types via, 168–170
    relative discharge characteristics, 168, 169
    relative head characteristics, 170
    relative power characteristics, 168, 169
  kinds of, 139–144
    general, 140–143
      operating characteristics, 140–141, 161–164
      universal characteristics, 141–143
    geometric factors, 139
    kinematic factors, 139
    linear, 143–144, 160–161
    mode of operation, 139
  model parameters, conversion of to full-scale equipment, 151–159
    efficiency of full-scale turbine, 154–157
      hydraulic efficiency correction formula, 155, 157–159
      kinematic viscosity of water, 156
      Reynolds number, 158
      von Karman formula, 158
    hydraulic energy losses, 152–153
      hydraulic efficiency, 153
    mechanical losses, 153–154
      mechanical efficiency, 154
    turbine efficiency, 154
    volumetric losses, 153
      volumetric efficiency, 153

model tests, 144–148, 156
cavitation rig, 146–148
coefficient, 147
Venturi flow meter, 146
power test rig, 144
brake rotor, 145
efficiency of, 145
runaway, 164–166
combinator dependence, 166
turbine development, 59–60
turbine head, 17–21; *see also* specific components
turbine installation, 209–212
draft tube cone lining, 210
insert parts, 210–211
steel scrolls, 211
removable parts, 211
runners, 212
turbine shaft, 212
turbine cover, 212
turbine operation, 213–216
abrasive wear, 215–216
availability factor, 213
cavitation erosion, 214
reliability, 213
turbine selection, for hydroelectric power plants, 171–200
hydroelectric unit, 171–173
electric generator, 171
synchronous speed, 172
nomenclature, of reaction turbines, 173–185
axial-flow adjustable blade horizontal turbines, 179, 181
axial-flow adjustable blade vertical turbines, 177–180
axial-flow turbines, propeller-type, 182
mass or weight, 182, 184, 185
mixed-flow adjustable blade turbines, 178, 179, 181, 182
radial-axial-flow turbines, 182, 183
range chart, 176–178
specific speed, 176–177, 179
adjustable blade turbines, 176
axial-flow bulb-type turbines, 177
radial-axial turbines, 176
turbine type marks, 173–176
operation characteristics, 197–200
load curve, 198
determination of average efficiency, 198–199
load distribution, 197–198
relative increment, 197
total, 199
turbine elevation, 200
operation curves, 196, 197
Pelton turbines, peculiarities of, 191–196
capacity, 192
dimensions, 194
efficiency, 192, 193
flow rate, 191–192
jets, 192
optimal reduced rotational speed, 191
specific speed of, 192, 193
powerhouse of HEPP, 173
reduced characteristic parameters, use of, 185–190
calculation procedure, 185–187
turbine characteristic, utilized area of, 187
turbine shafts, 55–56
turbine type, 86–90
determination of, 86
discharge ratio, 89
power ratio, 89
similarity laws of, 86–88, 90
speed ratio, 89
velocity parallelograms, 87
unitary parameters, *see* reduced parameters

VAB, *see* vertical axial-flow pump, adjustable blades
vacuum groundwater lowering installations, 360–361
VAF, *see* vertical axial-flow pump, fixed blades

Verkhne-Tuloma (Russia) hydroelectric power plant, 37, 38
vertical axial-flow pump, adjustable blades (VAB), *see* impeller pumps
vertical axial-flow pump, fixed blades (VAF), *see* impeller pumps
vertical hydroelectric units, 171, 172

water motion, mode of in turbine runner, 97–99
  circulation, 98, 99
  Kutta-Joukovski theorem, 98
  lift force, 98
  reduced parameters, 99
  runner blades, 99
water pressure (energy), 8–13
well pumps, 346–350
  with immersion electric motor, 348–350
    construction of, 348
    nomenclature of, 349–350
  with transmission shaft, 346–348
    construction of, 346–347
    nomenclature of, 347, 348

Zagorsk hydroelectric power plant (Russia), 385, 386, 388
Zeisk hydroelectric power plant (Russia), 43, 44